Cancer Field Surgery in Gynecologic Oncology

Principles and Practice

Michael Höckel
Rainer Kimmig
Ulrich Behn

Springer

Cancer Field Surgery in Gynecologic Oncology

Michael Höckel • Rainer Kimmig
Ulrich Behn

Cancer Field Surgery in Gynecologic Oncology

Principles and Practice

Springer

Michael Höckel
Leipzig School of Radical Pelvic Surgery
Leipzig, Germany

Ulrich Behn
Universität Leipzig
Institut für Theoretische Physik
Leipzig, Germany

Rainer Kimmig
Universitätsfrauenklinik Essen
Westdeutsches Tumorzentrum
Essen, Germany

ISBN 978-3-031-83029-7 ISBN 978-3-031-83030-3 (eBook)
https://doi.org/10.1007/978-3-031-83030-3

Preface

This book project marks a state in a long-term scientific and clinical enterprise that has achieved insights and results to be structured and summarized. When it became apparent that traditional concepts of local cancer progression had to be abandoned due to incompatibilities with clinical facts, a new approach, the ontogenetic cancer field model, evolved. Pursuing the development of the female reproductive system to map its ontogenetic anatomy provided clues for local spread patterns of lower genital tract carcinomas. The model unveils a so far hidden order of cancer: Tumors propagate locally within tissues, which are determined by successive de-differentiation of the cancer cells, a reversion of the corresponding normal cell type's differentiation trajectory during morphogenesis. This model stringently explains the discrepancies in the traditional isotropic cancer spread concept. Moreover, a precise understanding of the complex anatomy of the subperitoneum and a different view on the perineum arose from the study of their ontogenetic pathways. It renders the conventional surgical anatomy of dissection-driven artifacts and arbitrary tissue boundaries obsolete.

Linking the cancer field model to mechanisms of peripheral immune tolerance of normal and transformed cells and respecting the network architecture of the lymphatic system based on its development allowed an unequivocal interpretation of the pattern of lymph nodal metastasis with regard to first, second, and third immunologic defense lines as observed with carcinomas of the lower genital tract.

The clinical translation of this new paradigm of ontogenetic cancer fields into ontogenetic cancer staging and cancer field surgery with immunologic defense line-directed lymph node dissection totally dispensing with adjuvant radiotherapy has led to sustainable superior treatment results, now manifested with more than one thousand patients in our centers. Since 2005, the new principles and practice are taught at the Leipzig School of Radical Pelvic Surgery. Many colleagues from all over the world have attended the courses held in Leipzig, Germany, and implemented cancer field surgery in their armamentarium. Each course increased the demand not only of practicing colleagues but also of medical students interested in a deeper understanding of solid cancers to compile the educational contents in a textbook. When the superior results of cancer field surgery passed the test of time and many other centers were able to reproduce them, this book project was finally started. The book aims to fulfill three goals: the reader should (1) understand the logic of the cancer field model, (2) become familiar with the ontogenetic anatomy

of the female pelvis and perineum, and (3) be enabled to practice cancer field surgery. Co-authored by Rainer Kimmig, who developed robotic cancer field surgery to treat endometrial cancer, the book introduces the optimal technical approaches available to date to operate gynecologic cancer according to the paradigm.

The book is divided into two parts: Basics and Clinics. Although the Basics part provides useful information to practice cancer field surgery by introducing the reader into the paradigm of ontogenetic cancer fields, the comprehension of this rather ambitious text is not essential to become able to reproduce the novel surgical techniques. The Clinics part describes cancer field surgery for the treatment of gynecologic cancer step by step, elucidating all aspects of its perfect performance.

Figures in the form of schematic and anatomical drawings as well as photographs are placed at high priority. Two artists, Nikolaus Lechenbauer and Mara Sandrock, accomplished this demanding task with their personal aesthetic signatures to inform and engage the reader. Mara Sandrock and Angela Steller took the step-by-step procedural photographs mastering the challenge of depicting the deep pelvis with highest precision and resolution.

The paradigm of ontogenetic cancer fields claims general validity. The theoretical physicist Ulrich Behn thoroughly tested its arguments for consistency and co-authored a brief discourse of the cancer field model in a broader context at the end of this book.

The authors are indebted to Professor Bahriye Aktas, Chairwoman of the Women's Hospital at the University of Leipzig, for continuous support. M.H. is partucularly grateful to Professor Thomas Kahn, former Director of the Institute of Radiology, University of Leipzig for providing the MRI scans, to Professor Lars-Christian Horn, Institute of Pathology, University of Leipzig for producing the microphotographs of the histological sections and to Katja Schmidt for her kind long-term care of our patients. We thank the Stiftung Gynäkologische Forschung at the University Hospital of Essen for funding. The editorial and publishing efforts of Springer Nature are acknowledged.

Leipzig, Germany — Michael Höckel
Essen, Germany — Rainer Kimmig
Leipzig, Germany — Ulrich Behn

Contents

List of Abbreviations

ACM	Anterior cloacal mesoderm/mesenchyme
APC	Antigen presenting cell
Breg	Regulatory B cell
CAg	Cancer antigen
CLM	Caudal lateral mesoderm/mesenchyme
cN	Clinical nodal state
ECM	Extracellular matrix
ECS	Extracapsular spread
EMMR	Extended mesometrial resection
FIGO	International Federation of Gynaecology and Obstetrics
ICG	Indocyanine green
iLND	Immunologic defense line-directed lymph node dissection
LEER	Laterally extended endopelvic resection
MHC	Major histocompatibility complex
oT, oN	Ontogenetic tumor and nodal stage
pMHC	Peptide-major histocompatibility complex
PMMR	Peritoneal mesometrial resection
pT, pN	Pathological tumor and nodal state
PTAg	Peripheral tissue antigen
R0, 1, 2	Resection margin without, with microscopic, with macroscopic cancer
Tc	Cytotoxic T cell
Th	Helper T cell
TMMR	Total mesometrial resection
Treg	Regulatory T cell
VFR	Vulvar field resection

Introduction

1

Cancer, the malignant disease of multicellular animals (Metazoa), is complex at all scales: the malignantly diseased organism, the malignant tumor, the cancer cell, and the cancer cell epigenome and genome. With each piece of insight, cancer research reveals more open questions. Complexity reduction, like breaking down cancer into hallmarks [1], has been mandatory to deal with the disease both clinically and scientifically. However, complexity reduction bears an inherent risk of drawing incorrect *general* conclusions. In oncology, this became evident with concepts such as sequential genomic hits driving malignant progression [2], tumor angiogenesis [3], and antitumor immune responses pharmacologically exploited to cure cancer [4, 5], to name just a few. Whereas the accumulation of mutations in distinct genes was confirmed for cancer initiation in some tumor types, the identification of mutations causative for metastasis, the most common cause of cancer lethality, could not be identified to date, making illusory the notion that drug cocktails active against all driver mutations are a curative treatment. Likewise, intense research to elucidate the molecular mechanism of tumor angiogenesis and to interfere with the formation of new blood vessels necessary for cancer growth resulted in drugs prolonging the lives of patients with certain tumor situations but did not succeed in permanent disease control, as had been hoped [6]. Similarly, although long-term disease control has been achieved with current immunotherapeutic approaches for individual cancer patients, many interventions failed, rendering this treatment as a final victory in the fight against cancer prematurely optimistic [7].

Another example of complexity reduction in oncology is the idea of randomly continuous, i.e., *isotropic local tumor spread* (Fig. 1.1). The microscopic invasion of peritumoral tissues by single cancer cells or cell clusters is an essential pathological feature of malignancy. Cancer cell infiltration occurs interstitially, within lymph or blood vascular spaces, or along nerve fibers. It is generally assumed that the direction of spread is unpredictable and that progression proceeds irrespective of tissue borders. As a clinical consequence, the surgical resection of solid malignant tumors is performed as a *wide excision*, including a metrically defined circumferential margin of microscopically uninvolved tissue (Fig. 1.2). Margin width is measured and reported by the pathologist investigating the surgical specimen. If the tumor board considers the margin width too narrow, re-excision or adjuvant (chemo)radiation is recommended. Likewise, planning of primary radiotherapy for local tumor control integrates a circumferential mantle of macroscopically tumor-free tissue into the target volume determined by radiologic imaging.

However, the tenet of continuous isotropic local tumor spread has to be rejected due to its incompatibility with numerous clinical data reported for many cancer types. If the concept of

M. Höckel et al., *Cancer Field Surgery in Gynecologic Oncology*,
https://doi.org/10.1007/978-3-031-83030-3_1

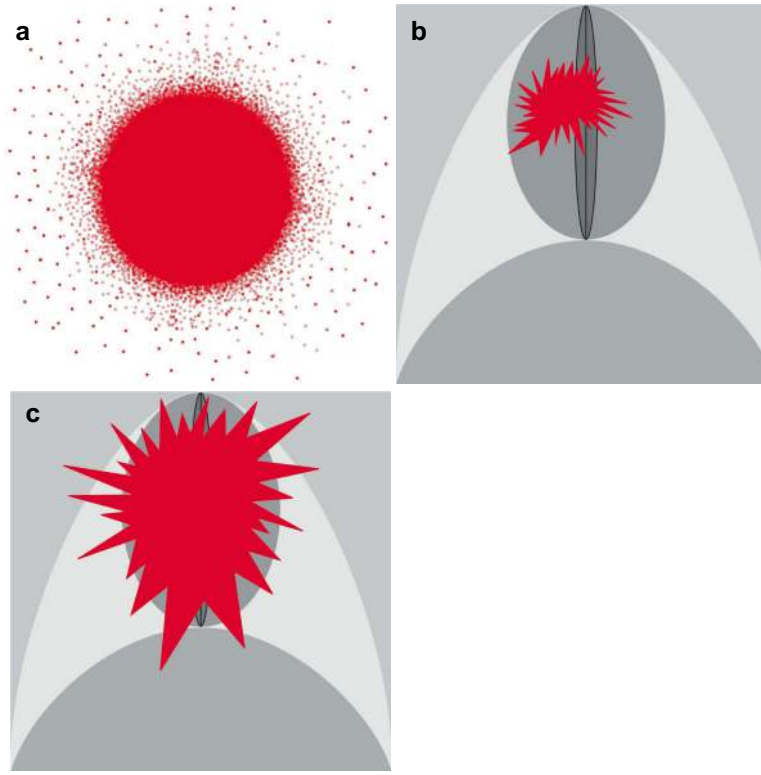

Fig. 1.1 Schematic illustration of the current view on local tumor spread. (**a**) According to the isotropic model, microscopic cancer foci are considered to follow a random diffusive pattern. (**b**, **c**) Malignant tumor (red) propagation ignores tissue borders (shades of grey)

isotropic local tumor propagation were correct, then margin width would be a robust predictor of local tumor recurrence. However, this is not the case. Table 1.1 lists the predictive relevance of margin width for vulvar and breast cancers as examples. Likewise, a prospective randomized investigation on the significance of the extent of parametrial resection, comparing two types of radical hysterectomy for the surgical treatment of cervix carcinoma FIGO stages IB and IIA, could not demonstrate better local control for the more extensive surgery [18].

The lack of robustness of margin width to predict local recurrence can be simply explained by assuming *anisotropy in local tumor spread*, which results from permissive and nonpermissive tissues for the propagation of individual cancer (Fig. 1.3). In order to test this hypothesis, we generated local tumor landscapes by mapping the probability of pelvic and perineal tissues to be infiltrated by cervix and vulvar carcinomas (Figs. 1.4 and 1.5). The data were derived from more than 600 carcinomas of the uterine cervix FIGO stages IB-IVA and vulvar carcinomas FIGO stages IB and II that were resected with clear surgical margins. Conventional topographic anatomy was applied in the transverse sections of the midpelvis and the superficial and deep perineum. The tissues were color-coded as heat maps, representing infiltration probability based on the histopathological findings in the surgical specimens. Anisotropic local spread patterns become clearly evident from these maps. Whereas the paracervical involvement of cervical carcinoma was about 80%, it dropped to 20% at the ureteral and mesureteral borders and increased to 70% distal to the ureters at the bladder adventitia and mesentery. Ventral cervix cancer propagation to the bladder wall was twice as frequent as dorsal spread into the mesorectum, despite their similar proximity to the cervix, the site of cancer origin.

Tumor landscapes of vulvar carcinomas demonstrated anisotropic spread patterns as well. As an example, cancers presenting their main tumor mass in the peripheral subcompartment (i.e., the preputium, interlabial sulcus, and lateral perineum), and therefore presumably originating

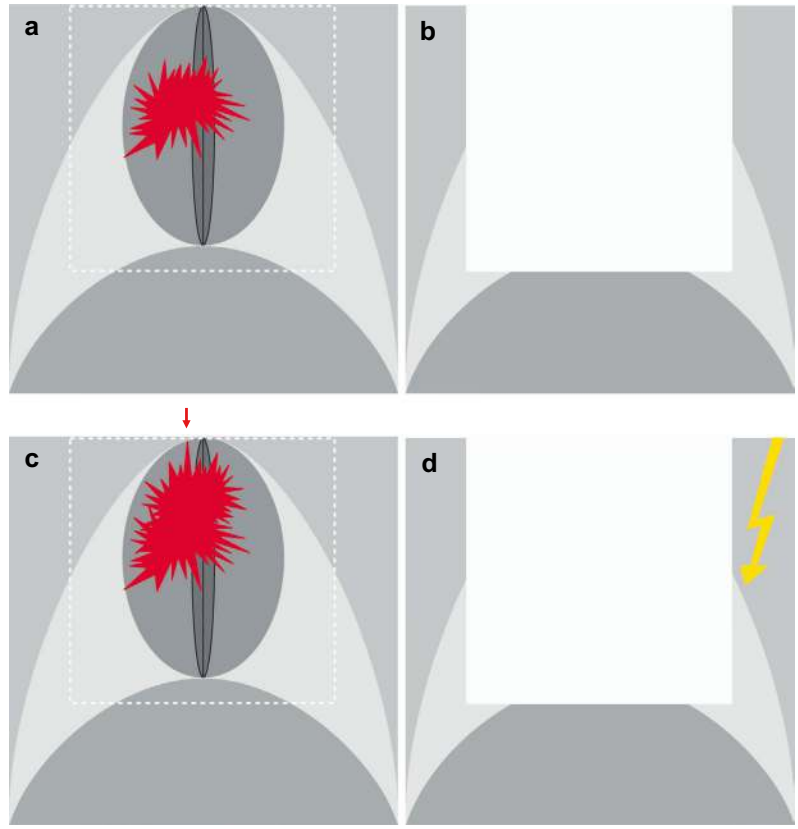

Fig. 1.2 Schematic illustration of wide tumor excision. (**a**, **b**) A malignant tumor (red) is resected with a circumferential margin of microscopically cancer-free tissue (shades of grey within the dotted frame). (**c**, **d**) If the resection margin is considered to be too narrow (arrow), re-excision or postoperative adjuvant radiotherapy is recommended. White areas represent resected tissues

Table 1.1 Inconsistent results of surgical margin width to predict local recurrence

Breast cancer	
Wider surgical margins lower the risk of local recurrence	
Vicini et al. [8]	$n = 507$
Local control with breast-conserving surgery is not improved by wider tumor-free margins	
Antonini et al. [9]	$n = 1724$
Jones et al. [10]	$n = 1616$
Odds of local recurrence are not associated with margin width	
Houssami et al. [11]	$n = 14{,}571$ (meta-analysis)
Vulvar cancer	
Close (<8 mm) margin predicts local recurrence	
Heaps et al. [12]	$n = 91$
Close (<8 mm) margin does not predict local recurrence	
Groenen et al. [13]	$n = 93$
Cancer-free margin width is not related to local recurrence	
Baiocchi et al. [14]	$n = 205$
Nooij et al. [15]	$n = 148$
Woelber et al. [16]	$n = 289$
Te Grootenhuis et al. [17]	$n = 287$

there, exhibited an 18% probability of peripheral spread into the labia majora, compared to a 34% probability of central spread into the labia minora, glans clitoridis, and central perineum. Likewise, directly underlying deep structures, such as the corpus or crura of the clitoris, were found to be infiltrated in only 12% of the cases. The logical consequences of these findings suggest a more adequate principle for cancer surgery, namely the removal of a malignant tumor by resecting tissues permissive for its local spread. Alternatively, the resection of the tumor with wide cancer-free margins within its permissive tissues and with just clear margins (R0) at the border toward the nonpermissive tissues should be considered (Fig. 1.6). Cancer surgery, according to this concept, prevents local recurrences despite the preservation of tissues close to the tumor if they are nonpermissive. The development of this idea as a new *paradigm of ontogenetic cancer fields* and its translation into cancer field surgery for the locoregional control of carcinomas are the subjects of this book.

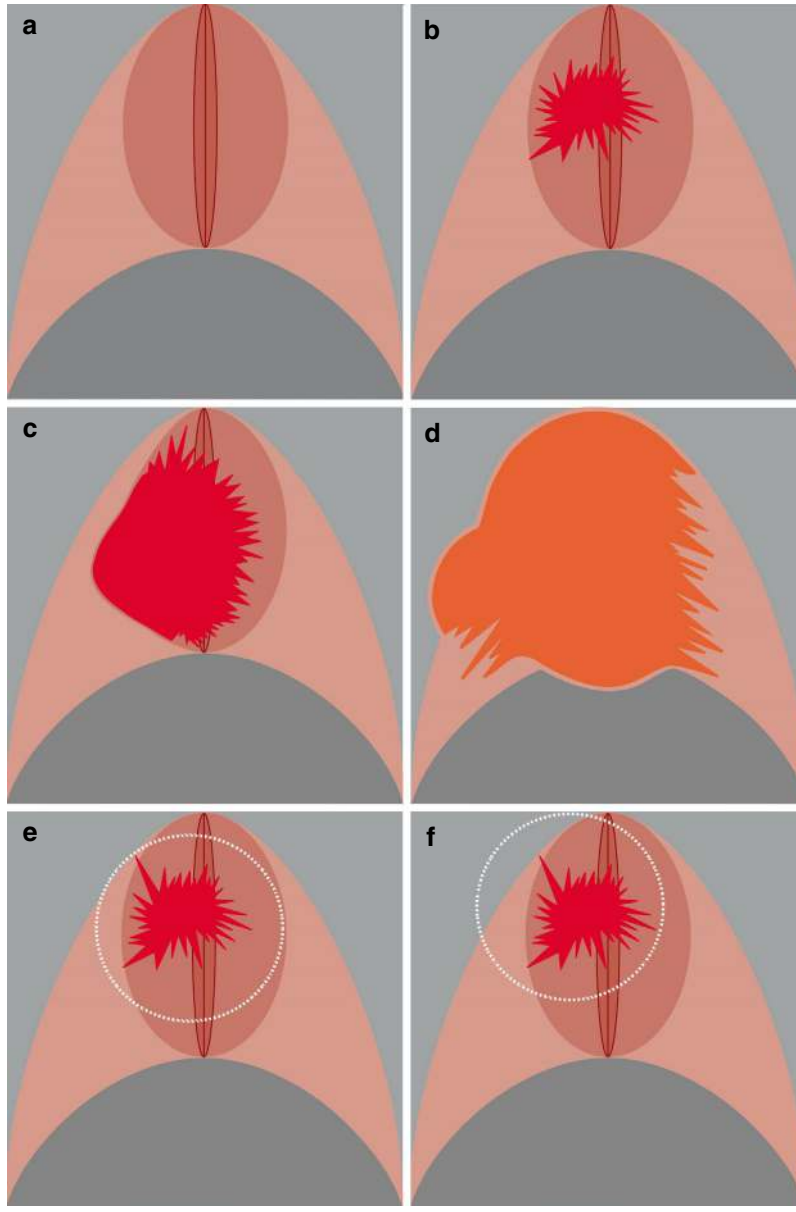

Fig. 1.3 A schematic illustration of anisotropic local tumor propagation that causes the lack of robustness in the resection margin width. (**a**) A hierarchy of permissive regions for local tumor spread, which are colored in three shades of pink. Grey areas are nonpermissive. (**b**) A malignant tumor that originated in the shallow elliptic area (e.g., an epithelium) spreads randomly within the larger elliptic area, representing the first cancer field. (**c**) The tumor, exhibiting the first stage of malignant progression, distorts but does not transgress the first cancer field. (**d**) Malignant progression opens up the next cancer field, which again is distorted but cannot be transgressed. (**e**) A narrow resection margin at the border to nonpermissive tissue indicates no risk of local recurrence. (**f**) A narrow resection margin within permissive tissue indicates a high risk of local recurrence. As situations (**e**, **f**) cannot be distinguished by the pathologist, the predictive significance of margin width is not robust

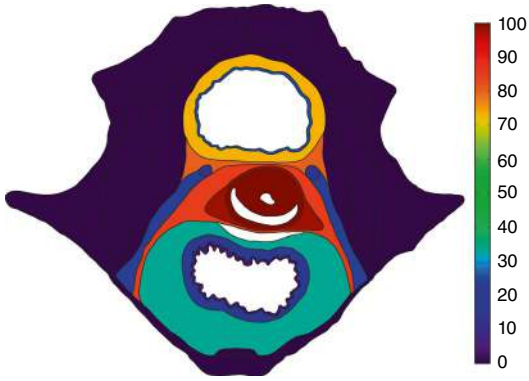

Fig. 1.4 An anatomical landscape of local cancer spread, showing the probability of tumor infiltration by heat map coloring (percent scale to the right). The spread of cervix carcinomas is demonstrated in a midpelvic transverse plane. Data are obtained from n = 565 cervix carcinomas, FIGO stages IB - IVA operated with clear surgical margins

The paradigm, which is outlined in Part I, includes three concepts: ontogenetic anatomy, the local cancer field model, and the regional cancer field model. *Ontogenetic anatomy* and the *cancer field model for local tumor spread* are the topics of Chap. 2. Ontogenetic anatomy maps the mature tissue derivatives of the morphogenetic fields associated with the stepwise development of a cell type from the phylotypic state to maturity. The cancer field model relates tissues permissive to the local spread of the transformed cell type, the cancer fields, to the mature derivatives of the morphogenetic fields of the nontransformed cell type.

The steps in the development of the uterus, vagina, and vulva; the corresponding lineage-associated morphogenetic fields; and their mature

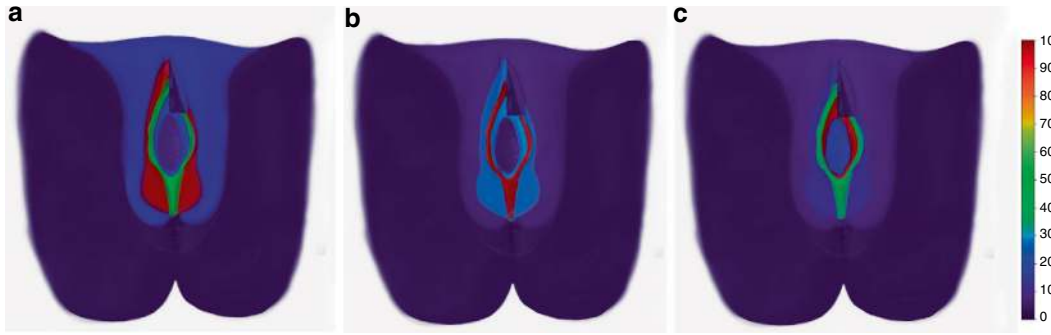

Fig. 1.5 Anatomical landscapes of the local spread of vulvar cancer color-coded as heat maps. The carcinomas originated in the peripheral (**a**), intermediate (**b**), and central (**c**) vulvar subcompartments. Heat maps were constructed from the histopathological assessment of 60 (**a**), 112 (**b**), and 78 (**c**) patients with vulvar carcinoma FIGO stages IA–IIIC resected with clear surgical margins. The topographic perineal anatomy is colored according to the scale bar on the right to express the frequency of local tumor involvement. Anisotropic tumor spread according to the ontogenetic anatomy is evident

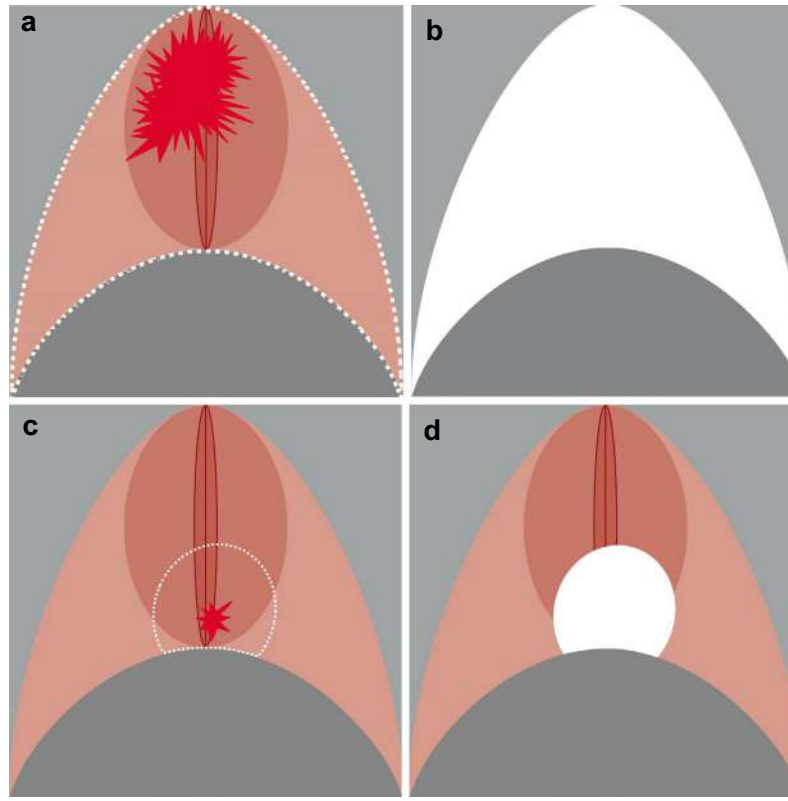

Fig. 1.6 A schematic illustration of the new principle of cancer surgery. (**a**, **b**) The complete tissue permissive for local tumor spread is resected. At the border to the nonpermissive tissue, a narrow resection margin is sufficient. (**c**, **d**) The tumor is resected with wide margins within its permissive tissue, but only a narrow resection margin is demanded at the border. White areas represent resected tissues

tissue derivatives from the phylotypic state to terminal differentiation are described in Chaps. 3 and 4. Color-coding these tissues in conventional topographical anatomic illustrations represents their ontogenetic anatomy, which highlights the territories permissive for the spread of the corresponding carcinomas. Surgical treatment tailored to the cancer field enables maximum local tumor control with minimal treatment-related morbidity as tissues outside the individual cancer field, which could be functionally or aesthetically significant, can be preserved despite their immediate proximity to the malignant lesion.

Epithelial cancers, i.e., carcinomas, have a significant risk of regional metastasis at the time of their clinical diagnosis. Except for very early disease stages, it is therefore mandatory to integrate regional tumor control into a treatment plan with curative intent. Current clinical practice for carcinoma of the lower female genital tract applies surgery as the most accurate means to assess the nodal state. Sentinel lymph node biopsy following dye and/or radionuclide application has been established for vulvar and endometrial cancers and is under investigation for cervix cancer to detect or exclude lymph node metastases. If metastases are histopathologically proven, surgical treatment alone is considered insufficient for regional tumor control, and adjuvant or radical radiotherapy is recommended. However, postoperative adjuvant radiation thwarts failure analysis. As a consequence, this convention has impeded improvements in the surgical control of regional disease. Topographically mapped therapeutic (immune defense-line-directed) lymph node dissection completely dispensing with adjuvant radiotherapy in cases of histopathologically proven lymph node metastasis enabled us to accurately determine the patterns of regional spread in cancer of the lower female genital tract. From these pathoanatomical results, an ontogenetic cancer field model for regional tumor propagation has been deduced and prospectively tested.

The *regional cancer field model* is the subject of Chap. 5. This model refers to mechanisms of peripheral immune tolerance that "export" and extend the local cancer field to the draining

lymph nodes and thus enable released competent carcinoma cells to form metastases. From the interrelation between the tissue representing the local tumor bed and the complex network of the lymphatic system, lymph nodes at risk for metastases can be identified. The ontogenetic anatomy of the lymphatic system describes the first, second, and third peripheral immunologic defense lines for any tissue of interest. Chapter 6 discusses the ontogenetic anatomy of the lower human body's lymphatic system, providing clues for the regional progression of carcinomas of the lower genital tract.

Part II of this book is devoted to the clinical translation of the ontogenetic cancer field paradigm into a new practice for diagnosing and surgically treating gynecologic malignancies. In Chap. 7, the diagnostic management of *ontogenetic gynecologic cancer staging* is introduced. Chapters 8, 9, 10, and 11 present detailed descriptions of the different types of *cancer field surgery*: total and extended mesometrial resections, peritoneal mesometrial resections, and laterally extended endopelvic resections, vulvar field resections, all combined with immunological defense line-or peripheral immune network-directed lymph node dissection (iLND). These new surgical techniques that apply ontogenetic anatomy differ significantly from conventional procedures that are based on empirical and arbitrary concepts of tissue topography. Traditional surgical anatomy of the subperitoneal tissues considering so-called "ligaments" and "spaces" is founded on dissection artifacts with major variations between surgeons and substantial deviations from the tissue borders established by ontogenesis. Likewise, conventional topographic anatomy and ontogenetic anatomy of the vulva vary in many aspects.

Chapter 12 introduces selected surgical procedures for the anatomical reconstruction of the vulva, optimally combined with cancer field surgery. Each procedure in Chaps. 8, 9, 10, 11, and 12 is demonstrated step-by-step with essential intraoperative illustrations. In-depth descriptions of the clinical management of vulvar, vaginal, cervix, and endometrial carcinomas according to the ontogenetic cancer field paradigm include preoperative, intraoperative, and postoperative aspects. Possible intra- and postoperative complications are specified and recommendations are provided on how to deal with them. For all tumor entities, clinical management algorithms regarding indication and treatment are set up in Chap. 13. Long-term outcome data of large cohorts of patients with gynecologic carcinomas treated by cancer field surgery are presented as well. From the systematic pathoanatomical analysis of treatment failures without interference by adjuvant radiation, the limits of cancer field surgery are elaborated. The results are another strong support for the ontogenetic cancer field paradigm.

Finally, a short epilogue resumes the hitherto unrecognized aspects of solid malignant tumors, which are evident from the paradigm of ontogenetic cancer fields: the *cancer paradox* and the *order of cancer*. Becoming aware of this may help in comprehending and treating cancer.

References

1. Hanahan D, Weinberg RA. Hallmarks of cancer: the next generation. Cell. 2011;144:646–74. https://doi.org/10.1016/j.cell.2011.02.013.
2. Vogelstein B, Kinzler KW. The path to cancer – three strikes and you're out. N Engl J Med. 2015;373:1895–8. https://doi.org/10.1056/NEJMp1508811.
3. Folkman J. Tumor angiogenesis: therapeutic implications. N Engl J Med. 1971;285:1182–6. https://doi.org/10.1056/NEJM197111182852108.
4. Okazaki T, Honjo T. PD-1 and PD-1 ligands: from discovery to clinical application. Int Immunol. 2007;19:813–24. https://doi.org/10.1093/intimm/dxm057.
5. Sharma P, Wagner K, Wolchok JD, Allison JP. Novel cancer immunotherapy agents with survival benefit: recent successes and next steps. Nat Rev Cancer. 2011;11:805–12. https://doi.org/10.1038/nrc3153.
6. Carmeliet P, Jain RK. Molecular mechanisms and clinical applications of angiogenesis. Nature. 2011;473:298–307. https://doi.org/10.1038/nature10144.
7. Hegde PS, Chen DS. Top 10 challenges in cancer immunotherapy. Immunity. 2020;52:17–35. https://doi.org/10.1016/j.immuni.2019.12.011.
8. Vicini FA, Eberlein TJ, Connolly JL, Recht A, Abner A, Schnitt SJ, et al. The optimal extent of resection for patients with stages I or II breast can-

cer treated with conservative surgery and radiotherapy. Ann Surg. 1991;214:200–5. https://doi.org/10.1097/00000658-199109000-00002.
9. Antonini N, Jones H, Horiot JC, Poortmans P, Struikmans H, Van den Bogaert W, et al. Effect of age and radiation dose on local control after breast conserving treatment: EORTC trial 22881-10882. Radiother Oncol. 2007;82:265–71. https://doi.org/10.1016/j.radonc.2006.09.014.
10. Jones HA, Antonini N, Hart AAM, Peterse JL, Horiot J-C, Collin F, et al. Impact of pathological characteristics on local relapse after breast-conserving therapy: a subgroup analysis of the EORTC boost versus no boost trial. J Clin Oncol. 2009;27:4939–47. https://doi.org/10.1200/JCO.2008.21.5764.
11. Houssami N, Macaskill P, Marinovich ML, Dixon JM, Irwig L, Brennan ME, et al. Meta-analysis of the impact of surgical margins on local recurrence in women with early-stage invasive breast cancer treated with breast-conserving therapy. Eur J Cancer. 2010;46:3219–32. https://doi.org/10.1016/j.ejca.2010.07.043.
12. Heaps JM, Fu YS, Montz FJ, Hacker NF, Berek JS. Surgical-pathologic variables predictive of local recurrence in squamous cell carcinoma of the vulva. Gynecol Oncol. 1990;38:309–14. https://doi.org/10.1016/0090-8258(90)90064-r.
13. Groenen SM, Timmers PJ, Burger CW. Recurrence rate in vulvar carcinoma in relation to pathological margin distance. Int J Gynecol Cancer. 2010;20:869–73. https://doi.org/10.1111/IGC.0b013e3181df7423.
14. Baiocchi G, Mantoan H, de Brot L, Badiglian-Filho L, Kumagai LY, Faloppa CC, et al. How important is the pathological margin distance in vulvar cancer? Eur J Surg Oncol. 2015;41:1653–8. https://doi.org/10.1016/j.ejso.2015.09.024.
15. Nooij LS, van der Slot MA, Dekkers OM, Stijnen T, Gaarenstroom KN, Creutzberg CL, et al. Tumour-free margins in vulvar squamous cell carcinoma: does distance really matter? Eur J Cancer. 2016;65:139–49. https://doi.org/10.1016/j.ejca.2016.07.006.
16. Woelber L, Griebel L-F, Eulenburg C, Sehouli J, Jueckstock J, Hilpert F, et al. Role of tumour-free margin distance for loco-regional control in vulvar cancer – a subset analysis of the Arbeitsgemeinschaft Gynäkologische Onkologie CaRE-1 multicenter study. Eur J Cancer. 2016;69:180–8. https://doi.org/10.1016/j.ejca.2016.09.038.
17. Te Grootenhuis NC, Pouwer AW, de Bock GH, Hollema H, Bulten J, van der Zee AGJ, et al. Margin status revisited in vulvar squamous cell carcinoma. Gynecol Oncol. 2019;154:266–75. https://doi.org/10.1016/j.ygyno.2019.05.010.
18. Landoni F, Maneo A, Cormio G, Perego P, Milani R, Caruso O, et al. Class II versus class III radical hysterectomy in stage IB-IIA cervical cancer: a prospective randomized study. Gynecol Oncol. 2001;80:3–12. https://doi.org/10.1006/gyno.2000.6010.

Part I

Basics: The Paradigm of Ontogenetic Cancer Fields

2 Ontogenetic Anatomy and the Cancer Field Model of Local Tumor Progression

Cancer is a complex disease affecting nearly all species of the biological kingdom of multicellular animals (Metazoa). Current insights into metazoan evolution, development, regeneration, and repair are briefly considered to introduce the concepts of ontogenetic anatomy and the local cancer field model.

The evolution of Metazoa, which started about 600 million years ago, brought forth the novel biological feature of multiple somatically inheritable epigenetic states of the genome representing different *cell types*. Multiple temporarily stable noninheritable epigenetic states representing *cytotypes*, in addition to those replicated by cell division, had already existed in advanced unicellular animals. During the development of all multicellular animals, transitions of cell types are driven toward decreased plasticity and increased specificity, herein termed *cell type differentiation*. The stepwise developmental pathway forms a cell type *differentiation trajectory*. Bifurcations in developmental pathways structure a branched pedigree from the zygote (fertilized egg cell) to all mature cell types of the organism. The plasticity of inheritable and noninheritable states allows *transdifferentiation* between cell types and cytotypes to various degrees. Transdifferentiation between cell types is also termed *transdetermination*.

The comparison of extant choanoflagellates, akin to the Urchoanozoon—the most advanced unicellular animal—with Porifera (sponges), akin to the Urmetazoon—the earliest multicellular animal—illustrates evolutionary novelties [1]. Choanoflagellates exhibit multiple resident and mobile states of cytodifferentiation (cytotypes) induced by extrinsic signals, reproduce sexually, and form structured cell aggregates. Transdifferentiation between cytotypes occurs unidirectionally if the resident choanoflagellate adheres to a substrate and bidirectionally in motile states. However, only one state is somatically inheritable [2].

Sponges exhibit two somatically inheritable cell states (cell types) that are interrelated through transdetermination: archeocytes and choanocytes. Both cells are totipotent and differentiate into ten mature cytotypes [3]. In sexual sponge reproduction, choanocytes and archeocytes develop from the zygote through a one-step bifurcational differentiation trajectory.

Sponges also reproduce asexually from archeocytes that are liberated from the parent organism [4].

Hydra, another multicellular animal that arose very early in evolution, develops three somatically inheritable cell states (cell types) during its embryogenesis: ectodermal, endodermal, and interstitial cells [5]. Hydra reproduces sexually as well as asexually. With sexual reproduction, the zygote proceeds through a pathway of three bifurcations to the three cell types, which differentiate further into 15 cytotypes [6]. Asexual reproduction occurs through continuous bud

M. Höckel et al., *Cancer Field Surgery in Gynecologic Oncology*,
https://doi.org/10.1007/978-3-031-83030-3_2

formation and the detachment of buds from the parent organism. The three cell types continuously substitute the cells that are physiologically lost. Later in metazoan evolution, undifferentiated stem cells without organelles and specialized cytoplasm and various partly differentiated progeny arose as inheritable cytotype states of a cell type, in addition to differentiated cytotypes with or without replicable abilities. Together, they establish linear or branched cytotype trajectories for each cell type.

Figure 2.1a shows the tentative cell type differentiation trajectories in early human development based on morphological evidence [8]. Three-dimensional (3D) cultured early human embryos are currently used to gain deeper insights into these early events of human development [9–11].

Another essential feature of animal multicellularity, in addition to the developmental pedigree of cell types, which is conceptually important for ontogenetic anatomy and the cancer field model, is the *topoanatomical identity* of pattern-forming cell types realized by the habitats of their populations at anatomically distinct locations.

Cell type differentiation, associated with the emergence of spatially distinct habitats, starts with the first segregation into the trophectoderm and the inner cell mass detectable in the human conceptus at the 16-cell stage after four cleavage divisions. Trophectoderm cells with apical polarity are situated on the surface of the conceptus, and the apolar cells of the inner cell mass are confined to the internal space. Due to differences in tension, lower tension polar cells proceed to the surface and higher tension apolar cells are pushed into the inner conceptus [12, 13]. Hydraulic fracturing of the trophectoderm cell contacts and the confluence of the intercellular fluid lead to blastocoel formation [14].

By the second lineage bifurcation, epiblast and primitive endoderm populations (hypoblast) appear, generating their habitats at the future contact site of the blastocyst with the decidual surface of the uterus, known as the embryonic pole. The initially mixed epiblast and primitive endoderm cells segregate again as a consequence of differences in polarity: the hypoblast along the trophoblast surface toward the ab-embryonic pole and the epiblast along the trophoblast surface toward the embryonic pole [13]. The third lineage bifurcation, visible after blastocyst implantation, directs the epiblast and primitive endoderm populations along the proximodistal axis with regard to the precursor cell type population: the secondary epiblast as the proximal inner embryonic pole population and the amnioblast as the distal inner embryonic pole population; the visceral primitive endoderm as the proximal inner ab-embryonic pole population and the umbilical vesicoblast as the distal inner ab-embryonic pole population.

Figure 2.1b illustrates the spatial habitats of cell types that emerged after three bifurcations in a 9-day human blastocyst completely implanted into the maternal decidua.

Human cell-type differentiation trajectories exhibit a multitude of bifurcations to reach the terminal developmental stage. Their populations topographically occupy more and more specified territories, forming the mature human anatomy. Prior to *determination*, cells of a distinct type and state can transgress from their habitat into an adjacent anatomical territory and adopt the type of the cell population to which they immigrated. This transdetermination plasticity enables integrated morphogenetic actions and smoothens territorial borders [15, 16]. The combined anatomical territories that are permissive for a predetermination cell type, due to its topoanatomical plasticity, form its *morphogenetic field.* With each step in cell type differentiation, territorial plasticity decreases, while specificity in terms of the spatial interaction of the cell type with the environment increases, resulting in the formation of more and more anatomical details in the embryo and fetus. Plasticity of different cell lines abrogates with the state of *determination*, the end of the embryonic period in general and the early fetal period for sex-dependent structures. The morphogenetic field of a cell type is then restricted to its habitat and is termed *anatomical compartment*, but cell fate progression continues. Different progeny populations occupy subcom-

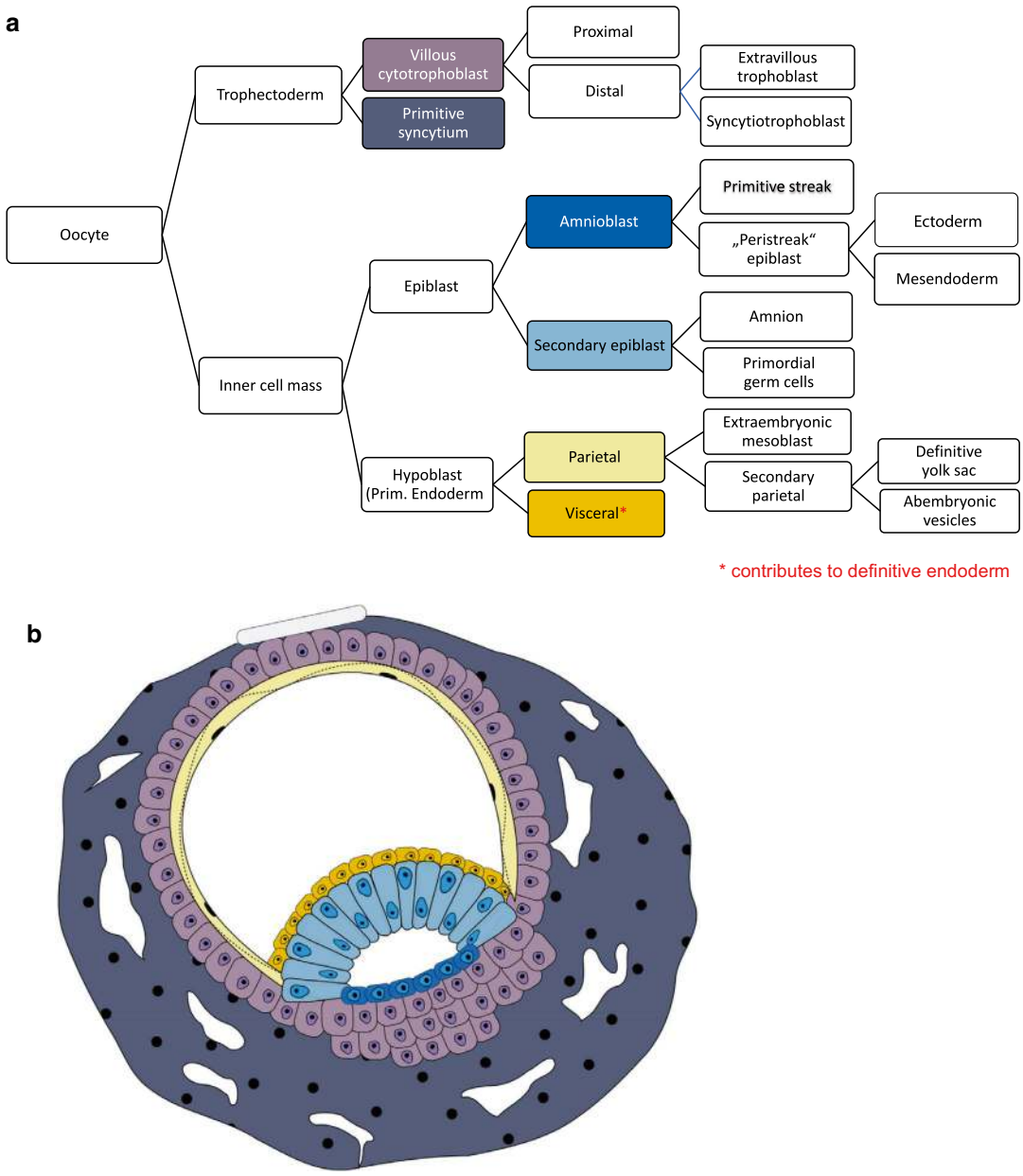

Fig. 2.1 (**a**) Tentative cell type differentiation trajectories for early human development, Carnegie stages 1–6. (**b**) Early anatomical territories representing the spatial habitats of the populations of six cell types after two or three bifurcations visible in a 9-day human blastocyst, color-coded as in (**a**) (modified after [7])

partments at different scales. The postdetermination differentiation trajectory no longer exhibits binary bifurcations, as was the case with cell fate decisions prior to the determined state. Figure 2.2 schematically illustrates this concept for the postphylotypic metazoan morphogenesis relevant to ontogenetic anatomy and the cancer field model, as indicated below. Herein it is assumed that (1) transitions in the differentiation trajectories of adjacent cell populations are interdependent; i.e.,

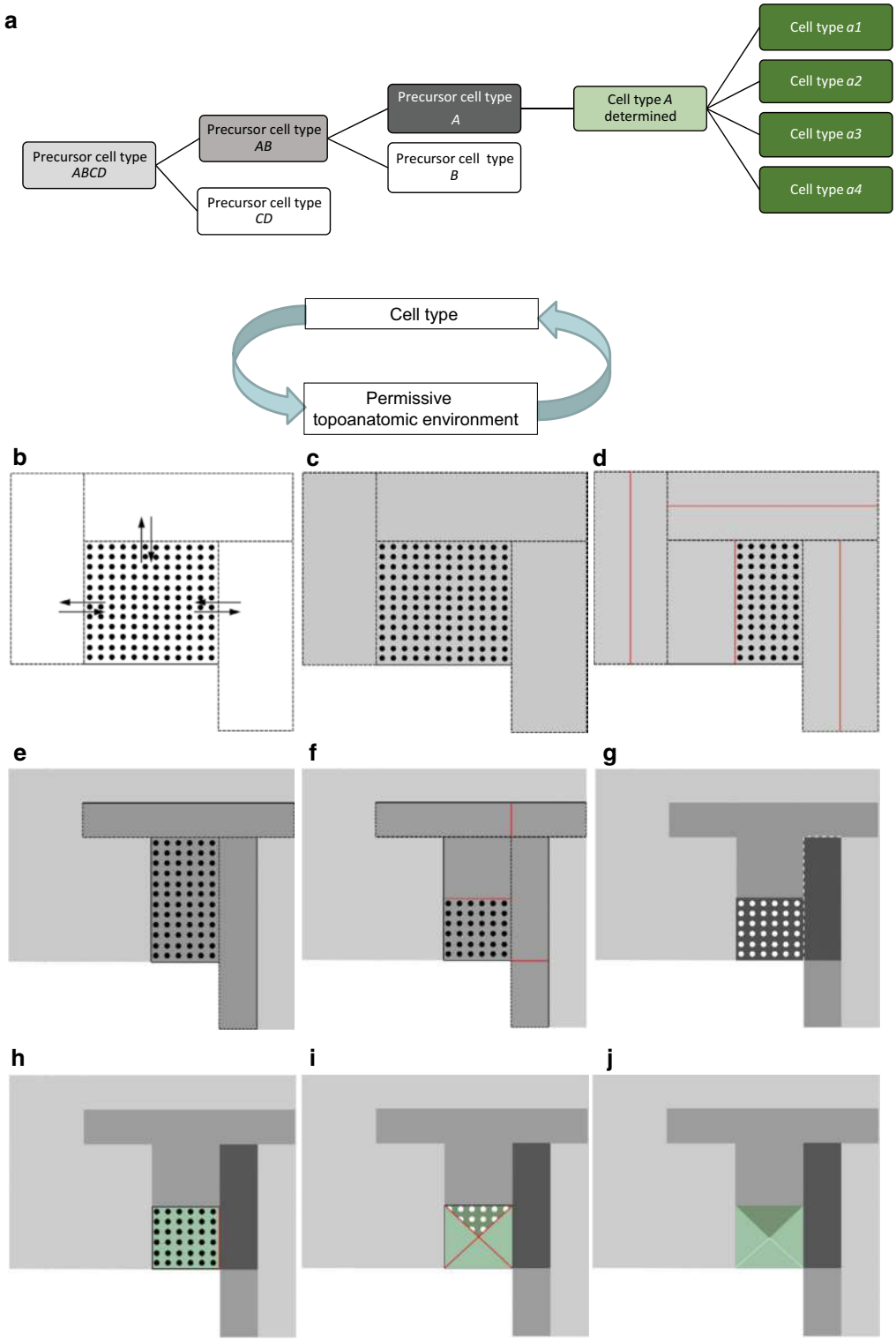
a
Precursor cell type ABCD
Precursor cell type AB
Precursor cell type CD
Precursor cell type A
Precursor cell type B
Cell type A determined
Cell type a1
Cell type a2
Cell type a3
Cell type a4
Cell type
Permissive topoanatomic environment
b
c
d
e
f
g
h
i
j

a differentiation step of one cell type is associated with a differentiation step of the abutting cell types. (2) Transdetermination between the two descendants of a precursor cell type and transgression into their habitats do not occur.

Mapping the mature tissue derivatives from the morphogenetic fields related to a cell type lineage at successive developmental states, from the phylotypic period to maturity, is the foundation of *ontogenetic anatomy*. Ontogenetic anatomy is expressed in two modes: in one mode, the spatial habitats of multiple determined cell types, compartments, and subcompartments are delimited. The other mode indicates the mature derivatives of the postphylotypic developmental steps for one cell type. It is accomplished by the color-coding of topographic anatomical illustrations.

Figure 2.3 shows the cell type differentiation trajectory for the uterine cervix, beginning with the nephrogenic cords as the precursor cell population of the mesonephric system at Carnegie stage 11, and the corresponding ontogenetic anatomy in a midpelvic transverse plane in the female human. The cell type differentiation trajectory of the peripheral vulvar subcompartment from the cloacal membrane cell population and the corresponding ontogenetic anatomy of the human female perineum are illustrated in Fig. 2.4. Details of the developmental history on which the ontogenetic anatomic maps are based are subjects of Chaps. 3 and 4.

Key features of the cancer field model for local tumor spread, which are derived from findings of those fields:

- Carcinoma phenotypes propagate locally within a hierarchy of topographically defined permissive tissue regions, termed *cancer fields*.
- The cancer fields are the mature derivatives of the *morphogenetic fields* established by the stepwise developmental pathway of the untransformed cell type.
- Within the cancer field, invasive and intravasive permeation of the tumor is random, but transgression of the field borders does not occur.
- Malignant progression opens up new cancer fields in hierarchical order, dictated by the reversion of the developmental pathway of the untransformed cell type.

Why is ontogenetic anatomy important to decipher the topography of local cancer spread? Biological mechanisms of repair and regeneration in multicellular animals are considered to provide the answer. Metazoa can regenerate damaged or lost tissues to various degrees, ranging from the restoration of the whole organism in

Fig. 2.2 Schematic classification of morphogenetic fields during postphylotypic cell type differentiation. (**a**) Differentiation trajectory from a postphylotypic precursor cell type *ABCD* to mature cell types, *a1–a4*. (**b**) Precursor cell type *ABCD* (points) and cells of different adjacent cell type populations can transgress habitat borders (dotted lines) and change cell type identity. (**c**) The habitat of the precursor cell type *ABCD* and the habitats of all adjacent cell types with transdetermination potential form the morphogenetic field of the cell type *ABCD* (light grey). (**d**) Transition to the next differentiation state produces two new cell types (precursor cell types *AB* and *CD*), generating two habitats with borders that can no longer be transgressed (red lines). Concomitantly, cell-type transitions of the adjacent cell populations occur. (**e**) The habitat of precursor cell type *AB* and the habitats of adjacent cell types with transdetermination potential form the morphogenetic field of the *AB* cell type (middle grey). (**f**) Transition of precursor cell type *AB* to the next differentiation state, the precursor cell type *A*, and generation of its habitat. (**g**) The habitats of precursor cell type *A* and the adjacent cell population with transdetermination potential form the morphogenetic field of the precursor cell type *A* (dark gray). (**h**) Determination of cell type *A*. The habitat of its population is fixed as an anatomical compartment (light green); its borders can no longer be transgressed by cell type *A* and adjacent sessile cell populations. (**i**) Further postdetermination lineage specification of cell type *A* into cell types *a1–a4* allocates subcompartments (dark green) to these cell type populations (shown for cell type *a1*). (**j**) The mature derivatives of the morphogenetic fields are mapped and color-coded for the representation of ontogenetic anatomy

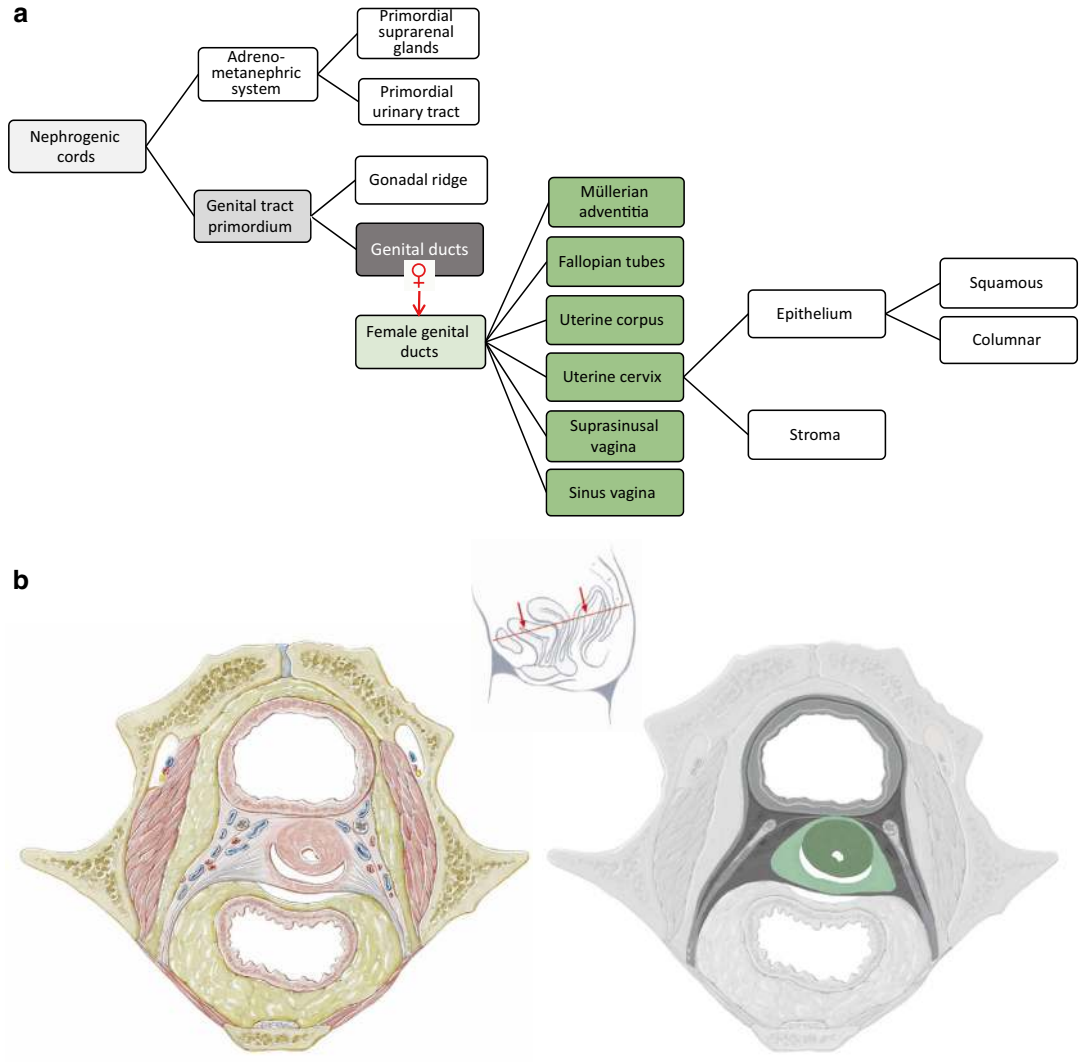

Fig. 2.3 Ontogenetic anatomy of the uterine cervix. (**a**) Cell type differentiation trajectory of uterine cervix epithelial and stromal cells starting from the nephrogenic cords. (**b**) The midpelvic transverse plane (inset) has been color-coded to map the mature tissue derivatives of the morphogenetic fields related to the developmental stages

phylogenetically earliest animals, such as sponges or hydra, to wound repair with substitution by scar formation in higher animals, such as mammals [17]. If the whole body of a sponge is fragmented into single cells, the suspension of these cells can regenerate the complete organism [18]. Dissociated hydra cells in suspension can also regenerate the complete organism [5]. Urodeles (salamanders and newts) are capable of complete limb and tail regeneration after amputation through a process that mirrors embryonic development after adult cells proximal to the site of tissue loss have undergone cell type dedifferentiation and produced an immature blastema [19].

The dedifferentiation of mature cell types through "backward" transitions of the somatically inheritable states, reversing their differentiation trajectories, is a general and essential (canonical) mechanism of regeneration and repair [20]. Although Porifera can completely regenerate from the totipotent archeocyte, hydra

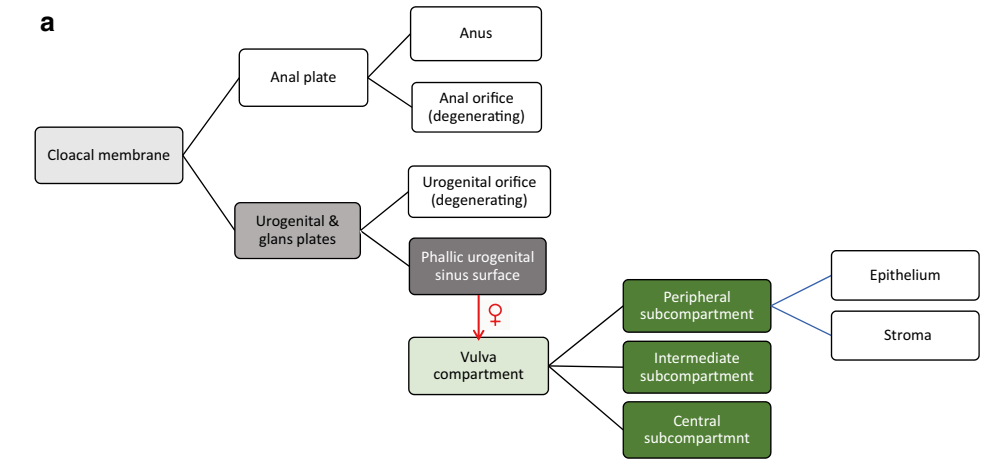

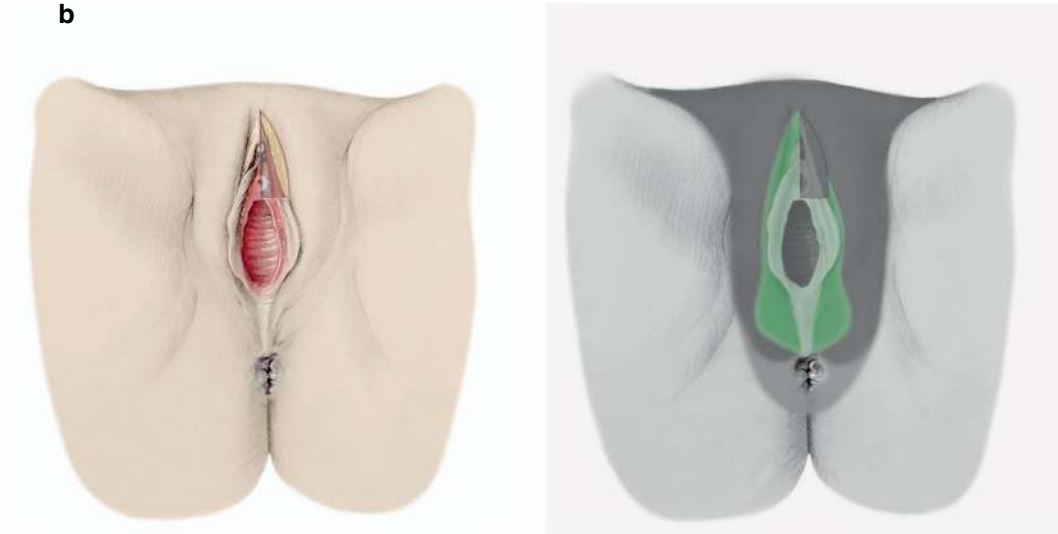

Fig. 2.4 Ontogenetic anatomy of the peripheral vulvar subcompartment. (**a**) Cell type differentiation trajectory of the epithelial and stromal cells of the vulva's peripheral subcompartment, starting from the cloacal membrane. (**b**) The perineum has been color-coded to map the mature tissue derivatives of the morphogenetic fields related to the developmental stages

mandates the dedifferentiation of mature cell types to restore a new organism from a single cell. As the regenerative potential of higher animals such as mammals is restricted, lost functional tissues are mainly substituted by scars. Nevertheless, the dedifferentiation of cell types during repair has been demonstrated for a multitude of mammalian responses to injury, such as wound healing of the skin [21] and the regeneration of the peripheral nerves [22], esophagus [23], colon [24], and liver [25]. A consequence of cell type dedifferentiation includes the extension of topoanatomical identity and an increase in the plasticity of the cell type, which enlarges the anatomical territory permissive to colonization by its population.

Transformed (i.e., cancer) cells permanently destroy their habitat by their uncontrolled proliferation, initiating and maintaining an inflammation and futile repair process. Malignant tumors therefore have been termed "wounds that do not heal" [26]. The cancer field model claims that in

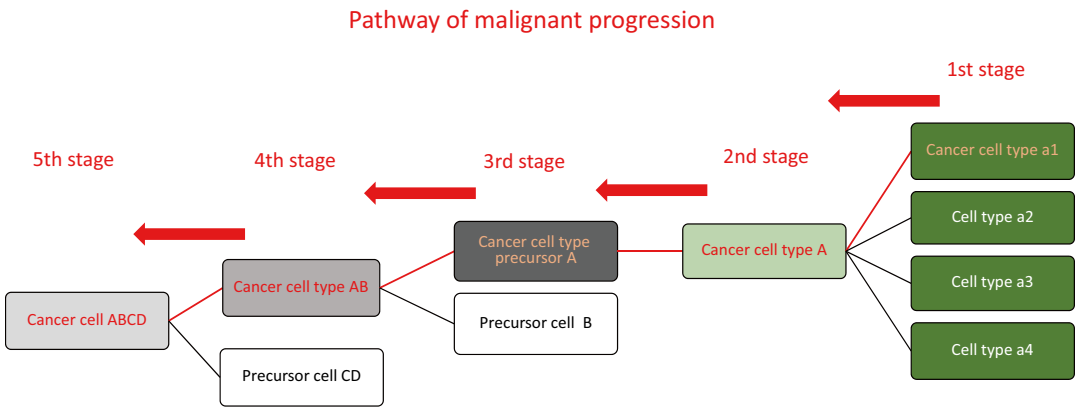

Fig. 2.5 Steps of cancer cell type dedifferentiation of the transformed cell type *a1* (compare with Fig. 2.2). The cancer field model considers the stepwise dedifferentiation of the transformed cells, due to the constant disruption of homeostasis and futile attempts at repair, as the pathomechanism for malignant progression

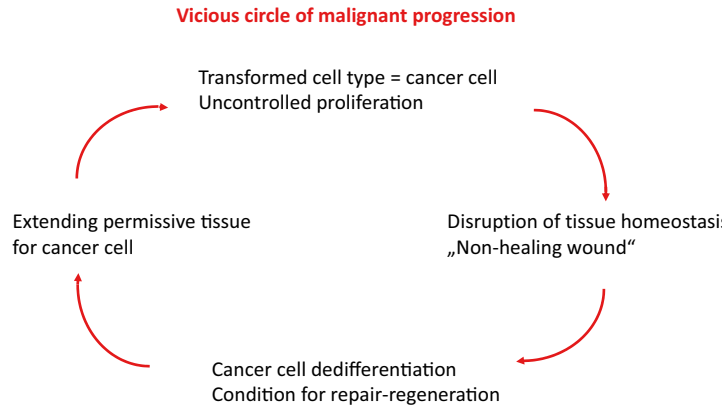

Fig. 2.6 Malignant progression as a vicious circle of the cancer paradox. The attempt of transformed cells to restore the disturbed tissue homeostasis caused by their uncontrolled proliferation through dedifferentiation extends the tissue permissive for the cancer cells and thus increases their destructive potential

addition to the normal cells of the tumor bed, transformed cells dedifferentiate themselves, attempting to repair the disruption of homeostasis (Fig. 2.5) [27]. Paradoxically, dedifferentiation extends the cancer cell's topoanatomical identity, causing the destruction of even more tissues through uncontrolled proliferation, which further propels dedifferentiation for futile repair (Fig. 2.6). This vicious circle of the *cancer paradox* drives malignant progression and ends in a catastrophe for the organism if not halted by external intervention. The state of dedifferentiation within the reverse differentiation trajectory of the corresponding normal cell type determines the topoanatomical identity and plasticity of the transformed cells. Consequently, local progression of malignant tumors occurs within permissive territories, the *cancer fields*, represented by the mature tissue derivatives of the morphogenetic fields, which are related to the differentiation trajectory of the corresponding untransformed cell type in reverse sequence (Fig. 2.7). This hierarchical principle of tumorigenesis unveils an *order of cancer* that is clinically exploited with *ontogenetic staging* and *cancer field surgery*.

The identification of malignant cells within the mature derivatives of a differentiation state-associated morphogenetic field mapped by ontogenetic anatomy defines the ontogenetic stage of cancer and predicts the extension of its potential local spread. Resection of the lesion can thus be tailored to the cancer field to achieve maximum local control at minimal treatment-related morbidity since all tissues outside the cancer field can be preserved.

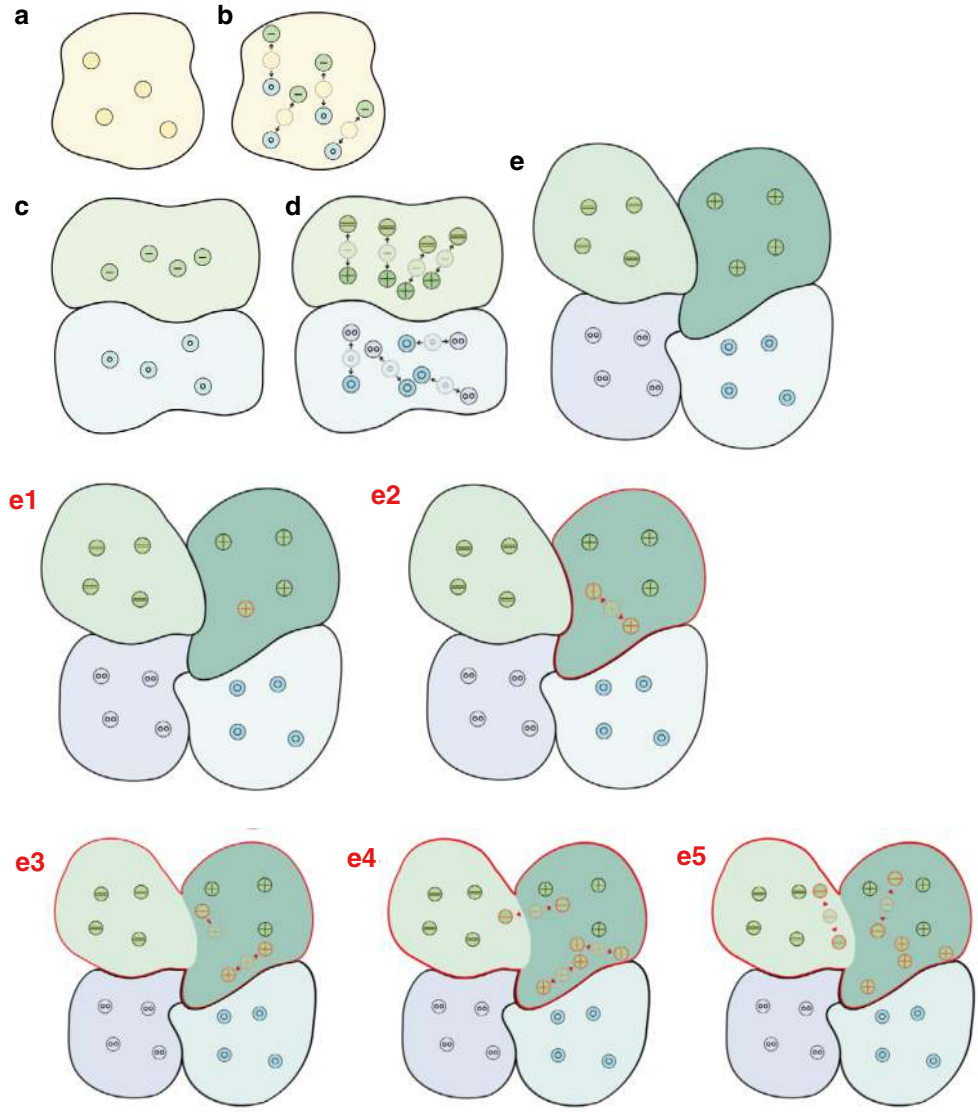

Fig. 2.7 Schematic demonstration of cell type differentiation and habitat formation during metazoan morphogenesis (**a**–**e**) and progressive cancer cell propagation during tumorigenesis by the dedifferentiation of the cancer cells, as proposed by the cancer field model (**e1**–**e8**). (**a**) Developmental cell population (yellow) within its anatomical territory (black borderline). Topoanatomical plasticity is not considered in this scheme. (**b**–**e**) Cell type differentiation results in the formation of two new cell types (black arrows). The populations of each new cell type generate their spatial habitats by changing and expanding the anatomical territory of the precursor cell type. Spatial order and specificity are increasing. Cell type differentiation finally terminates at developmental homeostasis, with mature cells occupying a cell type habitat. (**e1**–**e2**) A normal adult cell type (black "+") is transformed into a founding cancer cell (red "+"). The transformed cell type is no longer confined to its location and proliferates (red arrowheads) within the habitat of the cell type as the first cancer field (dark green, red borderline). (**e3**–**e5**) Further disruption of homeostasis by uncontrolled proliferation induces dedifferentiation of the cancer cell, adopting the topoanatomical identity of the precursor state of the normal cell (red "-", red arrow). Along with this step, the territory permissive for cancer cell colonization increases by including the mature habitat of the precursor cell type's progeny, which represents the next cancer field (red borderline). (**e6**–**e8**) Continued uncontrolled cancer cell proliferation induces the next step of dedifferentiation (arrow, yellow circle area), i.e., malignant progression further expanding the cancer field (red borderline). As a consequence, cancer propagates within a sequence of anatomical territories determined by the development of the normal cell type from which the cancer cell originated. (**f**) Normal cell type differentiation trajectory (black arrows) and reversed trajectory of transformed cell type dedifferentiation as malignant progression (red arrows)

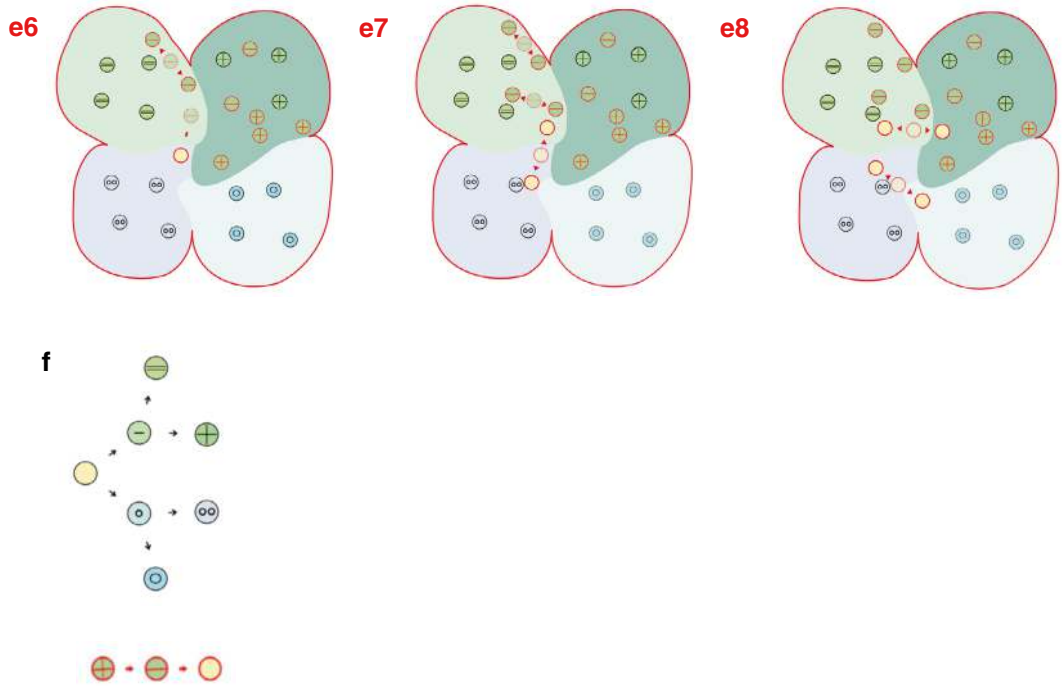

Fig. 2.7 (continued)

The ontogenetic cancer field model is also useful for understanding the limits of surgical treatment, e.g., when the resection of the potential cancer field would cause unacceptable morbidity or is not compatible with life at all. Figures 2.8 and 2.9 exemplarily illustrate the cancer fields of ontogenetic stages 1–4 of cervix carcinoma and the peripheral subcompartment of vulvar carcinoma. It is evident that ontogenetic stages 1 and 2 of both cervix and vulvar carcinomas are proper candidates for surgical therapy, whereas stages 3a and higher demand resective extensions with significant functional consequences and morbidity. Resection of the complete oT4 cancer field is not compatible with life.

The cancer field model has been verified through the analysis of the local spread patterns of more than 1000 primary carcinomas of the lower female genital tract (uterine cervix, vagina, and vulva) derived from the histopathological assessment of surgical specimens of cancers resected with clear margins (R0) [28–30]. This has been shown by the landscapes of local tumor spread for both cervix and vulvar cancers. The probability of malignant infiltration of the pelvic tissues by cervix cancer and of perineal tissues by vulvar cancer, based on the histopathological investigation of surgical specimens, has been highlighted by mapping in a midpelvic transverse plane and the superficial and deep perineum (Fig. 1.4 in Chap. 1). As can be verified, the tumor landscapes of the cervix and vulvar cancers are in good accordance with the corresponding ontogenetic anatomical maps in Figs. 2.3 and 2.4.

Additional supportive evidence for the model comes from the high-resolution topographical analysis of local recurrences observed in cervical and vulvar carcinomas treated by cancer field surgery without adjuvant radiation. The topography of the recurrent tumors is clearly related to the pretreatment cancer field of the primary tumor (see Chap. 13).

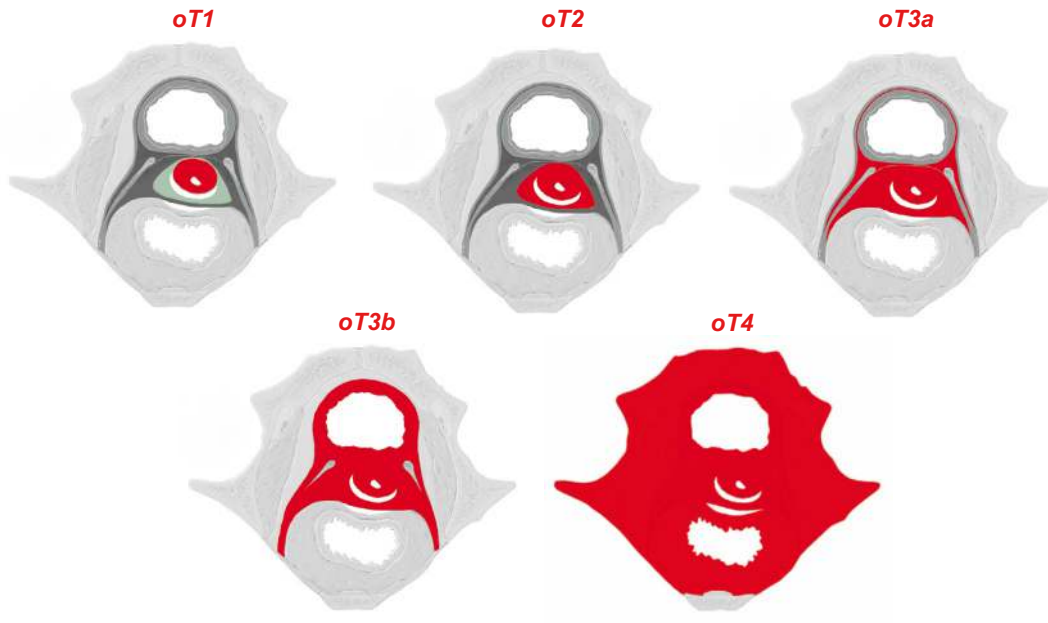

Fig. 2.8 Cancer fields of progressing carcinoma of the uterine cervix. oT, ontogenetic stages

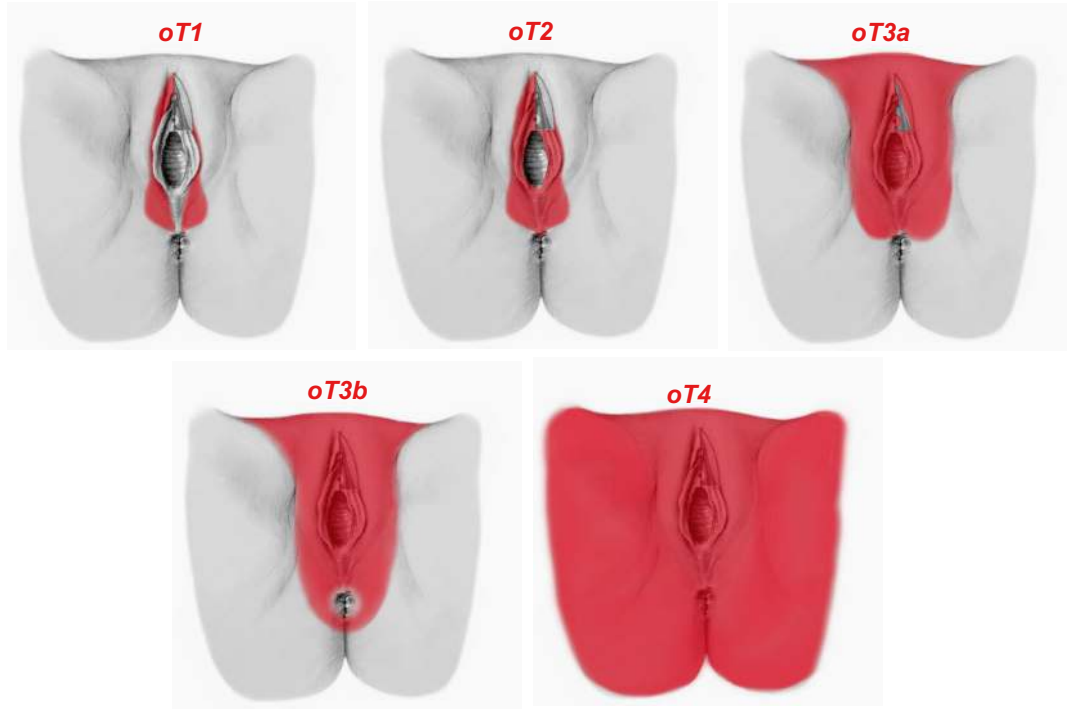

Fig. 2.9 Cancer fields of progressing carcinoma originating in the peripheral subcompartment of the vulva. oT, ontogenetic stages

References

1. Brunet T, King N. The origin of animal multicellularity and cell differentiation. Dev Cell. 2017;43:124–40. https://doi.org/10.1016/j.devcel.2017.09.016.
2. Sebé-Pedrós A, Degnan BM, Ruiz-Trillo I. The origin of metazoa: a unicellular perspective. Nat Rev Genet. 2017;18:498–512. https://doi.org/10.1038/nrg.2017.21.
3. Funayama N. The cellular and molecular bases of the sponge stem cell systems underlying reproduction, homeostasis and regeneration. Int J Dev Biol. 2018;62:513–25. https://doi.org/10.1387/ijdb.180016nf.
4. Ereskovsky AV, Renard E, Borchiellini C. Cellular and molecular processes leading to embryo formation in sponges: evidences for high conservation of processes throughout animal evolution. Dev Genes Evol. 2013;223:5–22. https://doi.org/10.1007/s00427-012-0399-3.
5. Martin VJ, Littlefield CL, Archer WE, Bode HR. Embryogenesis in hydra. Biol Bull. 1997;192:345–63. https://doi.org/10.2307/1542745.
6. Hobmayer B, Jenewein M, Eder D, Eder M-K, Glasauer S, Gufler S, et al. Stemness in *Hydra* – a current perspective. Int J Dev Biol. 2012;56:509–17. https://doi.org/10.1387/ijdb.113426bh.
7. Sadler TW. Langman's medical embryology. 9th ed. Philadelphia: Lippincott Williams & Wilkins; 2004.
8. O'Rahilly R, Müller F. Developmental stages in human embryos. Washington: Carnegie Institution of Washington; 1987.
9. Hemberger M, Hanna CW, Dean W. Mechanisms of early placental development in mouse and humans. Nat Rev Genet. 2020;21:27–43. https://doi.org/10.1038/s41576-019-0169-4.
10. White MD, Plachta N. Specification of the first mammalian cell lineages in vivo and in vitro. Cold Spring Harb Perspect Biol. 2020;12:a035634. https://doi.org/10.1101/cshperspect.a035634.
11. Xiang L, Yin Y, Zheng Y, Ma Y, Li Y, Zhao Z, et al. A developmental landscape of 3D-cultured human pre-gastrulation embryos. Nature. 2020;577:537–42. https://doi.org/10.1038/s41586-019-1875-y.
12. Lim HY, Alvarez YD, Gasnier M, Wang Y, Tetlak P, Bissiere S, et al. Keratins are asymmetrically inherited fate determinants in the mammalian embryo. Nature. 2020;585:404–9. https://doi.org/10.1038/s41586-020-2647-4.
13. Zhu M, Zernicka-Goetz M. Principles of self-organization of the mammalian embryo. Cell. 2020;183:1467–78.
14. Dumortier JG, Le Verge-Serandour M, Tortorelli AF, Mielke A, de Plater L, Turlier H, et al. Hydraulic fracturing and active coarsening position the lumen of the mouse blastocyst. Science. 2019;365:465–8. https://doi.org/10.1126/science.aaw7709.
15. Dahmann C, Oates AC, Brand M. Boundary formation and maintenance in tissue development. Nat Rev Genet. 2011;12:43–55. https://doi.org/10.1038/nrg2902.
16. Rothmann J, Jarriault S. Developmental plasticity and cellular reprogramming in Caenorhabditis elegans. Genetics. 2019;213:723–57. https://doi.org/10.1534/genetics.119.302333.
17. Gurtner GC, Werner S, Barrandon Y, Longaker MT. Wound repair and regeneration. Nature. 2008;453:314–21. https://doi.org/10.1038/nature07039.
18. Ereskovsky A, Borisenko IE, Bolshakov FV, Lavrov AI. Whole-body regeneration in sponges: diversity, fine mechanisms, and future prospects. Gene. 2021;12:506. https://doi.org/10.3390/genes12040506.
19. Stocum DL. Mechanisms of urodele limb regeneration. Regeneration. 2017;4:159–200. https://doi.org/10.1002/reg2.92.
20. Wells JM, Watt FM. Diverse mechanisms for endogenous regeneration and repair in mammalian organs. Nature. 2018;557:322–8. https://doi.org/10.1038/s41586-018-0073-7.
21. Li Y, Long J, Zhang Z, Yin W. Insights into the unique roles of dermal white adipose tissue (dWAT) in wound healing. Front Physiol. 2024;15:1346612. https://doi.org/10.3389/fphys.2024.1346612.
22. Nocera G, Jacob C. Mechanisms of Schwann cell plasticity involved in peripheral nerve repair after injury. Cell Mol Life Sci. 2020;77:3977–89. https://doi.org/10.1007/s00018-020-03516-9.
23. Jiang M, Li H, Zhang Y, Yang Y, Lu R, Liu K, et al. Transitional basal cells at the squamous-columnar junction generate Barrett's oesophagus. Nature. 2017;550:529–33. https://doi.org/10.1038/nature24269.
24. Yui S, Azzolin L, Maimets M, Pedersen MT, Fordham RP, Hansen SL, et al. YAP/TAZ-dependent reprogramming of colonic epithelium links ECM remodeling to tissue regeneration. Cell Stem Cell. 2018;22:35–49. https://doi.org/10.1016/j.stem.2017.11.001.
25. Deng X, Zhang X, Li W, Feng R-X, Li L, Yi G-R, et al. Chronic liver injury induces conversion of biliary epithelial cells into hepatocytes. Cell Stem Cell. 2018;23:114–22. https://doi.org/10.1016/j.stem.2018.05.022.
26. Dvorak HF. Tumors: wounds that do not heal. N Engl J Med. 1986;315:1650–9. https://doi.org/10.1056/NEJM198612253152606.
27. Ge Y, Gomez NC, Adam RC, Nikolova M, Yang H, Verma A, et al. Stem cell lineage infidelity drives wound repair and cancer. Cell. 2017;169:636–50. https://doi.org/10.1016/j.cell.2017.03.042.
28. Höckel M, Hentschel B, Horn L-C. Association between developmental steps in the organogenesis of the uterine cervix and locoregional progression of cervical cancer: a prospective clinicopathological

analysis. Lancet Oncol. 2014;15:445–56. https://doi.org/10.1016/S1470-2045(14)70060-9.

29. Höckel M, Trott S, Dornhöfer N, Horn L-C, Hentschel B, Wolf B. Vulvar field resection based on ontogenetic cancer field theory for surgical treatment of vulvar carcinoma: a single-centre, single-group, prospective trial. Lancet Oncol. 2018;19:537–48. https://doi.org/10.1016/S1470-2045(18)30109-8.
30. Höckel M, Wolf B, Schmidt K, Mende M, Aktas B, Kimmig R, et al. Surgical resection based on ontogenetic cancer field theory for cervical cancer: mature results from a single-centre, prospective, observational, cohort study. Lancet Oncol. 2019;20:1316–26. https://doi.org/10.1016/S1470-2045(19)30389-4.

3 Ontogenetic Anatomy of the Female Genital Ducts: Local Progression of Cervix Carcinoma

As detailed in the previous chapter, ontogenetic anatomy maps mature tissues with respect to their postphylotypic development. One mode to express ontogenetic anatomy is by adding a fourth dimension of information to the three-dimensional (3D) topographic anatomical depiction of the structures, indicating the degree of developmental kinship, which is determined by the distance on the developmental path or on the cell type differentiation trajectory, i.e., the number of cell type transitions from the precursor cell population to the mature cell population. At each developmental stage, populations of a single cell type establish their habitats within distinct anatomical territories and assemble structures therein. During the embryonic and early fetal periods, many cell types are not determined, i.e., phenotypically not fixed, as they are able to adopt the fates of neighboring cell populations when they enter their habitats, a phenomenon termed transdetermination. Based on the concept of postphylotypic metazoan morphogenesis, prior to cell type determination, a cell population and all adjacent cell populations exhibiting transdetermination potential make up a *morphogenetic field*. After determination, morphogenetic fields are confined to the habitats of the cell populations, represented by topographically distinct cell type *compartments* and *subcompartments*. The generation of an ontogenetic anatomical map for the tissue of interest thus necessitates identifying its founder cell population in the phylotypic period first. Next, the developmental path of that cell population, its differentiation trajectory, must be known. This process should be tracked from the onset of organogenesis (corresponding to Carnegie stage 11 in human embryogenesis) to maturity. Cell type transitions occur as bifurcations until determination. The determined cell population may then segregate into several terminal subpopulations. For each developmental stage of a distinct cell type from Carnegie stage 11 to maturity, the morphogenetic fields have to be topographically outlined in the embryo and fetus. Their mature tissue derivatives, i.e., compartments and subcompartments, are finally color-coded in the topographic anatomical presentation.

The prerequisite for constructing ontogenetic anatomical maps is having precise topographical information on all morphogenetic fields at all developmental stages, from the beginning of organogenesis to maturity, in relation to a distinct cell type. Since currently available published sources do not completely provide the necessary information, several knowledge gaps still have to be filled by projections. However, these projections must fit into a network of existing morphological data, allowing trial-and-error approaches. Additional clues can be derived from the morphogenetic principle that cell type differentiation trajectories mark segregations of the habitats at

M. Höckel et al., *Cancer Field Surgery in Gynecologic Oncology*,
https://doi.org/10.1007/978-3-031-83030-3_3

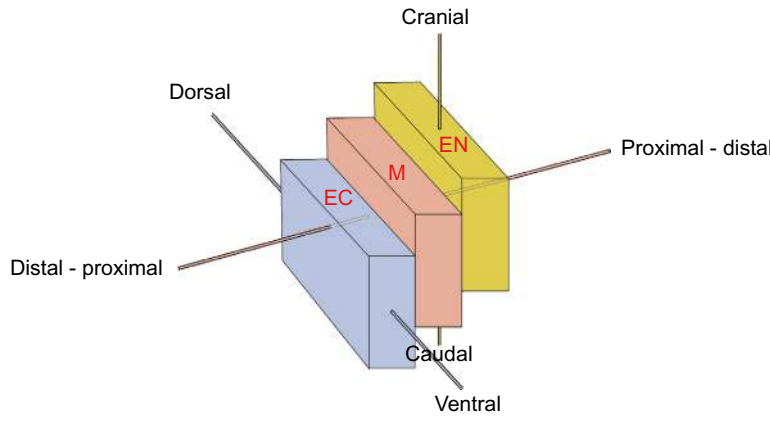

Fig. 3.1 Topographical axes of cell type segregation during its postphylotypic differentiation trajectory. *EC* ectoderm, *M* mesoderm, *EN* endoderm

proximodistal, dorsoventral, and craniocaudal axes [1]. Proximodistal segregation is applied to mesenchymes interacting with either ectodermal or endodermal derivatives; craniocaudal segregation is valid for endodermal linear tubular structures, such as the gut and the urethrovesical canal; and dorsoventral segregation relates to ectodermal tissues (Fig. 3.1). Moreover, the local interaction of adjacent cell populations in terms of induction and competence—which are known phenomena in embryology—is recognized. At the time of this writing, some uncertainty remains, but the available morphological data are sufficient to identify the ontogenetic anatomy of the female genital tract and perineum, as demonstrated by its successful application in gynecologic oncology.

3.1 Cell Type Differentiation Trajectories Related to the Female Genital Tract

The founder cell type of the genital tract at the beginning of organogenesis in the phylotypic period is derived from the lower trunk intermediate mesoderm forming the bilateral *nephrogenic cords* at the dorsolateral flanks of the embryo. These structures extend from the level of somite 8 beneath the pericardio-peritoneal canals to the level of the caudal hindgut, where they can no longer be discriminated from adjacent cell populations. Adjacent to the ectoderm, the primordial mesonephric ducts are integral to the nephrogenic cords as solid rods (Fig. 3.2).

The cell type differentiation trajectory from the nephrogenic cords at Carnegie stage 11 to the mature female genital tract is shown in Fig. 3.3. Nephrogenic cord cell populations differentiate into mesonephric cytotypes. Undifferentiated mesonephric cells segregate into the precursor populations of the *adrenometanephric system* and the *primordial genital tract* observable around Carnegie stage 14. Undifferentiated primordial genital tract cells bifurcate into the *gonadal ridge*, the precursor populations of the gonads and of the *genital ducts*, indicated by the appearance of the Müllerian duct at about Carnegie stage 17. During the remaining embryonic and early fetal periods in the female, the genital duct cell populations become determined and further develop into the *Müllerian system*. It terminally differentiates into the cell populations, forming the fallopian tubes, the uterine corpus, the cervix, the suprasinus and sinus vagina, and the surrounding Müllerian adventitia. Cell type differentiation continues: in

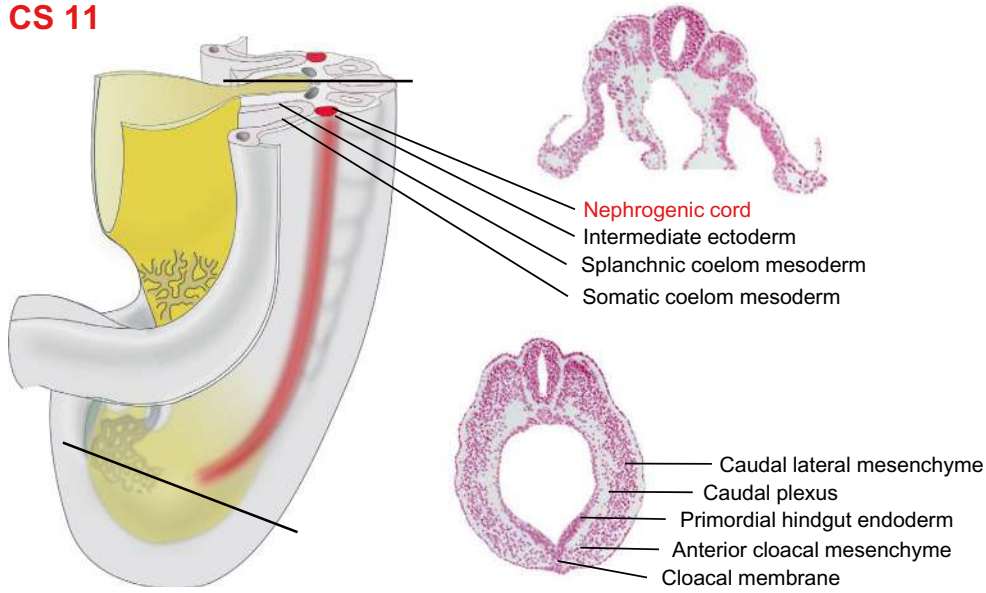

Fig. 3.2 Nephrogenic cords as founder cell populations of the genital ducts (red) approaching the primitive hindgut (yellow) at Carnegie stage 11. Schematic depiction of the lower trunk (left) and transverse sections (right) at the level of somite 8 and close to the caudal pole (from [2])

the cervix, the epithelium segregates from the stroma, and the epithelium finally exhibits two cell types: squamous and columnar cells. Gonadal ridge cells are determined in the female to an ovarian cell fate. Its population is restricted to the ovarian compartment. Continued cell type differentiation generates ovarian cortex, medullahilum, and rete ovarii cell types, which occupy the corresponding subcompartments. Cell type differentiation within the subcompartments progresses, e.g., to ovarian surface epithelium cells and to follicles and stroma cells in the cervix. For each of the three predetermination developmental stages, the adjacent cell populations make up the stage-associated morphogenetic fields. The cell type differentiation trajectories of the most relevant interacting cell populations are indicated in Fig. 3.4.

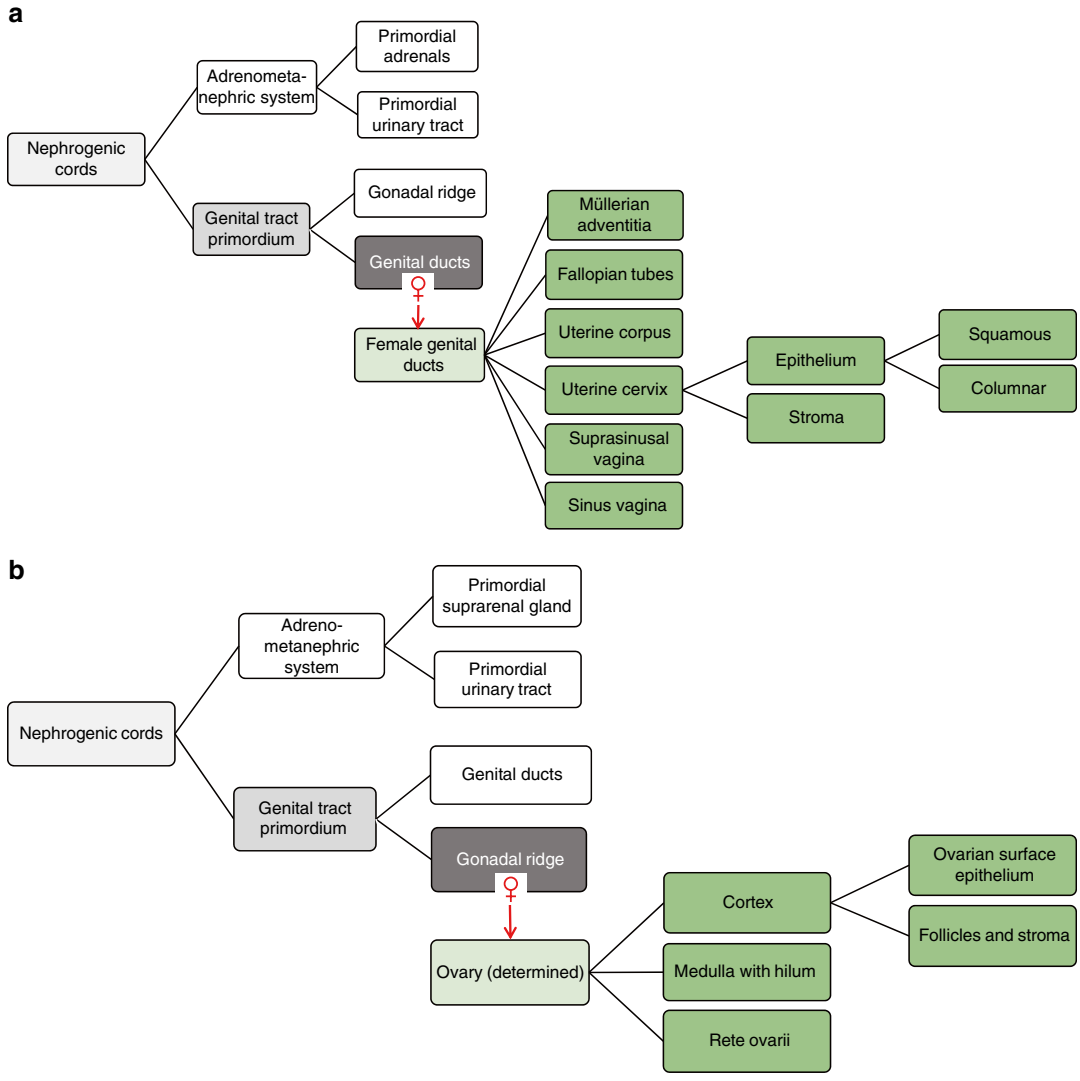

Fig. 3.3 Differentiation trajectories of the cell types forming the female genital tract from the nephrogenic cords at Carnegie stage 11, (**a**) to the mature Müllerian system, (**b**) to the mature ovarian compartment

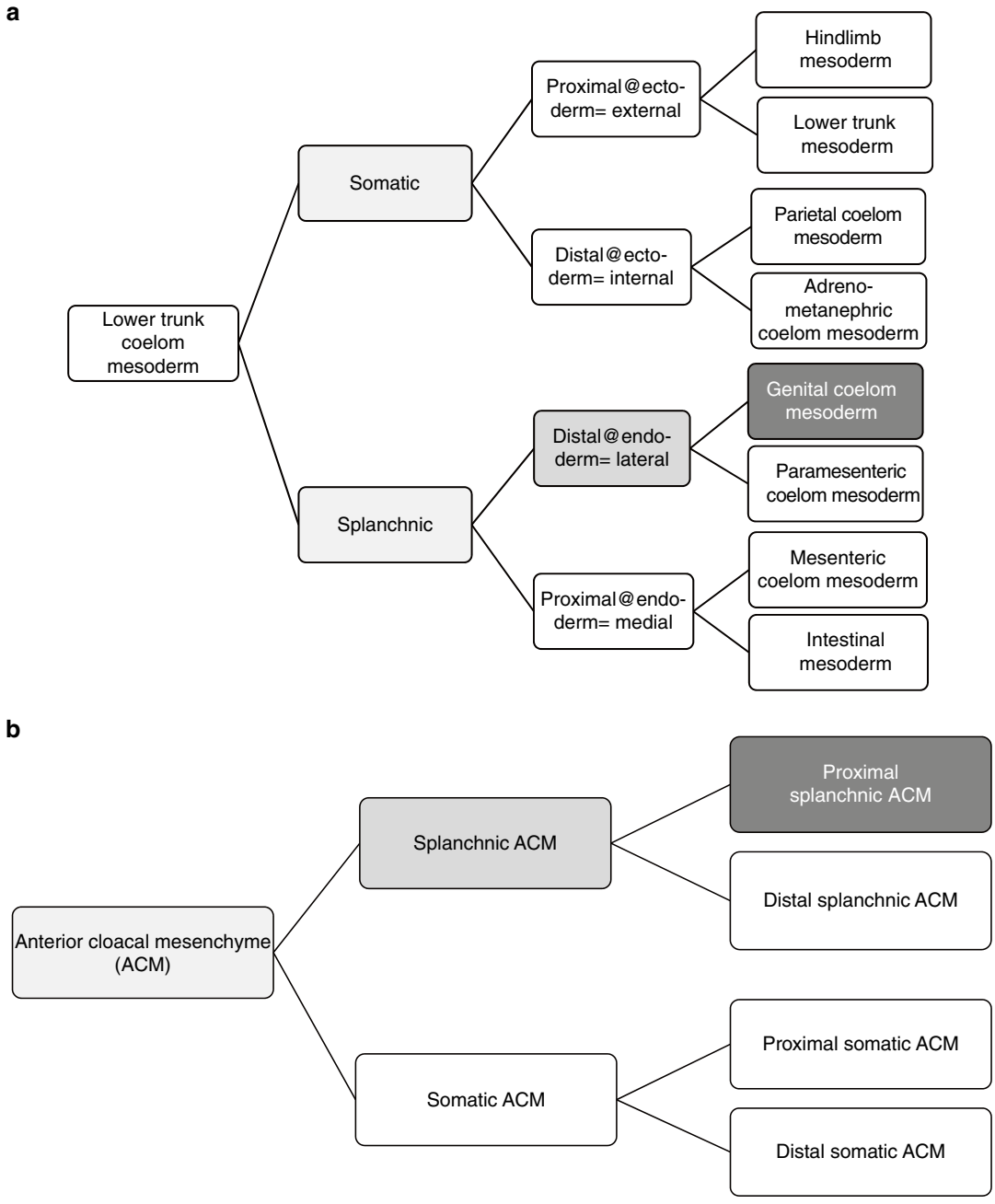

Fig. 3.4 Differentiation trajectories of associated cell types involved in the morphogenesis of the female genital ducts by forming morphogenetic fields with the population of the genital duct cell type from Carnegie stage 11 to maturity. (**a**) Lower trunk coelom mesoderm. (**b**) Anterior cloacal mesenchyme (ACM). (**c**) Hindgut endoderm. (**d**) Cloacal membrane/plate

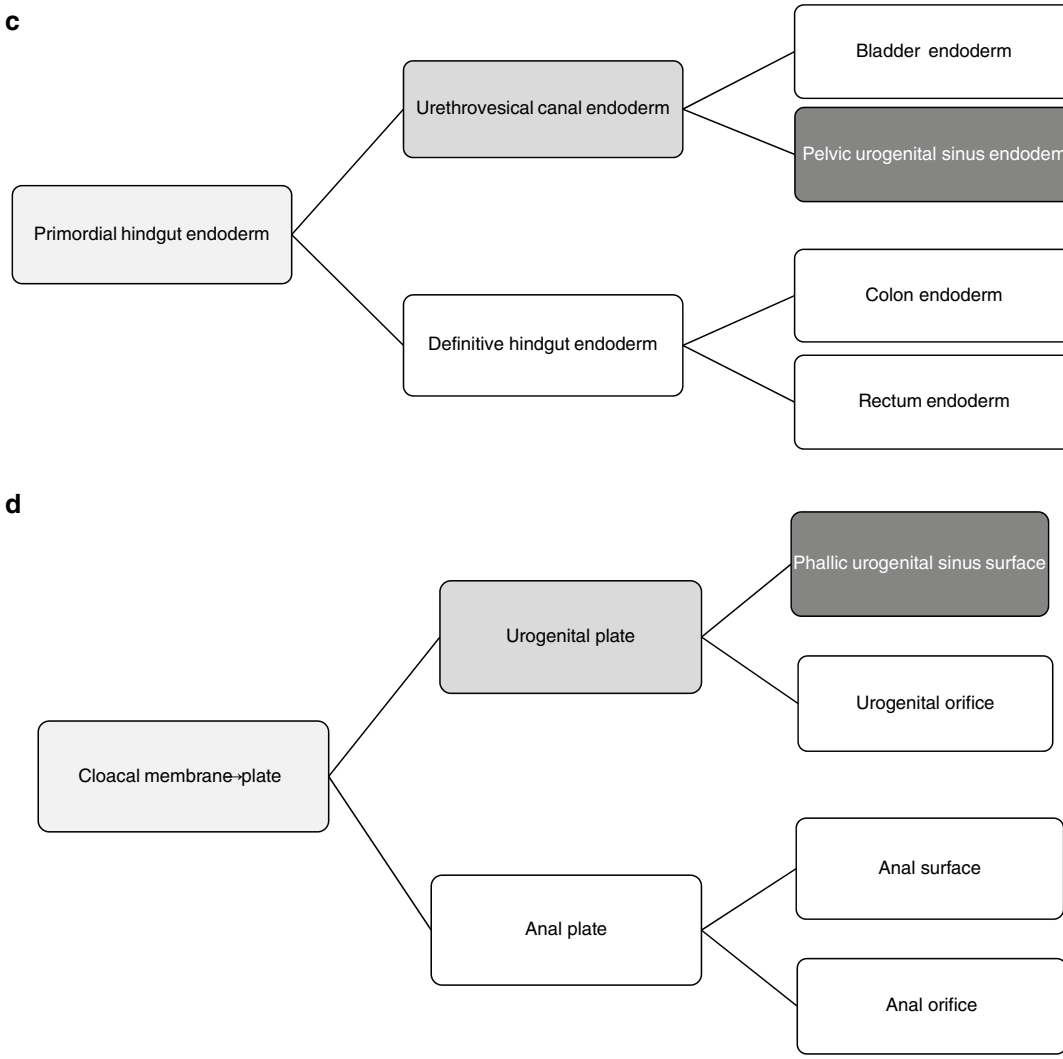

Fig. 3.4 (continued)

3.2 Mesonephric Morphogenetic Field

As can be observed in embryos of Carnegie stage 11, the nephrogenic cords contact many other cell populations, which together establish their morphogenetic field. In the cranial part, juxtaposed populations include intermediate ectoderm, splanchnic coelom (lateral plate) mesoderm, and somatic coelom (lateral plate) mesoderm. The caudal part of the nephrogenic cord population cannot be morphologically discriminated from caudal lateral mesoderm (CLM), caudal plexus, primordial hindgut endoderm, anterior cloacal mesenchyme (ACM), and cloacal membrane cells (Fig. 3.2) [2]. The morphogenetic actions within this field include the formation of the mesonephros I°, an early organ consisting of numerous nephrotomes with tubuloglomerular structures connected to the arterial (dorsal aorta) and venous (cardinal vein) circulation and to the mesonephric duct by Carnegie stage 13 [3]. Mesonephros morphogenesis is associated with the formation of the mesonephric ridge, which shifts the early organ away from the somites and the ectoderm cranially (Fig. 3.5) [2].

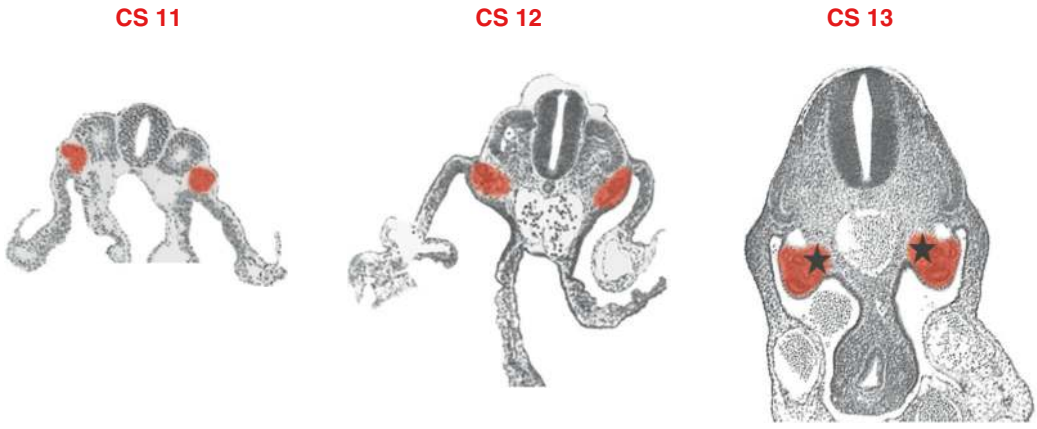

Fig. 3.5 Development of the mesonephric system during Carnegie stages 11–13—cranial aspects. Mesonephric cords covered by splanchnic and somatic coelom mesoderm bulge into the abdominal cavity as bilateral mesonephric ridges displaced laterally from the ectoderm and dorsally from the somites. Bilateral dorsal aortae unite in the sagittal midline. Nephrogenic cords form the mesonephric ducts and nephrotomes with functional tubuloglomerular structures. Stars at the CS13 panel indicate the location of the adrenocortical-gonadal precursor tissue complex; mesonephric tissues are highlighted by red coloring (from [2])

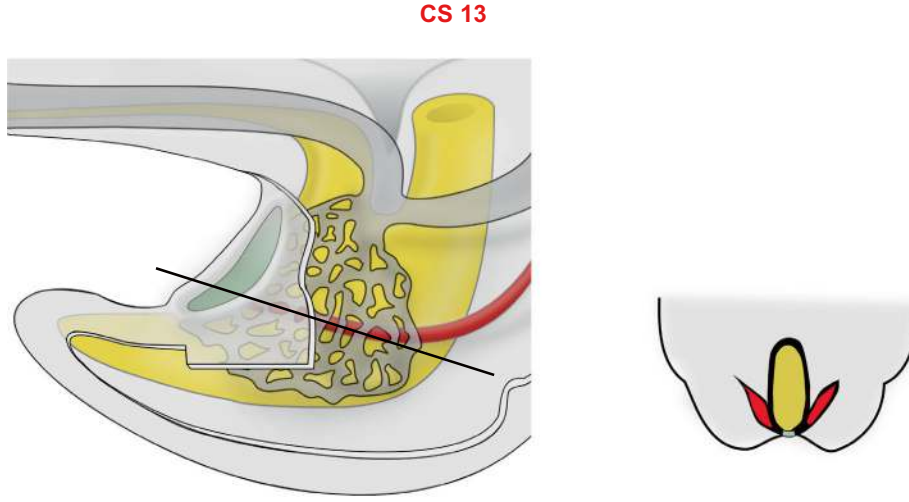

Fig. 3.6 Development of the mesonephric system—caudal aspects. Anatomical drawing of the caudal trunk at Carnegie stage 13. The mesonephric ducts (red) are formed primarily as solid rods anastomosing with the primitive hindgut (yellow) at the lateral cloacal membrane (green), establishing the cloaca. Lumen formation in the distal mesonephric ducts proceeds cranially. The cloaca and the mesonephric ducts are vascularized by the dorsal plexus from the umbilical artery anastomosed with the internal iliac artery. The right panel shows the transverse section at the plane indicated on the left panel

Caudally, the mesonephric duct, which develops from a solid rod, anastomoses to the peripheral cloaca at the cloacal membrane (Fig. 3.6) [4]. The cloaca and the caudal mesonephric ducts receive blood vessels from the bilateral caudal plexus, which have developed at the connection of the umbilical arteries to the dorsal aortas laterally to the cloaca. Medially to the mesonephros above the level of the aortic bifurcation the adrenogonadal primordium is located. The craniodorso-medial pre-adrenocortical and the caudo-ventro-lateral pregonadal parts are contin-

uous at this developmental stage, as shown in investigations of bovine embryos [5]. In the human embryo, functional cytodifferentiation of these cell populations is not visible at that stage (Fig. 3.5).

3.3 Primordial Genital Tract Morphogenetic Field

Next in the cell type differentiation trajectory undifferentiated mesonephric cells segregate into primordial genital tract and adrenometanephric cells as new founder populations that become morphologically visible around Carnegie stage 14 in the upper peripheral and lower central regions of the mesonephric ridges.

The next bifurcations of the cell type differentiation trajectories of other cell populations forming the mesonephric morphogenetic field relevant for further development, as shown in Fig. 3.4, are the following: the distal hindgut endoderm segregates into ventral urethrovesical canal and dorsal definitive hindgut populations. ACM segregates into internal endoderm-associated splanchnic and external ectoderm-associated somatic populations. The cloacal plate cells segregate into ventral urogenital plate and dorsal anal plate populations. The somatic and splanchnic coelom mesoderms of the lower trunk bifurcate into proximal and distal populations, depending on the distance of the abutting ectoderm and endoderm. The segregation of the adrenometanephric and primordial genital tract cell populations is accompanied by the segregation of the juxtaposed lateral plate (coelom) mesoderm populations. Whereas adrenometanephric cells abut to and interact with the distal somatic coelom mesoderm, the genital tract populations constitute a morphogenetic field, together with the distal splanchnic coelom mesoderm (Fig. 3.7). Caudally, the morphogenetic field of the primordial genital tract system includes the splanchnic ACM, the urethrovesical canal endoderm, and the urogenital plate.

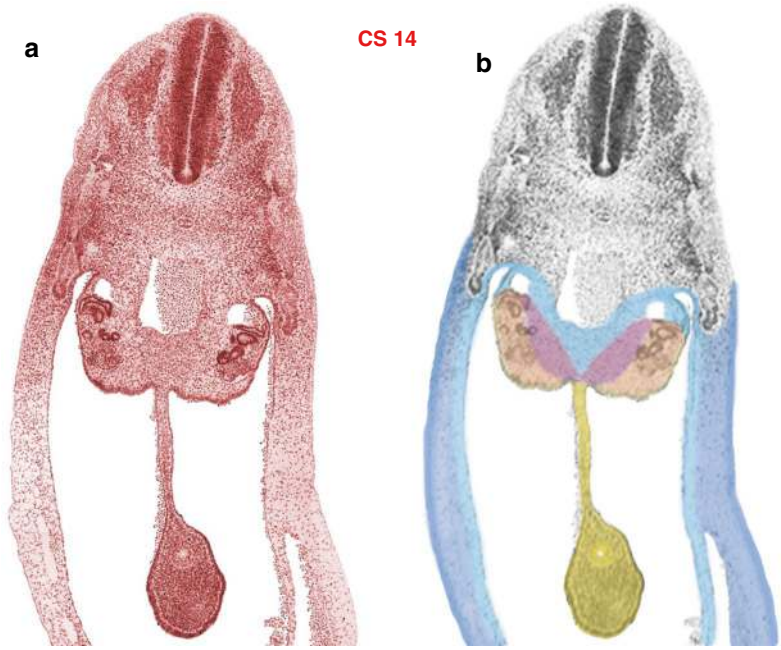

Fig. 3.7 Transverse section through an embryo Carnegie stage 14 at the midlevel of the lower trunk. (**a**) Histological section from the Virtual Embryo Project [2]. (**b**) Presumed anatomical territories representing the genital tract primordium separated from the adrenometanephric system are color-coded: dark yellow, proximal splanchnic coelom mesoderm with hindgut mesoderm; light yellow, distal splanchnic coelom mesoderm; pink, primordial genital tract (mesonephros II°); purple, undifferentiated adrenometanephric tissue; light blue, distal somatic coelom mesoderm; dark blue, proximal somatic coelom mesoderm with ectoderm

The morphogenetic actions within this field—the dorsomedial shift of the caudal mesonephric ducts, anastomosed to the cloaca concomitantly with the cloacal septation, and the sprouting of the ureters (Fig. 3.8), which roughly occur during Carnegie stages 14–17, determine the main bauplan of the pelvis.

Above the primordial pelvis, the gonadal ridges develop and attract germ cells (Fig. 3.9).

At the cloacal-hindgut transition dorsally to the estuary of the allantois, the urethrovesical canal endoderm interacts with the splanchnic ACM and the proximal splanchnic coelom mesoderm interacts with the hindgut endoderm in the midsagittal plane and separates the anterior urethrovesical canal from the definitive hindgut. This process advances caudalward [4, 7]. Within this "septum," a horseshoe-shaped caudal extension of the coelomic cavum originates, connecting the early urorectal pouch to the peritoneal cavity. This might be achieved by the separation of the distal from the proximal splanchnic coelom mesoderms. Concomitantly, the mesonephric ducts are shifted dorsomedially. The urorectal pouch extends caudally below the level of the anastomoses of the mesonephric ducts to the urethrovesical canal, which finally establishes the sinusal tubercle. A bridge of primordial genital

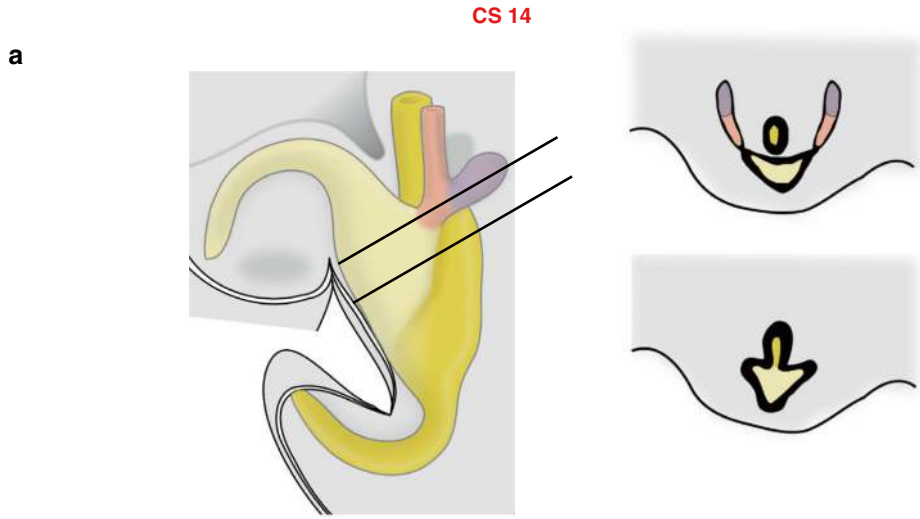

Fig. 3.8 Schematic anatomical drawings illustrating cloacal septation at Carnegie stages 14, 15, and 16 (modified from [4]). The separation of the urethrovesical canal (light yellow) anteriorly and the definitive hindgut (dark yellow) posteriorly with interposed mesonephric ducts (pink) proceeds craniocaudally through the interactions of the splanchnic ACM with the urethrovesical canal endoderm, of the proximal splanchnic coelom mesoderm with the hindgut endoderm, and of both the splanchnic ACM and distal splanchnic coelom mesoderm with the mesonephric ducts. Mesonephric ducts anastomosed to the urethrovesical canal endoderm are shifted dorsomedially. Proximal and distal splanchnic coelom mesoderms generate the primary urorectal pouch, which extends caudally below the level of the anastomoses. Ureteral buds sprout from the proximal mesonephric ducts, forming the metanephric system (purple). (**a**) At Carnegie stage 14, ureteral sprouts (purple) appear dorsolaterally at the distal mesonephric ducts (pink). The urethrovesical canal endoderm (light yellow) and the distal hindgut endoderm (dark yellow) line the cloaca. Bilateral mesenchymal cloacal folds of the splanchnic ACM and the distal and proximal coelom mesoderm approach each other in the midsagittal plane, initiating urorectal septation cranially. (**b**) At Carnegie stage 15, urorectal septation has proceeded approximately halfway. Distal mesonephric ducts have been transformed into a common outlet with the ureters. Common outlets are lined by the urethrovesical endoderm. The tailgut has disappeared. Early kidneys have been formed. (**c**) At Carnegie stage 16, the septation is almost completed. Common outlets for the mesonephric ducts and ureters have been integrated into the urethrovesical canal, the precursor of the trigone. Ureteral anastomoses have been shifted cranially, mesonephric duct anastomoses medially. As a consequence, vascularization of the genital ducts from the cloacal plexus has to traverse the ureters (supraureteral) and will be integral to the urethrovesical canal at lower levels (infraureteral). The right panels show transverse sections of two levels, indicated in the left panel

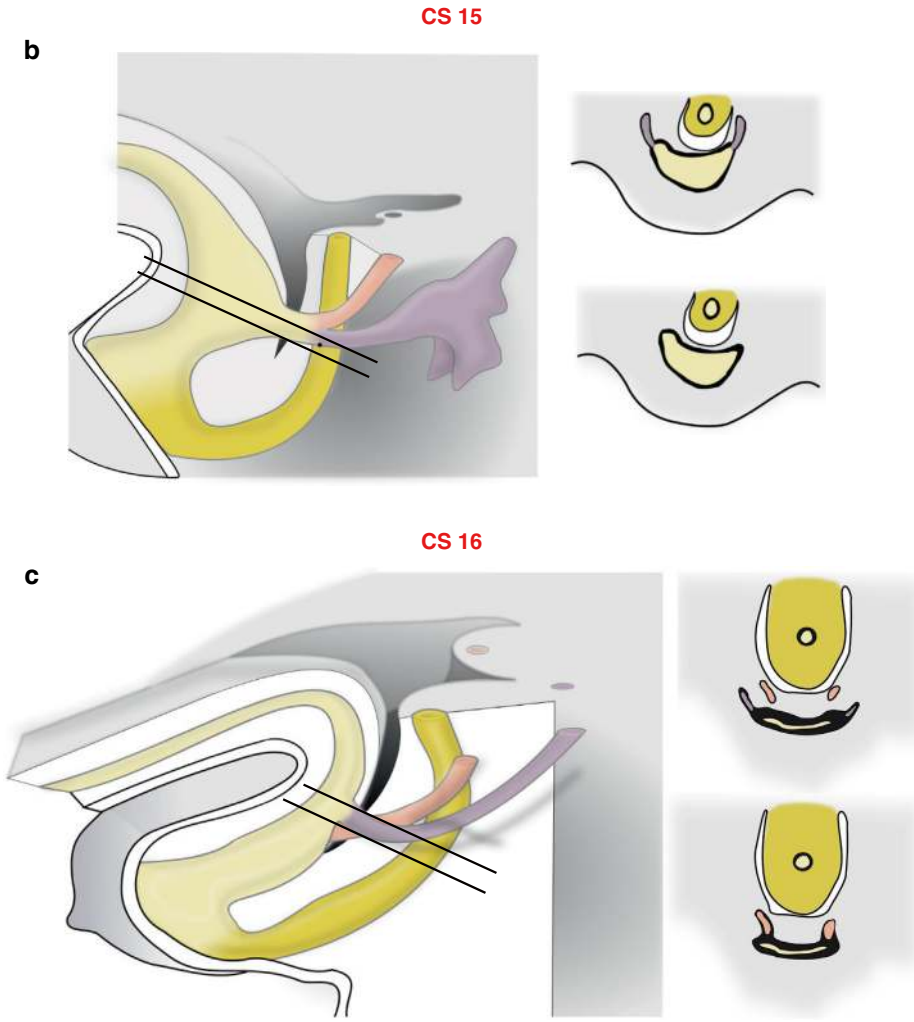

Fig. 3.8 (continued)

tract tissue abutting the urogenital plate is assumed to exist below the anastomosis of the mesonephric ducts, with the urethrovesical canal within the splanchnic ACM. Simultaneously, the metanephric system is formed. Ureteric sprouts arising dorsolaterally from the distal mesonephric ducts contact the metanephric blastema of the adrenometanephric cell collective to generate the early kidneys [3, 4, 8]. The growth and differentiation of the kidney-ureter complexes are accompanied by their ascension, guided by the distal somatic coelom mesoderm. The epithelium of the distal mesonephric ducts, which have been the common outlets for both the mesonephric ducts and the ureters, is replaced by the urethrovesical canal endoderm [9]. Both common outlets are integrated into the urethrovesical canal, shifting the ureters cranialward and the mesonephric ducts medially. By this process, the trigone precursor is formed [10]. This morphogenetic process allows a direct vascularization of the mesonephric (and later the paramesonephric) ducts from the lateral caudal plexus only by a supraureteral route. Infraureteral vascularization of the genital ducts has to occur via bladder vessels. Likewise, the formation of the early urorec-

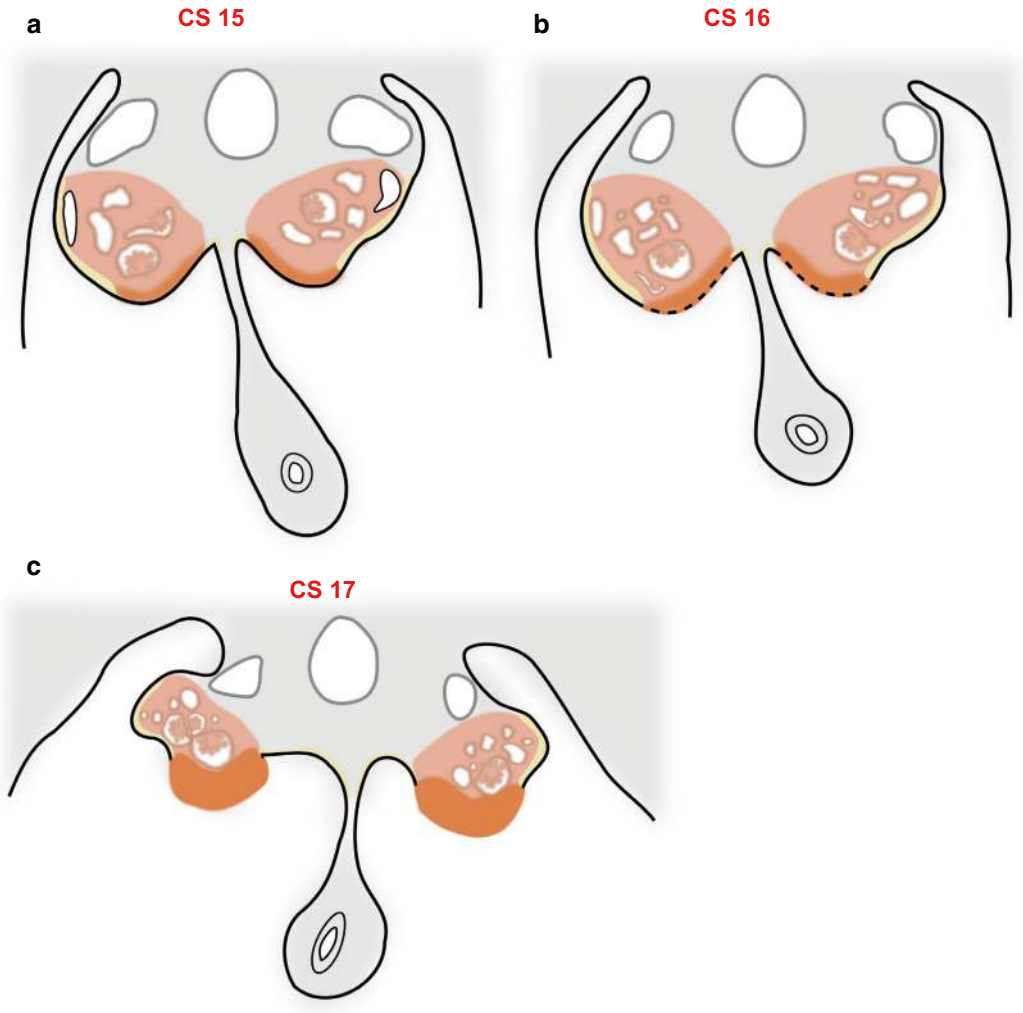

Fig. 3.9 The gonadal precursors develop on the medial sides of the urogenital ridges through the interaction of the primordial gonadal tract cells (mesonephros II°) with the distal splanchnic coelom mesoderm, attracting primordial germ cells. (**a**) Carnegie stage 15: the distal splanchnic coelom mesoderm (yellow) is specified by the mesonephros (mesonephros II°) (pink) of the primordial genital tract at the medial sites of the mesonephric ridges and proliferates, forming gonadal ridge epithelial-like (GREL) cells (orange). (**b**) Carnegie stage 16: at the gonadal ridges, the epithelial basement membrane is fragmented, allowing intermingling between coelom-derived GREL cells (orange) and mesonephric II° stroma (pink) to form the gonadal precursors. (**c**) Carnegie stage 17: the gonadal ridge epithelial basement membrane is completely absent. Gonadal precursor tissue has approached the mesonephric corpuscles and is displaced more laterally from the intestinal mesentery. Primordial germ cells have entered the gonadal precursor tissue and proliferate (not shown). Preformed connections of the gonadal precursor tissues with the mesonephros II° establish the gonadal rete (not shown) (according to [6])

tal pouch prevents a major lateral vascularization of the distal hindgut, which later becomes the rectum.

Along with the bifurcation of the mesonephric cell type, the adrenogonadal primordium is segregated into the gonadal and suprarenal gland precursors. The ascending kidneys dislodge the adrenal primordia, a part of the adrenometanephric system, from the gonadal blastema, which is part of the primordial genital tract [5]. The gonadal tissues are formed through the interaction of the gonadal primordium with the abutting

distal splanchnic coelom mesoderm, located ventromedially to the mesonephric corpuscles. The medial sides of the mesonephric ridges become the gonadal ridges (Fig. 3.9) [3, 8]. At the gonadal ridges, the distal splanchnic coelom epithelium specifies, proliferates, and dissolves its basal membrane (except at the periphery), allowing intermingling with stroma cells from the mesonephric gonadal precursor and the immigration of primordial germ cells [6].

Upon contact with the gonadal environment, primordial germ cells proliferate. As the developing gonad and the genital tract-associated mesonephros II° are part of a common morphogenetic field, future contacts between the gonads and genital ducts through the gonadal rete, which are functional in the male phenotype, are preformed at this developmental stage.

3.4 Genital Duct Morphogenetic Field

The final predetermination bifurcation in the cell type differentiation trajectories originating from the nephrogenic cords segregates the genital tract primordium (mesonephros II°) cells into the gonadal and the genital duct precursor populations and the adrenometanephric cells into the suprarenal gland and the kidney/ureter precursor populations (Fig. 3.3). The differentiated mesonephroi begin to regress. Collateral bifurcations (Fig. 3.4) segregate the distal splanchnic coelom mesoderm into genital and paramesenteric coelom mesoderm derivatives. The splanchnic ACM segregates into proximal and distal populations in relation to the endoderm. The urethrovesical canal endoderm segregates into cranial bladder and caudal urogenital sinus endoderms. Urogenital plate cells segregate into peripheral and central cell populations. The genital duct morphogenetic field now encompasses genital coelom mesoderm, proximal splanchnic ACM, urogenital sinus endoderm, and peripheral urogenital plate cells abutting the mesonephric ducts and their periductal mesenchyme.

The main morphogenetic action within the genital ducts' morphogenetic field during the sexually indifferent phase around Carnegie stages 17–23 is the formation of the bilateral paramesonephric or Müllerian ducts and their distal fusion to the sinusal tubercle. Lateral to the gonadal ridges in the projection of the mesonephric ducts, genital coelom mesoderm thickens to form the Müllerian ridge on both sides of the embryo. At the level of the cranial end of the mesonephric duct, the Müllerian ridge coelom invaginates the primordial genital tract mesenchyme toward the duct to initiate the paramesonephric (Müllerian) ducts [11].

At the invagination of the cranial Müllerian ridge, genital coelom cells delaminate and assemble the initial Müllerian duct as a solid rod. Both Müllerian ducts elongate caudalward through the proliferation of their tip cells. Periductal mesenchyme is supplemented by the delamination of the genital coelom mesoderm. The Müllerian ducts develop a lumen and an ostium in connection with genital coelom invagination [11]. Below the caudal poles of the primordial gonad system, the paramesonephric ducts cross the mesonephric ducts and continue their caudal migration parallel to each other, surrounded by a common mantle of periductal mesenchyme (Fig. 3.10). The paramesonephric ducts finally fuse to the dorsal wall of the urogenital sinus at the sinusal tubercle in continuity with the mesonephric ducts, which are anastomosed to the urogenital sinus endoderm [3, 4, 8, 12]. At the end of the embryonic period corresponding to Carnegie stage 23, the topography of the pelvic precursor tissues, as shown in Fig. 3.11, provides a template for the complex architecture of the subperitoneum, as illustrated later in this chapter.

The development of the genital ducts within their morphogenetic field before determination continues during the early fetal period, now depending on the individuum's sex. In the female, it is characterized by the formation of the tubal fimbriae at the proximal ends of the paramesonephric ducts, the cranialward fusion of the two distal paramesonephric ducts forming the uterovaginal canal, and the connection of the distal ends of the fused paramesonephric ducts to the peripheral phallic urogenital sinus endosurface (Fig. 3.12). The latter results from the interaction of the sinuvaginal bulbs (representing the tissue complex of the terminal paramesonephric ducts

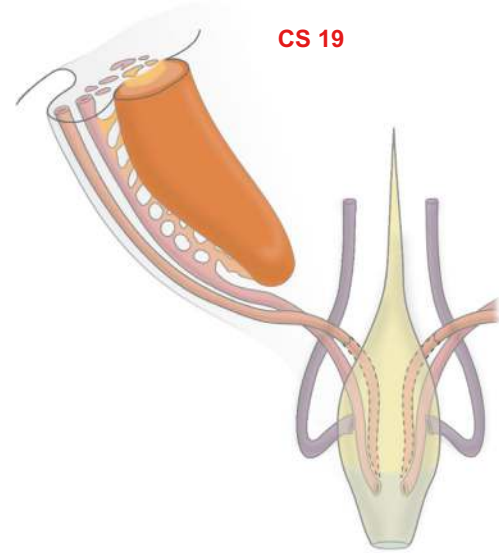

Fig. 3.10 Formation of the paramesonephric (Müllerian) ducts in the human embryo at Carnegie stage 19. Semischematic anatomical drawing to illustrate the topographic relations between the Müllerian ducts (pink), mesonephric (Wolff) ducts (pink), and distal ureters (purple). The Müllerian ducts, which had been initiated in the cranial mesonephric ridges laterally to the Wolffian ducts, elongate adjacent to the latter. Below the lower pole of the gonads (orange), the Müllerian ducts cross the Wolffian ducts to proceed caudalward, medially to the latter. By Carnegie stage 23 the Müllerian ducts have met the sinusal tubercle of the pelvic urogenital sinus (dotted lines). The gonadal ridge cell population (orange) is now distinct from the genital ducts and periductal mesenchyme

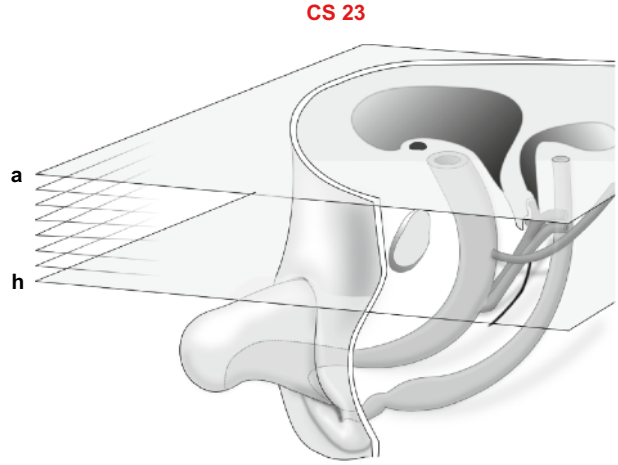

Fig. 3.11 Photohistographs of craniocaudal serial transverse sections of a female embryo at Carnegie stage 23. The levels of sections (**a**–**h**) are indicated in the schematic drawing. The subperitoneal tissue architecture is determined dorsally by the horseshoe-shaped splanchnic coelom structures separating the hindgut and its mesentery from the genital ducts and periductal mesenchyme through the primordial urogenitorectal peritoneal pouch (**b**–**h**). Ventrally, the confluence of the genital ducts and the urogenital sinus mesenchymes is apparent (**f**, **g**, **h**). The course of the distal ureters and their mesureters to their connections with the bladder can be followed (**a**–**e**). The genital duct mesenchyme is encased by the proximal splanchnic ACM ventrolaterally and by the genital coelom mesoderm dorsolaterally (**b**–**h**). Prominent plexus of blood vessels are dispersed in the proximal splanchnic ACM (**b**–**h**). Autonomic nerve tissue (arrows) can be noted in the hypogastric coelom mesoderm laterally and dorsally to the genital coelom mesoderm intermingling with the ACM ventrally. The tissues forming the genital duct morphogenetic unit are colored as follows: pink, genital ducts mesenchyme; green, proximal splanchnic ACM; yellow, genital coelom mesoderm; yellow-green, pelvic urogenital sinus

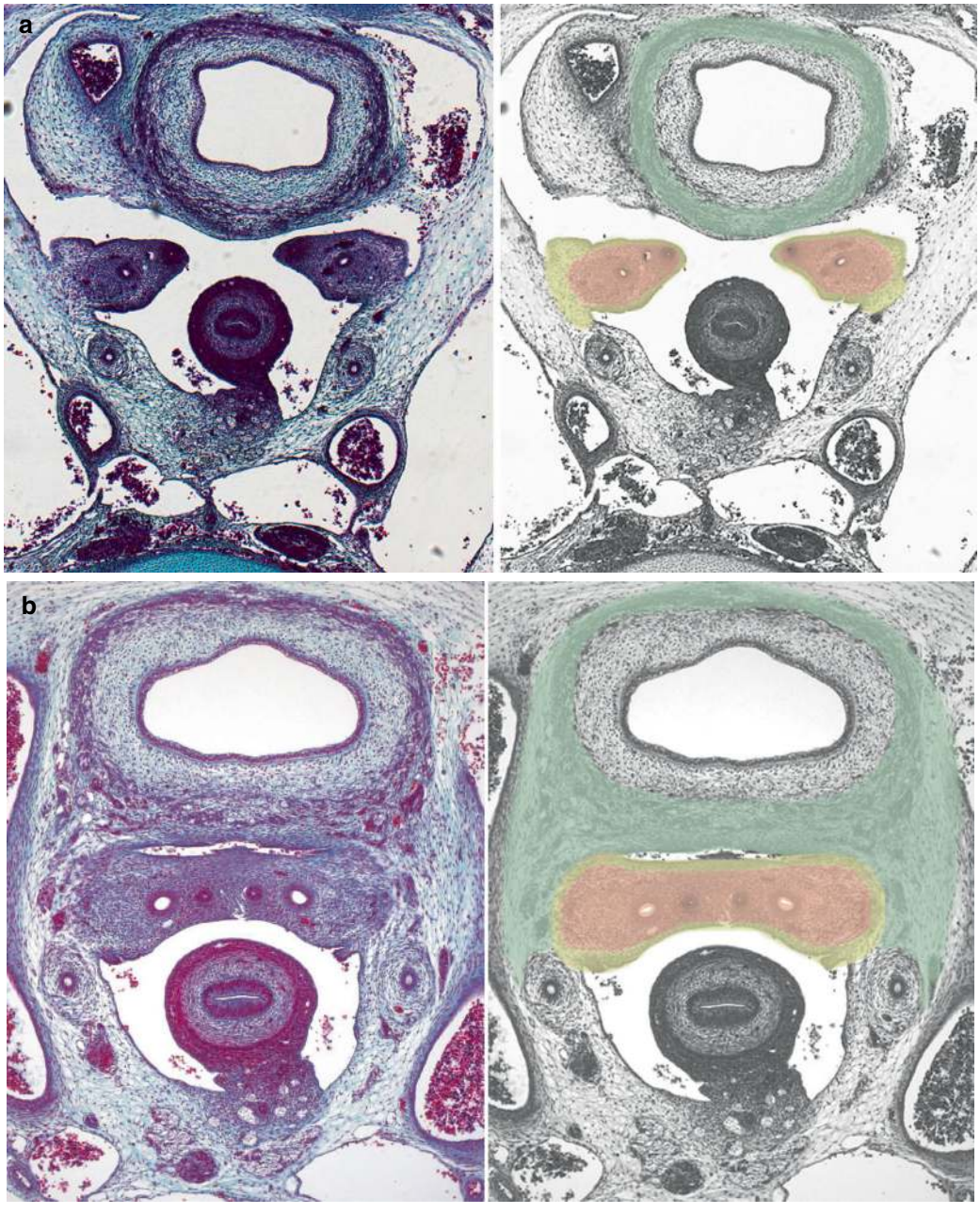

Fig. 3.11 (continued)

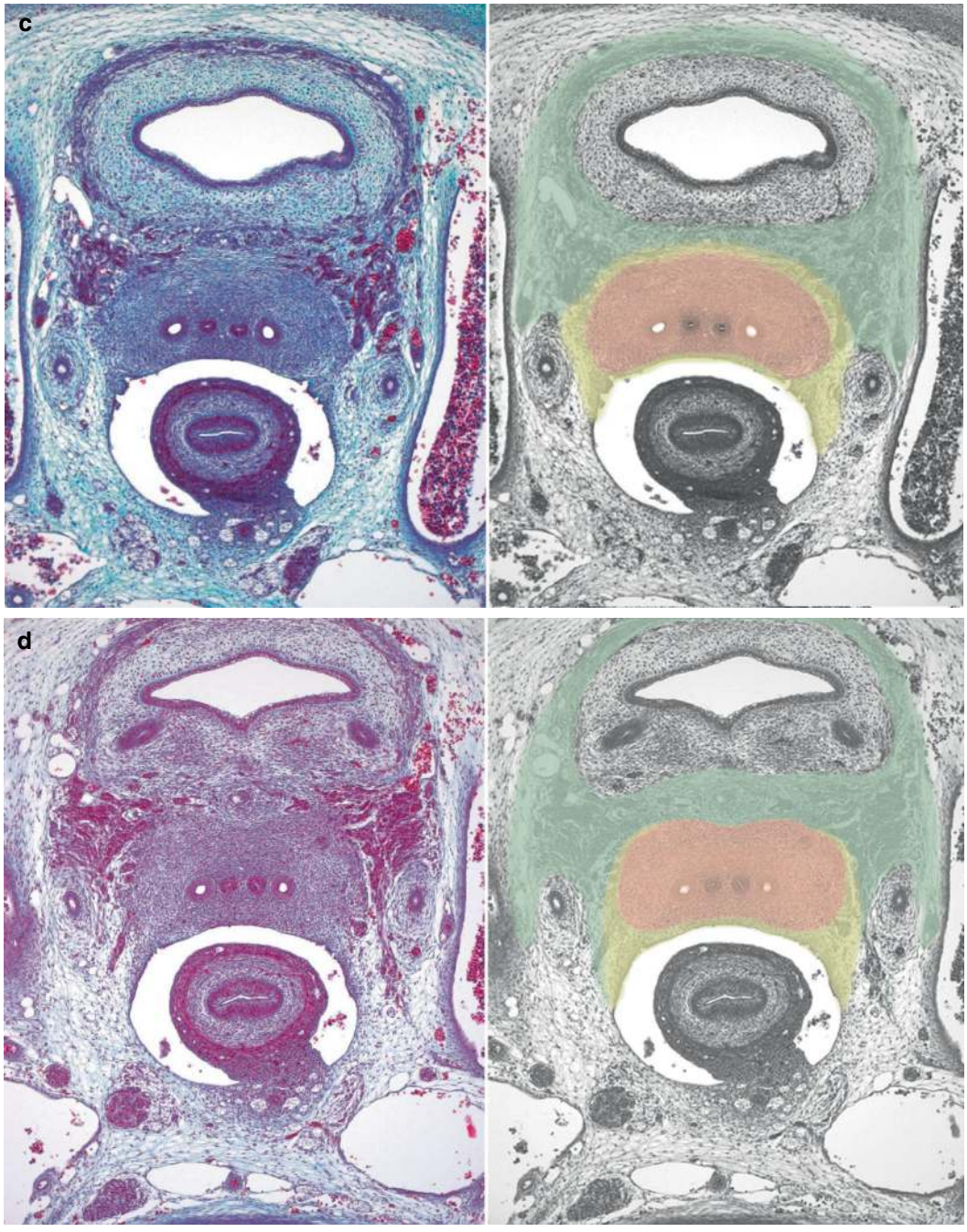

Fig. 3.11 (continued)

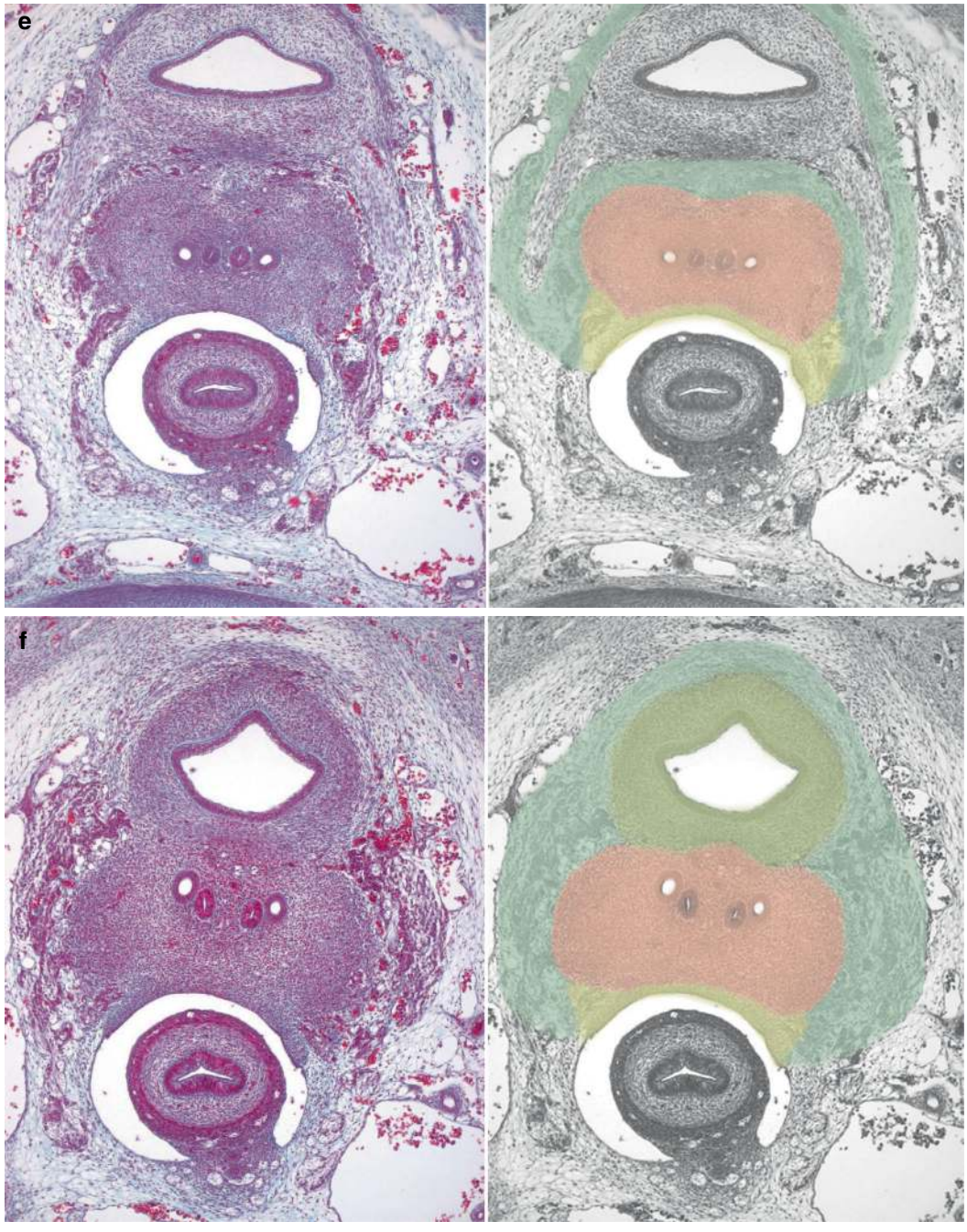

Fig. 3.11 (continued)

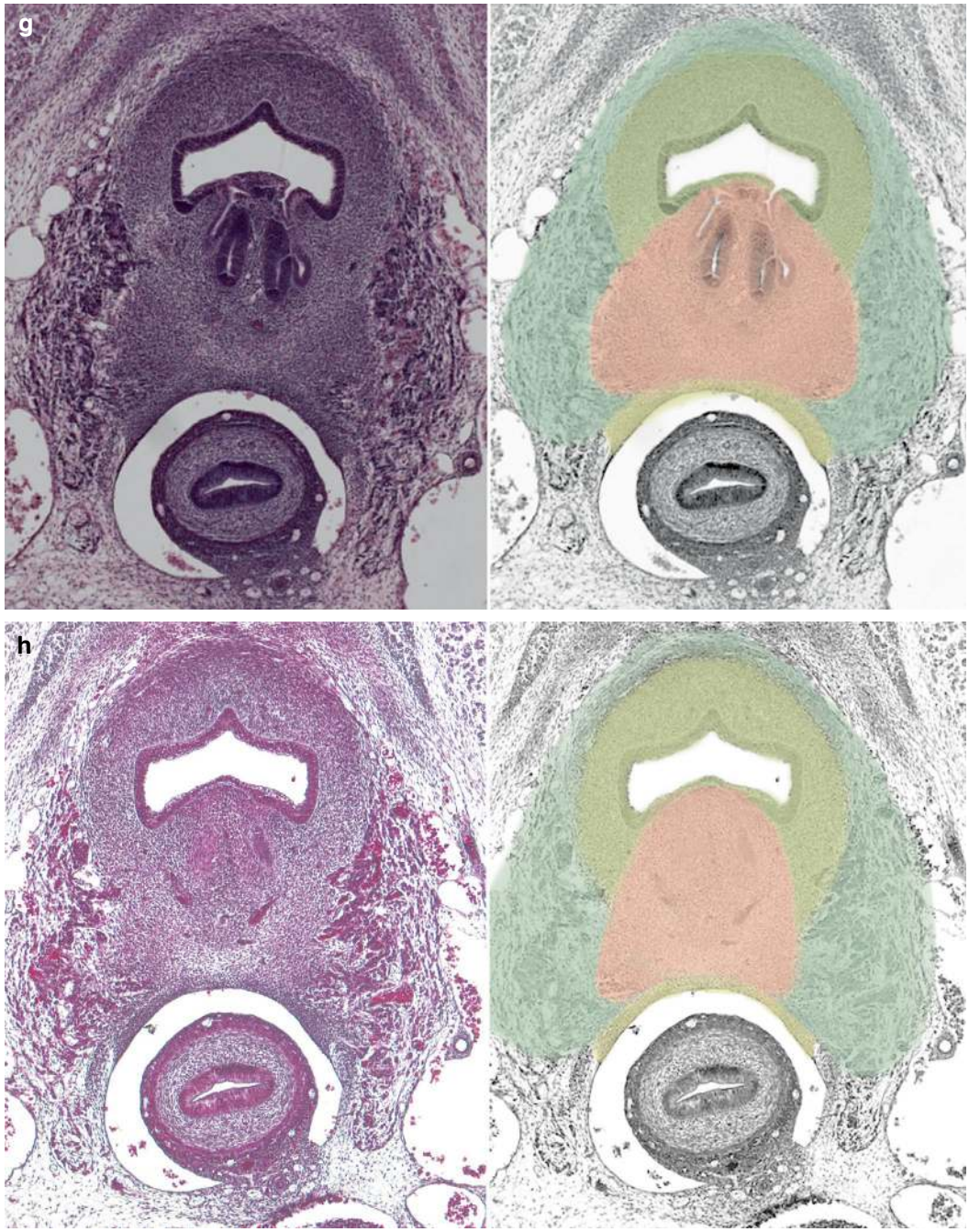

Fig. 3.11 (continued)

anastomosed with the degenerating mesonephric ducts and the periductal mesenchyme) with the proximal splanchnic ACM, urogenital sinus endoderm, and the phallic urogenital sinus endosurface, which is the primordial vestibulum of the developing vulva. The united distal paramesonephric ducts are primarily occluded and appear as a vaginal plate [9, 12].

During the descent of the sinuvaginal bulbs within the urogenital sinus mesenchyme (proximal splanchnic ACM), the primordial urorectal peritoneal pouch begins to obliterate caudocrani-

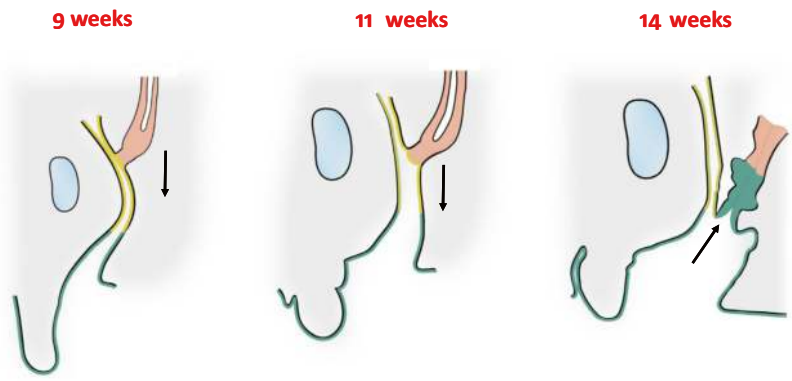

Fig. 3.12 Schematic depiction of the formation of the distal (sinus) vagina and its connection to the phallic urogenital sinus endosurface in the female fetus (modified from [9]). Midsagittal sections at 9, 11, and 14 weeks of gestational age. Bilateral sinuvaginal bulbs that are formed by paramesonephric and degenerating mesonephric ducts within the proximal splanchnic ACM move caudalward along the posterior urethral (pelvic urogenital sinus) endoderm. At their final position, the phallic urogenital sinus endoderm grows within the proximal splanchnic ACM toward the sinuvaginal bulbs, encasing their tip, and fuses with the paramesonephric ducts' epithelium. Yellow, pelvic urogenital sinus (urethral) epithelium; green, phallic urogenital sinus (vulvar) epithelium; pink, paramesonephric epithelium, sinuvaginal bulb

ally up to the level of the bladder neck and the transition of the sinus to the suprasinus vagina. The suprasinus vagina elongates.

3.5 Müllerian Compartment

The formation of the vaginal orifice in the vestibule at around 14 weeks is considered the morphological marker for the determined state of the genital duct cell population in the female. The genital ducts and their periductal mesenchyme (mesonephros III°) now make up the genital duct (Müllerian) compartment, representing the morphogenetic field.

The morphogenetic actions within the Müllerian compartment include the continued degeneration of the mesonephric ducts and the regionalization of the Müllerian ducts by specification of the mantle mesenchymes of the Müllerian subcompartments: the sinus and suprasinus vagina, the cervix, the corpus, and the tubes, which are all covered with Müllerian adventitia (Fig. 3.13). The most caudal Müllerian subcompartment, the sinus vagina and its adventitia, is encased by pelvic urogenital sinus mesenchyme derived from the proximal splanchnic ACM. The suprasinus vagina and cervix and their adventitias are covered anteriorly by vascular mesocolpoi/mesometria derived from the proximal splanchnic ACM and posteriorly by ligamentous mesocolpoi/mesometria derived from the genital coelom mesoderm. Uterine corpus and tubes with their adventitias are enveloped by serosa and mesenteries, which are also derived from the genital coelom mesoderm. The forma-

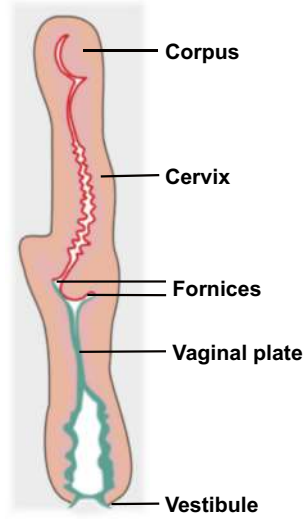

Fig. 3.13 Regionalization of the paramesonephric (Müllerian) duct system demonstrated in a midsagittal section of a female fetus at 18 weeks (modified from [12]). Tubularization of the vaginal plate starting distally at the vestibule is completed at week 18 when the appearance of the vaginal fornices marks the vaginocervical transition

tion of a lumen in the vaginal plate starts at the distal sinus vagina and is completed at about 18 weeks. The appearance of the vaginal fornix at that time marks the cervicovaginal transition. Cervicocorporal transition becomes grossly and histologically distinct at about 22 weeks. In the early fetal period, the epithelium of the distal vaginal plate displays molecular markers, indicating an origin from the urogenital sinus distinct from all other epithelia of the Müllerian compartment. The urogenital sinus-derived epithelium ascends and finally covers the whole vagina and ectocervix by about 21 weeks [12].

Within the cervical subcompartment, rudimentary glands are formed through outpouchings of the columnar epithelium into the stroma starting at about 14 weeks. By 20 weeks, significant elongation and branching of the cervical glands occur [12].

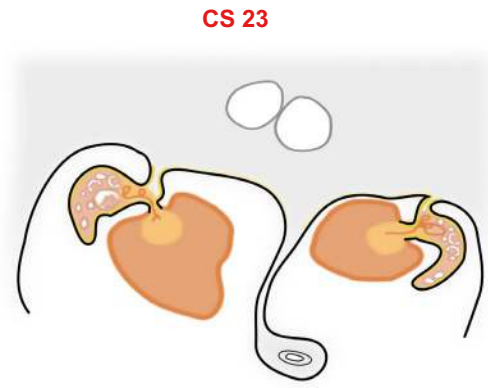

Fig. 3.14 Formation of the ovarian compartment. At Carnegie stage 23, primordial ovaries (orange) exhibiting cortical and medullary regionalization have been formed. At the hilum, the ovarian surface epithelium abuts the mesothelium of the genital peritoneum (darker yellow). The rete ovarii, representing gonadal ridge-associated mesonephros III°, extends into the future mesovarium, separated from the genital duct-associated mesonephros III° (pink). The paramesenteric peritoneum extends between the bowel mesentery and the mesovarium (lighter yellow)

3.6 Primordial Gonad Morphogenetic Field and Ovarian Compartment

The primordial gonad morphogenetic field comprises the gonadal ridge, genital coelom mesoderm, and primordial germ cells. The gonadal ridge cells have been separated from the genital duct-associated mesonephros III cell population by the previous bifurcation in the cell differentiation trajectory (Fig. 3.3).

The morphogenetic actions within this field generate the first sex-specific anatomical structures. In the female phenotype, the proliferating germ cells, supporting cells, and interstitial cells expand the ovarian tissue mass, which further bulges into the peritoneal space [6, 13, 14]. Regionalization into the ovarian cortex and medulla is imminent (Fig. 3.14). Interaction with the genital coelom mesoderm at the base of the primordial ovary leads to the formation of the hilum, serving as a neurovascular entry zone and also connecting the intra- and extraovarian rete, which are mesonephric remnants. Whereas the mesonephric ducts degenerate in the female, the ovarian rete persists as a structure of, so far, an unknown function [15]. The supporting cells differentiate into granulosa cell precursors. Germ cells and adjacent granulosa cells form ovigenous cords, encased by basal laminas. Continuous with the ovigenous cords, a basal lamina forms below the ovarian surface cells, supporting the ovarian surface epithelium. Granulosa cells secrete paracrine factors, which recruit and differentiate steroidogenic theca cells. The theca cells are derived from the interstitial cells of the ovary and from the extraovarian rete later in development [16]. The ovigenous cords are fragmented into smaller assemblies and finally into primordial follicles, which consist of a meiotically arrested oocyte and surrounding granulosa cells, encased by a basal lamina. The fragmentation of the ovigenous cords and the formation of the primordial follicles start at the cortex-medulla transition and proceed toward the ovarian surface. Concomitantly with the formation of the continuous ovarian surface epithelium and underlying basal lamina, a tunica albuginea is established. Details about folliculogenesis, as well as the morphological and functional aspects of ovulation and corpus luteum formation, are beyond the scope of this book. The ovarian compartment is finally determined, and a border toward the genital coelom mesoderm derivatives, such as the

mesovarium, is set up during the fetal period. However, the exact time of reaching determination is not known. Three spatial subcompartments of the ovary are discernable:

- The cortex covered by the ovarian surface epithelium with underlying tunica albuginea containing the follicles
- The medulla encased by the cortex, except at the hilus, which is directly overlaid by the ovarian surface epithelium and tunica albuginea
- The rete ovarii with its extraovarian part extending into the mesovarium

At the hilum, the ovarian surface epithelium meets the mesothelium of the genital peritoneal compartment, which includes the mesovarium.

3.7 Ontogenetic Anatomy of the Subperitoneum

The role of ontogenetic anatomy in assigning the habitats of multiple determined cell types to mature anatomical structures as *ontogenetic compartments* and *subcompartments* is demonstrated with the subperitoneum.

The stepwise development of the female genital tract outlined above allows a new understanding of its 3D structural relations to adjacent organs and to their supply and support tissues, which is not based on dissection artifacts dividing the pelvic subperitoneum into so-called ligaments, spaces, leaves, etc. As a consequence, much more surgical precision can be applied to completely remove intercalated lymph nodes and, eventually, tertiary lymphoid tissues at risk for metastases yet preserving essential neurovascular structures (see Chaps. 5 and 6). The topographic subperitoneal pelvic anatomy in the female can be approached using a model of a posterior and an anterior system of seven more or less horseshoe-shaped parallel shells, two of which meet at the lower genital tract, i.e., the uterus and vagina (Fig. 3.15). The posterior part represents four derivatives of the coelom mesoderms. The anterior part of the subperitoneal shell model consists of three derivatives of the splanchnic ACM. Starting in the posterior sagittal midline, the rectum is bordered by the innermost posterior shell, the mesorectum, which is derived from the proximal splanchnic mesoderm. A denser anterior mesorectum can be discriminated from the lateral and posterior parts.

The second posterior shell in the proximodistal axis is formed by the distal splanchnic coelom mesoderm, which gives rise to the pararectal fasciae continuous with the ligamentous mesometria and mesocolpoi. The inferior hypogastric plexus lateral to these structures is proposed to be derived from the distal somatic coelom mesoderm.

The fourth posterior shell in the proximodistal direction is made up of bilateral mesureters, delicate sheets that coat the ureters and provide their neurovascular support. Their precursor tissue is the distal somatic coelom mesoderm.

The dorsal anterior shell consists of the vascular mesometria and mesocolpoi, with intercalated lymph nodes draining the lower genital tract. It can be separated from the bilateral bladder mesenteries and dorsal adventitia. Both shells are derivatives of the proximal splanchnic ACM. The ventral anterior shell is represented by the bladder peritoneum, visceral endopelvic fascia, and distal urogenital mesentery with the obliterated umbilical artery. The distal urogenital mesentery can also contain intercalated lymph nodes, which drain the lower genital tract. The precursor tissue is the distal splanchnic ACM.

In the model of the subperitoneal pelvic shells, the lower genital tract (cervix and vagina) is located in the fusion zone of the second posterior shell, the ligamentous mesometrium and mesocolpos, and the dorsal anterior shell, which corresponds to the vascular mesometrium and mesocolpos. The vascular mesometrium crosses the ureter-mesureter complex anteriorly. The distal mesureter separates the upper mesocolpos from the bladder mesentery. The lower mesocolpos is connected to the bladder mesentery with regard to arterial supply and lymphatic drainage. Branches of the inferior hypogastric plexus radiate medially to supply the genital tract (plexus of Frankenhäuser) and superolaterally to the ureterovesical junction and the bladder.

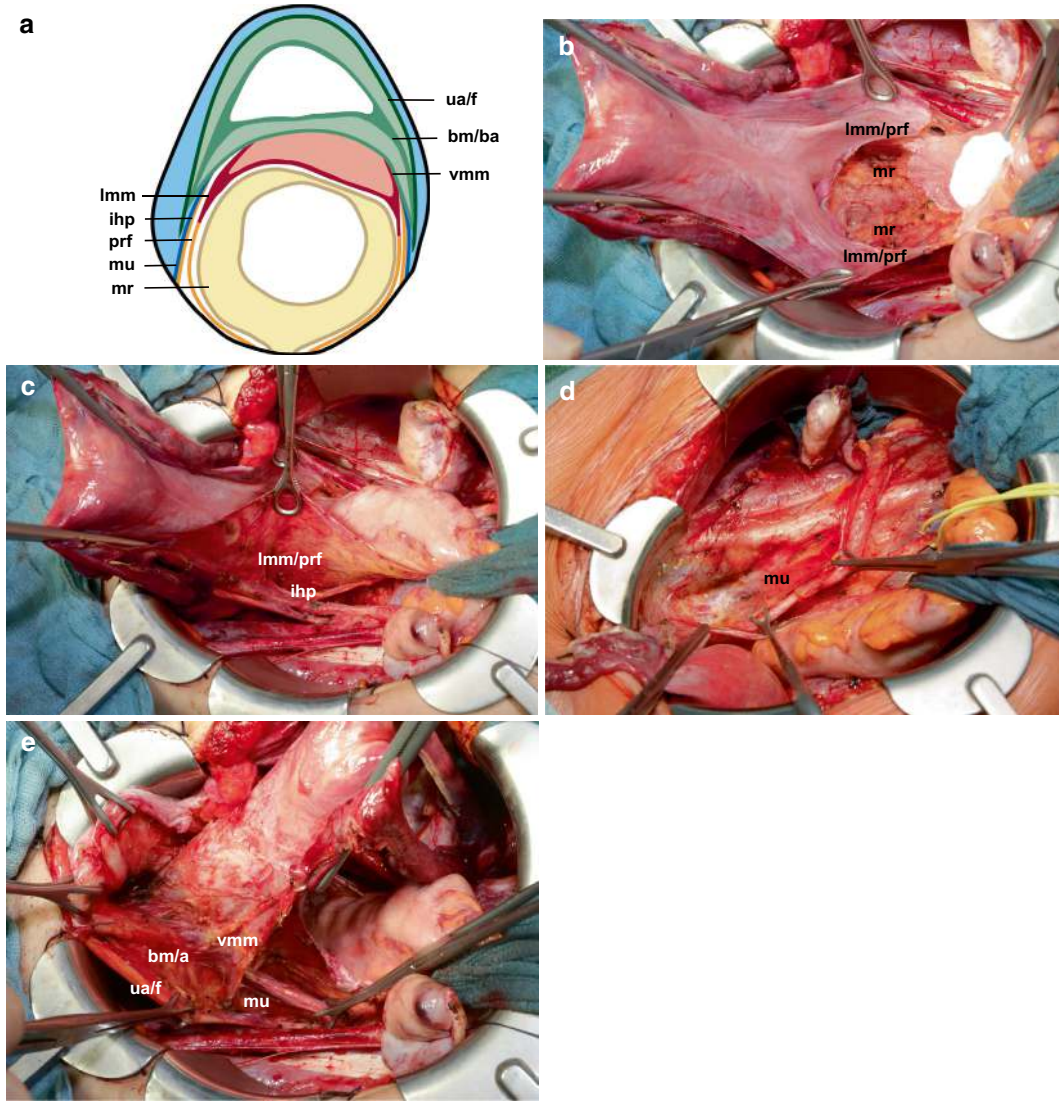

Fig. 3.15 Shell model of the female subperitoneum based on ontogenetic anatomy. Four posterior shells are derived from the lower trunk coelom mesoderm. Three anterior shells originate from splanchnic anterior cloacal mesenchyme. The second posterior and the dorsal anterior shells meet at the lower genital tract (cervix uteri and vagina). (**a**) Schematic illustration. (**b**) The mesorectum (mr), as the first posterior shell, and the bilateral complex of the pararectal fascia and ligamentous and peritoneal mesometrium (prf), as the second posterior shell, are shown. (**c**) Lateral to the pararectal fascia-ligamentous mesometrium/mesocolpos complex, the third posterior shell containing the distal hypogastric nerve and inferior hypogastric plexus (ihp) is demonstrated. (**d**) The mesureter (mu) as the fourth posterior shell is presented. (**e**) The left dorsal anterior shell comprised of the vascular mesometrium (vmm) has been separated from the bladder mesentery/adventitia (bm/a), which is still adherent to the ventral anterior shell, represented by the umbilical artery and the visceral endopelvic fascia (ua/f). The bladder mesentery as the intermediate anterior shell and the ventral anterior shell have not been detached here. The distal mesureter is dissociated from the bladder mesentery and the vascular mesometrium

3.8 Mature Derivatives of Morphogenetic Fields Forming the Female Genital Tract

Mature tissues derived from the morphogenetic fields of each developmental step can be deduced from cell type differentiation trajectories (Table 3.1, Fig. 3.3). Mature derivatives developing from the cell populations of the *mesonephric morphogenetic field* comprise almost the whole lower trunk, in particular the genital tract with ovaries, the perineum with anus and vulva, the urinary tract, the bladder and urethra, the suprarenal glands, the bowel, all urogenital and intestinal mesostructures, the retro- and subperitoneum, the pelvic floor, the pelvic and abdominal walls, and the legs, including all associated systemic structures (vascular system, lymphatic system, nervous system).

Table 3.1 Mature tissues derived from the morphogenetic fields generating the Müllerian compartment from the nephrogenic cords at Carnegie stage 11

Mesonephric morphogenetic field
Abdominal and pelvic walls, perineum with anus and vulva, legs, pelvic floor
Peritoneum, retroperitoneum, and subperitoneum
Urinary organs, suprarenal glands, and support tissues
Reproductive tract organs and support tissues
Bowel and support tissues
Primordial genital tract morphogenetic field
Reproductive tract organs
Urinary bladder and urethra, urethral sphincter
Pubourethral ligament, endopelvic fascia, bladder peritoneum
Urogenital mesentery
Vulva, vestibular bulb, Buck's fascia
Genital peritoneum, serosa, and "ligaments"
Paracolorectal retro-/subperitoneum and peritoneum
Genital ducts morphogenetic field
Müllerian compartment
Vascular mesometria/mesocolpoi
Genital serosa, peritoneum and peritoneal mesenteries (mesovar, mesosalpinx, peritoneal mesometrium)
Ligamentous mesometria/mesocolpoi
Periurethral tissue and urethra, bladder adventitia, and proximal mesenteries
Vulva, vestibular bulb
Müllerian compartment
Uterine tubes, uterine corpus, uterine cervix, suprasinusal and sinus vagina, Müllerian adventitia

The mature derivatives of the *primordial genital tract morphogenetic field* are the genital tract with ovaries, including the serosa, genital peritoneum, and "ligaments"; the paracolorectal subperitoneum-retroperitoneum-peritoneum complex; the vulva compartment; the bladder and urethra; and the urogenital mesenteries with umbilical arteries, endopelvic fascia, and bladder peritoneum.

The mature derivatives of the *genital ducts morphogenetic field* are the genital ducts compartment, vulva compartment, vestibular bulbs, urethra and periurethral tissue, bladder adventitia and proximal mesenteries, vascular mesometria/mesocolpoi, genital serosa, mesovar, mesosalpinx, peritoneal and ligamentous mesometria/mesocolpoi, proximal round proper ovarian and infundibulopelvic ligaments, and fimbriae. The mature derivatives of the female genital ducts or *Müllerian compartment* are the bilateral fallopian tubes and adventitia, the corpus uteri and adventitia, the cervix uteri and adventitia, and the sinus and suprasinus vagina and adventitia.

The ontogenetic anatomy of the *Müllerian compartment* with its subcompartments is demonstrated by color-coding the topographical anatomy of the pelvic organs and the supporting tissues to indicate their developmental kinship. We have used shades of green and grey for that purpose: dark green for the subcompartment, light green for the compartment, dark grey for the tissues developed from the predetermination morphogenetic field, and middle and light grey for those matured from the morphogenetic fields of the previous developmental steps.

The Müllerian compartment and its subcompartments can be illustrated in 3D (Fig. 3.16). For the additional depiction of the derivatives of the predetermination morphogenetic fields, 2D illustrations at defined pelvic planes have to be selected. Figures 3.17, 3.18, and 3.19 show the ontogenetic anatomy of the suprasinus vagina, cervix, and corpus uteri in three transverse planes of the pelvis.

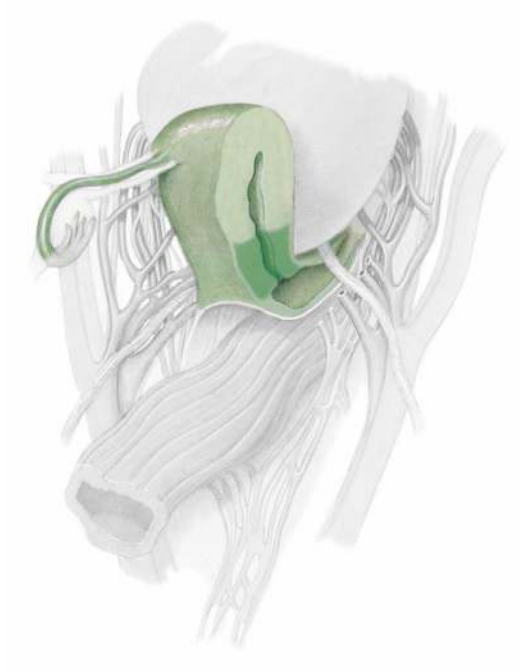

Fig. 3.16 Semischematic 3D depiction of the Müllerian compartment (light green) with its cervix subcompartment (dark green). Genital serosa and subserosa, bladder peritoneum, mesorectum, and mesureter are omitted. Some visceral branches of the right internal iliac vessel system are cut

The suprasinus vagina (Fig. 3.17) is coated by Müllerian adventitia, another Müllerian subcompartment, indicating a first-degree developmental kinship. Tissues of second-degree kinship to the vagina are the bladder adventitia and proximal mesenteries and the ligamentous and vascular mesocolpoi, including the rectovaginal septum. The bladder wall, endopelvic fascia, distal bladder mesentery exhibit third-degree kinship to the vagina. All other tissues are of fourth-degree kinship.

The uterine cervix, as shown in the plane of Fig. 3.18, is bordered circumferentially by Müllerian adventitia, representing first-degree developmental kinship. The Müllerian tissues abut to the bladder adventitia, proximal mesentery, and vascular mesometria anterolaterally and to the ligamentous mesometria and cervical serosa dorsally, which are all tissues of second-degree developmental kinship. The bladder wall, distal bladder mesentery, and visceral endopelvic fascia are tissues of third-degree kinship, and all other pelvic tissues, including the mesureters, ureters, and mesorectum, have a fourth-degree developmental kinship to Müllerian tissues, although they may be spatially close to the Müllerian compartment.

The uterine corpus, as the next Müllerian subcompartment in the cranial direction, is an intraperitoneal structure. As depicted in Fig. 3.19, it is encased by circumferential adventitia as another Müllerian subcompartment, indicating first-degree developmental kinship. Uterine serosa and peritoneal mesometria are of second-degree kinship. Pararectal peritoneum is of third-degree developmental kinship. All other pelvic tissues are of fourth-degree kinship.

The sinus vagina, as the most caudal, and the bilateral uterine tubes, as the most cranial Müllerian subcompartments, as well as the ovarian compartments, are not shown in the color-coded anatomical maps. The sinus vagina is encased by Müllerian adventitia, exhibiting first-degree kinship. The urethra, periurethral and perivaginal tissues derived from the proximal splanchnic ACM represent second-degree kinship. The endopelvic fascia, pubourethral ligament, and rectovaginal septum are of third-degree and all other neighboring tissues are of fourth-degree kinship. The developmental kinship of the uterine tubes to the adjacent tissues corresponds to that of the uterine corpus.

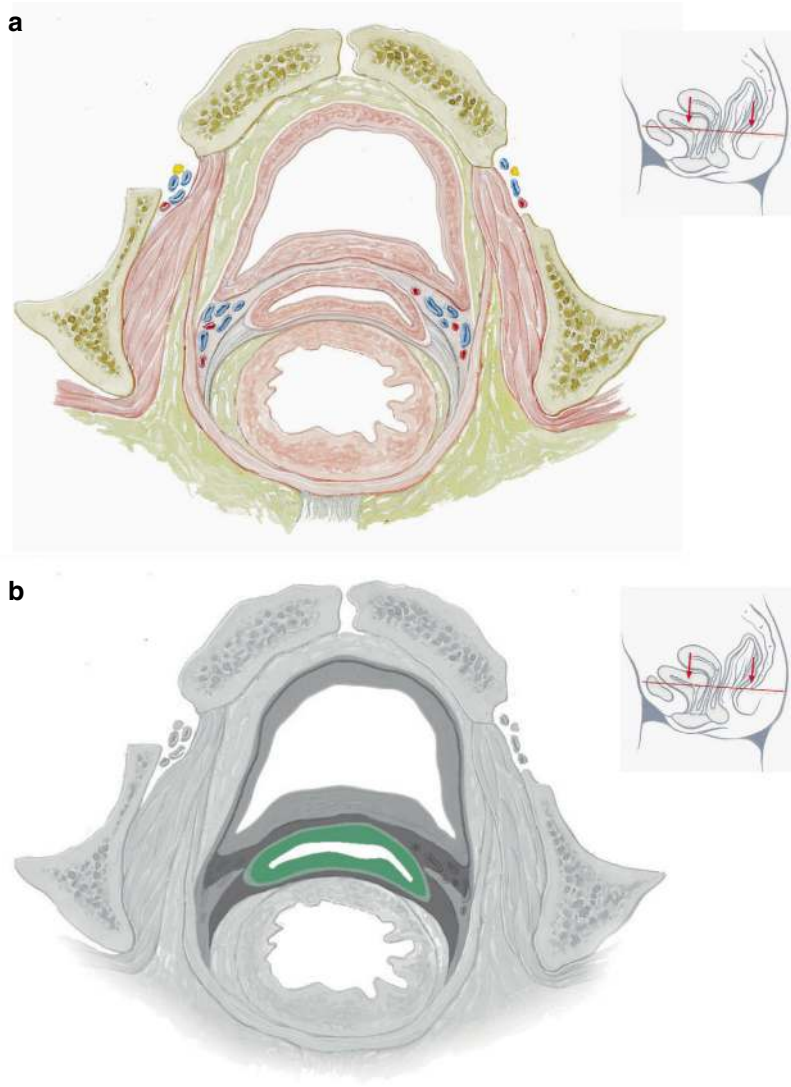

Fig. 3.17 Ontogenetic anatomy of the vagina illustrated in a transverse section of the pelvis at the level indicated in the inset. (**a**) Topographical anatomy. (**b**) Color code of ontogenetic kinship: dark green, vagina; light green, Müllerian adventitia; dark grey, mature tissue derivatives of the genital duct morphogenetic unit; middle grey, mature tissue derivatives of the primordial genital tract morphogenetic unit; light grey, mature tissue derivatives of the mesonephric morphogenetic unit

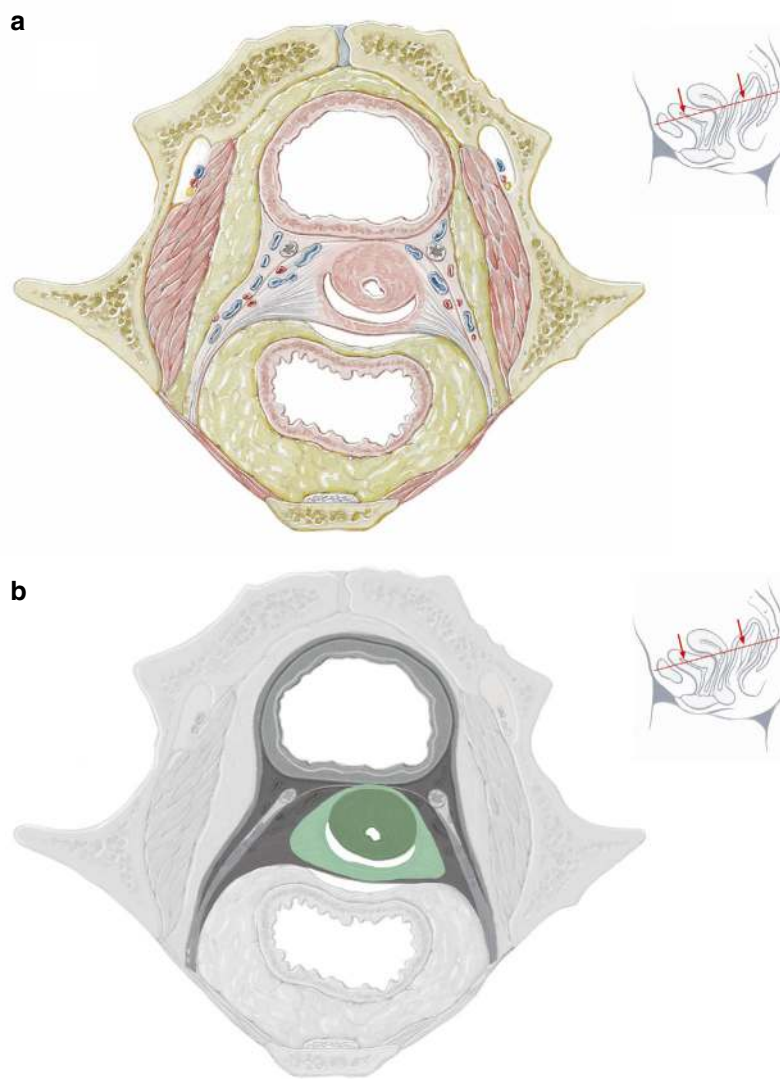

Fig. 3.18 Ontogenetic anatomy of the uterine cervix illustrated in a transverse section of the pelvis at the level indicated in the inset. (**a**) Topographical anatomy. (**b**) Color code of ontogenetic kinship: dark green, uterine cervix. Otherwise, the color code as given in Fig. 3.17

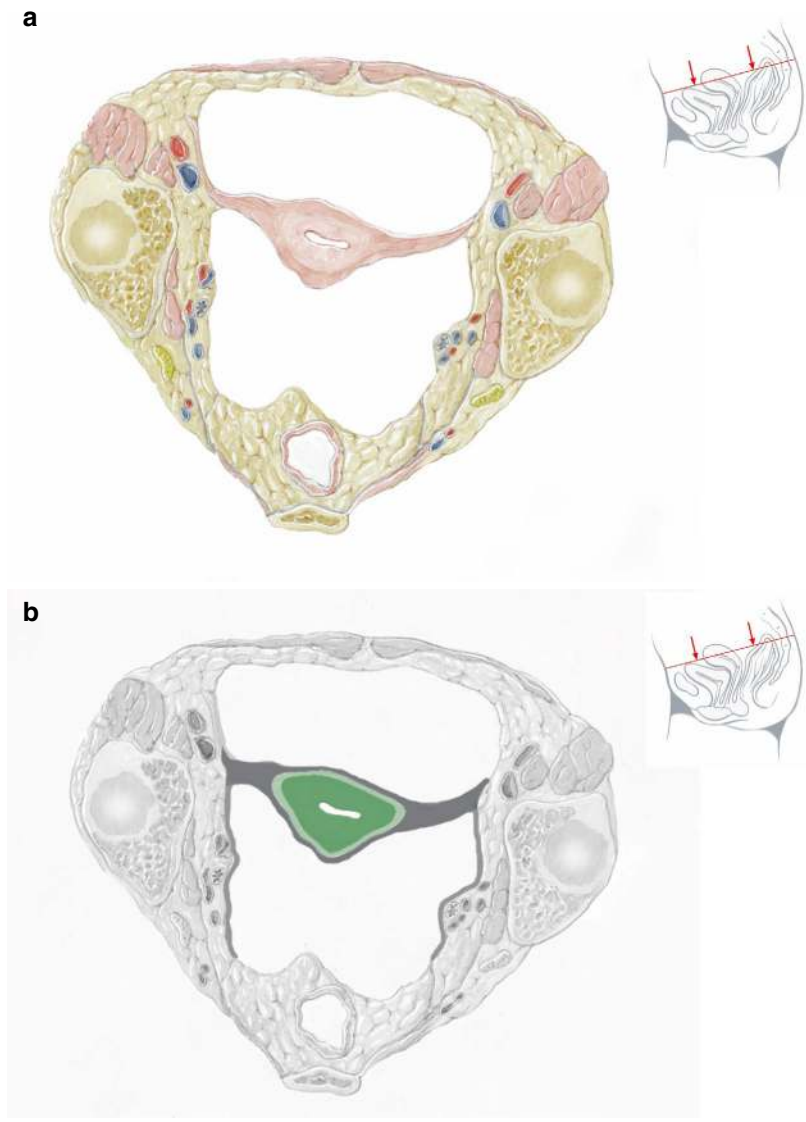

Fig. 3.19 Ontogenetic anatomy of the uterine corpus illustrated in a transverse section of the pelvis at the level indicated in the inset. (**a**) Topographical anatomy. (**b**) Color code of ontogenetic kinship: dark green, uterine corpus. Otherwise, the color code as given in Fig. 3.17

3.9 Local Cancer Fields of Carcinomas of the Suprasinus Vagina, Uterine Cervix, and the Endometrium

The ontogenetic cancer field model claims a stepwise local tumor progression within tissues following the order of developmental kinship in reverse. Tissues that have matured from the subcompartments, compartments, and morphogenetic fields before determination, associated with the differentiation trajectory of the cell type from which the malignant tumor originated, are termed *cancer fields. The ontogenetic (oT) staging system* was implemented to indicate the degree of malignant progression by assigning macroscopic or microscopic neoplastic tissue to the most advanced cancer field.

The oT-stage-associated cancer fields for carcinoma of the suprasinus vagina, uterine cervix, and endometrium are demonstrated in the transverse planes of the pelvis, from caudal to cranial, in Figs. 3.20, 3.21, and 3.22.

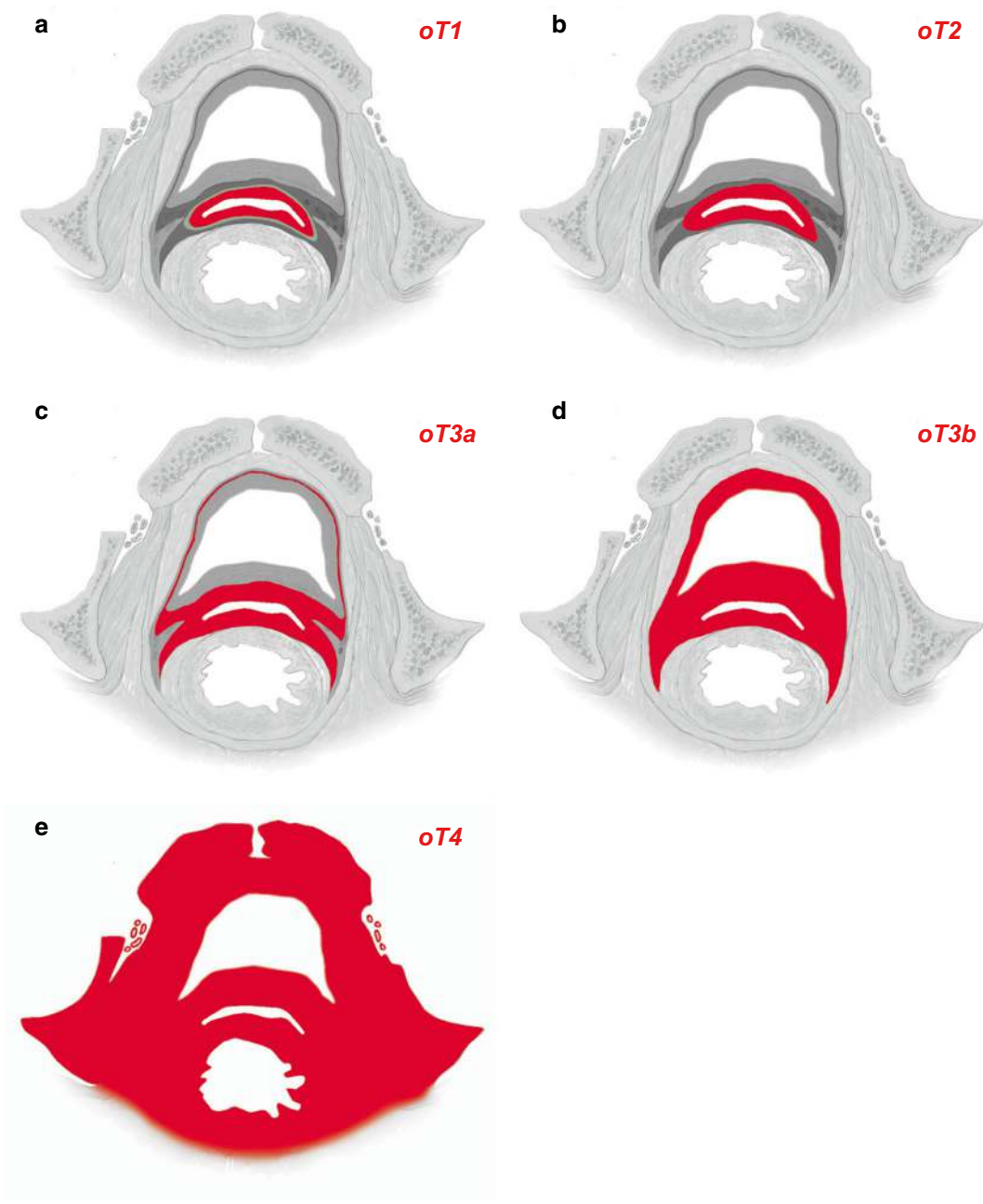

Fig. 3.20 Ontogenetic tumor stage (oT)-associated cancer fields of vaginal carcinoma demonstrated in the transverse pelvic plane of Fig. 3.17. (**a**) oT1, (**b**) oT2, (**c**) oT3a, (**d**) oT3b, (**e**) oT4

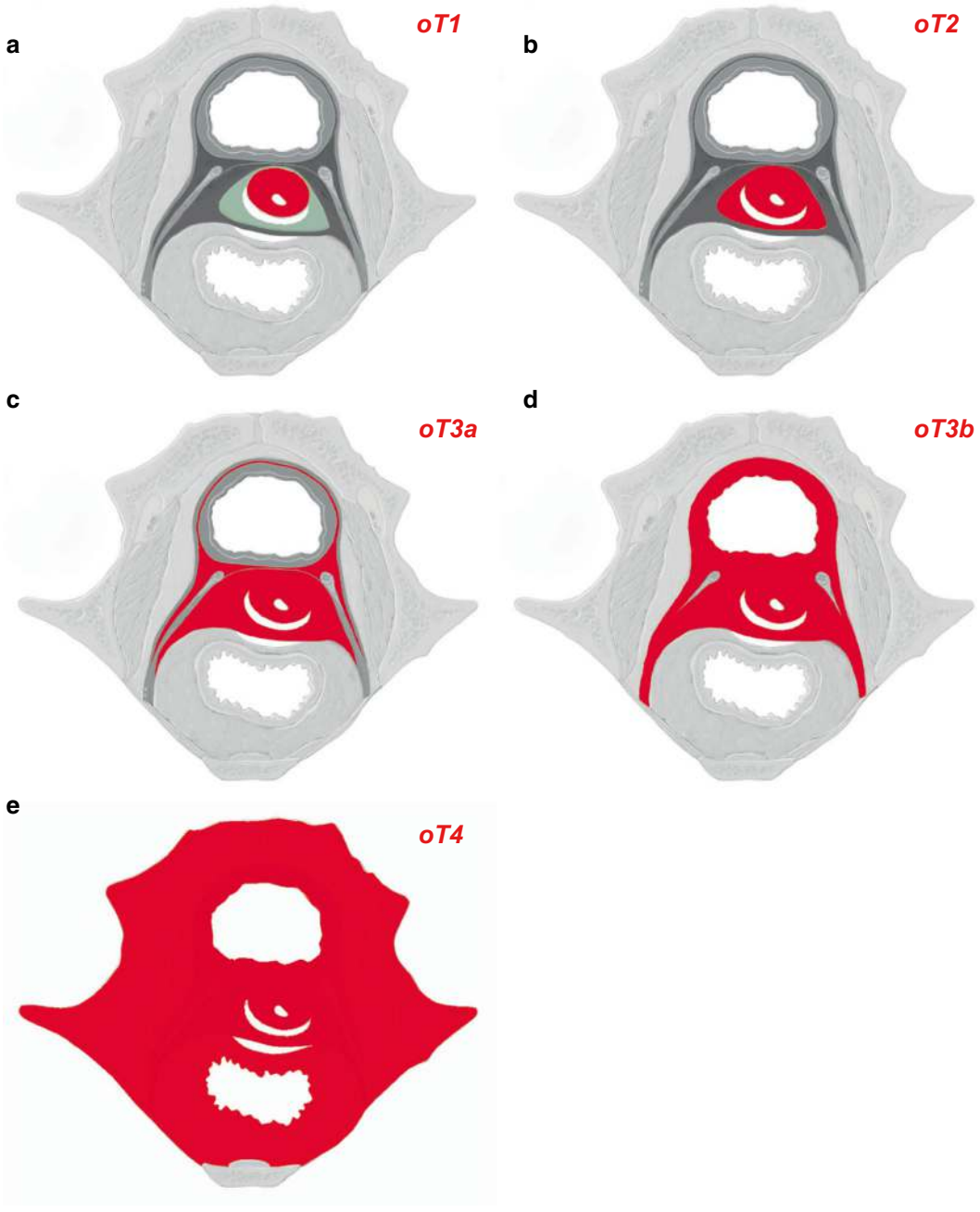

Fig. 3.21 Ontogenetic tumor stage (oT)-associated cancer fields of cervix carcinoma demonstrated in the transverse pelvic plane of Fig. 3.18. (**a**) oT1, (**b**) oT2, (**c**) oT3a, (**d**) oT3b, (**e**) oT4

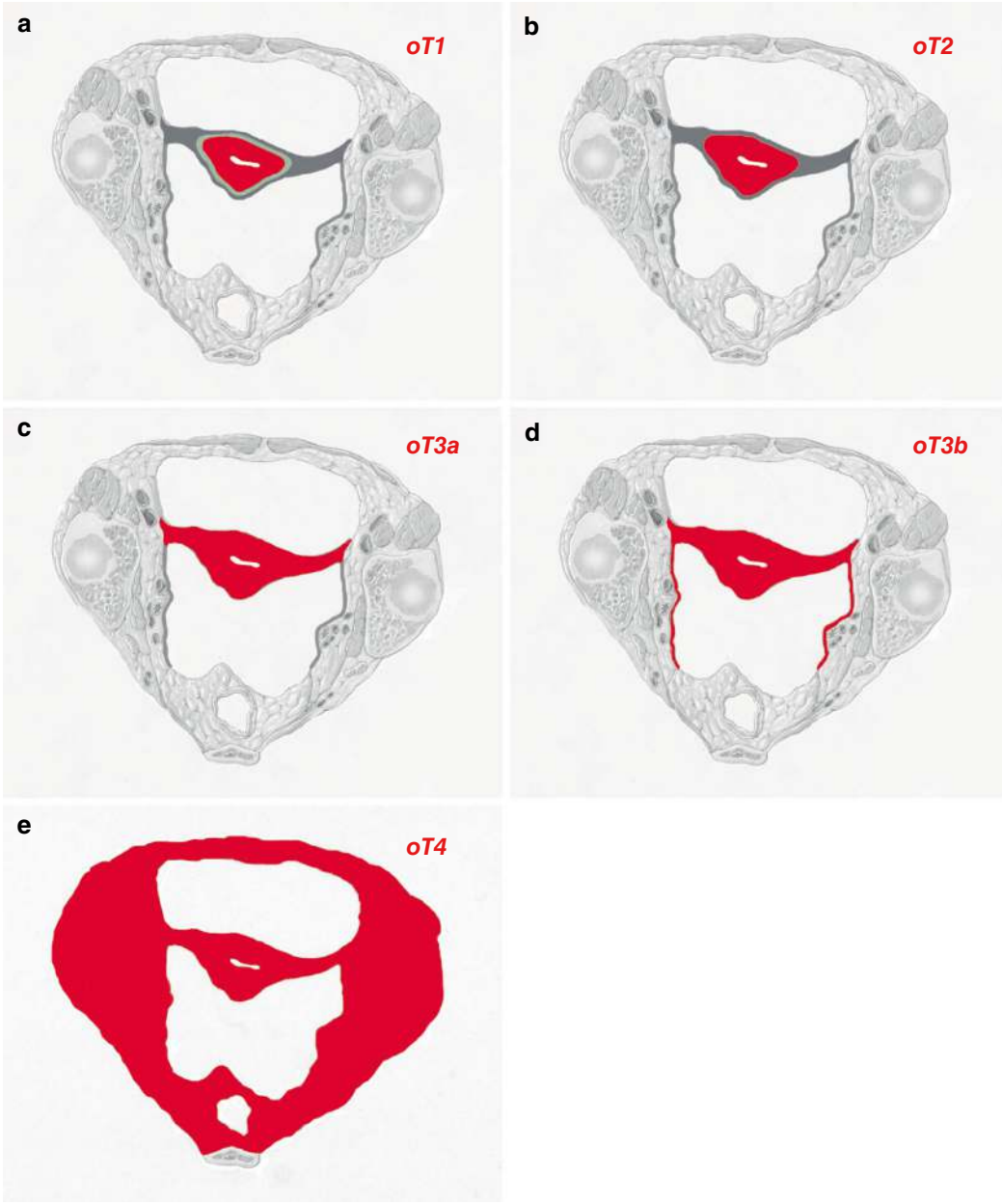

Fig. 3.22 Ontogenetic tumor stage (oT)-associated cancer fields of endometrium carcinoma demonstrated in the transverse pelvic plane of Fig. 3.19. (**a**), oT1, (**b**) oT2, (**c**) oT3a, (**d**) oT3b, (**e**) oT4

3.10 Landscape of Local Cervical Carcinoma Progression

As mentioned in the introduction (Chap. 1), we have mapped the probability of infiltrating cervical cancer in a transverse plane of the midpelvis from the histopathological results of 565 surgical specimens of cervical carcinoma FIGO stages IB-IVA. All tumors had been resected by cancer field surgery with clear margins. The frequency of tumor involvement was indicated by overlaying a heatmap of rainbow colors on the topographic anatomical depiction of the pelvic tissues at that plane (Fig. 1.4a). It is evident that the tumor landscape is not compatible with an isotropic tumor spread model. Computational modeling confirmed the best relation of local tumor spread to developmental kinship, as predicted by the ontogenetic cancer field model shown in Fig. 3.18b [17].

3.11 Local Cancer Fields of Ovarian Carcinoma

According to the ontogenetic cancer field model, oT1 ovarian cancers are confined to one of the three ovarian subcompartments: cortex, medulla, rete ovarii. oT2 cancers involve at least two subcompartments; their cancer field is the complete ovarian compartment. The oT3a cancer field includes the derivatives of the genital coelom mesoderm, which are the genital peritoneum and subperitoneum, in addition to the ovarian compartment. Ovarian malignant tumors must progress to an oT3b stage to infiltrate any tissue of the Müllerian compartment. The oT3b cancer field also comprises the bladder peritoneum and the derivatives of the paramesenteric coelom mesoderm, represented by the pararectal and paracolic peritoneum and subperitoneum. All peritoneal structures and the bowel are part of the oT4 cancer field.

According to current morphological and molecular pathological findings, the origin of ovarian carcinoma is the fimbrial or tubal epithelium in the majority of cases and less frequently the ovarian surface epithelium [18, 19]. For a carcinoma of fimbrial or tubal origin, the cancer field model demands malignant progression to ontogenetic stage 3b to infiltrate the adjacent ovary. This is in accordance with the clinical fact that these tumors most often exhibit extensive peritoneal spread at diagnosis. For ovarian carcinomas that originated from the ovarian surface epithelium, larger ovarian tumor masses and detection at earlier stages are to be expected from applying the cancer field model.

The uterine tubes are subcompartments of the Müllerian compartment. In order to infiltrate the tubal serosa, the carcinoma must progress to an oT3a stage. Even at this advanced stage of malignant progression, a tubal carcinoma would not be able to invade the ovarian stroma, according to the cancer field model. Clinical evidence suggests that preinvasive serous tubal intraepithelial carcinoma (STIC) sheds tumor foci on the adjacent ovarian surface, which may also be internalized into the ovary as cargo of epithelial inclusion cysts. The malignant progression of these ovarian STIC deposits is obviously faster than the progression of the orthotopic lesions [20]. The cancer field model predicts that a focal infiltration of tubal carcinoma into the abutting ovary or the reverse situation without simultaneous multifocal peritoneal involvement—which would be a common feature if the isotropic local cancer spread model was valid—should be the exception.

References

1. Gilbert SF. Developmental biology. 7th ed. Sunderland: Sinauer Associates; 2003.
2. Gasser RF. The virtual human embryo. 2001. http://www.ehd.org/visual-human-embryo.
3. O'Rahilly R, Müller F. Developmental stages in human embryos. Washington: Carnegie Institution of Washington; 1987.
4. Keibel F. Zur Entwicklungsgeschichte des menschlichen Urogenitalapparates. In: Archiv für anatomie und entwicklungsgeschichte. Leipzig: Veit et Comp; 1896. p. 55–156.
5. Wrobel K-H, Süß F. On the origin and prenatal development of the bovine adrenal gland. Anat Embryol. 1999;199:301–18. https://doi.org/10.1007/s004290050230.
6. Rotgers E, Jorgensen A, Yao HH-C. At the crossroads of fate – somatic cell lineage specification in the fetal

gonad. Endocr Rev. 2018;39:739–59. https://doi.org/10.1210/er.2018-00010.
7. Hynes PJ, Fraher JP. The development of the male genitourinary system. I. The origin of the urorectal septum and the formation of the perineum. Br J Plast Surg. 2004;57:27–36. https://doi.org/10.1016/j.bjps.2003.08.019.
8. O'Rahilly R, Müller F. Human embryology and teratology. New York: Wiley; 2001. p. 317–43.
9. van der Putte SC. The development of the perineum in the human. Adv Anat Embryol Cell Biol. 2005;177:1–131.
10. Batourina E, Tsai S, Lambert S, Sprenkle P, Viana R, Dutta S, et al. Apoptosis induced by vitamin A signaling is crucial for connecting the ureters to the bladder. Nat Genet. 2005;37:1082–9. https://doi.org/10.1038/ng1645.
11. Jacob M, Konrad K, Jacob HJ. Early development of the Müllerian duct in avian embryos with reference to the human. Cells Tissues Organs. 1999;164:63–81. https://doi.org/10.1159/000016644.
12. Robboy SJ, Kurita T, Baskin L, Cunha GR. New insights into human female reproductive tract development. Differentiation. 2017;97:9–22. https://doi.org/10.1016/j.diff.2017.08.002.
13. Austria T, Dubeau L. Embryological insights into the origin of epithelial cancers of the female reproductive tract. Cold Spring Harb Perspect Med. 2023;13:a040642.
14. Hummitzsch K, Hatzirodos N, Irving-Rodgers HF, Hartanti MD, Perry VEA, Anderson RA, et al. Morphometric analyses and gene expression related to germ cells, gonadal ridge epithelial-like cells and granulosa cells during development of the bovine fetal ovary. PLoS ONE. 2019;14:e0214130. https://doi.org/10.1371/journal.pone.0214130.
15. McKey J, Anbarci DN, Bunce C, Ontiveros AE, Behringer RR, Capel B. Integration of mouse ovary morphogenesis with developmental dynamics of the oviduct, ovarian ligaments, and rete ovarii. elife. 2022;11:e81088. https://doi.org/10.7554/eLife.81088.
16. Liu C, Peng J, Matzuk MM, Yao HH-C. Lineage specification of ovarian theca cells requires multicellular interactions via oocyte and granulosa cells. Nat Commun. 2015;6:6934. https://doi.org/10.1038/ncomms7934.
17. Kubitschke H, Wolf B, Morawetz E, Horn L-C, Aktas B, Behn U, et al. Roadmap to local tumour growth: insights from cervical cancer. Sci Rep. 2019;9:12768. https://doi.org/10.1038/s41598-019-49182-1.
18. Löhmussaar K, Kopper O, Korving J, Begthel H, Vreuls CPH, van Es JH, et al. Assessing the origin of high-grade serous ovarian cancer using CRISPR-modification of mouse organoids. Nat Commun. 2020;11:2660. https://doi.org/10.1038/s41467-020-16432-0.
19. Zhang S, Dolgalev I, Zhang T, Ran H, Levine DA, Neel BG. Both fallopian tube and ovarian surface epithelium are cells-of-origin for high-grade serous ovarian carcinoma. Nat Commun. 2019;10:5367. https://doi.org/10.1038/s41467-019-13116-2.
20. Yates MS, Meyer LA, Deavers MT, Daniels MS, Keeler ER, Mok SC, et al. Microscopic and early-stage ovarian cancers in *BRCA1/2* mutation carriers: building a model for early BRCA-associated tumorigenesis. Cancer Prev Res. 2011;4:463–70. https://doi.org/10.1158/1940-6207.CAPR-10-0266.

4 Ontogenetic Anatomy of the Female External Genitalia: Local Progression of Vulvar Carcinoma

The principles and procedural aspects for generating ontogenetic anatomic maps have been introduced in Chaps. 2 and 3. Briefly, the differentiation trajectory for the mature cell type of interest must be identified. For each developmental step, the cell population of this cell type and all abutting populations of cell types, which can be adopted by transdetermination, must be localized. Together, these cell populations make up a developmental-stage-associated morphogenetic field. The mature tissue derivatives of the morphogenetic fields, from the beginning of organogenesis to the terminal stage, are color-coded within their topographic anatomic representation.

4.1 Cell Type Differentiation Trajectory Related to the Female External Genitalia

The precursor cell population of the vulva at Carnegie stage 11, the beginning of organogenesis, forms the cloacal membrane, located at the ventral caudal pole of the embryo proximal to the tailbud (Fig. 4.1) [1–5]. The differentiation trajectory from the cloacal membrane cell population at Carnegie stage 11 to the mature vulva is shown in Fig. 4.2. The cloacal membrane cells having formed the cloacal plate segregate into anterior urogenital-glans plates and posterior anal plate populations. Both progenies bifurcate further into peripheral and central populations. Whereas the latter degenerate to produce the urogenital and anal orifices, the former are direct precursors of the vulva in the female and of the anus in both sexes. The vulva results from the determined populations of the phallic urogenital sinus ecto- and endosurface as an ontogenetic compartment consisting of three subcompartments: peripheral, intermediate, and central. Each subcompartment exhibits epithelial-stromal zonation. For the three developmental stages before determination, the adjacent cell populations encompassing the morphogenetic fields and their developmental pathways are shown in Fig. 4.3.

M. Höckel et al., *Cancer Field Surgery in Gynecologic Oncology*,
https://doi.org/10.1007/978-3-031-83030-3_4

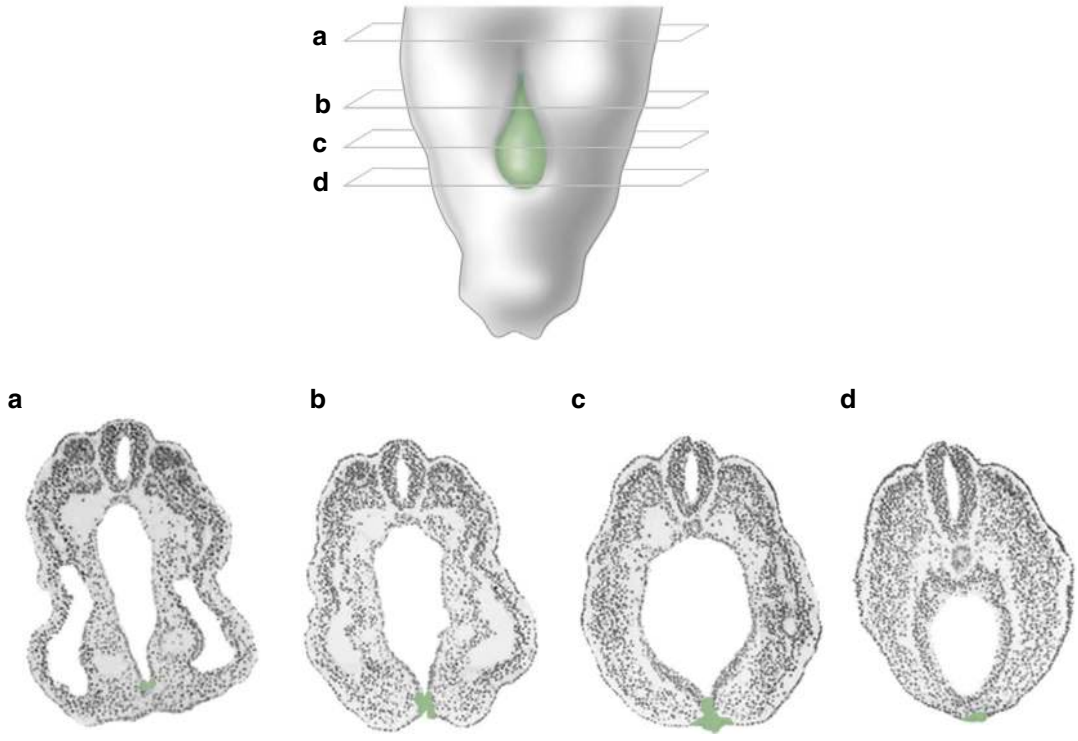

Fig. 4.1 Cloacal membrane of a human embryo at Carnegie stage 11. Four parallel transverse sections (**a**–**d**) demonstrate the cloacal membrane (green) and adjacent cell populations encompassing the cloacal plate morphogenetic field at that developmental stage (modified from [1, 2])

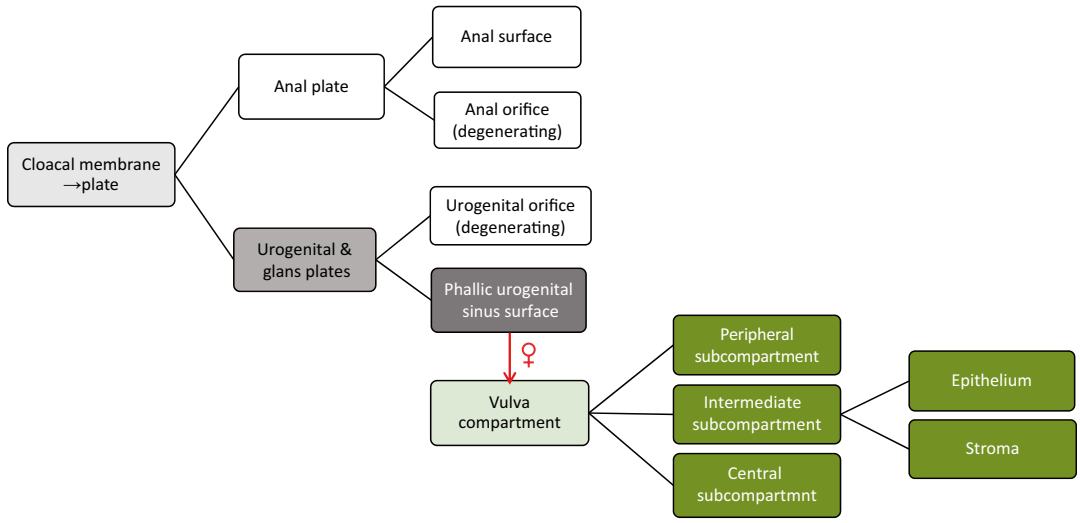

Fig. 4.2 Differentiation trajectories of the cell types forming the vulva from the cloacal membrane at Carnegie stage 11 to maturity

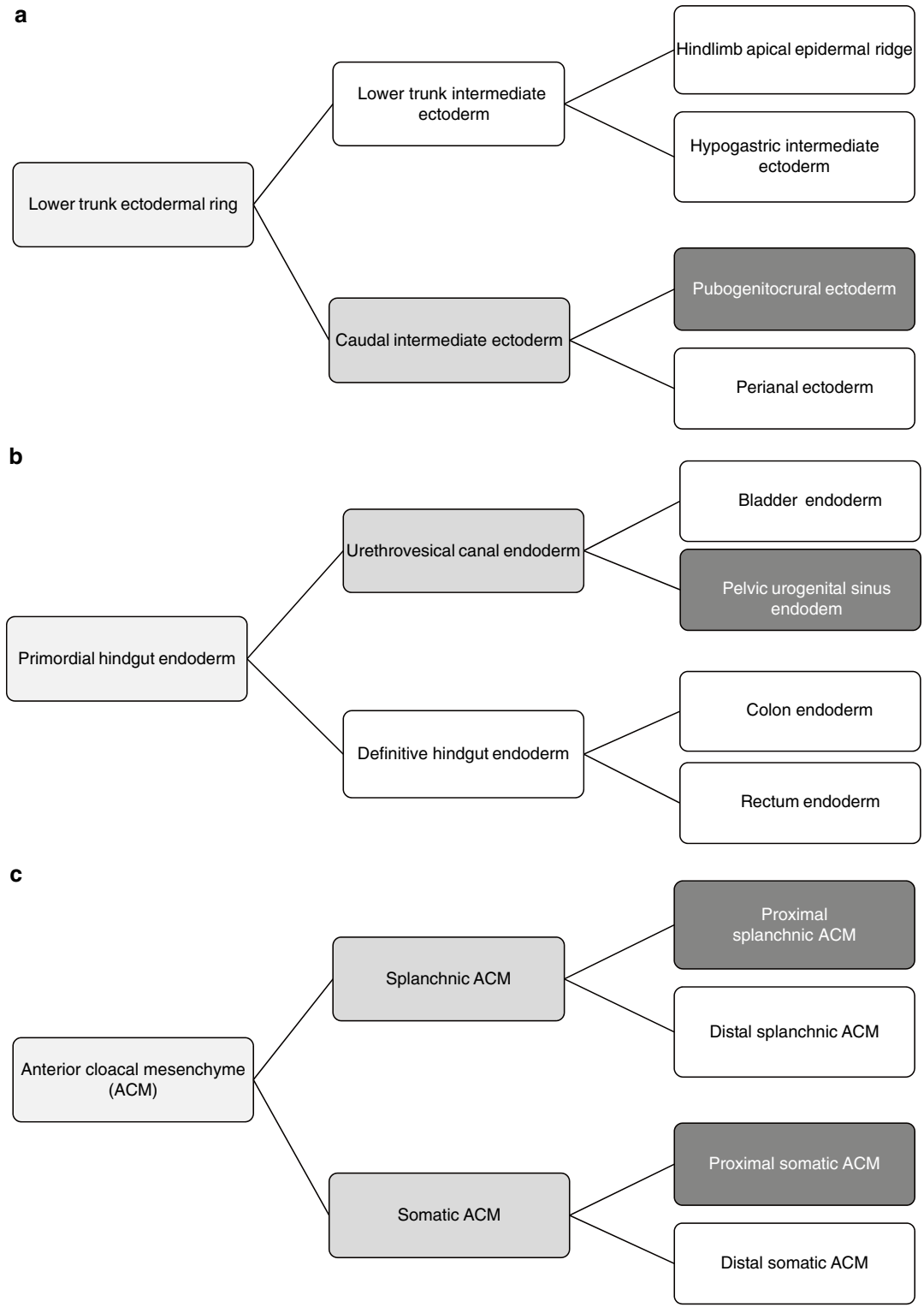

Fig. 4.3 Differentiation trajectories of associated cell types involved in the morphogenesis of the vulva from Carnegie stage 11 to determination. (**a**) Lower trunk ectodermal ring. (**b**) Hindgut endoderm. (**c**) Anterior cloacal mesenchyme (ACM). (**d**) Caudal lateral mesoderm (CLM). (**e**) Nephrogenic cords

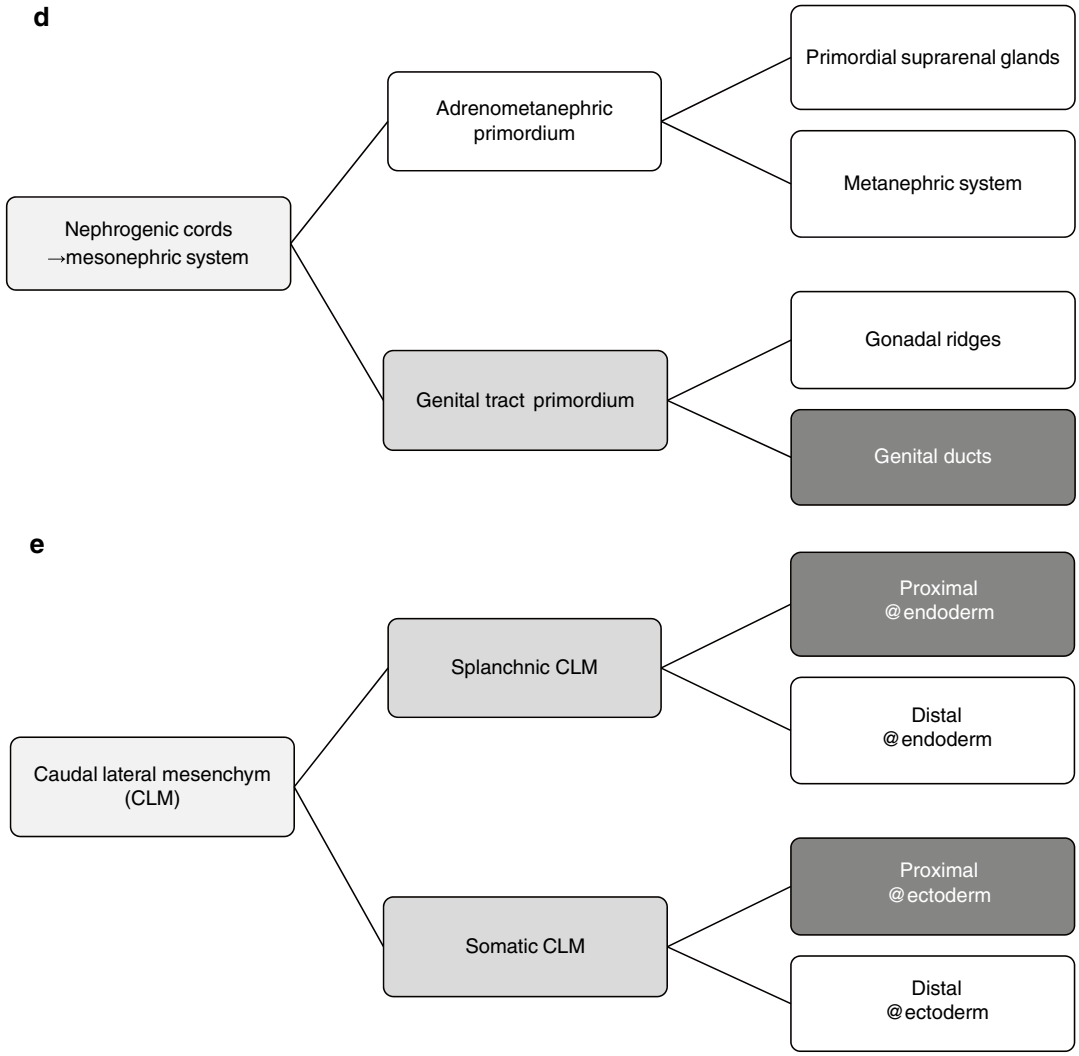

Fig. 4.3 (continued)

4.2 Cloacal Membrane/Plate Morphogenetic Field

The cloacal membrane develops caudally to the primitive streak of the embryonic disc at the transition to the connecting stalk. Upon loss of the mesoderm, the ectoderm and endoderm abut each other at this location [6]. At Carnegie stage 11, these cell populations, together with the juxtaposed lower trunk ectodermal ring [7], primary hindgut endoderm, anterior cloacal mesenchyme (ACM), nephrogenic cords, and caudal lateral mesoderm (CLM), represent the cloacal plate morphogenetic field. The morphogenetic actions of the cloacal membrane cell population during Carnegie stages 11–13 are not very pronounced. The ecto- and endodermal cells of the cloacal membrane appear as one proliferating phenotype, forming the cloacal plate [1–5]. Cloacal plate cells are involved in anastomosing the mesonephric ducts with the cloaca, which occurs in direct proximity to the cloacal plate (Fig. 4.4). The proliferation of the ACM and, to a lesser degree, of the CLM accentuates the bilateral sagittal cloacal folds connected by a shallow coronary groove flanking the cloacal plate. The lower pole

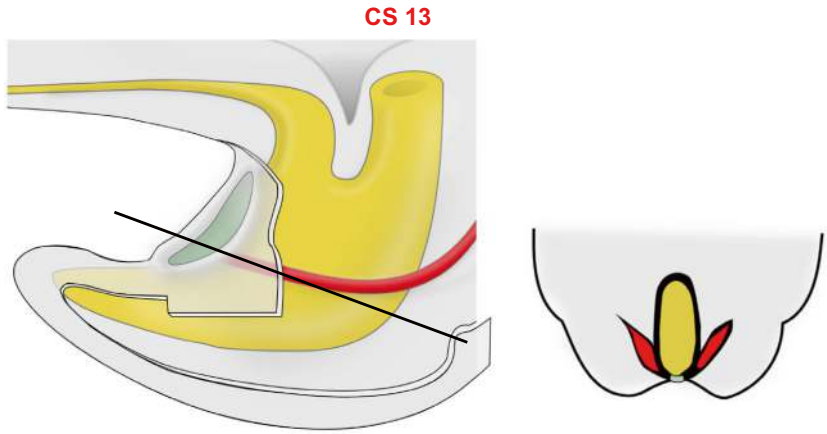

Fig. 4.4 Fusion of the mesonephric duct to the primordial hindgut at the lateral cloacal membrane on the right side. Schematic 3D depiction of the cloaca with cranial allantois and caudal tailgut of an embryo at Carnegie stage 13. The mesonephric duct connects to the cloaca at the level of the cloacal membrane. The right panel shows the transverse section at the level indicated on the left

of the embryo bends toward the umbilical stalk, and a caudal prominence containing an endodermal recessus (a "tail" with a "tailgut") emerges. Bilateral limb buds appear projecting to the location of somites 25–29.

4.3 Urogenital and Glans Plate Morphogenetic Field

Interaction of the cloacal plate cell population with the adjacent ACM ventrally and CLM dorsally is associated with its segregation into the urogenital and glans plate and the anal plate cell types (Fig. 4.2) [8]. Concomitantly, the next generation of cell types abutting the urogenital and glans plate cell population is established by bifurcations: the lower trunk ectodermal ring segregates into the lower trunk and caudal intermediate ectoderm, the primary hindgut endoderm segregates into urethrovesical canal and definitive hindgut endoderms, the ACM into splanchnic and somatic populations, and mesonephric cells into primordial genital tract and adrenometanephric populations (Fig. 4.3). The urogenital and glans plate cells establish the next morphogenetic field, together with the caudal intermediate ectoderm, urethrovesical canal endoderm, somatic and splanchnic ACMs, and primordial genital tract mesenchyme.

The morphogenetic actions within this morphogenetic field, visible during Carnegie stages 14–17, are demonstrated in Fig. 4.5. Proliferating somatic and splanchnic ACMs form the urogenital eminence, which, at its lower side, is midsagittally separated by the urogenital and glans plate. By interacting with the caudal intermediate ectoderm and somatic ACM, urogenital and glans plate cells spread over the eminence as a cap with an epithelial tag [2, 5].

As a collateral morphogenetic action, bilateral genital swellings are beginning to form. For that, somatic ACM interacting with caudal intermediate ectoderm proliferates laterally to the urogenital eminence at both sides. Another important collateral morphogenetic event at that stage is urorectal septation. As described in Chap. 3, the bilateral frontal proliferating splanchnic ACM, which interacts with the urethrovesical endoderm, and the proximal splanchnic coelom mesoderm, which interacts with the definitive hindgut endoderm, meet and unite in the sagittal midline. This process advances caudally. The separation of the proximal from the distal splanchnic coelom mesoderm generates the primordial urorectal pouch. Although not observable, it is assumed that mesonephric mesenchyme maintains contact with the urogenital-glans plate despite the craniodorsal translocation of the anastomoses of the mesonephric ducts with the urethrovesical canal.

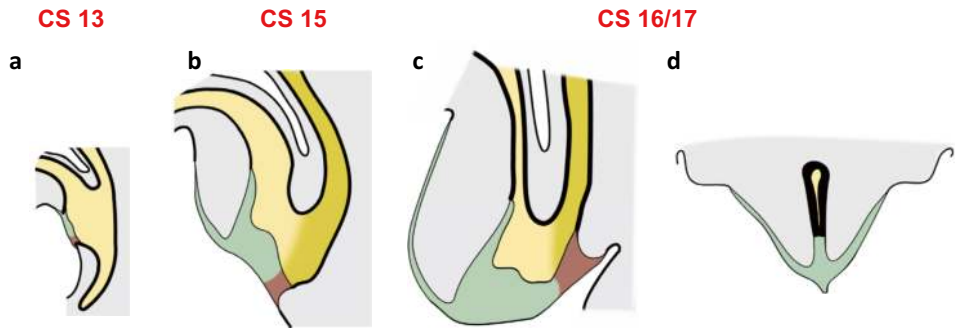

Fig. 4.5 Morphogenetic actions involving the urogenital and glans plate morphogenetic field during Carnegie stages 14–16/17. (**a**–**c**) Midsagittal sections showing the formation of the urogenital eminence with ecto- and endosurfaces covered by urogenital and glans plate cells. Urorectal septation by mesenchymal folds of splanchnic ACM ventrally and splanchnic coelom mesoderm dorsally covered with urethrovesical and definitive hindgut endoderm proceeds caudally toward the border of the urogenital and glans and anal plates. (**d**) Transversal section through the urogenital eminence with urogenital and glans plate. Bilaterally, the genital swellings appear. Green, urogenital and glans plate cells; brown, anal plate; grey, mesenchymes; fine black lines, ectoderm; prominent black lines, endoderm

The development of the anus and posterior perineal region occurs within a different morphogenetic field, consisting of the anal plate cell population, the somatic and splanchnic CLMs, the definitive hindgut endoderm, and the caudal intermediate ectoderm. A prominent postanal fold becomes visible, and the "tail" with the "tailgut" regresses.

4.4 Phallic Urogenital Sinus Morphogenetic Field

The next step in the development of the external genitalia is indicated by the bifurcation of the urogenital-glans plate cell population into peripheral and central types (Fig. 4.2). The central cell population degenerates creating the primordial urogenital orifice. The peripheral cell population generates the external and internal surfaces of the phallic urogenital sinus. The collateral bifurcations are the following: the caudal intermediate ectoderm segregates into an anterior pubogenitocrural and a posterior perianal population; the urogenital canal endoderm into a pelvic urogenital sinus and bladder endoderm; the somatic and splanchnic ACMs into proximal and distal populations related to the ectoderm and endoderm, respectively; and the primordial genital tract into genital ducts and gonadal populations (Fig. 4.3).

The morphogenetic field associated with the phallic urogenital sinus surface cell population also includes the pubogenitocrural ectoderm, urogenital sinus endoderm, proximal somatic and splanchnic ACMs, and genital duct mesenchyme. The morphogenetic actions within the phallic urogenital sinus morphogenetic field relate to the still sexually indifferent embryo during Carnegie stages 18–23, followed by events specific for the male and female phenotypes in the early fetal period.

The major morphogenetic actions during Carnegie stages 18–23 are:

- The distal anterior urorectal septation and the formation of the primordial perineum
- The establishment of distinct phallic urogenital sinus subsurface stroma tissues

During the early fetal period in the female phenotype, the following morphogenetic actions are discernable:

- Further opening of the urogenital orifice
- Lengthening and broadening of the perineum
- Subtotal prepuce formation
- Formation of the vaginal orifice

The bilateral frontal folds of the proximal splanchnic ACM fusing midsagittally proceed caudally to reach the peripheral urogenital-glans plate at around Carnegie stage 18, completing the distal urorectal septation (Fig. 4.6). United bilateral proximal splanchnic and somatic ACMs cov-

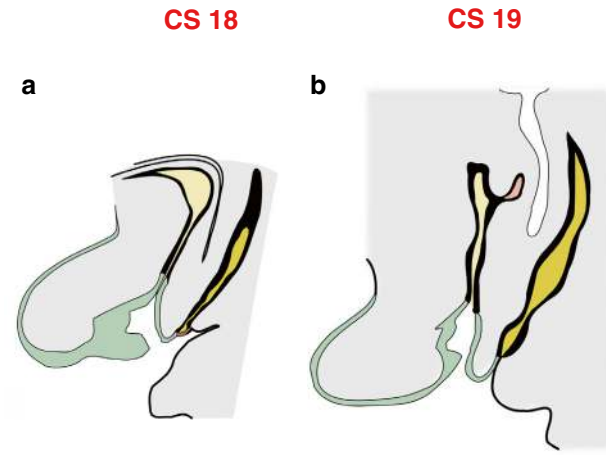

Fig. 4.6 Midsagittal sections demonstrating the completion of the distal urorectal septation and the formation of the perineum in the human embryo within the phallic urogenital sinus morphogenetic field at Carnegie stages 18 (**a**) and 19 (**b**). Color codes as indicated in Fig. 4.5. Details of the complex morphological actions of this process are given in the text

ered by urogenital sinus surface cells form the primordial perineum. Simultaneously, the urogenital orifice is established by the degeneration of the central urogenital plate cell populations. The morphogenetic actions associated with the posterior aspects of the distal urorectal septation forming the primordial anus proceed within a different morphogenetic field and are not considered here.

The interaction of phallic urogenital sinus surface cells with proximal somatic and splanchnic ACMs forms the peripheral (lateral) phallic shaft and the primordial vestibule mesenchymes, respectively. The interaction of intermediate phallic urogenital surface cells with both proximal somatic and splanchnic ACMs forms the mesenchymes of the primordial glans surface, urogenital labia, and midsagittal perineum. The primordial perineum and anus, both being concealed between the genital tubercle and the postanal swelling at Carnegie stage 18, gradually bulge outward and become visible by Carnegie stage 23 [5].

Collateral morphogenetic actions of the pubogenitocrural ectoderm and the proximal somatic ACM further shape the bilateral genital swellings. The pelvic urogenital sinus (primordial urethra) is formed from the urogenital sinus endoderm and proximal splanchnic ACM. The latter also generates the precursor tissues of the corpus spongiosum with bulbi vestibulares and both greater vestibular glands. The distal somatic ACM forms the corpora cavernosa. Both distal somatic and splanchnic ACMs receive myogenic cells from the sacral somites to establish the superficial and deep perineal muscles and fasciae, respectively [5]. Peripheral anal plate cells interacting with proximal somatic and splanchnic CLMs form the anus and anal canal.

Figure 4.7 shows the serial transverse sections of a human female embryo at Carnegie stage 23. The phallic urogenital sinus morphogenetic field is represented by its surface cells, the externally adjacent genitocrural ectoderm and the internally adjacent urogenital sinus endoderm, the proximal splanchnic and somatic ACMs, and the genital duct mesenchyme.

During the early fetal period, the phallic urogenital sinus manifests as either a female or male phenotype.

In the female, this morphogenetic process is characterized by four main events: sagittal lengthening of the urogenital orifice, subtotal prepuce formation, extension of the (gynecologic) perineum, and formation of the vaginal introitus [5, 9, 10].

The further opening of the phallic urogenital sinus is the result of epithelial-mesenchymal interactions between the phallic urogenital sinus surface cells and proximal somatic and splanchnic ACMs. It occurs in the caudocranial direction, resembling an "opening zipper," during weeks 9 and 10 (Fig. 4.8a, b).

The prepuce formation, initiated by the interaction of the phallic urogenital sinus surface cells with the proximal somatic ACM, starts at about 12 weeks. The shift of the phallic urogenital sinus surface over the glans surface is subtotal in the

female, occurring only at the dorsal site. Ventrally, the glans surface proceeds into the urogenital labia, precursors of the labia minora (Fig. 4.8c). During the early fetal period, the gynecologic perineum extends in the anteroposterior axis. The posterior parts of the bilateral genital swellings, precursors of the labia majora, temporarily approach each other.

The interaction of the inner phallic urogenital sinus surface with the proximal splanchnic ACM, the urogenital sinus endoderm, and the sinuvaginal bulbs (a complex of Müllerian ducts, degenerating Wolffian ducts, and periductal stroma) results in the generation of the vaginal introitus and the hymen by around 14 weeks, as described in Chap. 3 (Fig. 3.12). Whereas the hymenal

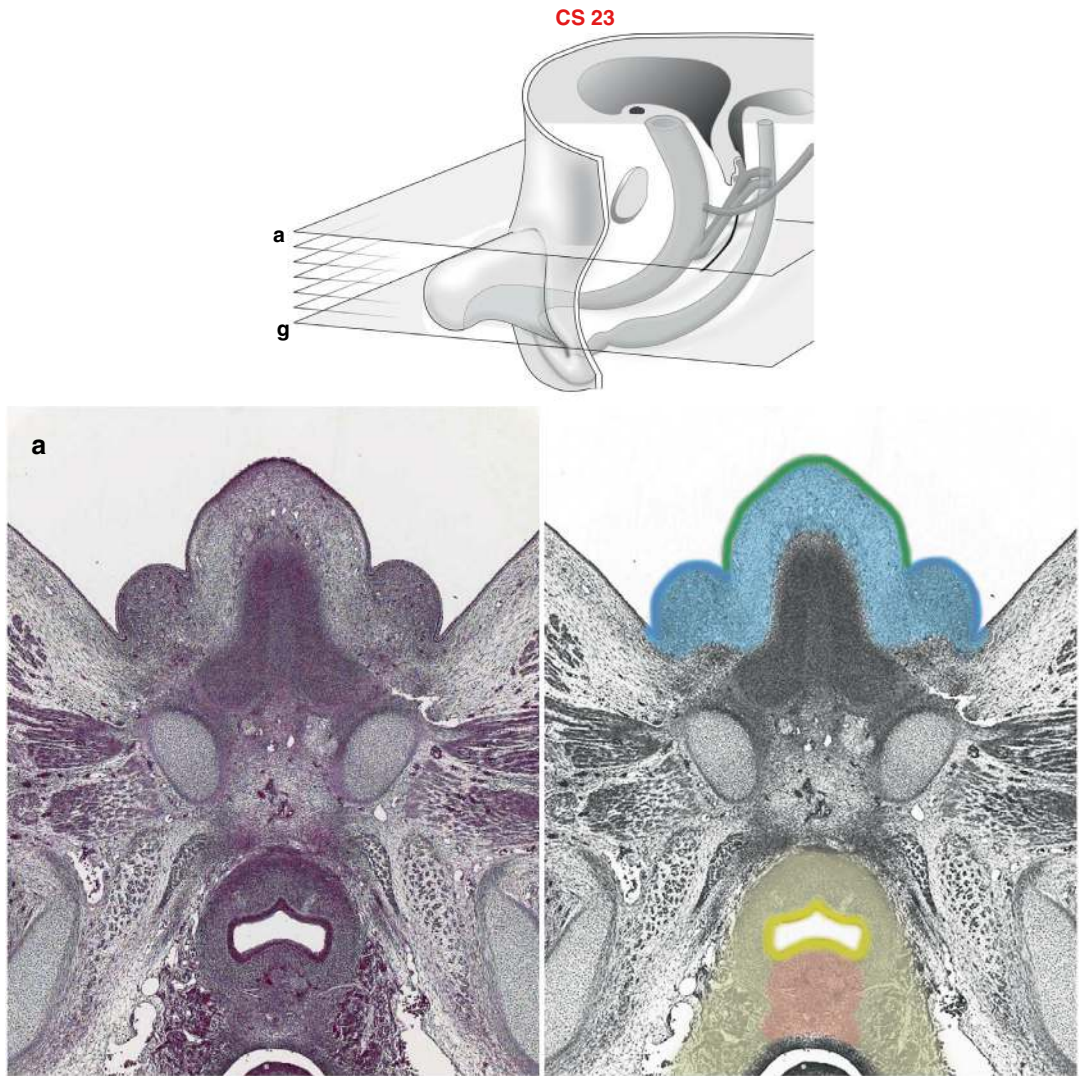

Fig. 4.7 Color-coded photomicrographs of serial transverse sections of a female human embryo at Carnegie stage 23 demonstrating the phallic urogenital sinus morphogenetic field. The levels of the sections (**a**–**g**) are indicated in an anatomical drawing of the midsagittal section. The different tissues making up the morphogenetic field are color-coded as follows: green, phallic urogenital sinus surface cells; blue, pubogenitocrural ectoderm; yellow, urogenital sinus endoderm; blueish, proximal somatic ACM; light yellow, proximal splanchnic ACM; reddish, genital ducts mesenchyme

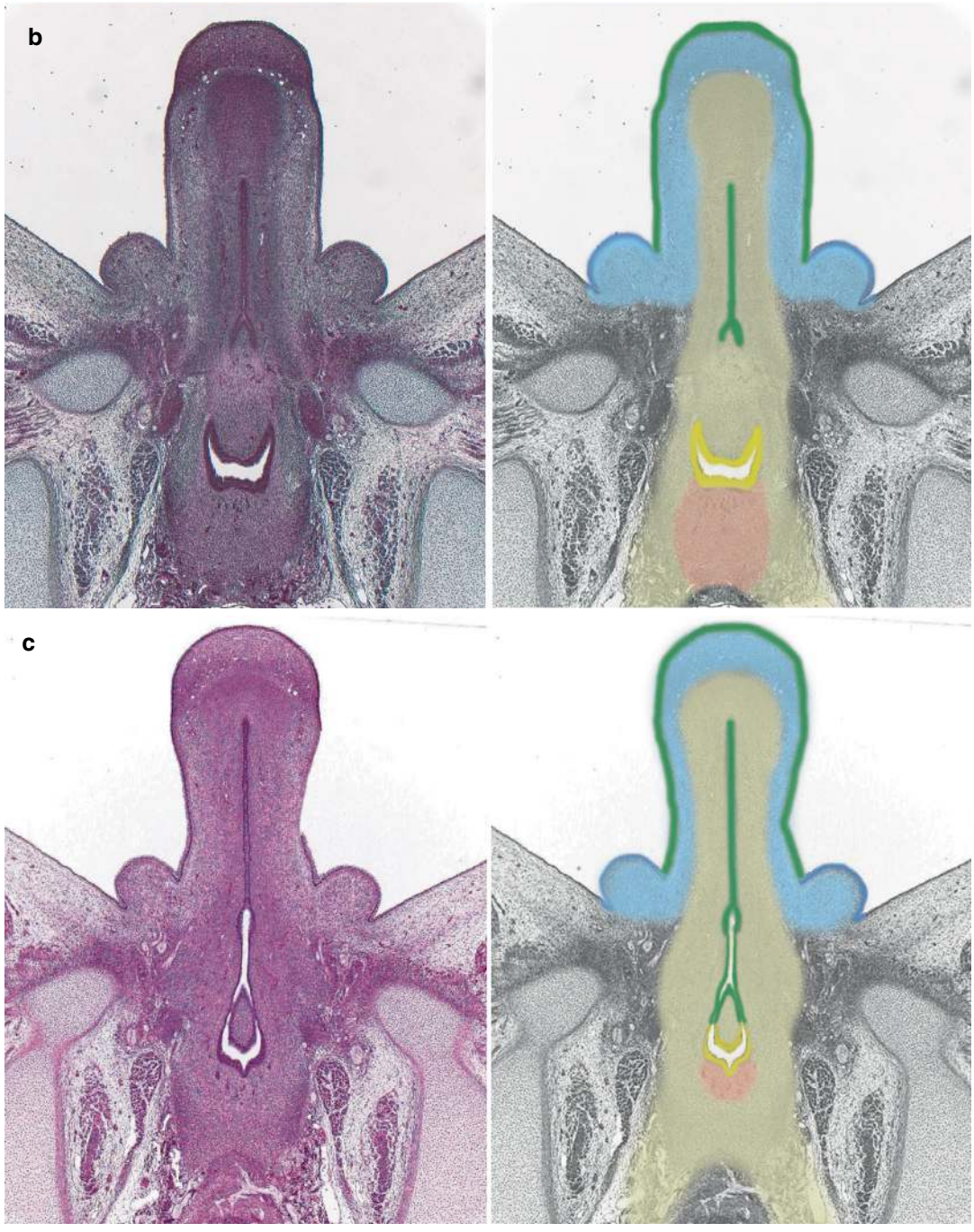

Fig. 4.7 (continued)

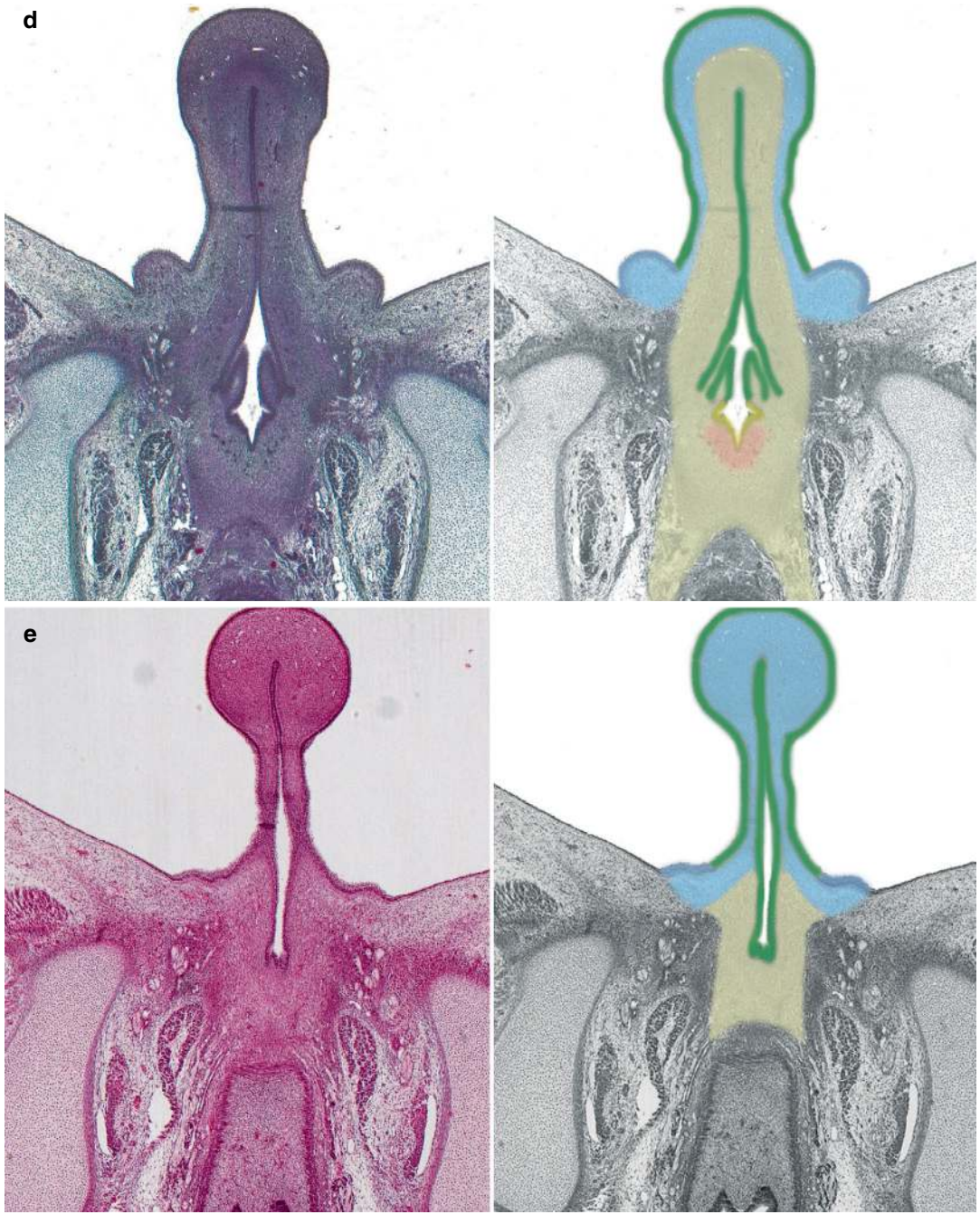

Fig. 4.7 (continued)

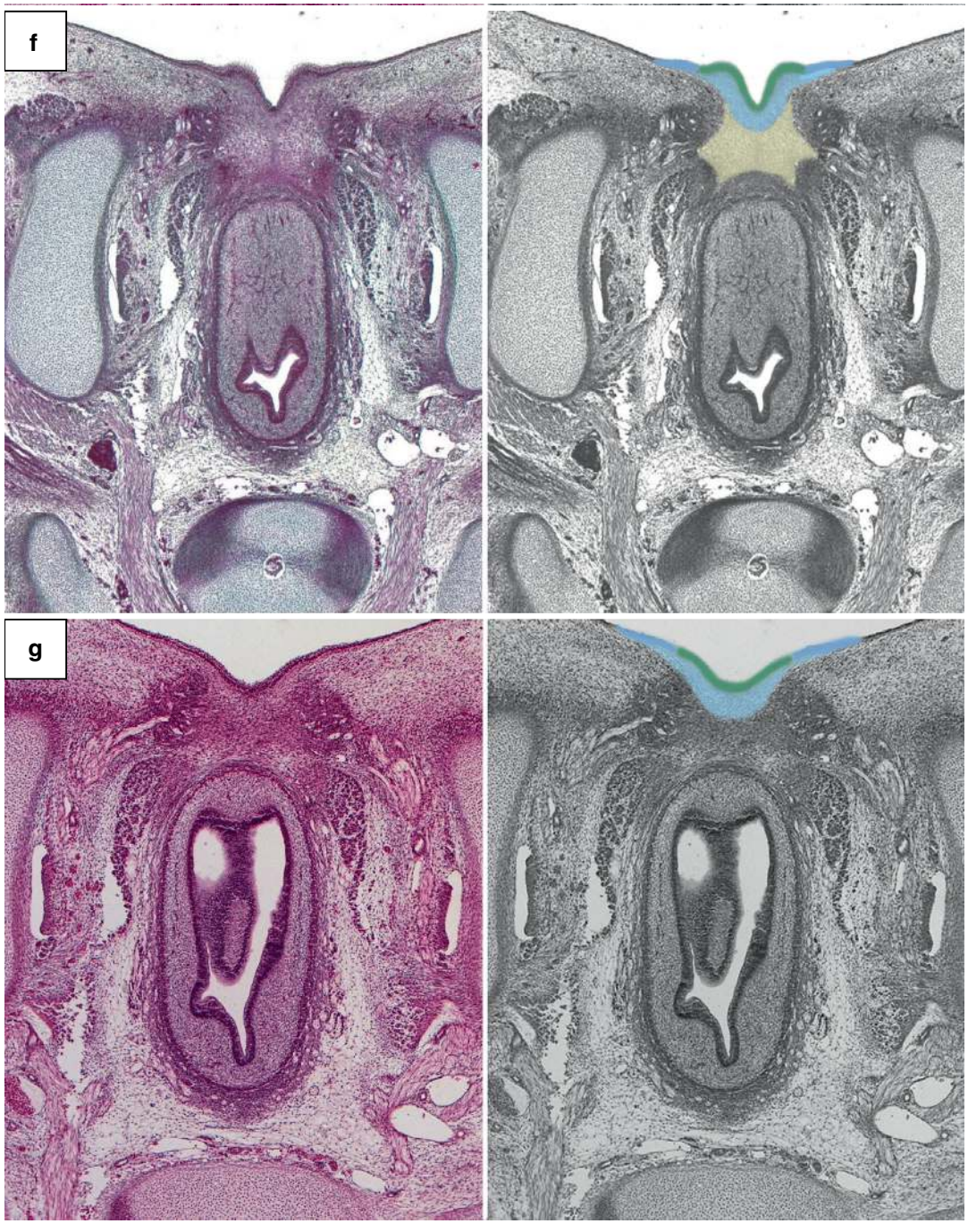

Fig. 4.7 (continued)

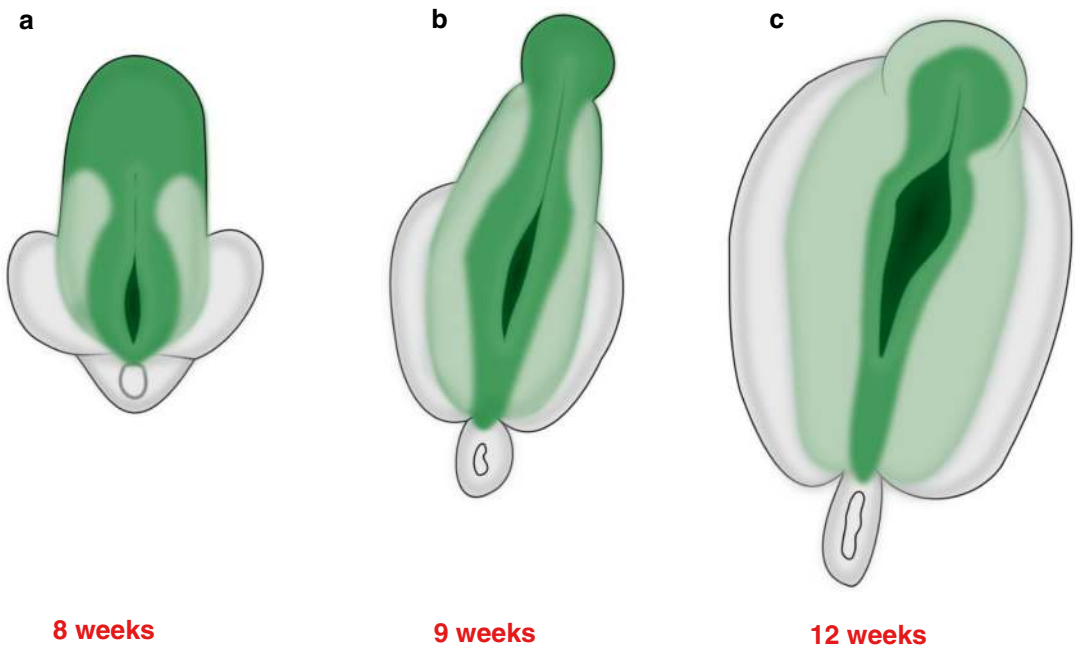

Fig. 4.8 External phallic urogenital sinus in the female at 8 weeks (**a**), 9 weeks (**b**), and 12 weeks (**c**), showing the opening of the vestibular plate, the broadening of the base of the phallic urogenital sinus, subtotal prepuce formation, and sagittal extension of the gynecologic perineum. The phallic urogenital sinus surface tissues are color-coded as follows: light green, peripheral zone; middle green, intermediate zone (glans-labia); dark green, central zone

stroma is of Müllerian origin, the hymenal epithelium is derived from the phallic urogenital sinus endosurface. The formation of the vaginal introitus is associated with the broadening of the gynecologic perineum. By this process, the posterior genital swellings are distended and shifted anteriorly. The inclination of the corpora cavernosa, forming the primordial clitoridal body and crura from the distal somatic ACM, can be observed in the female fetus between weeks 13 and 14.

4.5 Vulvar Compartment

Determination of the phallic urogenital sinus surface cells and integral mesenchyme in the female results in the formation of the vulvar compartment. Its maturation produces a wedge-shaped central perineal surface region containing the urinary and vaginal orifices. It is covered by the squamous cell epithelium and is devoid of hair and fatty tissue. The subsurface mesenchymes established in the previous developmental stage define three subcompartments in the proximodistal axis: a peripheral subcompartment that includes the prepuce, interlabial sulcus, and lateral gynecologic perineum; an intermediate subcompartment consisting of the cutaneous glans clitoridis, the bilateral labia minora, and a linear or V-shaped central perineal zone that projects into the ventral anus between about 11 and 1 o'clock; as well as a central subcompartment represented by the vestibulum with the urethral meatus and the hymen (Fig. 4.9). The type of epithelium in the three subcompartments differs, being keratinized in the peripheral and nonkeratinized in the central subcompartment. The epithelium of the intermediate subcompartment is keratinized squamous laterally and nonkeratinized squamous medially. The border between the two epithelia is visible as the line of Hart. While the epithelium of the central subcompartment is generally not pigmented, the pigmentation of the intermediate and peripheral subcompartment occurs at variable intensity.

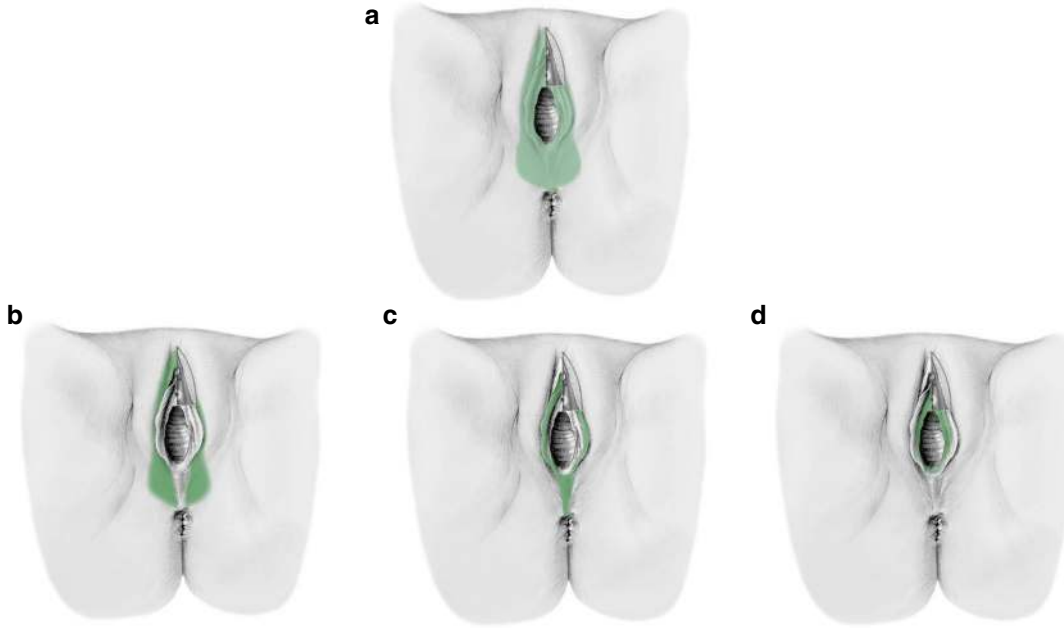

Fig. 4.9 Anatomical drawings of the vulvar compartment (**a**) and its three subcompartments (**b**–**d**) in the mature female. The peripheral vulvar subcompartment (**b**) includes the prepuce, interlabial sulcus, and lateral gynecologic perineum. The intermediate vulvar subcompartment (**c**) consists of the glans surface, bilateral labia minora, and medial gynecologic perineal surface protruding in the anus between about 11 and 1 o'clock. The central vulvar subcompartment (**d**) is represented by the vestibulum with the urethral meatus and the hymenal surface

4.6 Mature Derivatives from the Morphogenetic Fields Forming the Female External Genitalia

From the cell type differentiation trajectory (Fig. 4.2), the mature derivatives of the morphogenetic fields of each developmental step are ascertained (Table 4.1): the mature derivatives of the *cloacal membrane/plate morphogenetic field* in the female encompass all tissues of the superficial and deep perineum (vulvar compartment, anus, labia majora, genitocrural regions, urogenital diaphragm, ischioanal fossae), pubic and inguinal regions, abdominal and pelvic walls, legs, pelvic floor, genital tract, urinary tract, colorectum. The mature tissue derivatives of the *urogenital and glans plate morphogenetic field* in the female are the vulvar compartment; the labia majora; the inguinal, genitocrural, pubic, perianal, and inguinal skin; all erectile tissues of the vulva (including the corpus and crura of the clitoris), urethra and bladder, and genital tract; and all fasciae and muscles of the urogenital diaphragm.

The cell populations of the *phallic urogenital sinus morphogenetic field* mature in the female into the vulvar compartment; labia majora with anterior commissure; genitocrural, pubic, and inguinal skin; Dartos fasciae; erectile glans clitoridis and corpora spongiosa/vestibular bulbs; urethra; and Müllerian system with vagina as the closest subcompartment. The mature *vulvar compartment* consists of the peripheral, intermediate, and central subcompartments, as specified above.

It is evident that the ontogenetic vulva, as a derivative of the cloacal membrane, differs significantly from the anatomy of the vulva, described in textbooks as a basis for clinical practice (Fig. 4.10). Whereas the complete labia majora are considered part of the vulva in the traditional topographic and clinical anatomy, their main (lateral) parts represent a different compartment ontogenetically. Conversely, the complete genital perineum and even a ventral sector of the anus belong to the ontogenetic vulvar compartment, as well as the meatus urethrae and the hymen.

Table 4.1 Mature tissue derivatives of the successive morphogenetic fields starting with the cloacal membrane to form the ontogenetic vulvar compartment with its three subcompartments

Cloacal membrane/plate morphogenetic field
All tissues of the superficial and deep perineum, pubic and inguinal region, abdominal and pelvic walls, legs, pelvic floor, genital tract, urinary tract, and colorectum
Urogenital and glans plate morphogenetic field
Vulvar compartment; labia majora; genitocrural, perianal, pubic, and inguinal skin; all erectile tissues of the vulva, urethra and bladder, and genital tract; and all fasciae and muscles of the urogenital diaphragm
Phallic urogenital sinus morphogenetic field
Vulvar compartment; labia majora with anterior commissure; genitocrural, pubic, and inguinal skin; Dartos fasciae; erectile glans clitoridis; corpora spongiosa/vestibular bulbs; urethra; and Müllerian system with vagina as closest subcompartment
Vulvar compartment
Peripheral, intermediate, and central subcompartments
Peripheral vulvar subcompartment
Interlabial sulcus, prepuce, and lateral gynecologic perineum
Intermediate vulvar subcompartment
Glans clitoridis, labia minora, and central gynecologic perineum
Central vulvar subcompartment
Vestibular skin with urethral meatus and hymen

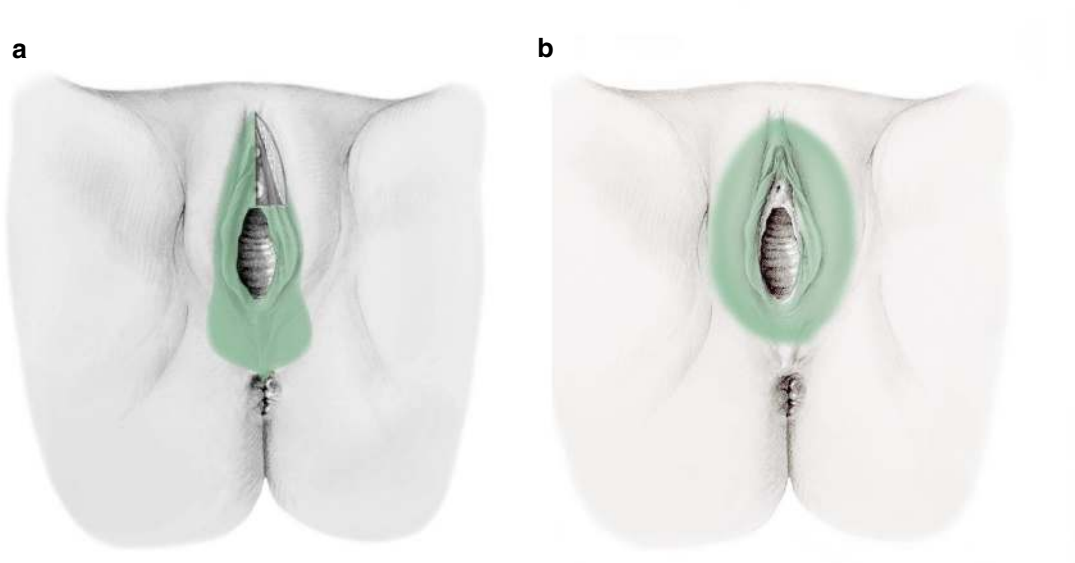

Fig. 4.10 Comparison of the ontogenetic vulvar compartment (**a**) with the tissues allocated to the vulva in textbook anatomy (**b**). As further specified in the text, major differences are evident

Using the green-grey color coding, as introduced before, the ontogenetic anatomy of the superficial and deep perineal tissues is displayed, highlighting their developmental kinship to the ontogenetic vulva. Figure 4.11 illustrates this with a window showing some deep tissues. The first degree of ontogenetic kinship for each of the vulvar subcompartments is represented by the adjacent subcompartment(s). Except for the anus between 1 and 11 o'clock, the vulva compartment is peripherally surrounded by tissues whose progenitors share the phallic urogenital sinus morphogenetic field, which are the labia majora with Dartos fat bodies and the genitocrural skin and subcutaneous fat. These tissues are therefore of second-degree ontogenetic kinship to the

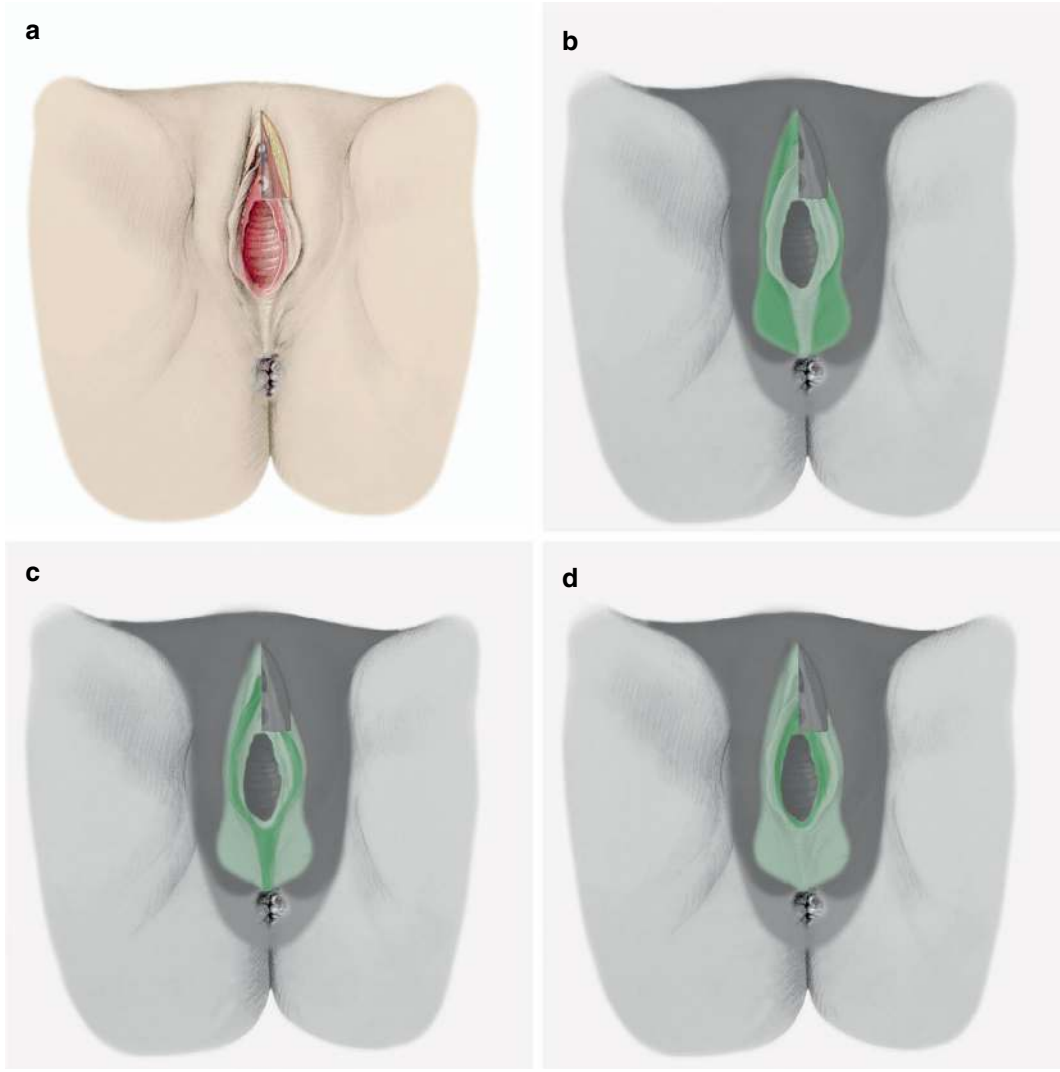

Fig. 4.11 Ontogenetic anatomy of the three subcompartments of the vulvar compartment, illustrated with a frontal view of the superficial perineum with a window showing deep perineal tissues. Conventional anatomical drawing (**a**), color-coded for the indication of the ontogenetic kinship of the peripheral (**b**), intermediate (**c**), and central (**d**) vulvar subcompartments to the adjacent tissues. Dark green, peripheral, intermediate, and central vulvar subcompartments; light green, vulvar compartment; dark grey, mature tissue derivatives of the phallic urogenital sinus morphogenetic field; middle grey, mature tissue derivatives of the urogenital eminence morphogenetic field; light grey, mature derivatives of the cloacal plate morphogenetic field

vulva. Likewise, the abutting urethra and vagina, the erectile glans clitoridis, and the corpora spongiosa-vestibular bulbs are of second-degree kinship as their precursors belong to the phallic urogenital sinus morphogenetic field.

The body and crura of the clitoris and the multiple fibromuscular tissues of the urogenital diaphragm, including the superficial (ischiocavernosus, bulbospongiosus, transverse) perineal muscles and the ensheeting Colles' fasciae, as well as Buck's fascia, the deep perineal muscles, and the external urethral sphincter muscles, have matured from precursors sharing the urogenital and glans plate morphogenetic field and are therefore of third-degree kinship to the ontogenetic vulva.

The precursors of the remaining perineal tissues, anus, anal canal, sphincters, and ischioanal fat body, are integral to the cloacal plate morphogenetic field, entailing a fourth-degree kinship to the ontogenetic vulva.

In addition to the perineal tissues, which are shown in Fig. 4.11, the ontogenetic relation of the deeper-located lower trunk tissues to the vulva compartment is the following: the complete Müllerian system is of second-degree kinship; the bladder, pubourethral ligament, and all subperitoneal mesotissues and ovaries are of third-degree kinship. The abdominal and pelvic walls, legs, and intestines have a fourth-degree kinship.

The ontogenetic anatomy of the vulva is the foundation for the categorization of local vulvar cancer progression as ontogenetic staging (oT). The oT stage-associated cancer fields for vulvar carcinoma correspond to the mature derivatives of the morphogenetic fields forming the ontogenetic vulvar compartment with its three subcompartments, listed in Table 4.1 and highlighted in the anatomical drawings of the female perineum in Fig. 4.12.

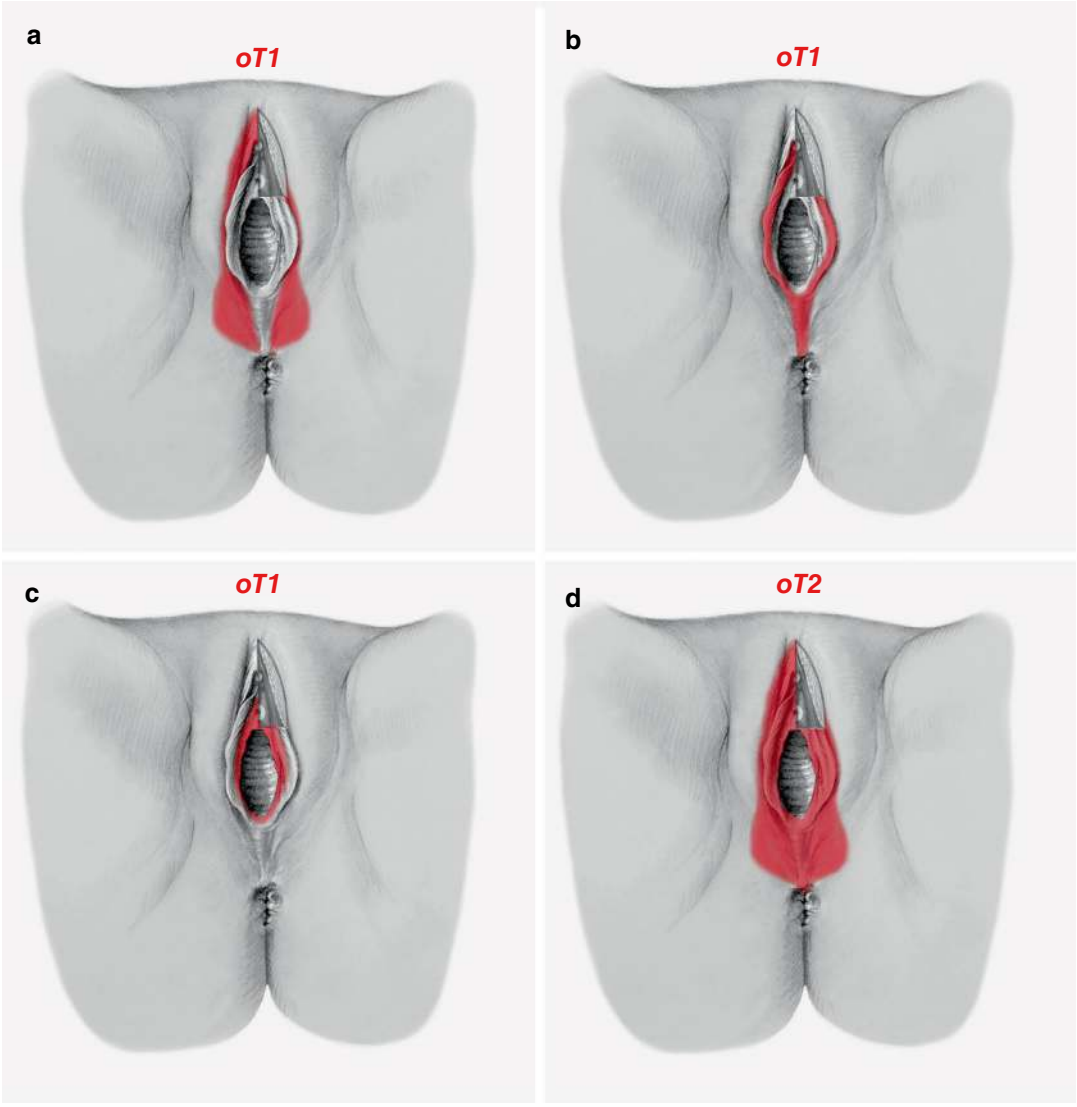

Fig. 4.12 Ontogenetic tumor stage (oT)-associated cancer fields of vulvar carcinoma shown with a frontal view at the perineum. (**a**–**c**) oT1, (**d**) oT2, (**e**) oT3a, (**f**) oT3b, (**g**) oT4

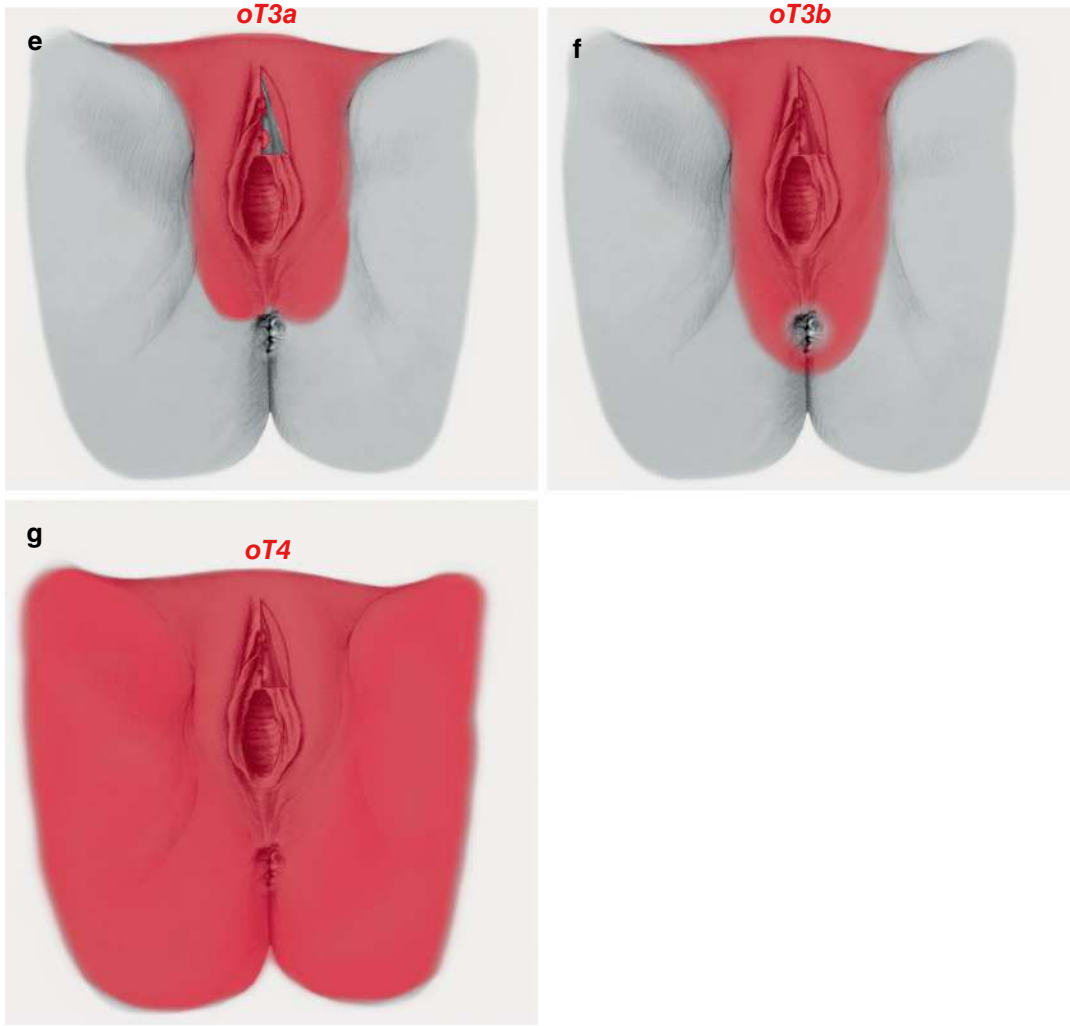

Fig. 4.12 (continued)

4.7 Landscapes of Vulvar Carcinoma Progression

As for cervical carcinoma, the validity of the ontogenetic cancer field model has also been supported for vulva carcinoma by the generation of local tumor landscapes. Anatomical heatmaps of the female perineum demonstrating the frequency of vulvar cancer, detected histologically in surgical specimens, have been established for carcinomas originating from the peripheral, intermediate, and central subcompartments of the vulvar compartment, see Fig. 1.5 in Chap. 1. Although the anatomical resolution is limited as a consequence of the relatively low number of cases, the anisotropy of local tumor spread is evident. Carcinomas of the peripheral and central vulvar subcompartments show a strikingly lower frequency of tumor involvement of the lateral (labia majora) and medial (urethra and vagina) tissues, which do not belong to the vulvar compartment, compared to the intermediate tissue, which is a vulvar subcompartment. Likewise, there is an abrupt drop in the frequency of carcinomas of the intermediate subcompartment at the anal part of the vulva toward the remaining anal region.

References

1. Gasser RF. The virtual human embryo. 2001. http://www.ehd.org/visual-human-embryo.
2. Keibel F. Zur Entwicklungsgeschichte des menschlichen Urogenitalapparates. In: Archiv anatomie entwicklungsgeschichte. Leipzig: Veit et Comp; 1896. p. 55–156.
3. O'Rahilly R, Müller F. Developmental stages in human embryos. Washington: Carnegie Institution of Washington; 1987.
4. Spuler A. Entwicklungsgeschichte des weiblichen Genitalapparates. In: Stöckel W, editor. Handbuch der gynäkologie. München: J.F. Bergmann; 1930. p. 439–90.
5. van der Putte SCJ. The development of the perineum in the human. In: Advances in anatomy, embryology and cell biology, vol. 177. Berlin: Springer; 2005. https://doi.org/10.1007/b138055.
6. Hassoun R, Schwartz P, Rath D, Viebahn C, Männer J. Germ layer differentiation during early hindgut and cloaca formation in rabbit and pig embryos. J Anat. 2010;217:665–78. https://doi.org/10.1111/j.1469-7580.2010.01303.x.
7. O'Rahilly R, Müller F. The origin of the ectodermal ring in staged human embryos of the first 5 weeks. Acta Anat. 1985;122:145–57. https://doi.org/10.1159/000145996.
8. Wang C, Wang JY, Borer JG, Li X. Embryonic origin and remodeling of the urinary and digestive outlets. PLoS ONE. 2013;8:e55587. https://doi.org/10.1371/journal.pone.0055587.
9. Baskin L, Shen J, Sinclair A, Cao M, Liu X, Liu G, et al. Development of the human penis and clitoris. Differentiation. 2018;103:74–85. https://doi.org/10.1016/j.diff.2018.08.001.
10. Overland M, Li Y, Cao M, Shen J, Yue X, Botta S, et al. Canalization of the vestibular plate in the absence of urethral fusion characterizes development of the human clitoris: The single zipper hypothesis. J Urol. 2016;195:1275–83. https://doi.org/10.1016/j.juro.2015.07.117.

5 The Ontogenetic Cancer Field Model for the Regional Spread of Carcinomas

The ontogenetic cancer field model for the regional progression of carcinomas considers the following aspects in order to map the *first-*, *second-*, and *third-line lymph node regions* as a hierarchically structured regional cancer field, expanding the local cancer field of an individual carcinoma:

- Locoregional links in immune surveillance and peripheral immune tolerance
- The development of the regional lymphatic system
- Topographical pattern analysis of a high number of nodal positive carcinomas

5.1 Locoregional Links in Immune Surveillance: Basic Aspects

A detailed description of the locoregional links in immune surveillance and peripheral immune tolerance, as an interaction of the regional lymph node with its tributary tissues involving (micro) anatomy, physiology, cellular, and molecular mechanisms, is far beyond the scope of this textbook. Only a brief overview of some known mechanisms is given herein. For further information, the reader may consult current textbooks on immunology (e.g., [1]) and more recent reviews (e.g., [2–6]).

A lymph node, as a secondary lymphatic organ, is anatomically structured by subcapsular and intranodal sinuses, a cortex with follicles, a paracortex, a medulla, and intranodal blood vessels [7, 8]. It is connected by afferent lymph vessels to its tributary tissues, which are immunologically surveilled by it. The downstream flow of lymph enables the fast passive transport of antigens—processed by professional antigen-presenting cells (APCs, mainly dendritic cells) as well as nonprocessed ones—to the lymph node. T cells meet antigens in the interfollicular zones and the paracortex. Antigens are presented by APCs to CD4+ T-helper (Th) cell receptors through major histocompatibility complex (MHC) class II molecules. Licensed APCs also offer antigens through major histocompatibility complex class I molecules to CD8+ cytotoxic T-cell (Tc) receptors. A licensed APC crosspresents an antigen to Th cells by MHC class II and to Tc cells by MHC class I. Dendritic cells transfer antigen-MHC complexes to lymph endothelial cells, reticular fibroblastic cells, and other stromal cells of the lymph node as well [9]. Pathological antigens recognized by a cognate T-cell receptor induce activation (priming), clonal expansion, and the differentiation of T cells into effector and memory subsets.

In the primary follicles of the cortex, antigens are presented to B cells by follicular dendritic cells, another subset of lymph node stroma cells. Unprocessed antigens can be directly bound by B-cell receptors. Additional stimulatory mechanisms, including contact with Th cells through

M. Höckel et al., *Cancer Field Surgery in Gynecologic Oncology*,
https://doi.org/10.1007/978-3-031-83030-3_5

the interaction of their T-cell receptor with antigens that are processed and displayed by MHC class II, initiate B-cell proliferation and differentiation into antibody-producing plasma and memory B cells, forming secondary follicles with germinal centers. Memory B cells, in particular, are able to digest the unprocessed antigen and present it via MHC class II to the cognate Th-cell receptor.

The interaction of APCs and lymphocytes is orchestrated by the lymph node stroma, which can archive antigens for the long term. Effector and memory T cells, memory B cells, and antibodies are released through the lymph node medulla to efferent lymph vessels, eventually to downstream lymph nodes in the chain, and finally to the lymphovascular junctions into the blood circulation. They exit the blood vessels at their target sites in the tributary tissue to exert their immunological function locally. Most of the memory B cells and a subset of memory T cells are retained in or re-enter the lymph node.

In addition to their function in combatting pathogens that attack the tributary tissue, draining lymph nodes are vital for *peripheral immune tolerance* as they supplement mechanisms of central immune tolerance to prevent autoimmune reactions and support local tissue repair/regeneration. Self-antigens of the tributary tissue are transported to the draining lymph node via afferent lymph vessels and are displayed by the tolerogenic dendritic and stroma cells of the node. Upon contact with a cognate receptor of naïve T cells, tolerance, i.e., the suppression of an immune response toward the self-antigen, is induced by complex mechanisms that involve the apoptosis of cytotoxic T cells and the differentiation of naive Th cells into exhausted, anergic, and peripheral regulatory T cells (Treg). Treg cells, specific to the tributary tissue's self-antigens, traffic through the efferent lymph and bloodstream to the tributary tissue to execute their immunosuppressive function there. Long-lived memory Treg cells recognizing self-antigens circulate with the lymph and the blood or persist both in lymph nodes and in the peripheral tissue from which the antigen was released. Peripheral immune tolerance is also supported by regulatory B-cell (Breg) populations, predominantly by generating an immunosuppressive cytokine and cell surface molecule milieu upon encountering an antigen and displaying it to cognate Tregs [10]. In animal studies, Breg cells have also been shown to convert resting CD4+ Th cells into immunosuppressive Treg cells [11]. A lymph node contains both memory Treg and memory Breg cells, recognizing self-antigens specific to its tributary tissue.

Whether activated to attack or tolerized by a peripheral antigen, the cognate T cell must be "informed" about the anatomical location of the antigen to act there. This topographic anatomical (topoanatomical) information is exerted through the imprinting of homing receptors specific to the tributary tissue when naïve T cells are primed by epigenetic interaction with the dendritic cells within the lymph node microenvironment [12–16]. However, the molecular mechanisms of topoanatomical information transfer are still unknown [17].

Disturbance of the tributary tissues' homeostasis by pathogens or injury necessitates augmented protection of the normal cells at the site of tissue damage from the provoked immune response to prevent autoimmune reactions, in addition to combatting the pathogens. This is accomplished by an expansion of the local Treg cell population from both central and peripheral sources specific to the normal tissue [18, 19]. In the draining lymph nodes, Treg cells are activated, clonally expand, and differentiate when encountering the tributary tissues' self-antigens, which had been liberated by direct or collateral damage. The self-antigens and their topoanatomical information are transferred to the node by APCs to be tolerized. If self-antigens "known" to the immune system are offered to memory Tregs in the draining lymph node(s), the tolerogenic response is accelerated and amplified. Treg cells activated in the lymph node traffic to the site of tissue disturbance, guided by homing receptors specific to that tissue. In addition to their immunosuppressive function, Treg cells participate in various mechanisms to restore tissue integrity

and homeostasis, including angiogenesis, lymphangiogenesis, and tissue remodeling, usually needed for wound healing and tissue repair/regeneration [20, 21].

If tissue homeostasis is impaired by a malignant tumor, cancer antigens (CAgs), in addition to normal tissue self-antigens, are released, processed, and transported to the draining lymph node. CAgs are considered to include cancer-associated and cancer-specific antigens here. Many CAgs presented in the lymph node are tolerized because of their structural similarities to the self-antigens of the tributary tissue and other cancer-inherent mechanisms involving immune-regulating molecules [22]. These and the released normal self-antigens induce the activation, clonal expansion, and differentiation of cognate Treg cells in the draining lymph node. Treg cells traffic to the tumor site via efferent lymphatics and blood vessels mediated by their homing receptors. In encountering the corresponding antigens at the local tumor site, which are also presented by cancer-associated fibroblasts in addition to the professional APCs, the Treg cells exert their multifaceted immunosuppressive and generative-restorative mechanisms, which are exploited by the cancer cells for further expansion [23, 24].

5.2 Regional Cancer Field Model

The regional cancer field model is founded on evidence that topoanatomical information characterizing the tributary tissue is transferred to the draining lymph node by the dendritic cells, together with the antigen-MHC complex. The tributary tissue's *topoanatomical code*, representing its topoanatomical identity, is imprinted on the T cells during the priming of the naïve subsets through interaction with lymph node stroma cells (lymphatic endothelial cells and reticular fibroblastic cells) sharing the cognate antigen [17]. The code is proposed here to be manifested in complementary l and r structures. The l-form is inherent in the stromal matrix of the tributary tissue and is also represented by the addressins of the lymphatic and blood vessels. The r-form is expressed on the surface of the tributary tissue's resident cells and of the T cells as homing receptors. The interaction of clonally proliferating Treg cells exhibiting the r-code with lymph node stroma cells is assumed to generate microareas in the extracellular matrix of the draining lymph node expressing the l-code, which mimics and therefore exports the local cancer field to the draining lymph node.

According to the regional cancer field model, a lymph node draining a malignant tumor is considered to undergo three phases for metastasis formation (Fig. 5.1): loading, activation, and colonization.

The *loading phase* occurs before the development of the local cancer by the continuous delivery of peripheral tissue antigens (PTAg), mainly from apoptotic normal cells to the draining lymph node. Due to the high cell turnover and production of apoptotic cells, the major source of peripheral self-antigens is the epithelium of the tributary tissue. Dendritic cells presenting these self-antigens, together with the tributary tissue's topoanatomical code interacting with lymph node stroma cells, induce the tolerogenic priming of T and B cells and produce Treg and Breg effector and memory cells. The peripheral tissue antigens archived by lymphatic endothelial cells and fibroblastic reticular cells [3] accomplish the long-term presence of Treg memory and Breg memory cells that remain in or re-enter the lymph node (Fig. 5.1a). Lymphatic endothelial cells lining the subcapsular and trabecular sinuses are assumed to be equipped with the tributary tissue's topoanatomical code in the l-form.

The *activation phase* is initiated by the local tumor liberating CAgs, PTAgs, extracellular vesicles, and bioactive molecular factors drained to the lymph node. In addition, bone-marrow-derived cells are attracted to supplement the reactive infiltrate. Activation, clonal expansion, and differentiation of Treg (memory) cells with cognate receptors for CAgs that are promiscuous with PTAgs or tolerized CAgs in concert with APCs and lymph node stroma cells are proposed to focally provide the tributary tissue's topoanatomical code in the l-form by ECM remodeling. Treg

cell proliferation and differentiation are accompanied by a supportive immunosuppressive cytokine milieu, angiogenesis, and lymphangiogenesis, which together execute the premetastatic conditioning of the draining lymph node (Fig. 5.1b).

This premetastatic conditioning enables the *colonization phase.* Competent clonogenic cancer cells recognizing their permissive topoanatomical code adhere at the subcapsular and trabecular sinus lymph endothelium and invade

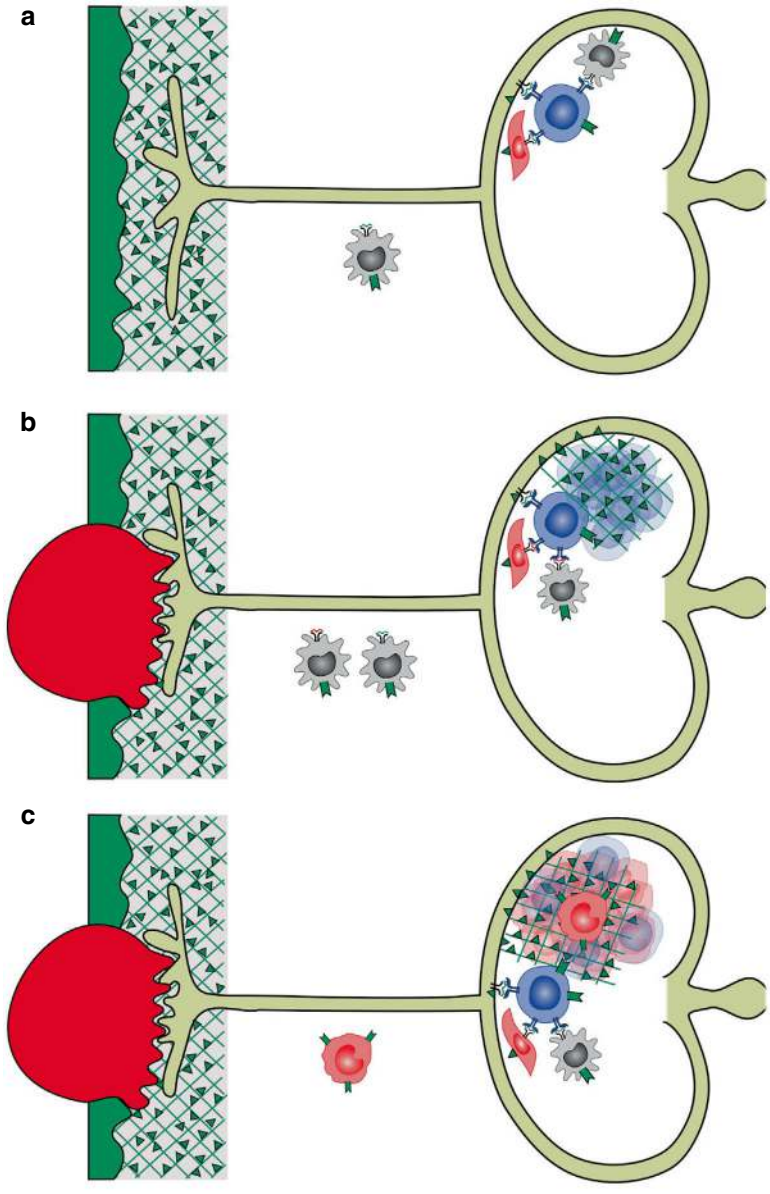

the underlying stroma, which provides the cancer field characteristics by means of the remodeled ECM, together with an immunosuppressive and tissue regenerative wound healing microenvironment (Fig. 5.1c). The density of these conditioned microareas in the draining lymph node and the flow density of competent clonogenic cancer cells are determinants of metastasis formation.

As the lymph node of a tributary tissue is "loaded" predominantly with epithelial self-antigens, its premetastatic conditioning by the described mechanisms should be particularly effective for epithelial cancers. It may explain the clinical observation that lymph node metastases are common in carcinomas but are rare in sarcomas, although other mechanisms essential for cancer cell colonization, which are different between epithelial and mesenchymal types, may contribute as well.

Most importantly, the regional cancer field model is consistent with the fact that whereas distant metastases are usually a late manifestation of carcinomas diagnosed either in locally advanced and recurrent disease or in a few cases of early disease after a long clinically uneventful interval, lymph node metastases are common findings in carcinomas of intermediate or even early stages. The tolerogenic immune reaction attracts cancer

Fig. 5.1 Schematic depiction of the regional cancer field model. (**a**) Lymph node loading with peripheral self-antigens and topographic anatomical information (topoanatomical code) of the tributary tissue. The tributary tissue (left)—predominantly the epithelium due to its permanent cell turnover—constantly releases self-antigens (green dashes), which are transported to the draining lymph node (right), both unprocessed and processed by dendritic cells (grey) as tolerogenic peptide-major histocompatibility complexes (pMHC). In addition to the dendritic cells, pMHCs are displayed at the node's stroma cells, particularly subcapsular and transverse sinus endothelial cells and reticular fibroblastic cells (pink). The tolerogenic dendritic cells entering the node also provide topoanatomical information related to the peripheral self-antigen (l-form of the tributary tissue's topoanatomical code; green triangles), to be stored in lymph node stroma cells. Naïve CD4+T cells (blue) encountering the pMHC by their cognate receptors are primed by the antigen-presenting cells to become effector and memory Treg cells as one major mechanism of peripheral immune tolerance. The priming process involves the induction of the tributary tissue's topoanatomical code in the r-form (green fork tag) as homing receptors of the Treg cells. Moreover, the pMHC self-antigens are archived by lymph node stroma cells, assuring their long-term presence in the node. Memory Treg cells are retained by binding to their cognate receptors, which are permanently displayed by the lymph node stroma. In that way, the draining lymph node is "loaded" with a multitude of Treg memory cells, which recognize the self-antigens of their tributary tissue. These cells also memorize the topographic anatomical identity of the self-antigens expressed by their imprinted homing receptors. Therefore, a lymph node is equipped with the occult site-specific code of its tributary tissue. (**b**) Lymph node activation by cancer antigens and peripheral tissue antigens and other substrates directly or indirectly produced by the local tumor. An invasive epithelial neoplasm (red) delivers tolerized cancer antigens (CAg; red dashes) and peripheral tissue antigens (PTAg; green dashes) to the draining lymph node by the carcinoma as a nonhealing wound. The antigens, processed by tolerogenic dendritic cells, enter the node together with the information of the tributary tissue's topoanatomical l-code (green triangle). PTAgs and tolerized CAgs induce the activation of the Treg memory cells equipped with the topoanatomical r-code of the tributary tissue as homing receptors (green fork tag). The regional cancer field model claims that cellular and extracellular changes in the lymph node stroma associated with the activation, proliferation, and differentiation of the Treg cells focally provide the tributary tissue's topoanatomical l-code to lymph node microareas. In concert with the actions of tumor-derived substrates, extracellular vesicles, and tumor-mobilized bone-marrow-derived cells (not shown), Treg cells execute supportive functions, such as lymphangiogenesis, angiogenesis, and immunosuppression, and thus accomplish premetastatic conditioning, extending the local cancer field to the draining lymph node. (**c**) Carcinoma cell colonization forming lymph node metastases. Competent clonogenic cancer cells with the topoanatomical r-code of the tributary tissue (green fork tag), mainly transported through afferent lymph vessels into the lymph node, which has been conditioned according to (**b**), meet the topoanatomical code of their local cancer field in the l-form (green triangles), a prerequisite for their colonization. Angiogenesis, lymphangiogenesis, remodeling of extracellular matrix, proliferation-promoting and immunosuppressive cytokines foster the formation of micro- and finally gross lymph node metastases

cells with metastasis-forming abilities and provides the topoanatomical code of the cancer field in the lymph node for proliferation, even in the earliest stage of malignant progression (oT1, see Chap. 2). Therefore, lymph node metastases can occur very early in the disease course.

As for the local cancer field model, the regional model is based on biological and clinical phenomena. Potential molecular mechanisms are outside of the scope of this textbook. In order to apply the regional cancer field model for the comprehension of the cancer type-specific pattern of lymph node metastases, the topographic relations between the tributary tissues and the draining lymph nodes displaying their peripheral antigens and topobiological codes must be known. Hints to the structural organization are obtained from the development of the lymphatic system and of the lymph nodes in humans. However, the definitive pattern of lymph node metastasis has to be confirmed from the histopathological results obtained from cancer field surgery without neoadjuvant or adjuvant radiation, performed in a high number of patients.

5.3 Development and Ontogenetic Anatomy of the Lymphatic System

In mammalian embryos, immature peripheral veins give rise to the lymph endothelium through interaction with adjacent mesenchyme. Minor contributions of lymph endothelium stem directly from the mesenchyme. At distinct sites, the specified endothelium evades from the veins into the abutting mesenchyme to form an initial lymph sac or plexus. Most lymph sacs originate along the cardinal vein system. Other sources are heart, skin, and mesentery precursors. Peripheral outgrowths of these lymph sacs—prelymphatics—spread centrifugally and anastomose with each other and with those derived from adjacent lymph sacs, forming a complex *lymphatic network* with major aggregations at the sites of previous lymph sac centers, the *lymph basins*. The venous connections to the lymph sacs disintegrate, except at communication with the jugular veins. The prelymphatics mature into three types of lymph vessels: capillary, precollector, and collector lymphatics [25–27].

Primary lymph nodes develop at the sites of the lymph basins by the evasion of hematopoietic lymphoid tissue inducer cells (LTis) from adjacent blood vessels. LTis cluster and intermingle with abutting mesenchymal cells (LTos), ultimately surrounded by the lymphatic endothelium. The primary lymph nodes of the lymph basins are connected by internodular lymphatics, forming a complex serial and parallel pattern. In addition to the primary lymph nodes, the *basin nodes*, secondary lymph nodes develop in association with lymph collectors as *intercalated nodes* [28]. Even in the mature organism, *tertiary lymphatic organs* composed of lymphoid-like stroma, APCs, and lymphocytes can be established at the local sites of chronic inflammation, i.e., in a tumor bed [29, 30].

The lymph system, founded on its multifocal origin from topographically defined lymph sacs, represents a modular network consisting of multiple topographically distinct *lymph territories*, each composed of a lymph basin with the primary lymph nodes and lymph collectors with the intercalated secondary nodes, as well as their peripheral precollector and capillary lymph vessels (Fig. 5.2a). Any tissue can be allocated to its lymph territory. The lymph produced at a tissue site flows through lymph capillaries, precollectors, and collectors to the basin of the lymph territory. Within a lymph territory, collateral and even reverse lymph flow may take place. Likewise, the lymph flow related to the lymph territories occurs both in series and in parallel to the lymphovenous connections of the ductus thoracicus and ductus lymphaticus dexter with the jugular veins. The direction of the lymph flow defines upstream and downstream relations within the lymphatic system [28].

According to the regional cancer field model, a lymph node directly connected to a tributary tissue by afferent lymphatics, represents a *first-line node* (Fig. 5.2b, c). It can be a basin node or an intercalated node. A lymph node can be first

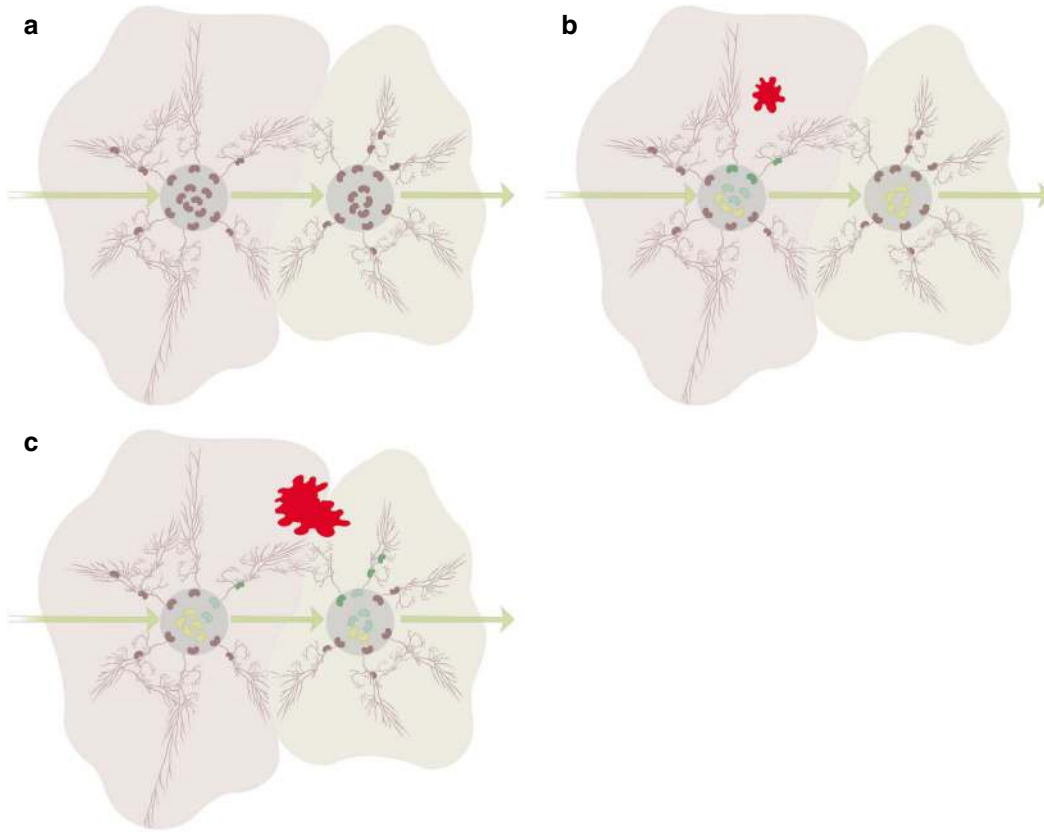

Fig. 5.2 (**a**) Schematic representation of an excerpt of the mature mammalian lymphatic system as a modular network of two lymph territories, with lymphatics and lymph nodes derived from two distinct lymph sacs. The main direction of lymph flow toward the lymphovenous connection is indicated by arrows. Lymphatics guide the lymph from the periphery of the lymph territory toward its center, acting as a basin. Lymph nodes are intercalated into the terminal (collector) lymph vessels and are concentrated in the lymph basins. (**b**) Classification of lymph nodes into first- (dark green), second- (light green), and third-line (yellow) nodes related to a carcinoma propagating within a distinct site of a lymph territory (red spot). (**c**) Classification of first-, second-, and third-line lymph nodes related to a carcinoma propagating within a distinct site involving two lymph territories

line to several tributary tissues. Lymph nodes indirectly connected to the tributary tissue by preceding lymph nodes within a chain integral to the same lymph territory are designated as *second line*, while further downstream nodes located in the adjacent lymph territory are considered *third line*. Lymph nodes of the first-line node's lymph territory, functionally not connected to a tributary tissue under normal lymph flow conditions but potentially at abnormal lymph flow, are considered third line as well. Second- and third-line nodes often receive lymph from several tissue sites that are immunologically monitored by them.

5.4 Patterns of Lymph Node Metastasis

Taking into consideration the proposed mechanism of regional metastasis formation, which involves the export of the local cancer field to the draining lymph nodes as a consequence of peripheral immune surveillance, it is evident that—according to the law of mass action—first-line nodes are at the highest risk of metastasis, as the highest area density of PTAg- and CAg-induced microareas with suitable characteristics meets the highest current density of competent clonogenic tumor cells there. More accurately,

this feature relates to the lymph node sector associated with an afferent lymph vessel from the corresponding tributary tissue. These first-line lymph nodes, with regard to a distinct tributary tissue, correspond to the so-called *sentinel nodes* of a malignant tumor infiltrating this tissue. However, this relation is only valid if the immune balance in the first-line node for the cancer cells is tolerogenic; otherwise, the cancer cells are destroyed, and metastasis formation is frustrated.

In the second- and third-line nodes downstream to the first-line node, the concentration of the PTAgs of the first-line node's tributary tissue and of the CAgs of the carcinoma confined to the tributary tissue is much lower due to the efferent lymph from other tributary tissues. Only carcinoma cells having left the first-line node enter the nodes next in the chain. Therefore, the probability of second-line lymph node metastases directly from the local tumor is small. The dilution effect should be even more pronounced in third-line nodes from adjacent different lymph territories compared to second-line nodes, where anastomoses and collaterals counteract it to some extent. However, a macrometastasis in the first-line node conditions the downstream nodes next in the chain in a similar way as the local tumor conditioned the first-line node before. Tolerized CAgs activating primed Treg cells with the topoanatomical code to proliferate and differentiate expand the cancer field to the second-line node, allowing competent clonogenic cancer cells derived from the first-line node to form a metastasis there.

The lymph node metastasis pattern beyond the colonization of first-line nodes is influenced by the complex lymph flow between individual nodes of a lymph territory with reverse and circular directions and between adjacent lymph territories. Upstream lymph node metastases may affect downstream lymph flow.

If the local carcinoma has progressed to higher ontogenetic stages (oT >2), the number of lymph nodes directly connected to the tumor bed increases. oT >2 carcinoma cells can colonize lymph nodes corresponding to second or even third defense lines with regard to tributary tissues representative for oT1 and 2 tumors. The downstream hierarchy of first-, second-, and third-line nodes, which is valid for early (oT1, 2) tumors, is not applicable in tumors of advanced ontogenetic stages. Based on the same argument, advanced progression of local carcinomas should confer a higher risk of regional disease in general as more lymph node regions are prone to forming metastases.

The clinically applied marker-guided sentinel node biopsy in low-volume carcinomas is largely in line with the regional cancer field model for oT1 tumors as the lymphatic clearance of the marker particles injected into the tumor and tumor bed is a proxy for the transport of PTAgs, Cags, and cancer cells into the draining lymph node(s), which are determinants of metastasis formation. Yet there is a conceptual risk of false-negative results in situations where lymph node metastases block the afferent lymph flow or the marked nodes are fibrotic and no longer immunologically active.

In conclusion, to realize the potential lymph node metastasis pattern for a carcinoma entity based on the regional cancer field model, the topographical identification of the tissues infiltrated by the local cancer and the ontogenetic tumor stage is necessary. The hierarchy of first-, second-, and third-line nodes within the lymphatic network draining the tumor bed determines the regional cancer field, i.e., the lymph nodes of potential metastasis formation for the individual tumor. Metastatic involvement of the first-line node(s) indicates a risk for second- and third-line nodes. Although metastases in the third-line nodes are often associated with second-line metastases, the presence of second-line metastases is not a mandatory prerequisite for the formation of third-line metastases. For carcinomas of lower ontogenetic stages (oT1, 2), the lymph node hierarchy is predictable and the extent of necessary therapeutic lymph node dissection to obtain regional tumor control can be ascertained intraoperatively by frozen section investigation. In locally advanced (oT >2) carcinomas, the wide distribution of potential first-line nodes primarily demands an extended lymph node dissection for regional tumor control. Regional disease patterns

of cervix and vulvar carcinomas, as approached with the cancer field model, are the topics of the following chapter.

References

1. Mak TW, Saunders ME, Jett BD. Primer to the immune response. 2nd ed. Burlington: Academic Press; 2014.
2. Arasa J, Collado-Diaz V, Halin C. Structure and immune function of afferent lymphatics and their mechanistic contribution to dendritic cell and T cell trafficking. Cells. 2021;10:1269. https://doi.org/10.3390/cells10051269.
3. Jalkanen S, Salmi M. Lymphatic endothelial cells of the lymph node. Nat Rev Immunol. 2020;20:566–78. https://doi.org/10.1038/s41577-020-0281-x.
4. Johnson LA. In sickness and in health: the immunological roles of the lymphatic system. Int J Mol Sci. 2021;22:4458. https://doi.org/10.3390/ijms22094458.
5. Oliver G, Kipnis J, Randolph GJ, Harvey NL. The lymphatic vasculature in the 21st century: novel functional roles in homeostasis and disease. Cell. 2020;182:270–96. https://doi.org/10.1016/j.cell.2020.06.039.
6. Randolph GJ, Ivanov S, Zinselmeyer BH, Scallan JP. The lymphatic system: integral roles in immunity. Annu Rev Immunol. 2017;35:31–52. https://doi.org/10.1146/annurev-immunol-041015-055354.
7. Fletcher AL, Acton SE, Knoblich K. Lymph node fibroblastic reticular cells in health and disease. Nat Rev Immunol. 2015;15:350–61. https://doi.org/10.1038/nri3846.
8. Saxena V, Li L, Paluskievicz C, Kasinath V, Bean A, Abdi R, et al. Role of lymph node stroma and microenvironment in T cell tolerance. Immunol Rev. 2019;292:9–23. https://doi.org/10.1111/imr.12799.
9. Harlé G, Kowalski C, Garnier L, Hugues S. Lymph node stromal cells: mapmakers of T cell immunity. Int J Mol Sci. 2020;21:7785. https://doi.org/10.3390/ijms21207785.
10. Catalán D, Mansilla MA, Ferrier A, Soto L, Oleinika K, Aguillón JC, et al. Immunosuppressive mechanisms of regulatory B cells. Front Immunol. 2021;12:611795. https://doi.org/10.3389/fimmu.2021.611795.
11. Rosser EC, Mauri C. Regulatory B cells: origin, phenotype, and function. Immunity. 2015;42:607–12. https://doi.org/10.1016/j.immuni.2015.04.005.
12. Fu H, Ward EJ, Marelli-Berg FM. Mechanisms of T cell organotropism. Cell Mol Life Sci. 2016;73:3009–33. https://doi.org/10.1007/s00018-016-2211-4.
13. Masopust D, Schenkel JM. The integration of T cell migration, differentiation and function. Nat Rev Immunol. 2013;13:309–20. https://doi.org/10.1038/nri3442.
14. Tough DF, Rioja I, Modis LK, Prinjha RK. Epigenetic regulation of T cell memory: recalling therapeutic implications. Trends Immunol. 2020;41:29–45. https://doi.org/10.1016/j.it.2019.11.008.
15. von Andrian UH, Mackay CR. T-cell function and migration. Two sides of the same coin. N Engl J Med. 2000;343:1020–34. https://doi.org/10.1056/NEJM200010053431407.
16. Wei S, Kryczek I, Zou W. Regulatory T-cell compartmentalization and trafficking. Blood. 2006;108:426–31. https://doi.org/10.1182/blood-2006-01-0177.
17. von Andrian UH, Mempel TR. Homing and cellular traffic in lymph nodes. Nat Rev Immunol. 2003;3:867–78. https://doi.org/10.1038/nri1222.
18. Grover P, Goel PN, Greene MI. Regulatory T cells: regulation of identity and function. Front Immunol. 2021;12:750542. https://doi.org/10.3389/fimmu.2021.750542.
19. Shao Q, Gu J, Zhou J, Wang Q, Li X, Deng Z, et al. Tissue Tregs and maintenance of tissue homeostasis. Front Cell Dev Biol. 2021;9:717903. https://doi.org/10.3389/fcell.2021.717903.
20. Arpaia N, Green JA, Moltedo B, Arvey A, Hemmers S, Yuan S, et al. A distinct function of regulatory T cells in tissue protection. Cell. 2015;162:1078–89. https://doi.org/10.1016/j.cell.2015.08.021.
21. Sjaastad LE, Owen DL, Tracy SI, Farrar MA. Phenotypic and functional diversity in regulatory T cells. Front Cell Dev Biol. 2021;9:715901. https://doi.org/10.3389/fcell.2021.715901.
22. Sharma P, Goswami S, Raychaudhuri D, Siddiqui BA, Singh P, Nagarajan A, et al. Immune checkpoint therapy – current perspectives and future directions. Cell. 2023;186:1652–69. https://doi.org/10.1016/j.cell.2023.03.006.
23. Paluskievicz CM, Cao X, Abdi R, Zheng P, Liu Y, Bromberg JS. T regulatory cells and priming the suppressive tumor microenvironment. Front Immunol. 2019;10:2453. https://doi.org/10.3389/fimmu.2019.02453.
24. Takeuchi Y, Nishikawa H. Roles of regulatory T cells in cancer immunity. Int Immunol. 2016;28:401–9. https://doi.org/10.1093/intimm/dxw025.
25. Betterman KL, Harvey NL. The lymphatic vasculature: development and role in shaping immunity. Immunol Rev. 2016;271:276–92. https://doi.org/10.1111/imr.12413.
26. Francois M, Oszmiana A, Harvey NL. When form meets function: the cells and signals that shape the lymphatic vasculature during development. Development. 2021;148:167098. https://doi.org/10.1242/dev.167098.
27. Yang Y, Oliver G. Development of the mammalian lymphatic vasculature. J Clin Invest. 2014;124:888–97. https://doi.org/10.1172/JCI71609.
28. Földi M, Földi E, Kubik S, editors. Lehrbuch der lymphologie. 6th ed. Urban & Fischer: Munich; 2005.

29. Buckley CD, Barone F, Nayar S, Bénézech C, Caamaño J. Stromal cells in chronic inflammation and tertiary lymphoid organ formation. Annu Rev Immunol. 2015;33:715–45. https://doi.org/10.1146/annurev-immunol-032713-120252.

30. Onder L, Mörbe U, Pikor N, Novkovic M, Cheng H-W, Hehlgans T, et al. Lymphatic endothelial cells control initiation of lymph node organogenesis. Immunity. 2017;47:80–92. https://doi.org/10.1016/j.immuni.2017.05.008.

6 Ontogenetic Anatomy of the Lower Human Body's Lymphatic System: Lymphatic Network of the Female Genital Tract—Regional Progression of Gynecologic Carcinomas

6.1 Lymph Sac-Derived Lymph Territories

Ontogenetic anatomy maps mature tissues with regard to their development. In the case of the human lymphatic system, ontogenetic *lymph territories* are topographically defined by their sites of origin, the *lymph sacs* and *plexus*, described in the previous chapter. The mature human lymphatic system consists of superficial and deep lymph territories. The collector vessels of the superficial lymph system draining the integument run in the direction of the larger subcutaneous veins. The collectors of the deep lymph system draining the body walls, extremities, and internal organs follow the courses of their supplying blood vessels. The collectors of the internal organs are located in their mesenteries or mesotissues. Primary lymph nodes are formed at the centers of the lymph territories, the lymph basins. Secondary lymph nodes are established peripherally and intercalated in the collector vessels, mainly in those of the deep lymph territories [1].

From the scarce sources of morphological information about the lymphatic system in the human embryo, it can be concluded that the lower body's lymphatic territories relevant to the drainage and immunologic surveillance of the genital tract and external genitalia originate from three bilateral lymph sacs—*lumbar*, *iliac*, and *inguinal*—and from the unilateral *mesenteric* lymph sac [2, 3].

The lumbar lymph sacs are formed dorsolaterally to the abdominal aorta. Lumbar prelymphatics either follow the adreno-nephroureteral blood vessels toward these primordial organs or grow into the lumbar body wall. Consequently, the basin nodes of the *lumbar lymph territory* are mainly found dorsally and laterally of the abdominal aorta and vena cava inferior and between these vessels from their bifurcations upward to the diaphragm. Intercalated nodes of the lumbar lymph territory exist in the adreno-nephroureteral mesenteries and in the subfascial lumbar body wall.

The unilateral mesenteric lymph sac arises ventral to the abdominal aorta. It matures into the *mesenteric lymph territory* with its basin lymph nodes, located at the ventral surface of the abdominal aorta and vena cava inferior and extending to the left paraaortic region. Multiple intercalated lymph nodes of the mesenteric lymph territory are distributed in the intestinal mesenteries, including the mesorectum, and in the omental structures. Mesenteric lymph nodes related to the surface and cranial tissues of the genital tract are intercalated in the collector lymph vessels of the peritoneal mesometrium (broad ligament), mesosalpinx, and mesovar and in the "infundibulopelvic ligament." A lymph drainage pathway from the surface and immediately adjacent tissues of the lower genital tract (lower corpus, cervix, vagina) is established in the ligamentous mesometria and mesocolpoi, pararectal fascia, and subperitoneum, which also

M. Höckel et al., *Cancer Field Surgery in Gynecologic Oncology*,
https://doi.org/10.1007/978-3-031-83030-3_6

contain intercalated lymph nodes. With respect to the lymphatic drainage of the genital tract and fixed surgical landmarks, we have settled the upstream border of both lumbar and mesenteric lymph basins at the most caudal point of the aortic bifurcation. Irrespective of their allocation to different lymph territories, the downstream periaortic nodes are then categorized into "aortic bifurcation," extending to the level of the origin of the inferior mesenteric artery, and "infrarenal," extending to the renal veins (Fig. 6.1a).

The bilateral iliac lymph sacs appear shortly after the lumbar lymph sacs. They encase the iliac vessels beginning at the aortic bifurcation and extend caudalward. Multiple anastomoses are formed between the prelymphatics of the iliac, lumbar, and mesenteric lymph sacs. Most basin nodes of the *iliac lymph territory* surround the iliac vessel system at the pelvic side walls, including the obturator vessels anteriorly and the lateral sacral vessels posteriorly. Considering their surgical identification from constant anatomical landmarks—a line at the external and common iliac vessel axis crossed by a line from the sciatic spine along the internal iliac axis at the iliac bifurcation—the iliac basin lymph nodes can be categorized into four subregions: external iliac, paravisceral (with anterior internal iliac,

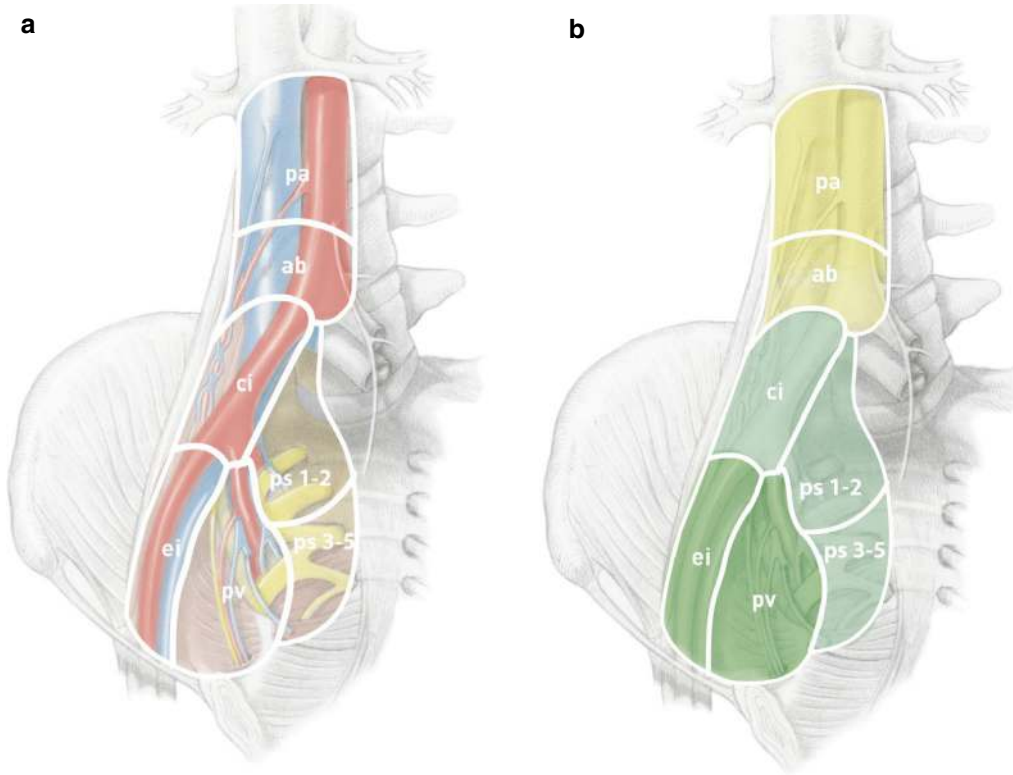

Fig. 6.1 Basin lymph node regions draining the Müllerian core compartment (without sinus vagina caudally and uterine fundus and tubes cranially). (**a**) Semischematic anatomical drawing of the infrarenal and right pelvic somatic retroperitoneum. *ei* external iliac, *pv* paravisceral, *ci* common iliac, *ps 1–2* upper presacral, *ps 3–5* lower presacral, *ab* aortic bifurcation, *pa* periaortic. (**b**) Color-coded hierarchy of basin lymph node defense lines for the Müllerian core compartment. Intense green, first-line node regions; light green, second-line node regions; yellow, third-line node regions

obturator, and internal pudendal nodes), common iliac, and presacrococcygeal (with posterior internal iliac, superior and inferior gluteal nodes, and lateral sacral nodes) (Fig. 6.1a). The intercalated nodes of the iliac lymph territories are widely spread in the subfascial musculoskeletal pelvic walls and the legs. Endopelvic intercalated nodes from the iliac lymph territories are located in the urogenital mesenteries, including the bladder mesentery, the vascular mesometria, and mesocolpoi, and in the urethrovesical mantle tissue (Fig. 6.2a, b).

By the end of the embryonic period, bilateral inguinal lymph plexus can be discerned in the subectodermal mesenchyme at the pubocrural transition. The inguinal lymph plexus are the precursors of the *inguinal lymph territory*, encompassing the superficial (suprafascial) layer of the lymphatic system, which supplies the dermis of the lower trunk, perineum, and legs. Their basin nodes are situated in the superficial inguinal regions. Most of the basin nodes are found in the femoral triangle, bordered by the inguinal ligament cranially and by the suprafascial projections of the intersecting sartorius and adductor longus muscles laterally and medially. A straight line in the projection of the greater saphenous vein perpendicularly crossed by a straight line at its estuary into the femoral vein at the hiatus saphenus is used to identify four quadrants of the superficial inguinal lymph node basin: superolateral—superomedial—inferomedial—inferolateral (Fig. 6.3a). Intercalated nodes in the subcutaneous collectors of the inguinal lymph territory exist at the flanks and the umbilicus. Small superficial popliteal nodes are found immediately below the fascia lata at the estuary of the vena saphena parva into the popliteal vein. According to our experience, lymph nodes intercalated into the collector vessels may also run through the labia majora to the superficial inguinal lymph nodes. The deep inguinal lymph nodes, located below the fascia lata medially to the femoral veins, are considered intercalated nodes of the iliac lymph territories, which are connected to the lacunar nodes, as most upstream nodes of the iliac lymph basin [3] (Fig. 6.3b).

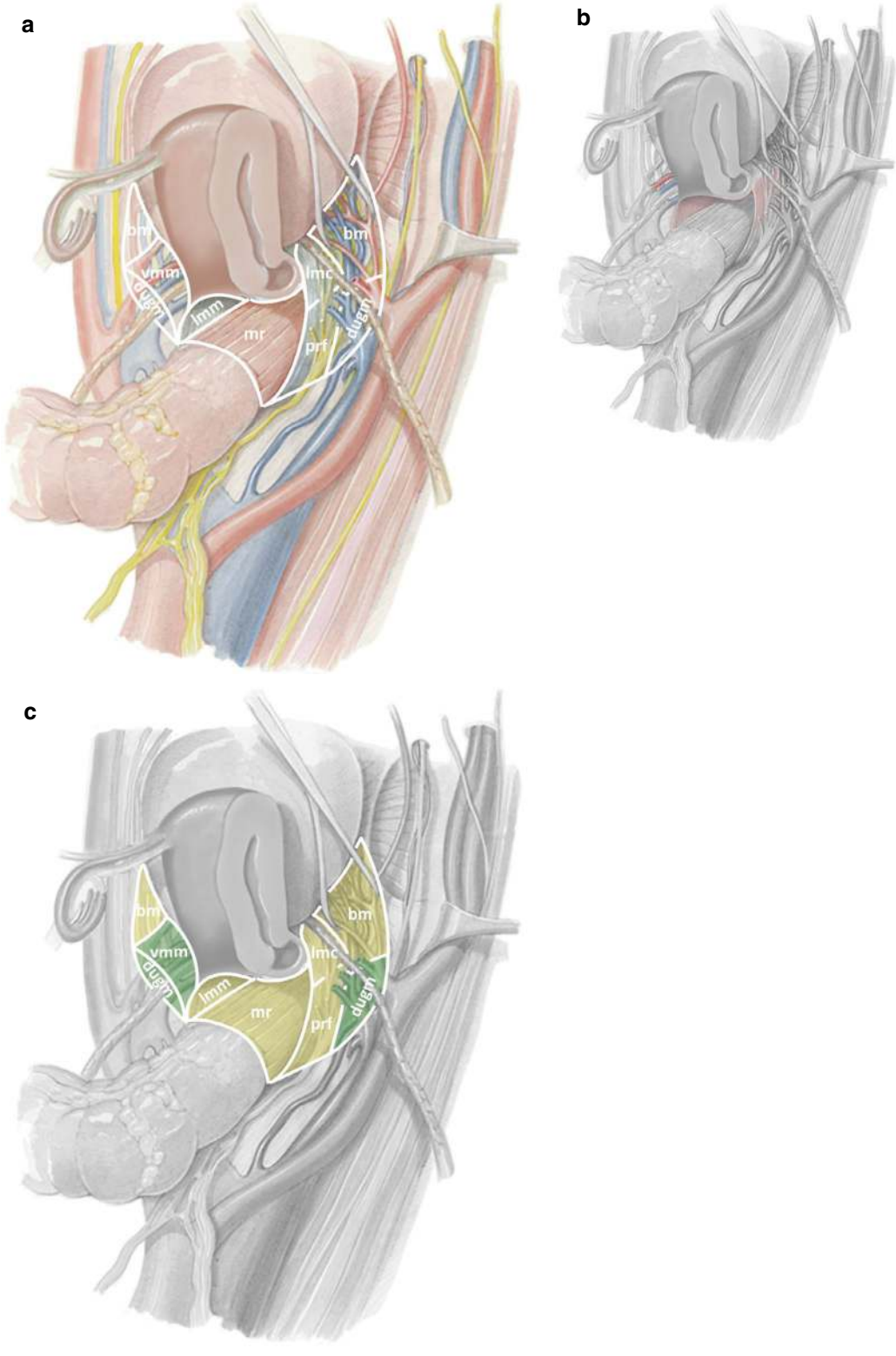

Fig. 6.2 Intercalated lymph node regions draining the Müllerian core compartment. (**a**) Semischematic drawing of the female endopelvis. (**b**) Vascular mesometrium/mesocolpos and ligamentous mesometrium/mesocolpos highlighted. (**c**) First-line intercalated lymph node regions highlighted in intense green. *vmm* vascular mesometrium, *vmc* vascular mesocolpos, *ugm* distal urogenital mesentery, *lmm* ligamentous mesometrium, *lmc* ligamentous mesocolpos, *bm* bladder mesentery, *pf* perirectal fascia, *mr* mesorectum

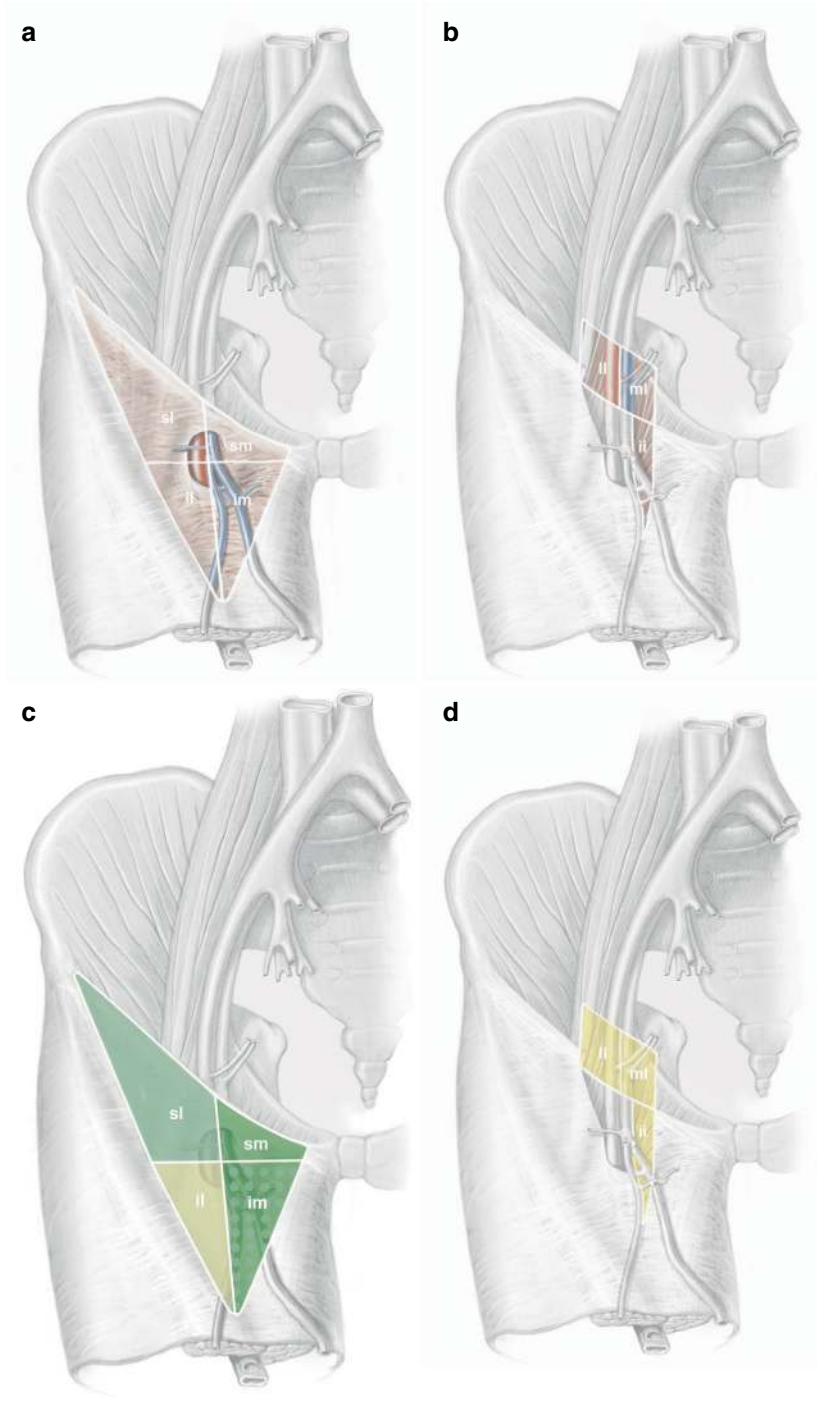

Fig. 6.3 Lymph node regions draining the ontogenetic vulvar compartment. (**a**) Anatomical drawing of the right femoral triangle bordered by the inguinal ligament and sartorius and adductor longus muscles. A line in the axis of the leg perpendicularly crossed at the hiatus saphenus by a second line marks the four quadrants of the superficial inguinal lymph node basin. *sl* superolateral, *sm* superomedial, *im* inferomedial, *il* inferolateral. (**b**) Anatomical drawing of the deep inguinal (ii), medial lacunar (ml), and lateral lacunar (ll) lymph node regions at the right side. (**c**, **d**) Color-coded hierarchy of inguinolacunar lymph node defense lines for the ontogenetic vulva. Intense green, first-line regions, *sm* superomedial, *im* inferomedial. Light green, second-line regions, *sl* superolateral. Yellow, third-line regions, *il* inferolateral, *ii* deep inguinal, *ml* medial lacunar, *ll* lateral lacunar

6.2 Hierarchy of Lymphatic Defense Lines

The modular network architecture of the lymph system derived from the developmental principles described above and the flow direction of the lymph fluid toward the lymphovenous communications at the jugular veins allow the categorization of both intercalated and basin lymph nodes into first, second, or third defense lines with regard to a distinct tributary tissue. As indicated in Chap. 5, *first-line nodes* are directly connected to the tributary tissue. *Second-line nodes* belong to the same lymph territory as the first-line nodes but receive the lymph fluid indirectly after passage through the first-line nodes. *Third-line nodes* are allocated either to a different lymph territory connected downstream to first- and second-line nodes or to lymph nodes of the same lymph territory, which normally do not receive lymph from that tissue but may participate in the lymph drainage under pathological conditions. The regional cancer field model considers this threefold defense-line categorization of lymph nodes with respect to the tissues infiltrated by a carcinoma. Based on the ontogenetic anatomy of the genital tract and external genitalia (see Chaps. 3 and 4) and on the ontogenetic anatomy of the draining lymphatic network, distinct lymph node regions for the formation of first-, second-, and third-line metastases can be predicted and surgically removed. Parietal first-line nodes draining the uterus can be specified by labeling techniques, e.g., indocyanine green injection into the uterine stroma.

6.3 Surgical Anatomy of the Lymphatic Drainage of the Uterine Corpus and Cervix Derived from Indocyanine Green (ICG) Visualization

The injection of indocyanine green dye into uterine stroma under defined conditions (see Chap. 9) enables the precise topographical identification of its lymph collectors and the associated first-line lymph nodes by their fluorescence under near infrared illumination. As demonstrated for endometrial carcinoma treated with minimally invasive robotic surgery, this elaborated surgical diagnostic procedure bears a high potential for reducing treatment-related morbidity without compromising regional cancer control. However, certain caveats should be considered with regard to the cancer field model:

- Based on the arguments presented in Chap. 5, lymph collector-guided identification of the nodal state of an individual carcinoma is only valid for the oT1 stage.
- Metastatic lymph nodes can shut down their afferent lymph flow and may therefore escape detection from dye injection.
- Short-term lymph flow following dye injection into the tumor and tumor bed tissues at nonphysiologic pressure is different from long-term flow under the interstitial pressure produced by the growing local tumor.

Nevertheless, long-term experience with this technique has generated sound knowledge of the complex lymphatic draining architecture of the uterine corpus and cervix [4–7].

Four lymphatic pathways from the uterus have been verified:

1. The upper iliac (ui) pathway
2. The lower iliac (li) pathway
3. The lower mesenteric (lm) pathway
4. The upper mesenteric (um) pathway

The *upper iliac pathway* (Fig. 6.4a–c) usually exhibits one or more main collector vessels running along the uterine artery and crossing over the ureter. Above the umbilical artery, two branches can be discerned. A more medial anterior branch passes the internal and external iliac arteries close to the bifurcation of the common iliac artery, reaching its first-line node(s) within the bifurcation medial to the external iliac artery. A more lateral posterior branch runs between the internal and external iliac veins to the first-line node(s), located laterally to the external iliac vein and ventrally to the obturator vessels. Second-line nodes of the upper iliac pathway are situated laterally to the external and common iliac ves-

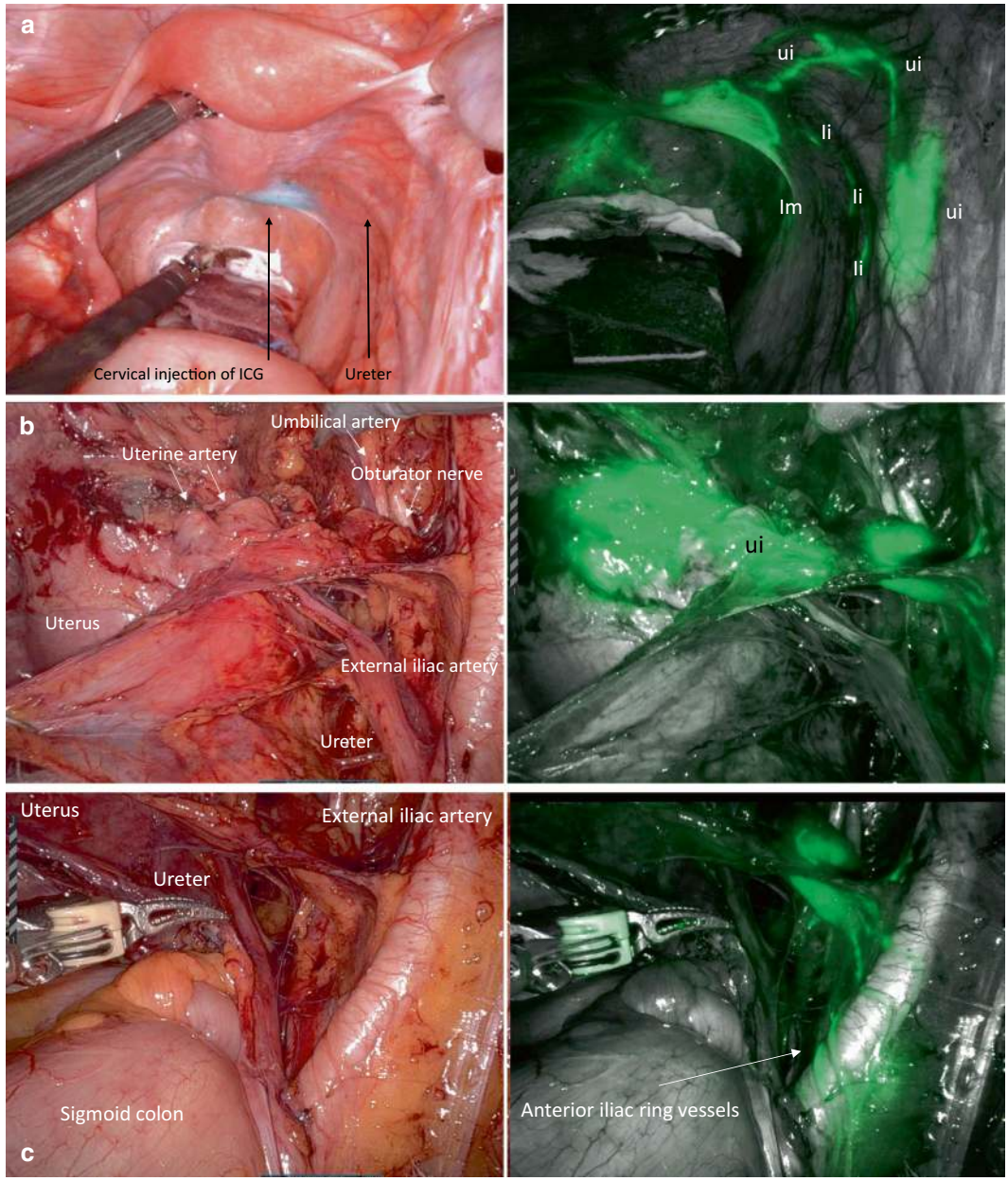

Fig. 6.4 Endopelvic situs at visible light (left) and with green fluorescence at near-infrared illumination (right) after injection of indocyanine green dye (ICG) into the uterine cervix extending into the serosa. (**a**) Lower mesenteric (lm) and lower (li) and upper iliac (ui) lymphatic pathways are demonstrated in the right panel. (**b**) Right upper iliac (ui) pathway. From the cervical ICG depot, uterine collector vessels transport ICG along the uterine artery to the first-line nodes medial to the external iliac vessels. (**c**) Right upper iliac pathway. First-line nodes medial to the external iliac and lymphatic "ring" vessels surrounding the external iliac artery anteriorly and dorsally are visible at near-infrared illumination

sels. They are connected to first-line nodes by anterior and posterior "ring vessels." Lumbar and mesenteric paraaortic nodes serve as third defense line. Upstream to the paraaortic region, draining is strictly ipsilateral. However, anastomoses between the right and left sides exist at the level of the inferior mesenteric artery and further downstream. Physiological lymph flow is directed from right to left.

The *lower iliac pathway* (Fig. 6.5a, b) runs dorsocaudally along the vaginal/deep uterine vein(s) within the infraureteral vascular mesocolpos, joined with the distal urogenital mesentery to the medial posterior internal iliac lymph nodes

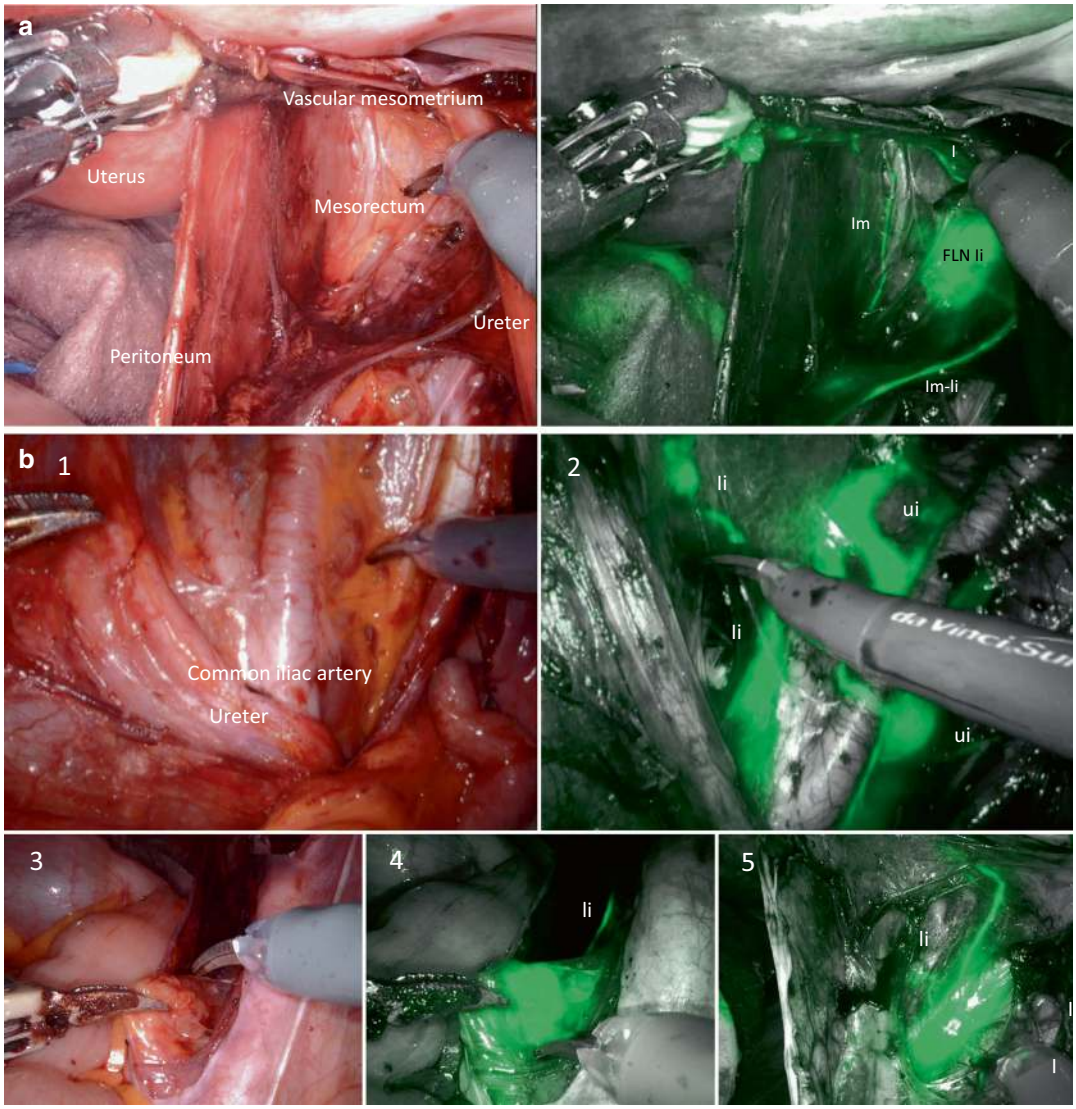

Fig. 6.5 Endopelvic situs at visible light (left) and with green fluorescence at near infrared illumination (right) after cervical injection of ICG. (**a**) Right lower iliac lymphatic pathway leading to a first-line node (FLN li). A collector vessel of the right lower mesenteric (lm) pathway and a lymph vessel connecting the lower iliac and mesenteric lymph territories (li-lm) are also visible. (**b**) Dissection of the right distal lower iliac pathway (li) along the internal iliac artery (panel 2) and mobilization of the associated first-line node (panels 3–5). The right distal upper iliac pathway with first-line node(s) is also visible (panel 2, ui)

(first-line), further to the lateral sacral and precoccygeal nodes (second line), and downstream to the lumbar paraaortic lymph node basins (third line). The drainage is side-specific to as far as the subaortic region, where anastomoses between the right and left lymph basins are present, directing the lymph flow from right to left under physiological conditions. In some patients, connections to collector vessels of the lower mesenteric lymph territory have been observed.

The *lower mesenteric pathway* (Figs. 6.4a, 6.5a, and 6.6) draining the dorsal serous and subserous cervicovaginal tissues and rectovaginal septum proceeds in the ligamentous mesometrium to the pararectal fascia. The first-line lymph nodes of these pericervicovaginal structures are eventually intercalated in these collectors.

The *upper mesenteric pathway* (Figs. 6.7, 6.8, 6.9, and 6.10) draining the uterine fundus accompanies the ovarian branch of the uterine artery to the mesovarium and the ovarian vessels within the "infundibulopelvic ligament." Here, two lymph collectors are regularly visible: one along the ovarian artery and another along the ovarian vein. On the right side, the first-line nodes receiving the lymph from the ovarian artery-associated collector are located in the right periaortic region ventral to the vena cava between the estuaries of the inferior mesenteric arteries and ovarian vein. On the left side, the collectors drain into first-line

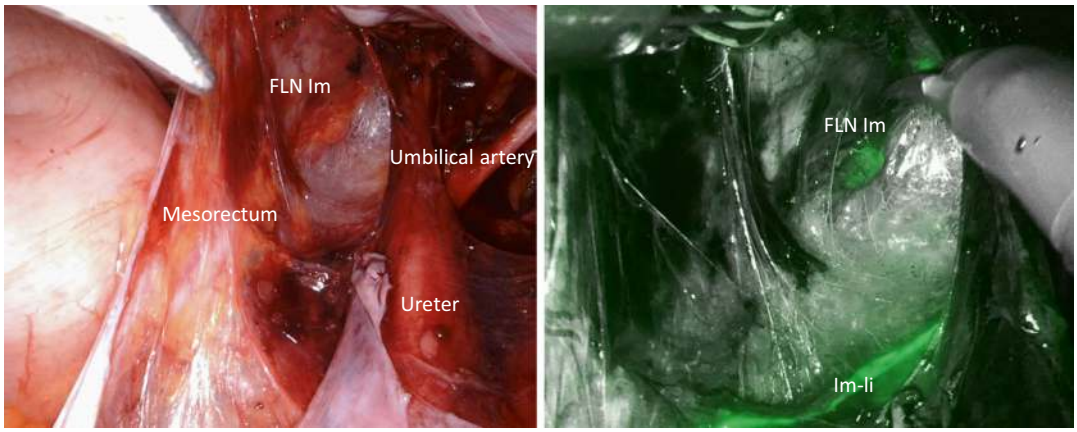

Fig. 6.6 Endopelvic situs at visible light (left) and with green fluorescence at near-infrared illumination (right) after cervical injection of ICG. Pararectal lymph node intercalated in the right lower mesenteric lymph pathway (FLN lm). A lymphatic vessel connecting lower mesenteric and iliac lymph territories (lm-li) is demonstrated. We did not diagnose single lymph node metastases of cervix carcinoma at this site. However, lymph node metastases of the lower mesenteric pathway occurred in oT3a, b and oT4 cervix carcinomas, together with metastases at other sites

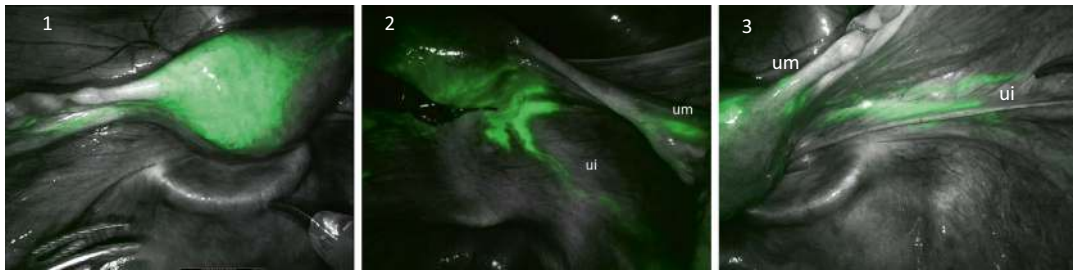

Fig. 6.7 Visualization of the proximal upper mesenteric pathways (um) after ICG injection into the uterine corpus. The upper iliac (ui) pathways in panels 2 and 3 are also visible

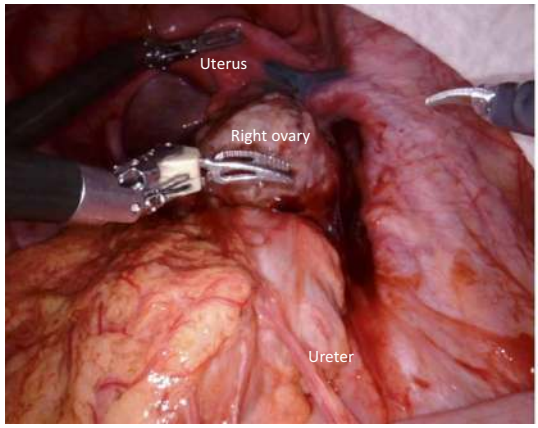

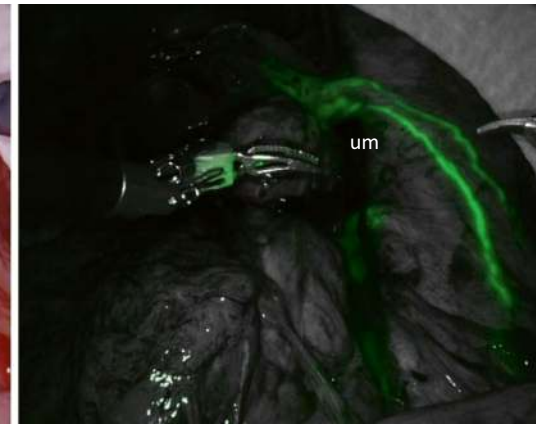

Fig. 6.8 Endopelvic situs at visible light (left) and with green fluorescence at near infrared illumination (right) after injection of ICG into the right mesovarium, highlighting the two lymph collectors of the right proximal upper mesenteric (um) pathway along the ovarian vessels

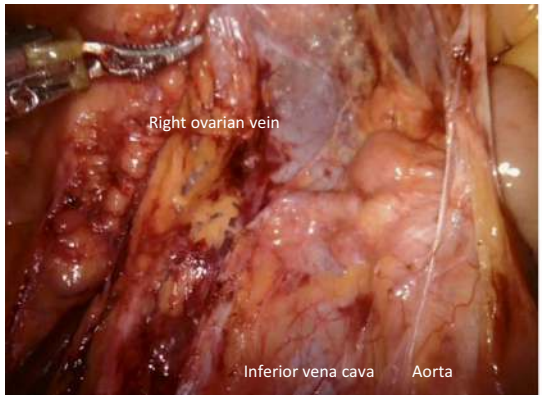

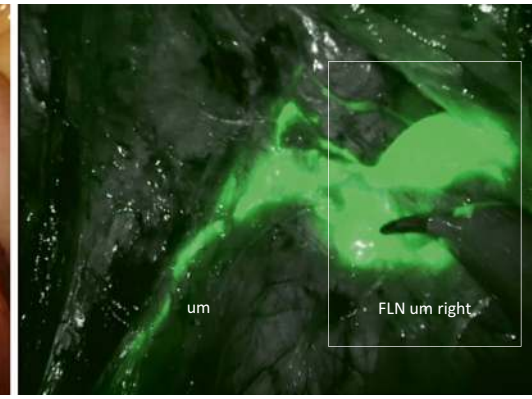

Fig. 6.9 Endopelvic situs at visible light (left) and with green fluorescence at near-infrared illumination (right) after mesovarian injection of ICG, demonstrating parietal first-line nodes of the right upper mesenteric (FLN um right) pathway

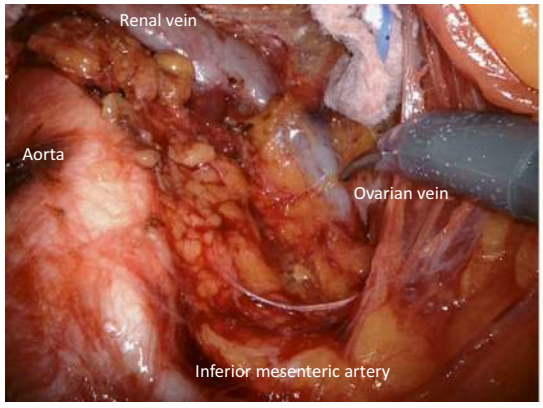

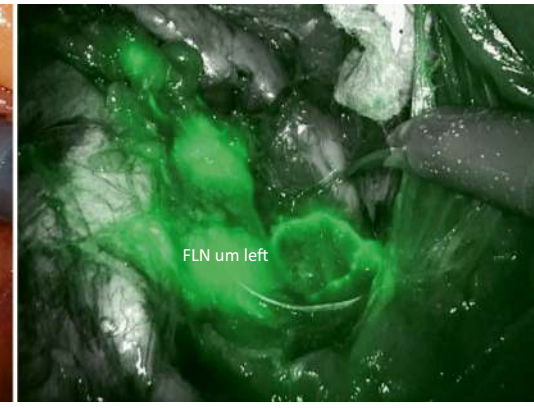

Fig. 6.10 Endopelvic situs at visible light (left) and with green fluorescence at near-infrared illumination (right) after mesovarian injection of ICG, showing parietal first-line nodes of the left upper mesenteric (FLN um left) lymphatic pathway

infrarenal nodes located on the left side of the aorta below the left renal vein.

All first-line nodes belong to the mesenteric periaortic regions. Figure 6.11 summarizes the four major lymphatic pathways observable after the injection of ICG into the uterine cervix, corpus, and mesovarium.

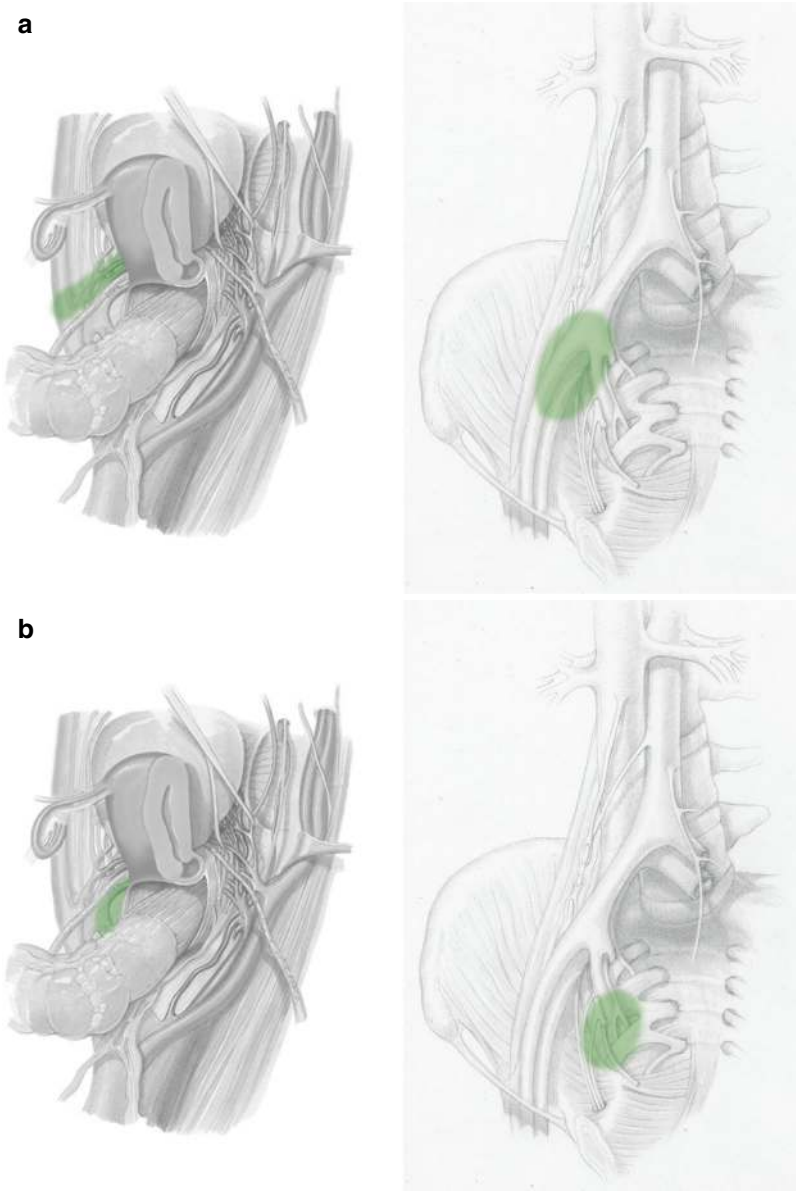

Fig. 6.11 Comprehensive representation of the four major lymphatic pathways identified after injection of ICG into the uterine cervix, corpus, and mesovarium. (**a**) Upper iliac. (**b**) Lower iliac. (**c**) Upper mesenteric. (**d**) Lower mesenteric

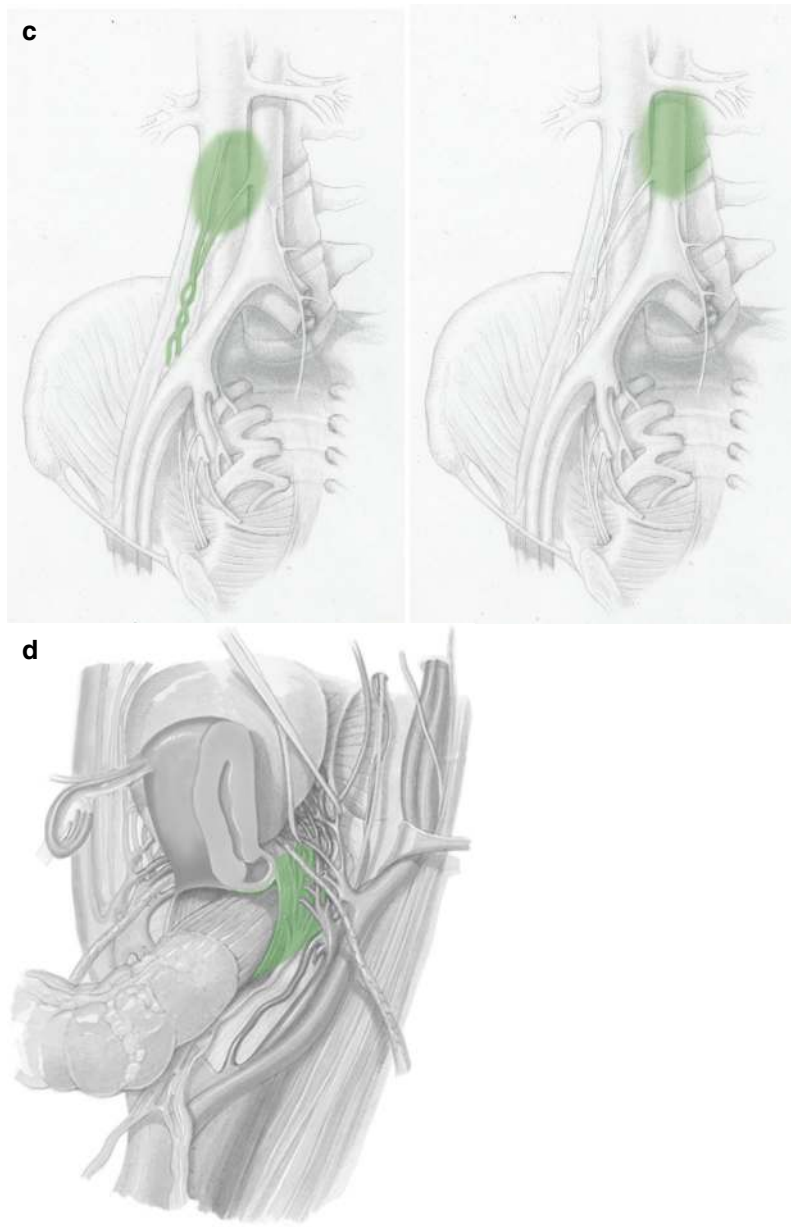

Fig. 6.11 (continued)

6.4 Regional Progression of Cervix Carcinoma

For cervix carcinoma confined to the cervical stroma (oT1), the lower basin nodes of the iliac lymph territory, i.e., external iliac and paravisceral, as well as nodes intercalated in the vascular mesometria-mesocolpoi and in the distal urogenital mesenteries connected to the basin nodes, are first line because any of these nodes can drain the cancer field directly. The upper basin nodes of the iliac lymph territory, i.e., the common iliac and presacrococcygeal, are typically second line, with rare exceptions. Further downstream, peri-

aortic nodes of the lumbar and mesenteric lymph sacs are third-line nodes as they are derived from different lymph sacs.

The oT2 cancer field of cervix carcinoma includes the complete Müllerian compartment. In addition to those of oT1 cancers, cervix carcinomas infiltrating the sinus vagina may also develop first-line metastases in the superficial inguinal lymph node regions. The infiltration of the uterine fundus extends the sites of first-line nodes to the intercalated lymph nodes in the peritoneal mesometrium, the infundibulopelvic ligament, and the mesenteric basin nodes. Second- and third-line nodes correspond to those of the cervix. Figures 6.1b and 6.2c display the first-, second-, and third-line regions of the basin and intercalated lymph nodes for cervix carcinomas of stage oT1 and the vast majority of stage 2. Cervix carcinomas that have propagated to infiltrate the sinus vagina caudally or the uterine fundus cranially have usually infiltrated non-Müllerian tissues and therefore are no longer confined to an oT2 stage. The oT3a cancer field of cervix carcinoma encompasses, in addition to the Müllerian compartment, the vascular and ligamentous mesometria and mesocolpoi, the bladder adventitia, the periurethral tissue, the vulva, the genital serosa, and the peritoneum (see Chap. 3). As a consequence, its direct lymph drainage is extended to the superficial inguinal, common iliac, and presacrococcygeal basin lymph nodes and to the intercalated nodes of the periurethral tissue and bladder mesentery, all becoming first-line nodes in addition to the first-line nodes for oT1 cervix carcinomas. Intercalated lymph nodes in the ligamentous mesometria/mesocolpoi and pararectal fascia are first line as well but have been detected only in the presence of other metastatic lymph node regions in our series by now. First-line nodes of oT3b cervix carcinomas correspond to those of oT3a stages. The oT4 cancer fields add the mesorectal and lumbar periaortic nodes to the first-line category.

From these ontogenetic anatomical considerations, several predictions can be made for the pattern of lymph node metastasis and its prognostic significance in cervical carcinoma:

1. Single metastases of oT1 and 2 cervical carcinomas (except fundal and sinus vaginal involvement) should be located in the external iliac, paravisceral, vascular mesometrial, and mesocolpic lymph node regions as well as in the distal urogenital mesentery. Single metastases of cervix carcinoma > oT2 may be detected in any of the locations described above.
2. The presence of first-line lymph node metastases increases the risk of second-line metastases, whose presence, in turn, increases the risk of third-line metastases.
3. Advanced oT stage is associated with the increased probability of lymph node metastasis in general, an increased number of lymph node metastases, and an increased number of involved lymph node regions.
4. The allocation of metastases to first-, second-, and third-line lymph nodes related to the oT1 and 2 (except fundal and sinus vaginal involvement) cancer fields is prognostically significant, allowing an ontogenetic staging system (oN) for cervix carcinoma.
5. According to the ontogenetic cancer field model, the extracapsular spread (ECS) of a lymph node metastasis indicates malignant progression corresponding to an oT stage that includes the perinodal tissues as permissive. For example, cancer cells of mesometrial lymph node metastasis with proven ECS must have progressed to at least the oT3a stage. The ECS of iliac and lumbar basin lymph nodes confirms an oT4 stage. Consequently, the detection of the ECS of lymph node metastases should have a negative influence on prognosis.

Lymph node metastases have been identified histopathologically from surgical specimens of cervical carcinomas treated with cancer field surgery and staged with regard to the ontogenetic anatomy, as described in Chap. 3. No postoperative adjuvant radiotherapy has been administered, and almost all (98%) patients have been followed for recurrent disease. Therefore, any lymph node metastases that had not been removed surgically should have been identified by the pattern of relapse.

The histopathological results of 589 patients with FIGO IB-IIB cervix carcinoma, oT stages 1–4 treated with total mesometrial resection (TMMR)/extended mesometrial resection (EMMR) and peripheral immune network-directed lymph node dissection (iLND) without adjuvant radiation, confirmed the predictions. Table 6.1 demonstrates the sites of first-line lymph node metastases detected at primary treatment. Recurrent cervical carcinoma, manifesting as lymph node metastases after a nodal negative state at primary treatment, was diagnosed in nine patients. The sites of recurrent first-line lymph node metastases in these patients were paravisceral-distal urogenital mesentery transition, $n = 6$, and mesometrium-mesocolpos, $n = 3$. Although infrequent, oT > 2 stage cervix carcinomas having progressed locally beyond the Müllerian compartment exhibited first-line metastases in the common iliac (2/51) and presacral (1/51) lymph node regions. Irrespective of the ontogenetic stage of their local tumors, 81 patients with metastases in the common iliac ($n = 44$) and presacrococcygeal ($n = 37$) regions had ipsilateral metastases in the mesometrial, external iliac, and paravisceral regions as a single site of upstream metastasis. Table 6.2 shows the sites of second-line lymph node metastases at primary treatment. Recurrent second-line lymph node metastases were identified in seven patients in the upper ($n = 2$) and lower ($n = 5$) presacral regions. Twenty-seven carcinomas with periaortic metastases (both of the lumbar and mesenteric lymph system) also had metastases in the first- and second-line lymph node regions. Nine patients with periaortic metastases had upstream metastases only in the Müllerian first-line defense regions. Recurrent third-line lymph node metastases occurred in the periaortic region in one patient and in the mesorectum in one patient. The fairly constant pattern of lymph node metastasis of cervix carcinoma, FIGO stages IB-IIB, in terms of first-, second-, and third-line metastases enables ontogenetic nodal staging (oN1, 2, 3).

Table 6.3 shows a positive correlation between the incidence of lymph node metastases, the number of lymph node metastases, and the num-

Table 6.1 First-line lymph node metastases of FIGO stage IB-IIB cervix carcinoma

	External iliac (%)		Paravisceral (%)		Mesometrial[a] (%)		Common iliac (%)			
oT	Right	Left	Right	Left	Right	Left	Right	Left	Presacral (%)	Total number of cases
1	5	32	17	10	31	7	–	–	–	41
2	10	25	28	25	8	5	–	–	–	40
3a	13.5	17	17	17	5	13.5	1.5	1.5	1.5	52

Numbers relate to 133 cases with lymph node metastases in a single anatomical region, as categorized
Results from 589 successive patients treated with TMMR/EMMR and iLND at the University of Leipzig and nine patients with pelvic relapses identified as lymph node metastases whose primaries were nodal negative
[a] Summarizes vascular mesometrium, vascular mesocolpos, and distal urogenital mesentery, the latter as a fusion zone to the internal iliac vessel system

Table 6.2 Single-site second-line lymph node metastases of FIGO stage IB-IIB cervix cancer related to a single site of first-line lymph node metastases

Site of first-line metastases	Site of second-line metastases	
Right side	Right common iliac	Presacrococcygeal
External iliac (6)	2	4
Paravisceral (5)	1	4
Mesometrial (3)	–	3
Left side	Left common iliac	Presacrococcygeal
External iliac (9)	5	4
Paravisceral (3)	1	2
Mesometrial (1)	–	1

Results from 589 successive patients treated with TMMR/EMMR and iLND at the University of Leipzig

Table 6.3 Relation of lymph node metastases to ontogenetic local stage (oT) in cervix carcinoma FIGO stages IB-IIB

oT stage	*n*	pN1 (%)	pM1 (LYM) (%)	Number of metastatic first-line regions	
				Median	Mean
1	228	11	1	1 (1–2)	1.3 ± 0.5
2	123	40	8	2 (1–4)	1.8 ± 0.9
3a+	41	83	27	3 (1–5)	2.9 ± 1.3

Results from 385 successive patients treated with TMMR/EMMR and iLND at the University of Leipzig

ber of involved nodal sites with the state of local tumor progression expressed as oT stage.

6.5 Regional Progression of Endometrial Carcinoma

The lymph node hierarchy of the lymphatic network surveilling the corporal Müllerian subcompartment, i.e., the endometrium and myometrium, is mainly determined by the upper pathway toward the iliac lymph territory, described in detail above. The lymphatic drainage of the uterine fundus additionally follows the ovarian vessel system via its uterine rami to the mesenteric periaortic lymph nodes. Therefore, this lymph node region is also first line for endometrial cancer infiltrating the uterine fundus.

From the analysis of 135 patients with endometrial cancer treated with peritoneal mesometrial resection and lymph collector-guided first-line lymph node dissection and, if nodal positive, followed by completing lymph node dissection, lymph node metastases were found in 16 cases (12%). Local cancers were restricted to the Müllerian compartment (oT1 and 2) in 11 patients. Seven of these had only metastases in the first-line node regions, detected by collector-guided lymph node dissection. One patient had metastases in the first- and second-line regions and three patients in the first-, second-, and third-line regions.

One of the patients with a locally advanced (oT > 2) tumor had only metastases in the iliac first-line regions, while another one exhibited metastases exclusively in the mesenteric first-line regions. The remaining oT > 2 tumors metastasized into the first- and second-line lymph node regions ($n = 1$) and into the first-, second-, and third-line regions ($n = 2$). No patients with negative first-line nodes, as determined using the collector-guided method, had a regional lymph node relapse.

Although the number of lymph node positive cases is low due to the early detection of endometrial carcinoma in the majority of patients, the preliminary analysis is in line with the regional cancer field model as outlined above.

6.6 Regional Progression of Vaginal Carcinoma

Lymph node defense lines of the suprasinus vaginal subcompartment are equivalent to those of the cervix subcompartment, described above. However, additional intercalated lymph nodes in the mesocolpos may act as first-line nodes as well. Carcinoma of the sinus vagina can exhibit first-line metastases in the superficial inguinal region.

6.7 Regional Progression of Vulvar Carcinoma

The lymph nodes directly connected to the ontogenetic vulvar compartment as a tributary region represent the first-line nodes of vulvar carcinomas at ontogenetic stages oT1 and 2. These are the basin nodes of the inguinal lymph territory, located in the superomedial and inferomedial quadrants of the superficial femoral triangle. Intercalated lymph nodes in the collector vessels transgressing the labia majora and the inguinogenital skin bridge may also contribute to the first defense line. Nodes of the superolateral quadrant are connected downstream to the superomedial and inferomedial quadrants' nodes and therefore represent secondary defense lines. The inferolat-

eral quadrant of the superficial inguinal lymph basin contains lymph nodes that drain the superficial leg tissues ([1]). These nodes are neither directly nor indirectly connected to the vulvar compartment but belong to the same lymph territory. They receive lymph from the vulva compartment only if the lymph flow is reversed and therefore represent third-line nodes. As outlined before, deep inguinal lymph nodes are considered intercalated nodes of the iliac lymph compartment. Both the deep inguinal lymph nodes and the downstream lacunar nodes of the most caudal iliac basin are third line for vulvar carcinoma of ontogenetic stages 1 and 2 as well (Fig. 6.3c, d).

Local progression to oT3a extends the cancer field of vulvar carcinoma to the adjacent skin and subcutaneous fat, vagina, and urethra, as well as to erectile tissues, such as the glans clitoridis and bulbus vestibularis, rendering iliac basin nodes first line, in addition to superficial and deep inguinal nodes.

Our clinical data with 65 nodal-positive vulvar carcinomas from 212 successively treated patients support the conclusions from ontogenetic anatomy. In 14 of 15 patients (93%) with a single mapped lymph node metastasis, this was located in the superomedial quadrant of the superficial inguinal basin. In one of the 15 patients, a single lymph node metastasis was found in the inferomedial quadrant. The corresponding local carcinoma had emerged in the peripheral subcompartment of the ontogenetic vulva. The superomedial and inferomedial quadrants of the superficial inguinal lymph node basin are the first defense lines in oT stages 1 and 2 vulvar carcinoma.

The selective resection of the superomedial and inferomedial quadrants may therefore substitute a complete superficial inguinal lymph node dissection in situations of noninformative radionuclide- or dye-guided sentinel lymph node dissection in oT stages 1 and 2 vulvar carcinoma. The inferomedial quadrant mainly harbored second-line metastases. In the presence of metastases in the right superomedial quadrant, second-line metastases were identified in the ipsilateral inferomedial and superolateral quadrants in 60% and 40% of cases, respectively; left superomedial metastases were accompanied by second-line metastases in the ipsilateral inferomedial and superolateral quadrants in 33% and 67% of cases, respectively.

Third-line metastases were identified in the inferolateral quadrant in only one patient and in the lacunar regions of the iliac lymph territory in three patients of our series ($n = 212$). A regional recurrence following cancer field surgery of vulvar carcinoma proved the existence of intercalated lymph nodes in the labium majus.

Table 6.4 lists the correlation of the incidence of lymph node metastases, the number of metastases, and the number of involved nodal sites with the ontogenetic tumor stage (oT).

Table 6.4 Relation of lymph node metastases to ontogenetic stage (oT) in vulvar carcinoma

					Number of metastatic first-line	
oT stage	n^a	pN+ (%)	pM1(LYM) (%)	n^b	Regions	Nodes
1	58	4	–	7	9	12
2	42	44	2	12	16	27
3a+	24	71	8	18	33	53

[a] Results from 124 successive patients treated with VFR and iLND at the University of Leipzig

[b] Results from 37 successive nodal-positive patients treated with VFR and iLND at the Universities of Leipzig and Essen

References

1. Kubik S, Kretz O. Anatomie des Lymphgefäßsystems. In: Földi M, Földi E, Kubik S, editors. Lehrbuch der lymphologie. 6th ed. Munich: Urban & Fischer; 2005. p. 1–150.
2. Töndury G, Kubik S. Zur ontogenese des lymphatischen systems. In: Altmann HW, Büchner F, Cotttier H, Grundmann E, Holle G, Letterer E, et al., editors. Handbuch der allgemeinen pathologie. Berlin: Springer; 1972. p. 1–38.
3. van der Putte SC. The development of the lymphatic system in man. In: Advances in anatomy, embryology and cell biology, vol. 51. Berlin: Springer; 1975. https://doi.org/10.1007/978-3-642-66090-0.
4. Kimmig R, Aktas B, Buderath P, Rusch P, Heubner M. Intraoperative navigation in robotically assisted compartmental surgery of uterine cancer by visualisation of embryologically derived lymphatic networks with indocyanine-green (IGC). J Surg Oncol. 2016;113:554–9. https://doi.org/10.1002/jso.24174.
5. Kimmig R, Iannaccone A, Aktas B, Buderath P, Heubner M. Embryologically based radical hysterectomy as peritoneal mesometrial resection (PMMR) with pelvic and para-aortic lymphadenectomy for loco-regional tumor control in endometrial cancer: first evidence for efficacy. Arch Gynecol Obstet. 2016;294:153–60. https://doi.org/10.1007/s00404-015-3956-y.
6. Kimmig R, Rusch P, Buderath P, Aktas B. Aortic utero-ovarian sentinel nodes and left infrarenal aortic lymph node dissection by ICG supported navigation. Gynecol Oncol Rep. 2017;20:22–3. https://doi.org/10.1016/j.gore.2017.02003.
7. Kimmig R, Buderath P, Rusch P, Mach P, Aktas B. Early ovarian cancer surgery with indocyanine-green-guided targeted compartmental lymphadenectomy (TCL, pelvic part). J Gynecol Oncol. 2017;28:e68. https://doi.org/10.3802/jgo.2017.28.e68.

Part II

Clinics: Cancer Field Surgery

7 Ontogenetic Staging of Gynecologic Cancer: Diagnostic Management and Findings

Like in conventional cancer staging, the individual tumor's ontogenetic stage (oT) is primarily determined clinically. In cases of operative treatment for locoregional tumor control, histopathologic assessment via intraoperative frozen section investigation, followed by an examination of the surgical specimen, determines the definitive tumor stage. The goal of ontogenetic staging is the identification of the local cancer field of the neoplasm according to the principles introduced in Chap. 2, i.e., assigning tissues infiltrated by the tumor to the anatomical compartments defined by the postphylotypic differentiation trajectory of the cell type from which the cancer originated. *Ontogenetic tumor stages* are classified into oT1, oT2, oT3a, oT3b, and oT4, corresponding to whether the malignant tumor is confined to the subcompartment, compartment, or the mature tissue derivatives of the three preceding morphogenetic fields of the normal cell type's trajectory.

Ontogenetic nodal staging indicates the metastatic occupation of the three lymph node defense lines of an ontogenetic compartment, as described in Chaps. 5 and 6. The oN1, oN2, and oN3 nodal stages designate lymph node metastases in, respectively, the first-, second-, and third-line lymph node regions related to the tissue compartment of the carcinoma's origin.

Diagnostic methods to be applied for ontogenetic cancer staging depend on the tumor type and the state of its progression, as well as on patient history and characteristics. The diagnostic armamentarium includes gynecologic inspection, palpation, radiologic and nuclear medicine imaging, endoscopy, and directed biopsies. The following management recommendations relate to the ontogenetic local and nodal staging of cervix, vaginal, endometrial, and vulvar carcinomas.

7.1 Cervix Carcinoma

Clinical oT staging of cervical carcinoma is determined through a disease-specific gynecological examination, which is optimally performed under anesthesia. Inspection methods are applied, including the use of a vaginal speculum; bimanual vaginal and rectovaginal palpation; cystoscopy; and, in rare cases, rectoscopy; eventually, diagnostic laparoscopy is also applied. Pelvic magnetic resonance imaging (MRI) should supplement the findings from the examination conducted under anesthesia. The role of sonography for ontogenetic local staging cannot be judged by the authors. Only in advanced stages (i.e., oT3b and oT4) or in the case of oN3, or when multiple macrometastases are detected by pelvic MRI is an investigation for distant metastases, preferably by positron emission tomography-computed tomography (PET/CT), indicated.

The inspection report should detail the appearance of the ectocervix and—if the neoplastic tissue is visible—describe the tumor's manifestation

M. Höckel et al., *Cancer Field Surgery in Gynecologic Oncology*,
https://doi.org/10.1007/978-3-031-83030-3_7

as exophytic, endophytic, ulcerative, or necrotic. It should provide an estimation of the tumor size in the transverse and frontal planes. The involvement of the vagina should be specified by location and extent.

Bimanual vaginal and rectovaginal palpation is performed with regard to the pelvic side to be assessed: the examiner's right hand for evaluating the midpelvis and right lateral pelvis and the left hand for the midpelvis and left lateral pelvis. Palpation findings to be reported are the estimated tumor size in the sagittal plane; the size, contour, and axis of the uterine corpus; and the presence of adnexal masses. Most importantly, the movability of the uterus should be classified bilaterally as normal, modestly limited, severely limited, or completely abolished (i.e., the uterus is fixed to the pelvic wall and floor). Likewise, both the vesicovaginal septum and the bilateral parametria should be graded as slightly, significantly, or completely indurated, shortened and thickened. Nodular structures within the parametria or at the pelvic walls should be documented as well. Finally, the palpated relation of the diseased genital tract to the rectum should be described. The examination under anesthesia includes cystoscopy in all cases except FIGO stage IB1, checking for discrete changes such as asymmetries of the trigone and of the ureteral ostia, local mucosal edema and atypical microvessels to massive alterations such as bullous edema of the mucosa, gross neoplastic tissue appearance or fistula formation. Rectoscopy is only indicated in palpable rectal tumor involvement and for diagnosing fistulae between the rectum and uterus or vagina. To confirm suspected peritoneal involvement, diagnostic laparoscopy is necessary.

It is recommended to have high-resolution pelvic MRI series of T2-weighted transverse and sagittal sections displayed in the operating room during the examination. The gynecologic oncologist assessing the patient's tumor should be able to evaluate her pelvic MRI scans with reference to the ontogenetic anatomy.

All information from inspection, palpation, cystoscopy (eventually rectoscopy and laparoscopy), and pelvic MRI should be integrated to determine the clinical ontogenetic tumor and nodal stage of the cervical carcinoma. The histopathological proof of malignancy, usually from the tissue obtained via core biopsies, is mandatory.

7.1.1 Histopathological Assessment

In addition to diagnosing cervix carcinoma from an incisional core or excisional cone biopsy, the role of the pathologist is essential during therapeutic surgery. Frozen section evaluation is necessary for first-line lymph node regions and, in the case of detection of metastases in oT1 and 2 stages, for third-line aortic bifurcation nodes as well (see Chap. 6). Considering local tumor progression, intraoperative investigation of the uterine corpus and the colpotomy site should be done to ascertain the adequacy of cancer field surgery for locoregional tumor control. The clinical and histopathological findings for each ontogenetic stage are as follows.

7.1.2 Stage oT1 Cancer Field

The tumor is limited to the cervical stroma.

7.1.2.1 Clinical Findings

By inspection, no vaginal involvement of the tumor can be noticed. Palpation reveals a completely mobile uterus without induration, shortening, or thickening of the parametria and the vesicovaginal or rectovaginal septum. The pelvic MRI in the T2 mode shows an uninterrupted dark cervical border zone in both transverse and sagittal planes and no evidence of tumor invasion of the uterine corpus (Fig. 7.1a, b). Tumor size can be more accurately determined by MRI than by clinical examination.

7.1.2.2 Histopathology

All microscopic tumor is restricted to the cervical stroma. The tumor front may reach but does not involve the cervical adventitia (Fig. 7.1c).

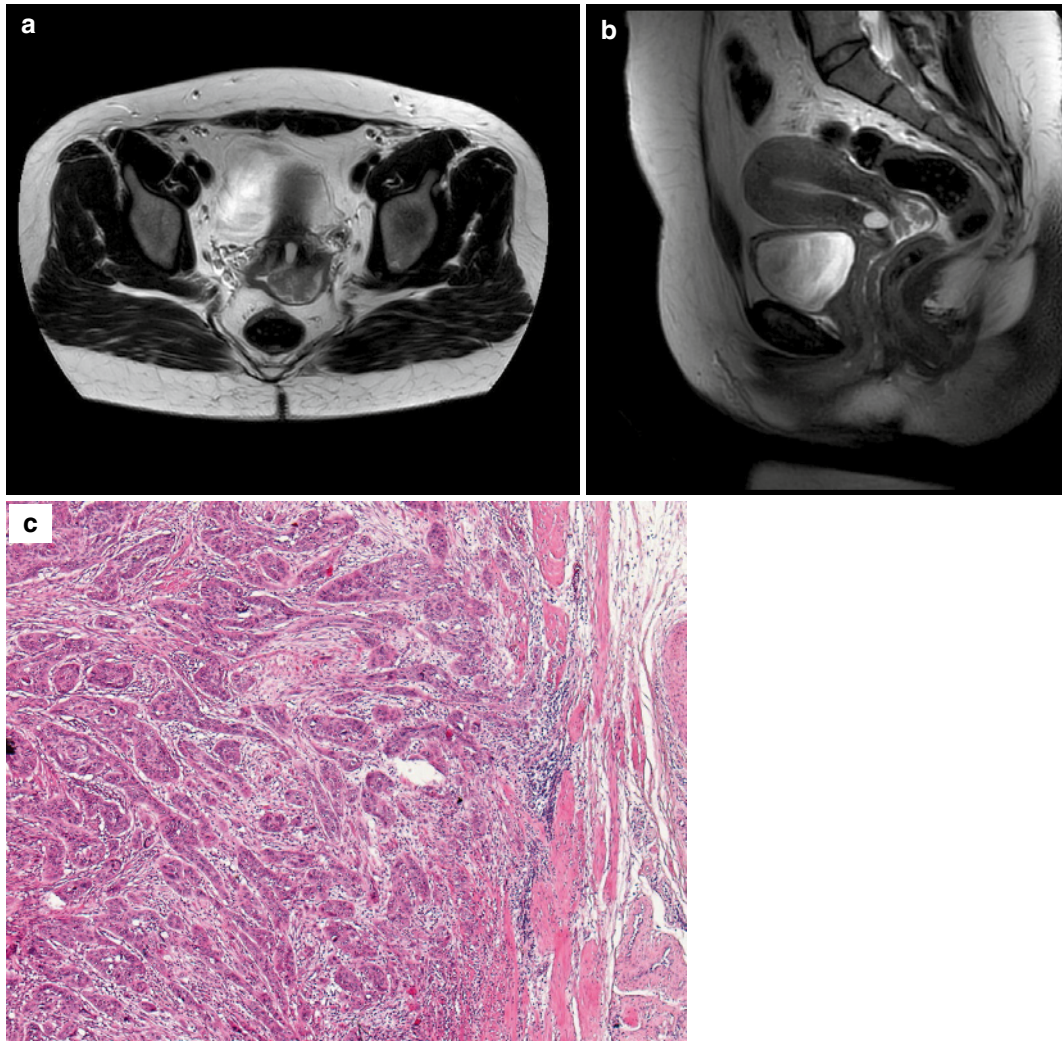

Fig. 7.1 oT1 cervix carcinoma. T2-weighted transverse (**a**) and sagittal (**b**) MRI scans show a tumor confined to the cervix. The main tumor mass is exophytic. Histopathological evaluation confirms malignant cells restricted to the cervical stroma (**c**)

7.1.3 Stage oT2 Cancer Field

The tumor is limited to the Müllerian compartment. In addition to the cervical stroma, the vagina, Müllerian adventitia, or corpus uteri are infiltrated either singly or in any combination. The uterine tubes are also part of the compartment; however, their distance to the cervix is usually too far to be involved at the oT2 stage.

7.1.3.1 Clinical Findings

Neoplastic tissue may be ascertained by speculum inspection at the ectocervix continuous or discontinuous with the vaginal mucosa. Suspicion of vaginal involvement should be ascertained by histopathological diagnosis from a targeted biopsy. Palpation may sense a modestly limited unilateral movability of the uterus, concomitantly with a beginning induration of the ipsilateral

parametrium and paracolpos compatible with an infiltrated Müllerian adventitia. No thickening of the vesicovaginal and vesicocervical septum should be obvious.

Cystoscopy should verify normal findings. Pelvic MRI is well suited for detecting an infiltration of the uterine corpus, but an accurate assessment of the early parametrial involvement of cervix cancer is not possible (Figs. 7.2a, b and 7.3a, b).

7.1.3.2 Histopathology

Invasion of the vagina either by mucosal or submucosal tumor propagation may be detected (Fig. 7.2c). Likewise, involvement of the uterine corpus can be manifest at the endo- or myometrium (Fig. 7.3c). Importantly, with respect to the paracervical tissue, the pathologist must discriminate between tumor infiltration of the cervical adventitia and of the abutting fatty tissue-containing mesometrium. Both situations repre-

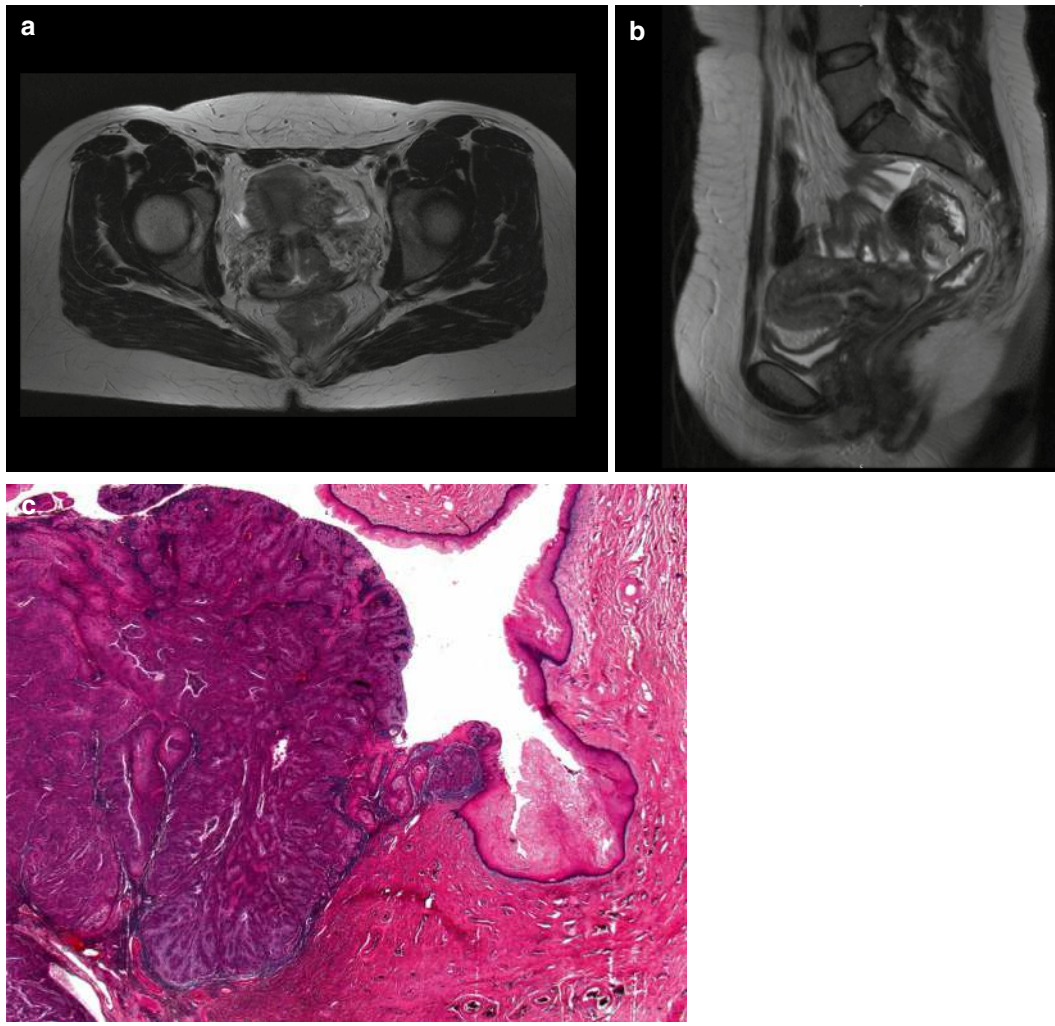

Fig. 7.2 oT2 cervix carcinoma with vaginal involvement. T2-weighted transverse (**a**) and sagittal (**b**) MRI scans show neoplastic tissue in the cervical stroma and adjacent vagina. Histopathology confirms the continuous spread of the cervix cancer to the vagina (**c**)

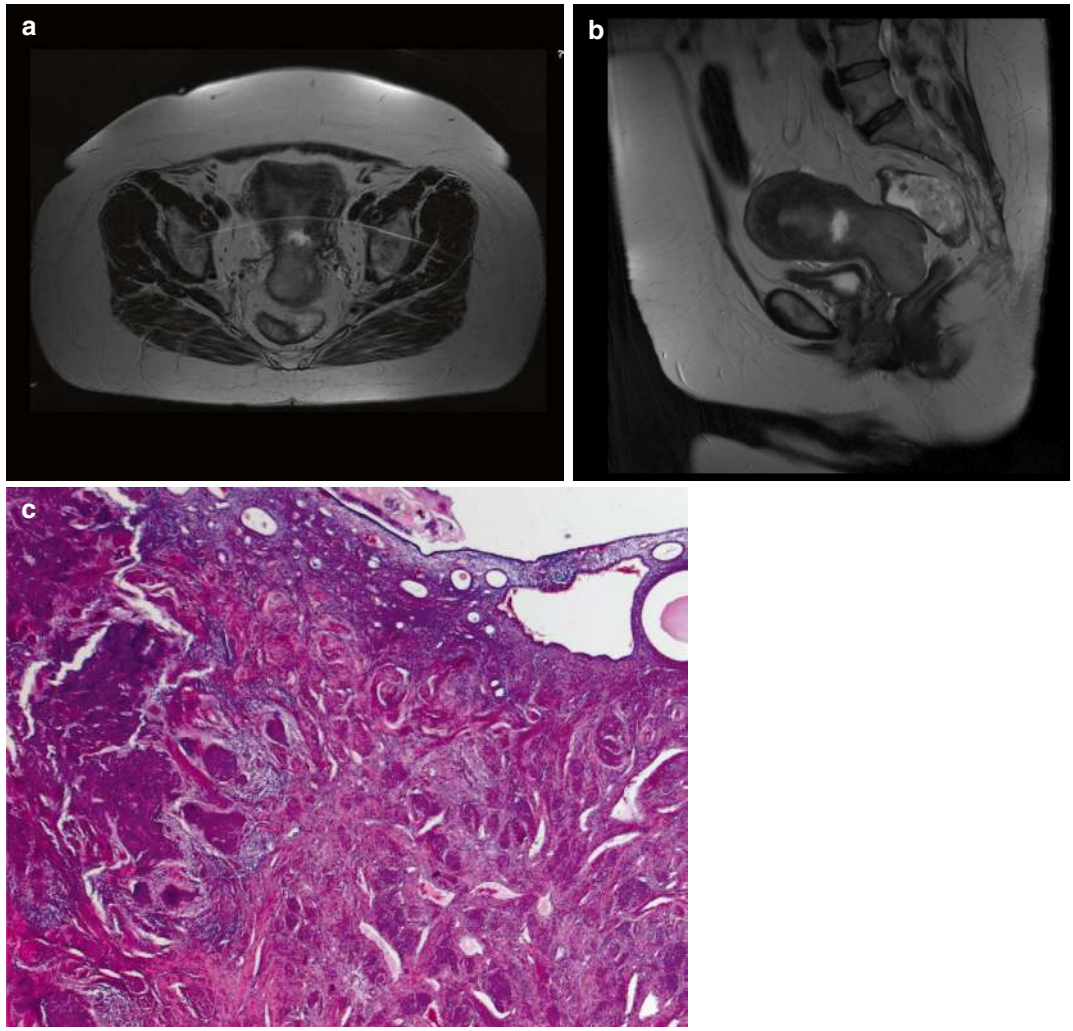

Fig. 7.3 oT2 cervix carcinoma with infiltration of the uterine corpus. T2-weighted transverse (**a**) and sagittal (**b**) MRI scans indicate the involvement of the uterine corpus by the cervix carcinoma. Histopathology demonstrates cervix carcinoma adjacent to the endometrium (**c**)

sent a pT2b stage but indicate different oT stages. To stage a cervix cancer as oT2, the most peripheral cancer cell collectives in the horizontal plane must be restricted to the cervical adventitia (Fig. 7.4). Lymphangiotic or hemangiotic tumor foci preceding the invasion front do not influence pT staging but are relevant in the oT staging system.

An oT2 stage demands that lymphangiotic and hemangiotic cancer cell clusters be restricted to the Müllerian compartment.

7.1.4 Stage oT3a Cancer Field

The cancer infiltrates any anatomical compartment derived from the Müllerian duct morphogenetic unit, including the bladder adventitia and proximal bladder mesenteries, paraurethral tissues, vulva, vascular and ligamentous mesometria and mesocolpoi, genital serosa, and mesenteries in addition to the Müllerian compartment.

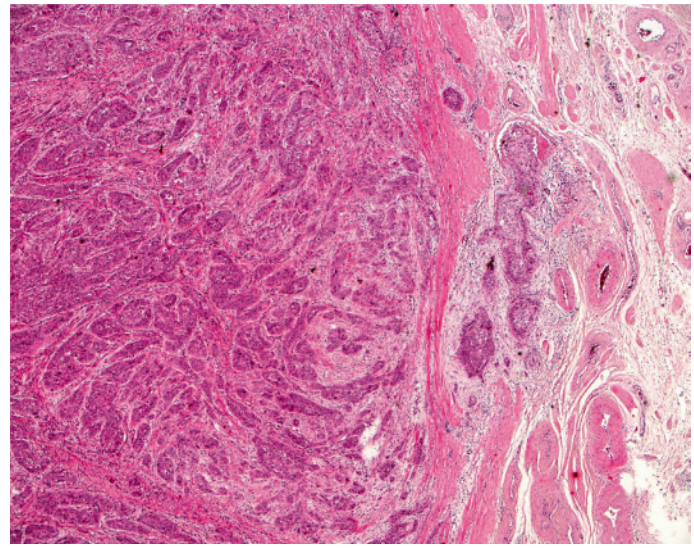

Fig. 7.4 Photomicrograph of an oT2 cervix carcinoma infiltrating the Müllerian adventitia but not the adjacent mesometrium, indicating a pT2b stage

7.1.4.1 Clinical Findings

Infiltration of the vulva by cervix carcinoma diagnosed from inspection confirms an oT3a stage. However, this situation is rare due to the long distance from the cervix. Most frequently, the oT3a stage is ascertained by systematic palpation, as described above. Stage oT3a cervix carcinomas severely limit the movability of the uterus, concomitantly with significant induration (shortening or thickening) of the parametrium, paracolpos, and vesicovaginal septum, indicating the infiltration of the vascular and ligamentous mesometria and mesocolpoi.

Cystoscopy may reveal a structural difference between both sides of the trigone as irregular prominence of the ureter ostium, indicating involvement of the bladder adventitia. Atypical microvessels can be identified at this prominent site as well. As mentioned for the oT2 stage already, pelvic MRI is currently not sufficiently accurate to diagnose mesometrial involvement in general. However, in addition to the findings from palpation, MRI may be informative (Figs. 7.5a, b, 7.6a, b, and 7.7a, b).

7.1.4.2 Histopathology

Microscopic verification of cervical cancer infiltration of the mesometrium, mesocolpos, Müllerian (sub)serosa, and bladder adventitia and mesentery is the mainstay for diagnosing an oT3a stage. The demonstration of malignant cells in these tissues, both in the interstitium and intravasally in the lymphatics and blood vessels, is indicative (Fig. 7.5c–e). Whether they are continuous with the main tumor mass or discontinuous does not influence ontogenetic staging.

7.1.5 Stage oT3b Cancer Field

The cancer infiltrates any compartment matured from the primordial genital tract morphogenetic field. These include the bladder muscle, with or without mucosal involvement; the bladder peritoneum; the distal urogenital mesenteries and umbilical arteries; the endopelvic fascia; the ovaries; and the paramesenteric retroperitoneum, subperitoneum, and peritoneum with the pararectal fascia, in addition to the oT3a cancer field.

7.1.5.1 Clinical Findings

As with earlier ontogenetic stages, the cervical cancer may infiltrate the vagina and the vulva. Palpation detects complete fixation to the pelvic sidewall or floor as the most frequent indication of an oT3b stage. Broad unilateral or bilateral induration of the parametria and paracolpoi can be traced to the laterocaudal fixation site. Vesicovaginal septum thickening is nearly always noticed. The rectum is often fixed to the tumor; however, rectal mucosa is observed as smooth and mobile.

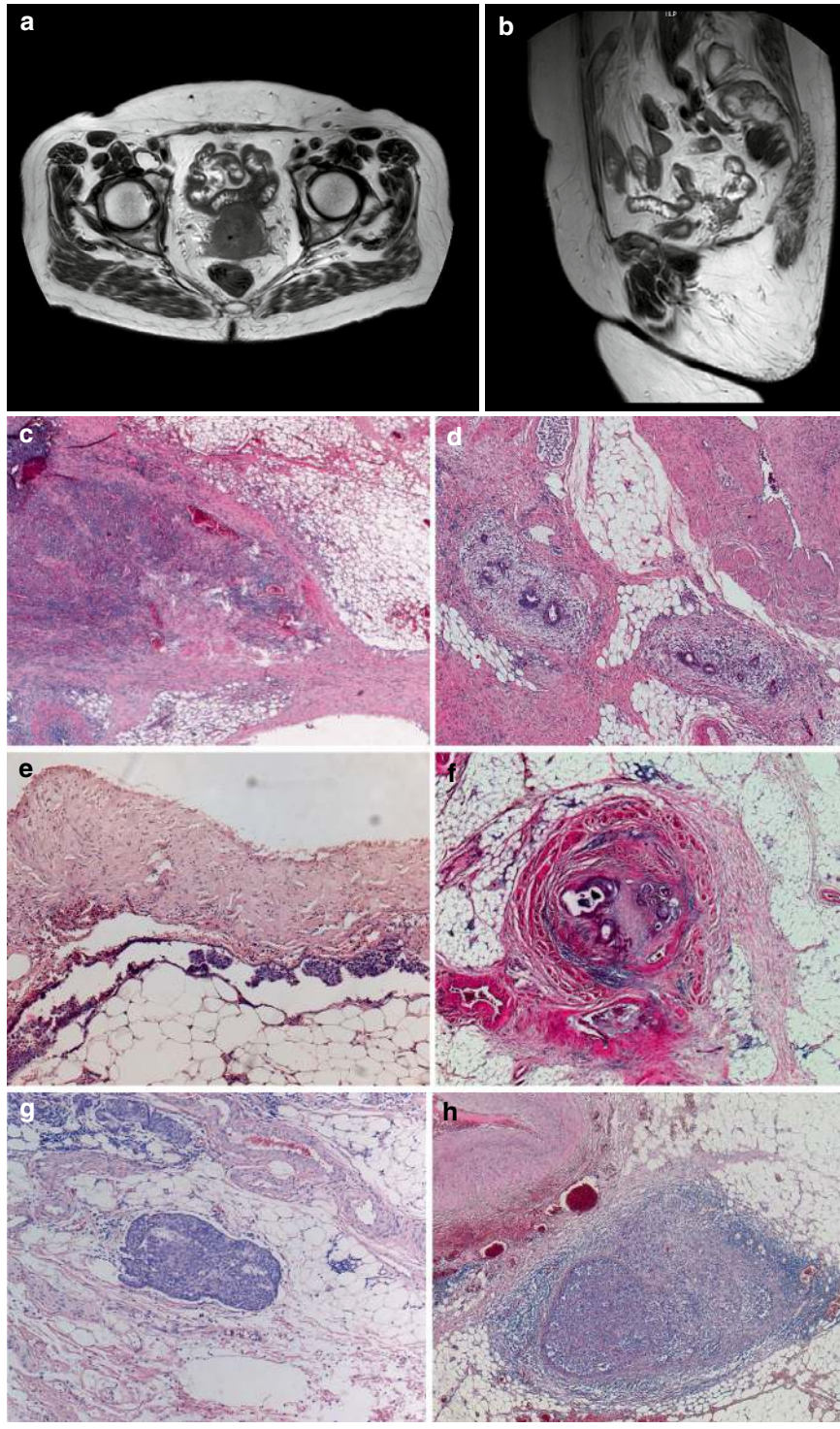

Fig. 7.5 oT3a cervix carcinoma infiltrating the vascular mesometrium. T2-weighted transverse (**a**) and sagittal (**b**) MRI scans demonstrate cervix cancer infiltrating the right vascular mesometrium. Histopathology is necessary to confirm an oT3a stage through the verification of cancer cells in the mesometrium, through either continuous spread in squamous cell carcinoma (**c**) and adenocarcinoma (**d**) or discontinuous spread in lymphatic spaces (**e**) or blood vessels (**f**). The carcinoma can evade lymphatic vessels (**g**) or intercalated lymph nodes (**h**) and propagate in the mesometrial tissue

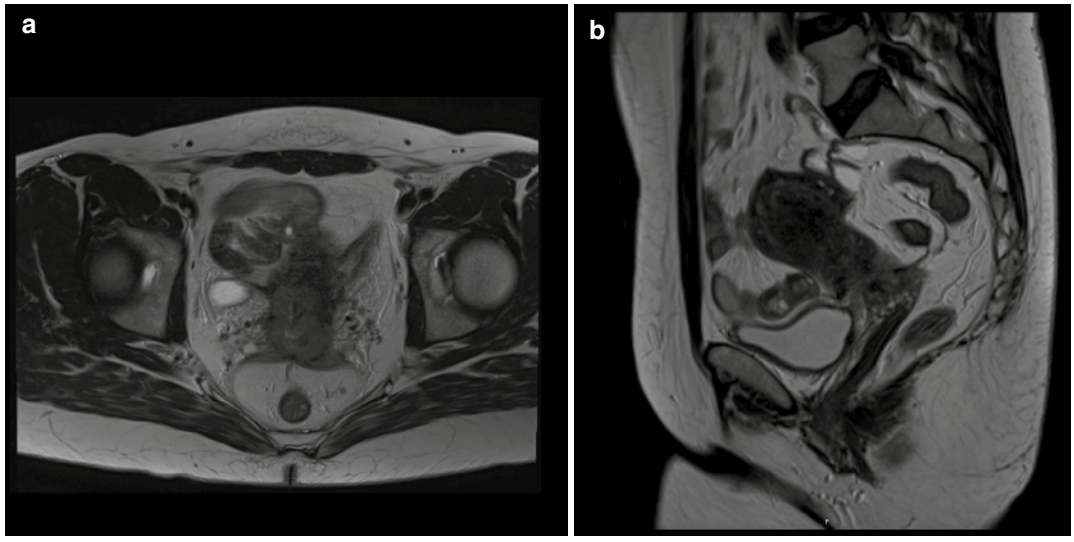

Fig. 7.6 oT3a cervix carcinoma infiltrating the ligamentous mesometria and rectovaginal septum. T2-weighted transverse (**a**) and sagittal (**b**) MRI scans show a cervix carcinoma spreading dorsolaterally through the ligamentous mesometria and mesocolpoi at both sides. Infiltration of the cervical (sub)serosa and bladder adventitia can also be noted

Cystoscopy may indicate either focal or bullous edema of the bladder mucosa, atypical vessels, or gross tumor infiltration. With rectoscopy, no signs of mucosal infiltration, stenosis, or irregular wall structure are found.

MRI shows extracervical tumor spread up to the border of the parietal (somatic) retro-, subperitoneum, and peritoneum; endopelvic fascia; and mesorectum, but there is no evidence of infiltration of these tissues (Figs. 7.8a, b, 7.9a, b, and 7.10a, b). Unilateral or bilateral ureteral dilatation is often present but not obligatory (Fig. 7.9a, b). Tumor involvement of the urethral and bladder wall with or without infiltration of the mucosal layer is often obvious with MRI (Figs. 7.11a, b, 7.12a, b). Bullous edema of the vesical mucosa can be ascertained (Fig. 7.11a, b). Gross ovarian involvement may be noticed. Occasionally, peritoneal thickening is seen at the bladder dome and in the posterior pelvis, but bowel involvement has to be excluded. In order to specify suspected peritoneal infiltration, it is necessary to perform diagnostic laparoscopy and to take biopsies at defined locations.

7.1.5.2 Histopathology

There is no unequivocal histopathological correlation for pelvic wall fixation. However, tumor infiltration of the umbilical artery is a histopathological correlate (Fig. 7.8c). Hydronephrosis is not associated with malignant infiltration of the mesureter or ureter (Fig. 7.9c). Infiltration of the muscularis or mucosa layer of the bladder confirms the oT3b stage (Figs. 7.11c and 7.12c). The detection of cervix carcinoma infiltration in the endopelvic fascia, bladder peritoneum, and ovarian stroma is indicative of oT3b (Fig. 7.13).

7.1.6 Stage oT4 Cancer Field

The most advanced ontogenetic local tumor stage is evident if the cancer infiltrates tissues derived from the mesonephric system morphogenetic field, in addition to the oT3b cancer field. These are most frequently the mesorectum and rectum with or without mucosal involvement, as well as the mesureter and ureter. oT4 cervix carcinomas

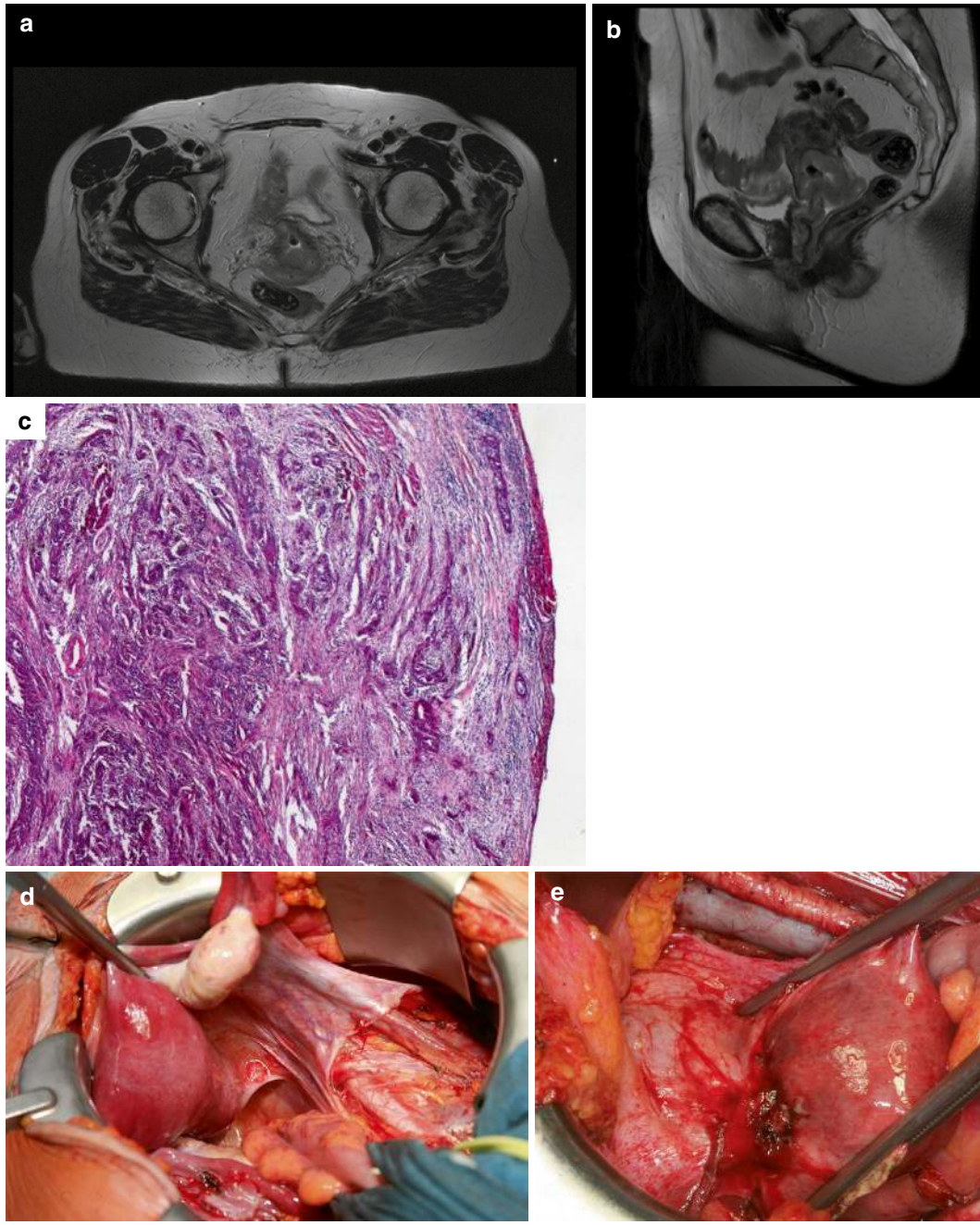

Fig. 7.7 oT3a cervix carcinoma infiltrating the cervical (sub)serosa. T2-weighted transverse (**a**) and sagittal (**b**) MRI scans demonstrate a carcinoma involving the (sub) serosa of the dorsal cervix without evidence of infiltration of the rectal peritoneum and mesorectum. Histopathology confirms infiltration of the cervical subserosa (**c**). Intraoperative visualization of cervix carcinoma infiltrating the right peritoneal/ligamentous mesometrium (**d**) and the left anterior uterine serosa and bladder adventitia (**e**)

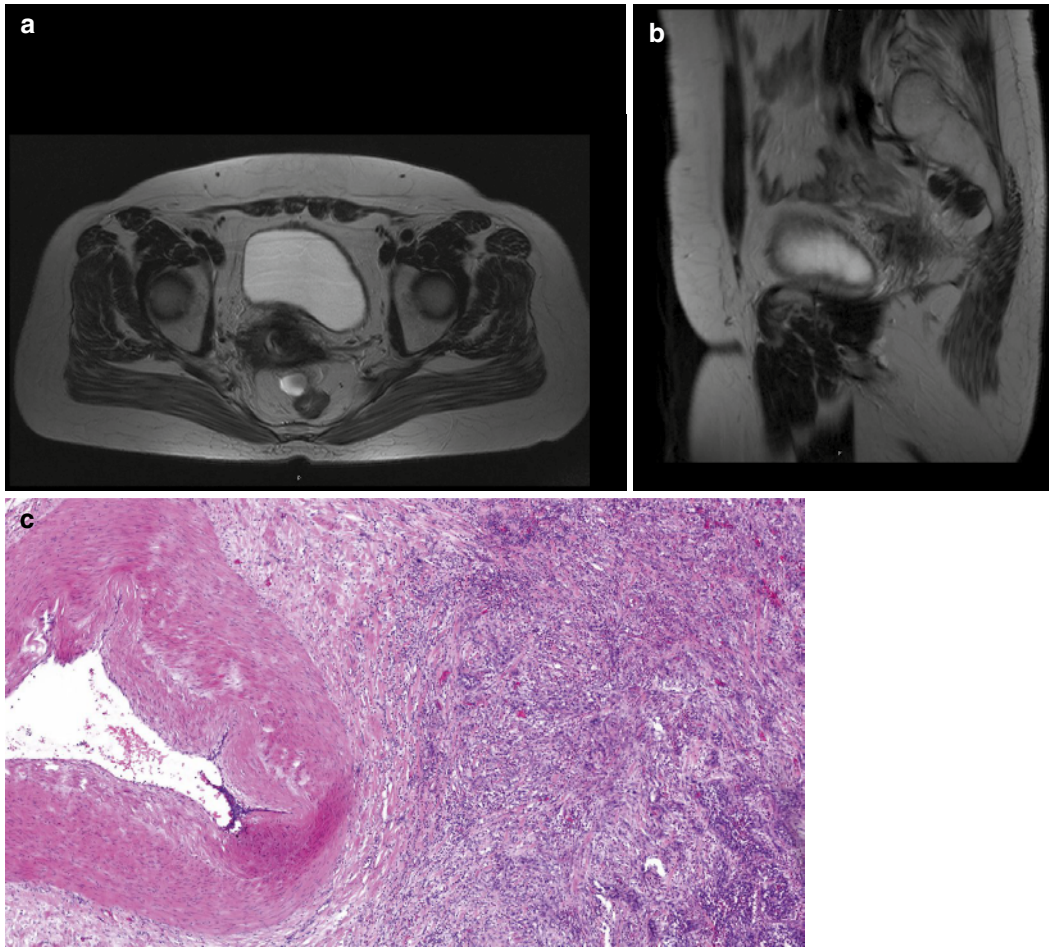

Fig. 7.8 oT3b cervix carcinoma infiltrating the right vascular mesometrium up to the border of the parietal (somatic) subperitoneum fixing the uterus broadly at the right pelvic sidewall. T2-weighted transverse (**a**) and sagittal (**b**) MRI scans demonstrate tumor formations approaching the border of the right somatic subperitoneum. The left proximal vascular mesometrium and the right ligamentous mesometrium appear to be infiltrated by the tumor as well. Histopathology demonstrates the early infiltration of the right proximal umbilical artery (**c**).

can infiltrate any pelvic and abdominal tissue, except the spinal column and adjacent autochthonous musculature.

7.1.6.1 Clinical Findings

Rectal and mesorectal tumor infiltration can be palpated and confirmed by core biopsies. Pelvic MRI is useful to detect these and other signs of the oT4 stage (Figs. 7.14a, b, 7.15a, b, 7.16a, b, 7.17a, b, and 7.18a, b). Enlarged mesorectal lymph nodes often represent metastases and indicate mesorectal or rectal tumor infiltration. Local spread to the intestinal or parietal peritoneum detected by diagnostic laparoscopy confirms an oT4 stage as well. Mesureteral and ureteral tumor infiltration often but not obligatorily causes ureteral constriction and hydronephrosis. However, sciatic pain is indicative of

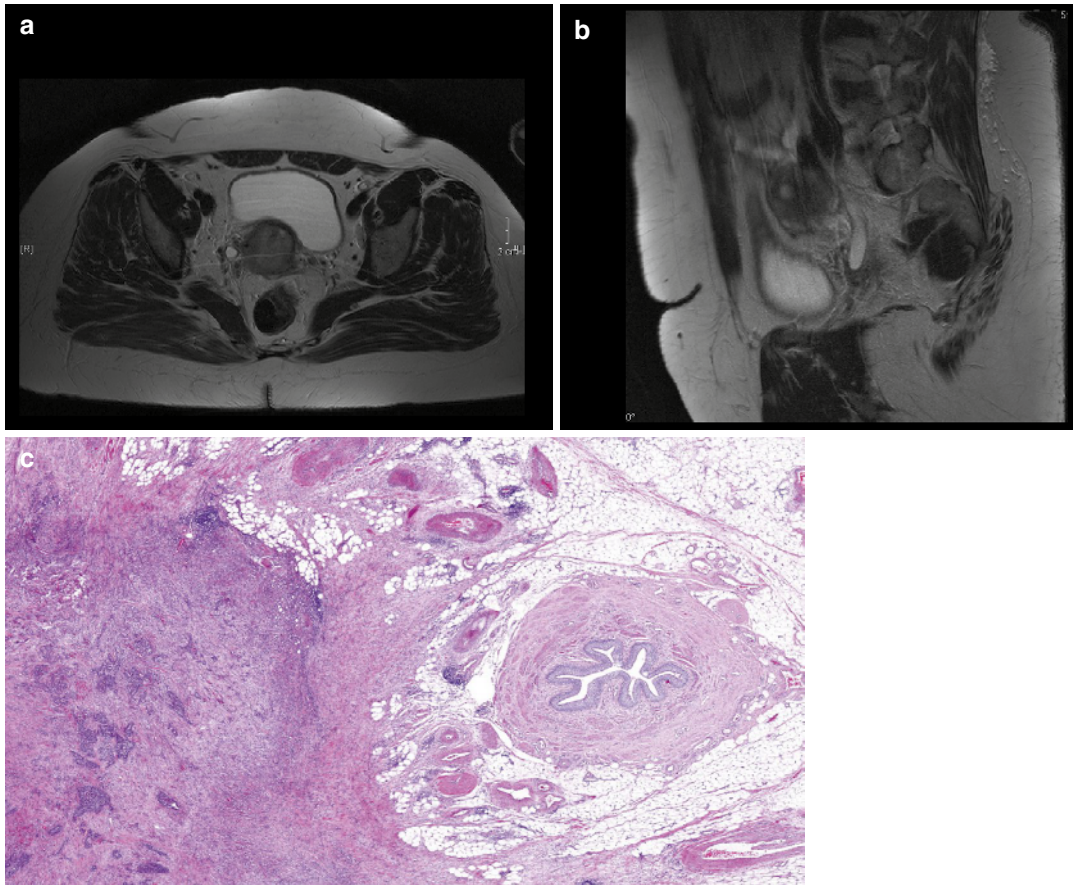

Fig. 7.9 oT3b cervix carcinoma infiltrating the right vascular mesometrium up to the border of the parietal (somatic) subperitoneum, causing hydronephrosis. T2-weighted transverse (**a**) and sagittal (**b**) MRI scans show tumor extension toward the right vessels of the bladder mesentery, encasing and obliterating the ureter. The dilated right proximal ureter is visible. Histopathology shows that the ureter and mesureter are not yet invaded by the carcinoma (**c**)

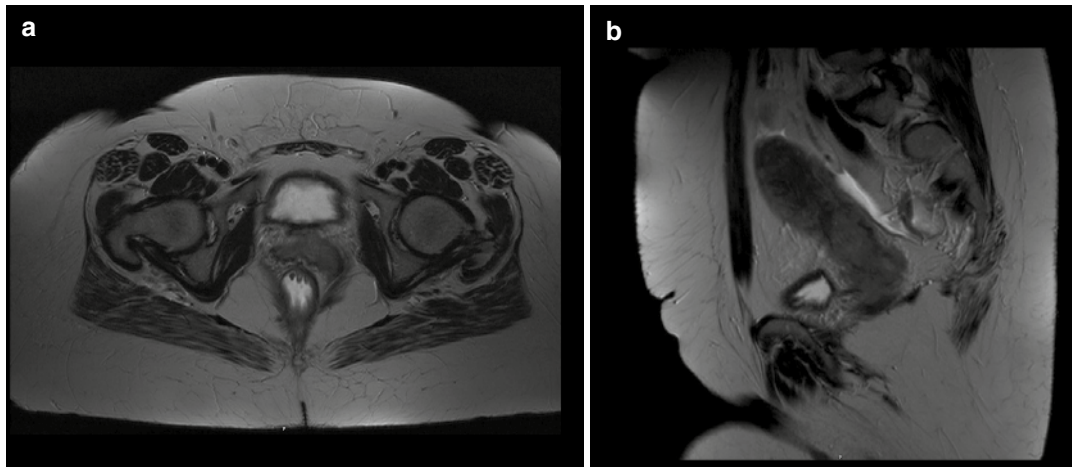

Fig. 7.10 oT3b cervix carcinoma infiltrating the left mesocolpos up to the parietal endopelvic fascia. T2-weighted transverse (**a**) and sagittal (**b**) MRI scans are compatible with the fixation of the vaginal tumor extension at the left levator ani muscle

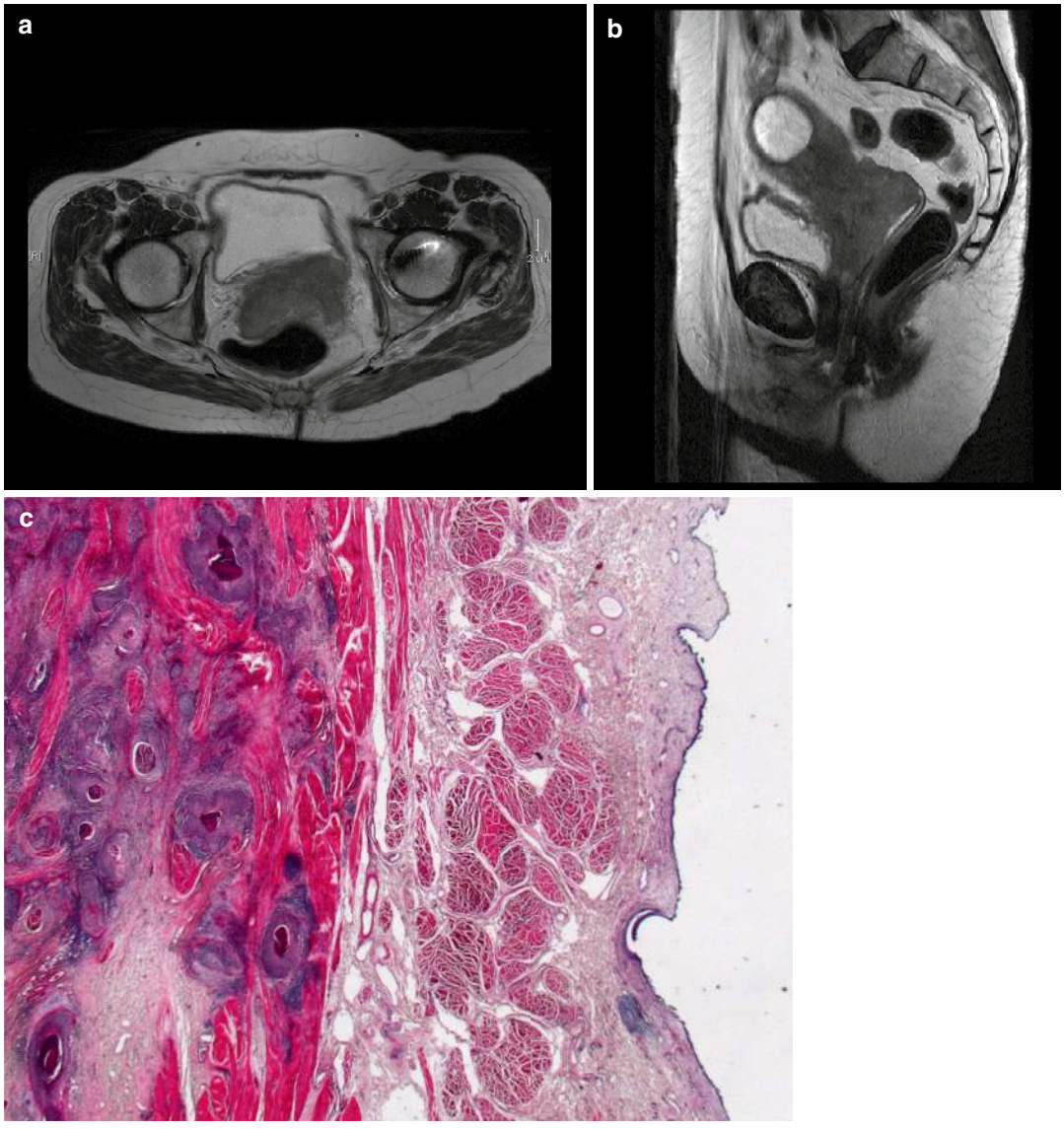

Fig. 7.11 oT3b cervix carcinoma infiltrating the bladder muscle above the bladder neck. T2-weighted transverse (**a**) and sagittal (**b**) MRI scans show tumor involvement of the supratrigonal bladder wall and bullous edema of the adjacent bladder mucosa. Histopathology proves the infiltration of the external vesical muscularis layer (**c**)

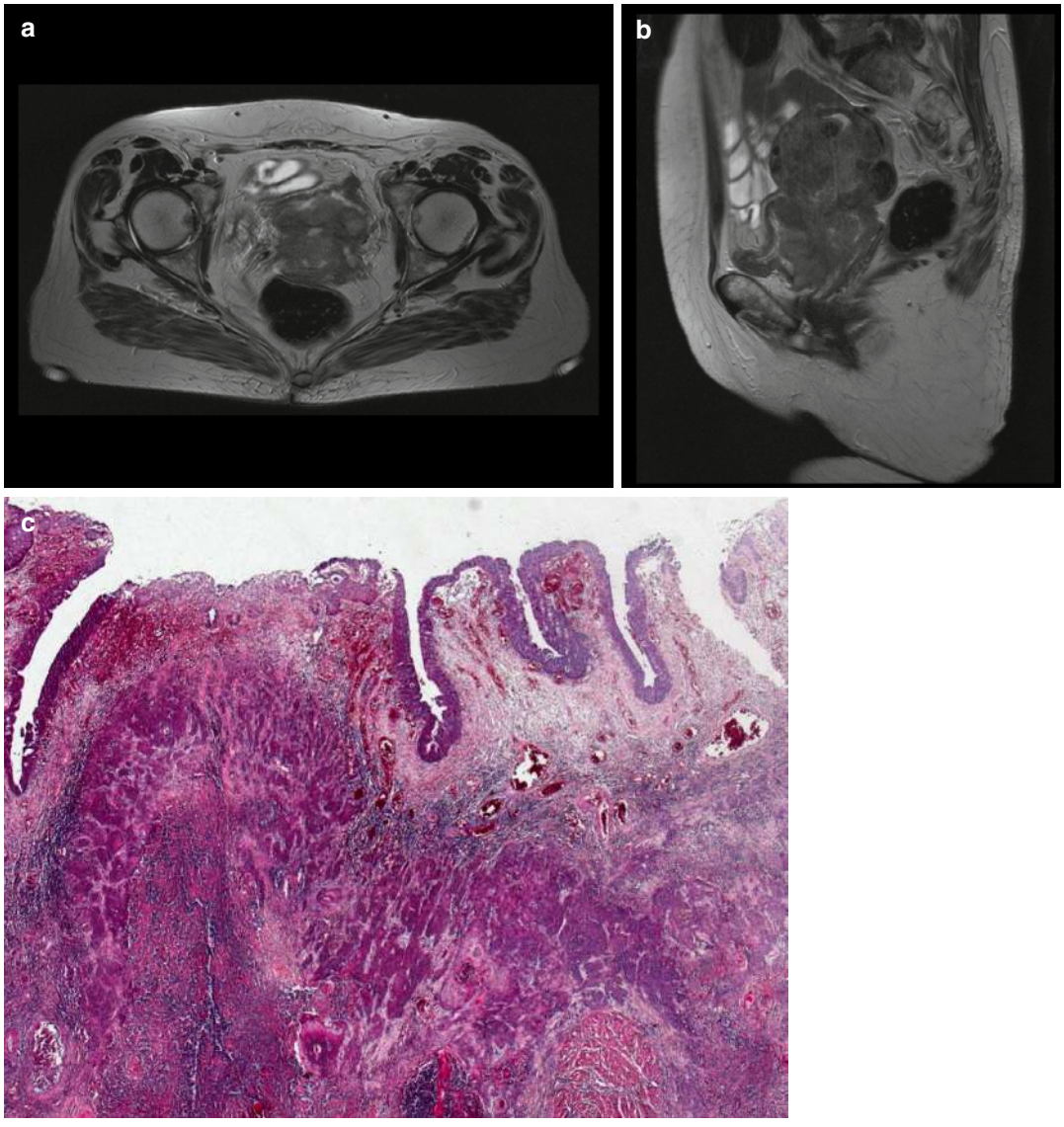

Fig. 7.12 oT3b cervix carcinoma infiltrating the bladder mucosa. T2-weighted transverse (**a**) and sagittal (**b**) MRI scans demonstrate the continuous spread of cervical carcinoma through the complete posterior bladder wall. Histopathology confirms the infiltration of the bladder mucosa (**c**)

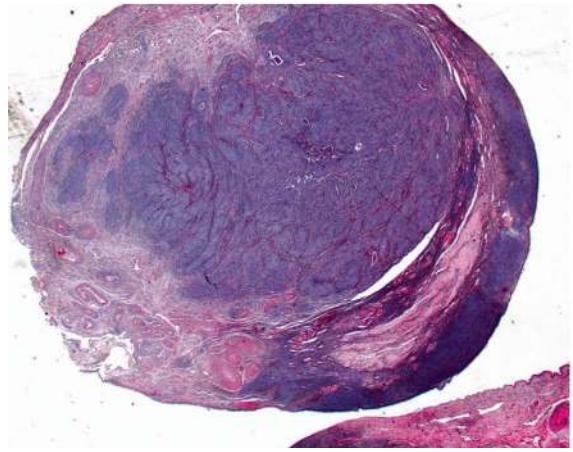

Fig. 7.13 Histopathological correlate of oT3b stage cervix carcinoma. Infiltration of the ovary correlates of oT3b stage cervix carcinoma. Infiltration of the ovary

infiltration of the parietal (somatic) subperineum or even of somatic pelvic wall structures. Likewise, (malignant) leg edema or thrombosis associated with tumor fixation at the ipsilateral pelvic sidewall demonstrates the involvement of the somatic subperineum.

7.1.6.2 Histopathology

The identification of cervical cancer cells in any of the abdominopelvic structures beyond the oT3b cancer field proves an oT4 stage. Figures 7.14c, 7.15c, 7.16c, Fig. 7.18c and 7.19a, b represent histopathological findings with cervical carcinoma infiltrating the oT4 cancer field.

7.1.7 Ontogenetic Regional Staging

Lymph node metastases can be diagnosed preoperatively by MRI (Fig. 7.20a, b). However, definitive proof is always obtained from histopathological assessment during and after cancer field surgery, as described by the treatment algorithms in Chap. 12. The ontogenetic nodal stage (oN1, oN2, oN3) is determined by the final histopathological report, which allocates lymph node metastases to first-, second-, and third-line regions, as described in Chap. 6. Extracapsular spread of lymph node metastases should also be

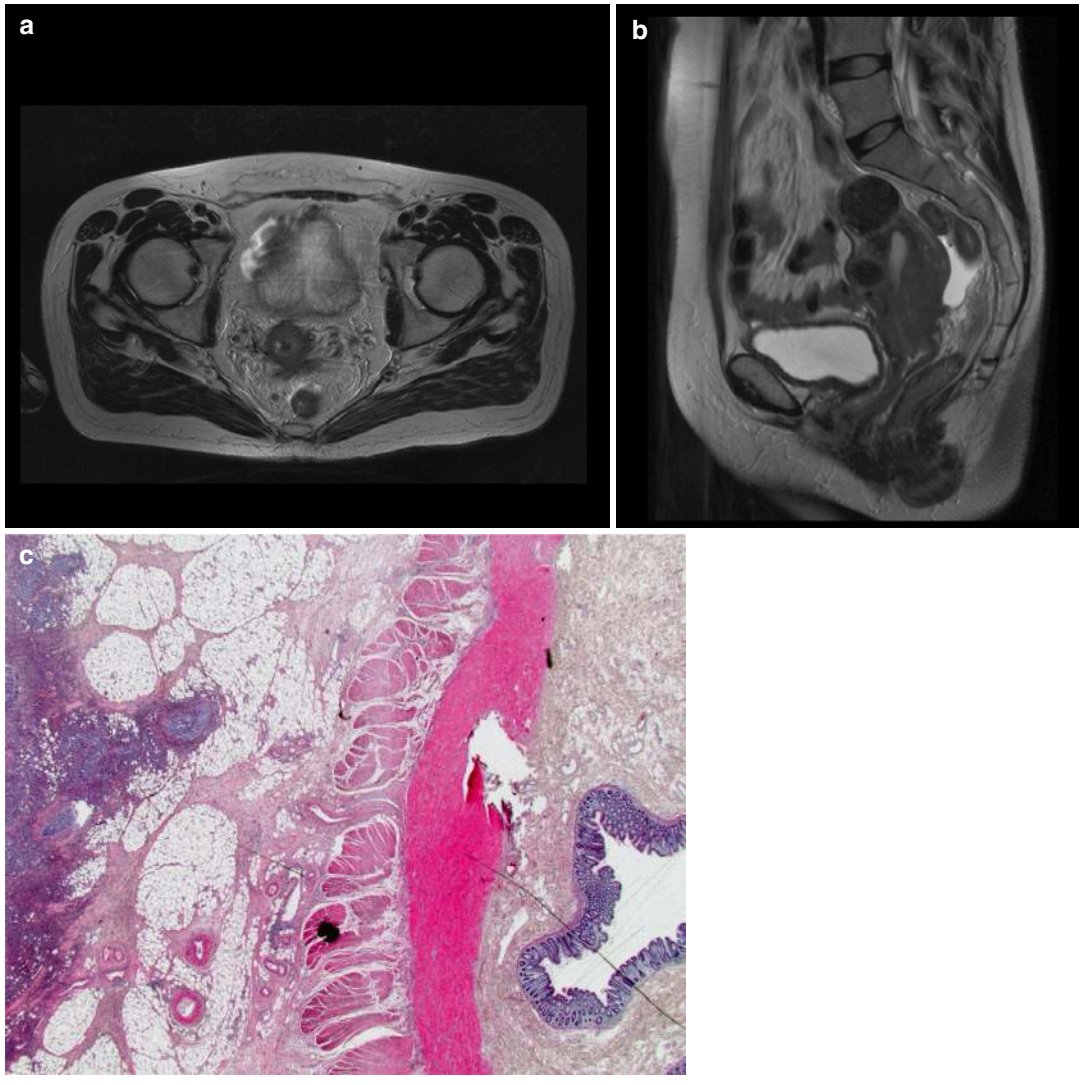

Fig. 7.14 oT4 cervix carcinoma infiltrating the mesorectum. T2-weighted transverse (**a**) and sagittal (**b**) MRI scans show continuous cervix carcinoma spread into the mesorectum with a prominent lymph node in the vicinity. Histopathology confirms mesorectal infiltration (**c**)

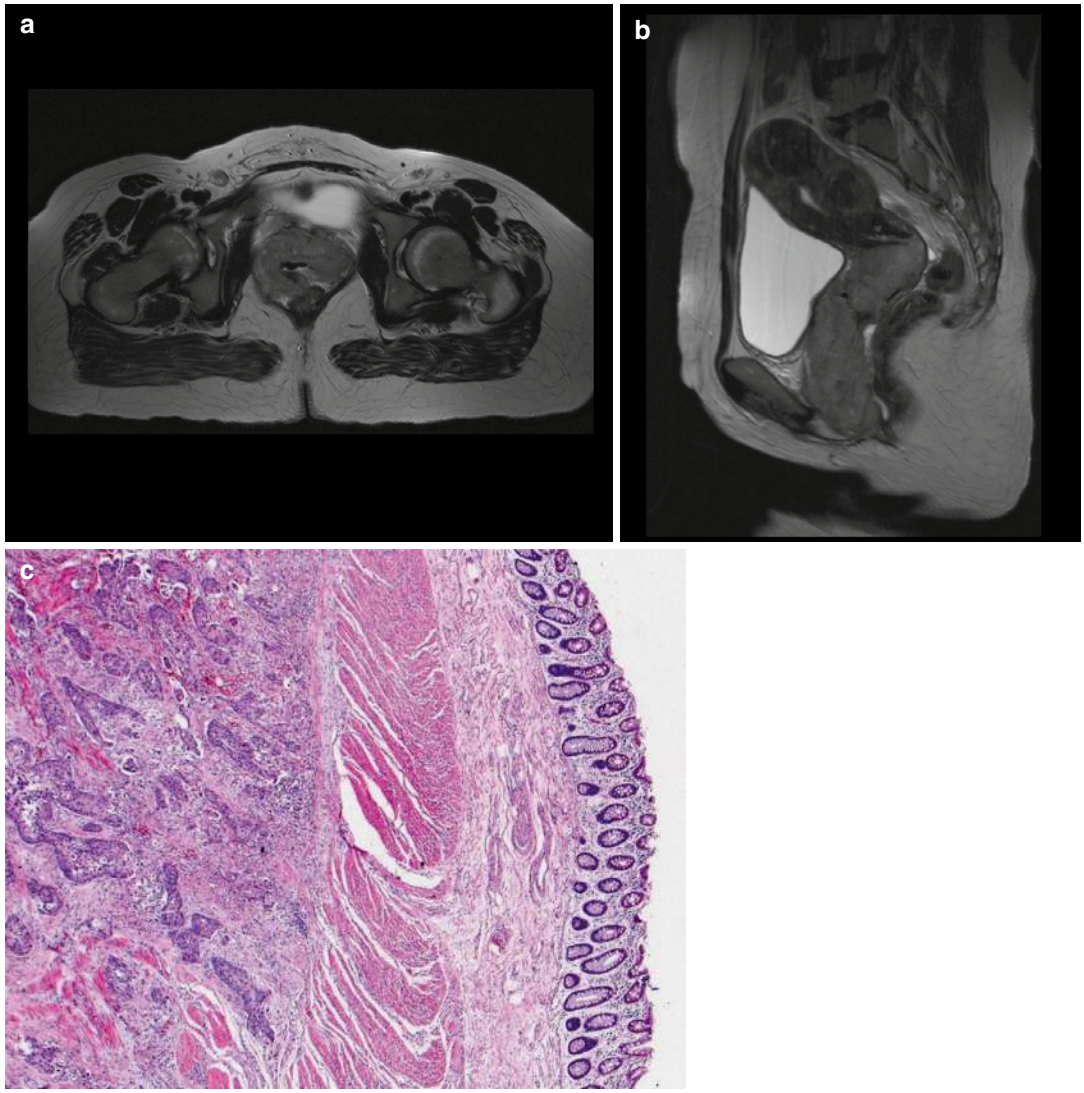

Fig. 7.15 oT4 cervix carcinoma infiltrating the rectal wall. T2-weighted transverse (**a**) and sagittal (**b**) MRI scans demonstrate cervix cancer approaching the rectal wall via massive vaginal extension. Histopathology verifies neoplastic involvement of the rectal muscle (**c**)

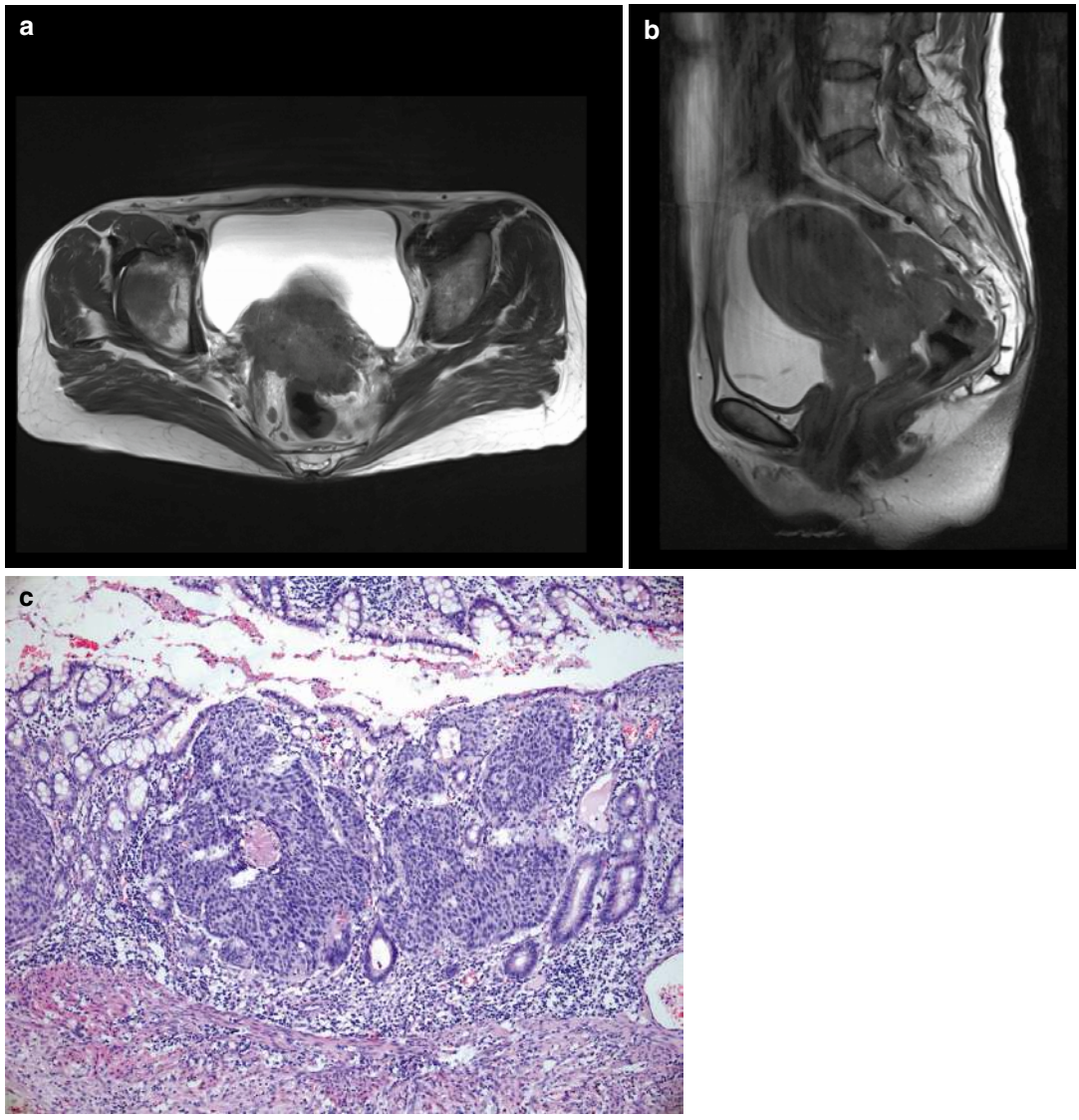

Fig. 7.16 oT4 cervix carcinoma infiltrating the rectal mucosa. T2-weighted transverse (**a**) and sagittal (**b**) MRI scans demonstrate broad extension of cervix carcinoma into the mesorectum and rectum, including the rectal mucosa, which is confirmed by histopathology (**c**)

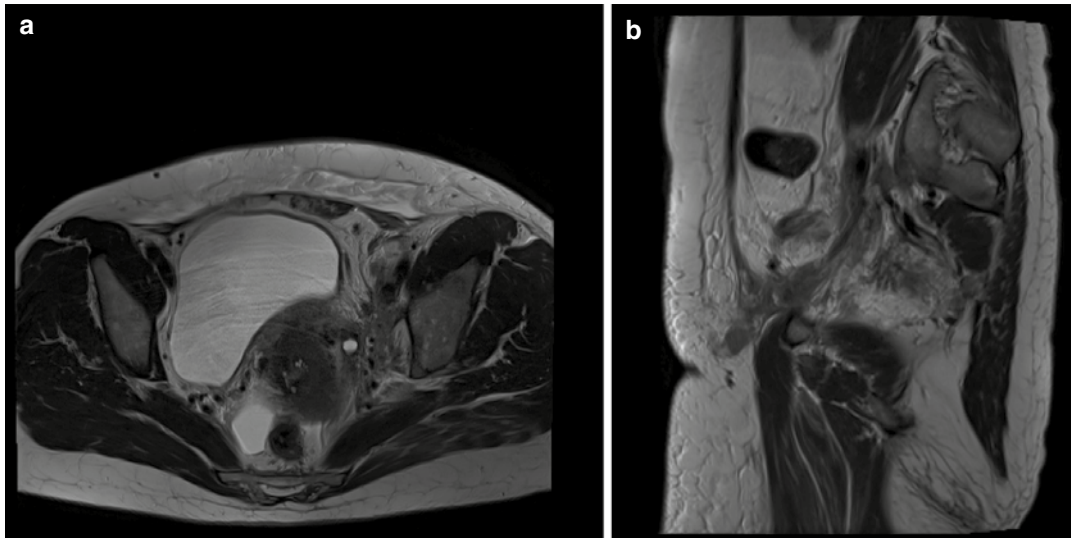

Fig. 7.17 oT4 cervix carcinoma infiltrating the left parietal (somatic) subperitoneum. T2-weighted transverse (**a**) and sagittal (**b**) MRI scans show lateral extension of a cervix carcinoma into the left somatic subperitoneum also encasing and constricting the ureter

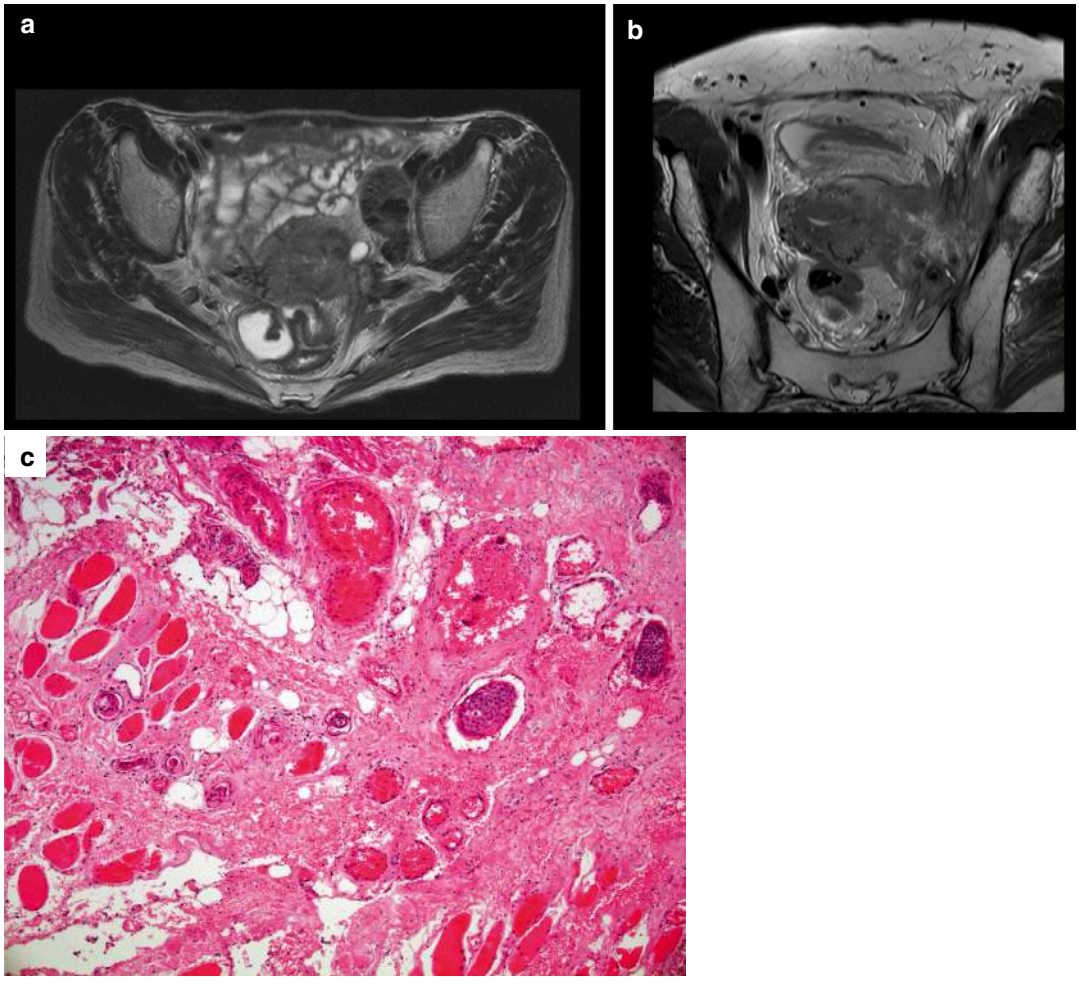

Fig. 7.18 oT4 cervix carcinoma infiltrating somatic pelvic wall tissues. T2-weighted transverse MRI scans demonstrate the infiltration of the left sciatic nerve (**a**) and the psoas muscle and os ilium (**b**) by cervix cancer. (**c**) Histological section of striated muscle infiltrated by cervix carcinoma

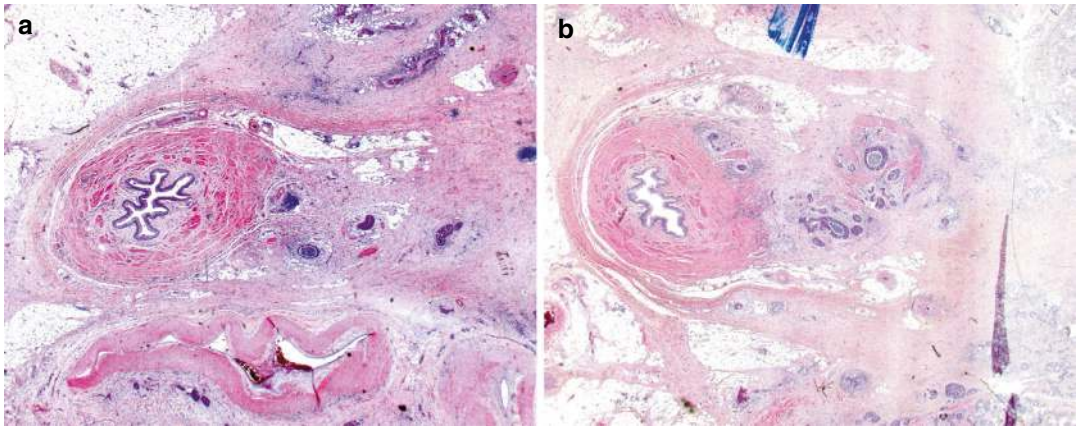

Fig. 7.19 oT4 cervix carcinoma infiltrating the mesureter and ureter. Photomicrographs demonstrating lymphatic infiltrates of cervix carcinoma into the mesureter (**a**) and ureter (**b**)

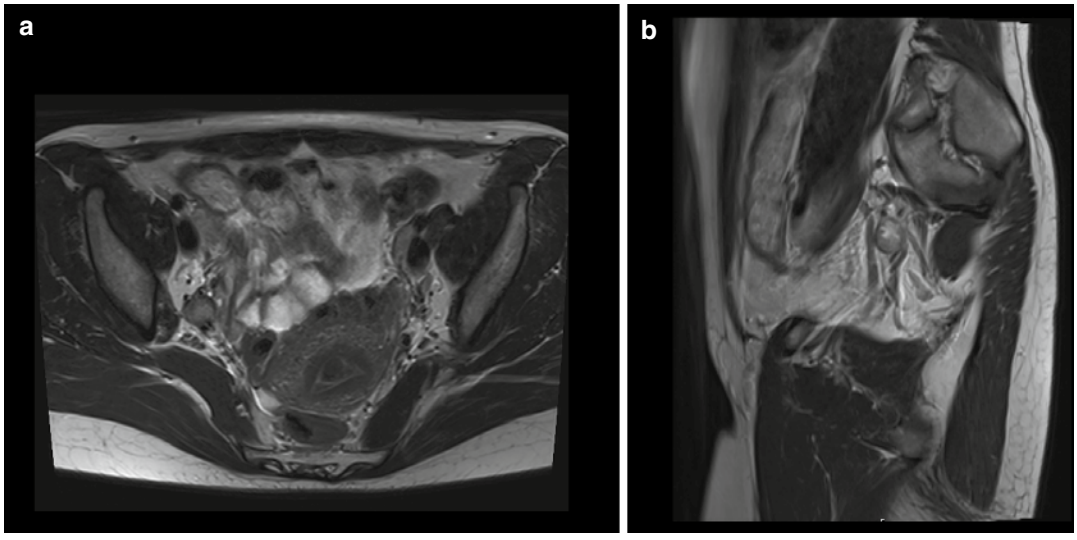

Fig. 7.20 Cervix carcinoma metastasis at the right sciatic nerve. T2-weighted transverse (**a**) and sagittal (**b**) MRI scans show an enlarged lymph node suspicious as metastasis lateral to the right internal iliac vessel system riding on the lumbar root of the sciatic nerve. Histopathology confirmed metastatic involvement of the node harvested with lymph node dissection

specified, in addition to the ontogenetic nodal stage.

7.2 Vaginal Carcinoma

The diagnostic procedures and principles for the clinical oT staging of vaginal carcinoma are the same as described for cervical carcinoma, including gynecologic examination under anesthesia, cystoscopy and (eventually) rectoscopy, pelvic MRI, and PET-CT (for advanced disease). The vaginal lesion suspected to be malignant should be exactly described in terms of location, size, appearance, consistency, and movability toward the urethra and bladder, rectum, and pelvic sidewalls and floor. Any involvement of the uterine cervix cranially or of the vulva caudally must be noted. The complete vaginal mucosa and ectocervix (if present) should be inspected for lesions in addition to the tumor and biopsies should be taken of all suspicious areas. Palpation of the inguinal regions for enlarged lymph nodes is also an integral part of the clinical assessment.

7.2.1 Stage oT1 Cancer Field

The tumor is limited to the vaginal wall.

7.2.1.1 Clinical Findings

The lesion is completely separated from the ectocervix cranially and from the vestibulum caudally. It is (semi-)mobile toward all adjacent tissues. MRI shows the confinement of the tumor to the vaginal wall (Fig. 7.21a, b).

7.2.1.2 Histopathology

The carcinoma is restricted to the muscularis layer of the vaginal wall (Fig. 7.21c).

7.2.2 Stages oT2–oT4

The cancer fields for vaginal and cervical carcinoma are the same: Müllerian compartment (oT2), mature derivatives of the Müllerian ducts (oT3a), primordial genital tract (oT3b), and mesonephric system (oT4) morphogenetic fields. They have been described in depth above.

The clinical findings can no longer discriminate between the two cancer entities if the lesion involves both the vagina and the cervix. MRI can be informative with regard to extra-Müllerian tissues infiltrated by the malignant neoplasm to determine the clinical ontogenetic stage (Figs. 7.22a, b, 7.23a, b, 7.24a, b, and 7.25a, b). Histopathology confirms the malignant involvement of the corresponding tissues. It may detect precursor VAIN III, suggesting vaginal carcinoma as a primary disease if both the uterine cervix and vagina are infiltrated. Likewise, oT3a carcinomas of the sinus vagina infiltrating the vulva compartment may be clinically indistinguishable from oT3a vulvar carcinomas infiltrating the vagina (Fig. 7.26). Again, the existence of associated dysplasia could be informative of cancer origin.

7.2.3 Ontogenetic Regional Staging

Ontogenetic nodal stages for individual vaginal carcinomas are derived from the definitive histopathological findings of the defense line-directed lymph node dissection. If the sinus vagina, with or without the vulva, is part of the total cancer field, inguinal lymph node metastases may be first line (see Chap. 6).

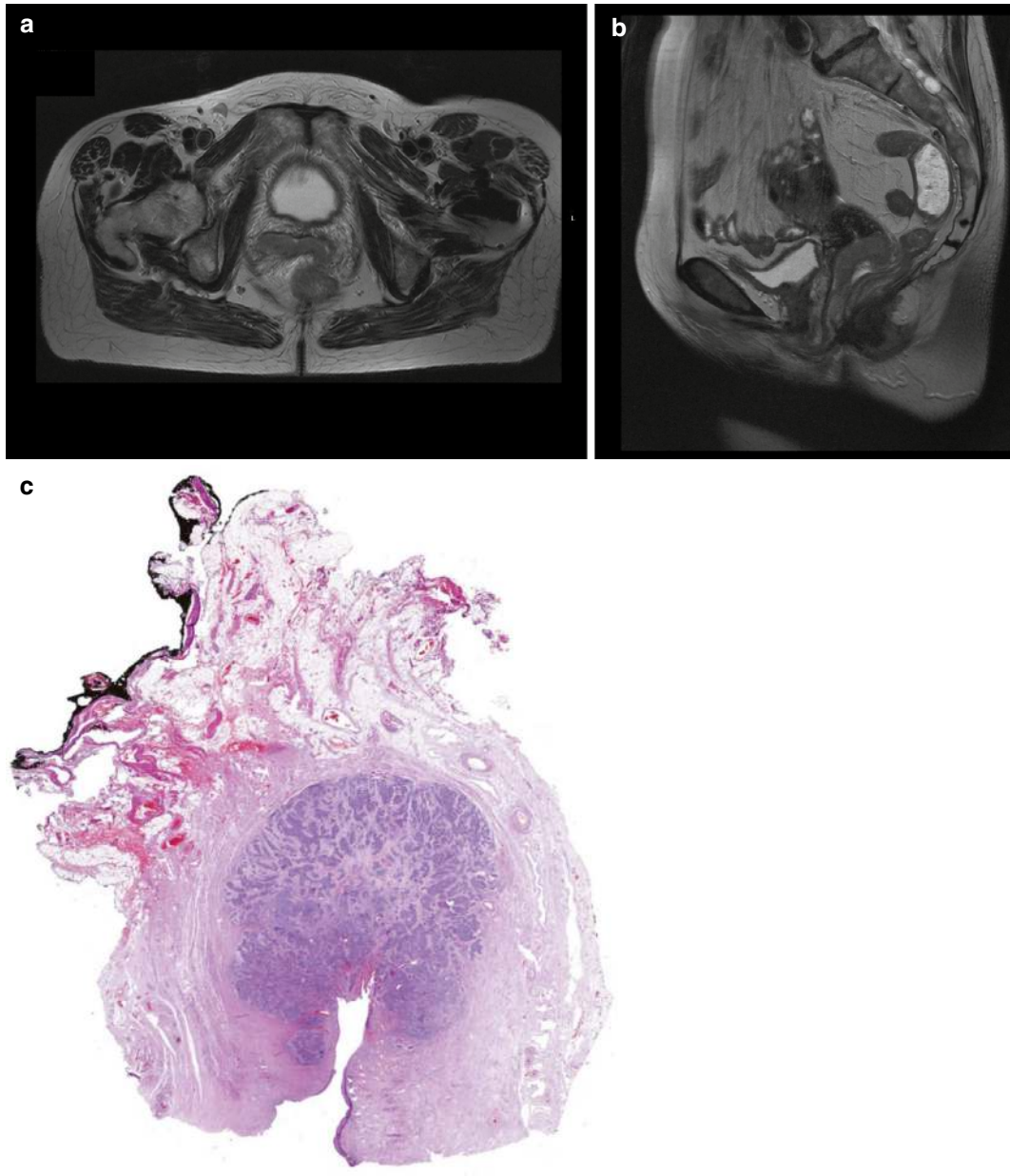

Fig. 7.21 oT1 vaginal carcinoma infiltrating the vaginal wall. T2-weighted transverse (**a**) and sagittal (**b**) MRI scans show a circumscribed tumor separate from the uterine cervix, confined to the vaginal wall. (**c**) Histopathology confirms the extension of the carcinoma into the muscularis layer of the vagina

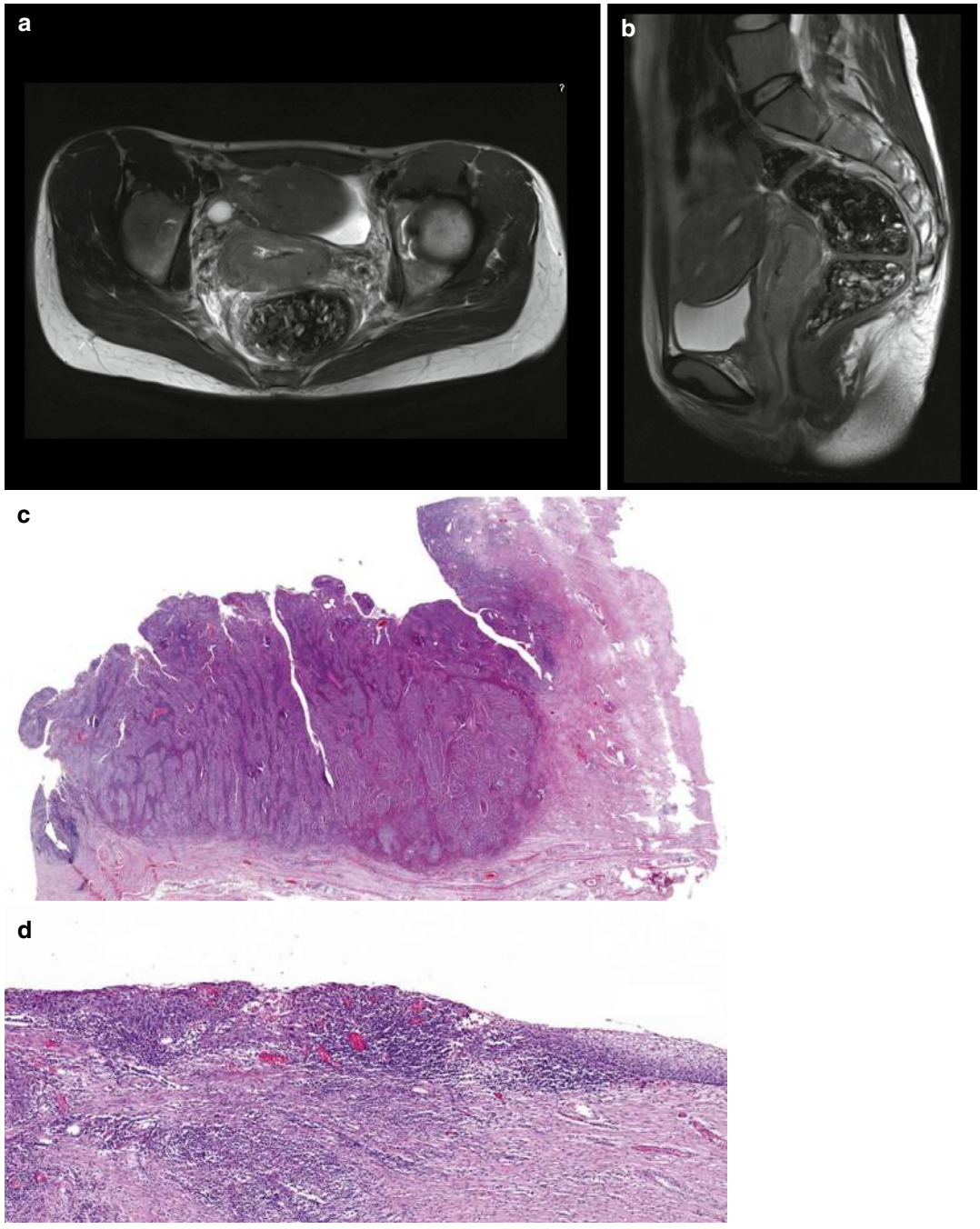

Fig. 7.22 oT2 vaginal carcinoma infiltrating the uterine cervix. T2-weighted transverse (**a**) and sagittal (**b**) MRI scans demonstrate neoplastic expansion to nearly the entire vaginal tube, reaching the ectocervix. Histopathology confirms VAIN III, in addition to the invasive vaginal carcinoma (**c**–**d**)

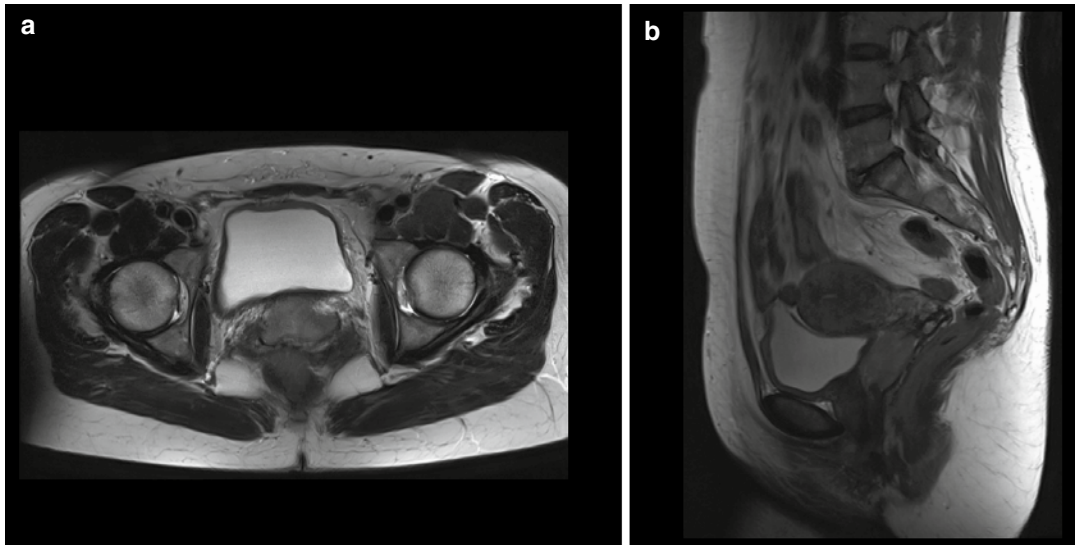

Fig. 7.23 oT3a vaginal carcinoma infiltrating the anterior mesocolpos. T2-weighted transverse (**a**) and sagittal (**b**) MRI scans show a vaginal tumor extending into the vesicovaginal septum

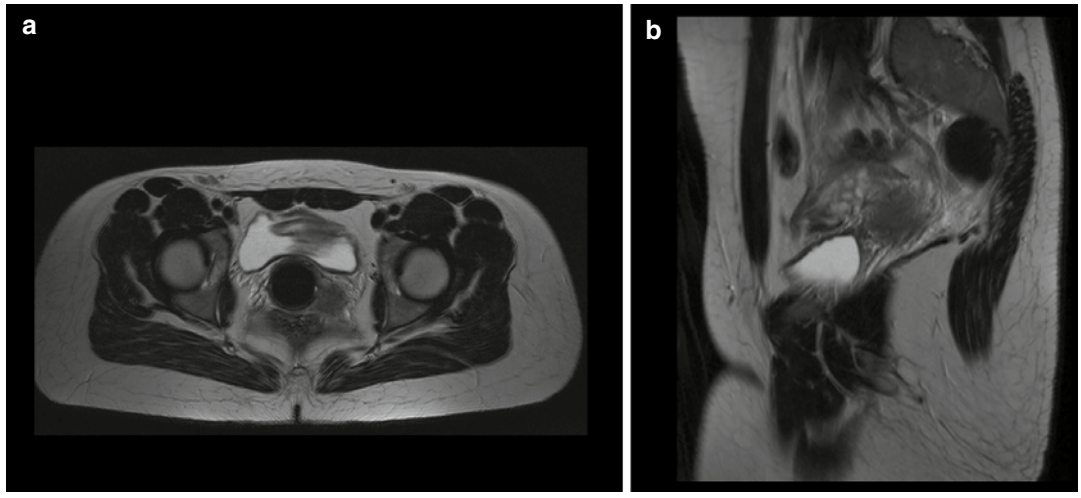

Fig. 7.24 oT3b vaginal carcinoma infiltrating the left mesocolpos and hypogastric subperitoneum. T2-weighted transverse (**a**) and sagittal (**b**) MRI scans demonstrate vaginal cancer spreading through the left mesocolpos to the pelvic wall. Here, the tumor is fixed, as assessed by palpation during examination under anesthesia

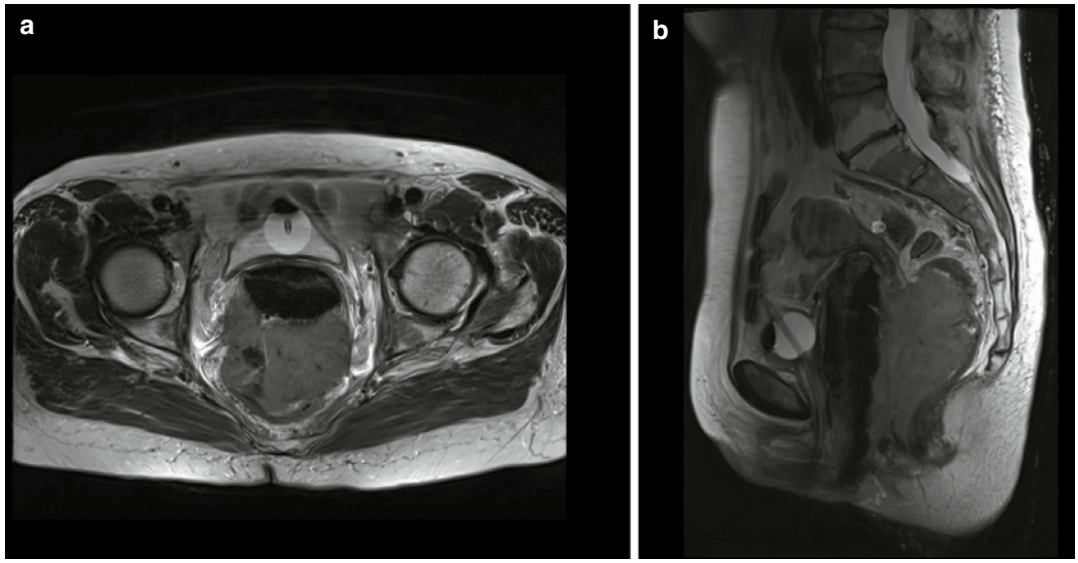

Fig. 7.25 oT4 vaginal carcinoma infiltrating the rectum. T2-weighted transverse (**a**) and sagittal (**b**) MRI scans show a large tumor of the dorsal vagina extending over a distance of more than 10 cm into the rectum

Fig. 7.26 oT3a carcinoma of the sinus vagina infiltrating the vulva. Photograph of a tumor ulcer involving the anterior sinus vagina and adjacent parts of the vulvar compartment

7.3 Endometrial Carcinoma

Irregular vaginal bleeding is the most frequent early symptom of endometrial carcinoma, which is confirmed by the histopathological diagnosis from an endometrium biopsy. Suspicion from the patient's history and sonography of the uterus mandates hysteroscopy and curettage of the uterine corpus and cervix, together with clinical examination under anesthesia. If cervical stroma involvement is suspected, corresponding core biopsies are taken as well. Likewise, any vaginal lesions suspicious of malignancy should be biopsied. In cases of deep myometrial or cervix stroma infiltration diagnosed via vaginal sonography or of hints of extracorporeal cancer spread and lymph node metastases, a pelvic MRI, including T2-weighted axial sagittal scans, should be ordered to plan the appropriate cancer field surgery.

Evidence of a locally advanced disease state (i.e., ontogenetic stage oT > 2) from the physical and sonographic assessment is an indication of the need to explore the pelvic and abdominal peritoneal sites to exactly describe the location of peritoneal lesions and biopsy them. This diagnostic procedure is usually performed immediately prior to the surgical therapy under the same anesthesia. Cystoscopy and rectoscopy are rarely necessary to characterize the local extent of endometrial carcinoma.

7.3.1 Histopathological Diagnostics

Preoperatively, the pathologist investigates the biopsies to determine the histological type and grade. The intraoperative role of the pathologist in cancer field surgery for endometrial cancer is to assess biopsies and surgical resection margins in locoregionally advanced disease and to diagnose lymph node metastases through frozen section investigation. Postoperatively, the local carcinoma spread with regard to interstitial and intravasal manifestation as well as in-transit metastases should be reported in terms of ontogenetic anatomy. The cancer fields of ontogenetic stages >1 correspond to those described for cervix carcinoma. Due to the different Müllerian subcompartments of the cancer's origin, field occupation patterns vary and the primary tumor cannot be determined with routine staining. Additional immunohistochemical assessment by the pathologist can clarify these situations.

Lymph node metastases should be allocated to the first-, second-, and third-line regions, and extracapsular spread must be reported. Molecular pathologic diagnostics, which are becoming increasingly important for planning systemic therapy, are beyond the scope of treatment with cancer field surgery.

7.3.2 oT1 Cancer Field

The tumor is limited to the corporal myometrium.

7.3.2.1 Clinical Findings

Abnormal bleeding from the cervical os may be noted. The uterus may be palpated as enlarged and of soft consistency; otherwise, clinical findings are normal. Vaginal sonography and hysteroscopy show endometrial thickening or foci of endophytic tumor manifestations in the uterine cavum (Fig. 7.27a).

7.3.2.2 Histopathology

Endometrial carcinoma is detected exclusively in the corporal myometrium (Fig. 7.27b).

7.3.3 oT2 Cancer Field

The tumor infiltrates the corporal and any other Müllerian subcompartment: cervix, vagina, uterine tube, and Müllerian adventitia.

7.3.3.1 Clinical Findings

Neoplastic tissue may be detected by gynecologic inspection in the endocervical canal, at the ectocervix, or at the vaginal mucosa. Palpation

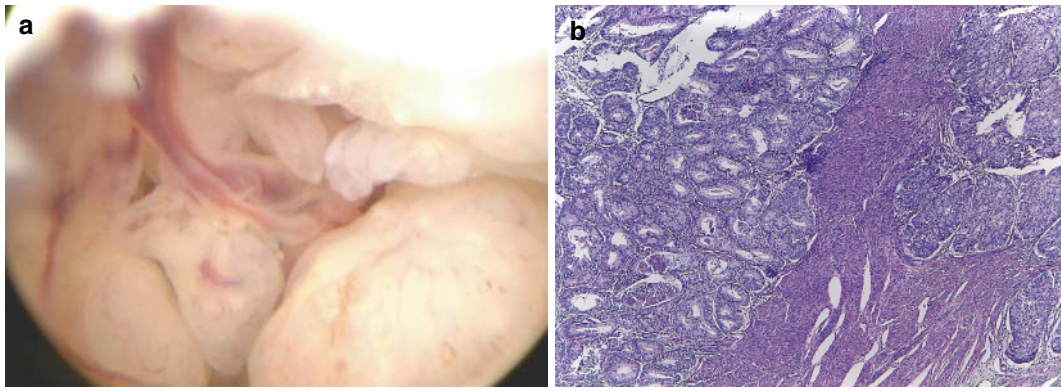

Fig. 7.27 oT1 endometrium carcinoma. (**a**) Hysteroscopic appearance. (**b**) Histopathology demonstrating myometrial infiltration

may identify an enlarged cervix or nodular structures within the vaginal wall. Vaginal sonography and hysteroscopy show tumor formations in the uterine cavum and cervix.

7.3.3.2 Histopathology

Endometrial carcinoma cells are found in addition to the corporal stroma in the cervical canal and stroma, Müllerian adventitia, vagina, and uterine tube. Discrimination between primary cervix and endometrial carcinoma in case of cancer infiltration of both Müllerian subcompartments needs immunohistologic typing.

7.3.4 oT3a Cancer Field

The tumor infiltrates any anatomical compartment derived from the Müllerian duct morphogenetic field (see above and Chap. 3). Endometrial carcinoma preferably colonizes the genital coelom compartment, i.e., Müllerian subserosa and serosa, peritoneal and ligamentous mesometria, mesosalpinx, and mesovar. The infiltration of the vascular mesometrium by endometrial carcinoma is a known manifestation of oT3a stage as well.

7.3.4.1 Clinical Findings

The cervix is often but not necessarily infiltrated, as assessed by inspection and palpation. Although parametrial shortening and thickening, which affect the movability of the uterus, can be identified in some instances, the main diagnostic evidence for the oT3a stage of endometrial carcinoma comes from the endoscopic assessment of the peritoneal and serosal surfaces. Ascites containing malignant cells is often present.

7.3.4.2 Histopathology

Endometrial cancer cells are identified in the Müllerian tissues, the uterine subserosa and serosa, the peritoneal mesometrium, the mesosalpinx, and the mesovar. Both ligamentous and vascular mesometria and mesocolpoi may be infiltrated by continuous and discontinuous tumor spread. In the cancer field model, the presence of endometrial carcinoma cells in lymphatics and blood vessels within these tissues is considered indicative of the colonizing ability of the malignant cells.

7.3.5 oT3b Cancer Field

The tumor infiltrates any anatomical compartment derived from the primordial genital tract morphogenetic field (see above and Chap. 3). Preferred occupation sites of the oT3b cancer field by endometrial carcinoma are the bladder peritoneum and the pararectal peritoneum with underlying tissues. Tumor infiltration of the vascular mesometrium may reach the umbilical artery. All sites of the oT3a cancer field may be included.

7.3.5.1 Clinical Findings

Endoscopic peritoneal assessment and pelvic MRI are necessary for the diagnosis of endometrial carcinoma foci at the peritoneal and subperitoneal sites, as indicated above. Malignant ascites is most often obvious.

7.3.5.2 Histopathology

Tissues of the oT3b cancer field biopsied by the surgeon are infiltrated by endometrial carcinoma, which is confirmed histopathologically.

7.3.6 oT4 Cancer Field

The tumor infiltrates any tissue matured from the nephrogenic cord morphogenetic field (see above and Chap. 3). Although almost all abdominopelvic structures are part of the oT4 cancer field, the most common sites infiltrated by endometrial cancer exceeding the oT3b field are the complete peritoneal cavity and the bowel.

7.3.6.1 Clinical Findings and Histopathology

Patients may present with abdominal distension and bowel obstruction. Malignant lesions at intestinal, omental, and parietal peritoneal sites biopsied during laparoscopy confirm the oT4 stage. Evidence of an advanced tumor stage is

obtained by physical examination, pelvic MRI, and endoscopic peritoneal assessment.

7.3.7 Ontogenetic Nodal Staging

At the time of this writing, the importance of ontogenetic nodal staging for endometrial carcinoma is not settled due to the relatively low number of nodal-positive cases treated so far with cancer field surgery. For oT1 and 2 carcinomas, the hierarchy of first-, second-, and third-line nodes should correspond to that of cervix carcinoma confined to the Müllerian compartment (see Chap. 6). First-line nodes of oT1 and oT2 endometrial carcinomas propagating within the uterine fundus and of oT3a tumors having invaded the corporal subserosa or serosa include the mesenteric periaortic nodes and sporadically intercalated nodes within the peritoneal mesometrium and the "infundibulopelvic ligament."

7.4 Vulvar Carcinoma

Ontogenetic tumor staging of vulvar carcinoma demands gross inspection of the perineum. Focal visualization with the colposcope, both without and with the application of acetic acid, may detect additional premalignant lesions. The consistency and movability of the local tumor are assessed by palpation. Likewise, the labia majora, genitocrural skin bridges, and inguinal regions are inspected and palpated for enlarged and fixed lymph nodes. In the case of locally advanced disease and suspected lymph node metastases, MRI offers important additional diagnostic information. Evaluation for distant metastases with PET-CT is indicated for oT stages 3b and 4, for oN3 stage, or if ulcerative inguinal pelvic lymph node metastases or skin metastases are evident.

The report of clinical findings should precisely describe the perineal situs based on its ontogenetic anatomy (see Chap. 4) according to the following protocol:

- Deviations from the normal perineal anatomy related to age, nutritional state, and obstetrical history, such as tissue malformations, defects, or scars from previous diseases or operations or signs of current pathology other than the suspected (or histopathologically proven) malignant lesions, e.g., lichen sclerosus
- The location of the lesion on the 12-h clock scale (Fig. 7.28a)
- The infiltrated tissues with regard to the ontogenetically defined vulvar subcompartment: peripheral—intermediate—central and adjacent nonvulvar compartments (Fig. 7.28b)
- The size of the lesion
- Its appearance as a tumor, flat ulcer, or tumor ulcer
- Its movability toward underlying tissues

In the case of multifocal disease, these features must be described for each lesion. The perineum should be photodocumented, demonstrating the complete extent of the lesion(s). To accomplish this, the spreading of the labia or the insertion of a vaginal speculum may be necessary.

The results of the clinical assessment of the inguinal regions, skin bridges, and labia majora should be reported for both sides, including the number of suspicious lymph nodes, their size, their consistency, their movability, and signs of skin involvement.

The mainstay for ontogenetic staging is pretherapeutic histopathological *vulvar mapping*, executed by systematically taking multiple topographically defined minute skin samples with punch biopsy devices. For the histopathological diagnosis of large tumors, core biopsies instead of punch biopsies should be preferred as the latter may not provide a representative sample or may miss vital tumor tissue due to necrosis.

Vulvar mapping for ontogenetic staging is performed according to the following systematics. The lesion is characterized as described. In addition to the clock scale projected on the vulvar compartment, four sectors are defined (Fig. 7.29a):

1. 11–1 o'clock: anterior
2. 1–5 o'clock: left
3. 5–7 o'clock: posterior
4. 7–11 o'clock: right

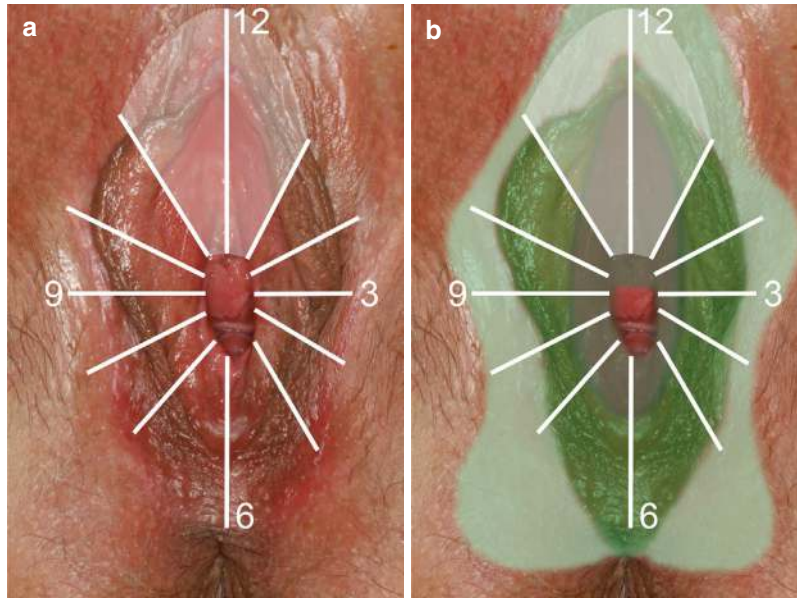

Fig. 7.28 Systematic clinical documentation of malignant vulvar lesions. (**a**) 12-hour clock scale centered at the vaginal orifice projected into a photograph of a female perineum. The scale is divided into four sectors: anterior, 11–1 o'clock (highlighted in the figure); left, 1–5 o'clock; posterior, 5–7 o'clock; right, 7–11 o'clock. (**b**) Ontogenetic anatomy of the vulva projected into the photograph (**a**), showing the peripheral, intermediate, and central subcompartments of the vulvar compartment in light, middle, and dark green coloring. Adjacent nonvulvar compartments are not highlighted in this picture. Their relation to the vulvar compartment, which becomes relevant in advanced stages (>oT2), is shown in Fig. 4.11

About 5 mm distance from the macroscopic perimeter of the lesion, a circumferential line is drawn.

Three categories of biopsies, distal—proximal—intralesional, are taken in that order. The distal biopsies are taken from the vulvar subcompartment(s) at all sectors not infiltrated by the tumor.

The proximal biopsies are located at the circumferential line around the tumor and encompass all subcompartments and nonvulvar compartments crossed by it. The biopsies should be directed toward the tissues that will be preserved by the planned cancer field surgery.

Finally, punch or core biopsies are taken from the malignant lesion at all the vulvar subcompartments and nonvulvar compartments infiltrated by it.

All biopsies are documented with regard to category, location on the clock scale and sector, vulvar subcompartment, or nonvulvar compartment (Fig. 7.29a–c). Importantly, dysplastic and neoplastic lesions should be characterized for HPV association (usual versus differentiated vulvar intraepithelial neoplasia, p16 positive versus negative carcinoma).

Following histopathological diagnosis from vulvar mapping, communication with the pathologist is necessary during the surgery for the intraoperative frozen section assessment of topographically defined lymph nodes and resection margins at subcompartment and compartment borders.

7.4.1 Stage oT1 Cancer Field

The histopathologically malignant lesion is confined to a site involving only one subcompartment, as determined clinically (Fig. 7.30a–c).

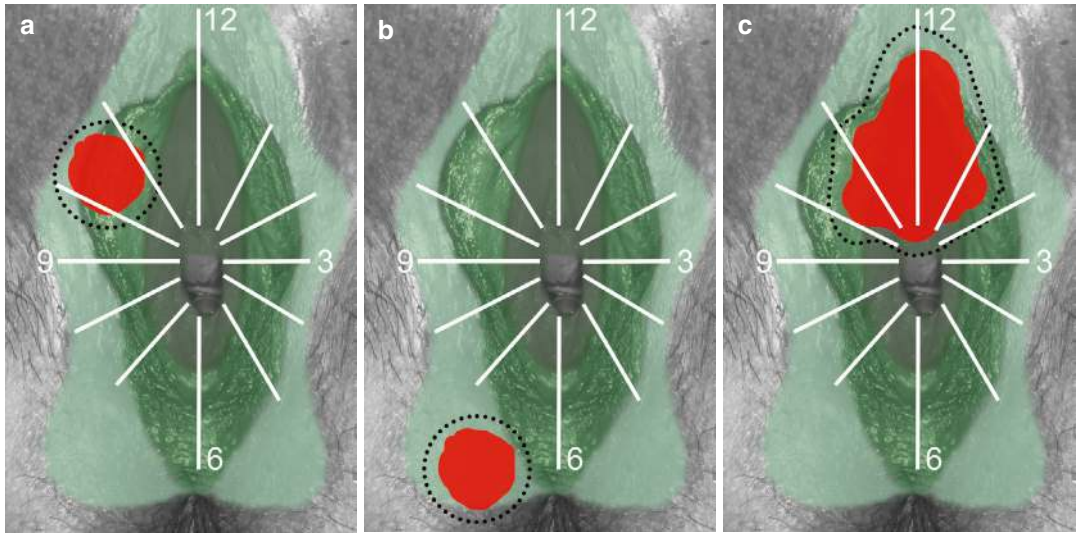

Fig. 7.29 Three examples of systematic vulvar mapping protocols. (**a**) 2 cm malignant lesion at 10–11 o'clock; right sector involving the intermediate subcompartment. Distal biopsies are taken from the intermediate subcompartment at the 12, 1–2, and 6 o'clock positions in the anterior, left, and posterior sectors. Proximal biopsies are taken from the peripheral subcompartment at 10 o'clock, from the intermediate subcompartment at 9–10 o'clock, and from the central subcompartment at 11–12 o'clock. A tumor biopsy is taken from the intermediate subcompartment at 10:30 o'clock. (**b**) 2 cm malignant lesion at 6–7 o'clock in the posterior sector involving the peripheral subcompartment. Distal biopsies are taken from the peripheral subcompartments at 9:30, 12 o'clock, and 3:30 positions in the right, anterior, and left sectors. Proximal biopsies are taken from the peripheral subcompartment at 7 o'clock, from the intermediate subcompartment at 6:30, from the anus at 6:30, and from the genitocrural skin at 7 o'clock. A tumor biopsy is taken from the peripheral subcompartment at 6:30. (**c**) 5 cm malignant lesion between 10 and 2 o'clock mainly in the anterior sector involving the intermediate and central subcompartments. Distal biopsies are taken from the intermediate and central subcompartments at 4:30, 6 o'clock, and 7:30 in the left, posterior, and right sectors. Proximal biopsies are taken at 12:30 from the peripheral subcompartment, at 2:30 from the central subcompartment, and at 9:30 from the intermediate subcompartment. Tumor biopsies are taken at 11:30 from the intermediate subcompartment and at 12 o'clock from the central subcompartment

The pathologist can only discriminate between keratinized and nonkeratinized squamous normal skin adjacent to the cancer, which is not sufficient to allocate a lesion to a single subcompartment.

7.4.2 Stage oT2 Cancer Field

The malignant lesion involves two or three subcompartments but is confined to the vulvar compartment (Fig. 7.31a, b). The infiltrated subcompartments again have to be determined clinically. Histopathological assessment has to ascertain that only cutaneous tissue is colonized by cancer cells.

7.4.3 Stage oT3a Cancer Field

The vulvar carcinoma infiltrates anatomical compartments derived from the phallic urogenital sinus morphogenetic field (Fig. 7.32a–c). Clinically, these tumors are still mobile but involve tissues adjacent to the vulva compartment, such as the labia majora, anterior commissure, genitocrural skin, vagina, and urethra. Histopathologically, any of the following tissues are infiltrated by cancer cells: subcutaneous fat, urethra, vagina, erectile glans clitoridis, and corpus spongiosus of the bulbus vestibularis.

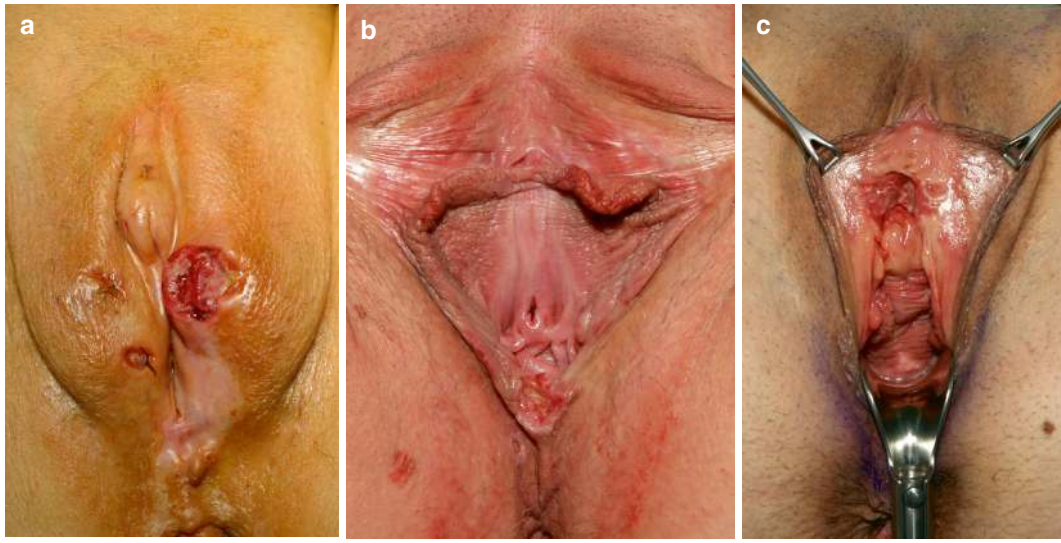

Fig. 7.30 Photographs of oT1 vulvar carcinomas infiltrating the peripheral (**a**), intermediate (**b**), and central (**c**) subcompartment exclusively

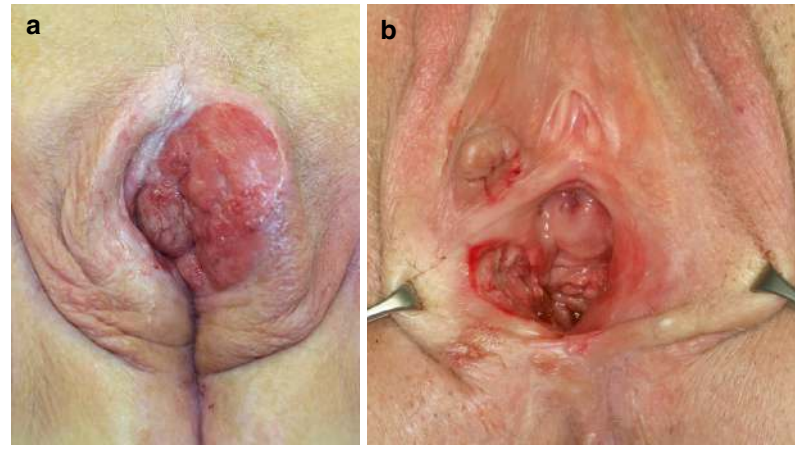

Fig. 7.31 Photographs of oT2 vulvar carcinomas infiltrating the vulvar compartment. (**a**) Tumor involves peripheral and intermediate subcompartments. (**b**) Tumor involves intermediate and central subcompartments

7.4.4 Stage oT3b Cancer Field

The vulvar carcinoma infiltrates anatomical compartments derived from the urogenital plate morphogenetic field (Fig. 7.33a, b). A clinical correlate of that stage is the fixation of the tumor to underlying tissues because the cancer may invade parts of the urogenital diaphragm, such as Colles' fascia, the perineal muscles, Buck's fascia, as well as the corpus or crura of the clitoris. This may then be confirmed histopathologically. Likewise, the infiltration of the rectovaginal septum (but not of the rectum) and of gluteal tissues represent an oT3b stage.

7.4.5 Stage oT4 Cancer Field

The vulvar carcinoma infiltrates tissues matured from the cloacal membrane morphogenetic field (Fig. 7.34a, b). oT4 vulvar cancers most often appear clinically as large tumor masses involving the pubic bones, anorectum, legs, and abdominal wall. Only rarely (e.g., in immunocompromised

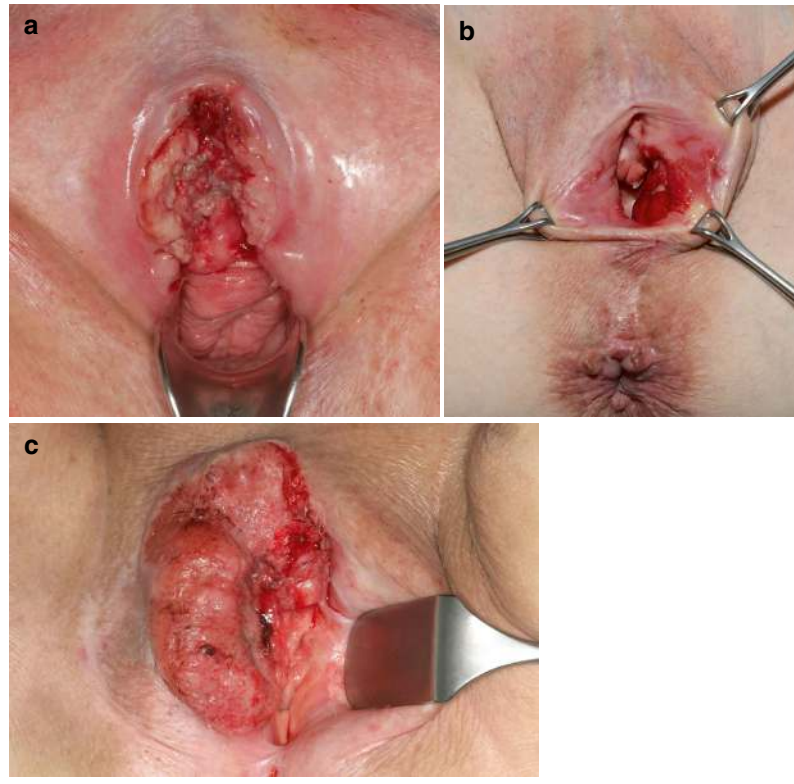

Fig. 7.32 Photographs of oT3a vulvar carcinomas infiltrating anatomical compartments derived from the phallic urogenital sinus morphogenetic field. (**a**) The tumor involves the urethra. (**b**) The tumor involves the vagina. (**c**) The tumor involves the labium majus

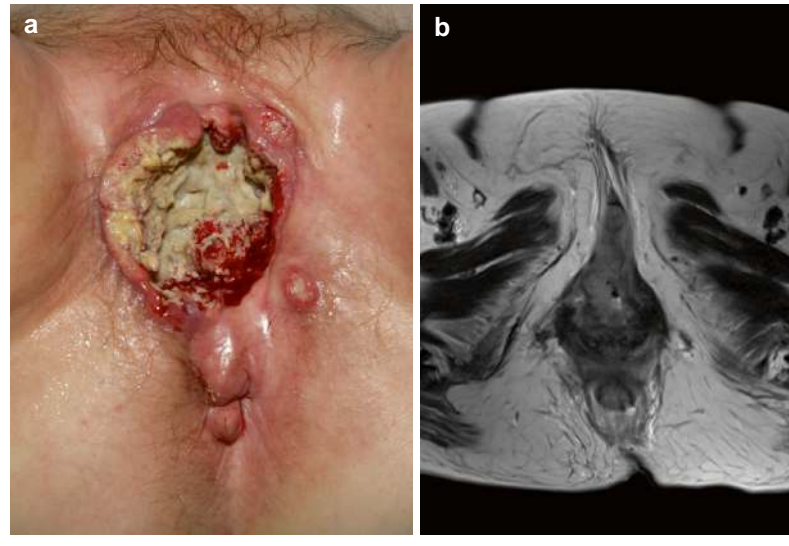

Fig. 7.33 oT3b vulvar carcinoma infiltrating tissues matured from the urogenital plate morphogenetic field. (**a**) Photograph of a vulvar carcinoma involving the labia majora, urethra, and erectile structures. (**b**) T2-weighted transverse MRI scan showing a vulvar carcinoma infiltrating the corpus and crura of the clitoris

patients) is infiltration of anal tissues observed with relatively low tumor volumes.

7.4.6 Ontogenetic Regional Staging

As with cervix and vaginal carcinomas, ontogenetic nodal stages in vulvar cancer are determined from the final histopathological report of the lymph node dissection by allocating lymph node metastases to first-, second-, and third-line regions (see Chap. 6). The extracapsular spread of inguinal lymph node metastases indicates the malignant progression of the vulvar carcinoma, corresponding to an oT3a stage.

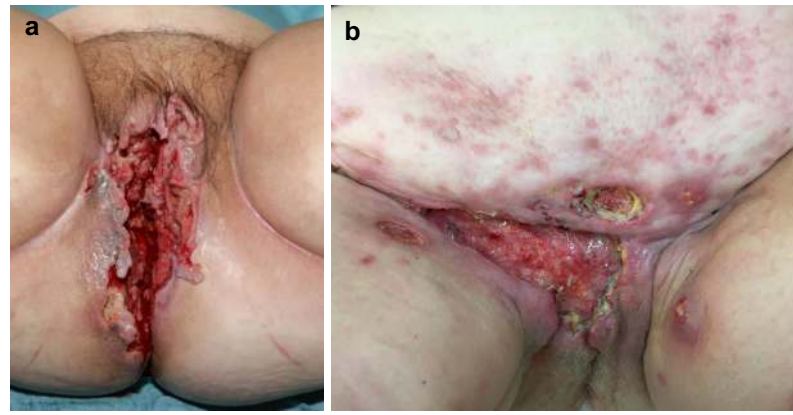

Fig. 7.34 Photographs of oT4 vulvar carcinomas infiltrating mature derivatives of the cloacal membrane morphogenetic field. (**a**) Tumor involves the anus, perianal, and gluteal regions. (**b**) Tumor involves abdominal and leg skin and subcutaneous tissue

8 Total and Extended Mesometrial Resections with Defense Line-Directed Lymph Node Dissection

The translation of the ontogenetic cancer field model into surgical treatments for cancer of the Müllerian compartment includes abdominal and abdominoperineal *total, peritoneal, and extended mesometrial resection (TMMR, PMMR, and EMMR)*. Fig. 8.1 provides a schematic overview of these procedures, which are combined with immunologic defense line-directed lymph node dissection, also termed peripheral immune network-directed lymph node dissection (iLND), in case of epithelial cancers, i.e., carcinomas, aiming to eliminate all locoregional clonogenic malignant cells. TMMR is designed for the treatment of cancer of the lower Müllerian compartment (cervix and vagina) while PMMR for that of the upper Müllerian compartment, i.e., endometrial carcinomas. Tubal carcinoma, because of its low prevalence, is not considered here.

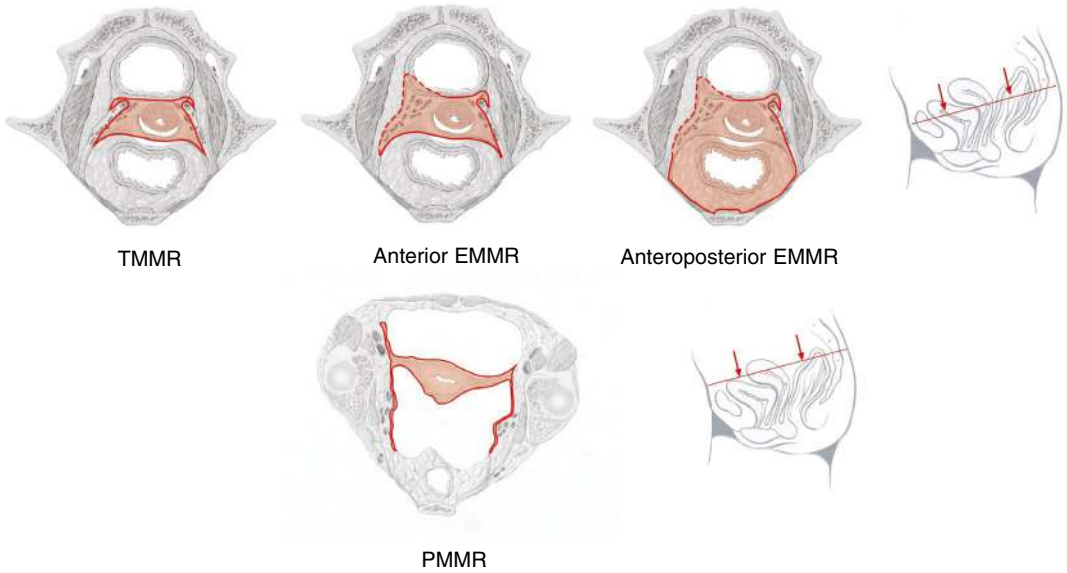

Fig. 8.1 Schematic overview of the different types of mesometrial resections based on ontogenetic anatomy. The tissues resected by these procedures are depicted in the transverse pelvic planes indicated in the sagittal plane panels on the right. *TMMR* total mesometrial resection, *EMMR* extended mesometrial resection, *PMMR* peritoneal mesometrial resection

M. Höckel et al., *Cancer Field Surgery in Gynecologic Oncology*,
https://doi.org/10.1007/978-3-031-83030-3_8

EMMR removes extra-Müllerian tissues in addition to the mesometria and mesocolpoi, which are already part of TMMR. The ovaries, which are extra-Müllerian tissues as well, are included in EMMR and PMMR generally and in TMMR if indicated or demanded by the patient. All abdominal mesometrial resections excise the complete Müllerian compartment, except a part of the vagina. If the distal (sinus) vagina has to be included, abdominoperineal techniques are applied.

TMMR and PMMR differ when it comes to the mesotissues removed in addition to the subtotal Müllerian compartment. The bilateral vascular mesometrium derived from the anterior cloacal mesenchyme (ACM) and the bilateral ligamentous mesometrium derived from the genital coelom mesoderm are part of both TMMR and PMMR specimens. Other mesotissues matured from the genital coelom mesoderm, i.e., peritoneal mesometrium, mesovarium, mesosalpinx, ovarian ligament proper, infundibulopelvic "ligament," and proximal round ligament, are generally integrated into the PMMR, whereas the genital coelom-derived ligamentous mesocolpos and the ACM-derived vascular mesocolpos are integral to TMMR. TMMR and EMMR are the subjects of this chapter, while PMMR is discussed in Chap. 9.

8.1 Total and Extended Mesometrial Resections and Peripheral Immune Network-Directed Lymph Node Dissection

TMMR should eliminate all local cancer cells of oT1 and oT2 tumors of the Müllerian compartment (Fig. 8.2). The risk of local recurrence of cervix carcinoma in the preserved functional part of the vagina was less than 1% in our series (four of 472 cases). The surgical removal of the complete cancer field of cervicovaginal carcinomas that progressed to oT3a necessitates anterior lateral endopelvic resection (LEER; see Chap. 10). The application of EMMR for the R0 resection of oT3a tumors is a compromise, as the urethra, bladder, and unilateral bladder mesentery are preserved to allow micturition. The "oncological prize" for the subtotal resection of the cancer field in oT3a cervical carcinomas is a local failure rate

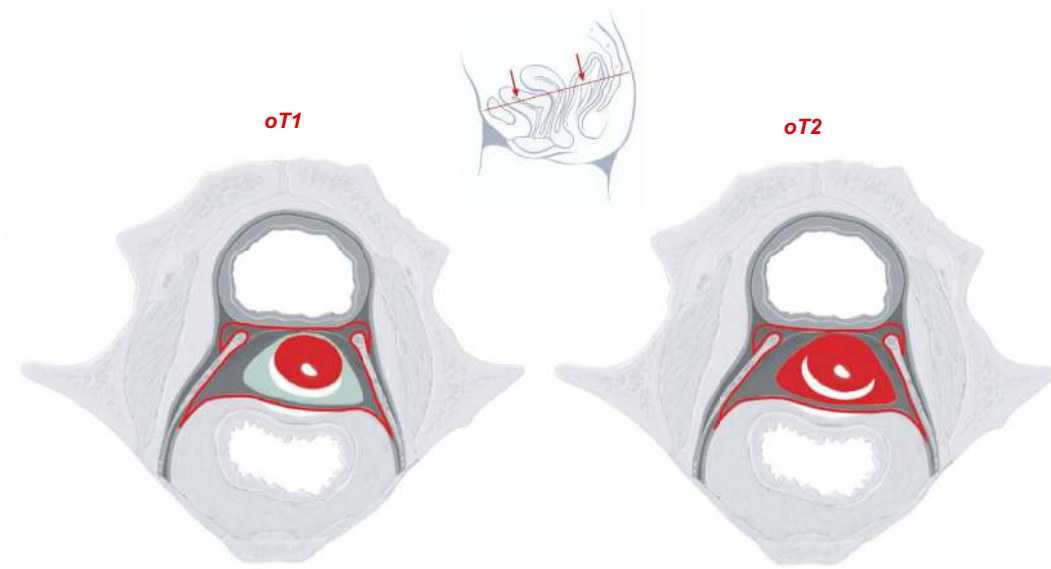

Fig. 8.2 Schematic illustration of the oT1 and oT2 cancer fields of cervix carcinoma within the borders of TMMR in the transverse pelvic plane, indicated in the sagittal plane panel

of 11%, according to our results with 111 patients. Whether radiotherapy, which includes the complete cancer field, is superior for the treatment of oT3a cervix carcinomas is not known at present (this topic will be discussed in Chap. 12).

According to the ontogenetic cancer field model, regional tumor control is the aim of *immunologic defense line-directed lymph node dissection also termed peripheral immune network-directed lymph node dissection (iLND)*, a procedure for the removal of first-, second-, and third-line lymph node regions, depending on the ontogenetic tumor stage of the local cancer and on metastatic lymph node involvement, which is assessed by intraoperative frozen section investigation (see Chap. 6). Regional tumor control is achieved through mesometrial resections that eliminate the intercalated nodes (Fig. 8.3a) and the additional excision of the basin nodes (Fig. 8.3b), according to the treatment algorithms described in Chap. 12, and fully dispensing with adjuvant radiotherapy.

For oT1 and oT2 cervix carcinomas confined to the Müllerian compartment, iLND clears all first-line lymph node regions containing both basin and intercalated nodes. The additional resection of second- and third-line nodes adheres to the algorithm given in Chap. 12. The regional failure rate of iLND was 3% (13/472) in our cohort.

With oT3a cervix carcinomas, single metastases can occur in first-, second-, and even third-line lymph node regions related to the Müllerian compartment as tributary tissue. The complete regional cancer field for oT3a carcinomas (e.g., intercalated lymph nodes in the bladder mesentery or in the pararectal subperitoneum and fascia) cannot be removed for functional reasons.

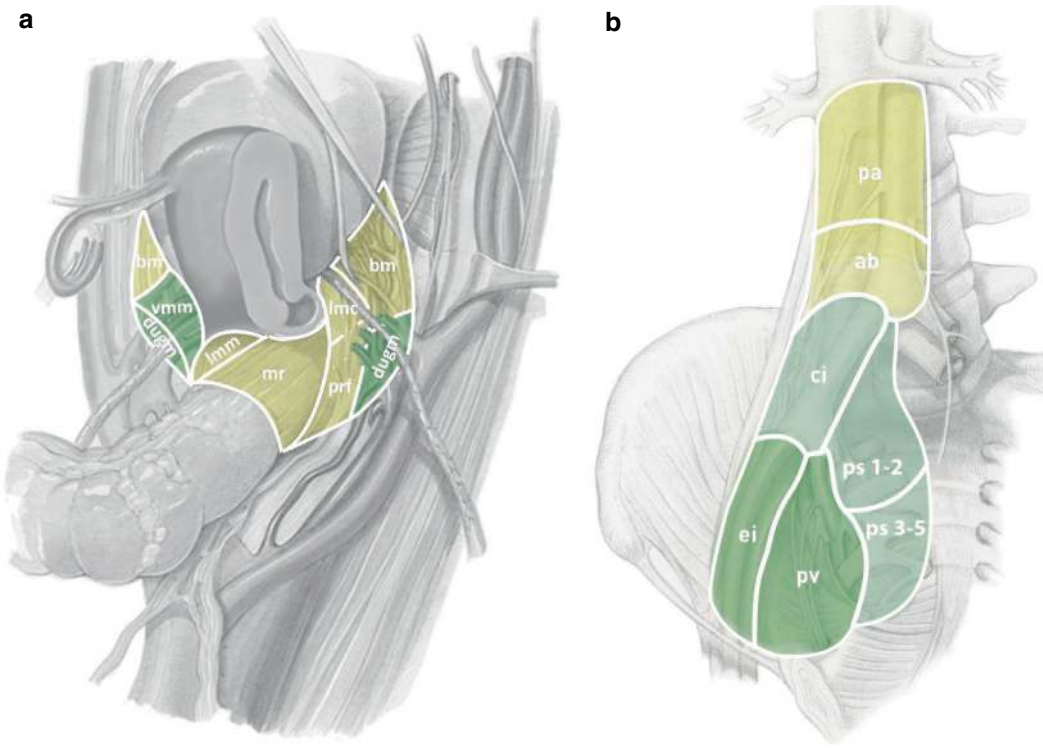

Fig. 8.3 Intercalated (**a**) and basin (**b**) lymph node regions categorized in first (intense green), second (light green), and third (yellow) defense lines for cervix carcinoma of ontogenetic stages oT1 and oT2. *vmm* vascular mesometrium, *lmm* ligamentous mesometrium, *lmc* ligamentous mesocolpos, *prf* pararectal fascia, *dugm* distal urogenital mesentery, *bm* bladder mesentery, *mr* mesorectum, *ei* external iliac, *pv* paravisceral, *ci* common iliac, *ps* presacral, *ab* aortic bifurcation, *pa* periaortic

The regional failure rate following iLND for oT3a cervix carcinoma was 5% (6/111) in our series.

All mesometrial resections are based on ontogenetic anatomy, which has been comprehensively demonstrated in Chap. 3. The subperitoneal tissue architecture is best approached by the anterior and posterior horseshoe shell system, as outlined there (Fig. 3.15a). All actions to be performed for cancer field surgery, in general, are categorized into four tissue manipulations: incision, dissection along developmentally defined planes, transection accompanied by sealing or ligating of blood vessels, and tissue adaptation and closure. Blunt separation of tissues is avoided.

The TMMR and EMMR techniques are founded on the author's (MH) experience with more than 1000 patients, who were followed for 20 years and longer. All steps of the procedures have been optimized, as described and illustrated, leaving no room for so-called "tips and tricks." Whenever anatomical variations would have an impact on the surgical techniques, it will be indicated, and the necessary modifications are described. The prerequisite for the optimal performance of cancer field surgery is a state-of-the-art operating room infrastructure, a selection of surgical instruments and equipment (as listed in Table 8.1) for the different procedures, patient preparation and positioning, as well as surgical team organization as described. Optimal perioperative anesthesiological performance is essential; however, this is beyond the scope of this textbook. Intraoperative dialogue with the pathologist is a mainstay of cancer field surgery. It must be ensured through professional and accurate communication during, after, and even sometimes before the procedure. The presentation of the surgical techniques will be followed by the description of important aspects of postoperative care as well as a compilation of potential complications and their clinical management. However, the means for the rehabilitation of patients are beyond the scope of this book. The long-term results of cancer field surgery for cancer of the female genital tract and the treatment algorithms are the subjects of Chap. 12.

Table 8.1 Nondisposable surgical instruments for executing TMMR/EMMR and iLND

Number	Instrument
	Cutting devices
1	Scalpel handle Nr. 4
2	Scalpel handle Nr. 4 L
2	Metzenbaum dissecting scissors curved, 230 mm
1	Metzenbaum dissecting scissors curved, 200 mm
1	Wertheim dissecting scissors curved, 230 mm
1	Ligature scissors serrated, curved, 230 mm
1	Ligature scissors serrated, curved, 180 mm
1	Surgical scissors straight, 145 mm
	Manual retractors
2	Fritsch abdominal retractor, 64 × 85 mm
2	Fritsch abdominal retractor, 34 × 50 mm
1	Doyen vaginal retractor, 120 × 60 mm
1	Doyen vaginal retractor, 90 × 60 mm
2	Bayonet retractor long, 180 × 40 mm
2	Bayonet retractor short, 150 × 35 mm
1	Cushing retractor 250 mm, small
1	Cushing retractor 250 mm, medium
1	Cushing retractor 250 mm, large
	Forceps
2	Tissue forceps, 250 mm
2	Tissue forceps, 200 mm
2	DeBakey atraumatic dissecting forceps 2.8 mm, 240 mm
2	DeBakey atraumatic dissecting forceps 2.0 mm, 200 mm
2	Waugh tissue forceps, 200 mm
2	Overholt dissecting forceps, 280 mm
1	Overholt dissecting forceps, fine pattern, 220 mm
1	Overholt dissecting forceps, fine pattern, 225 mm
2	Overholt-Geissendörfer dissecting forceps, 225 mm
	Clamps
6	Backhaus towel clamp, 110 mm
4	Mikulicz peritoneal forceps, 205 mm
6	Rochester-Ochsner artery forceps, straight
6	Rochester-Ochsner artery forceps, curved
4	Förster sponge forceps, 240 mm
2	Babcock grasping forceps, 220 mm
4	Babcock grasping forceps, 215 mm
6	Kocher-Ochsner artery forceps straight, 240 mm
4	Pean artery forceps straight, 260 mm
4	Bengolea artery forceps straight, 245 mm
2	Wertheim hysterectomy forceps, type Vienna, 240 mm

(continued)

Table 8.1 (continued)

Number	Instrument
2	Wertheim compression forceps, angled
1	Schröder uterine tenaculum forceps, straight
2	Maier sponge forceps curved, 262 mm
6	Maier sponge forceps straight, 265 mm
	Needle holders
2	DeBakey needle holder, 250 mm
2	DeBakey needle holder, 210 mm
2	Hegar needle holder, 245 mm
2	Hegar needle holder, 205 mm
	Additional devices for abdominal surgery
1	Cobb periosteal dissector, 10 mm
1	Cobb periosteal dissector, 13 mm
1	Cobb periosteal dissector, 19 mm
2	Kidney tray, 250 mm
1	Laboratory bowl, 0.4 L
1	Measuring cup, 1 L
	Additional devices for perineal surgery
6	Allis intestinal grasping forceps, 190 mm
1	Weitlaner retractor blunt, 255 mm
1	Weitlaner retractor blunt, 200 mm
1	Scherback vaginal specula set consisting of a handle, weight, and four blades
2	Perineal retractor 120°, blade size 20 × 70 mm
2	Perineal retractor 120°, blade size 30 × 50 mm
	Electrosurgical instruments
2	Electrosurgical pencil
2	Cutting electrode extension, length 16.5 cm, sharp
2	Bipolar coagulation forceps, tip 2.2 mm, length 22 cm
2	Bipolar coagulation forceps, tip 2.2 mm, length 25 cm
1	LigaSure curved jaw open sealer/dissector
	Bookwalter™ retractor system
1	Oval ring, medium
1	Segmented ring, medium
1	Table post
1	Post coupling
1	Horizontal flex bar
2	Balfour retractor
4	Kelly retractor blade, mini
4	Kelly retractor blade, small
4	Kelly retractor blade, medium
4	Kelly retractor blade, large
4	Kelly retractor blade, extra large
1	Malleable retractor blade, small
2	Malleable retractor blade, large
7	Tilt ratchet mechanism
2	Rotilt ratchet mechanism

8.2 Equipment

Although individual preferences and institutional restrictions often impact the selection of conventional surgical instruments, objective criteria for the optimal performance of cancer field surgery concerning precision, safety, and economy can be given. For the exposure of the deep subperitoneal tissues in the pelvis, particularly in an obese or morbidly obese patient, the most suitable retractor system in our experience is a Bookwalter™ set, as specified in Table 8.1. Providing symmetry is an important function of the system, necessitating the availability of four identical Kelly retractor blades for each size. Another type of surgical tool required for the performance of TMMR (as well as EMMR) are high-frequency vessel sealing devices. Bleeding of the parietal branches of the internal iliac vein during iLND bears a high risk for the patient and has to be strictly avoided. We found that the LigaSure™ curved jaw open sealer/divider is well designed for this as well as many other maneuvers of the procedure. Moreover, a straight bipolar coagulating forceps with a broad (i.e., 2 mm) tip facilitates the vessel stripping technique for iLND. The monopolar devices should be equipped with a blade extension of about 15 cm. The selection of high-frequency instruments is also listed in Table 8.1. We have identified the optimal set of conventional surgical instruments for TMMR/EMMR and iLND and specified them in Table 8.1.

For the manual dynamic exposition of the deep sub- and retroperitoneal tissues, we apply modified Breisky retractors, which originally had been developed for vaginal surgery by axially straightening the slightly curved blade. These devices, termed *bayonet blades* in the conventional instrument list in Table 8.1, are shown Fig. 8.4a,b. Likewise, 120° perineal retractors of different blade sizes are useful in the case of perineal surgery in abdominoperineal procedures (Fig. 11.3). Disposable devices used for TMMR/EMMR and iLND, in addition to the standard pads and towels, include elastic loops, tissue stripes, and a bowel bag. For urologic surgery with anterior EMMR, ureter stents should be

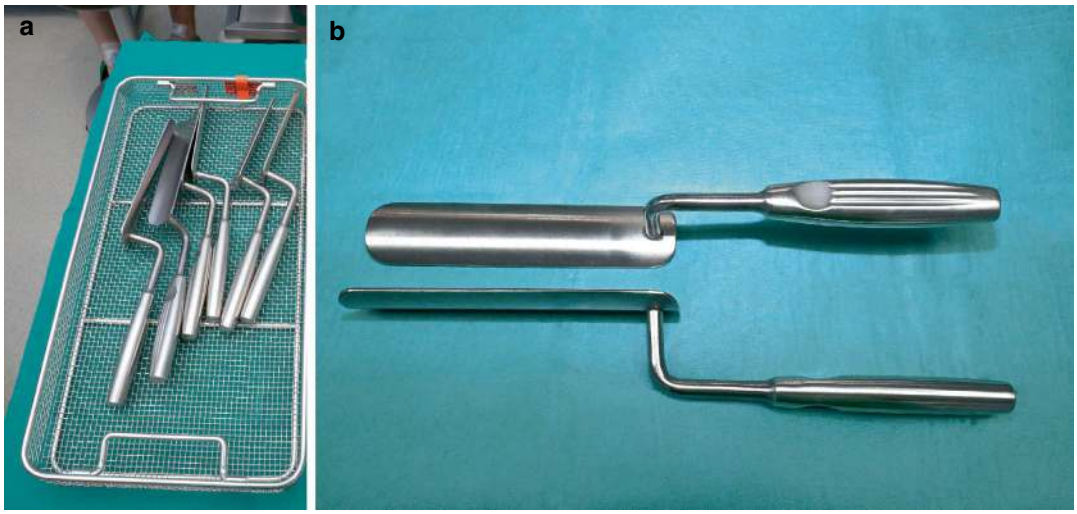

Fig. 8.4 Surgical instruments designed by the Leipzig School. (**a**, **b**) Bayonet retractors

available. Bowel surgery with posterior EMMR is performed with linear and circular stapling devices.

8.3 Patient Preparation and Positioning

Although considered obsolete in abdominal surgery, preoperative mechanical bowel preparation for TMMR and EMMR is recommended to reduce intraoperative bowel volume, which is of particular relevance in obese patients. The operating table must be variable in height, craniocaudal and right-left axes, as well as in leg-back angles. It is optimal to use adjustable bootleg holders for positioning the patient's legs. The knee joint angle should be about 100 degrees, and a straight line should lead from the patella toward the contralateral shoulder. Figure 8.5a–c demonstrates the patient's positioning for TMMR/EMMR. Both a Foley transurethral catheter and a transanal tube are inserted. The legs are cushioned with gel-filled pads against pressure from the surgical assistant's arms. The sagittal abdominal midline should be marked on the patient's skin before disinfection and draping as its accuracy may be blurred later at the time of skin incision due to the covering of anatomical references and positioning. Optimal intraoperative team economics are achieved when the surgeon stands on one side of the patient, with the co-surgeon opposite her or him, the surgical assistant seated between the patient's legs, and the scrub nurse assisting with the main instrument table placed above the head of the patient.

Fig. 8.5 Optimal patient and team positioning for TMMR and EMMR. (**a**) The patient's knee angle should be about 100°; legs must be placed in boot stirrups. (**b**) Foley catheter and bowel tube are inserted; a straight line leads from the patella to the contralateral shoulder; legs are covered with gel pads; sagittal abdominal midline is indicated. (**c**) Team positioning with the second assistant sitting between the patient's legs; main instrument table above the patient's head

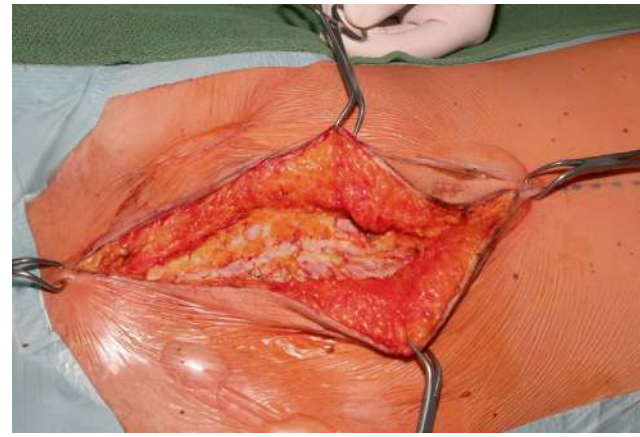

Fig. 8.6 Hypogastric midline laparotomy. The skin incision circumvents the umbilicus on the left side. It is extended into the epigastrium depending on the thickness of the abdominal fat layer and whether third-line lymph node dissection is mandatory. Both abdominal skin flaps are mobilized for 1–2 cm laterally at the fascia

8.4 Abdominal TMMR and iLND: Step-By-Step Procedure

Step 1: Laparotomy—intraperitoneal access (Fig. 8.6)

A midline hypogastric skin incision is made with the scalpel through the dermis, followed by the electric knife through the subcutaneous fat. Its lower pole is set to the pubic crest. The position of the upper pole depends on the thickness of the subcutaneous fat layer. For TMMR/EMMR and first- and second-line lymph node dissection, a rule of thumb is to extend the laparotomy to a distance corresponding to the thickness of the subcutaneous fatty tissue layer above the umbilicus. Both abdominal skin-fat flaps are mobilized about 1–2 cm laterally immediately above the rectus fascia, which is then incised exactly at the linea alba. The incision proceeds between the medial margins of the rectus abdominis muscles to the preperitoneal fat and the parietal peritoneum. The peritoneum is lifted and incised at the urachus, first cranialward and then caudalward toward the apex of the bladder dome. The caudal peritoneal incision deviates somewhat to the left to avoid the bladder until reaching the pubic crest. The margins of the incised hypogastric parietal peritoneum are then sutured to the skin at the symphysis (6 o'clock position) and at the left (3 o'clock) and right (9 o'clock) positions.

The standard technique of laparotomy has to be modified in cases of previous laparotomies—either longitudinal or transverse—or when encountering an umbilical hernia. In these situations, abdominal wall scarring and defects with protruding abdominal contents, as well as peritoneal adhesions, have to be considered and eventually treated.

Two Fritsch manual retractors are inserted bilaterally at the adhesion-free laparotomy sites, and movable parts of the omentum majus and small and large bowel are advanced over the epigastric skin, which enables the surgeon to explore the intraperitoneal pelvis and lower abdomen, as well as the intestines. The subperitoneum is systematically palpated for tumors and to assess the movability of the uterus.

Step 2: Retroperitoneal access; mobilization, wrapping, and retraction of the intestines (Figs. 8.7, 8.8, 8.9 and 8.10)

The parietal peritoneum is incised above the right psoas muscle at the pelvic inlet, just lateral to the ovarian vessels crossing the ureter. The peritoneal incision is advanced cranially in the right paracolic gutter up to the liver margin. Both the ovarian vessels and the ureter are exposed at the lower pole of the peritoneal incision, which is then guided medially parallel to the caudal radix mesenterii crossing the common iliac vessels at the bifurcation until reaching the sigmoid mesen-

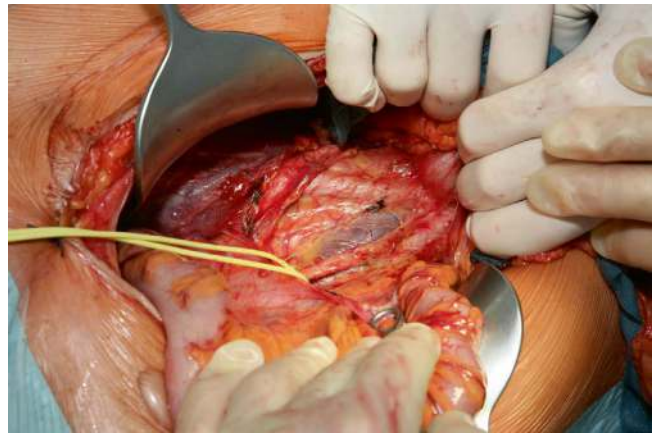

Fig. 8.7 Initial retroperitoneal access. The right parietal peritoneum has been incised above the psoas muscle at the pelvic inlet. The incision proceeded cranially within the right paracolic gutter and parallel to the caudal radix mesenterii to expose the right ovarian vessels, right ureter, and superior hypogastric plexus entwined by an elastic loop

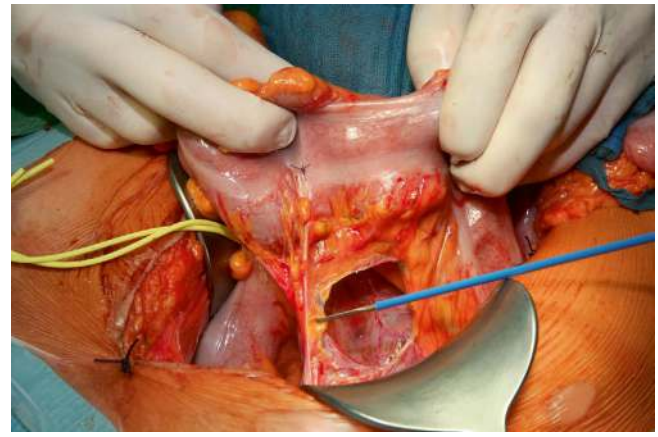

Fig. 8.8 Lysis of the connatal adhesions of the sigmoid colon. The adhesion site is marked by a fine suture in the taenia for peritoneal reconstruction at the end of the operation.

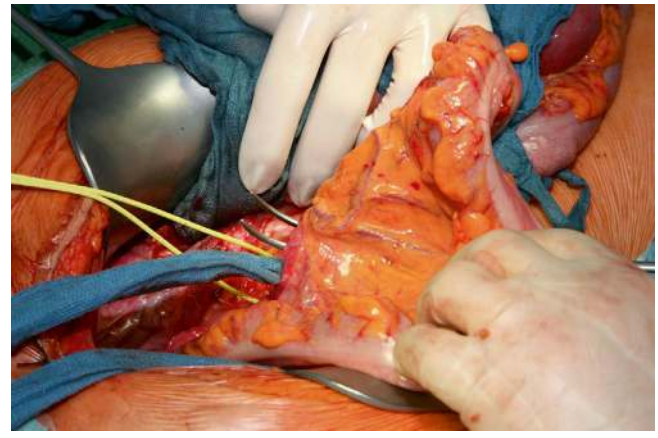

Fig. 8.9 Placement of tissue stripes at the rectosigmoid transition through a 5 cm tunnel in the mesosigmoid colon

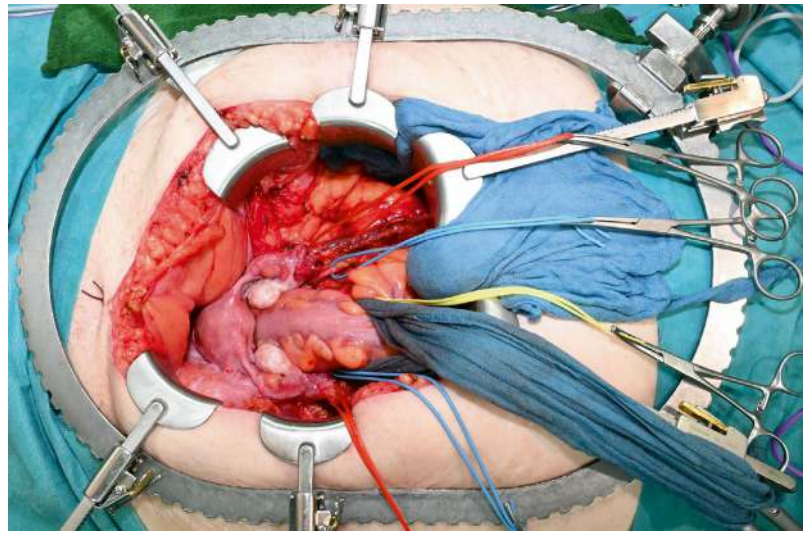

Fig. 8.10 Preparation of the endopelvic surgical field completed. The Bookwalter™ retractor system with an oval ring and six Kelly clamps of appropriate size have been set up. The intestines, except the rectosigmoid colon, are wrapped in a bowel bag and retained cranially

tery. Here, the plexus hypogastricus superior is identified and reined with a fine elastic loop (Fig. 8.7). Further exposing the right ovarian vessels and the ureter, the cecum with the appendix vermiformis is mobilized cranially.

On the left side, the connatal adhesions of the sigmoid colon are identified and lysed. That site is marked by a fine suture in the sigmoid taenia for the functional reconstruction of the connatal adhesions during the final laparotomy closure (Fig. 8.8). The lateral mesosigma is incised at the site of the adhesions, exposing the left ovarian vessels and the ureter. As on the right side, the peritoneal incision is advanced cranially within the left paracolic gutter. The left ovarian vessels and ureter are mobilized to approach the looped plexus hypogastricus superior. The mesosigma is then undermined, creating a tunnel of about 5 cm width to insert two fabric stripes, which will facilitate the mobilization and tension of the rectum at later stages of the operation (Fig. 8.9).

Now, dynamic abdominal wall retraction by the Fritsch devices is substituted with static retraction using the Bookwalter™ retractor system. The size of the six Kelly retractors is selected to fit the thickness of the abdominal walls. Two, usually the shortest, Kelly retractors are placed at the ischiopubic sites of the bony pelvis and another two larger blades at the acetabular sites. It is very important to ensure that the latter blades do not compress the femoral nerves. Therefore, they should not touch the iliopsoas muscles. The right large colon and most of the small bowel are packed into the bowel bag and retained with a large surgical towel before fixing another two blades with a three-dimensional (3D) ratchet to the retractor ring at about 10 o'clock and 2 o'clock positions (Fig. 8.10). The uterine corpus is grasped bilaterally at the proximal round and ovarian proper ligaments with two large Péan clamps allowing to keep it under tension in different directions as needed to perform the following steps.

Step 3: Subperitoneal access—bilateral (Figs. 8.11, 8.12 and 8.13)

The next maneuvers, i.e., genitoperitoneal transections, depend on the indication to include the ovaries in the TMMR. If the preoperative or early intraoperative diagnostics or the wish of the patient do not justify removal, the ovaries are retained. On both sides, the incision of the parietal peritoneum is advanced caudalward in the pelvis to the round ligaments, which are sealed and transected. Likewise, the mesosalpinx, the ligamenta ovarica propria, and the genital peritoneum above the level of the ureters are incised to mobilize both ovaries, together with the mesovaria and a stripe of peritoneal mesometrium

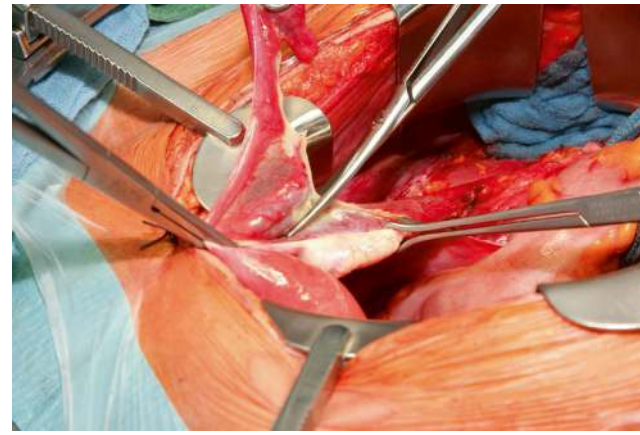

Fig. 8.11 Genito-peritoneal transections. If the ovaries are preserved, the mesosalpinx and the proper ovarian ligament are sealed and transected1

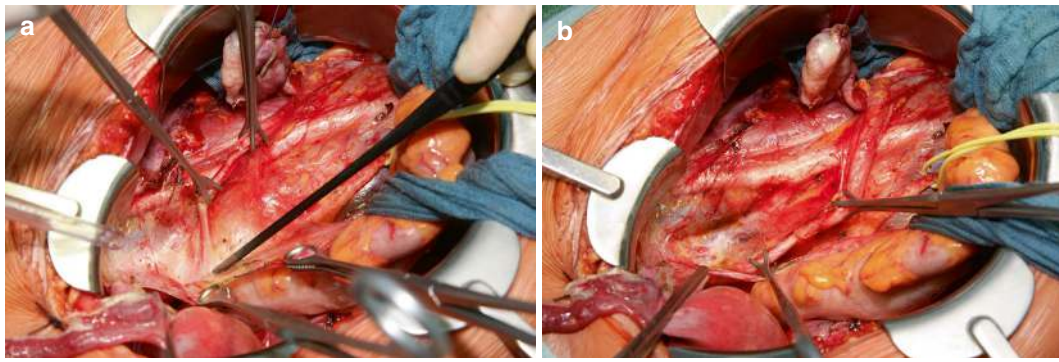

Fig. 8.12 Mobilization of the posterior pelvic ureter. (**a**) The right medial mesureter is dissected from the pararectal peritoneum/fascia and ligamentous mesometrium, exposing the hypogastric nerve and the inferior hypogastric plexus. (**b**) The right lateral mesureter is dissected from the posterior somatic subperitoneum, exposing the internal iliac artery and the estuary of the umbilical artery

cranially (Fig. 8.11). If ovariectomy is indicated, the ovarian vessels are sealed and cut on both sides at the level of the pelvic inlet, instead of the mesosalpinx and the ovarian proper ligament. To include the complete genital peritoneum, posterior lateral pelvic peritoneal incision is performed in projection of the ureter to the level of the vascular mesometrium. Ovariectomy for advanced cervix carcinoma necessitates the inclusion of the complete infundibulopelvic "ligament" to remove intercalated lymph nodes that may harbor metastases (see step 16). Now, the posterior pelvic ureters ensheeted by their mesureters are dissected medially from the pararectal peritoneum and fascia, which are continuous with the peritoneal and ligamentous mesometrium (Fig. 8.12a). The hypogastric nerves and, more ventrocaudally, the inferior hypogastric plexus are encountered and exposed. The lateral mesureteral dissection exposes the internal iliac arteries and the estuaries of the umbilical arteries in the somatic subperitoneum (Fig. 8.12b). Posterior mesureteral mobilization stops at the crossing of the upper vascular mesometria, which represent the distal medial surface of the urogenital mesentery. Anteriorly, the distally obliterated umbilical arteries are fully exposed toward the proximal medial umbilical fold of the anterior abdominal wall. The lateral surface of the urogenital mesentery, which is part of the visceral endopelvic fascia, is then dissected down to the parietal endopelvic fascia and the underlying levator ani muscles (Fig. 8.13). Both arci tendinei become visible. Lateral fascial defects may be encoun-

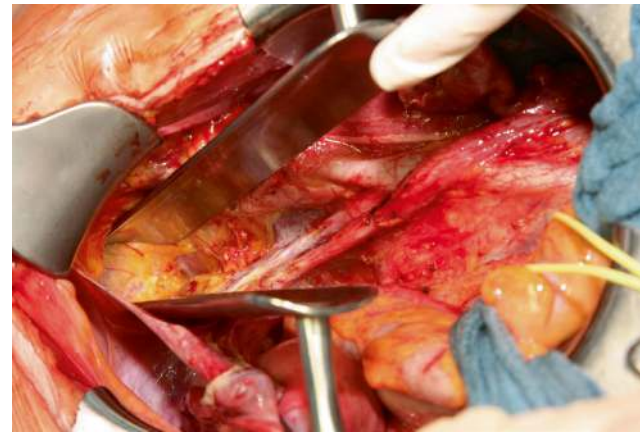

Fig. 8.13 Dissection of the lateral urogenital mesentery from the anterior pelvic retroperitoneum

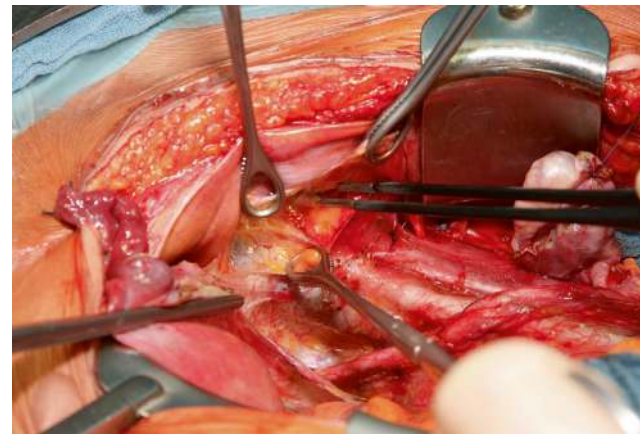

Fig. 8.14 The right retroinguinal fat is removed to expose the lacuna vasorum

tered. At the end of this step of the procedure, the posterior pelvic mesureters and the lateral and distal medial urogenital mesenteries are exposed.

Step 4: External iliac lymph node dissection—bilateral (Figs. 8.14 and 8.15)

Stretching the most caudal parietal peritoneum, the retroinguinal fatty tissue is removed to expose the lacuna vasorum (Fig. 8.14). The peritoneum is then fixed to the skin, similar to how it was done with other peritoneal sites facing the laparotomy. The Kelly retractor of the Bookwalter™ system is substituted by a small Fritsch retractor, to be manually used for dynamic traction during this and the next steps of the operation. The lymph fatty tissue is detached from the external iliac artery through adventitia stripping using straight broad-tipped bipolar forceps (Fig. 8.15). The resection primarily excludes the lacunar nodes and ends about 2 cm beyond the iliac bifurcation. The branches of the genitofemoral nerve should be preserved if they are not involved in metastatic or inflammatory lymph node conglomerates. Dissection then proceeds dorsocaudally along the medial surface of the psoas muscle to the level of the obturator nerve. The external iliac artery is then elevated to detach the lymph fatty tissue between this vessel and the external iliac vein, which is also subjected to adventitia stripping technique thereafter. If lymph node metastases are detected later during the frozen section investigation, the lacunar nodes are removed as well.

Step 5: Paravisceral lymph node dissection—bilateral (Fig. 8.16)

The paravisceral lymph fatty tissue is located in the deep anterior pelvic retroperitoneum below the external iliac vessels, extending laterally to the obturator internus muscle and dorsocaudally

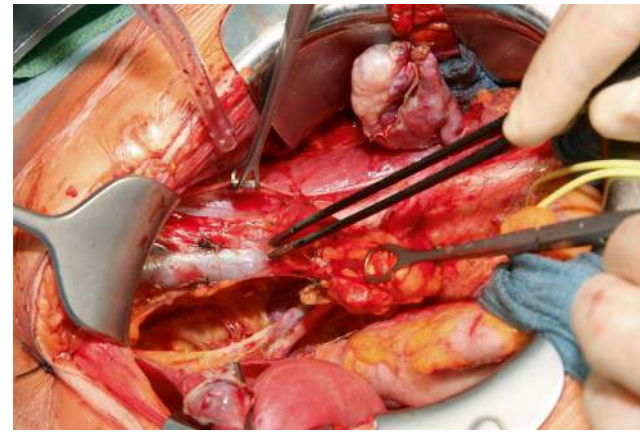

Fig. 8.15 External iliac lymph node dissection. The lymph fatty tissue is detached from the large vessels by bipolar adventitia stripping

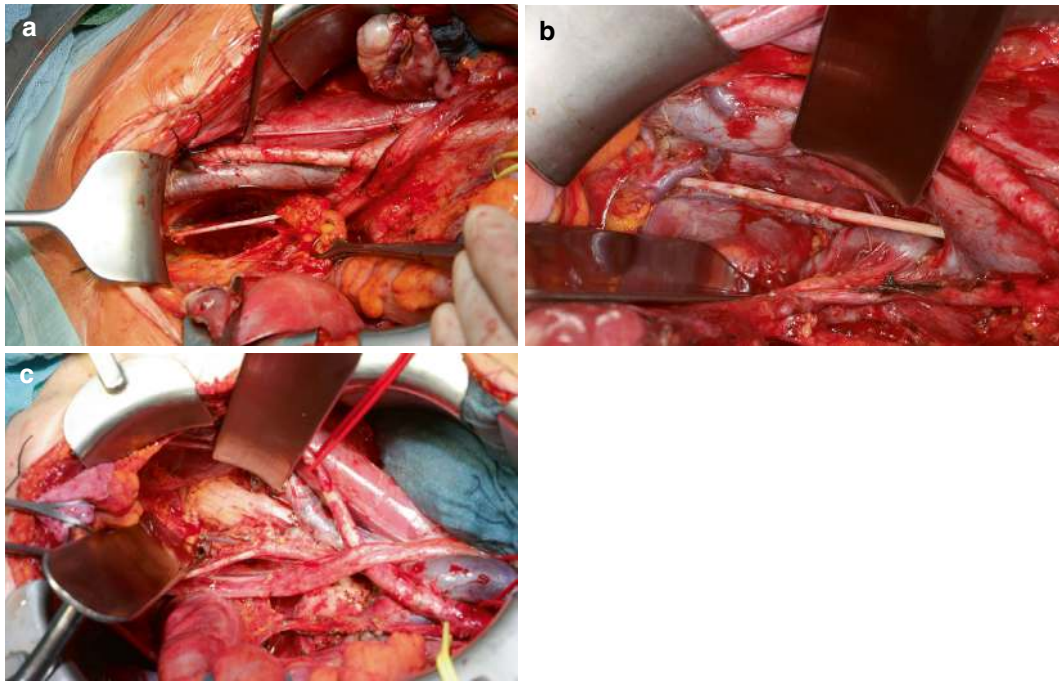

Fig. 8.16 Paravisceral lymph node dissection. (**a**) All paravisceral fatty tissue is removed. The level of the obturator nerve bisects the tissue into upper and lower parts. (**b, c**) Paravisceral lymph node dissection completed. The right pelvic floor and proximal sciatic nerve are exposed

to the parietal endopelvic fascia and levator ani muscles, as well as to the proximal sciatic nerve. This tissue is bordered medially by the visceral endopelvic fascia of the lateral urogenital mesentery and laterally by the obturator internus fascia. The obturator nerve, artery, and veins pass through the paravisceral lymph fatty tissue (Fig. 8.16a).

Dorsocranially, the paravisceral lymph fatty tissue abuts the internal iliac artery and vein with their anterior parietal branches, such as the pudenda interna and superior gluteal vessels. Ventrocaudally, it reaches to the obturator foramen (Fig. 8.16b). For the complete resection of this lymph node region, multiple parietal veins of

the internal iliac system are sealed and transected. The arteries can usually be preserved. This maneuver exposes the proximal sciatic nerve with its lumbar and first and second sacral roots (Fig. 8.16c).

The removal of the paravisceral lymph fatty tissue completes the dissection of the first-line basin lymph nodes. Together with the external iliac lymph node harvest, it is sent to the pathologist for frozen section evaluation.

Step 6: Vesicocervicovaginal separation (Fig. 8.17)

Following the peritoneal incision at the vesicouterine fold, the dorsal wall of the bladder dome is separated from the anterior cervix and proximal vagina by dissection within the bladder adventitia, and both organ systems are kept under tension (Fig. 8.17a). The dissection is advanced mediolaterally toward the bladder mesenteries, which are preserved. Caudally, the level of the ureterovesical junctions should be reached if the spread of cancer to the vagina is excluded (Fig. 8.17b). Otherwise, separation must proceed caudally to the level of the bladder neck. Non-neoplastic scarring, mostly due to a previous cesarean section, can impair the dissection. In these situations, the scar region should be circumferentially exposed and then transected. If the fibrosis connecting both organs is presumed to be caused by cancer invasion, the circumferentially exposed fibrotic zone, together with the adhering bladder parts, must be included in the mesometrial resection, rendering the procedure an extended mesometrial resection (EMMR; see below).

Step 7: Division of the urogenital mesentery—bilateral (Fig. 8.18)

According to the ontogenetic anatomy as described in Chap. 3, the urogenital mesentery is a composite structure consisting of the visceral endopelvic fascia, with the umbilical artery, bladder mesentery, and vascular mesometrium/mesocolpos traversed by the ureter-mesureter complex. The visceral endopelvic fascia-umbilical artery-bladder mesentery complex is dissected from the anterior bordering lamella of the vascular mesometrium to expose the uterine artery originating from the proximal umbilical artery or internal iliac artery and the (superficial) uterine vein(s) originating from the internal iliac vein. The posterior bordering lamella of the vascular mesometrium is separated from the lateral ureter-mesureter complex. During these dissections, venous connections may be encountered, which have to be sealed and transected.

The medial ureter-mesureter complex was separated from the ventral inferior hypogastric plexus during step 3 of the procedure. Figure 8.18 demonstrates the left urogenital mesentery divided into three components: (1) the bladder mesentery with the visceral endopelvic fascia and umbilical artery, (2) the vascular mesometrium, and (3) the ureter-mesureter complex. As with the previous step, the dissections can be hin-

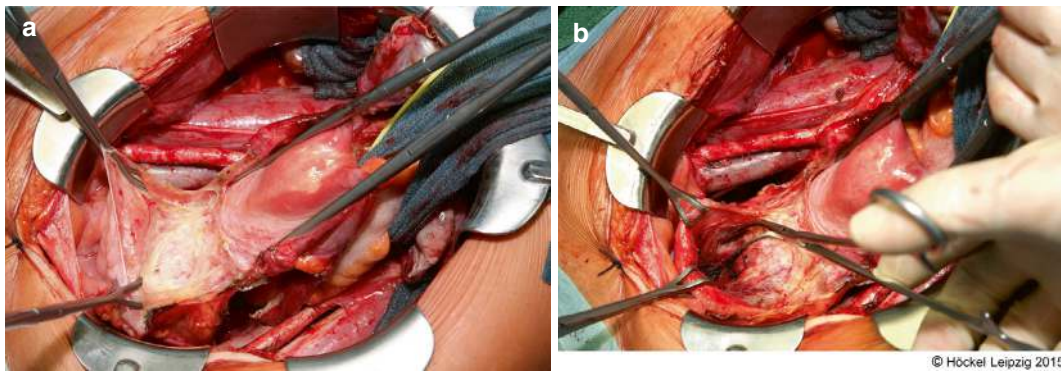

Fig. 8.17 Vesicocervicovaginal separation. (**a**) Both the bladder and the uterus are kept under tension to dissect the areolar tissue between the bladder dome (allantois bladder) and Müllerian adventitia. (**b**) Vesicocervicovaginal dissection proceeds craniocaudally and mediolaterally toward the ureterovesical junctions

Fig. 8.18 The left urogenital mesentery has been dissected into three tissue components: bladder mesentery with visceral endopelvic fascia and umbilical artery, vascular mesometrium, ureter with mesureter

dered by fibrosis. Although benign causes for these urogenital mesentery fibroses, such as endometriosis, are possible, this cannot be assured when treating cervicovaginal cancer. Therefore, fibrosis preventing the dissection of the intact mesostructures may necessitate the inclusion of the complete urogenital mesentery, as well as a part of the distal ureter, into the mesometrial resection specimen, rendering the procedure an EMMR (see below).

Step 8: Transection of the vascular mesometria/mesocolpoi—bilateral (Figs. 8.19, 8.20 and 8.21)

The fully exposed vascular mesometrium is sealed and transected laterally at the branching of the uterine artery and the (superficial) uterine vein(s) from the umbilical or internal iliac artery and internal iliac vein (Fig. 8.19a). The mesometrium flap containing the uterine vessels and lymph fatty tissue is mobilized medially and flipped dorsally above the ureter-mesureter complex (Fig. 8.19b). With dorsal tension of the mesometrial flap its anterior connection to the bladder adventitia and proximal bladder mesentery, including the vesicouterine venous plexus and the vaginal artery, is undermined immediately above the ureter-mesureter complex, sealed, and transected (Fig. 8.19c, d). To mobilize the ureter-mesureter complex laterally, approaching the vascular mesocolpos, the vaginal vein is exposed, sealed, and cut (Fig. 8.20). Now, the plexus hypogastricus inferior is detached from the pararectal fascia, continuous with the ligamentous mesometrium (Fig. 8.21a). The autonomous nerve branches deviating medially to the uterus and the proximal vagina (Frankenhäuser's plexus) are transected (Fig. 8.21b) in order to further lateralize the mesureter and expose the ligamentous mesocolpos (Fig. 8.21c), which forms a smooth tissue sheet together with the ligamentous mesometrium.

Step 9: Rectovaginal separation (Fig. 8.22)

With cranialward traction on the anterior rectum and the simultaneous lateral spreading of the residual deep dorsal peritoneal mesometrium, the rectouterine pouch is exposed. At its deepest point midsagittally, the peritoneum is incised (Fig. 8.22a). The incision is extended dorsolaterally on both sides of the mesorectum. The anterior rectum and anterolateral mesorectum are dissected from the ligamentous mesometria/mesocolpoi (Fig. 8.22b). The dissection is advanced laterally on both sides to about 3 and 9 o'clock at the mesorectal perimeter. The caudal extension depends on the planned location of the colpotomy. This maneuver can be spoiled by fibrotic tissue adherence due to pathological conditions such as (previous) pelvic inflammatory disease or endometriosis. If the fibrosis is caused by cancer spread, dorsally extended mesometrial resection may be necessary (described in the EMMR section).

Step 10: Transection of the ligamentous mesometria/mesocolpoi—bilateral (Fig. 8.23)

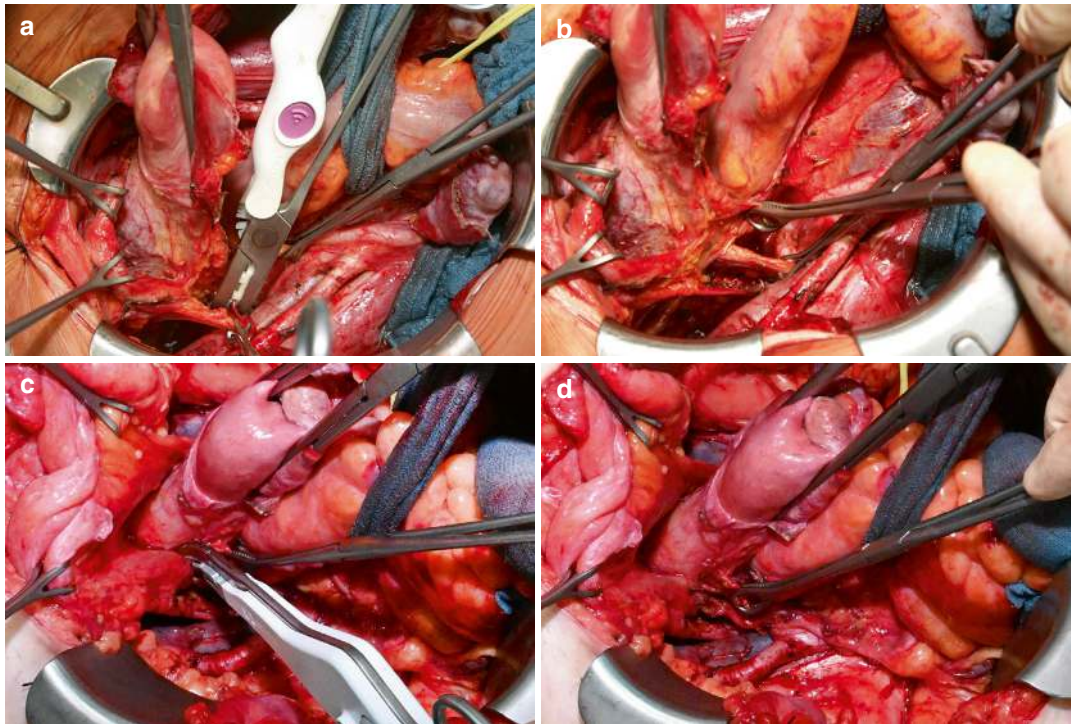

Fig. 8.19 (**a**) The left vascular mesometrium is sealed and transected laterally at the branching of the uterine artery and veins from the umbilical artery and internal iliac vein. (**b**) The mesometrium flap is flipped dorsomedially to cross the ureter, which is kept at dorsolateral tension. (**c, d**) The supraureteral anterior part of the vascular mesometrium containing the vesicovaginal venous plexus is undermined, sealed, and transected

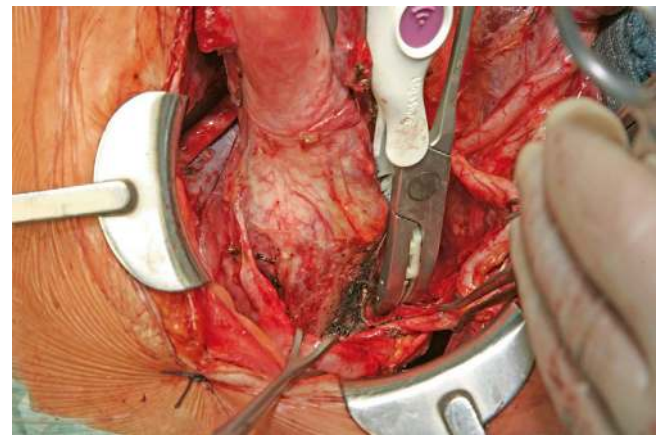

Fig. 8.20 The infraureteral vascular mesocolpos at the level of the deep uterine or vaginal vein is sealed and transected, taking care not to damage the laterally adjacent mesureter

With ventrocaudal traction on the uterus and ventrocranial traction on the rectum, the ligamentous mesometria/mesocolpoi-perirectal fascia complex is sealed and transected following the course of the hypogastric nerves and upper inferior hypogastric plexus—which had been mobilized laterally before—along the pelvic curvature up to the previous transection site of the vascular mesocolpos (Fig. 8.23a). After this maneuver, the subtotal Müllerian compartment encased by the genital serosa and peritoneal mesenteries and subperitoneally by vascular and ligamentous

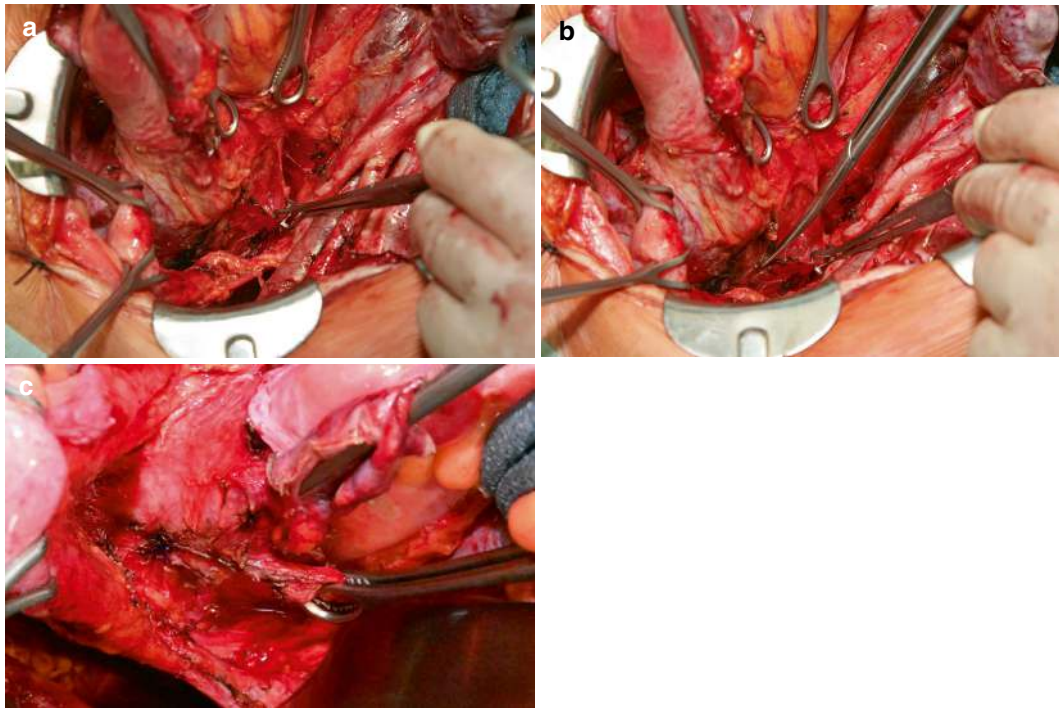

Fig. 8.21 (**a**) The left hypogastric plexus is detached from the ligamentous mesometrium/mesocolpos-perirectal fascia complex to expose its uterovaginal branches (plexus of Frankenhäuser). (**b**) These nerve branches are sealed and transected, again respecting the adjacent mesureter. (**c**) The left ligamentous mesometrium continuous with the upper mesocolpos is exposed

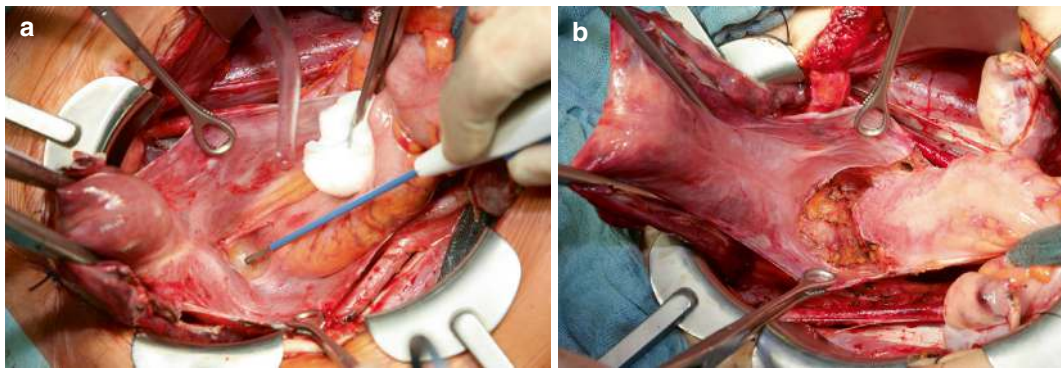

Fig. 8.22 (**a**) Incision of the rectovaginal peritoneal fold separating the rectal peritoneum from the pararectal peritoneum. (**b**) The perirectal fascia and ligamentous mesometrium/mesocolpos have been dissected from the mesorectum at the anterior hemicircumference of the rectum

mesometria/mesocolpoi is only connected to the distal vagina (Fig. 8.23b, c).

Step 11: Colpotomy (Fig. 8.24)

The colpotomy is facilitated by the prior uniting of the bilateral ligamentous and vascular mesometria/mesocolpoi with a suture at the dorsal uterus for better visibility. A rectangular Wertheim clamp is usually applied from the right side to temporarily obliterate the proximal vagina. Large tumor masses may demand the

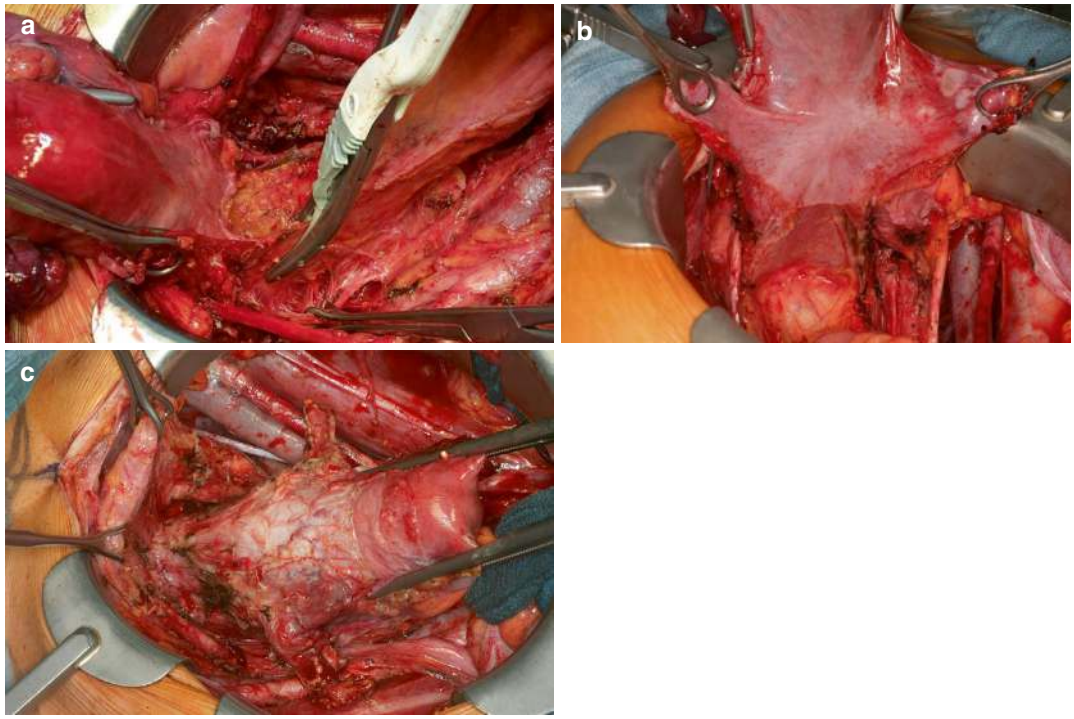

Fig. 8.23 (**a**) The ligamentous mesometria and mesocolpoi are sealed and transected from the pararectal fascia at about 3 and 9 o'clock of the mesorectal perimeter following the pelvic curvature and keeping the hypogastric nerves and inferior hypogastric plexus at lateral traction. (**b**) Subtotal Müllerian compartment with ligamentous mesometria/mesocolpoi "wings" viewed from posterior. (**c**) Subtotal Müllerian compartment with vascular mesometria/mesocolpoi "wings" viewed from anterior

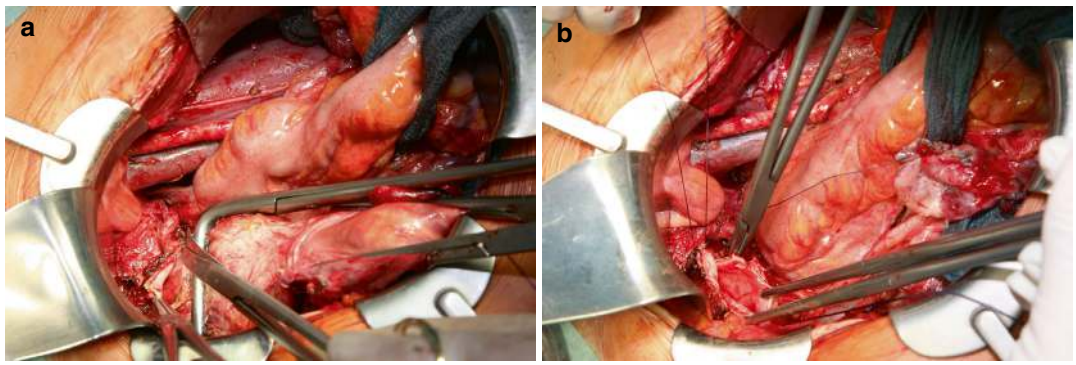

Fig. 8.24 (**a**) Anterior colpotomy is performed approximately 1 cm distal to the rectangular Wertheim clamp that closes the proximal vagina to prevent cancer cell spilling. (**b**) Colpotomy closure with a running inverting suture

placement of two clamps from both the right and left sides. Retracting the bladder with a blade, the colpotomy is started at the 12 o'clock position of the vaginal perimeter by point incision. The colpotomy is advanced to the 9 and 3 o'clock positions, and the distal anterior vaginal resection margin is grasped by large Kocher clamps and pulled ventrally (Fig. 8.24a). The posterior colpotomy is then done analogously. The TMMR specimen is sent for frozen section examination

to histopathologically assess the vaginal resection margin and the uterine corpus for neoplastic involvement. The colpotomy is closed by an inverting running suture (Fig. 8.24b).

Extensive lavage of the pelvis should be done to minimize the contamination associated with the colpotomy. Retrograde filling of the bladder with about 300 mL saline is done to check for focal defects of the adventitia and muscularis layers that need to be oversewn.

Step 12: Resection of intercalated lymph nodes in the distal urogenital mesentery—bilateral (Fig. 8.25)

Fatty tissue at the estuaries of the bladder vessels and umbilical artery to the internal iliac vessels (stars), which may contain intercalated lymph nodes, is removed, skeletoning the distal vesical arteries (Fig. 8.25a) and veins (Fig. 8.25b).

Step 13: Common iliac lymph node dissection—bilateral (Fig. 8.26)

As demonstrated in Chap. 6, defense line-directed lymph node dissection necessitates the removal of the parietal (basin) first-line lymph nodes for all cervix carcinomas to be treated with TMMR. If second-line lymph node dissection is indicated, the clearance of the common iliac lymph node regions is performed as the next step. Adventitia stripping is done along the common iliac artery, respecting and preserving the plexus hypogastricus superior, which had been exposed and grasped by an elastic loop already during step 2. The artery is detached from the common iliac vein to ensure completeness of the resection. Next, the common iliac vein is mobilized toward the psoas muscle, and all fatty tissue is removed along its course to expose the obturator nerve and

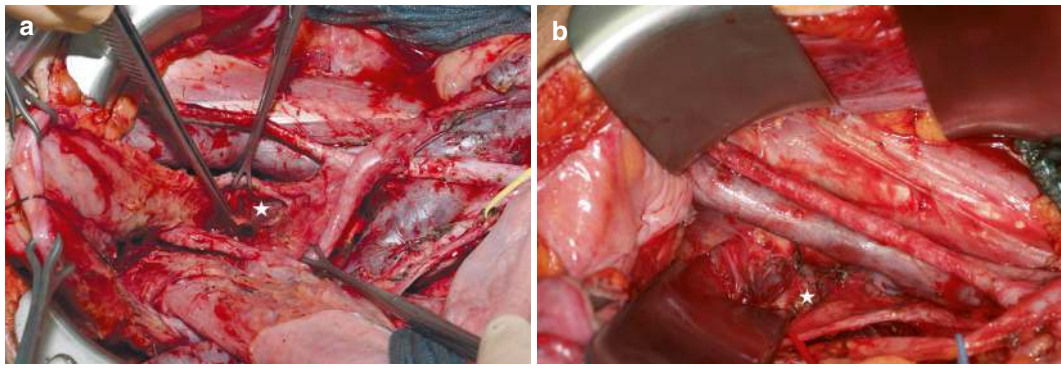

Fig. 8.25 Distal urogenital mesentery lymph node dissection. (**a**) Lymph fatty tissue at the proximal umbilical artery and distal internal iliac artery is removed. (**b**) Lymph fatty tissue at the estuaries of the bladder veins into the internal iliac vein is removed

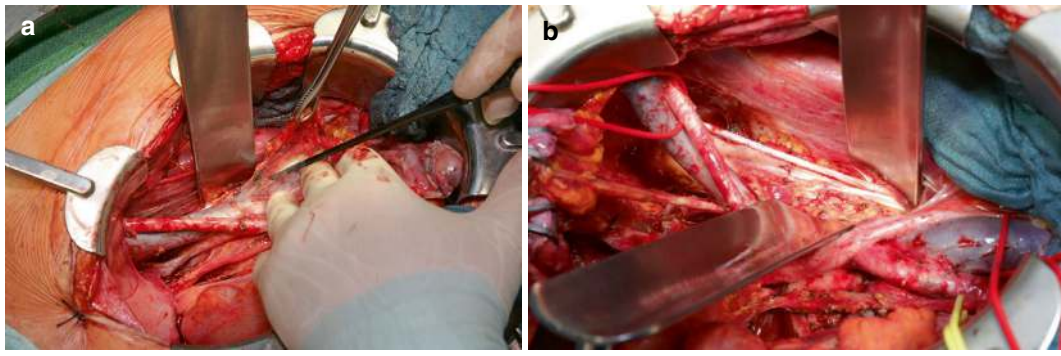

Fig. 8.26 Common iliac lymph node dissection. (**a**) The right common iliac vein is detached from the psoas muscle, and after sealing and transecting the iliolumbar veins, it is moved medially to completely harvest the lymph fatty tissue. (**b**) At the right pelvic inlet, the obturator nerve and the lumbar root of the sciatic nerve are exposed

the lumbar root of the sciatic nerve (Fig. 8.26a). After sealing iliolumbar veins, resection of the lymph fatty tissue below the large vein completes the common iliac lymph node dissection (Fig. 8.26b).

Step 14: Presacrococcygeal lymph node dissection—bilateral (Fig. 8.27)

Lymph fatty tissue is extirpated from the bifurcation of the common iliac veins caudalward to clear the promontorium first. Both the common iliac artery and vein should be elevated, e.g., by vessel loops, to ensure the completeness of the lymph node dissection toward the psoas muscle and the first sacral vertebra (Fig. 8.27a). Respecting the mesureter, and a ureter branch from the internal iliac artery in particular, the lymph fatty tissue dorsal to the internal iliac vessel system is resected. Presacrococcygeal lymph node dissection proceeds dorsally to the mesureter to remove both basin and intercalated lymph nodes. For the former, windows are created between the lateral sacral and the internal iliac veins to expose the lower sciatic nerve roots. Lymph node dissection has to respect the nervi splanchnici pelvici, which unite with the inferior hypogastric plexus. The pararectal fascia is the medial border of the presacrococcygeal lymph node dissection (Fig. 8.27b).

Step 15: Aortic bifurcation lymph node dissection (Fig. 8.28)

The resection of the lymph fatty tissues at the aortic bifurcation above, lateral to, and between the large vessels clears the caudal aorta abdominalis and the vena cava inferior up to the level of the origin of the inferior mesenteric artery. If not included in metastatic lymph node conglomerates, the major two nervi splanchnici lumbales are preserved (Fig. 8.28a). The mesureters change their direction when crossing the common iliac vessels from medial in the true pelvis to lateral in the lumbar region. Following the sealing and cutting of lumbar veins, both large vessels are elevated to remove the retrovascular lymph fatty tissue (Fig. 8.28b).

Step 16: Infrarenal periaortic lymph node dissection (Fig. 8.29) **and mesenteric periaortic lymph node dissection** (Fig. 8.30)

For the most extended execution of defense line-directed lymph node dissection, the laparotomy has to be advanced in the epigastric midline to the xyphoid process of the sternum. Again, the parietal peritoneum is sutured to the skin. Colon ascendens, duodenum, and colon descendens are mobilized further cranialward and above the skin level until the left renal vein is fully exposed. The bowel is temporarily kept in

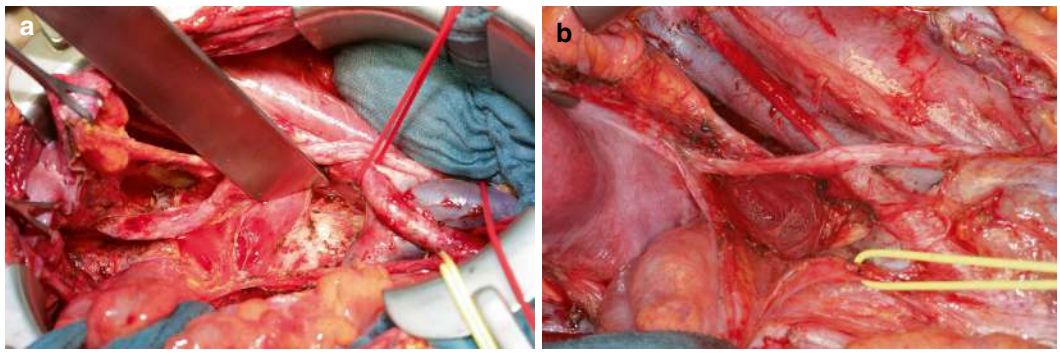

Fig. 8.27 Presacrococcygeal lymph node dissection. (**a**) Upper presacral lymph node dissection. The right common iliac vessels are elevated with elastic loops to remove all lymph fatty tissue at the level of S1 and S2. The mesureter and superior hypogastric plexus are preserved. (**b**) Lateral to the plexus hypogastricus inferior and dorsal to the mesureter, the lower presacral/precoccygeal lymph fatty tissue is removed, respecting the nervi splanchnici pelvici

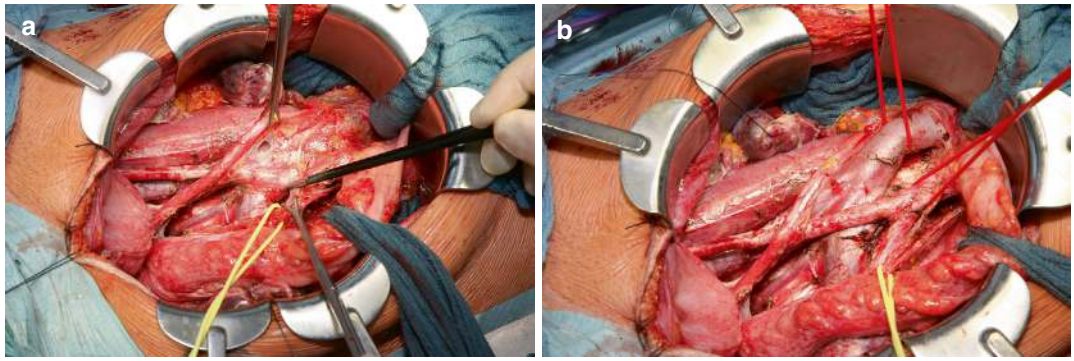

Fig. 8.28 Aortic bifurcation lymph node dissection. (**a**) Lymph fatty tissue encasing the venous and arterial bifurcation is removed, preserving the superior hypogastric plexus and the nervi splanchnici lumbales. (**b**) The large vessels are elevated with elastic loops to include the retrocaval and retroaortic lymph nodes into the resected tissue

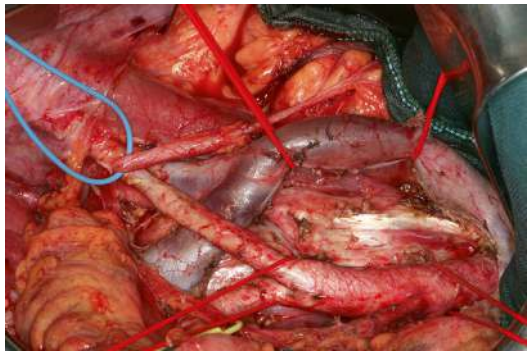

Fig. 8.29 Infrarenal periaortic lymph node dissection completed. Both large vessels are elevated with elastic loops after lumbar vessels have been transected. The right lumbar splanchnic nerve has been severed in this case; however, the left one is preserved

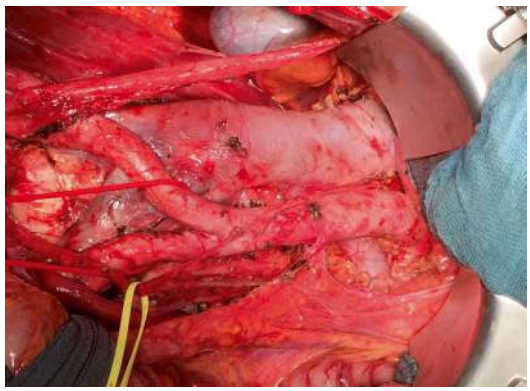

Fig. 8.30 Mesenteric periaortic lymph node dissection. Resection of the right ovarian vessels with associated aortocaval lymph nodes and of the left ovarian vessels with associated paraaortic lymph nodes. Retrocaval and retroaortic nodes remain in situ

this position by Kelly retractors fixed with 3D ratchets. The right ovarian vein and artery are sealed and cut at their estuary and origin, respectively, in order to completely remove the "infundibulopelvic ligament." All lymph fatty tissue above, lateral to, and between the large vessels is then resected from the level of the left renal vein to the aortic bifurcation that had been cleared already. Optimally, both the right and left, but at least the left, major lumbar splanchnic nerve(s) should be preserved. The inferior mesenteric artery is skeletonized proximally. Following the sealing and severing of lumbar veins, both the vena cava inferior and the aorta can be elevated with vessel loops to harvest the retrovascular lymph fatty tissue and expose the prevertebral fascia (Fig. 8.29). Lateral to the aorta, the left ovarian artery (which usually has been divided at this stage of the operation) and the left ovarian vein at its branching from the renal vein are identified medial to the renal pelvis and proximal ureter. The ovarian vein is sealed and transected, and the left "infundibulopelvic ligament" is dissected caudalward and removed.

In the case of oT2 cervix carcinomas infiltrating the uterine fundus and oT3a cancers without metastases in the aortic bifurcation region, infrarenal periaortic lymph node dissection can be substituted by *mesenteric periaortic lymph node dissection*. This procedure removes the right ovarian vessels with adjacent aortocaval lymph nodes and the left ovarian vessels with adjacent

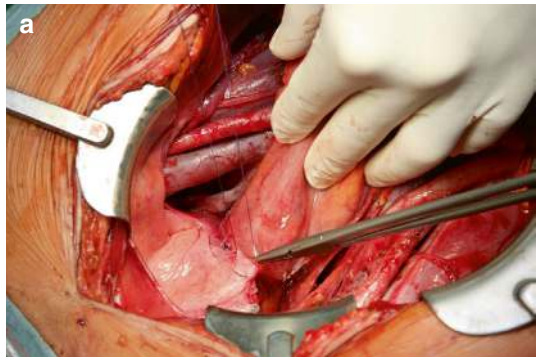

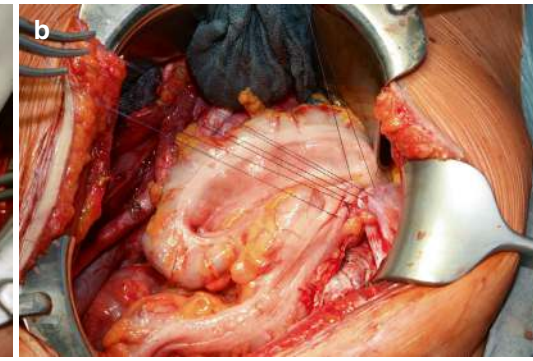

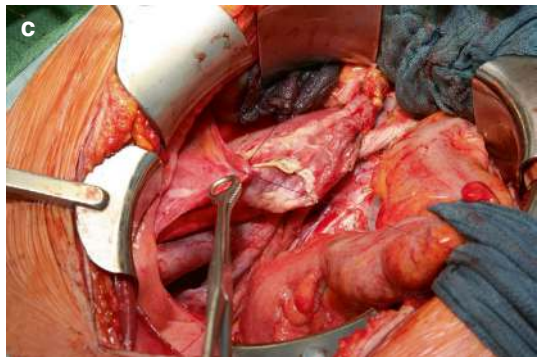

Fig. 8.31 Peritoneal reconstruction. (**a**) Bladder and rectum peritoneal flaps are united over the vaginal stump. (**b**) Connatal adhesions of the sigmoid colon are substituted by four sutures, adapting the mesosigma to the parietal peritoneum at the site previously marked. (**c**) Torsion-safe fixation of the ovaries at the pelvic inlet. The right ovary is sutured linearly over a distance of about 5 cm at the level of its original position by uniting preserved periovarial peritoneum with the remaining parietal peritoneum

periaortic lymph nodes (Fig. 8.30). Retrocaval and retroaortic lymph nodes remain in situ.

Although blood vessel anomalies can be encountered at all sites of the lymph node dissection, they are relatively frequent in the periaortic region. Large volume veins may be present, besides the vena cava and the renal and ovarian veins. Likewise, additional renal arteries supplying the lower kidney poles should be expected. If confluent lymph node metastases encase blood vessels or nerves to be preserved, stepwise detachment is facilitated by the application of Cobb periosteal dissectors equipped at the tip with sterile gel to reduce the friction.

Step 17: Peritoneal reconstruction and laparotomy closure (Figs. 8.31, 8.32 and 8.33)

After thorough lavage of the surgical field, the bladder and rectum peritoneal flaps are sutured over the vaginal vault as a presumed means to prevent infection (Fig. 8.31a). The connatal adhesions of the colon sigmoideum are substituted by four sutures uniting the lateral sigma serosa and the parietal peritoneum at the site marked before

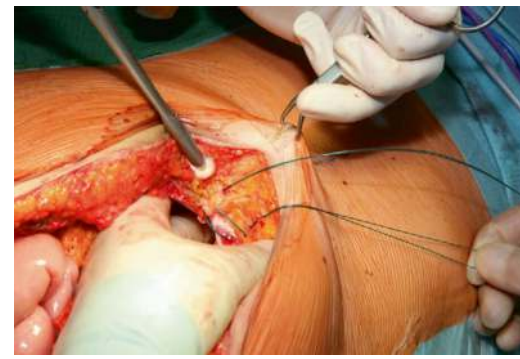

Fig. 8.32 Laparotomy closure with a running sling suture through all abdominal wall layers

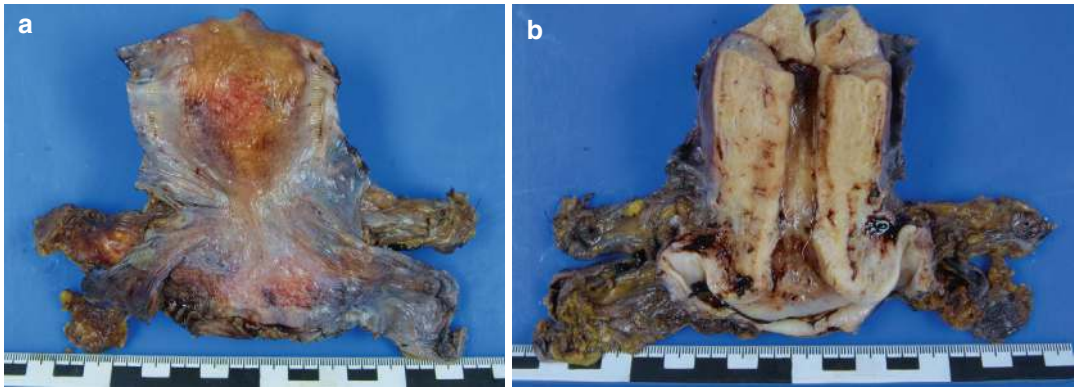

Fig. 8.33 Formalin-fixed TMMR specimen. The anterior uterus and vagina have been incised midsagittally. The characteristic four "wings" representing the vascular and ligamentous mesometria/mesocolpoi are spread laterally. (**a**) Posterior view. (**b**) Anterior view

(step 2) (Fig. 8.31b). If preserved, the ovaries are sutured to the parietal peritoneum at their previous pelvic locations. For torsion-safe fixation, the retained stripes of the periovarian genital peritoneum are linearly connected to the parietal peritoneal margins for about 5 cm (Fig. 8.31c). If abdominal drainage is applied, only soft devices, such as the Easy Flow system, should be used, ensuring that their ends cannot touch the stumps of the sealed parietal branches of the internal iliac veins. The laparotomy is closed by an absorbable running suture through all abdominal wall layers (Fig. 8.32). No sutures are placed into the subcutaneous fatty tissue. The skin may be stapled or closed by an intracutaneous suture.

The TMMR specimen exhibits the characteristic four "wings," representing the bilateral vascular mesometria/mesocolpoi and ligamentous peritoneal mesometria/mesocolpoi (Fig. 8.33).

8.5 TMMR on the Gravid Uterus (Fig. 8.34)

Depending on the gestational age, TMMR is carried out with the conceptus in situ or immediately following a cesarean section by midline hypogastric laparotomy and corporal uterotomy. After closure of the uterotomy with muscular sutures, the laparotomy is extended, and all steps of the standard TMMR are applied. The pregnancy-associated tissue changes rather facilitate the dissection at the tissue planes defined by ontogenetic anatomy (Fig. 8.34).

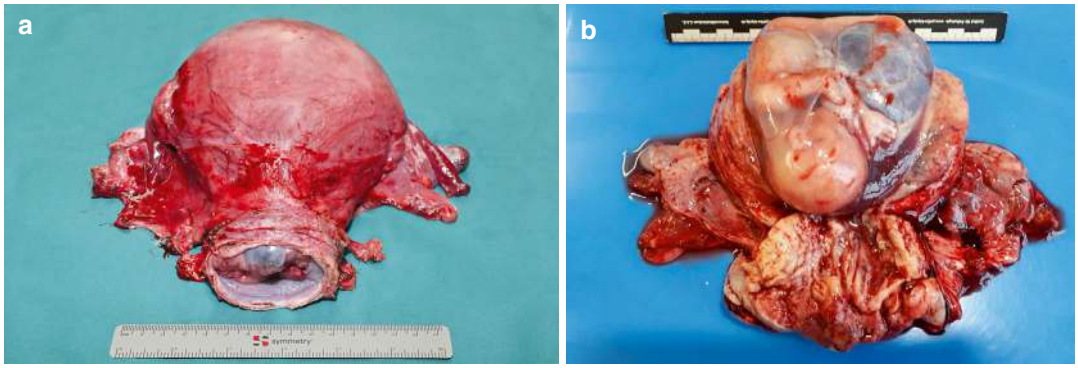

Fig. 8.34 TMMR on gravid uterus. TMMR specimen containing a 16-week gestational product. (**a**) Intact. (**b**) Ventrally incised

8.6 TMMR After Supracervical Hysterectomy

The modification of the TMMR procedure, as described when the uterine corpus had been removed for benign disease, is minor and relates to the means to initiate the subperitoneal access and to maintain differentiated tension on the cervix. The cervix cannot be grasped laterally with Péan clamps as it is done with the uterine corpus in place but has to be atraumatically held more medially, e.g., with Babcock clamps. If the ovaries are still in situ connected to the ovarian vessels and should be retained, they have to be freed from peritoneal adhesions and mobilized cranialward; otherwise, the ovarian vessels are sealed and transected to remove the residual adnexal structures completely. The incision of the pelvic peritoneum is extended along the psoas muscles to the stumps of the round ligaments. Remnants of the peritoneal mesometria (broad ligament) are mobilized medially toward the cervix, preserving their continuity.

8.7 TMMR After Total Hysterectomy (Fig. 8.35)

The resection of the proximal vagina, together with the vascular and ligamentous mesometria and mesocolpoi (Fig. 8.35), is indicated for posthysterectomy early carcinomas of the suprasinus vagina or—more often—when unexpectedly an early cervix carcinoma has been histopathologically detected in a total hysterectomy specimen. The prerequisite for the application of cancer field surgery in the latter case is an oT1 or oT2 stage carcinoma after a microscopically complete (R0) resection by the previous operation. Otherwise, radiotherapy is advocated to supplement the inadvertent treatment by simple hysterectomy.

Moreover, a late phase of posthysterectomy wound healing, i.e., about 6 weeks postoperatively, has to be awaited before dissection can be successfully performed. Generally, step 3 (subperitoneal access), step 6 (vesicocervicovaginal separation), and step 9 (rectovaginal separation) have to be modified, and traction is applied transvaginally, e.g., with a curved Maier clamp armed with a sponge.

Subperitoneal access is obtained similarly as described for TMMR after supracervical hysterectomy. Mobilization of the bladder dome is made significantly more difficult due to scarring from the hysterectomy. Usually, the vaginal apex is completely buried under the bladder and fixed to it by thick fibroses. Bladder injury may not be avoidable during vesicovaginal separation, and lesions have to be repaired according to urological principles and techniques. Likewise, rectovaginal separation may be hindered by posthysterectomy fibrosis.

Fig. 8.35 Formalin-fixed specimen of vaginal stump TMMR. View from below: the vascular and ligamentous mesometrial remnants and the mesocolpoi have been resected together with the vaginal vault after a previous inadvertent simple hysterectomy for early cervix carcinoma

To reduce the risk of postoperative vesicovaginal and rectovaginal fistula formation in high-risk cases, the application of an omentum majus flap elevating a part of the greater omentum and transposing it to the pelvis is advisable (see Chap. 10 for procedural details).

8.8 Abdominal EMMR

As outlined above, EMMR includes non-Müllerian adjacent tissues, in addition to the vascular and ligamentous mesometria/mesocolpoi, to ensure R0 resection in situations of distorted subperitoneal anatomy and unsuspected tumor extension (Fig. 8.1). For the vast majority of EMMRs, parts of the bladder and its unilateral mesentery are removed. In the latter case, a distal part of the ureter is also part of the EMMR specimen necessitating ureterovesiconeostomy. The resection of the complete urogenital mesentery, i.e., the vascular mesometrium/mesocolpos, together with the bladder mesentery, can only be done on one side to ensure sufficient bladder function. These procedures are designated as anterior EMMR. Less frequently, parts of the mesorectum and rectum have to be extirpated en bloc with the TMMR, rendering the procedures as posterior EMMR.

With anterior EMMR, steps 6, 7, and 8 have to be modified, as well as steps 9, 10, and 11 with posterior EMMR. All other maneuvers correspond to the standard TMMR technique.

8.9 Anterior EMMR

8.9.1 Modification of TMMR Step 6

If during step 6 focal fibrosis due to suspected neoplastic infiltration spoils the vesico-Müllerian separation, the zone of vesicouterine adherence must be circumferentially exposed by adventitia dissection. Full-thickness bladder wall excision should then include a 1–2 cm wide margin of the uninvolved bladder wall, which is only possible in focal adherence zones located medially at the dorsal bladder wall.

8.10 Modification of TMMR Steps 7 and 8: Unilateral (Fig. 8.36)

If the division of the urogenital mesentery into bladder mesentery, vascular mesometrium, and mesureter is spoiled due to fibrosis, whether of a malignant or nonmalignant cause, the complete ipsilateral urogenital mesentery and the distal ureter must be transected to ensure locoregional tumor control at this site. Therefore, all visceral arterial and venous branches of the internal iliac vessel system are sealed and transected (Fig. 8.36a). The umbilical artery is also cut at its obliterated part. The ureter is transected 1–2 cm proximal from its entry into the urogenital mesentery. A slice biopsy of the ureter is sent for frozen section assessment, and the proximal ureter is temporarily splinted with a soft catheter

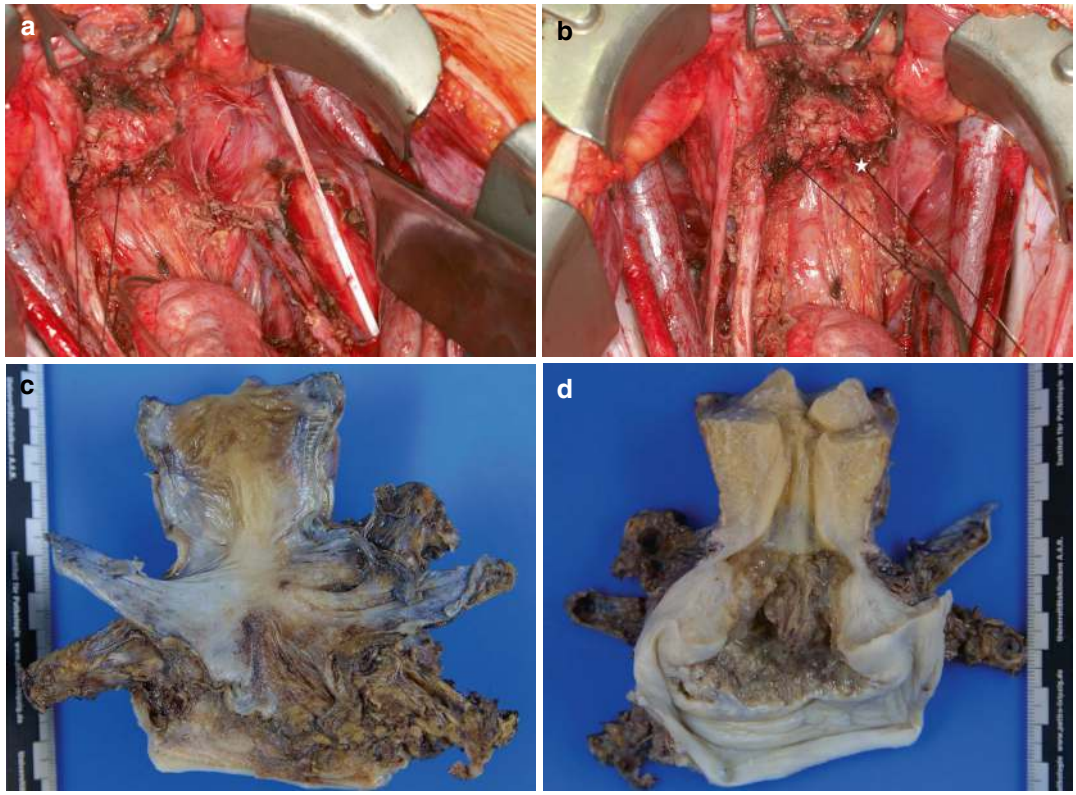

Fig. 8.36 Anterior EMMR, including the right urogenital mesentery. (**a**) The right urogenital mesentery, including the umbilical artery, all bladder vessels, and the distal ureter, have been resected. (**b**) The lower branches of the right ventral inferior hypogastric plexus are preserved (star). A temporary soft stent has been inserted into the right ureter. Traction on the closed vaginal stump is exerted with two stay sutures. (**c**, **d**) EMMR specimen cut ventrally in the sagittal plane after formalin fixation, posterior and anterior views. The complete right urogenital mesentery, including a part of the distal ureter, is part of the specimen. Compare with the vascular and ligamentous mesometrium and mesocolpos on the left side

(Fig. 8.36b). The complete urogenital mesentery is sealed and transected from the bladder adventitia and muscle. The distal ureter is cut at the vesicoureteral junction, and its lumen is closed. As the resection plane is ventral and lateral to the inferior hypogastric plexus, it is preserved together with its branches leading to the bladder neck and urethral sphincter. The anterior EMMR specimen clearly shows the difference between the vascular mesometrium and the complete urogenital mesentery (Fig. 8.36c, d).

8.11 Urologic Repair and Reconstruction (Fig. 8.37)

The bladder defect is elevated and stretched with two stay sutures pulling it in the transverse direction. If the defect is close to the ostium of the ureter, a pigtail catheter is inserted. The bladder defect is closed in two layers, one with a running suture to adapt the mucosa and another with interrupted sutures for the muscularis and adven-

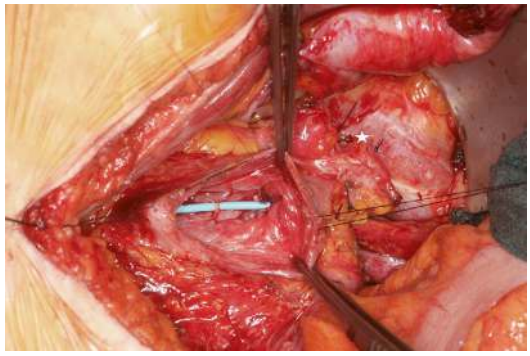

Fig. 8.37 Ureterocystoneostomy after anterior EMMR, including the right urogenital mesentery. The mobilized bladder has been fixed to the right psoas muscle (star). Vesicostomy shows the anastomosis of the ureter, which has been pulled through a submucous tunnel. A stent has been inserted

titia layers. The retrograde filling of the bladder up to 300 mL with saline ensures water tightness.

If the distal ureter has to be resected, ureterovesiconeostomy is performed with the psoas hitch or Boari technique. As the ureteral length is usually only reduced by about 5 cm, fixation of the psoas muscle can even be omitted in cases that allow tension-free ureterovesical anastomosis.

The bladder is mobilized by the incision of the peritoneum at the vesicoparietal fold. If necessary, the ipsilateral bladder dome is fixed to the psoas muscle with two or three sutures without severing the genitofemoral nerve(s) (Fig. 8.37). The bladder wall is incised longitudinally between two stay sutures. A submucosal tunnel of about 4 cm is created in the direction of the previous ostium, through which the distal ureter is pulled into the bladder. The temporary ureter splint has been removed before. After spatulation for about 5 mm, the ureter end is fixed to the bladder mucosa with interrupted sutures. A stent or splint is then inserted and pushed up to the renal pelvis. If a splint is used, it is brought out through the abdominal wall through a small stab wound. The cystostomy is closed with a running suture of the mucosa and with interrupted muscularis/adventitia sutures probing the width of the entry site of the ureter. For details, see textbooks on urologic surgery.

8.12 Posterior EMMR

8.12.1 Modification of TMMR Steps 9–11

This posterior extension of the TMMR can be necessary for locoregional tumor control if rectovaginal separation is frustrated by fibrosis and potential neoplastic infiltration of the ligamentous mesometria/mesocolpoi or by intercalated lymph nodes in the pararectal subperitoneum or even the mesorectum. With anteverted traction of the uterus, the proximal part of the rectum is dissected at the posterior mesorectal surface from the hypogastric nerve plate, and the rectal and pararectal peritoneum is incised about 5 cm cranial to the obliterated pouch of Douglas. The mesorectum is circumferentially sealed and transected to completely expose the muscularis layer of the rectum, which is aseptically divided by a GIA cutting and stapling instrument. The uterus is then kept at retroverted tension for the colpotomy, followed by grasping both the anterior and the posterior vaginal wall with large Kocher clamps. The posterior wall of the retained vaginal stump is dissected from the anterior mesorectum caudally for about 2–3 cm, keeping the rectum at upward tension. The ligamentous mesocolpoi are sealed and cut bilaterally in a retrograde direction, with the exposed plexus hypogastrici inferiores kept laterally. By this maneuver, the distal rectum is circumferentially exposed, to be divided by a linear stapling instrument with a fixed or adjustable cutting plane.

Rare situations may demand both anterior and posterior EMMRs (Fig. 8.38a, b).

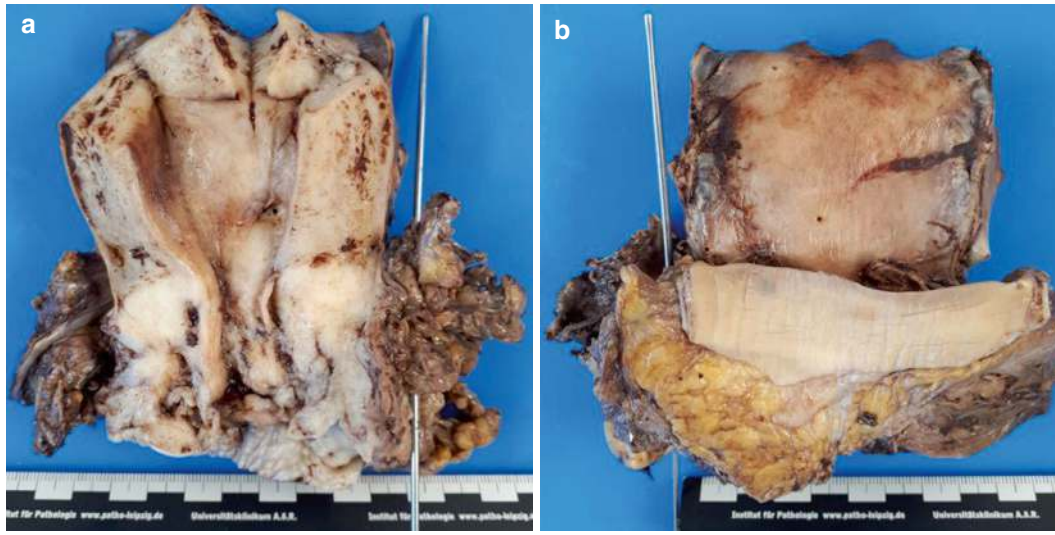

Fig. 8.38 Anterior and posterior EMMR for R0 resection of FIGO IIB cervix carcinoma infiltrating the left urogenital mesentery and ligamentous mesometrium-perirectal fascia complex. Formalin-fixed EMMR specimen cut ventrally in the sagittal plane. The left umbilical artery, the bladder mesentery and distal ureter (probe), and the middle third of the rectum with the mesorectum, perirectal fascia, and rectal peritoneum supplement the total mesometrial resection. (**a**) Posterior view. (**b**) Anterior view

8.13 Rectal Reconstruction

Low rectal end-to-end anastomosis is performed with a circular stapling instrument. The closed proximal rectum is opened by excising the tissue with the staple line. A purse string suture is applied and tightened after introducing the anvil, which has been removed from the instrument.

The circular stapling instrument with the recessed trocar tip is then introduced transanally to the level of the staple line. A small incision is made in the distal rectum at the midpoint of the linear staple line. The trocar tip is advanced through this incision and then removed from the instrument, which is connected to the anvil shaft thereafter. The instrument is closed and fired. After opening and removing the instrument, the tissue rings are inspected for completeness. The rectal anastomosis is checked for hemostasis and tested for air tightness. For details, see textbooks on colorectal surgery.

8.14 Abdominal Mesometrial Resections for Carcinomas Infiltrating the Suprasinus Vagina (Figs. 8.39)

The complete suprasinus vagina and its vascular and ligamentous mesocolpoi can be included in the abdominal mesometrial resection specimen. The procedure is carried out as described with standard or modified TMMR steps 6–10. However, the vesicocervicovaginal separation (step 6) has to be advanced to the level of the bladder neck, and the rectovaginal separation (step 9) has to be continued to reach the distal (urogenital sinus-associated) rectovaginal septum. Both vascular and ligamentous mesocolpoi are sealed and transected as a unit down to the level of the levator ani muscles extending step 10 (Fig. 8.39a). The complete suprasinus vagina, together with its mesocolpoi, is part of the TMMR specimen (Fig. 8.39b).

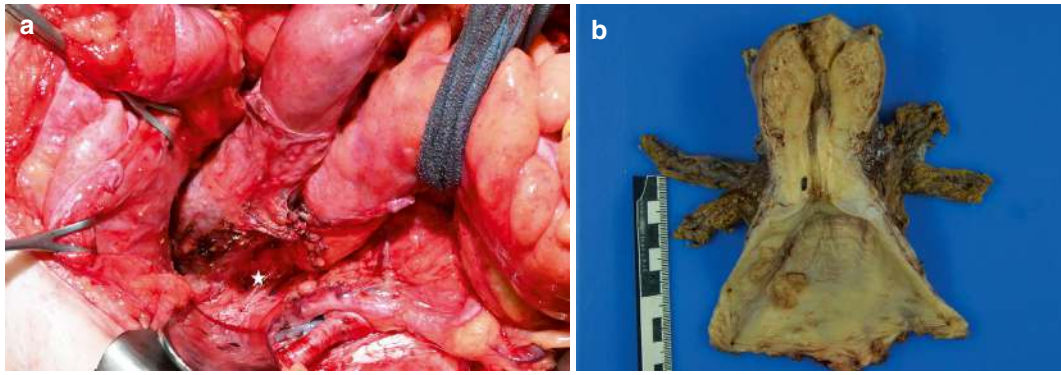

Fig. 8.39 TMMR for oT1 carcinoma of the suprasinus vagina. (**a**) Intra-abdominal view demonstrating the left vascular mesometrium and mesocolpos, which have been sealed and transected down to the pelvic floor. The anterior branches of the inferior hypogastric plexus innervating the bladder and the ipsilateral mesureter have been completely preserved (star). (**b**) Fixed TMMR specimen anteriorly cut in the midsagittal plane, demonstrating the four "wings" of vascular and ligamentous mesometria/mesocolpoi and stage oT1 carcinoma at the lower right suprasinus vaginal wall

8.15 Abdominoperineal Mesometrial Resections

If the distal (sinus) vagina has to be included in the mesometrial resections for the local control of oT2 vaginal carcinomas, additional perineal access is mandatory. Instead of performing the colpotomy (step 11), the patient is brought into the lithotomy position, and the vestibulum of the vulva is incised immediately distal to the hymenal remnants in the vulvar vestibulum, preserving the bulbi vestibulares laterally. The subsequent surgical technique corresponds to the resection of the sinus vagina as described in Chap. 11. For the abdominal withdrawal of the TMMR specimen, the vaginal introitus is closed by sutures or staples to prevent cancer cell spilling.

According to our (limited) experience with colon sigmoideum flaps, we do not advocate this technique for functional vaginal reconstruction. We rather perform an introital plasty with uni- or bilateral paralabial flap(s) as described in Chap. 12.

8.16 Postoperative Management

The following recommendations are given for the management of patients with an uneventful postoperative course after TMMR and EMMR. Postoperative monitoring is carried out at the discretion of the anesthesiologist. The majority of the patients can be brought to the regular ward a few hours up to one night after the procedure. The patients are usually equipped with a patient-controlled analgesia set, which is removed at postoperative day 2 or 3 and is substituted by oral metamizole, paracetamol, or ibuprofen on demand by the patient. Physiotherapeutic support is given to all patients during their stay at the hospital. The patients are mobilized as soon as they wish and are able to, usually on the day after the operation. Anticoagulation prophylaxis with 4500 IE low molecular weight heparin daily is started 6 h after the surgery, continued for the whole hospital stay, and advised for 1 month.

The patients receive tea or soup during the first 2 days and light meals after purgative treatment with sorbitol. Regular meals are given on the patient's demand. The intraabdominal drainage is usually removed on day 2 or 3.

Clinical laboratory diagnostics, including blood count, renal function, liver enzymes, and inflammatory and coagulation parameters, are performed on postoperative day 1. Coagulation parameters are additionally determined prior to removing the patient-controlled analgesia device. Sonography of the pelvis and the kidneys is performed on day 3 and during the discharge examination (see below). The laparotomy wound is redraped with a translucent dressing after 2 days and inspected daily.

The transurethral Foley catheter is removed on day 4. Spontaneous micturition and residual urine drawn by a single-use catheter are thereafter controlled by protocol until the repeated residual volume is less than 50 mL.

In the case of bladder reconstruction for EMMR, the Foley catheter is left for 7 days, and micturition training is delayed accordingly. The bladder is inspected by cystoscopy. Protective ureteral stents applied with EMMR are removed after 4 weeks, followed by sonographic control for ureteral obstruction. After ureteral reimplantation, retrograde urethrocystography and cystoscopy are performed by the urologist on days 7–10. In the uneventful course, the transurethral catheter is removed, and the ureteral stent remains for another 3 weeks.

The clinical discharge examination includes inspection and palpation of the abdomen, inspection of the vaginal vault with specula, vaginal and rectovaginal palpation, and sonography of the kidneys and pelvis after spontaneous micturition.

After discharge from the hospital, care for the patient is left to her gynecologist. Skin staples are removed stepwise on days 10 and 12. The intracutaneous laparotomy suture is left in situ.

8.17 Management of Complications

This compilation encompasses both early and late complications related to TMMR and EMMR. Early complications occurring during the postoperative hospital stay and thereafter for about 4 weeks are considered below. The management of late complications can only be sketched briefly within the scope of this textbook. Moreover, complications not directly related to the surgical procedure, such as pneumonia, convulsions, heart or brain infarction, and hypertensive crisis, are not considered here.

8.17.1 Urinary

Urinary infection is treated with antibiotics and high fluid intake. Urinary retention, as manifested with residual urine volumes of >50 mL after removal of the transurethral catheter at postoperative day 4, necessitates intermittent catheterization following spontaneous micturition. Patients are encouraged and trained to catheterize themselves and to document the volumes of spontaneous and residual urine. If urinary retention persists, cholinergic and inhibiting adrenergic medication is added to self-catheterization.

Urinary incontinence can indicate vesicovaginal or ureterovaginal fistulas to be diagnosed and treated as described below. Aggravation of preexisting stress incontinence observed as a late event should be verified by clinical and urodynamic investigation.

The diagnosis of postoperative hydronephrosis, urinoma, and urinary fistulas by sonography, pathological creatinine concentration in the ascites, or clinical evidence demands further assessment by cystoscopy, antegrade or retrograde urography, computed tomography (CT) or magnetic resonance imaging (MRI), and urologic intervention. Ureteral strictures are managed by

retrograde insertion of ureteral stents, which are left in situ for about 3 months. Small ureteral lesions are also treated with ureteral stents, as well as bladder and pelvic drainage for spontaneous closure. Therapy of persisting urinoma and extended ureteral lesions requires relaparotomy and ureterocystoneostomy.

Vesicovaginal fistulas are initially managed by bladder drainage. If spontaneous closure is not achieved, surgical repair by the vaginal or abdominal route is mandatory.

8.17.2 Intestinal

Enterocolitis caused by *Clostridium difficile* necessitates antibiotic therapy with clindamycin. Unspecific infections are treated symptomatically by anticholinergic medication and fluid substitution. Early ileus manifestations are mainly functional, i.e., paralytic. A gastrointestinal tube is inserted, fluid is substituted, and cholinergic medication is administered. Upon symptom persistence, CT imaging is performed to exclude mechanical bowel obstruction, which is usually a late complication. Mechanical bowel obstruction not resolving by conservative treatment demands relaparotomy and surgical treatment.

8.17.3 Laparotomy and Colpotomy Healing

Infected laparotomy wounds have to be opened to the fascial level in the majority of cases. A wound smear is taken for microbiological testing, and the fascia closure is inspected and eventually palpated for competence. If the fascial closure is intact, the wound is cleaned from pus and debris. Regular antiseptic lavages of the wound bed, accompanied by systemic antibiotic treatment, should result in the formation of granulation tissue without clinical signs of persistent infection. Vacuum wound dressings may be administered to expedite this process. Depending on the size and appearance of the wound at that stage, it is decided whether a secondary closure by suturing is done or the wound is left for secondary healing.

Dehiscence of the abdominal fascia is a surgical emergency necessitating the complete removal of the fascial suture and systematic exploration of the peritoneal situs. Smears for microbiological testing are taken from the peritoneum and from the fascial and epifascial tissues. Any intraabdominal cause for the laparotomy dehiscence has to be identified and treated. After thorough lavage of the abdomen and pelvis and the placement of at least two large volume drains contralaterally in the epigastrium and pelvis, the fascial wound margins are excised and readapted by suturing. An absorbable mesh may be oversewn on the fascia following lateral mobilization of the subcutaneous fatty tissue to stabilize the resuture. If the laparotomy dehiscence occurred for noninfectious reasons, the skin wound is closed as well; otherwise, it is left open and treated as described above.

Incisional hernias and keloid formation are late complications of laparotomy healing following TMMR/EMMR. Their management is beyond the scope of this textbook.

Partial or total dehiscence of the colpotomy may be suspected if persistent vaginal watery discharge is noticed in the early postoperative period. Speculum examination ascertains the diagnosis. The fluid passing the dehiscent colpotomy should be tested for creatinine to exclude a urinoma. Unless the small bowel is protruding through the dehiscent colpotomy, secondary healing can be awaited. Otherwise, relaparotomy, reclosure of the colpotomy, and placement of an omentum majus flap above the vaginal stump are indicated.

8.17.4 Vascular

Significant (>300 mL) postoperative bleeding demands relaparotomy to identify the source of the bleeding and control it. If bleeding vessels are

not found, anticoagulative medication may have been causative and should be stopped. All coagulated and noncoagulated blood remains have to be removed intraabdominally and from the abdominal wall wound. After the placement of peritoneal and subcutaneous drains, the laparotomy is closed again in layers.

Lymphascos can sometimes lead to significant abdominal volume expansion, which may not be tolerable for the patient. Paracentesis accompanied by albumin substitution is then indicated.

Lymphoceles have to be treated by CT- or sonography-guided drainage only if they are symptomatic due to infection or pressure effects. Deep venous thrombosis and thromboembolic events necessitate therapeutic heparinization.

Lower body lymphedema can affect any part of the leg and the pubic region with variable onset, extent, and duration. Compression therapy relieves the symptoms. Patients are advised to take a prophylactic antibiotic medication in case of any injury of the lower body to prevent erysipelas, which can aggravate the lymphedema. If erysipela is diagnosed, antibiotic therapy is mandatory. Severe lymphedemas of the leg can be surgically treated by transplantation of vascularized lymph node chains from the omentum majus to the inguinal regions or lymphovenous anastomoses.

8.17.5 Neuronal

TMMR/EMMR exposes the genitofemoral, obturator, and sciatic nerves. Lesions of the fine branches of the genitofemoral nerve cannot always be avoided and may cause dumbness of the inner thighs, which may persist for weeks to months. Encasement of the obturator nerve by metastatic lymph node conglomerates may necessitate the resection of the involved part of the nerve, which may cause weakness of the adductor muscles, usually without significant ambulatory impairment.

Clinically apparent lesions of the sciatic nerve did not occur in our series. Although the femoral nerve is not touched during the operation, paresis caused by retractor compression has been observed. These patients needed physiotherapy and walkers for several months, but their restraint finally resolved completely. In all situations of postoperative disturbances of sensitivity and leg motor functions, assessment by the neurologist is indicated.

The umbilical artery is exposed from its origin from the internal iliac artery to the proximal medial umbilical fold. Dissection of the lateral urogenital mesentery along the visceral endopelvic fascia proceeds down to the pelvic floor, exposing the parietal endopelvic fascia, the levator ani muscle, and the arci tendinei.

9 Peritoneal Mesometrial Resection, Lymph-Collector-Guided First-Line Lymph Node Dissection and Extended Procedures

Five major differences between endometrial carcinoma and cervix carcinoma have to be respected for the design of cancer field surgery with the goal of controlling this tumor entity locoregionally:

1. The carcinomas originate in a different Müllerian subcompartment.
2. Due to the symptom of abnormal vaginal bleeding, most carcinomas of the endometrium are diagnosed at an early stage.
3. Peritoneal cancer cell dissemination is an important mechanism of local spread with advanced endometrial carcinomas.
4. The majority of patients with endometrial carcinoma are morbidly obese, including individuals with excessive body mass index.
5. Primary radiotherapy is not an alternative to surgery for the locoregional control of endometrial carcinoma.

Although the cancer fields of oT > 1 tumors of endometrial and cervix carcinomas are the same (see Chaps. 3 and 6), their occupation by malignant tissue is different. oT2 endometrial carcinomas infiltrate the vagina and the Müllerian adventitia less frequently than cervix carcinomas. oT > 2 endometrial carcinomas more frequently involve derivatives of the genital coelom mesoderm than oT > 2 cervix carcinomas, both by continuous and discontinuous spread. Malignant colonization of derivatives of the anterior cloacal mesenchyme occurs less often with endometrial carcinoma and is then mostly confined to the vascular mesometria and the peritoneum of the vesicouterine transition. As the tumor mass is limited to the Müllerian compartment in oT2 tumors, the regional spread is similar in endometrial and cervix carcinomas, following the hierarchy of first-, second-, and third-line lymph nodes as described in Chap. 6. The mesenteric lymphatic pathway to superficial sites of the periaortic region in oT > 2 carcinomas infiltrating the uterine fundus is more important in endometrial carcinoma than in cervix carcinoma. Consequently, more mesenteric aortic lymph nodes are first line in local and advanced endometrial carcinoma.

Considering the histopathological characteristics of 135 consecutive endometrial carcinoma cases [1], 84% of the tumors would have been locoregionally controlled by treatment with simple hysterectomy and adnexectomy and 93% by simple hysterectomy with adnexectomy and immunologic defense line-directed lymph node dissection. Three percent of the patients presented with disseminated peritoneal carcinosis, totally excluding locoregional control through surgical treatment. Therefore, about 13% of endometrial carcinoma patients can be expected to benefit from cancer field surgery. Although the risk of lymph node metastases and extracompartmental local tumor propagation can be estimated by pretreatment diagnostic findings, we favor applying cancer field surgery to all patients with

M. Höckel et al., *Cancer Field Surgery in Gynecologic Oncology*,
https://doi.org/10.1007/978-3-031-83030-3_9

endometrial carcinoma with oT ≤ 2 stages and selected patients with oT > 2 stages to achieve maximum locoregional control without adjuvant radiotherapy at minimized treatment-related morbidity.

Peritoneal mesometrial resection (PMMR) involves the removal of the complete Müllerian compartment, except for most of the vagina. The PMMR specimen includes the complete genital peritoneum (Müllerian serosa, peritoneal mesometrium, mesosalpinx, mesovar, ovarian surface, proximal round ligament, proper ovarian ligament, proximal infundibulopelvic ligament, rectouterine peritoneal fold), the vesicouterine peritoneal fold, and the vascular mesometria. *Extended peritoneal mesometrial resection* may further comprise the bladder peritoneum, the pararectal peritoneum and ligamentous mesometria (*type A*), the vascular mesocolpoi and the ligamentous mesometria and mesocolpoi (*type B*), or a combination of these tissues (*type AB*). All peritoneal mesometrial resections are primarily performed with lymph collector-guided pelvic first-line lymph node dissection. Evidence of (sub)serous or (sub)peritoneal tumor involvement or infiltration of the uterine fundus mandates additional collector-guided periaortic first-line lymph node dissection. The histological proof of lymph node metastases is considered an indication for extending the lymph node dissection, as described with total mesometrial resection (TMMR) in Chap. 8.

The author (RK) developed appropriate techniques for the robot-assisted minimally invasive approach to PMMR and extended PMMR type A, both with lymph collector-guided pelvic and periaortal first-line lymph node dissection [1–5]. Given that more than 50% of endometrial cancer patients to be treated are morbidly obese and exhibit other comorbidities, avoiding large laparotomies while carrying out these procedures and maintaining locoregional tumor control is a significant advantage. There is also evidence that robotic surgery further reduces morbidity compared to classical laparoscopy [6]. Meanwhile, due to the technical support, the learning curve for robotic surgery is shorter and the conversion rate to laparotomy lower, especially in patients with high BMI, implying that robotic surgery is the technique of choice for the surgical treatment of most endometrial cancer patients. However, only for endometrial carcinomas exhibiting deep infiltration of the cervical stroma, vascular mesometria and mesocolpoi, and vagina, requiring extended peritoneal mesometrial resection types B or AB for local tumor control, may open surgery still be indicated. Likewise, large-volume lymph node metastases should be resected via laparotomy access (see treatment algorithm in Chap. 13).

9.1 Equipment

Irrespective of the robotic device used (the author initially used the da Vinci SI, followed by the da Vinci Xi system of Intuitive Surgical Inc.), the procedure will be performed with monopolar scissors, a bipolar instrument like Maryland forceps, and a grasper, e.g., Prograsp™. To avoid cancer spill, no uterine manipulator with an intrauterine probe should be applied. We favor the HOHL uterine manipulator (Karl Storz SE&Co. KG), fixing the cap only to the cervix by suture after closing the cervix as described below. For the injection of the indocyanine green (ICG) dye, we use an IOWA trumpet originally designed for pudendal anesthesia in obstetrics by injection into the uterine corpus transcervically.

9.2 Patient Preparation and Positioning

For robotic surgery, the patient is brought to a 30-degree Trendelenburg position. Downsliding of the patient is avoided by using shoulder support or a vacuum mattress. Legs should be positioned either on flat leg holders or in adjustable bootleg holders to reduce the risk of compartment syndrome in long-lasting surgeries. To mark the lymph collectors draining the uterine corpus and the connected pelvic first-line lymph nodes, 1 mL of ICG at a concentration of 1.66 mg/mL is injected into the uterine cervix at the 3 and 9 o'clock positions. For collector-guided periaor-

tic first-line lymph node dissection, the injection has to be done into the uterine fundus and middle corpus both on the right and left sides, each with 0.5 mL. Prior to the injection, coagulation of the fallopian tubes should be performed to avoid intraperitoneal cancer cell dissemination.

Following the application of ICG, the cervical canal will be closed by a Z-suture at the external os. A sponge soaked with 96% ethanol is fixed at the cervix with the same suture. Then the cap of the HOHL manipulator is placed around the cervix, and the sponge is fixed with the remaining part of the suture along the hollow tube around the grip. The intention of these measures is to reduce local cancer cell spills.

9.3 Peritoneal Mesometrial Resection and Lymph Collector-Guided Pelvic First-Line Lymph Node Dissection

9.3.1 Standard Procedure Step-by-Step

Step 1: Positioning of the trocars for robotic surgery (8 mm) and assistant trocar (10 mm) (Fig. 9.1).

Step 2: Systematic exploration of the pelvic and abdominal peritoneal surfaces and of ICG distribution (Fig. 9.2). Ascites is sucked off to be examined cytologically. All peritoneal sites clinically suspicious for cancer involvement should be biopsied and sent to histopathological assessment with the exact anatomical description. These results, together with the pretreatment diagnostic findings (see Chap. 7), determine the type of peritoneal mesometrial resection to be performed, i.e., standard PMMR or extended peritoneal mesometrial resections, types A, B, or AB (see treatment algorithms in Chap. 13).

Step 3: Both Fallopian tubes are coagulated at their isthmic parts (Fig. 9.3).

Step 4: Incision of the parietal peritoneum lateral and parallel to the right infundibulopelvic ligament (Fig. 9.4).

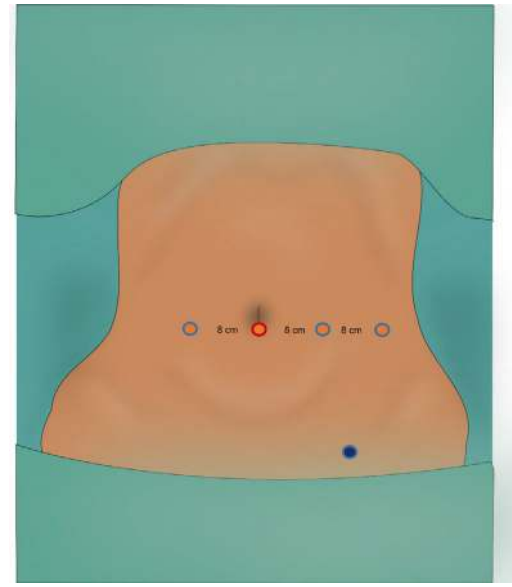

Fig. 9.1 Topography of trocar sites in da Vinci Xi; our da Vinci 8 mm ports are placed at the umbilical level and an assistant 10 mm port in the lower abdomen

Step 5: Sealing and transection of the right infundibulopelvic ligament at about 5 cm cranial to the ovary (Fig. 9.5).

Step 6: Sealing and transection of the right round ligament at the level of the external iliac vessels (Fig. 9.6).

Step 7: Ventral continuation of the incision at the border between genital and bladder peritoneum (distal to the vesicouterine fold) and dissection of the bladder adventitia from the vesicocervical septum (Fig. 9.7). Dissection of the right peritoneal mesometrium from the bladder mesentery.

Step 8: Identification of the fluorescent lymphatic collector vessels and connected parietal pelvic first-line nodes medial to the external iliac vessels (Fig. 9.8).

Step 9: Dissection of the right first-line nodes at the medial aspect of the external iliac artery ventral and dorsal to the external iliac vein down to the origin of the uterine artery en bloc (Fig. 9.9).

The distal vascular mesometrium is dissected from the bladder mesentery anteriorly and from the mesureter posteriorly (Fig. 9.10).

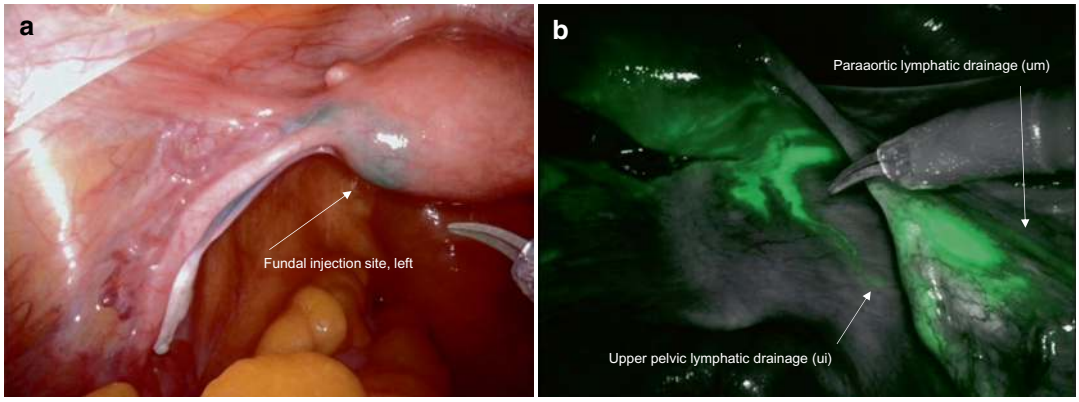

Fig. 9.2 (**a**) Endopelvic situs under visible light, showing the left uterine fundus and adnexa after fundal injection of ICG (arrow). (**b**) Right endopelvic situs under near-infrared illumination, demonstrating the upper mesenteric (um) and upper iliac (ui) lymph drainage by green fluorescence after transcervical corporal injection of ICG

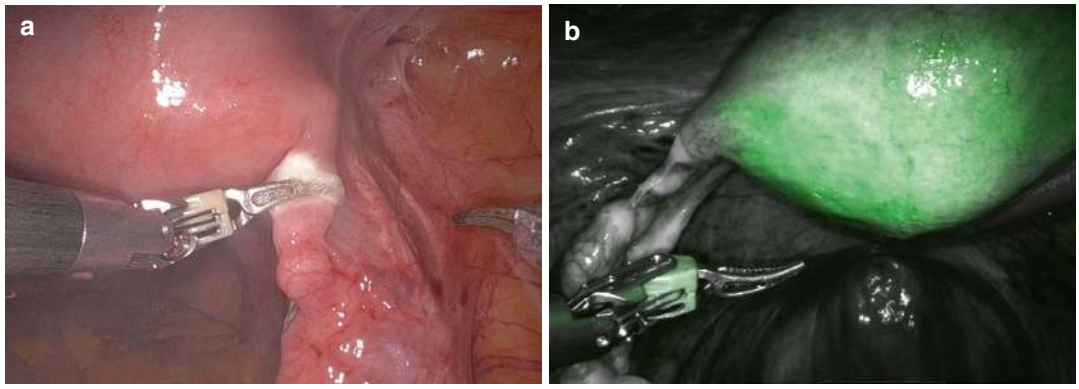

Fig. 9.3 Coagulation of fallopian tubes. (**a**) At visible light illumination on the right side. (**b**) ICG fluorescence at near-infrared illumination on the left side

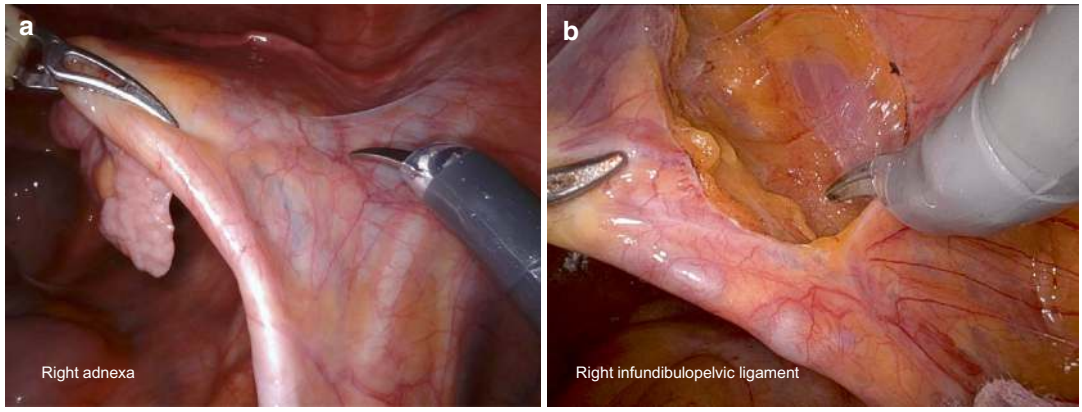

Fig. 9.4 (**a**) Incision into the parietal peritoneum lateral to the right infundibulopelvic ligament. (**b**) Beginning exposure of the right pelvic retroperitoneum

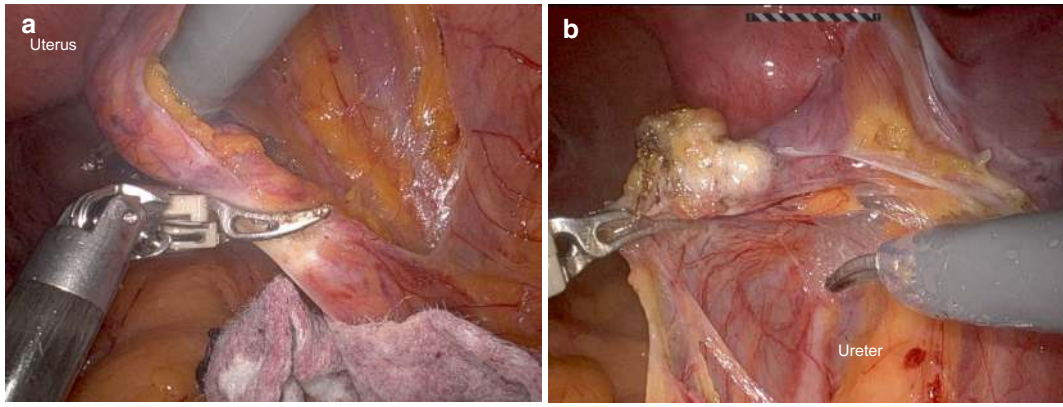

Fig. 9.5 (**a**) Sealing of the right infundibulopelvic ligament. (**b**) Right infundibulopelvic ligament transected

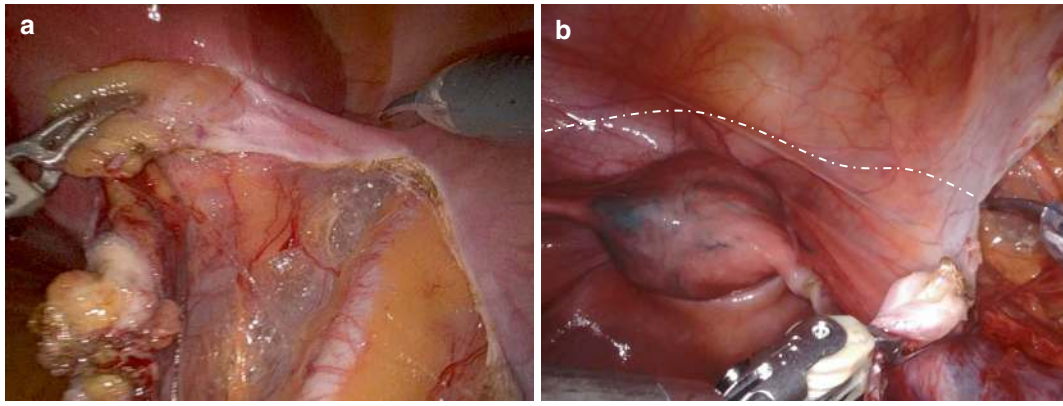

Fig. 9.6 (**a**) Further caudal incision into the right pelvic parietal peritoneum toward the round ligament. (**b**) Right round ligament transected. Projected incision of bladder peritoneum demonstrated

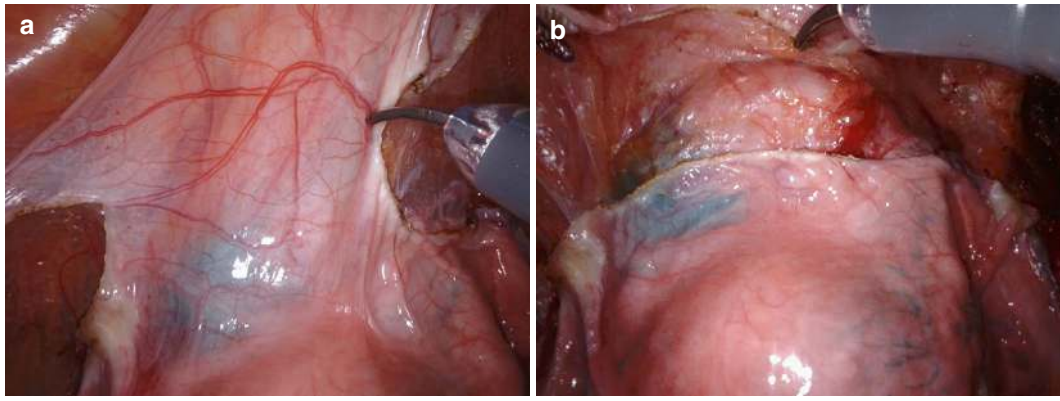

Fig. 9.7 (**a**) Incision into the bladder peritoneum distal to the vesicouterine fold (from the uterine perspective). (**b**) Dissection of the bladder adventitia from the vesicocervical septum, which corresponds to the anterior mesometrium/mesocolpos in terms of ontogenetic anatomy

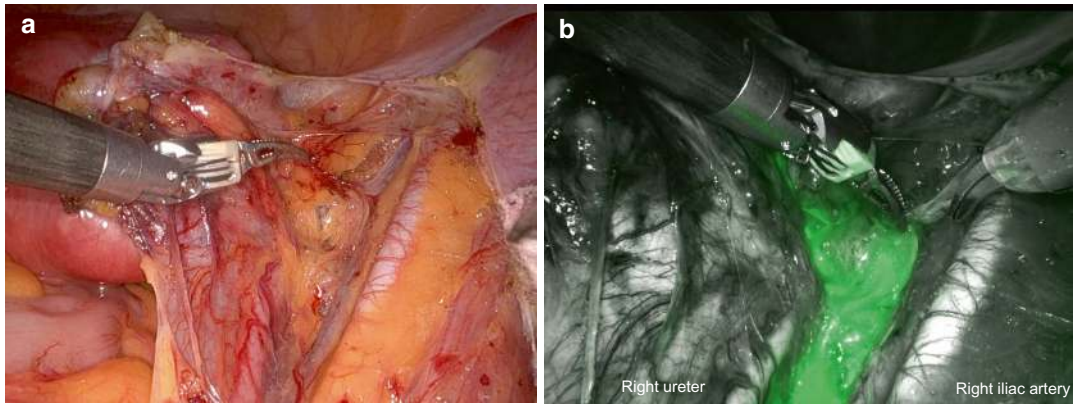

Fig. 9.8 (**a**) Dissection of the right peritoneal mesometrium from the bladder mesentery. (**b**) At near-infrared illumination identification of the collector vessels of the upper iliac lymphatic pathway and the first-line lymph nodes by green fluorescence

Deposition in an endobag to be sent for histopathologic investigation (Fig. 9.11).

Step 10: Exposition of the right vascular mesometrium containing the uterine artery and veins, together with lymph fatty tissue; sealing and transecting its origin from the umbilical artery and internal iliac vein (Fig. 9.12).

Step 11: Transection of the right posterior genital peritoneum to the rectouterine peritoneal fold and dissection of the right ureter, together with its mesureter, along the pararectal peritoneum and fascia; sealing and transection of the ureter vessels branching from the vascular mesometrium (Fig. 9.13).

Step 12: Transection of the vesicouterine vessel connections medial to the ureter and mobilization of the ureter laterocaudally (Fig. 9.14).

Step 13: Incision of the bladder peritoneum distal to the vesicouterine fold at the left side and completion of the separation of the bladder adventitia from the uterus and dissection of the distal left vascular mesometrium from the bladder mesentery (Fig. 9.15).

Step 14: Sealing and transection of the left round ligament at the level of the external iliac vessels.

Step 15: Incision of the parietal peritoneum lateral and parallel to the left infundibulopelvic ligament and mesosalpinx.

Step 16: Sealing and transection of the left infundibulopelvic ligament approximately 5 cm cranial of the ovary.

Step 17: Identification of the fluorescent lymphatic collector vessels and connected parietal pelvic first-line nodes on the left side medial to the external iliac vessels.

Step 18: En bloc resection of the left first-line nodes from the medial aspect of the external iliac artery ventral and dorsal of the external iliac vein down to the origin of the uterine artery. Deposition in an endobag to be sent for frozen section investigation.

Step 19: Transection of the left posterior genital peritoneum toward the rectouterine peritoneal fold and dissection of the left ureter, together with its mesureter, along the pararectal peritoneum and fascia; sealing and transection of left ureter vessels branching from the vascular mesometrium.

Step 20: Complete exposition of the left vascular mesometrium; sealing and transection at the origin from the umbilical artery/internal iliac vein.

Step 21: Transection of the left vesicouterine vessel connections medial to the ureter and mobilization of the ureter laterocaudally.

Step 22: Incision of the rectal peritoneum distal to the rectouterine transition on the left side and dissection of the remaining rectouterine fold

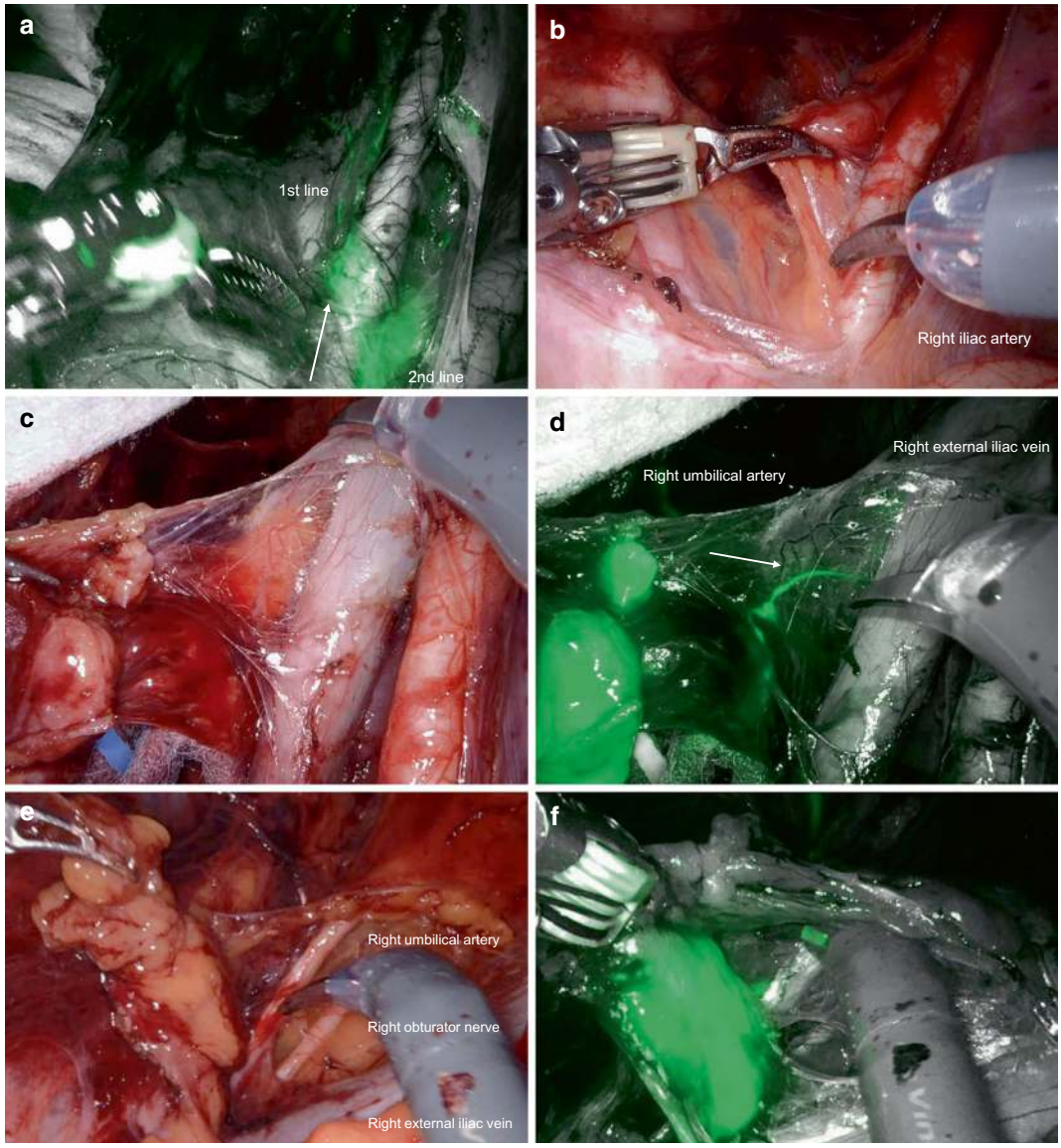

Fig. 9.9 (**a**) At near-infrared illumination sealing of the anterior internodal lymph vessels connecting the right external iliac first-line to the second-line nodes (arrow). (**b**) Dissection of the right external iliac first-line lymph node(s) from the medial aspect of the external iliac vessels starting at the common iliac bifurcation. (**c**) Continuing the first-line node dissection along the external iliac vein distally. (**d**) Following the lymphatic channel(s) dorsally (arrow) to the posteromedial first-line lymph nodes of the upper iliac pathway at near-infrared illumination. (**e**) Further caudal dissection of the posteromedial first-line nodes of the upper iliac pathway ventral to the obturator nerve. (F) ICG fluorescence confirms the first-line nodes medial to the external iliac vein

peritoneum and the left ligamentous mesometrium from the mesorectum, completely exposing the proximal posterior vaginal wall (Fig. 9.16).

Step 23: Colpotomy starting dorsally from left to right and ventrally from right to left (Fig. 9.17). The PMMR specimen is placed into an endobag to retrieve it, together with all remaining endobags and sponges, through the vagina.

Step 24: Suture of the colpotomy with V-lock 3-0 (Fig. 9.18).

Step 25: Lavage and control of the surgical field.

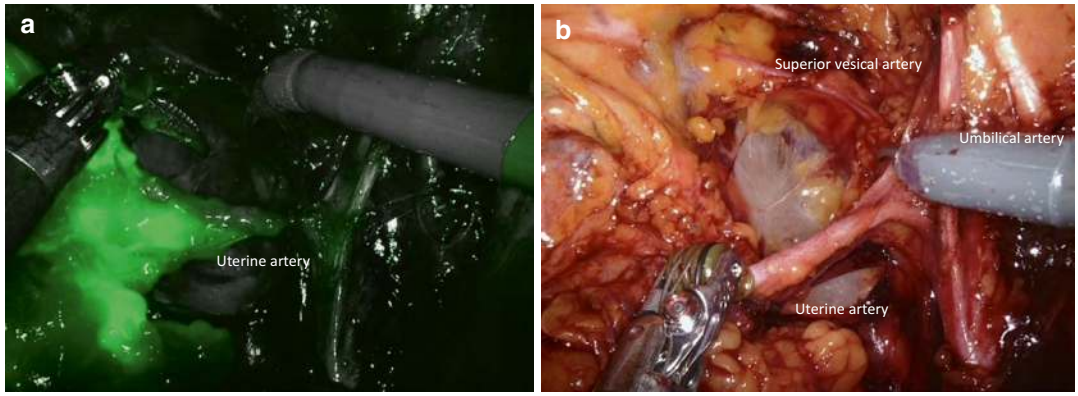

Fig. 9.10 (**a**) First-line nodes of the upper iliac pathway mobilized medially ventral to the uterine artery, shown with ICG fluorescence. (**b**) Dissection of the distal vascular mesometrium from the bladder mesentery anteriorly and the mesureter posteriorly

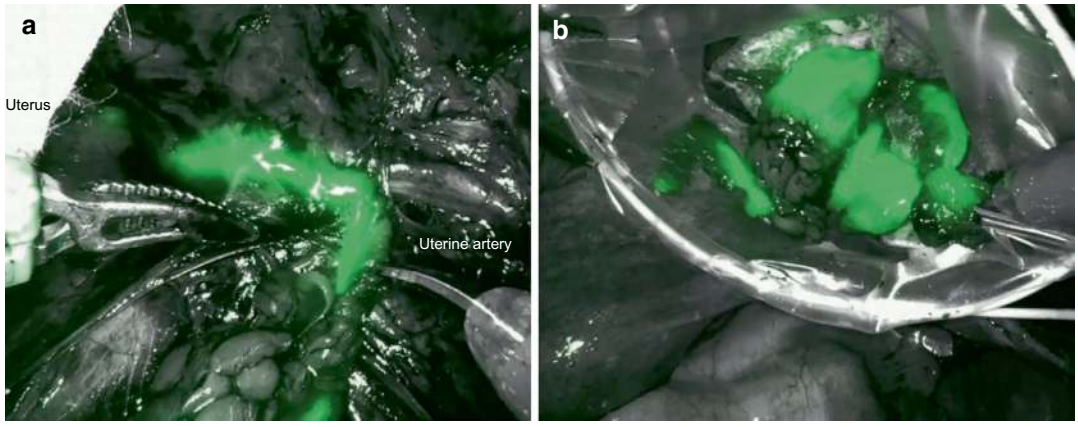

Fig. 9.11 (**a**) Transection of the proximal upper iliac collector vessel(s) demonstrated with ICG fluorescence. (**b**) Harvest of the upper iliac first-line nodes in an endobag

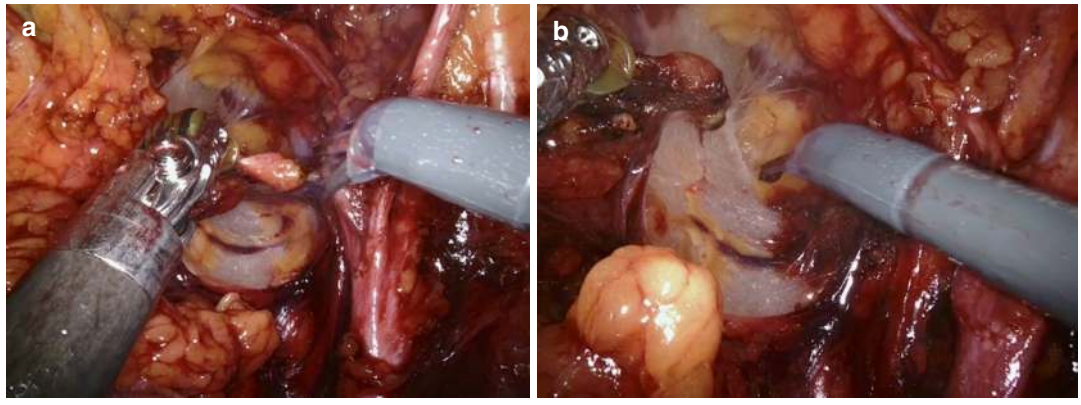

Fig. 9.12 (**a**) Sealing and transection of the right vascular mesometrium at the origin of the uterine artery and the estuary of the superficial uterine vein. (**b**) The transected right vascular mesometrium is lifted ventrally

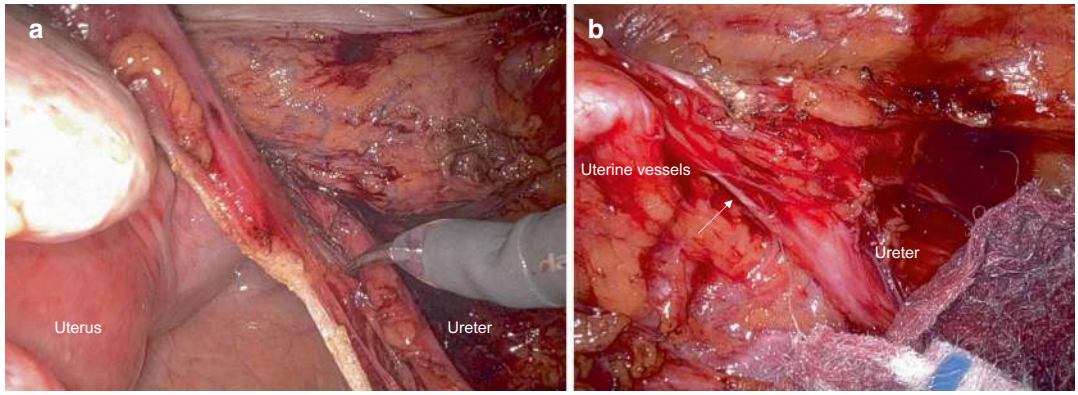

Fig. 9.13 (**a**) Dissection of the right ureter-mesureter complex from the pararectal peritoneum/fascia toward the vascular mesometrium. (**b**) By pulling the vascular mesometrium dorsomedially, the ureteral vessel (arrow) branching from the uterine artery is exposed to be sealed and transected

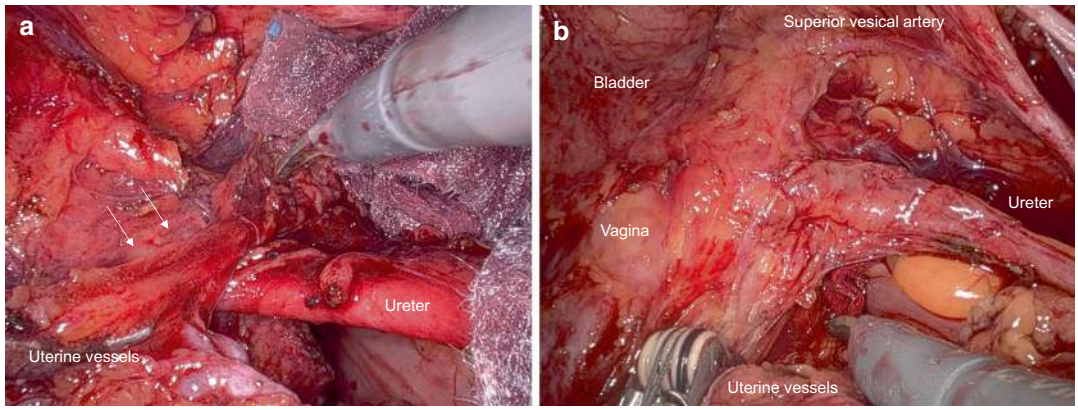

Fig. 9.14 (**a**) Dissection of the vascular mesometrium from the ureter to prepare the sealing and transection of the vesicovaginal vessel plexus. (**b**) Lateral mobilization of the right ureter, distancing it from the ligamentous mesocolpos

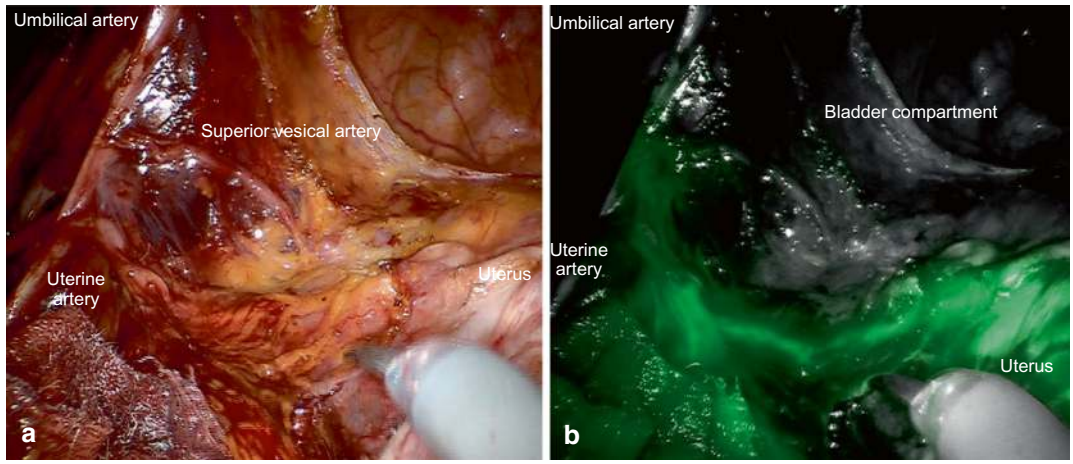

Fig. 9.15 (**a**) The left vascular mesometrium has been dissected from the bladder mesentery. (**b**) At near-infrared illumination, ICG fluorescence indicates collector vessels from the uterus in the left vascular mesometrium

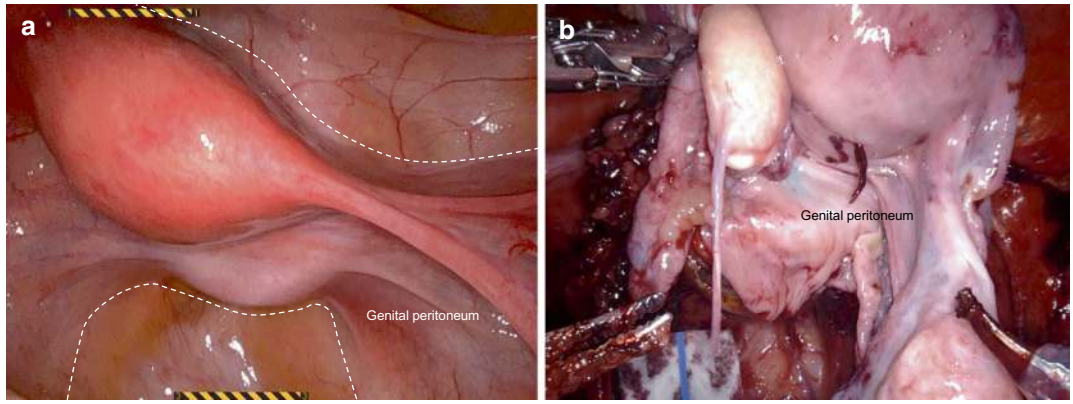

Fig. 9.16 (**a**) Peritoneal incision lines ensuring the inclusion of the complete genital peritoneum in the PMMR specimen. (**b**) Mobilized PMMR specimen prior to colpotomy

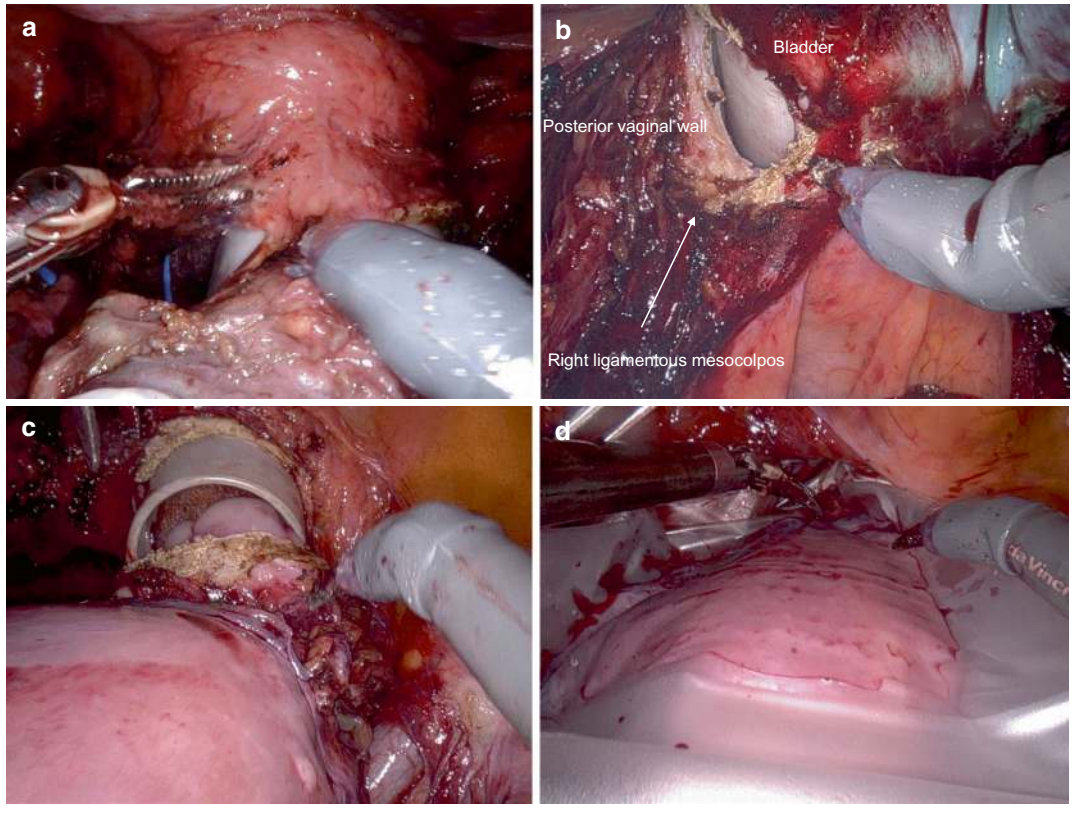

Fig. 9.17 (**a**) Clockwise colpotomy starting in the dorsal vaginal wall about 1 cm ventral of the left vascular mesocolpos. (**b**) Transection of the posterior vaginal wall from left to right. (**c**) Completed colpotomy unveils the uterine cervix covered by an alcohol-soaked sponge within the HOHL manipulator cap. The cervical canal had been closed by suture prior to the trocar insertion. (**d**) Vaginal extraction of the PMMR specimen wrapped in an endobag

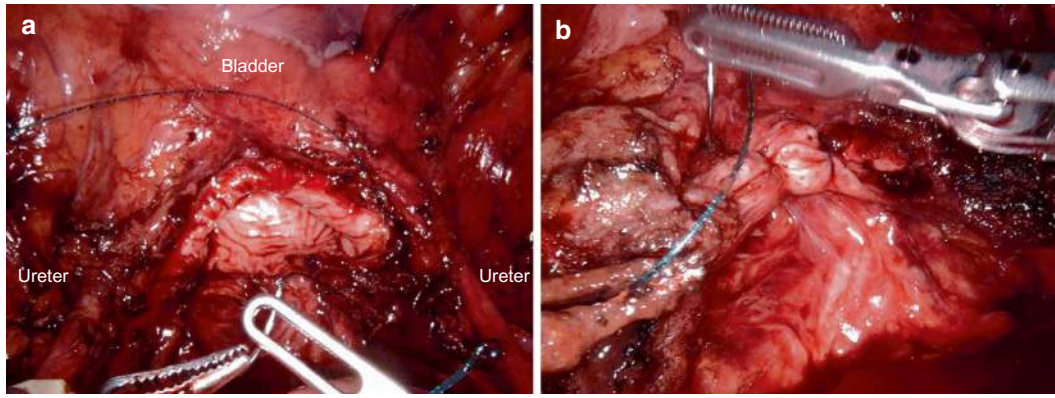

Fig. 9.18 (**a**) Closure of the colpotomy with a 3-0 barbed suture. (**b**) Closure completed

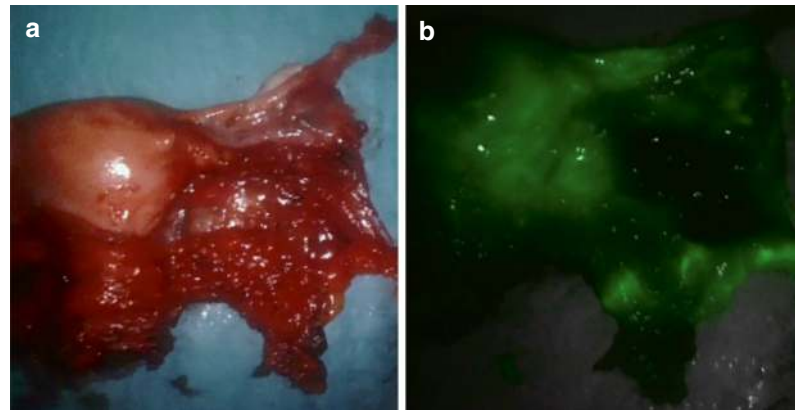

Fig. 9.19 (**a**) PMMR specimen consisting of the uterus, vascular mesometrium, adnexa, and genital peritoneum. (**b**) Near-infrared illumination demonstrates collector vessels of the upper iliac pathway in the vascular mesometrium

Step 26: Preparation of the specimen on a plate for histopathological assessment (Fig. 9.19).

9.4 Lymph Collector-Guided Periaortic First-Line Lymph Node Dissection

Step 27: ICG injection into the right ovary or mesovarium (Fig. 9.20) to identify the collector vessels of the right upper mesenteric pathway (Fig. 9.21).

Step 28: Cranialward mobilization of the right infundibulopelvic bundle, together with the lymphatic tissue, by the sealing and transection of the anastomoses to the colonic vessel system and the ovarian artery and vein at the level of the aorta and vena cava (Fig. 9.22).

Step 29: The right infundibulopelvic ligament is then resected together with the associated right para-aortic and pericaval mesenteric first-line nodes, guided by the ICG labeling (Figs. 9.23 and 9.24).

Step 30: ICG injection into the left ovary or mesovarium to identify the collector vessels of the left upper mesenteric pathway (Fig. 9.25).

Step 31: Exposition of the left renal vein and sealing and transection of the left ovarian vein (Fig. 9.26).

Step 32: The left ovarian vein is then mobilized caudalward, together with the ICG-labeled left para-aortic mesenteric (first-line) nodes (Fig. 9.27).

Step 33: Sealing and transection of the left ovarian artery and mobilization of the complete left infundibulopelvic ligament by transection of the colonic vessel anastomoses (Fig. 9.28).

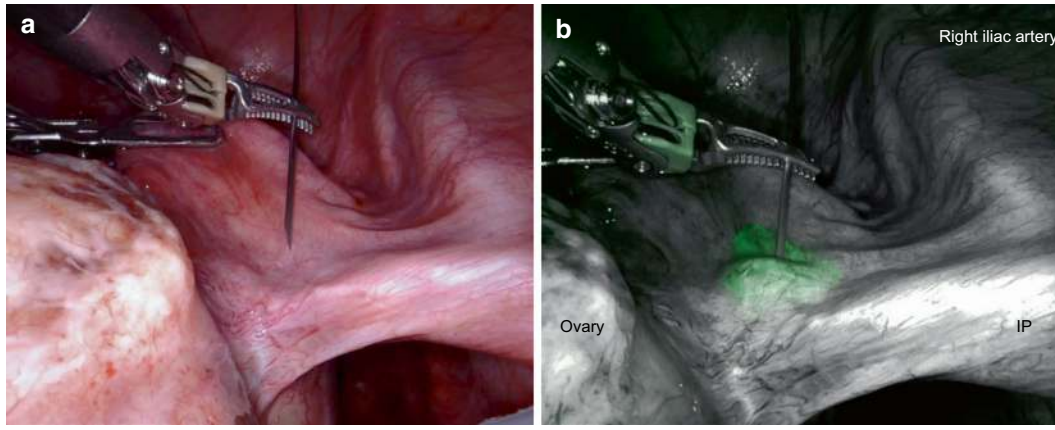

Fig. 9.20 Transabdominal injection of ICG into the right mesovarium. (**a**) At visible light illumination. (**b**) ICG fluorescence at near-infrared illumination

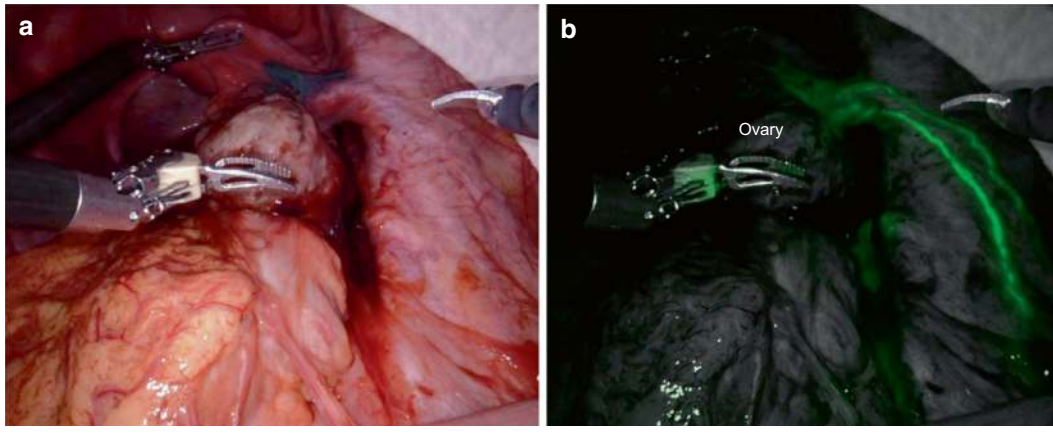

Fig. 9.21 Right infundibulopelvic ligament after injection of ICG into the right mesovarium. (**a**) At visible light illumination. (**b**) ICG fluorescence at near-infrared illumination demonstrates collector vessels of the upper mesenteric pathway

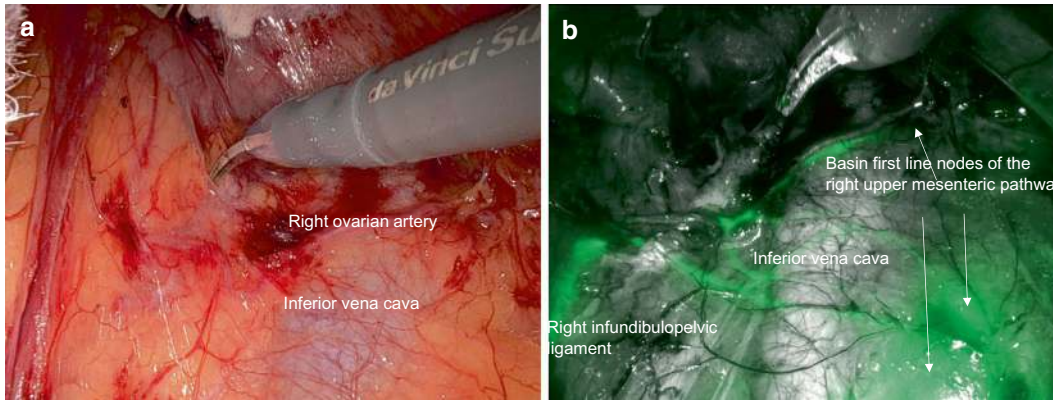

Fig. 9.22 Collector vessels and first-line nodes of the right upper mesenteric pathway. (**a**) At visible light illumination. (**b**) ICG fluorescence at near-infrared illumination

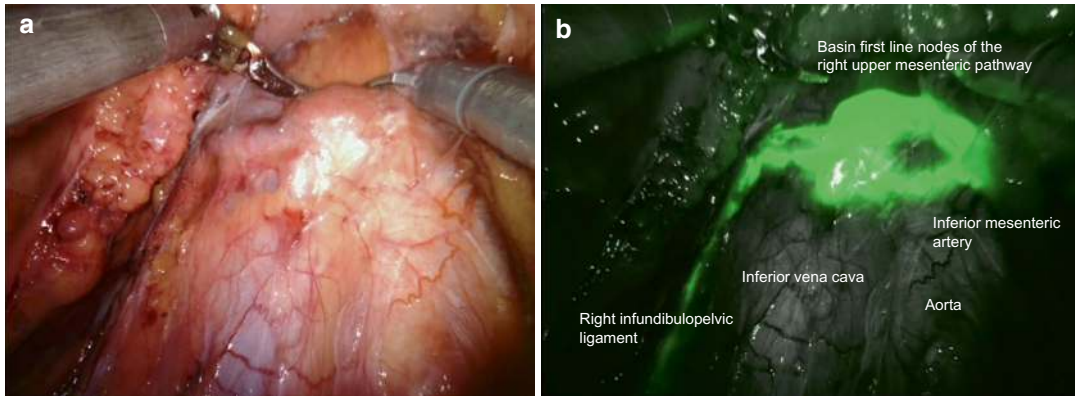

Fig. 9.23 First-line nodes of the right upper mesenteric pathway draining the uterine fundus and the right ovary. (**a**) At visible light illumination. (**b**) ICG fluorescence at near-infrared illumination

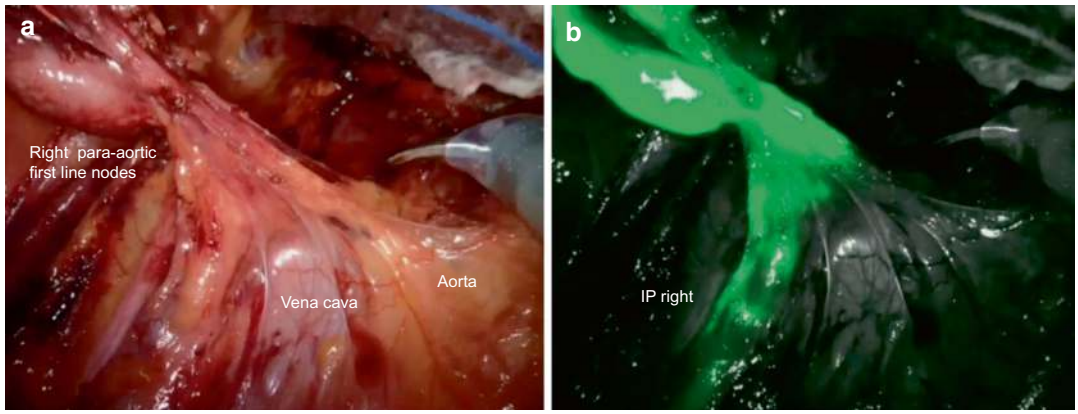

Fig. 9.24 Dissection of the right upper mesenteric basin first-line nodes in connection with the infundibulopelvic ligament. (**a**) At visible light illumination. (**b**) ICG fluorescence at near-infrared illumination

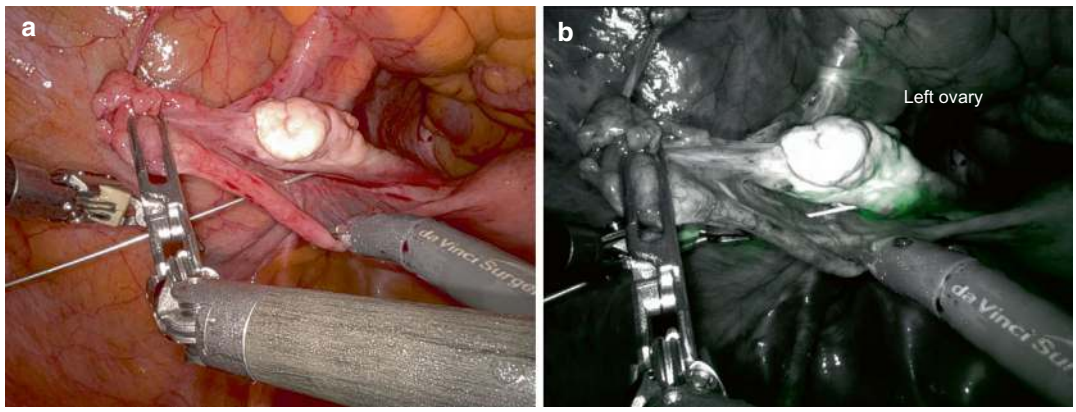

Fig. 9.25 Transabdominal injection of ICG into the left ovary. (**a**) At visible light illumination. (**b**) ICG fluorescence at near-infrared illumination

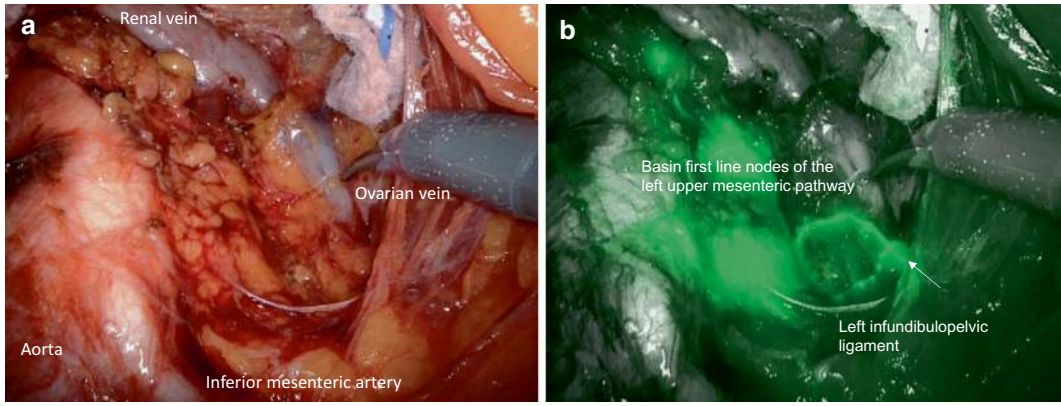

Fig. 9.26 Collector vessels and basin first-line nodes of the left upper mesenteric pathway draining the uterine fundus and left ovary. (**a**) At visible light illumination. (**b**) ICG fluorescence at near-infrared illumination

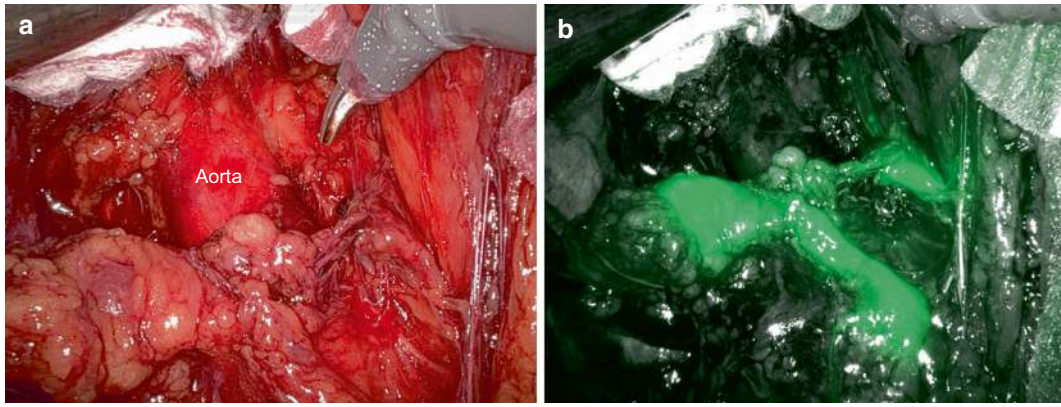

Fig. 9.27 Dissection of the left upper mesenteric basin first-line nodes, including collector vessels from the left infundibulopelvic ligament. (**a**) At visible light illumination. (**b**) ICG fluorescence at near-infrared illumination

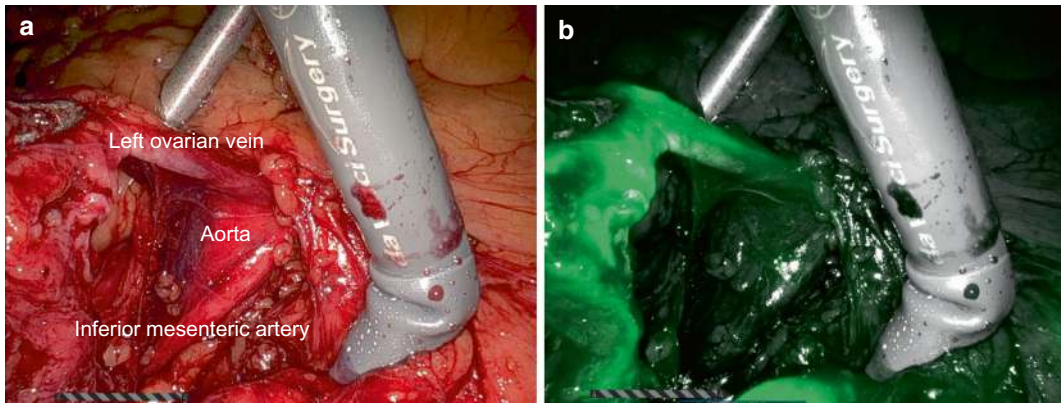

Fig. 9.28 Dissection of the left infundibulopelvic ligament together with upper mesenteric basin first-line nodes. (**a**) At visible light illumination. (**b**) ICG fluorescence at near-infrared illumination

9.5 Second- and Third-Line Lymph Node Dissection

If indicated, second-and third-line nodes are removed as described for cervical cancer in Chap. 8. However, lymph node dissection is performed by minimally invasive surgery, preferably by robotic surgery as well.

9.6 Closures

Apart from closure of the vagina with continuous V-lock 3-0 suture, no closure of peritoneal surfaces is performed. No drains are placed routinely.

9.7 Extended Peritoneal Mesometrial Resection: Type A

This procedure should be performed if endometrial carcinoma infiltration of tissues derived from the genital coelom mesoderm is detected in addition to the corporal tumor spread. Both bladder peritoneum and pararectal peritoneum are included.

9.8 Extended Peritoneal Mesometrial Resection: Type B

This procedure is recommended for endometrial carcinoma infiltrating the deep cervix stroma, vascular mesometrium, and vagina, necessitating additional resection of the vascular and ligamentous mesometrium and mesocolpoi. Type B extended peritoneal mesometrial resection corresponds to TMMR with ovariectomy as detailed in Chap. 8.

9.9 Extended Peritoneal Mesometrial Resection: Type AB

This procedure aims to control endometrium carcinoma locally if the tumor involves the deep cervical stroma, vascular mesometria, and vagina, as well as tissues derived from the coelom mesoderm. Type AB extended peritoneal mesometrial resection represents a TMMR with ovariectomy and additional resection of the bladder and pararectal peritoneum. The anterior and posterior incision lines are set distally to those indicated in steps 6 and 9 of the standard procedure, as previously described for type A extended peritoneal resection.

9.10 Secondary PMMR and Lymph Collector-Guided Pelvic and Periaortic Lymph Node Dissection

Patients with histopathological intermediate and high-risk factors diagnosed in simple hysterectomy specimens should receive complete surgical treatment according to the paradigm of ontogenetic cancer fields. After bilateral ICG injection into the mesometria through the vaginal vault, the pelvic first-line lymph nodes, vascular mesometria, and vaginal apex are resected. In patients at risk for metastatic spread through the upper mesenteric pathways, ICG is also injected into the infundibulopelvic ligaments, and periaortic first-line lymph node dissection is performed. The surgical techniques are adjusted to the primary procedure as described above [7].

9.11 Postoperative Management

General clinical and laboratory patient surveillance and examination before discharge correspond to the description in Chap. 8. The transurethral catheter is withdrawn within 24 hours. Residual urine after micturition is checked sonographically.

9.12 Management of Complications

Venous injuries and bleeding during robotic surgery are handled by compression, bipolar coagulation, application of TachoSil®, or suture. Arterial injuries demand bipolar coagulation or

sutures. Injuries of the bladder, ureter, and bowel are repaired minimally invasively as well. Consultation with a urologist or general surgeon may be needed.

The management principles of postoperative complications adhere to those presented in Chap. 8 for TMMR/EMMR. However, wound complications following robotic surgery are rare and less significant due to the small wound size. Moreover, most of the complications that need surgical intervention can also be treated by minimally invasive surgery.

9.13 Cancer Field Surgery for Early-Stage Tubal Carcinoma

The clinical translation of the paradigm of ontogenetic cancer fields for the surgical treatment of tubal cancer FIGO stages I and II is PMMR with defense line-directed pelvic and periaortic lymph node dissection, as described for endometrium carcinoma with fundal involvement. Due to the increased risk for peritoneal cancer dissemination (which is discussed for ovarian carcinoma below), adjuvant systemic treatment has to be considered an essential element to control this malignant disease.

9.14 Cancer Field Surgery for Early-Stage Ovarian Carcinoma

Contrary to cancer of the lower female genital tract, the local spread pattern of ovarian carcinoma is determined mainly by peritoneal dissemination [8, 9]. Outgrowths of transformed cell collectives detached from the tumor surface transit through the peritoneal fluid and attach to remote peritoneal sites. Here, the cancer outgrowths, which resemble organoids, can invade the submesothelial tissues if they correspond to the ontogenetic stage-associated cancer field and form peritoneal metastases. However, the ovarian cancer spread pattern is complicated by the fact that particularly high-grade serous ovarian carcinoma outgrowths attached to the peritoneal surface of primary nonpermissive sites can survive and advance in malignant progression. Upon reaching an oT4 stage, the outgrowths can invade any peritoneal site and form macrometastases.

The cancer field model for regional tumor spread considers immunologic defense lines defined by the lymphatic network for which the cancer field is tributary. First-line lymph nodes surveilling the ovarian compartment are connected to the upper mesenteric and upper iliac lymphatic pathways. First-line nodes of the upper mesenteric pathway, which is the main route, are located in the mesenteric periaortic lymph basin and may be intercalated in the infundibulopelvic ligament. The upper iliac route of the ovarian lymphatic drainage includes intercalated nodes of the vascular mesometrium and the basin nodes of the iliac bifurcation. Second-line nodes exist upstream and in the mesenteric and iliac lymph territories. Third-line nodes are located downstream in the mesenteric and iliac lymph territories or in the lumbar lymph territories.

High-grade serous ovarian carcinomas are the dominant ovarian cancer type (designated as type II) accounting for about 70% of all ovarian cancer cases [10]. Research during the last decade identified transformed fallopian tube secretory epithelial cells progressing to serous tubal intraepithelial carcinoma (STIC) as the origin of the majority (>80%) of high-grade serous ovarian carcinomas [11, 12]. STIC outgrowths rapidly undergo malignant progression in contact with the ovarian surface epithelium. According to the cancer field model, they have to reach the oT3b stage to invade the ovary. At that stage, they can also infiltrate various peritoneal sites when disseminated from there. Progression to the oT4 stage enables metastasis formation at any peritoneal site, which is clinically evident in most advanced ovarian cancer patients. The remaining ~20% of high-grade serous ovarian carcinomas originate from the ovarian surface epithelium. The cancer field model predicts that they become manifest with larger intraovarian tumor masses of fulminant growth. Type I ovarian tumors, including endometrial, mucinous, clear cell, and low-grade serous carcinomas, are also expected

to progress with larger ovarian tumor masses, albeit slower. In summary, the feature of peritoneal dissemination and the possibility of malignant progression of cancer outgrowths attached to (but not invading) peritoneal surfaces render the spread pattern of ovarian carcinoma rather unpredictable.

The goal of locoregional tumor control of ovarian carcinoma should be achievable with cancer field surgery for oT1, 2, and 3a stages, which encompass FIGO stages IA, B, C, and IIA. The corresponding procedures are total mesogonadal resection (TMGR) for oT1 and 2 ovarian carcinomas and peritoneal mesometrial resection (PMMR) for oT3a cases. Both operations are combined with immunologic defense line-directed pelvic and periaortic lymph node dissection. FIGO stages IC and IIA cases should receive postoperative adjuvant chemotherapy to lower the risk of peritoneal recurrences outside of the genital peritoneum [13, 14].

TMGR removes the ontogenetic ovarian compartment, together with the fallopian tube, infundibulopelvic ligament, broad ligament, proper ovarian ligament, and vascular mesometrium. PMMR includes the uterus (because of its serosa as a cancer field) in addition to the tissues extirpated with TMGR. The procedures are optimally performed with robotic assistance. With oT1 and 2 ovarian carcinomas, immunologic defense line-directed pelvic and periaortic lymphadenectomy can be carried out, guided by the ovarian lymph collectors that are visible at near-infrared illumination after indocyanine green injection. If metastases are detected intraoperatively in the first-line nodes, second- and third-line nodes have to be removed as well.

The exact topography of first-line lymph node metastases should be mapped prospectively. Together with the location of eventual lymph node recurrences, the spatial pattern of the regional spread of oT1 and 2 ovarian carcinomas has to be established in the future. With oT3a ovarian carcinoma, at least first- and second-line nodes have to be resected primarily.

From the paradigm of ontogenetic cancer fields it can be concluded that cancer field surgery is not applicable to the majority of ovarian carcinoma cases, which are those exceeding an oT3a stage. Even oT1 and 2 stages confined to the ovarian compartment and oT3a ovarian carcinomas may escape local control by the pathomechanism of peritoneal dissemination as described above.

However, based on the reported postoperative courses of conventional treatment, improvement in the regional tumor control of FIGO stages I and IIA and the local control of FIGO stage IIA ovarian carcinomas can be expected [15]. The overall recurrence rate of FIGO stages I and IIA ovarian carcinoma might be reduced by up to 30% (corresponding to 6% in absolute terms). Calculated from the incidence of low-grade, low-stage ovarian carcinomas [10], about 20% of ovarian cancer patients could benefit from cancer field surgery and defense line-directed lymph node dissection—a prospect that is worth considering for clinical testing.

References

1. Buderath P, Dang TM, Kimmig R. Cancer-field surgery for endometrial cancer by robotic peritoneal mesometrial resection and targeted compartmental lymphadenectomy (PMMR+TCL). J Gynecol Oncol. 2025;36:e13. https://doi.org/10.3802/jgo.2025.36.e13.
2. Buderath P, Rusch P, Mach P, Kimmig R. Cancer field surgery in endometrial cancer: peritoneal mesometrial resection and targeted compartmental lymphadenectomy for locoregional control. J Gynecol Oncol. 2021;32:e7. https://doi.org/10.3802/jgo.2021.32.e7.
3. Kimmig R, Aktas B, Buderath P, Wimberger P, Iannaccone A, Heubner M. Definition of compartment-based radical surgery in uterine cancer: modified radical hysterectomy in intermediate/high-risk endometrial cancer using peritoneal mesometrial resection (PMMR) by M Höckel translated to robotic surgery. World J Surg Oncol. 2013;11:198. https://doi.org/10.1186/1477-7819-11-198.
4. Kimmig R, Iannaccone A, Aktas B, Buderath P, Heubner M. Embryologically based radical hysterectomy as peritoneal mesometrial resection (PMMR) with pelvic and para-aortic lymphadenectomy for loco-regional tumor control in endometrial cancer: first evidence for efficacy. Arch Gynecol Obstet. 2016;294:153–60. https://doi.org/10.1007/s00404-015-3956-y.

5. Kimmig R, Thangarajah F, Buderath P. Sentinel lymph node detection in endometrial cancer—anatomical and scientific facts. Clin Obstet Gynaecol. 2024;94:102483. https://doi.org/10.1016/j.bpobgyn.2024.102483.
6. Liu H, Cao Y, Li L, Bai Y, Liu J. Effectiveness of robotic surgery for endometrial cancer: a systematic review and meta-analysis. Arch Gynecol Obstet. 2022;305:837–50. https://doi.org/10.1007/s00404-021-06229-x.
7. Buderath P, Elgharib M, Kimmig R. Peritoneal mesometrial resection with lymphadenectomy following prior hysterectomy in intermediate/high-risk endometrial cancer: feasibility and safety. Arch Gynecol Obstet. 2024;309:1569–74. https://doi.org/10.1007/s00404-023-07275-3.
8. Farsinejad S, Cattabiani T, Muranen T, Iwanicki M. Ovarian cancer dissemination—a cell biologist's perspective. Cancers. 2019;11:1957. https://doi.org/10.3390/cancers11121957.
9. Ritch SJ, Telleria CM. The transcoelomic ecosystem and epithelial ovarian cancer dissemination. Front Endocrinol. 2022;13:886533. https://doi.org/10.3389/fendo.2022.886533.
10. Singh N, McCluggage WG, Gilks CB. High-grade serous carcinoma of tubo-ovarian origin: recent developments. Histopathol. 2017;71:339–56. https://doi.org/10.1111/his.13248.
11. Löhmussar K, Kopper O, Korving J, Begthel H, Vreuls CPH, van Es JH, et al. Assessing the origin of high-grade serous ovarian cancer using CRISPR-modification of mouse organoids. Nature Comm. 2020;11:2660. https://doi.org/10.1038/s41467-020-16432-0.
12. Zhang S, Dolgalev I, Zhang T, Ran H, Levine DA, Neel BG. Both fallopian tube and ovarian surface epithelium are cells-of-origin for high-grade serous ovarian carcinoma. Nature Comm. 2019;10:5367. https://doi.org/10.1038/s41467-019-13116-2.
13. Kimmig R, Buderath P, Mach P, Rusch P, Aktas B. Surgical treatment of early ovarian cancer with compartmental resection of regional lymphatic network and indocyanine-green-guided targeted compartmental lymphadenectomy (TCL, para-aortic part). J Gynecol Oncol. 2017a;28:e41. https://doi.org/10.3802/jgo.2017.28.e41.
14. Kimmig R, Buderath P, Rusch P, Mach P, Aktas B. Early ovarian cancer suergery with indocyanine-green-guided targeted compartmental lymphadenectomy (TCL, pelvic part). J Gynecol Oncol. 2017b;28:e68. https://doi.org/10.3802/jgo.2017.28.e68.
15. Deng T, Huang Q, Wan T, Luo X, Feng Y, Huang H, et al. The impact of lymph node dissection on survival in patients with clinical early-stage ovarian cancer. J Gynecol Oncol. 2021;32:e40. https://doi.org/10.3802/jgo.2021.32.e40.

10 Laterally Extended Endopelvic Resections

Laterally extended endopelvic resection (LEER) represents cancer field surgery for locally advanced carcinomas, i.e., ontogenetic stages >2 of the Müllerian compartment. Due to the severe disturbances of body integrity and function resulting from the extensive LEER procedure, we deem its indication justified if:

- Locoregional tumor control provides a curative chance for the patient.
- There is no radiotherapeutic treatment alternative.

Anterior LEER extirpates the entire oT3a and most of the oT3b cancer fields of uterovaginal carcinomas (see Chaps. 3 and 7) (Fig. 10.1). Anteroposterior (total) LEER removes the whole oT3b cancer field and includes parts of the oT4 cancer field, such as the mesorectum and rectum, enabling excision with tumor-free margins (R0) in selected oT4 cases (Fig. 10.2). Most of these advanced tumors are fixed to the pelvic sidewall and floor through continuous and discontinuous dorsolateral spread within the urogenital mesenteries and the ligamentous mesometria/mesocolpoi. If the infiltration approaches or seizes the umbilical artery and visceral endopelvic fascia (see Fig. 7.8c), tumor-associated fibrosis leads to the fixation of the internal iliac vessel system (Fig. 10.3). Likewise, cancer spread through the ligamentous mesocolpos approaching or seizing the parietal endopelvic fascia induces fixation to the levator ani muscles (Fig. 10.4). A third, albeit less frequent, mechanism for pelvic wall fixation is mediated through large basin lymph node metastases adhering to the urogenital mesentery (Fig. 10.5).

LEER integrates the pelvic floor muscles and the internal iliac vessel system into the resection of the pelvic hollow organs (Fig. 10.6). Originally developed empirically by the author to remove Müllerian cancers fixed to the pelvic wall with microscopically tumor-free margins (R0), the procedure has proved to strictly adhere to the cancer field model, as demonstrated in 102 patients with cervicovaginal and 11 patients with endometrial carcinomas [1–3].

The vascular and muscular resection ensures the complete removal of the urogenital mesenteries and endopelvic fasciae comprising most of the oT3b cancer field. However, the infiltration of somatic retroperitoneal and pelvic wall structures (blood vessels, nerves, muscles, bones) (Figs. 7.18 and 7.19) represents contraindications for LEER, as further specified in Chap. 13. According to the regional cancer field model presented in Chaps. 5 and 6, defense line-directed lymph node dissection of advanced (>oT2) carcinomas mandates the extirpation of the complete first-, second-, and third-line basin lymph nodes

M. Höckel et al., *Cancer Field Surgery in Gynecologic Oncology*,
https://doi.org/10.1007/978-3-031-83030-3_10

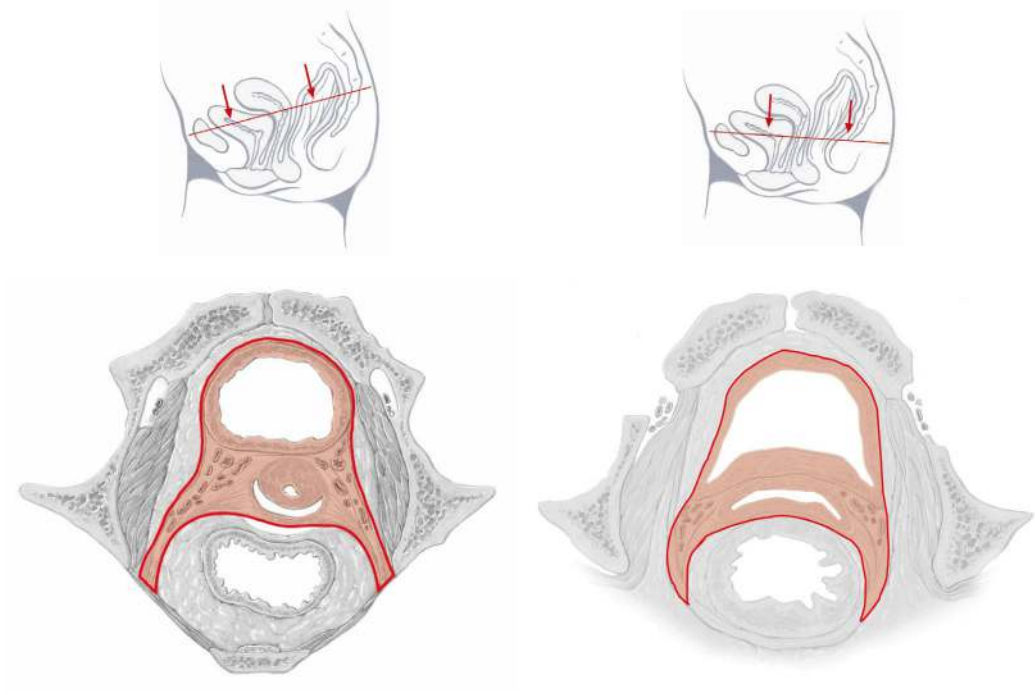

Fig. 10.1 Schematic representation of anterior laterally extended endopelvic resection (LEER) with the two transverse pelvic planes as indicated in the panels with the sagittal sections

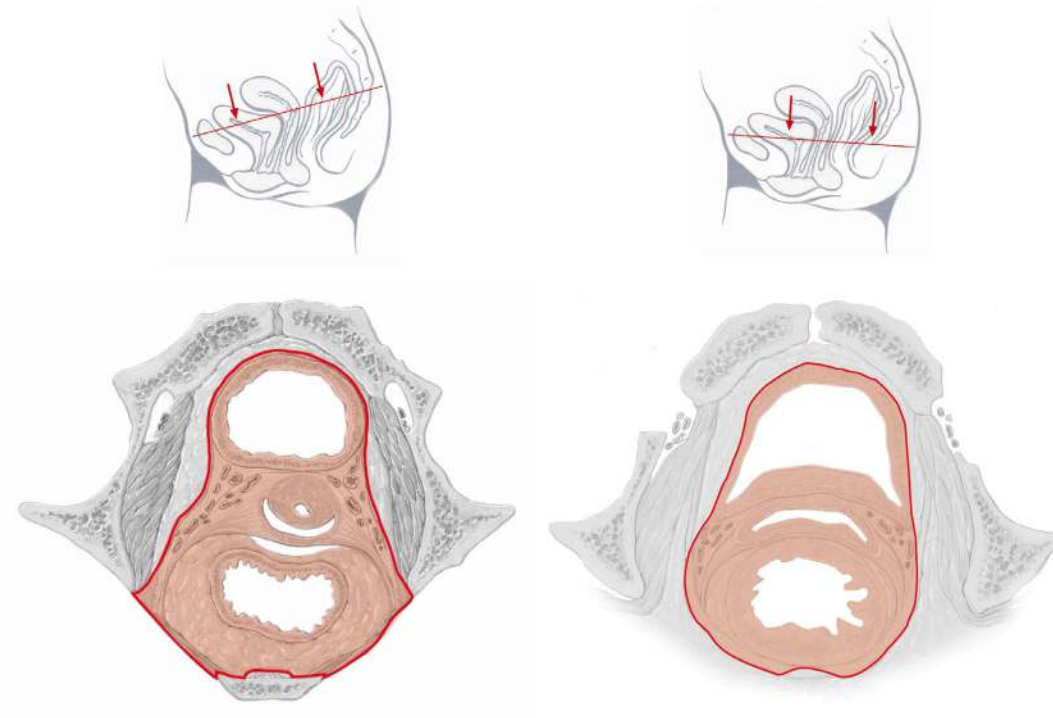

Fig. 10.2 Schematic representation of anteroposterior (total) LEER within the two transverse pelvic planes as indicated in the panels with the sagittal sections

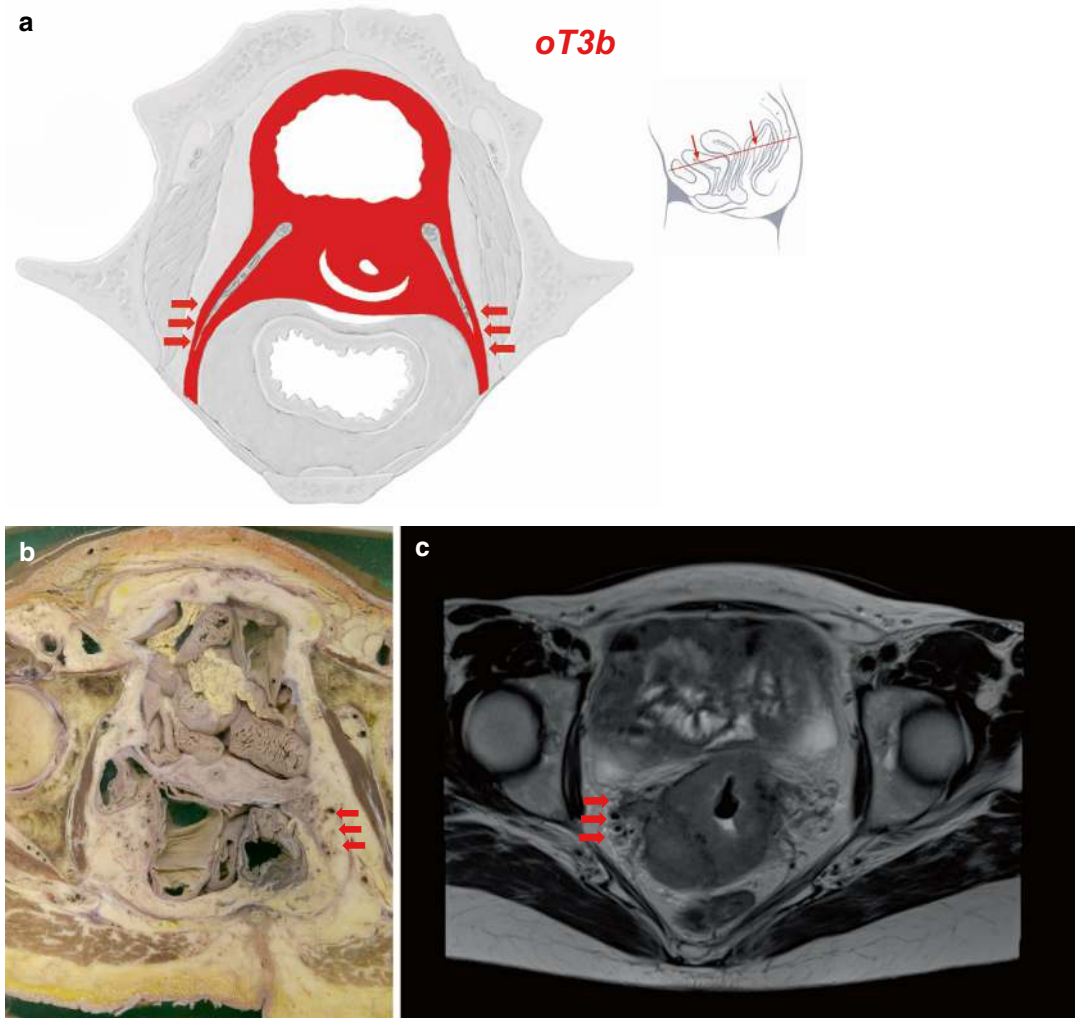

Fig. 10.3 Pathoanatomical mechanisms of cervix cancer fixation. Fixation at the internal iliac vessel system. (**a**) Schematic representation of the oT3b cancer field abutting the internal iliac vessel system (arrows) in the transverse pelvic plane as indicated in the panel with the sagittal section. (**b**) Potential fixation site at the transition of the left urogenital mesentery to the internal iliac vessel system demonstrated in a transverse pelvic section of a formalin-fixed female body. (**c**) T2-weighted transverse MRI scan shows oT3b cervix carcinoma spreading in the right urogenital mesentery to the internal iliac vessel system (arrows). Clinically, broad fixation of the tumor-inflated cervix to the right pelvic wall was palpated

(related to the Müllerian compartment) in addition to the intercalated nodes within the subperitoneum, since first-line metastases may be located at each of the corresponding anatomic regions (Fig. 10.7a–d). Carcinoma involvement of the urogenital sinus and perineal tissues adds the superficial and deep inguinal lymph node regions as potential sites of first-line metastases (Fig. 10.8a–d).

Primary restoration of urinary and intestinal functions, reconstruction of the pelvic floor and of vulva/perineum, and therapeutic angiogenesis of the denuded pelvis are essential elements of the LEER procedures.

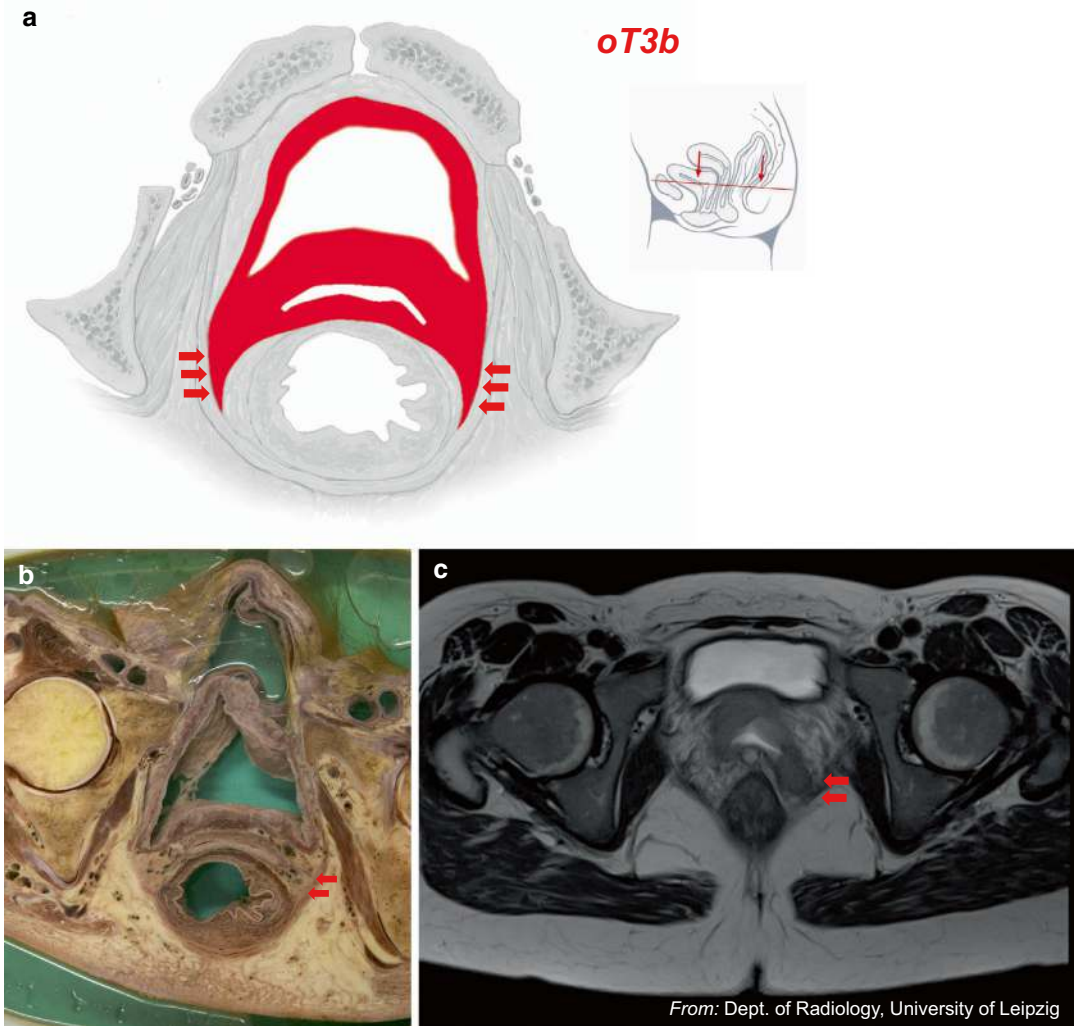

Fig. 10.4 Pathoanatomical mechanisms of cervix cancer fixation. Fixation at the levator ani muscle. (**a**) Schematic representation of the oT3b cancer field abutting the levator ani muscle (arrows) in the transverse pelvic plane as indicated in the panel with the sagittal section. (**b**) Potential fixation site at the left levator ani muscle and its overlying parietal endopelvic fascia, demonstrated in a transverse pelvic section of a formalin-fixed female body. (**c**) T2-weighted transverse MRI scan shows oT3b cervix carcinoma spread within the vagina and mesocoplos to the left levator ani muscle (arrows). Clinically, broad fixation of the tumor to the left pelvic wall was palpated

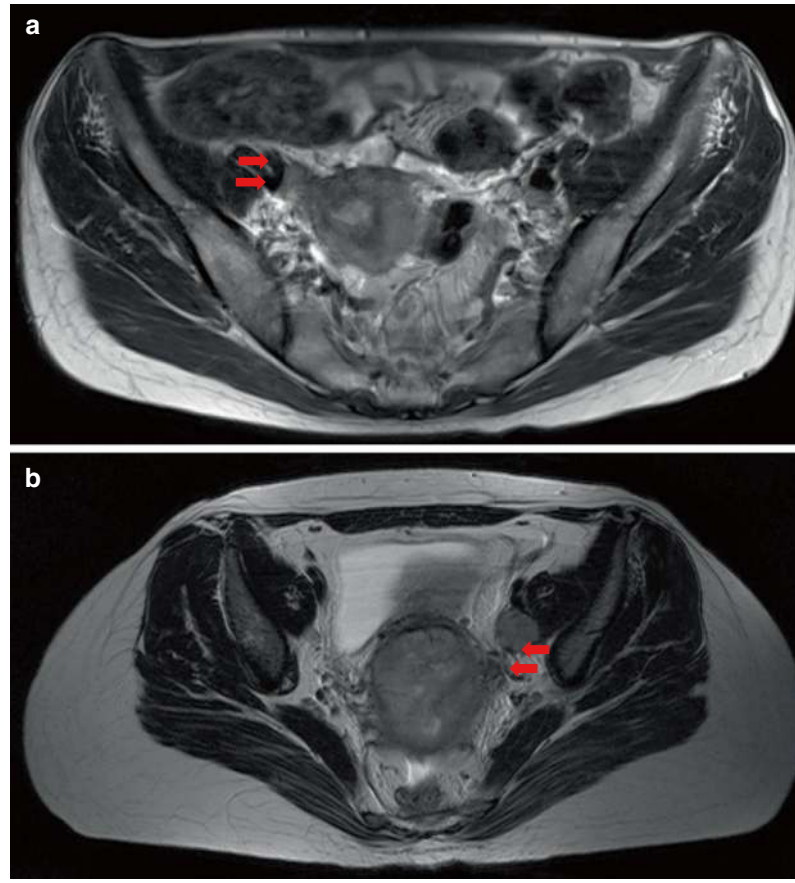

Fig. 10.5 Pathoanatomical mechanisms of cervix cancer fixation. Fixation at basin lymph node metastases. (**a**) Right external iliac lymph node metastasis adhering to the peritoneal mesometrium. (**b**) Left paravisceral lymph node metastasis adhering to the vascular mesometrium

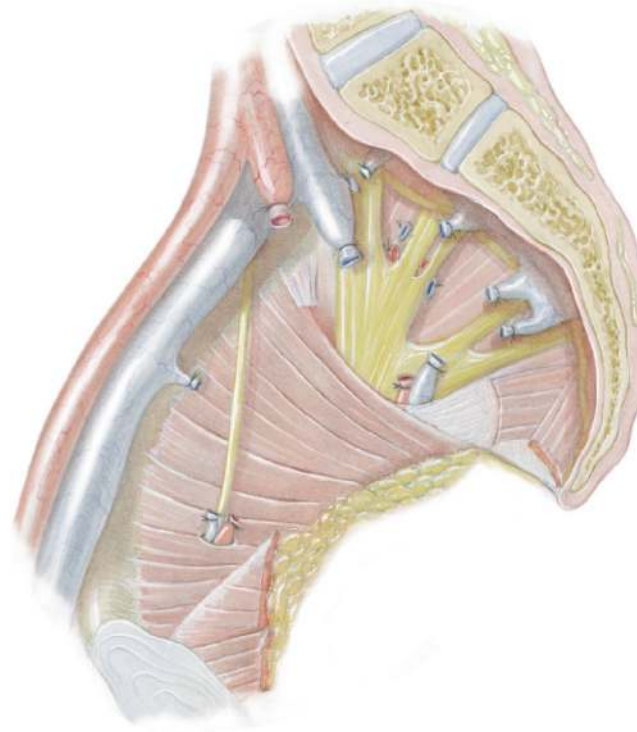

Fig. 10.6 Semischematic anatomical demonstration on the right parietal hemipelvis of the surgical mainstay of LEER, the resection of the internal iliac vessel system and levator ani muscle

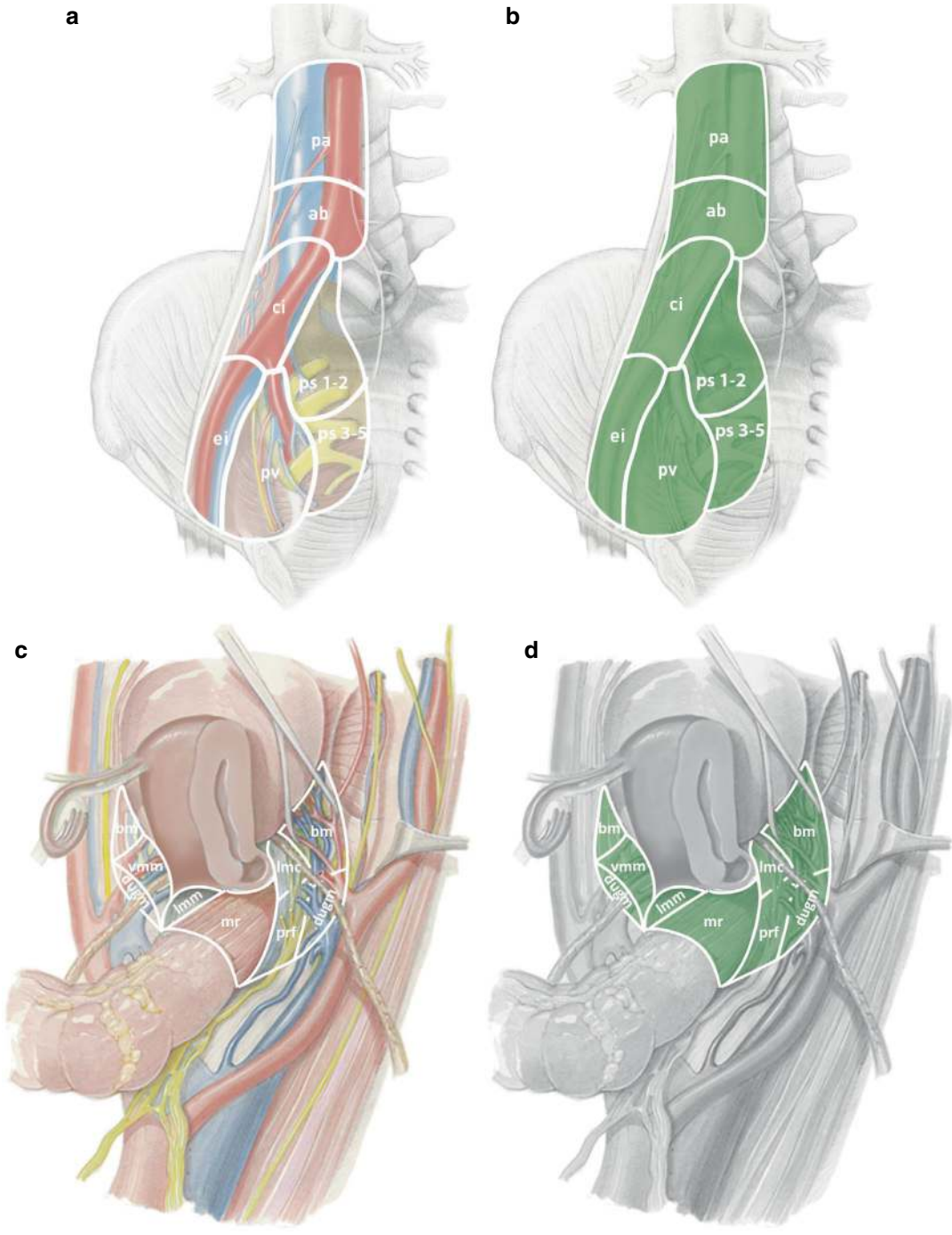

Fig. 10.7 Basin and intercalated lymph node regions, which can harbor first-line metastases in oT > 2 cervicovaginal carcinoma. First-line lymph node regions are highlighted with intense green coloring. (**a**, **b**) Infrarenal and right pelvic retroperitoneum. ei, external iliac; pv, paravisceral; ci common iliac; ps, presacral; ab, aortic bifurcation; pa, periaortic. (**c**, **d**) Semischematic drawing illustrates the subperitoneum. bm, bladder mesentery; ugm, urogenital mesentery; vmm, vascular mesometrium; lmm, ligamentous mesometrium; lmc, ligamentous mesocolpos; prf, pararectal fascia/hypogastric subperitoneum; mr, mesorectum. Compare with Figs. 6.1 and 6.2

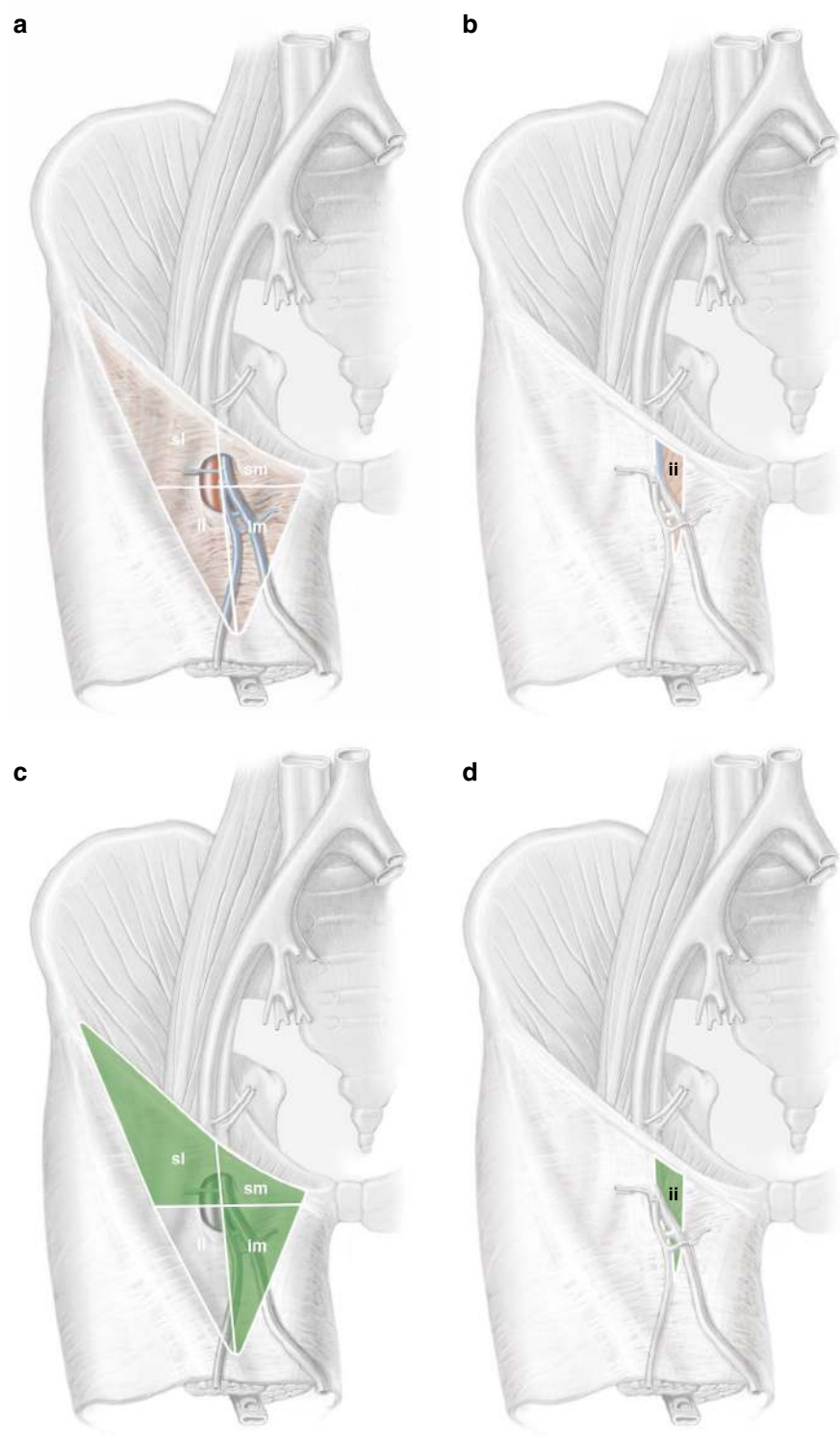

Fig. 10.8 Basin lymph node regions, which can contain first-line metastases in oT > 2 cervicovaginal cancer infiltrating the sinus vagina/urethra and vulva/perineum. (**a**) Anatomical drawing of the right superficial inguinal lymph node region. (**b**) Anatomical drawing of the right deep inguinal lymph node regions. (**c**, **d**) Sites of first-line lymph node metastases. *sl* superolateral quadrant of femoral triangle, *sm* superomedial quadrant, *im* inferomedial quadrant, *il* inferolateral quadrant, *ii* deep inguinal

10.1 Equipment

The instruments and devices compiled for the total mesometrial resection (TMMR)/extended mesometrial resection (EMMR) and VFR procedures in Chap. 8 (Table 8.1) and Chap. 11 (Table 11.1) are also optimal for LEER.

10.2 Patient Preparation and Positioning

In addition to bowel preparation, as noted for TMMR/EMMR in Chap. 8, four potential skin sites for urinary and bowel stomata should be marked on the patient's hypo- and epigastrium in the sitting position. Positioning directives given for TMMR/EMMR in Chap. 8 are also valid for LEER.

10.3 Anterior LEER: Step-by-Step Procedure Illustrated in a Patient

Step 1. Laparotomy—peritoneal access: the first step corresponds to the maneuvers as described for TMMR/EMMR. Previous pelvic and abdominal surgery, radical hysterectomy in particular, may have caused extensive and thick peritoneal adhesions. Their surgical lysis bears a risk of intra- or postoperative bowel lesions. In these situations, the use of monopolar ball pencils for peritoneal adhesiolysis is recommended. Systematic exploration of the peritoneal situs should focus on signs of extragenital and extraparamesenteric peritoneal tumor involvement, which should be sampled for frozen section pathological investigation. Confirmation of this diagnosis is not compatible with a curative treatment chance by LEER, this therapy must then be abandoned.

Step 2. Retroperitoneal access: the principles and techniques of this step are the same as those given for TMMR/EMMR in Chap. 8. Retroperitoneal fibrosis of various degrees, due to previous radiotherapy, retroperitoneal surgery, or both, may be encountered. Dilatation and thickening of the ureter is a frequent finding. If still existing, the ovarian vessels are sealed and cut at the level of the pelvic inlet.

Step 3. Subperitoneal access—bilateral: this step complies with TMMR, including ovariectomy. However, it may also be hampered by severe subperitoneal fibrosis from previous treatment. Cobb periosteal dissectors must often be applied to mobilize the ureters. The pelvic mesureters do not have to be preserved with LEER. The identification and exposition of umbilical arteries as the most important landmarks for access to the anterior pelvic retroperitoneum are essential. In the majority of cases, dissection along the visceral endopelvic fascia covering the anterior surface of the urogenital mesentery down to the parietal endopelvic fascia at the levator ani muscles is possible despite subperitoneal fibrosis, but it can be spoiled by cancer conglomerates of local tumor or intercalated and basin lymph node metastases. In this situation, one has to proceed to the next steps.

Step 4. External iliac lymph node dissection—bilateral.

Step 5: Paravisceral lymph node dissection—bilateral: the complete extirpation of the parietal first-line lymph node regions is performed according to the description for TMMR/EMMR. Subperitoneal fibrosis and malignant tumors may significantly impede the maneuvers. Gel-coated Cobb periosteal dissectors are helpful for exposing the iliaca externa vessels, the obturator nerve, and the iliaca interna vessels with their parietal branches. The parietal branches of the internal iliac vessel system have to be clearly identified, sealed, and cut to expose the proximal sciatic nerve with its lumbosacral roots.

Step 6. Transection of the distal pelvic ureters (Fig. 10.9): the ureters are transected about 2 cm proximal to their entry into the urogenital mesentery (Fig. 10.9). A slice biopsy of the transection site is sent for frozen section investigation. The ureters are splinted with soft catheters to drain the urine before urinary reconstruction.

Step 7. Resection of the internal iliac vessel system—bilateral (Fig. 10.10): the iliac artery is sealed and transected about 1–2 cm distal from

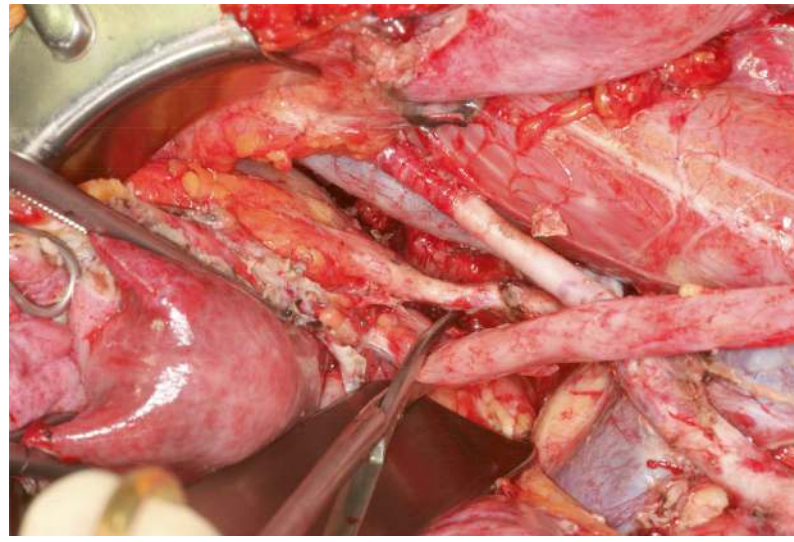

Fig. 10.9 Transection of the right distal ureter approximately 3 cm in front of its entry into the urogenital mesentery

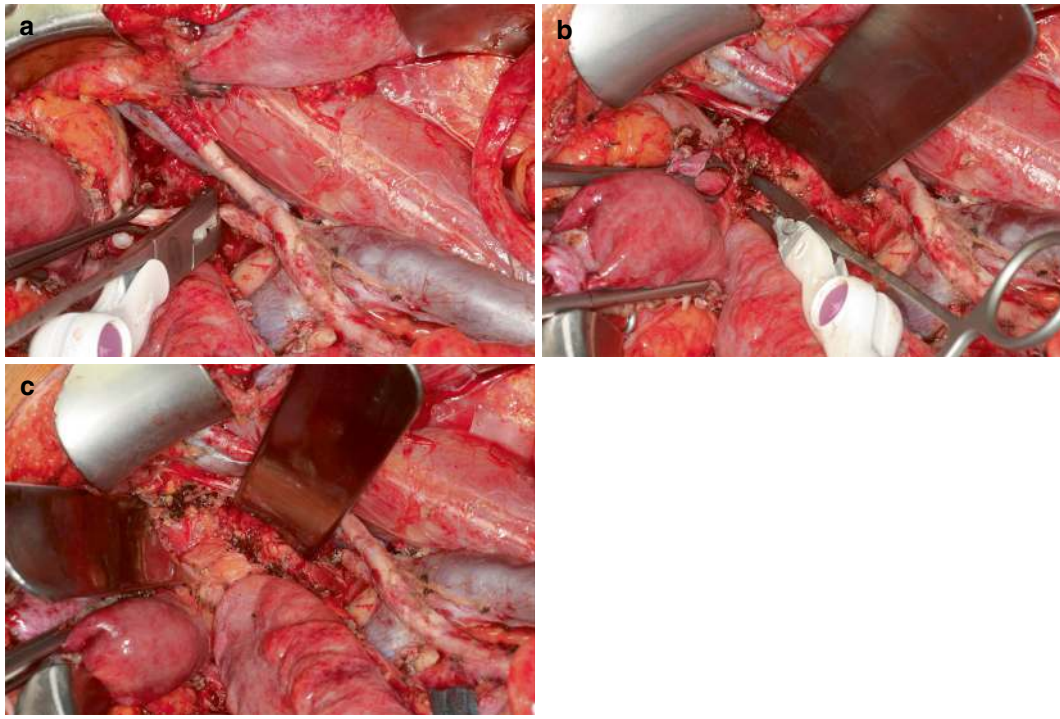

Fig. 10.10 Transection of the right internal iliac vessel system with parietal and visceral branches. (**a**) The internal iliac artery is sealed and transected. Its posterior trunk with the origin of the superior gluteal artery may be preserved. (**b**) After the sealing and transection of the right internal iliac vein, its parietal branches that remained after the paravisceral lymph node dissection are sealed and cut. (**c**) Vascular resection completed

its origin (Fig. 10.10a). Thereafter, the internal iliac vein is severed in the same way. Additional parietal branches that had not been accessed in the previous step, e.g., lateral sacral veins, are now sealed and cut (Fig. 10.10b). The urogenital mesentery is then mobilized medially up to the level of the inferior hypogastric plexus (Fig. 10.10c).

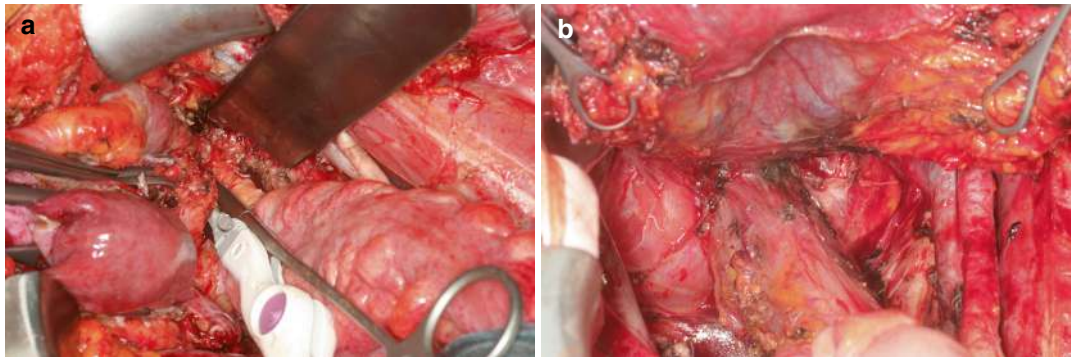

Fig. 10.11 Recto-Müllerian separation and transection of the ligamentous mesometria and proximal mesocolpoi. (**a**) The right urogenital mesentery is pulled ventrally for the sealing and transection of the right ligamentous mesometrium and mesocolpos. (**b**) Both urogenital mesenteries with internal iliac vessels have been grasped by Förster forceps and pulled ventrally to demonstrate the transection sites of the ligamentous mesometria and mesocolpoi at the anterolateral mesorectum

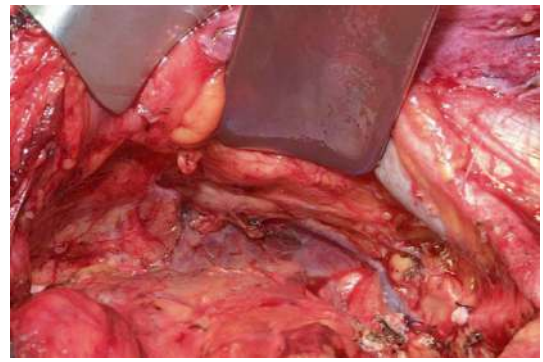

Fig. 10.12 The bladder covered by peritoneum and visceral endopelvic fascia has been separated from the parietal tissues, except from the pubourethral ligament. The intraoperative view to the right side is shown

Steps 8 and 9. Recto-Müllerian separation and transection of the ligamentous mesometria/proximal mesocolpoi (Fig. 10.11): these steps of the anterior LEER are performed like steps 9 and 10 of TMMR/EMMR but are extended caudally to reach the level of the levator ani muscles (Fig. 10.11a, b). All anterior branches of the inferior hypogastric plexus are transected, along with the transection of the proximal ligamentous mesocolpoi. However, the posterior branches of the plexus hypogastrici inferiores are preserved for rectal innervation.

Step 10. Bladder mobilization (Fig. 10.12): after incision of the bladder peritoneum in projection of the pubic symphysis and the anterior rami of the pubic bones, including the transection of the obliterated umbilical arteries and the urachus, dissection proceeds along the visceral endopelvic fascia toward the bladder neck, anterior proximal urethra, and pubourethral ligament, meeting the parietal endopelvic fascia. The complete visceral endopelvic fascia covering the anterior urogenital mesenteries bilaterally and the anterior bladder wall in between, as well as the anterior pelvic floor, are now exposed (Fig. 10.12).

Step 11. Muscular transection—bilateral (Fig. 10.13): depending on the tumor load of the urogenital mesenteries, the muscular incision is made at the arcus tendineus fasciae pelvis, the arcus tendineus levatoris ani, or even further lateral into the obturator internus muscle below the obturator nerve (Fig. 10.13a). The incision is extended anteriorly toward the symphysis and

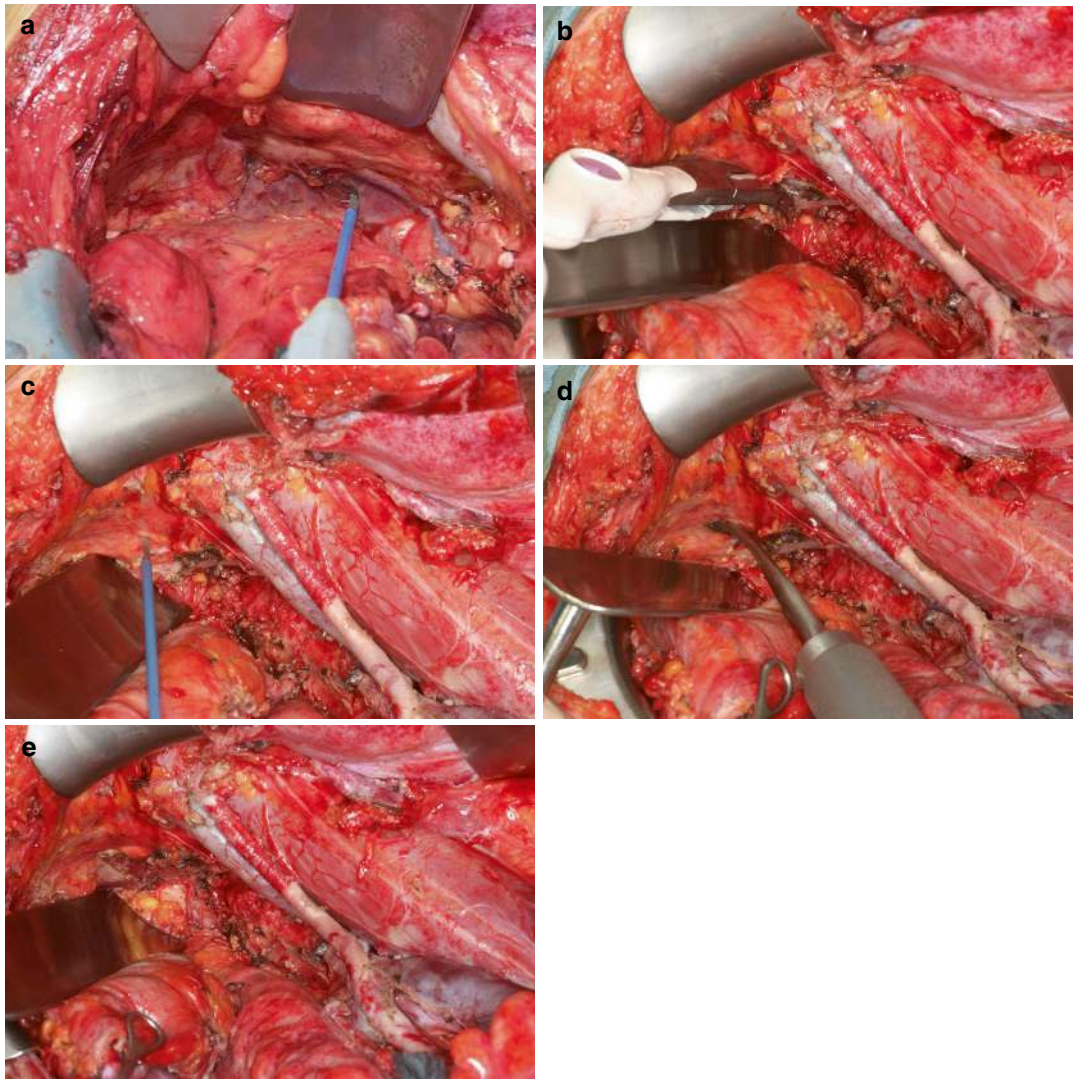

Fig. 10.13 Muscular dissection demonstrated at the right side. (**a**) In this patient, the parietal endopelvic fascia and underlying levator ani muscle are incised at the arcus tendineus fasciae pelvis. (**b**, **c**) The transection proceeds anteriorly and posteriorly, accompanied by the sealing of the muscle tissue. (**d**) With the use of a Cobb periosteal dissector, the levator ani muscle is separated from the underlying fatty tissue of the ischiorectal fascia. (**e**) Muscular dissection completed

posteriorly toward the sciatic spine optimally with the LigaSure™ curved jaw open sealer/divider (Fig. 10.13b). The bilateral anterior muscular transection terminates just lateral to the pubourethral ligament (Fig. 10.13c). The symphyseal connections of the levator ani muscles will be sealed and cut together with the pubourethral ligament during the perineal phase of the anterior LEER.

The posterior transection of the levator ani muscles proceeds to the midrectum bilaterally. If parts of the obturator muscles are included, the muscle must be transected before it leaves the endopelvis. The muscle flaps are then mobilized medially from the fibrofatty tissues of the ischiorectal fossa toward the hiatus genitalis with the use of Cobb periosteal dissectors (Fig. 10.13d, e).

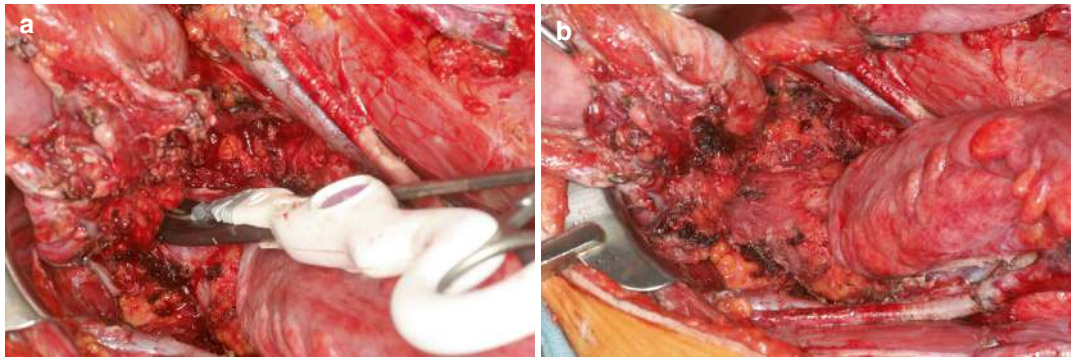

Fig. 10.14 Transection of the distal ligamentous mesocolpoi. (**a**) Sealing and cutting of the right distal ligamentous mesocolpos. (**b**) After the completion of this maneuver, the anterior LEER will proceed from the perineal route

Step 12. Transection of the distal mesocolpoi—bilateral (Fig. 10.14): the transection of the distal mesocolpoi from the bilateral mesorectum (Fig. 10.14a) completes the abdominal part of the anterior LEER (Fig. 10.14b).

Step 13. Perineal incision (Fig. 10.15): before the patient can be moved into the lithotomy position, the retractors of the Bookwalter™ system have to be removed, and the ring must be disconnected. The location of the perineal skin incision depends on the caudal extension of the malignant tumor. If the most caudal cancer involvement is cranial to the sinus vagina, the perineal incision is placed just distal to the hymenal remnants and the urethral meatus (Fig. 10.15a). If the inclusion of the ontogenetic vulva is deemed necessary for local tumor control, the perineal incision is performed at the ridges of the labia majora, anterior commissure, lateral gynecologic perineum, and ventral anal skin between 11 and 1 o'clock, as with total vulva field resection (see Chap. 11). Extravulvar superficial perineal tissues, such as the labia majora or labiocrural skin, rarely have to be integrated into anterior LEER procedures.

The anterior hemicircumference of the anal sphincter muscles is separated from the fatty tissue of the ischioanal fossa. The bulbospongiosus muscles covering the bulbi vestibulares are dissected from the vulva skin to be completely exposed (Fig. 10.15b). The urogenital diaphragm is reached lateral to the bulbospongiosus muscles. In oT3b carcinomas infiltrating the perineum, the clitoridal ligament is sealed and cut, and the body and crura of the clitoris are detached from the symphysis and the inferior rami of the pubic bones. In all anterior LEERs, the anovestibular septum is transected proximal to the external anal sphincter, and the distal anterior rectum is separated from the dorsal sinus vagina and abutting periurethrovaginal tissues in the midsagittal plane to reach the abdominal surgical field. The urogenital diaphragm is then transected along the peripheral margins of the bulbi vestibulares/bulbospongiosus muscles. After bilateral transection of the pubourethral ligament (Fig. 10.15c), the anterior LEER specimen can usually be extruded through the perineal defect (Fig. 10.15d). If the specimen is too bulky, it is removed abdominally. After thorough lavage, the peritoneal wound is temporarily closed superficially with skin staples (Fig. 10.15e).

Step 14. Common iliac lymph node dissection—bilateral.

Step 15. Presacrococcygeal and pararectal lymph node dissection—bilateral.

Step 16. Aortic bifurcation lymph node dissection.

Step 17. Infrarenal lymph node dissection.

Steps 14–17 correspond to those with TMMR/EMMR, described and illustrated in Chap. 8.

The patient is placed in a supine position, and the Bookwalter™ retractor system is set in again.

Figure 10.16 a–d shows pelvic intraoperative views of anterior LEERs.

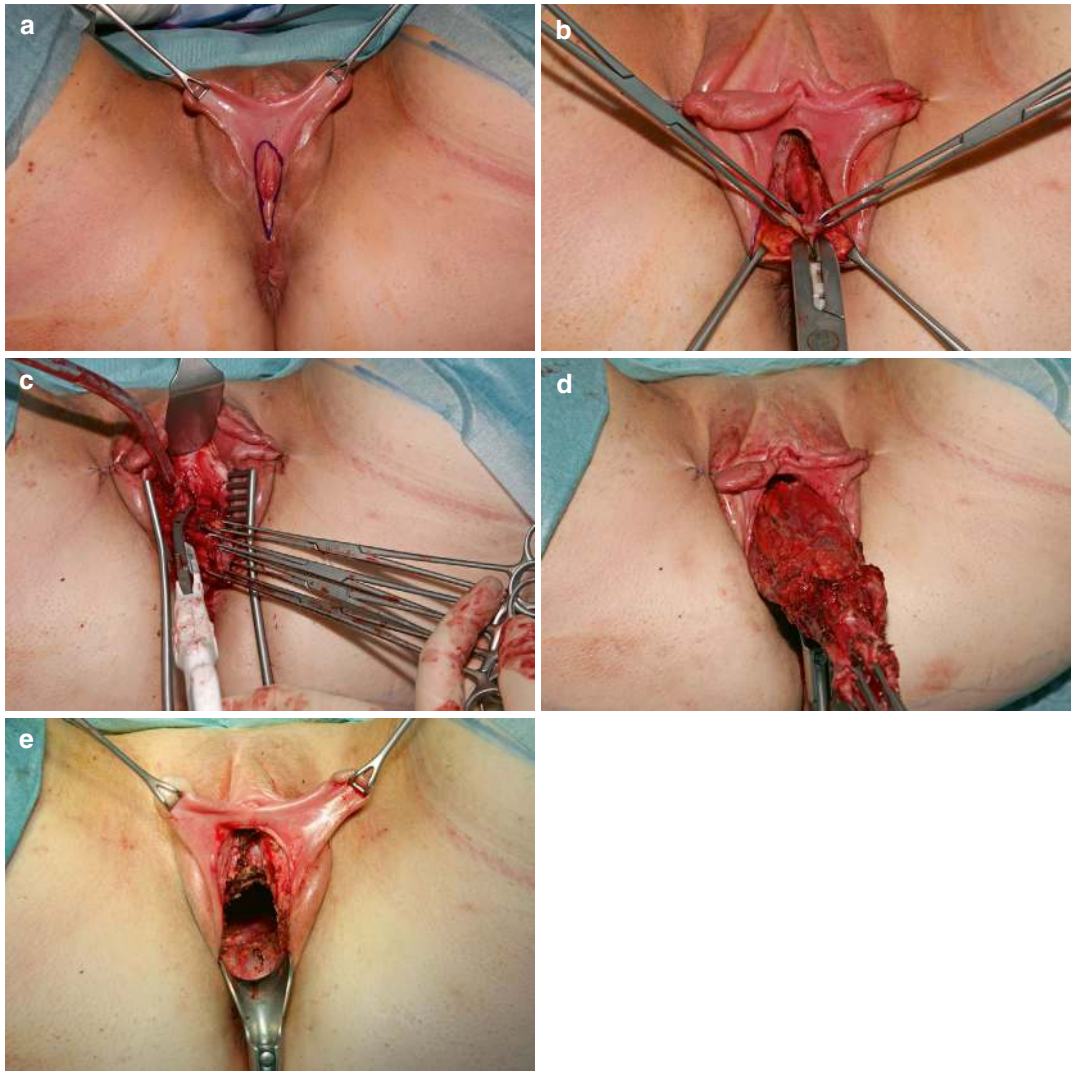

Fig. 10.15 Perineal part of anterior LEER. (**a**) Marking of the skin incision line. In this case, the vulvar compartment could be preserved. The skin incision is planned just distal to the hymenal remnants and the urethral meatus. (**b**) The anterior hemicircumference of the sphincter ani muscle and the bulbi vestibulares encasing both the vaginal introitus and the distal urethra have been exposed, and the anovestibular septum is transected. (**c**) The urogenital diaphragm and the pubourethral ligament are sealed and transected laterally to the bulbi vestibulares. (**d**) The anterior LEER specimen is extruded transperineally. (**e**) Perineal defect after anterior LEER. It is temporarily closed by skin staples to continue the abdominal part of the anterior LEER and is reconstructed by skin flap(s) thereafter

Step 18. Urinary diversion: a urological consultant should perform this step. The technique applied depends on his or her experience and the patient's preference. However, the use of irradiated bowel parts to produce a urinary conduit or pouch is strongly discouraged. For preirradiated patients, who represent the majority of cases, the transverse colon is the safest option as a source of bowel flaps for urinary diversion.

Step 19. Endopelvic angiogenic carpet with an omentum majus flap and laparotomy closure: the significantly denuded inner pelvis is

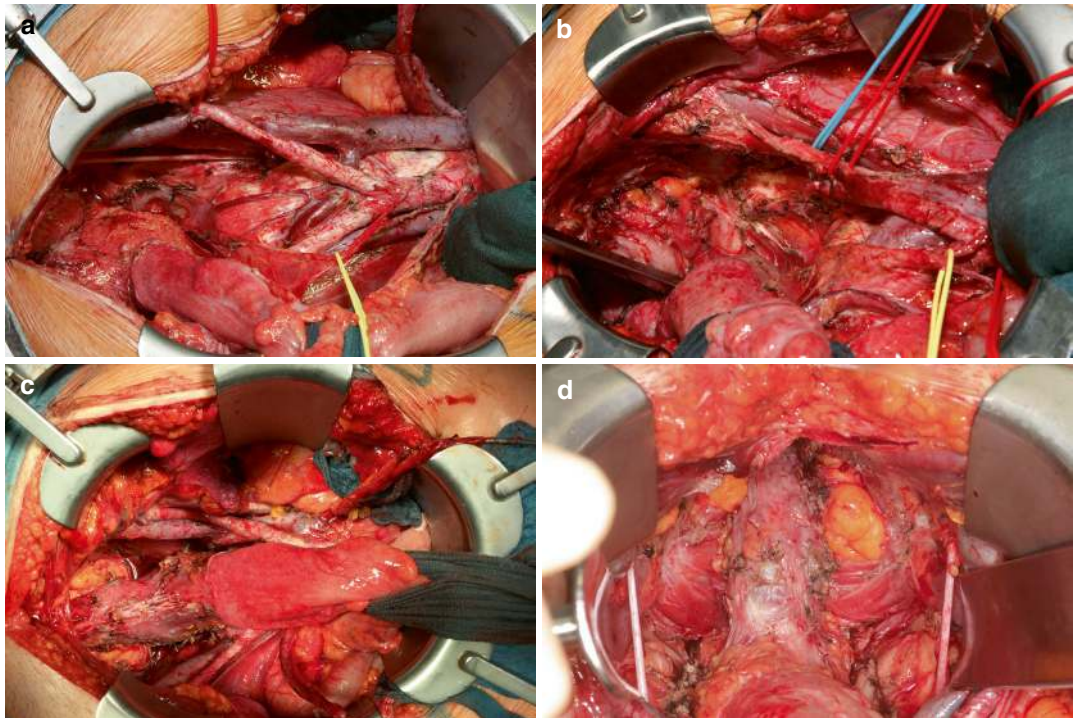

Fig. 10.16 Intraoperative views into the pelvis after anterior LEER and first-, second-, and third-line (with respect to the Müllerian compartment) lymph node dissection in three different patients. (**a**) At the right pelvic wall, the internal iliac vessel system and all parietal lymph nodes have been resected. The superior hypogastric plexus with two nervi splanchnici lumbales and the hypogastric nerves have been preserved (yellow band). The rectum and its right lateral mesorectum are exposed. (**b**) Similar perspective as in *a* in a pelvis with severe therapy-induced retroperitoneal fibrosis. (**c**) Horizontal intraoperative view into the pelvis after anterior LEER and lymph node dissection. Both pelvic ureters are splinted with catheters. The fatty tissue of the ischiorectal fossa is exposed. (**d**) Vertical intraoperative view into the pelvis of the same patient, as in *c*, demonstrating the transection sites in the lower endopelvis. The anterior halves of the levator ani muscles have been removed, exposing the fatty tissue of the ischiorectal fossae. At the lateral mesorectum, the ligamentous mesometria and mesocolpoi have been sealed and transected

prone to abscess and excessive adhesion formation, which may cause severe bowel complications. The risk is particularly high in the irradiated patient. The lining of the pelvic walls and floor with unirradiated angiogenic tissue of high immune competence as represented by the omentum majus is essential to reduce those risks. Established techniques described in surgery textbooks are illustrated with total LEER below (Fig. 10.20a–f).

The flap is sutured to the rim of the remaining parietal peritoneum, the mesorectum, and the pubic bones. Large volume flaps in obese patients are also useful to obliterate the hiatus genitalis. The connatal adhesions of the sigmoid colon are functionally restored as described in Chap. 8.

After thorough abdominopelvic lavage and the placement of Jackson-Pratt draining catheters in the deep pelvis and adjacent to the ureter anastomoses for urinary diversion, the laparotomy wound is closed with a running Smead-Jones suture of the musculofascial layer, which should be supported by epi- and hypogastric abdominal layer mattress sutures for abdominal tension release. The skin is then stapled or adapted by an intracutaneous suture.

Step 20. Inguinal lymph node dissection: if the sinus vagina and the vulva or any additional urogenital sinus and perineal tissues are infiltrated by the malignant tumor, inguinal lymph node dissection may be indicated for regional tumor control. The treatment-related risk of

severe lymphedema formation has to be considered for the decision according to the principles of defense line-directed lymph node dissection (see Chaps. 5 and 6). The surgical techniques to be applied are described in Chap. 11.

Step 21. Perineal plasty: the goal of the perineal plasty is the safe obliteration of the hiatus genitalis and the creation of a vaginal mold in those patients whose vulva could be preserved. In patients who need the inclusion of the ontogenetic vulva or even genitocrural tissues into the anterior LEER, perineal plasty aims to anatomically reconstruct the vulva as well.

The patient is again brought into the lithotomy position. For vaginal mold construction, a unilateral paralabial island flap is elevated from the genitocrural region (see Chap. 12). Anatomical vulva reconstruction demands additional surgical techniques, which are also described in Chap. 12.

10.4 Total LEER: Step-by-Step Procedure Demonstrated Post-mortem

Step 1. Laparotomy—peritoneal access.

Step 2. Retroperitoneal access.

Step 3. Subperitoneal access.

Step 4. External iliac lymph node dissection—bilateral.

Step 5. Paravisceral lymph node dissection—bilateral.

Step 6. Transection of the distal pelvic ureters.

Step 7. Resection of the internal iliac vessel system—bilateral.

These steps correspond to the anterior LEER procedure as described above.

Step 8. Rectosigmoid transection and posterior pelvic dissection (Fig. 10.17): after transection of the proximal superior mesenteric plexus (Fig. 10.17a), the sigmoid mesentery is divided at the rectosigmoid transition, and the superior rectal vessels are sealed and transected (Fig. 10.17b). Division of the bowel is accomplished with a GIA cutting and stapling device (Fig. 10.17c). Contrary to the total mesorectal excision (TME), the pelvic autonomous nerves are integrated into the resection with total LEER. The superior hypogastric plexus and the hypogastric nerves are dissected from the presacral fascia down to the coccyx with ventral traction of the rectum (Fig. 10.17d). Any venous presacrococcygeal connections are sealed and cut. The dorsolateral dissection proceeds lateral to the inferior hypogastric plexus toward the coccygeus muscles. The nervi splanchnici pelvici are transected, allowing complete mobilization of the rectum, together with the mesorectum-pararectal fascia-plexus hypogastrici inferiores complex ventrally (Fig. 10.17e). The following pictures illustrate surgical steps of a total LEER performed in a corpse fixed with the Thiel method.

Step 9. Bladder mobilization.

Step 10. Muscular transection—bilateral (Fig. 10.18): these steps correspond to steps 9 and 10 as described for anterior LEER (Figs. 10.13 and 10.18a–c). However, the posterior transection of the levator ani muscles proceeds to a level behind the rectum (Fig. 10.18d).

Step 11. Perineal incision, dissection, and transection (Fig. 10.19): the anterior perineal skin incision and the resection of the deep tissues related to the vulva in different extensions, depending on the caudal invasion front of the tumor, are carried out as outlined for anterior LEER.

For total LEER, the posterior perineal skin incision has to circumcise the anus, which has been closed beforehand with a purse string suture (Fig. 10.19a–c). The bilateral levator ani muscles are dissected from the fatty tissue of the ischioanal/rectal fossa until reaching the abdominal surgical level (Fig. 10.19d). Dorsally, the anococcygeal ligament is sealed and transected (Fig. 10.19e). When the abdominal surgical field is approached at the level of the coccygeal tip, the transection is continued ventralward as described with anterior LEER. The total LEER specimen can then be delivered through the perineal defect (Fig. 10.19f–h).

Step 12. Common iliac lymph node dissection—bilateral.

Step 13. Presacrococcygeal lymph node dissection—bilateral.

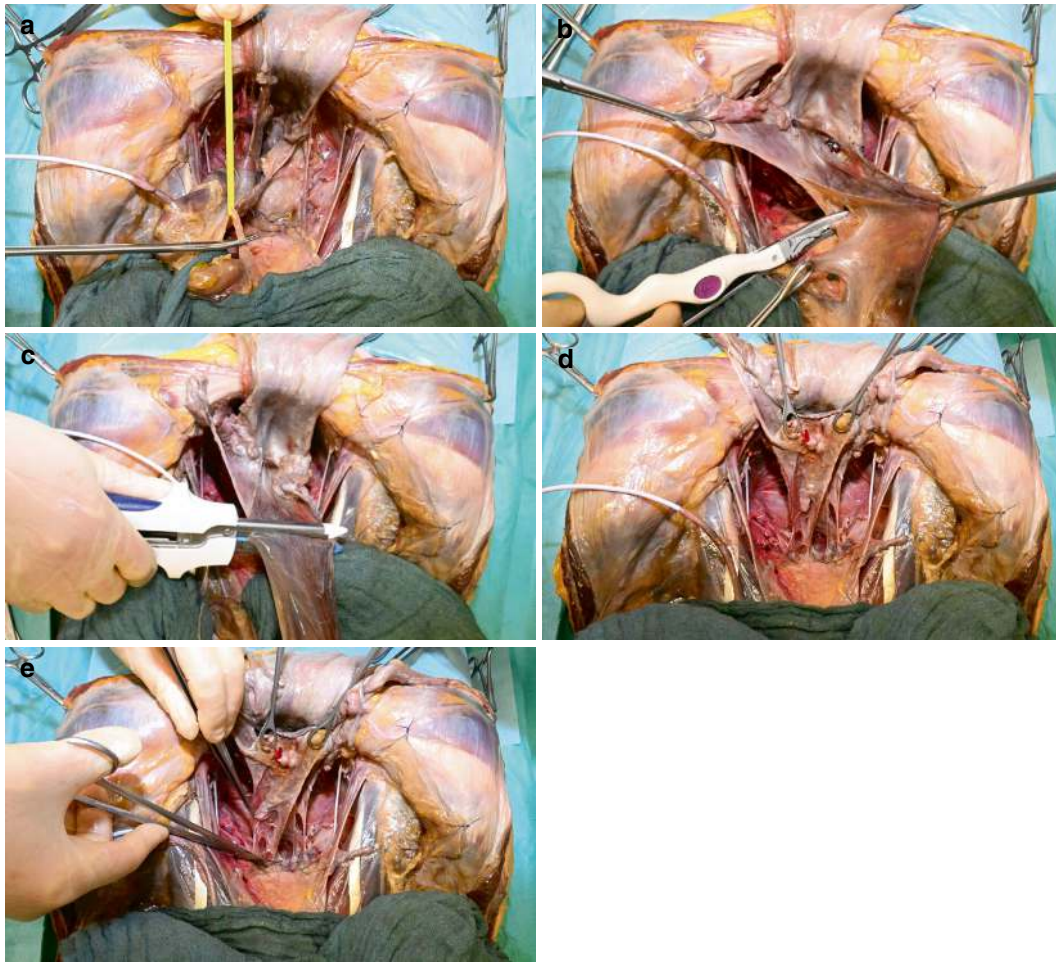

Fig. 10.17 Rectosigmoid transection and posterior pelvic dissection. (**a**) Transection of the proximal superior hypogastric plexus. (**b**) Sealing and transection of the sigmoid mesentery with the inferior mesenteric artery at the rectosigmoid transition. (**c**) Sterile division of the bowel at the rectosigmoid transition with a GIA device. (**d**) Dorsolateral dissection at the sacral fascia, exposing the pelvic splanchnic nerves. (**e**) Transection of the pelvic splanchnic nerves and further ventral mobilization of the hypogastric plexus-pararectal fascia-mesorectum-rectum complex toward the origin of the levator ani muscles

Step 14. Aortic bifurcation lymph node dissection.

Step 15. Infrarenal lymph node dissection.

Steps 12–15 correspond to TMMR/EMMR as specified in Chap. 8.

Figure 10.20 demonstrates the denuded pelvis after the completion of the resective part of a total LEER.

Step 16. Urinary diversion: it corresponds to anterior LEER.

Step 17. End colostomy: depending on the technique used for urinary diversion and on the distance of the colon end to the abdominal surface, it has to be decided whether the inferior mesenteric artery should be sealed and severed to further mobilize the sigmoid colon for colostomy construction. The potential bowel exit sites overlying the rectus muscle in the epi- and hypogastrium have been marked preoperatively on the patient's skin in the sitting position. Commonly,

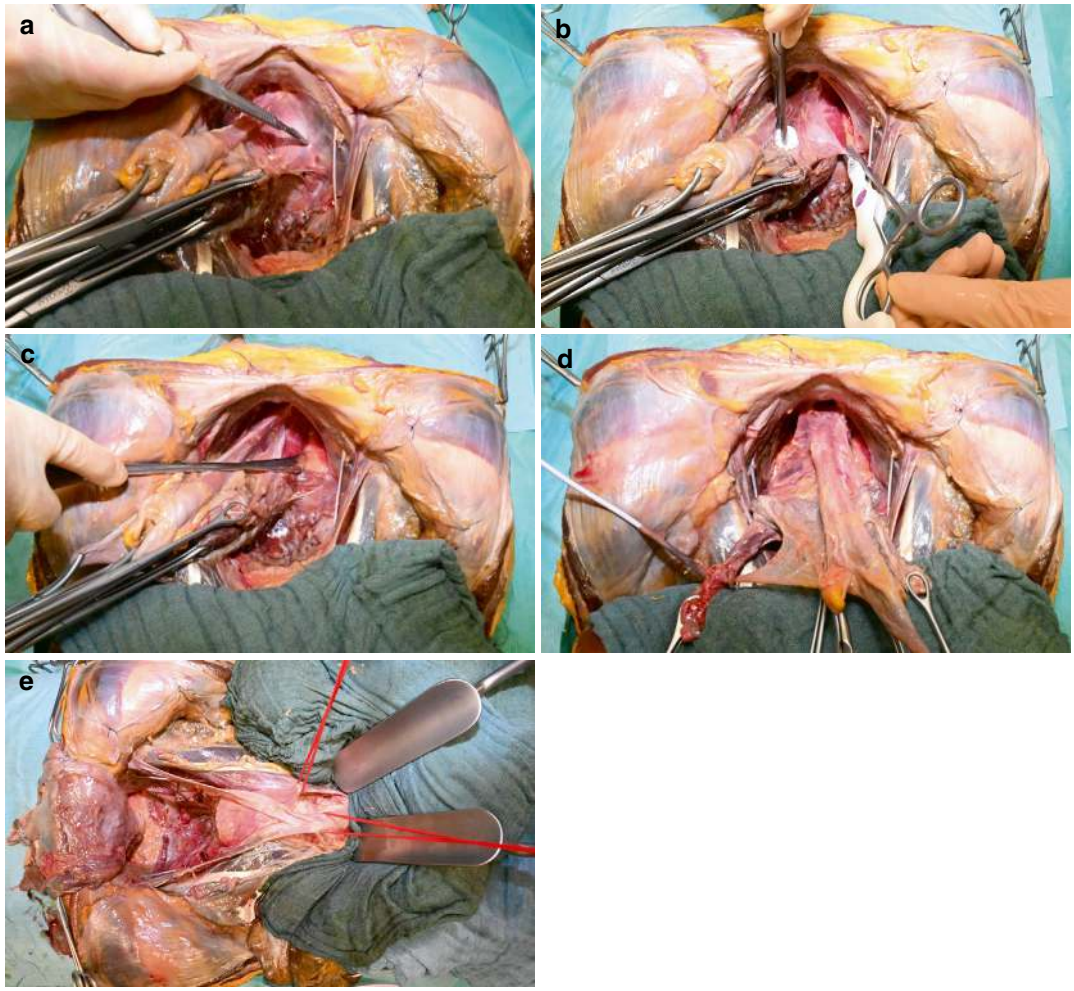

Fig. 10.18 Muscular transection. (**a**) Incision of the obturator fascia/endopelvic fascia. (**b**) Transection of the levator ani muscle at its insertion. (**c**) Medial dissection of the levator ani muscle at the ischiorectal fatty tissue by use of a periosteal dissector. (**d**) Posterior view into the pelvis after the completion of the abdominal part of total LEER

the urinary exit is on the right and the feces exit on the left side.

At the site selected for the colostomy, a circular disc of skin is excised, followed by the removal of the subcutaneous fatty tissue in projection of the skin disc. The rectus sheet is exposed, and a cruciate incision of about 4 cm is made. The muscle is split parallel to its fibers, and the underlying parietal peritoneum is incised. The peritoneum is sutured to the four triangles of the rectus sheet opening that have resulted from the cruciate incision with the sutures and needles left in place. The end of the colon is then delivered through the stab wound in the abdominal wall as far as to ensure a nonkinking tension-free intraabdominal terminal bowel when the laparotomy wound is closed. At this position, the bowel is fixed with four fascioperitoneal sutures in the seromuscular layer. For details of the surgical techniques, see corresponding textbooks.

Step 18. Endopelvic angiogenic carpet with an omentum majus flap and laparotomy closure (Fig. 10.21): the greater omentum is detached from the transverse colon (Fig. 10.21a, b). If this

bowel part was used for urinary diversion, this has been accomplished in part already. The omentum majus flap may be pedicled with the right, left, or bilateral gastroepiploic vessels as the source. Depending on the optimal design in the individual patient, the corresponding vascular connections to the greater curvature of the stomach are sealed and cut (Fig. 10.21c).

Guided along the paracolic gutter(s), the distal mono- or bipedicled flap is spread to cover the endopelvic surface and fixed to the remnants of the parietal peritoneum laterally, to the posterior symphysis and pubic bones anteriorly, and to the promontory dorsally (Fig. 10.21d–f).

The left (part of the) omentum majus flap is guided within the paracolic gutter lateral to the terminal intraabdominal colostomy. The part of the omentum flap passing the bowel is adapted to the bowel serosa and parietal peritoneum in order to obliterate the hiatus between the bowel and abdominal wall.

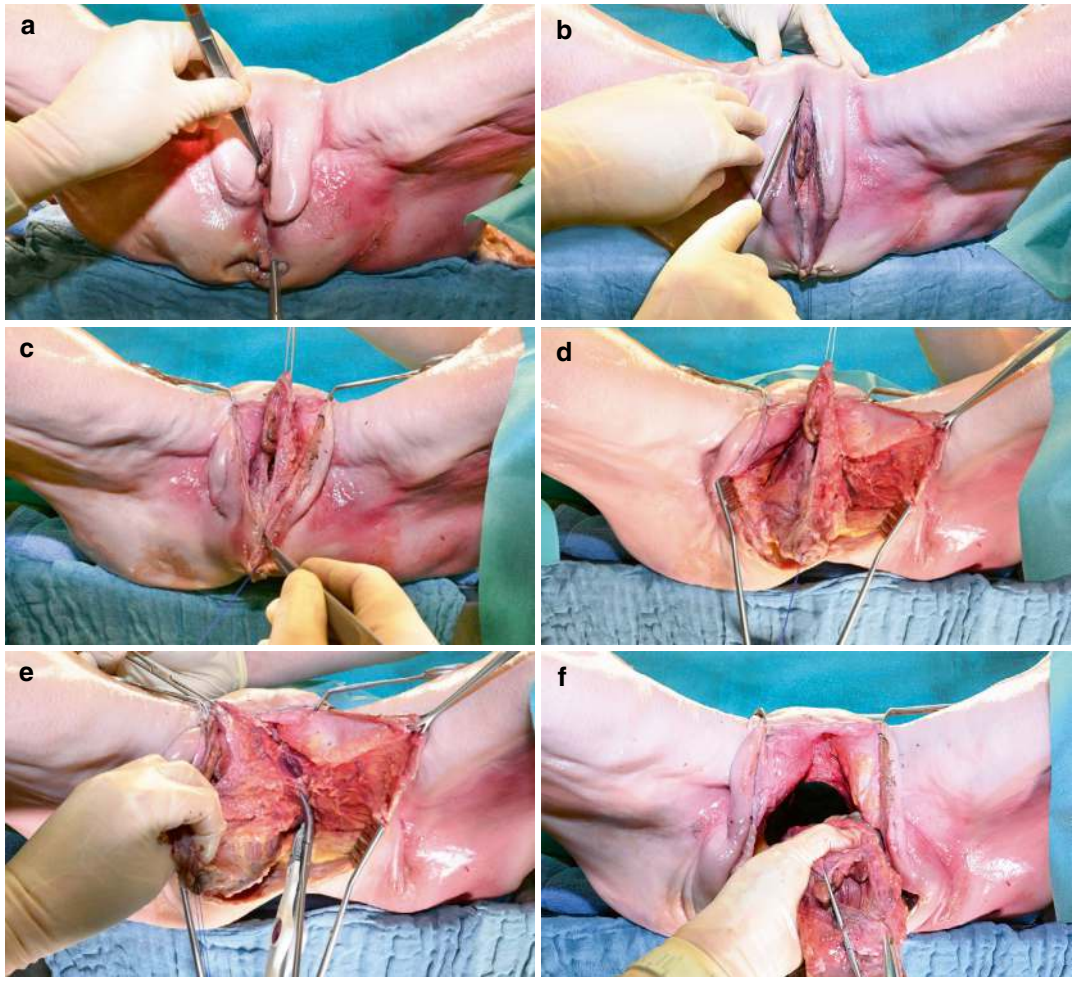

Fig. 10.19 Perineal incision, dissection, and transection. (**a**) The anal orifice is closed by a purse-string suture. (**b**) Perineal incision, including the vulva compartment. (**c**) The anal sphincter is circumcised. (**d**) The levator ani muscles have been circumferentially dissected from the ischiorectal fatty tissue. (**e**) The anococcygeal ligament has been completely transected, uniting the abdominal and perineal surgical fields. (**f**) The total LEER specimen is removed transperineally. (**g**) Total LEER specimen. (**h**, **i**) Perineal soft tissue and pelvic floor defect after total LEER

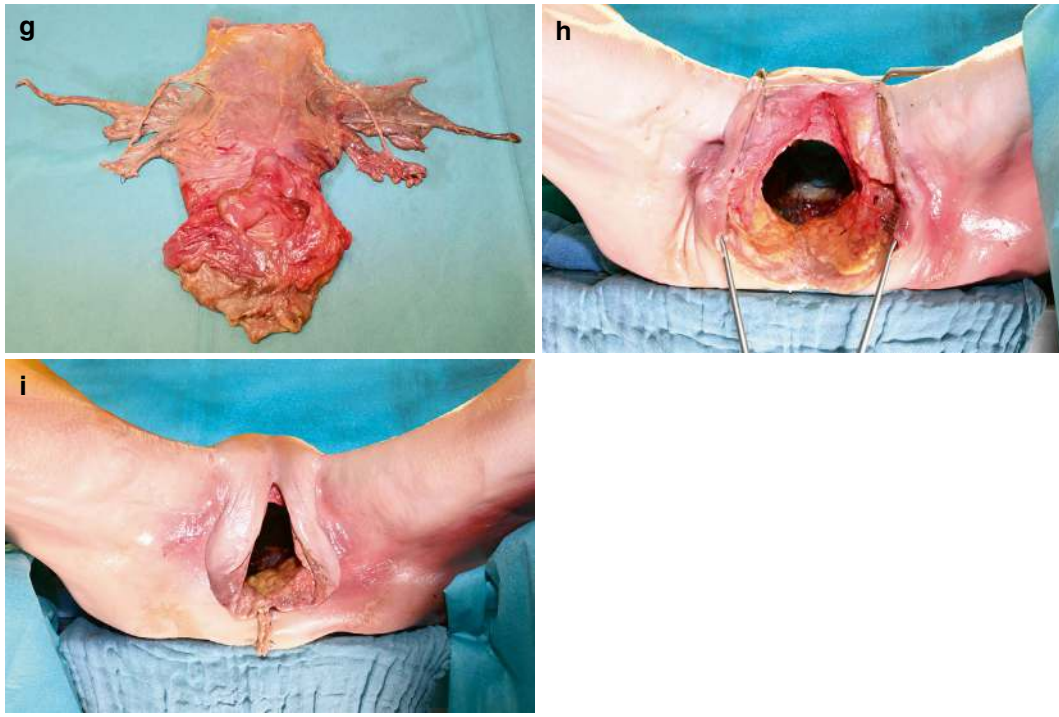

Fig. 10.19 (continued)

Fig. 10.20 Intraoperative view into the pelvis after total LEER and first-, second-, and third-line (with respect to the Müllerian compartment) lymph node dissection in a patient. Both proximal sciatic nerves are exposed below the obturator nerves. The internal iliac vessel systems have been transected below the superior gluteal arteries, which have been preserved. The levator ani muscles have been completely integrated into the surgical specimen, exposing the ischiorectal fatty tissue

After the closure of the laparotomy wound as described, the exteriorized colon is transected at the level of the skin surface and fixed with mucocutaneous sutures.

Step 19. Inguinal lymph node dissection: this potential step corresponds to the anterior LEER procedure as well.

Step 20. Perineal plasty (Fig. 10.22): the perineal defect after total LEER is not only superficially larger than that after anterior LEER but is also functionally different since the caudal support of the abdominal contents is lost. Although the external and internal soft tissue defect could be covered by composite flaps, such as the gluteal thigh or the gracilis musculocutaneous flap, wound dehiscence would pose a significant risk for perineal bowel prolapse. Therefore, a two-layer perineal reconstruction by inner muscle and outer skin flaps is recommended. The pelvic floor is substituted by a gracilis muscle flap, and the perineal skin defect is

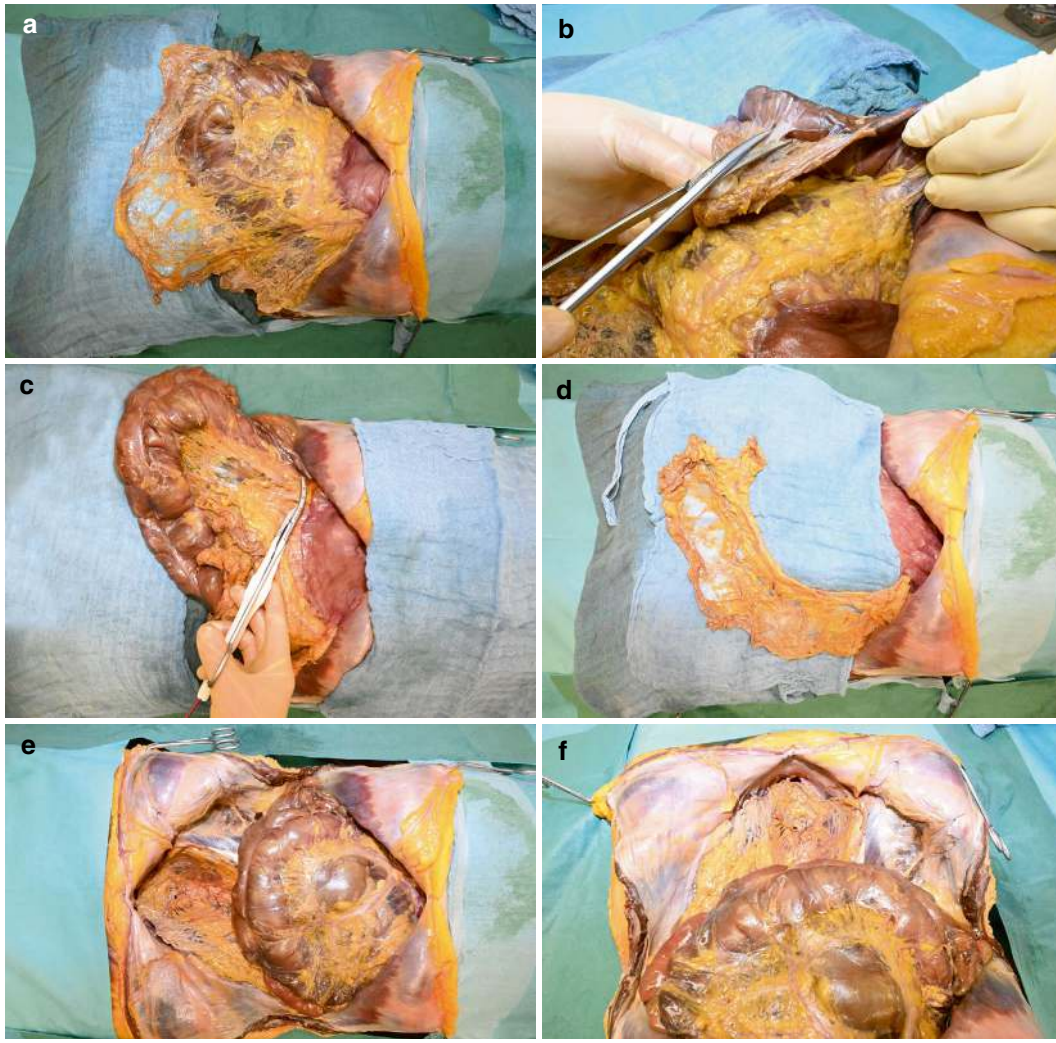

Fig. 10.21 Pelvic omental carpet. (**a**) Complete omentum majus spread out. (**b**) Dissection of the omentum majus from the transverse colon. (**c**) The right gastroepiploic vessels and their gastric branches are sealed and transected. (**d**) Omentum majus flap pedicled on the left gastroepiploic vessels spread out. (**e**, **f**) Fixed omentum majus flap completely covering the endopelvic surface

closed primarily or with two V-Y gluteal fold advancement flaps.

To elevate a gracilis muscle flap, a straight line is drawn on the stretched leg of the patient from the pubic tubercle to the ipsilateral medial femoral epicondyle (Fig. 10.22a), indicating the ventral border of the gracilis muscle.

The site of entry of the major vascular pedicle, i.e., the medial femoral circumflex vessels, is marked at that line 8–10 cm distal to the pubic tubercle. The skin incision directed toward the middle of the genitocrural fold starts at the distal medial thigh and runs for about 5 cm (Fig. 10.22b).

The subcutaneous tissue is mobilized to expose the fascia lata. The fascial incision uncovers the sartorius muscle (Fig. 10.22c). Upon upward displacement of the longitudinal sartorius muscle fibers, the round tendon of the gracilis muscle can be palpated and grasped (Fig. 10.22d). The gracilis muscle is then elevated for about 10 cm, from distal to proximal, through the successive widening of the skin, subcutaneous

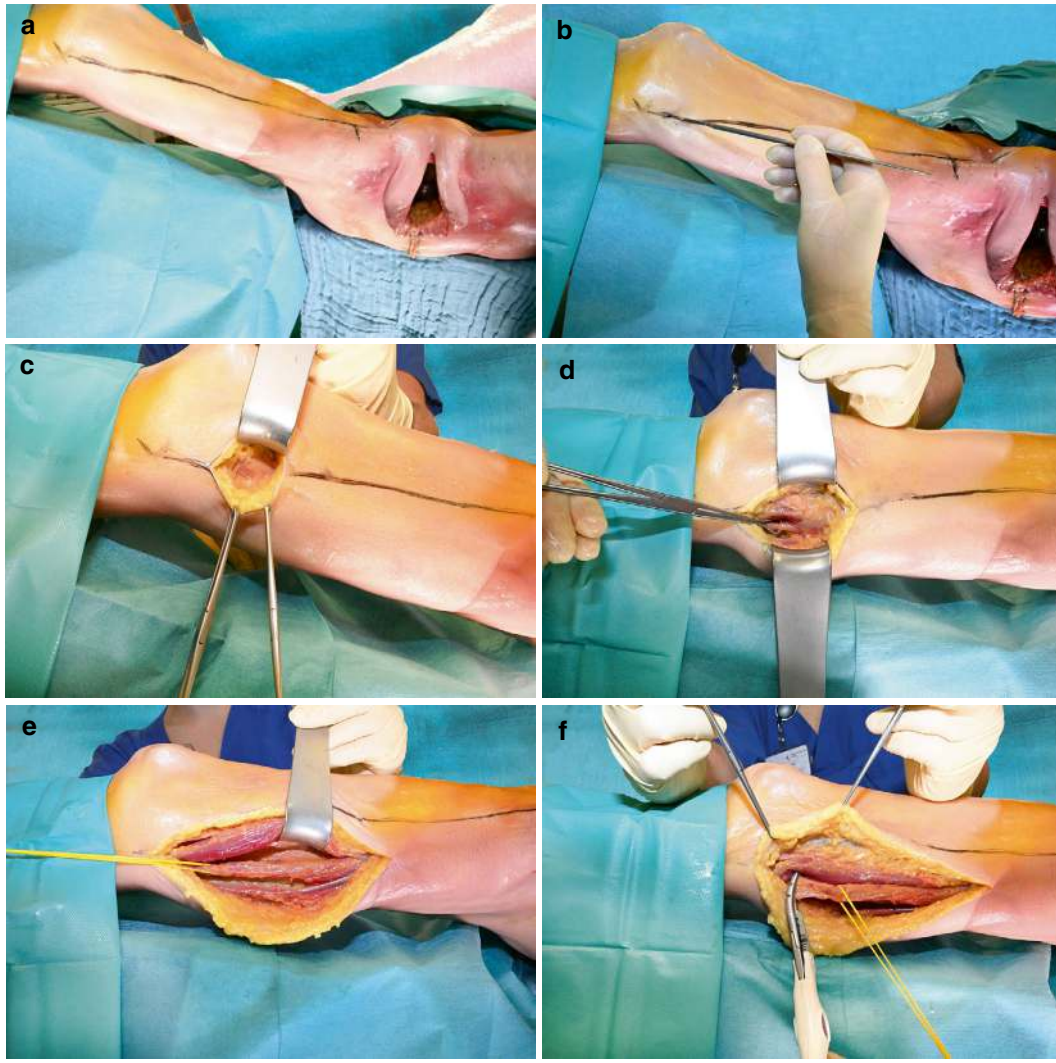

Fig. 10.22 Reconstruction of the pelvic floor by a spiralized gracilis muscle flap. (**a**) A straight marker line connecting the pubic tubercle with the medial femoral epicondyle has been drawn. The expected site of the appearance of the medial femoral circumflex vessels is indicated as well. (**b**) Initial skin incision at the distal medial thigh just proximal to the medial femoral epicondyle. (**c**) Deepening of the initial incision through the subcutaneous fatty tissue to expose the fascia lata and underlying sartorius muscle. (**d**) After incision of the fascia lata and ventral mobilization of the sartorius muscle, the round tendon of the gracilis muscle can be identified by palpation and grasped with a clamp. (**e**) Proximal extension of the incision of the skin, subcutaneous fatty tissue, and fascia lata in the gracilis muscle's midline axis to further expose the muscle that is still connected to its insertion at the medial proximal tibia. (**f**) Transection of the gracilis tendon. (**g**) Fixation of the tendon stump to the adjacent Sartorius muscle. (**h**) Further proximal exposition and mobilization of the gracilis muscle toward its origin, with particular attention to the site of its major vascularization by the medial circumflex femoral vessels. In the living, the complete skin incision, as shown in the post mortem demonstration, should be reduced to two shorter incisions: a distal one from the level of the medial epicondyle of the femur to the transition of the distal to the medial third of the thigh and a proximal one from the genitocrural fold to the transition of the proximal to the medial third of the thigh. (**i**) A subcutaneous tunnel is made below the ipsilateral genitocrural fold and labium majus. (**j**) The gracilis muscle flap is rotated counterclockwise through the genitocrural/labium majus tunnel into the perineal defect. (**k**) Spiralized flap fixed to the inferior margin of the symphysis and fibrofatty ischiorectal tissue. (**l**) Skin closure of the donor site and perineal defect

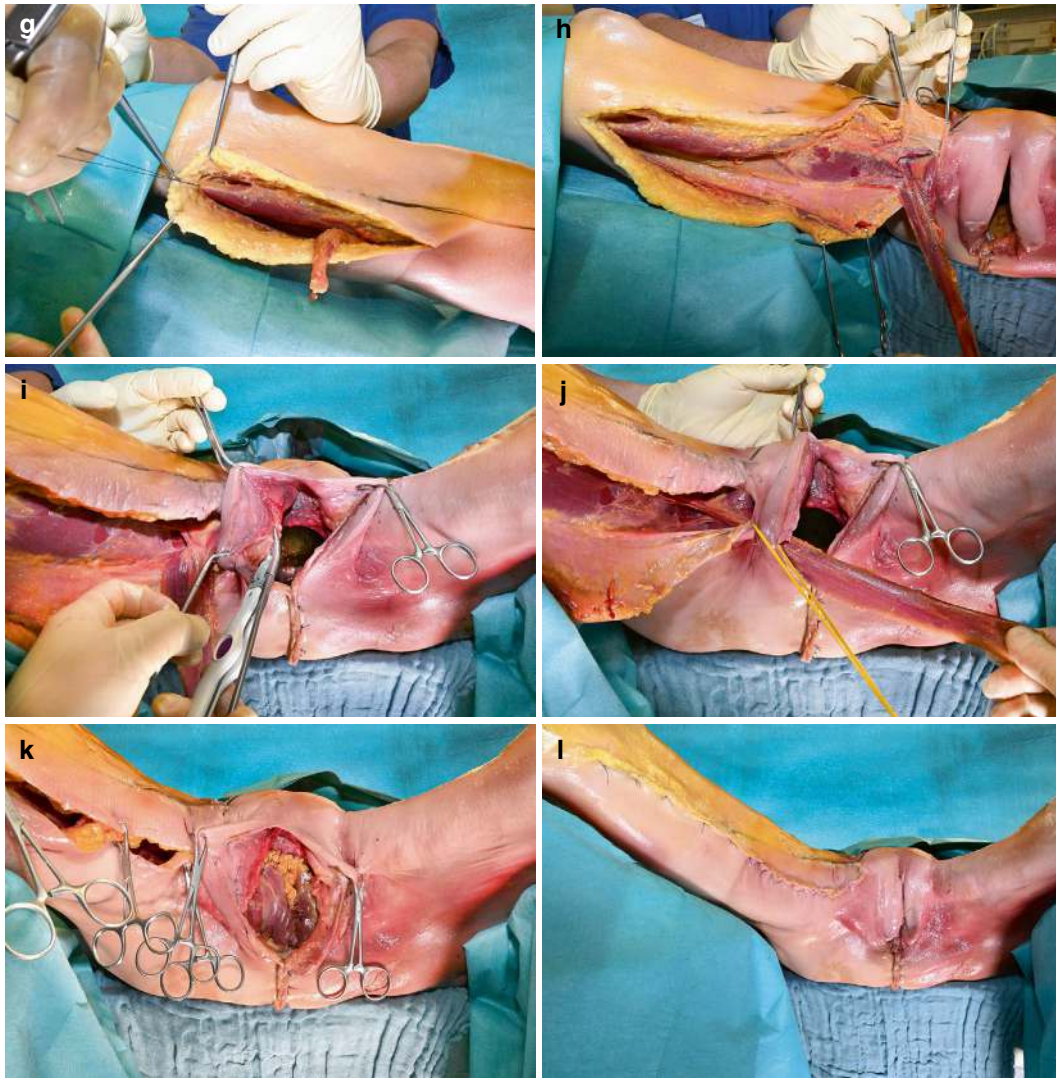

Fig. 10.22 (continued)

fat, and fascial incisions in the projection of the midline of the flat muscle mass (Fig. 10.22e). Only minor vessels approaching the deep surface of the muscle from above have to be sealed and cut. A second incision through the skin, subcutaneous fat, and fascia is made proximally along the projected midline of the gracilis muscle, starting about 5 cm distal to the genitocrural fold and passing the indicated site of the vascular pedicle to expose the proximal gracilis muscle and the anteriorly adjacent adductor longus muscle. Distally, the gracilis tendon is transected, and the tendon stump is sutured to the sartorius muscle (Fig. 10.22f, g). The gracilis muscle flap can then be mobilized through the medial thigh tunnel between the distal and proximal skin incisions, exteriorized, and further elevated up to the entry point of the medial femoral circumflex vessels at the border between the adductor longus muscle and the anterior deep surface of the gracilis muscle, which represents the center of the arc of rotation of the flap (Fig. 10.22h). A second

subcutaneous tunnel is made in the genitocrural region and below the labium majus entering the perineal defect of the total LEER (Fig. 10.22i). The gracilis muscle flap is rotated counterclockwise through the genitocrural tunnel into the perineal defect (Fig. 10.22j). It is spiralized from distal to proximal to create a muscular plate, which is fixed to the inferior symphysis and to fibrous structures of the ischiorectal fossa (Fig. 10.22k) to abut to the caudal position of the omentum majus flap. After the placement of a suction drain, the proximal and distal incisions of the donor site are closed with interrupted skin sutures (Fig. 10.22l).

Depending on the extent of the skin and subcutaneous tissue defect, the perineal wound can be closed primarily or restored with bilateral V-Y advancement flaps from the medial thigh or gluteal fold.

10.5 Postoperative Management

Postoperatively, patients are monitored at the intensive care unit due to the complexity and length of the surgery. Most LEER patients can be transferred to the intermediate care unit or to the regular ward after 24 hours, equipped with a gastrointestinal tube. Many aspects of postoperative management correspond to that of TMMR/EMMR patients (see Chap. 8). The gastrointestinal tube is positioned above the patient's level on the third postoperative day and removed before oral nutrition is started if the intestinal passage appears not to be disturbed. Special postoperative care is necessary for the urinary diversion. The fluid drained from the abdomen/pelvis is checked daily for creatinine. Urinary flow through the ureteral splints is monitored as well. Sonography of the kidneys is done regularly to rule out hydronephrosis. If a colon flap has been applied for urinary diversion, lavage for extensive mucus production has to be done. If a urinary splint is nonproductive, retrograde injection of a few milliliters of saline should remove plugs. The ureteral splints are withdrawn stepwise after about 3 weeks; only when the first has been successfully removed is the maneuver administered to the second one. Colostomy function is monitored awaiting feces discharge by the second postoperative week.

About 3–4 weeks after surgery, the patient is trained to handle the colostomy and the urinary stoma in the uneventful postoperative course.

The drain from the donor site of the gracilis muscle flap is withdrawn when its daily production is less than 50 mL. All skin sutures are removed stepwise in the second postoperative week.

10.6 Management of Complications

Tribute to the extended operation, particularly when performed in the irradiated patient, is a high probability of postoperative complications, mainly due to infections or ischemic pathomechanisms. Most of these complications demand reoperation in the early postoperative course.

10.6.1 Laparotomy Healing

Infection and dehiscence of the laparotomy wound is the most frequent complication in LEER patients. Its management is described in Chap. 8.

10.6.2 Perineal Wound Healing

Flap dehiscence due to infection or partial flap necrosis necessitates the debridement of nonviable tissue. Secondary healing is awaited with daily wound care. Secondary adaptation of clean wounds may expedite the healing process. After total LEER, vacuum wound dressing may be advantageous. Late complications appearing as perineal hernia have been observed with pudendal thigh flaps. These patients tolerated the caudal bulging and did not want surgical correction.

Pelvic abscess formation occurred—often repeatedly—in the early total LEER series when the patient's anus and distal rectal stump were

left in situ. Together with a risk of secondary rectal carcinoma, this frequent complication consolidated the indication of the abdominopelvic technique for all total LEER cases, which led to a significant reduction in pelvic abscess formation. If abscess drainage is not sufficient to solve the problem in the long run, obliteration of fixed postoperative pelvic sinuses by transposed well-vascularized tissue is advisable.

10.6.3 Urinary

Complications of the urinary diversion are frequent and severe. Ureterointestinal anastomosis insufficiency and bowel flap and ureter necrosis are early complications, while ureteral stricture, hydronephrosis, parastomal hernia, stone formation, and secondary malignancies are among the late complications. Their management is an affair of the urologist and beyond the scope of this textbook.

LEER patients need lifelong care by a urologist in the maintenance of the urinary diversion, even in the uncomplicated course.

10.6.4 Intestinal

The management of enterocolitis and early postoperative ileus is described in Chap. 8. Peritonitis, bowel perforations, anastomosis insufficiency require emergency relaparotomy, lavage, repair and eventual resection, internal or (additional) external feces diversion, and placement of large-volume abdominal drains.

Rectoperineal fistulas in anterior LEER patients have to be primarily treated with a loop colostomy. Whether the fistula can be successfully repaired thereafter is uncertain in the irradiated patient.

Early colostomy dehiscence can be managed conservatively if the exteriorized bowel is vital; otherwise, surgical revision is indicated.

Late intestinal complications of LEER are mechanical bowel obstruction (as outlined for TMMR/EMMR in Chap. 8), colostomy strictures, and parastomal hernias, which have to be treated surgically.

Vascular and neuronal complications are managed as described for TMME/EMMR in Chap. 8. Although LEER leads to major disruptions of the patients' physical integrity, most of them are able to cope well with the sequelae of the therapy when surviving the malignant disease, as evident from their self-assessment.

References

1. Höckel M. Long-term experience with (laterally) extended endopelvic resection (LEER) in relapsed pelvic malignancies. Curr Oncol Rep. 2015;17:1–6. https://doi.org/10.1007/s11912-014-0435-8.
2. Höckel M, Hentschel B, Horn L-C. Association between developmental steps in the organogenesis of the uterine cervix and locoregional progression of cervical cancer: a prospective clinicopathological analysis. Lancet Oncol. 2014;15:445–56. https://doi.org/10.1016/S1470-2045(14)70060-9.
3. Höckel M, Wolf B, Hentschel B, Horn L-C. Surgical treatment and histopathological assessment of advanced cervicovaginal carcinoma: a prospective study and retrospective analysis. Eur J Cancer. 2017;70:99–110. https://doi.org/10.1016/j.ejca.2016.10.016.

11 Vulvar Field Resection and Immunolgic Defense Line-Directed Lynph Node Dissection

Different types of vulvar field resection (VFR) and immunologic defense line-directed lymph node dissection (iLND) have been developed with the aim of obtaining local tumor control and regional tumor control in the case of lymph node metastases without adjuvant radiation. These procedures are based on the ontogenetic anatomy of the female external genitalia and their lymphatic drainage, applying the cancer field model of locoregional tumor progression as presented in Chaps. 4 and 6.

Vulvar field resections are performed as total, partial (i.e., anterior, lateral, posterior), focal, and extended versions (Fig. 11.1), depending on the oT stage of the disease and on additional diagnostic information, such as multicentricity, dysplasia, and nodal state, according to the treatment algorithms presented in Chap. 13.

Total VFR removes the complete ontogenetic vulva compartment, while partial VFRs leave parts of it in situ. The risk that the patient will develop a secondary vulvar carcinoma later in life after partial VFR is accepted, as the probability that a second carcinoma will originate in the remnants of her vulva compartment is lower than the default probability. Due to the alertness of the patients, secondary cancer is usually detected in an early stage. The resection of the sinus vagina according to the principles of cancer field surgery can be performed solely or in combination with VFR or total mesometrial resection (TMMR). Extended VFR includes adjacent tissues beyond the ontogenetic vulva. Cancer field resections remove the tumor with wide margins only within its ontogenetic stage-associated cancer field. At its borderline, R0 resection even with close margins is sufficient. As the borderlines between the ontogenetic vulvar subcompartments are often blurred, particularly in patients affected with lichen sclerosus or in older-age patients, partial VFR should always involve the adjacent vulvar subcompartments in addition to the part of the vulvar subcompartment infiltrated by the tumor.

The planning of regional treatment depends on the oT stage and clinical inguinal findings. According to the algorithm of cancer field surgery (Chap. 13), radionuclide-guided sentinel lymph node biopsy is restricted to oT1 vulvar carcinomas with clinically unsuspicious inguinal regions. Regional cancer field surgery for vulvar carcinoma and carcinoma of the sinus vagina comprises procedures of increasing extension (Fig. 11.2):

M. Höckel et al., *Cancer Field Surgery in Gynecologic Oncology*,
https://doi.org/10.1007/978-3-031-83030-3_11

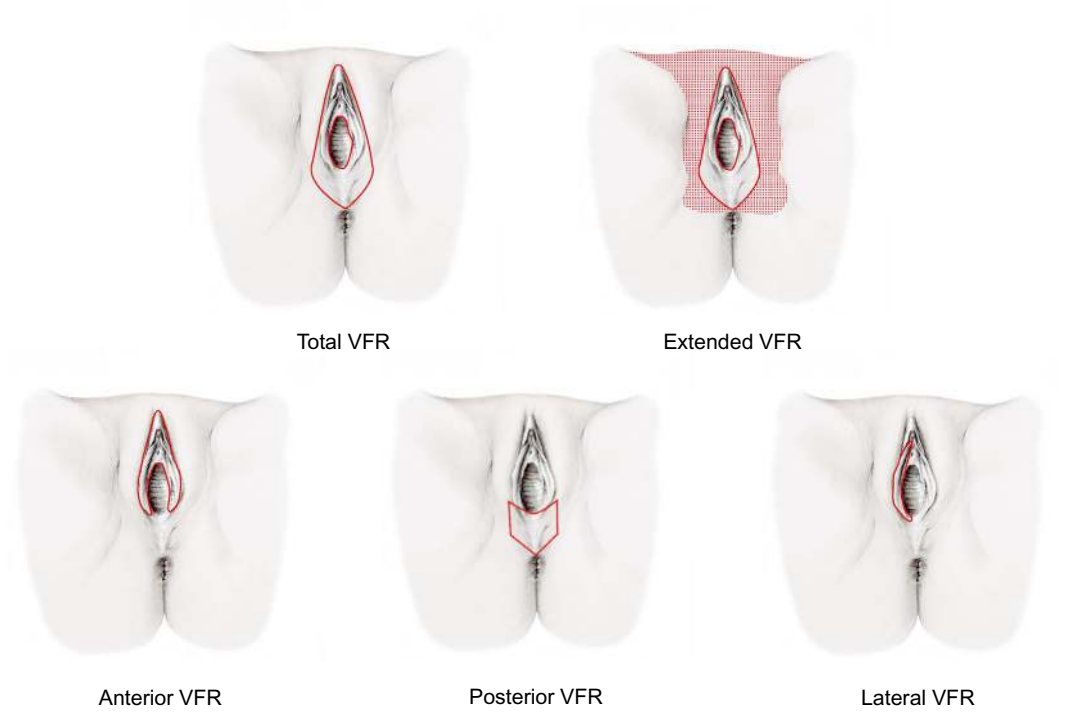

Fig. 11.1 Overview of the external incision lines of the different extensions of vulvar field resection (VFR) as indicated in the figure

- Superomedial quadrantectomy resecting only the superficial inguinal lymph nodes confined to the superomedial quadrant of the female triangle (Fig. 11.2a).
- First-line lymph node dissection removing the superomedial and inferomedial quadrants (Fig. 11.2b).
- First- and second-line lymph node dissection, including the superolateral quadrant (Fig. 11.2c).
- First-, second-, and third-line lymph node dissection clearing all superficial inguinal lymph nodes, the deep inguinal nodes, and the lacunar nodes (Fig. 11.2d, e).

Anatomical sentinel node biopsy is performed as superomedial quadrantectomy for oT1 cN0 carcinomas of the central and intermediate vulvar subcompartments and as first-line lymph node dissection for oT1 cN0 carcinomas of the peripheral vulvar subcompartment.

Otherwise, the first-, second-, and third-line nodes are resected according to the algorithm based on the results of the intraoperative frozen section investigation (see Chap. 13). Surgical reconstruction, as an essential supplement in cancer field surgery of vulvar carcinoma and of third-line lymph node dissection, is dealt with in Chap. 12.

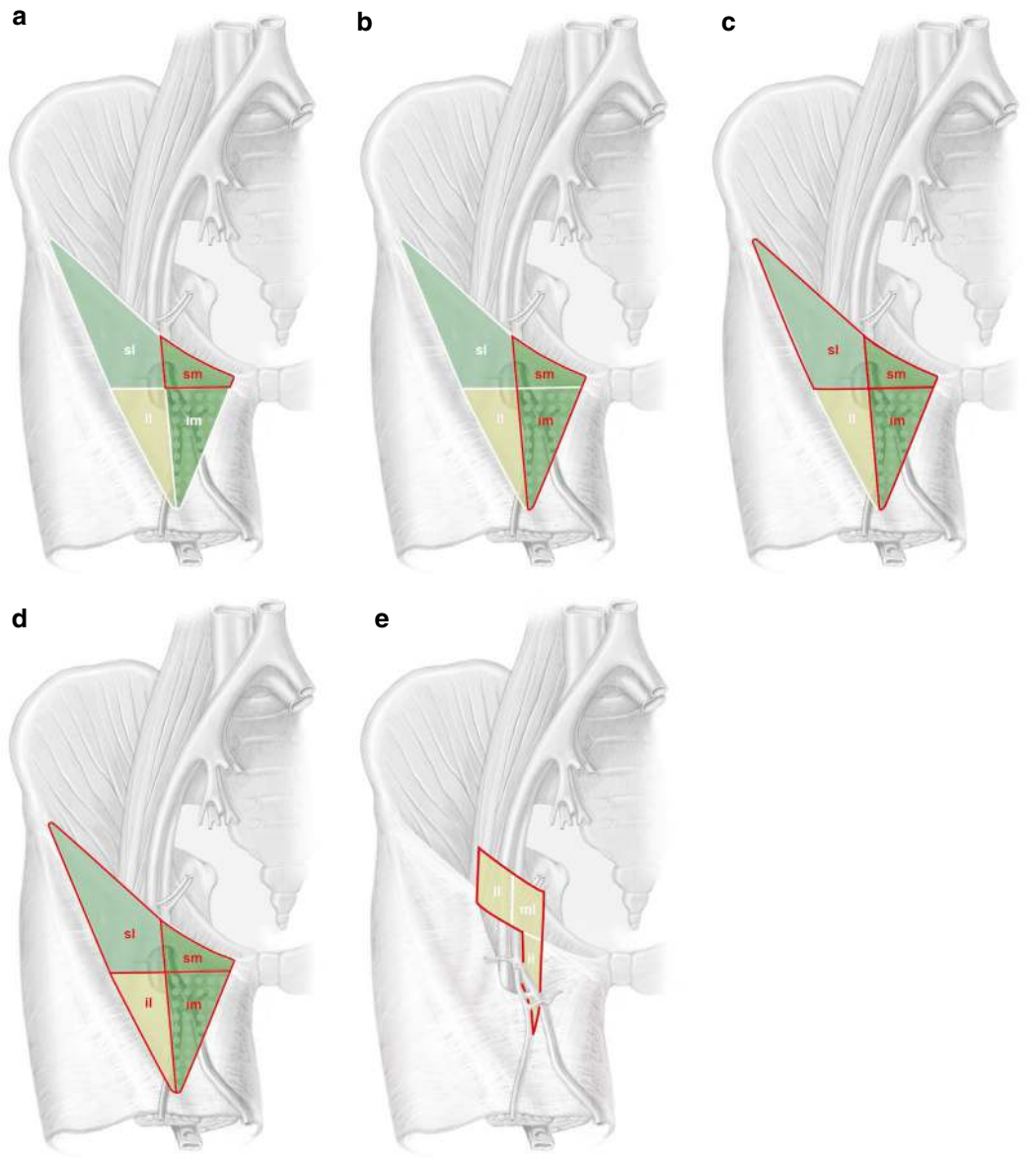

Fig. 11.2 Color-coded lymph node defense line hierarchy of the ontogenetic vulvar compartment as the basis for the lymph node dissection of vulvar carcinoma, demonstrated on the right side. First-line node regions are colored intense green, second-line light green, and third-line yellow. The red line delimits the extent of lymph node dissection. (**a**) Superomedial quadrantectomy. (**b**) First-line LND. (**c**) First- and second-line LND. (**d**) First-, second-, and third-line LND of the superficial inguinal lymph node basin. (**e**) Third-line LND of the deep inguinal and lacunar lymph node regions

11.1 Equipment

A set of surgical instruments, which we consider optimal for performing all types of VFR and iLND, is listed in Table 11.1. Monopolar and bipolar electrosurgical devices are obligatory. We also found the LigaSure™ curved jaw sealer/divider very useful. Allis clamps as well as Gillies hooks are particularly important for the precise performance of the dissection steps at ontogenetic tissue surfaces.

Table 11.1 Nondisposable surgical instruments to perform VFR and iLND

Number	Instrument
	Cutting devices
1	Scalpel handle Nr. 4
2	Scalpel handle Nr. 4 L
2	Metzenbaum dissecting scissors curved, 230 mm
1	Metzenbaum dissecting scissors curved, 200 mm
1	Wertheim dissecting scissors curved, 230 mm
1	Ligature scissors serrated, curved, 230 mm
1	Ligature scissors serrated, curved, 180 mm
1	Surgical scissors straight, 145 mm
	Retractors
2	Roux wound retractor, small
4	Roux wound retractor, medium
2	Roux wound retractor, large
2	Bayonet retractor short, 150 × 35 mm
2	Scherbak vaginal specula set with handle, weight, and three blades:
	80 × 30 mm, 85 × 35 mm, 85 × 40 mm
1	Kristeller vaginal speculum, upper blade 18 mm
1	Kristeller vaginal speculum, upper blade 26 mm
1	Kristeller vaginal speculum, upper blade 32 mm
2	Perineal retractor 120°, blade size 20 × 70 mm
2	Perineal retractor 120°, blade size 30 × 50 mm
2	Perineal retractor 120°, blade size 35 × 80 mm
1	Weitlaner retractor blunt, 200 mm
1	Weitlaner retractor blunt, 255 mm
	Forceps
2	Tissue forceps, 250 mm
2	Tissue forceps, 200 mm
2	DeBakey atraumatic dissecting forceps, 2.8 mm, 240 mm
2	DeBakey atraumatic dissecting forceps, 2.0 mm, 200 mm
2	Waugh tissue forceps, 200 mm
1	Overholt dissecting forceps, fine pattern, 220 mm
1	Overholt dissecting forceps, fine pattern, 225 mm
2	Overholt-Geissendörfer dissecting forceps, 225 mm
	Clamps
6	Backhaus towel clamp, 110 mm
8	Allis intestinal grasping forceps, 190 mm
8	Rochester-Ochsner artery forceps, straight
8	Rochester-Ochsner artery forceps, curved
4	Förster sponge forceps, 240 mm
2	Babcock grasping forceps, 220 mm
2	Babcock grasping forceps, 215 mm
6	Kocher-Ochsner artery forceps straight, 240 mm
2	Pean artery forceps straight, 240 mm
2	Bengolea artery forceps straight, 245 mm
2	Maier sponge forceps curved, 262 mm
6	Maier sponge forceps straight, 265 mm
2	Schröder uterine tenaculum forceps straight, 250 mm
	Probes, hooks, and spikes
1	Sims malleable uterine probe, 4 × 330 mm
1	Simon fistula hook, 220 mm, one tooth
1	Simon fistula hook, 220 mm, two teeth
2	Gillies hook, 180 mm
2	Redon spike, 190 mm
	Needle holders
2	Hegar needle holder, 245 mm
2	Hegar needle holder, 205 mm
2	Hegar-Mayo-Seeley needle holder
2	Wertheim needle holder, 240 mm
	Additional devices
2	Kidney tray, 250 mm
1	Laboratory bowl, 0.4 L
1	Measuring cup, 1 L
	Electrosurgical instruments (Medtronic)
2	Electrosurgical pencil
2	Cutting electrode extension, length 16.5 cm, sharp
2	Bipolar coagulation forceps, tip 2.2 mm, length 22 cm
2	Bipolar coagulation forceps, tip 2.2 mm, length 25 cm
1	LigaSure™ curved jaw open sealer/dissector

Fig. 11.3 Compilation of 120° lateral blades of different sizes and forms for manual perineal retraction (see Table 11.1)

For the radionuclide-guided sentinel biopsy, a Geiger counter with a probe covered by a sterile wrapping must be available.

For inguinal and perineal tissue exposition, Weitlauer retractor and a set of Scherbak vaginal specula with handles, weights, and blades of different sizes are recommended. We have also designed 120° lateral retractor blades of different sizes, as shown in Fig. 11.3, which proved to be efficient. A sterile pen to mark the incision lines is helpful as well. Adjustable bootleg holders are mandatory for the optimal positioning of the patient.

11.2 Patient Preparation and Positioning

Bowel preparation must ensure an empty rectum during the procedure and for some time afterward to reduce feces contamination of the surgical wound. Shaving of the pubic hair is necessary for the exact identification of the ontogenetic vulva. For inguinal and eventually lacunar lymph node dissection, the patient is kept supine with her legs bent dorsally for 10–20 degrees. The legs are lifted to the lithotomy position for the perineal procedure. During the whole operation, the knee angle should be about 100 degrees.

Ontogenetic staging and treatment algorithms for vulvar carcinoma are described in Chaps. 4, 7, and 13. Lymph node dissection is done prior to the perineal procedure to minimize contamination of the inguinal surgical fields.

11.3 iLND: Step-by-Step Procedures

Irrespective of the extent of the lymph node dissection, the inguinal landmarks to be identified by palpation are drawn on the patient's skin (Fig. 11.4). These are the femoral triangle with the inguinal ligament and the femoral vessels. The projected estuary of the greater saphenous vein into the femoral vein (hiatus saphenus) is taken as an intersection point of two perpendicular straight lines, defining the four quadrants of the superficial inguinal lymph fatty tissue: superomedial—superolateral—inferomedial—inferolateral. The skin incision line should then be designed considering these landmarks, depending on the planned extent of lymph node dissection.

Superomedial quadrantectomy and first-line lymph node dissection, removing the superomedial and inferomedial quadrants, are performed to obtain the most precise diagnostic information. It represents the complete regional treatment in the nodal-negative patient. First-, second-, and eventually third-line lymph node dissection is therapeutic for all cases with regional disease, abandoning adjuvant radiotherapy.

During preoperative history taking, it must be clarified whether the patient had any previous surgery affecting the inguinal regions, such as treatments for hernia or leg venous diseases, as these procedures lead to significant disturbance of the inguinal anatomy, which has to be known preoperatively.

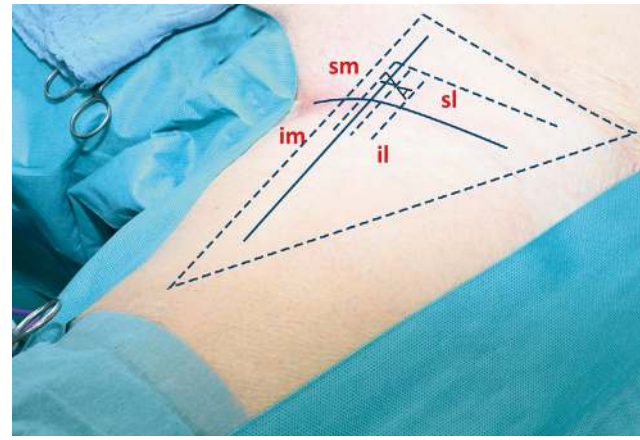

Fig. 11.4 Skin markings to plan incision for iLND in patients with vulvar carcinoma. *V* femoral vein, *A* femoral artery, *sm* superomedial, *im* inferiomedial, *sl* superolateral, *il* inferolateral

11.4 Superomedial Quadrantectomy and First-Line Lymph Node Dissection (Fig. 11.5)

Step 1: Skin Incision (Fig. 11.5a, b).

A curved incision line of about 3–4 cm in length is drawn, accessing the superomedial (Fig. 11.5a) and both supero- and inferomedial quadrants (Fig. 11.5b) as projected onto the skin. It is usually located at the medial inguinal fold or somewhat below it. The incision is advanced through the dermis and subcutaneous fat to expose Scarpa's fascia. Dissection along Scarpa's fascia with the cranial skin wound margin pulled upward proceeds to expose the medial inguinal ligament and the smooth fasciae of the pubic and Dartos fat pads. Laterally, the superficial epigastric vein is exposed and liberated from the fatty tissue. With the caudal skin wound margin kept under tension, dissection along Scarpa's fascia is accomplished for about 3 cm caudally.

Step 2: Exposition of the Saphenous Hiatus (Fig. 11.5c).

The superficial epigastric vein is followed caudally to the hiatus saphenus into the femoral vein.

Here, the estuary of the greater saphenous vein is exposed.

Step 3: Extirpation of the Superomedial Quadrant of the Femoral Triangle (Fig. 11.5d, e).

The cranial projection of the greater saphenous vein axis and a perpendicular line crossing at the hiatus saphenus define the superomedial quadrant of the superficial inguinal lymph fatty tissue. It is removed en bloc by sealing and cutting the lymph fatty tissue along the projected borders and lifted from the cribriform fascia. Care should be taken not to transect individual lymph nodes; any lymph node within the transection plane should be included in the biopsy specimen, which is sent to frozen section assessment by the pathologist.

Step 4: Extirpation of the Inferomedial Quadrant to Complete First-Line Lymph Node Dissection (Fig. 11.5f, g).

The caudal skin flap is further elevated for about 4 cm, and the saphenous vein is exposed over a length of about 6 cm. Medially, dissection should follow the bordering membrane of the Dartos fat body. The lymph fatty tissue along and medial to the exposed saphenous vein is then removed en bloc for histopathologic frozen section assessment (Fig. 11.5f). If the saphenous vein is bifurcated, its lateral branch defines the border of lymph fatty tissue transection (Fig. 11.5g).

Step 5: Inguinal Wound Closure.

After lavage and placement of a suction drainage, wound closure is done with interrupted subcutaneous-corium sutures and skin staples or with an intracutaneous suture.

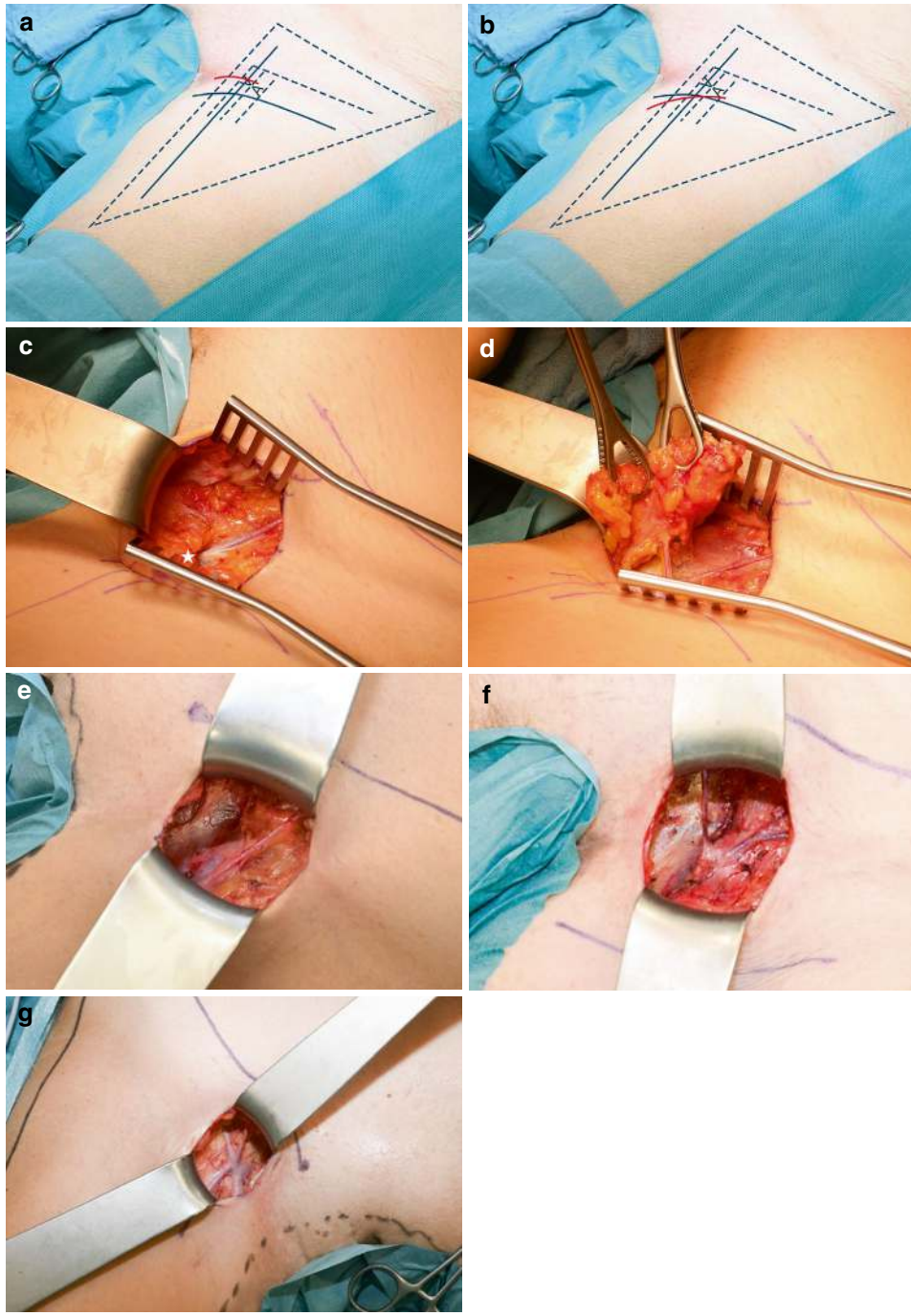

Fig. 11.5 Superomedial quadrantectomy and inguinal first-line lymph node dissection, demonstrated on the left side (**a**–**f** view from the left). (**a**) Planning of the skin incision for superomedial quadrantectomy. (**b**) Planning of the skin incision for inguinal first-line lymph node dissection. (**c**) Exposition of the superficial epigastric vein as a landmark leading to the hiatus saphenus (star). (**d**) Resection of the superomedial quadrant still connected to the hiatus saphenus by the superficial pudendal vein. (**e**) Superomedial quadrantectomy completed. (**f**) Inguinal first-line lymph node dissection completed. Both supero- and inferomedial quadrants of the femoral triangle have been removed. Superficial epigastric and circumflex iliac veins are preserved. (**g**) Right hiatus saphenus with two branches of the saphenous vein. The lateral branch defines the border of the inferomedial quadrant (view from the caudal)

11.5 First- and Second-Line Lymph Node Dissection (Fig. 11.6)

Step 1: Skin Incision (Fig. 11.6a, b).

The incision line should overlay the superomedial, superolateral, and inferomedial quadrants of the femoral triangle as marked on the skin (Fig. 11.6a). It is usually placed in the medial two thirds of the inguinal folds and is extended for a few centimeters into the inner thigh. The dermis and subcutaneous fatty tissue are incised into Scarpa's fascia, which is exposed at the complete incision line (Fig. 11.6b).

Step 2: Exposition of the Saphenous Hiatus (Fig. 11.6c).

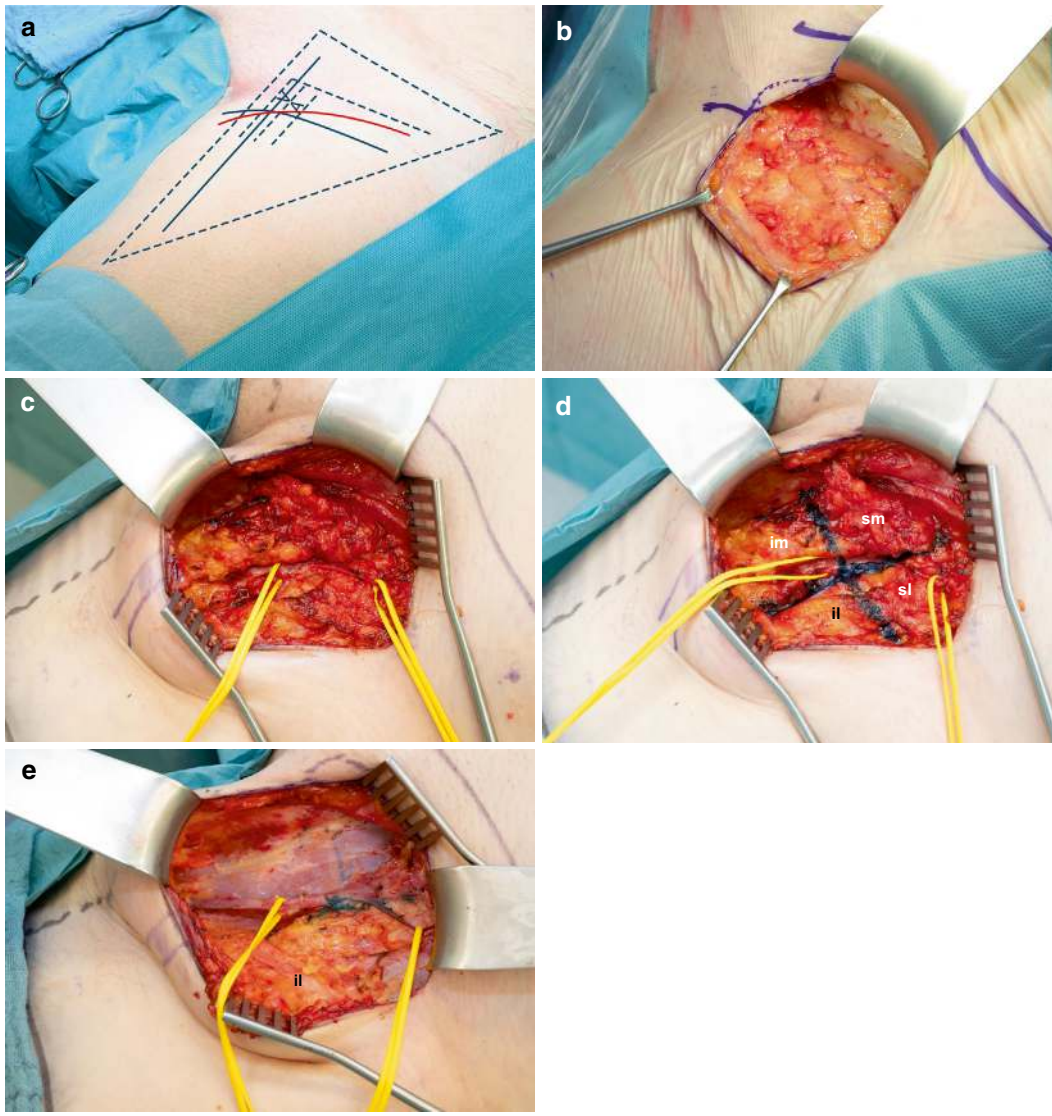

Fig. 11.6 Inguinal first- and second-line lymph node dissection demonstrated on the left side. (**a**) Planning of the skin incision. (**b**) Scarpa's fascia covering the superficial inguinal lymph nodes is exposed. (**c**) Superficial epigastric and great saphenous veins are exposed. (**d**) Two perpendicular lines intersecting at the hiatus saphenus have been marked with methylene blue, delineating the supero- (sm) and inferomedial (im) and the supero- (sl) and inferolateral (il) quadrants of the femoral triangle. (**e**) The inguinal first- and second-line lymph nodes have been completely removed, preserving the greater saphenous and superficial epigastric veins as well as the inferolateral quadrant of the superficial inguinal lymph nodes (view from the left)

This step corresponds to the first-line lymph node dissection, except for its more lateral extension.

Steps 3–5: Extirpation of the Superomedial, Superolateral, and Inferomedial Quadrants of the Femoral Triangle (Fig. 11.6d, e).

The two perpendicular straight lines defining the four quadrants of the femoral triangle can now be drawn on the inguinal lymph fatty tissue with methylene blue (Fig. 11.6d). The inferomedial, superolateral, and superomedial quadrants are completely removed against the bordering fasciae, preserving the exposed veins (Fig. 11.6e). The lymph fatty tissue is sealed and cut at the marked borderlines of the inferolateral quadrant and at the caudal border of the inferomedial quadrant. After marking the lymph fatty tissue at the medial superior cornu of the saphenous hiatus with a suture to indicate the Rosenmüller node, the specimen is handed over to the pathologist for frozen section examination.

Step 6: Inguinal Wound Closure.

This step corresponds to the first-line node dissection.

11.6 First-, Second-, and Third-Line Lymph Node Dissection (Figs. 11.7 and 11.8)

Steps 1–5 correspond to the first- and second-line lymph node dissection, except that the inferolateral quadrant is included.

Step 6: Extirpation of the Deep Inguinal Lymph Node(s).

The cribriform fascia and the fascia lata immediately medial to the femoral vein are incised for about 7 cm, and the lymph fatty tissue between this vessel and the adductor longus muscle is removed, exposing the pectineus muscle. Figure 11.7 shows the femoral triangle after complete extirpation of the superficial and deep inguinal lymph nodes.

Step 7: Retroperitoneal Access (Fig. 11.8a, b).

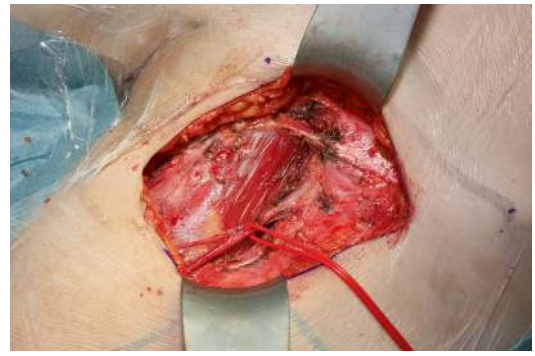

Fig. 11.7 Resection of the deep inguinal lymph node(s) in addition to the superficial inguinal nodes demonstrated at the left femoral triangle. Saphenous vein reined with an elastic loop. The fascia lata has been incised medially to the proximal femoral vein to harvest the deep inguinal lymph node(s), exposing the pectineus muscle

The inguinal ligament is incised in the direction of its fibers 1–2 cm proximal to its caudal margin. The upper fascial flap is temporarily sutured to the overlying skin margins (Fig. 11.8a). Fibers of the internal oblique and the transverse abdominal muscles are pushed apart, and the deep inferior epigastric vessels are identified and entwined with an elastic loop (Fig. 11.8b).

Step 8: Extirpation of the Lacunar Lymph Nodes (Fig. 11.8c).

The femoral artery and vein merging into the external iliac vessels are liberated from their encasing fascia sheets, respecting the inferior epigastric and deep iliac circumflex vessels. Medially to the external iliac vein, the pecten of the pubic bone is exposed. The lymph fatty tissue medial and lateral to the large vessels over a distance of about 5 cm proximal to the level of the symphysis is removed and sent to the pathologist designated as medial and lateral lacunar lymph nodes.

Step 9: Inguinal Wound Closure.

The inguinal ligament is resutured to the oblique aponeurosis. Skin closure corresponds to the first- and second-line lymph node dissection.

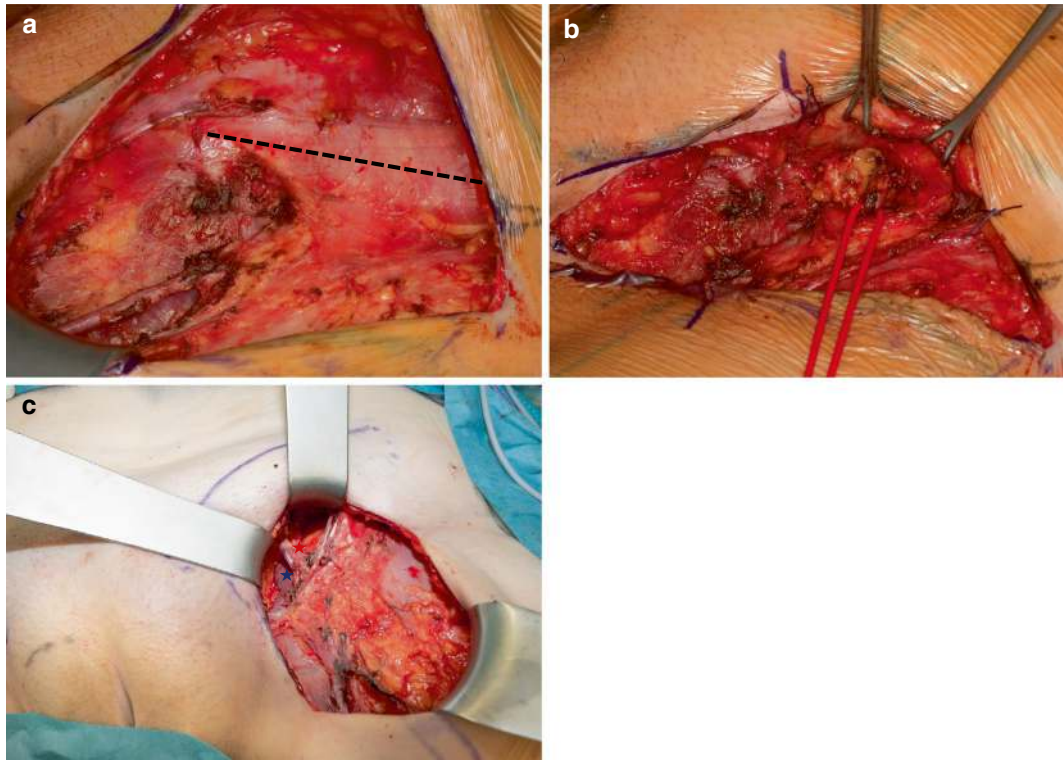

Fig. 11.8 Left lacunar lymph node dissection. (**a**) Incision line of the inguinal ligament (view from the left). (**b**) The deep epigastric vessels are exposed and reined with an elastic loop (view from the left). (**c**) The medial and lateral lacunar lymph nodes have been extirpated, exposing the distal external iliac vein (blue star) and artery (red star) (view from caudal)

11.7 Extended Inguinopubic Surgery (Fig. 11.9)

Lymph node metastases with extracapsular spread infiltrating the subcutaneous fat and dermis and those fixed to the cribriform fascia necessitate their wide excision en bloc with the underlying fascia lata and adjacent inguinal, pubic, and genitocrural soft tissues. The exposed proximal femoral vessels are protected by a medially transposed sartorius muscle flap. Large skin defects, with or without fascial defects, are best covered by a tensor fasciae latae flap (see Chap. 12).

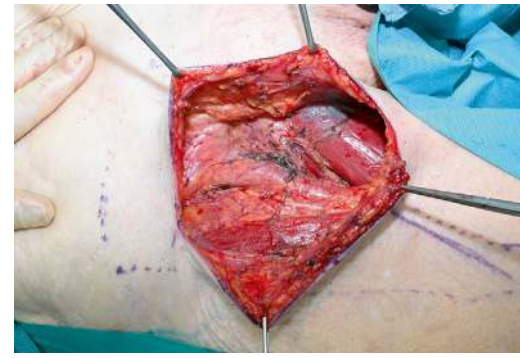

Fig. 11.9 Extended inguinal lymph node dissection demonstrated on the right side. The superficial inguinal lymph nodes with metastases exhibiting extracapsular spread have been removed en bloc with the overlying skin and the complete fascia lata of the femoral triangle (view from the right)

11.8 Total VFR: Step-by-Step (Figs. 11.10, 11.11, 11.12, 11.13, and 11.14)

Step 1: Peripheral Incision (Fig. 11.10).

With the patient in the lithotomy position, the incision line is first marked with a pen. It is located bilaterally at the crests of the labia majora, converging at the anterior commissure. Posteriorly, the incision line is widened to a level that follows the lateral border of the labia majora. At the ventral anal margin, the incision line bends medially to include the sector of the anal skin between 11 and 1 o'clock. The superficial (epidermal) incision is done with a scalpel and is subsequently deepened with a monopolar electric knife.

Fig. 11.10 Peripheral incision line for total VFR

Step 2: Lateral Dissection (Fig. 11.11).

The lateral peripheral skin incision is further deepened by dissection along the medial border of the Dartos fat bodies (Fig. 11.11a) down to Colles' fascia, covering the bulbospongiosus muscles on both sides. Veins connecting the Dartos bodies to the ontogenetic vulva are sealed and transected (Fig. 11.11b). At about 4 and 8 o'clock, the deep dissection is moved further laterally, guided by the bulbospongiosus muscles toward the superficial transverse perineal muscles, which are exposed at their insertion at the perineal body (Fig. 11.11c).

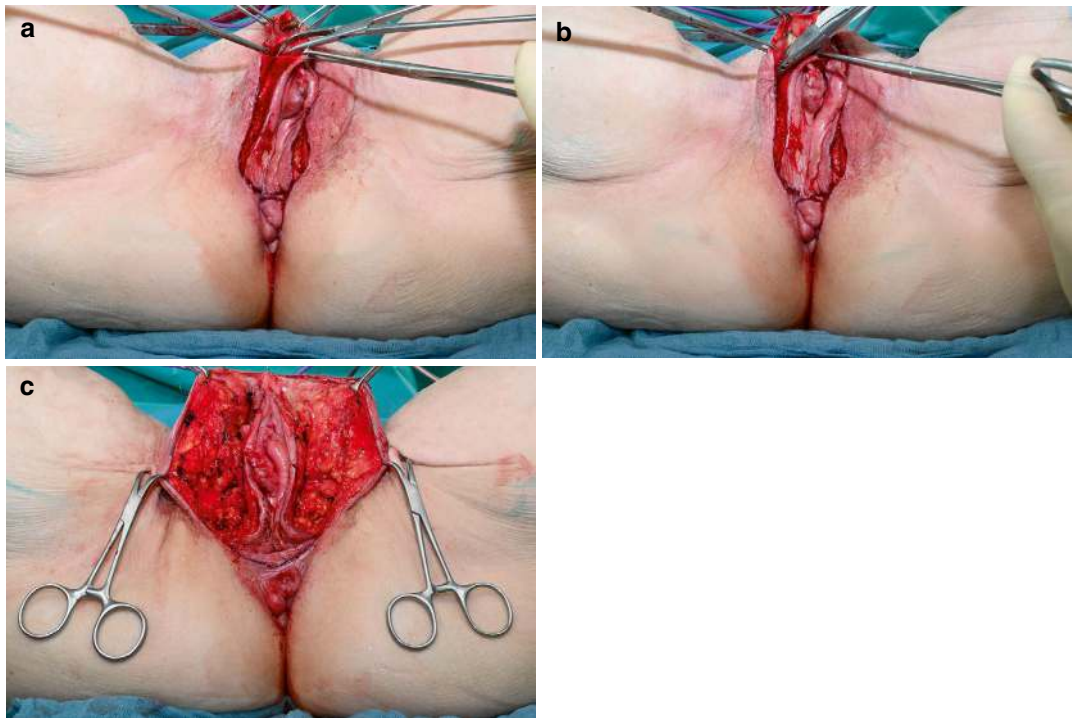

Fig. 11.11 Total VFR: lateral dissection. (**a**) Dissection from the right Dartos fat body after peripheral skin incision. (**b**) Veins connecting the Dartos fat body to the ontogenetic vulva are sealed and transected. (**c**) Lateral dissection completed

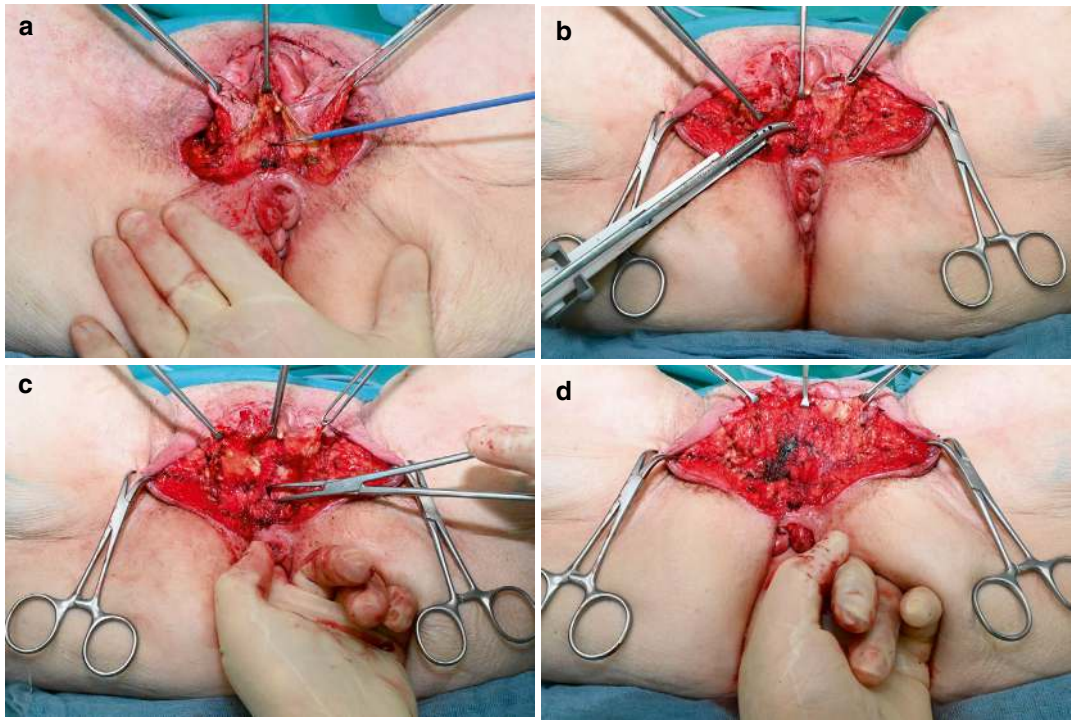

Fig. 11.12 Total VFR: posterior dissection. (**a**) The anal skin between 11 and 1 o'clock has been incised, exposing the underlying sphincter muscle. (**b**) The right origin of the bulbospongiosus muscle has been sealed and transected to widen the perineal body. (**c**) Dissection of the anovestibular and distal rectovaginal septum from the anal canal and rectum. (**d**) Posterior dissection completed

Step 3: Posterior Dissection (Fig. 11.12).

The anal skin between 11 and 1 o'clock and adjacent perineal skin are dissected from the superficial musculus sphincter ani and central perineal "tendon" (Fig. 11.12a). The origins of the bulbospongiosus muscles are incised to widen the perineal body (Fig. 11.12b). With a finger placed in the rectum pushing it downward, the anovestibular and distal rectovaginal septum are dissected from the anterior anal canal and rectal wall, starting in the midline and proceeding laterally to the medial borders of the bulbi vestibulares (Fig. 11.12c, d).

Step 4: Central Incision and Transection (Fig. 11.13).

The central incision is located in the distal (sinus) vagina immediately proximal to the hymenal remnants. It starts at 6 o'clock, pushing the rectum posteriorly with the finger still in place. A small stab incision is made in the vaginal wall with the monopolar knife from the antimucosal side (Fig. 11.13a). Transection is then advanced bilaterally by sealing and cutting toward the meatus urethrae externus immediately medial to the bulbi vestibulares, which are preserved (Fig. 11.13b). The vaginal skin is incised about 5 mm proximal to the external urethral orifice (Fig. 11.13c).

Step 5: Anterior Dissection and Transection (Fig. 11.14).

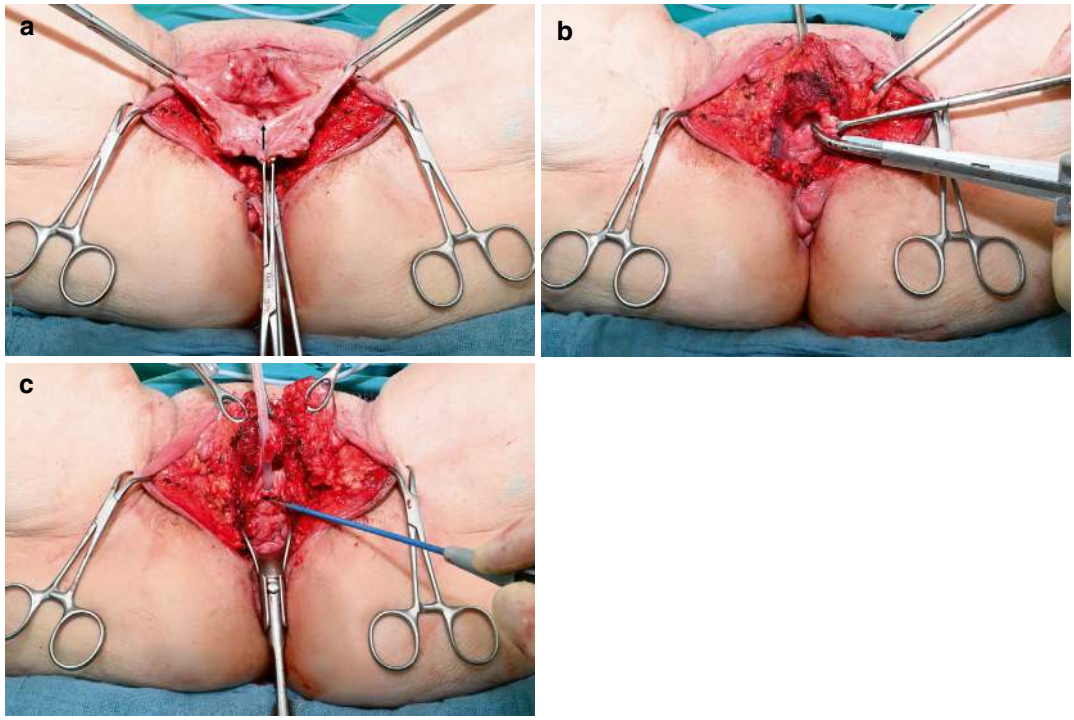

Fig. 11.13 Total VFR: central incision and transection. (**a**) A small stab wound has been placed into the 6 o'clock position of the sinus vagina just proximal to the hymen (arrow). (**b**) The transection proximal to the hymen is advanced toward the meatus urethrae, preserving the bulbi vestibulares. (**c**) Vaginal incision just proximal to the meatus urethrae

At the 12 o'clock position, the peripheral skin incision is deepened by the transection of the clitoridal ligament (Fig. 11.14a). The body of the clitoris, the insertions of the bulbospongiosus muscles, and the medial parts of the clitoridal crura are exposed by dissection. The glans clitoridis is transected to include its complete skin in the total VFR specimen (Fig. 11.14b). The suprarurethral spongiosus sling is preserved.

The anterior distal urethra is mobilized from the sling of the vestibular bulbi overlying it. Pulling the blocked Foley catheter downward the anterior hemicircumference of the distal urethra is incised (Fig. 11.14c). Upon upward traction of the Foley catheter, the posterior hemicircumference of the distal urethra is incised and transected to accomplish the total VFR (Fig. 11.14d). The VFR specimen is removed with the Foley catheter encased by the meatus urethrae externus to be intraoperatively assessed by the pathologist for resection margins (Fig. 11.14e). After surgical removal of the complete ontogenetic vulvar compartment, the labia majora and all deep erectile tissues, such as the clitoridal body and bulbi vestibulares, are preserved (Fig. 11.14e).

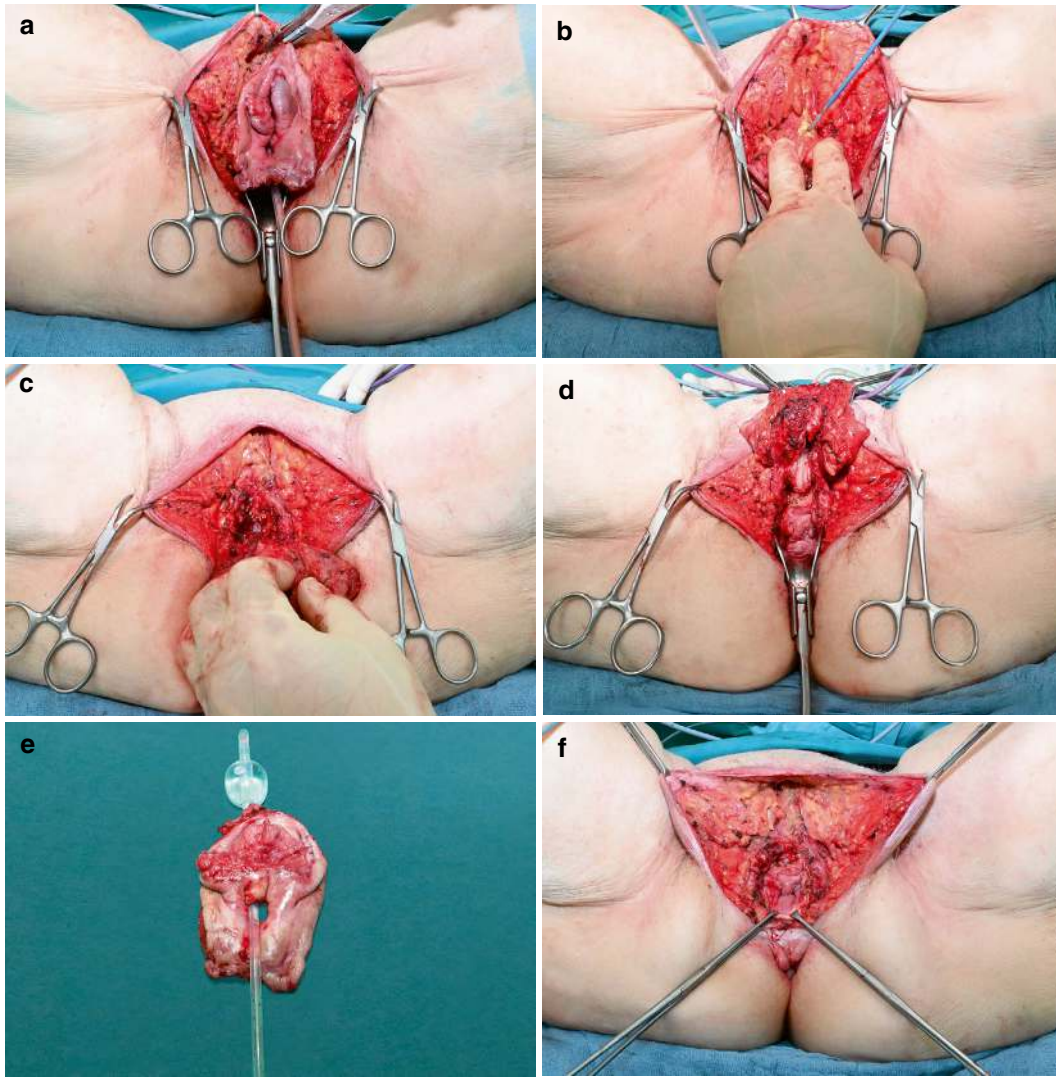

Fig. 11.14 Total VFR: anterior dissection and transection. (**a**) Sealing and transection of the clitoridal ligament. (**b**) After the exposition of the clitoridal body, it is incised distally to include the glans clitoridis in the VFR specimen. (**c**) The distal urethra is incised anteriorly just proximal to the meatus. (**d**, **e**) After completion of the urethral transection posteriorly, the total VFR specimen can be removed, together with the Foley catheter, to be assessed by the pathologist. (**f**) Total VFR completed

11.9 Anterior VFR: Step-by-Step (Figs. 11.15 and 11.16)

The procedure is described for oT1 and oT2 vulvar carcinomas involving the intermediate subcompartment. For oT1 cancers of the peripheral and the central subcompartments, parts of the corresponding central and peripheral subcompartments may be preserved, i.e., the meatus urethrae and the anterior commissure, respectively.

Step 1 (peripheral incision) and step 2 (lateral dissection) correspond to those of the total VFR, except that the peripheral skin incision and the lateral dissection are performed only from about 8 to 4 o'clock.

Fig. 11.15 Anterior VFR for oT1 vulvar carcinoma of the inferomedial subcompartment and oT2 carcinomas. Peripheral incision line between 8 and 4 o'clock

Step 3: Central Incision and Transection (Fig. 11.17).

The peripheral incision bends inward through all three subcompartments at 8 and 4 o'clock to become the central incision on both sides proximal to the hymenal remnants (Fig. 11.17a). The bulbi vestibulares are under visual control during that maneuver and should not be severed (Fig. 11.17b). The central incision converges anteriorly at a few millimeters proximal to the urethral meatus (Fig. 11.17c), which is included in the anterior VFR specimen (Fig. 11.17d, e).

Step 4: Anterior Dissection and Transection (Fig. 11.18).

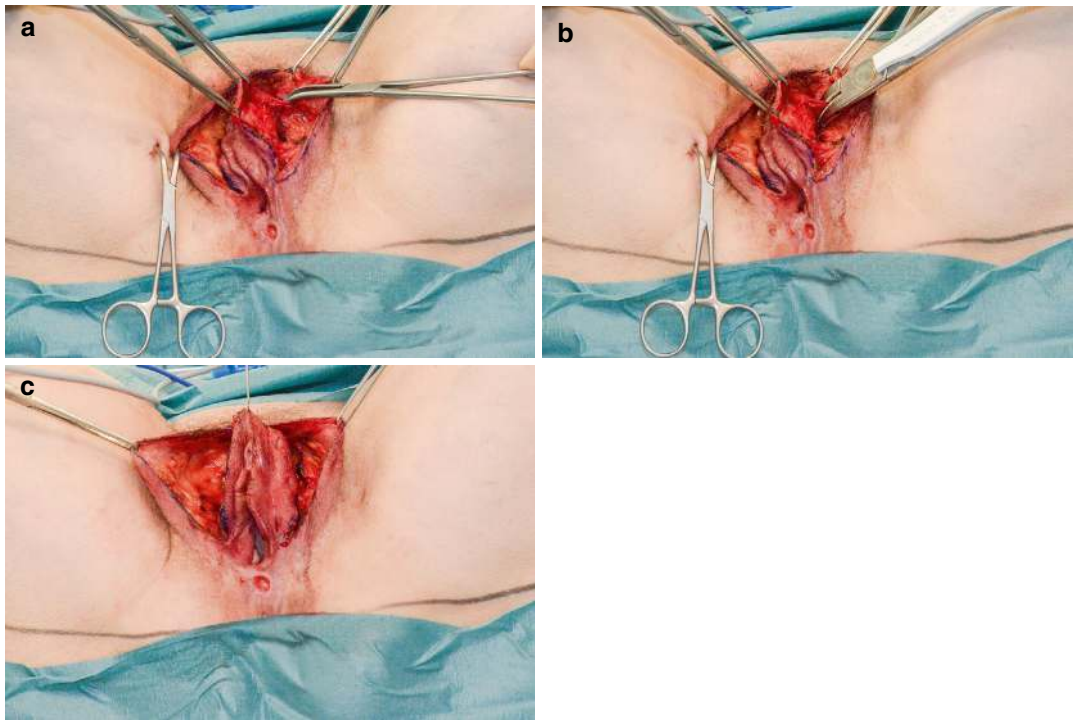

Fig. 11.16 Anterior VFR: lateral dissection. (**a**) Dissection along the medial border of the left Dartos fat body. (**b**) Sealing and transection of veins connecting the Dartos fat body to the vulvar compartment. (**c**) Bilateral dissection completed

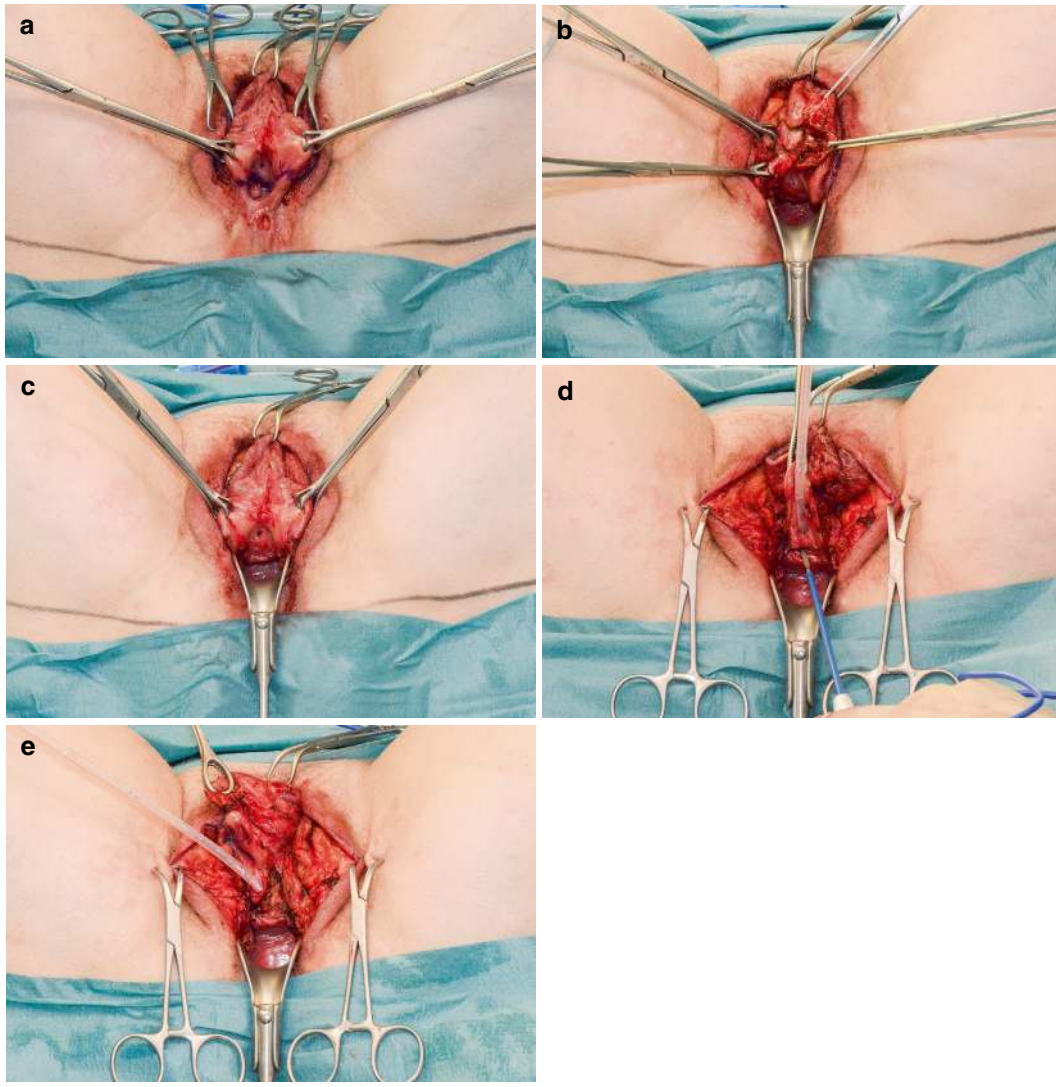

Fig. 11.17 Anterior VFR: central incision and transection. (**a**) Central incision line marked at 8 and 4 o'clock positions. (**b**) The bulbi vestibulares (the right one grasped with Babcock clamps) are preserved. (**c**) Central transection advanced toward the meatus urethrae. (**d**) Posterior urethral incision just proximal to the meatus. (**e**) Left bulbus vestibularis (corpus spongiosus) covered by the bulbospongiosus muscle, separated from the distal urethra

Anterior dissection is carried out as in a total VFR. After transection of the ligamentum clitoridis (Fig. 11.18a) and the glans clitoridis (Fig. 11.18b), the dissection is advanced caudally at the surface of the supraurethral spongiosus sling and further to the distal anterior urethra, which is transected a few millimeters proximal to the meatus (Fig. 11.18c). The anterior VFR specimen is fixed on a tray, and the intracompartmental resection margin is inked for histopathological assessment according to the cancer field paradigm (Fig. 11.18d). After anterior VFR, the complete posterior and parts of the lateral vulvar compartments, as well as the labia majora and the deep erectile tissues, are retained (Fig. 11.18e).

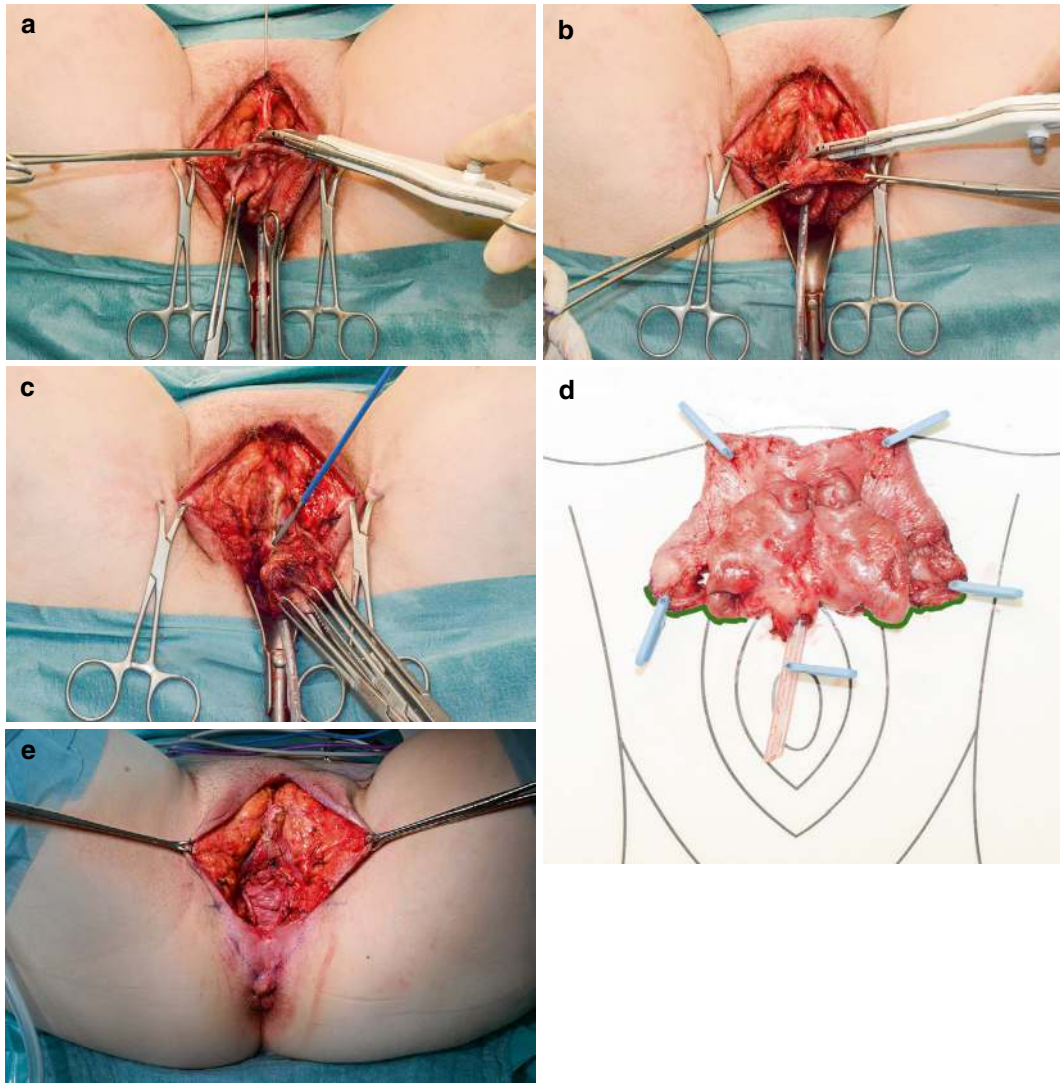

Fig. 11.18 Anterior VFR: anterior dissection and transection. (**a**) Sealing and transection of the ligamentum clitoridis. (**b**) Sealing and transection of the glans clitoridis. (**c**) Anterior incision of the urethra just proximal to the meatus. (**d**) Anterior VFR specimen fixed on a tray. The intracompartmental resection margin has been inked. (**e**) Anterior VFR completed

11.10 Lateral VFR: Step-by-Step

All surgical steps for the lateral VFR correspond to or can be deduced from the previous demonstrations.

Step 1: Lateral Incision.

The skin is incised at the crest of the labium majus, starting at the anterior commissure and proceeding posteriorly to circumvent the ipsilateral gynecologic perineum in the projection of the lateral border of the labium majus and at the anal margin.

Step 2: Lateral Dissection.

This corresponds to the unilateral maneuver with total VFR.

Step 3: Medial Incision.

The vulvar skin is incised at the base of the ipsilateral prepuce, and the frenulum of the labium minus is transected. The incision is advanced posteriorly through the anterior vestibulum, bypassing the urethral orifice and just proximal to the hymenal remnants. Traversing the midline of the gynecologic perineum, the medial incision meets the lateral one.

Step 4: Medial Dissection.

From cranial to caudal, the following tissues are partially exposed by advancing the medial incision lateralward: clitoridal body, bulbospongiosus muscle with bulbus vestibularis, and external anal sphincter muscle. The dissection proceeds at Colles' fascia to meet the surgical field of the lateral dissection, and the specimen of the lateral VFR can be withdrawn for examination by the pathologist.

11.11 Posterior VFR: Step-by-Step (Figs. 11.19 and 11.20)

A special technique of posterior VFR has been designed for oT1 vulvar carcinoma of the intermediate subcompartment, which is the most frequent form of posterior vulvar cancer. The incision figure is planned for anatomical reconstruction with bilateral perianal Limberg flaps (see Chap. 12).

Step 1: Planning of the "Double Rhomboid" Incision (Fig. 11.19).

The incision follows the geometry of two cranially directed Limberg rhomboids (defined by equally sized rectangles with 60° and 120° angles) sharing the medial midline sides. The side length of the double rhomboid depends on the tumor diameter, which should ascertain its wide

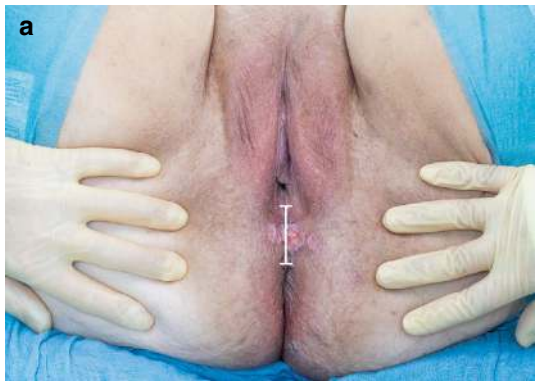

Fig. 11.19 Posterior VFR (double rhomboid): incision planning. (**a**) oT1 vulvar cancer of the intermediate subcompartment for which the technique is indicated. The distance between the hymen at 6 o'clock and the anal skin at 12 o'clock determines the individual side length of the 60°–120° rhomboid for the patient. (**b**) A double rhomboid (open book) figure with the individual side lengths drawn on a sterile paper is placed on the patient's perineum. (**c**) Double rhomboid Limberg biflap incision lines are marked

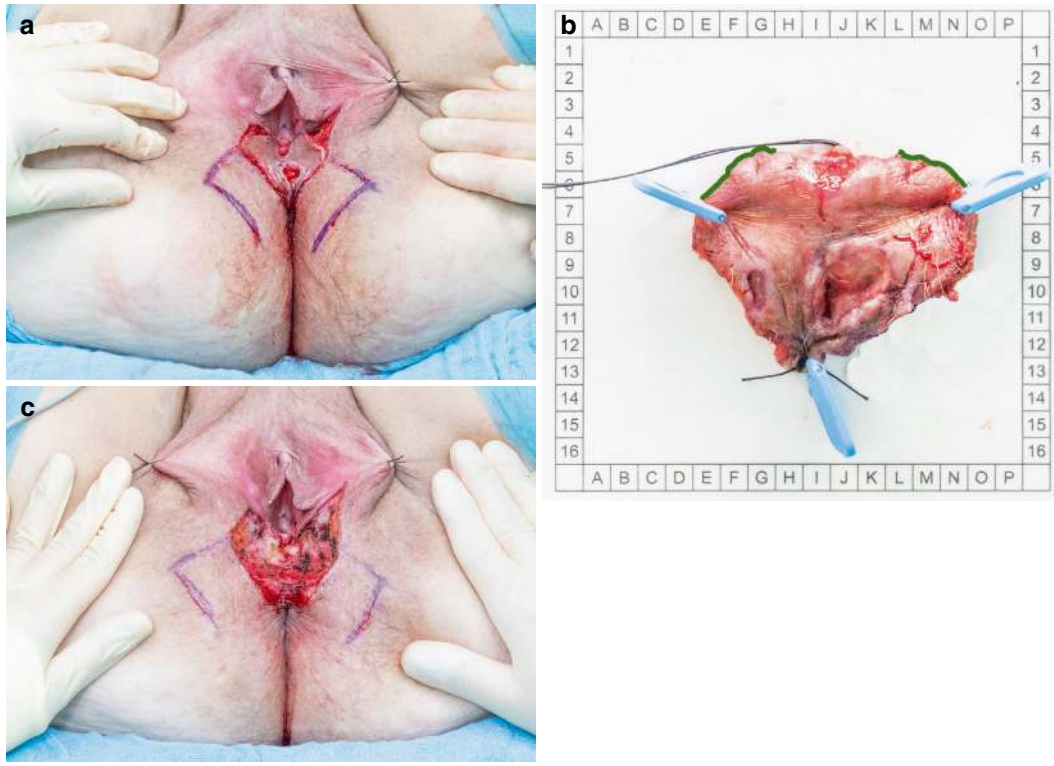

Fig. 11.20 Posterior VFR: incision and transection. (**a**) The incision follows the marked lines to expose the central perineal tendon and the ventral hemicircumference of the anal sphincter muscle. (**b**) Posterior VFR specimen fixed on a tray. Intracompartmental resection margins have been inked. (**c**) Perineal soft tissue defect after posterior VFR to be covered by bilateral Limberg flaps (Chap. 12)

excision with a clinically uninvolved margin of at least 1 cm. The maximum length is considered to be 4 cm.

The individualized double rhomboid incision figure is first drawn on a sterile sheet of paper, then cut out and attached to the patient's perineal and posterior vulvar surface (Fig. 11.19a, b) to mark the incision figure adjusted to three dimensions (Fig. 11.19c). The incision follows the marked line exactly to transect the anal and perineal dermis and the mucosa of the posterior vagina.

Step 2: Posterior Dissection.

Dissection for posterior VFR corresponds to step 3 of total VFR.

Step 3: Central Incision and Transection (Fig. 11.20).

The central incision is performed as described in step 4 of total VFR. However, it should follow the upper "V" of the double rhomboid incision line, instead of the posterior hymenal remnants (Fig. 11.20a). The double rhomboid posterior VFR extirpates the posterior intermediate and central vulvar subcompartments completely but retains parts of the posterior peripheral subcompartments (Fig. 11.20b, c).

In other situations of posterior vulvar carcinoma, cancer field resection corresponds to modified steps 1, 2, 3, and 4 of the total VFR.

11.12 Focal VFR (Fig. 11.21)

According to the principle of cancer field surgery, very small lesions of vulvar carcinoma, i.e., pT1a tumors with limited dysplastic surroundings, can be treated with focal VFR, which removes only part of the vulvar subcompartment containing the lesion (Fig. 11.21a–c). Due to the only minor distortion of the vulvar contour resulting

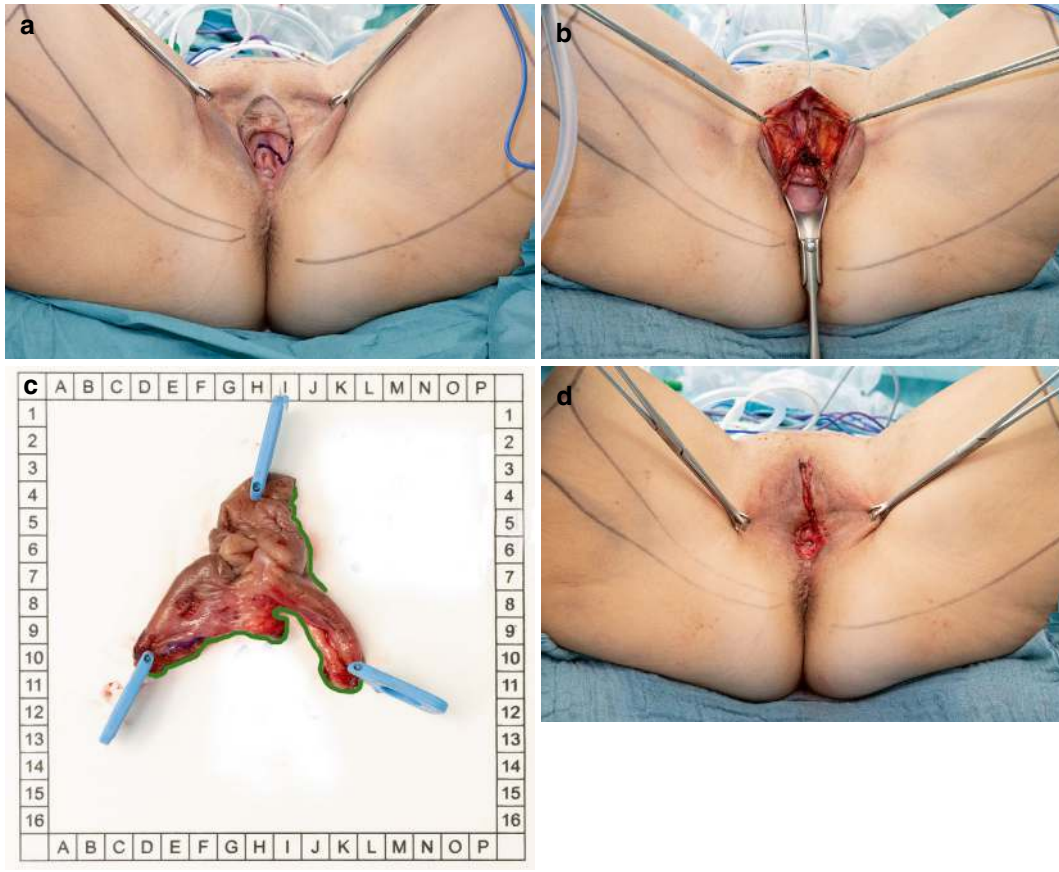

Fig. 11.21 Focal VFR for pT1a vulvar carcinoma at the glans clitoridis. (**a**) Peripheral and central incision lines. (**b**) Soft tissue defect comprising the anterior intermediate vulvar subcompartment. (**c**) Surgical specimen fixed on a tray. Intracompartmental resection margins have been inked. (**d**) Vulvar defect closed primarily

from focal VFR, primary wound closure often fulfills the demand to preserve the form and function of the organ (Fig. 11.21d).

11.13 Extended VFR (Fig. 11.22)

Extended vulvar field resections are mandatory for local tumor control if the ontogenetic stages exceed oT2. True local recurrences, particularly after adjuvant radiation, have often progressed to oT3a and higher stages (Fig. 11.22a). To include adjacent tissues in addition to the ontogenetic vulvar compartment, total VFR has to be extended peripherally and/or centrally. For peripheral extension (step 1 of total VFR), the peripheral incision is moved into the gluteal, perianal, genitocrural, labium majus, or inguinopubic region. Lateral resection (step 2 of total VFR) is then accomplished by deepening the skin incision to the fascia lata and mobilizing the skin fat flap centrally to reach Colles' fascia and the superficial perineal muscles. At the lateral margin of the bulbospongiosus muscles, Colles' fascia is incised, and the bulbi vestibulares are mobilized medially to be included in the surgical specimen. The urogenital diaphragm is sealed and transected laterally or to the bulbi vestibulares/bulbospongiosus muscles to approach and liberate the peripheral vaginal walls.

For central extension, steps 3–5 of total VFR are modified depending on the tissues to be additionally extirpated. By extended posterior dissection (step 3 of total VFR), the complete anterior

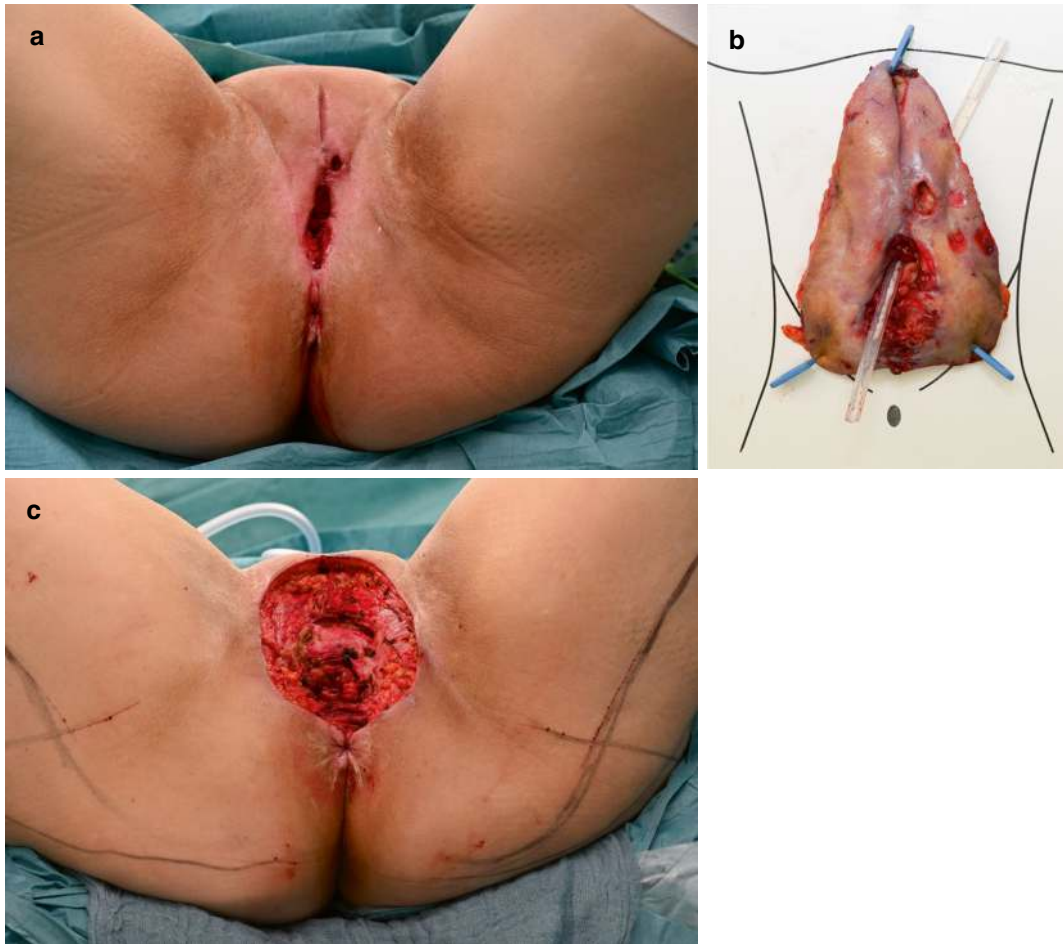

Fig. 11.22 Extended VFR. (**a**) Local relapse of a vulvar carcinoma after standard surgery and adjuvant radiotherapy. oT3a stage is manifest from the infiltration of the left labium majus. (**b**) Extended VFR specimen, which includes the labia majora, the anterior commissure, all deep erectile tissues, the distal urethra, the sinus vagina, and parts of the urogenital diaphragm. (**c**) Perineal soft tissue defect after extended VFR. The anterior symphysis is completely exposed. The anal sphincter muscle is preserved

hemicircumference of the sphincter ani muscle and the anterior wall of the distal rectum are exposed. At the level demanded for wide tumor excision, the central incision (step 4 of total VFR) is performed by an antimucosal stab incision into the vaginal wall at 6 o'clock and bilateral advancement to reach the surgical field of the lateral dissection. Extended anterior dissection (step 5 of total VFR) mobilizes the clitoridal corpus with overlying cranial bulbospongiosus muscles and the proximal crura downward against the symphysis after sealing and transecting the clitoridal ligament and distal crura. The proximal urethra is exposed after mobilizing the supraurethral sling of the bulbi vestibulares and transected according to the needs of a wide tumor excision. The anterior urogenital diaphragm is incised to meet the level of the lateral transection. With a Foley catheter inserted into the residual urethra pulled upward, the anterior wall of the sinus vagina is dissected sharply to the anterior central incision to complete the extended VFR (Fig. 11.22b, c).

Extension of a VFR to include the anorectum is possible but rarely indicated. It necessitates a permanent loop colostomy and major

flap surgery for reconstruction. Vulvar carcinomas have to progress to an oT4 stage in order to infiltrate the anorectum, usually associated with large fungating and ulcerative local tumor masses and distant metastases that render these patients no longer curable (see Chap. 7). If radiotherapy is a treatment option for local tumor control, it should be preferred over surgery. Patients with relapse or persistence of vulvar carcinoma after radiotherapy can benefit from this excessive perineal surgery. The technical details of that procedure are beyond the scope of this textbook.

11.14 Resection of the Sinus Vagina (Fig. 11.23)

The complete surgical removal of the most caudal Müllerian subcompartment as a stand-alone procedure is indicated for oT1 carcinomas of the sinus vagina, a rare clinical situation. More often than as a stand-alone operation, the sinus vagina has to be resected together with the suprasinus vagina through abdominoperineal TMMR or as central extensions of an extended VFR.

For the exclusive resection of the sinus vagina, the distal central incision is performed in the

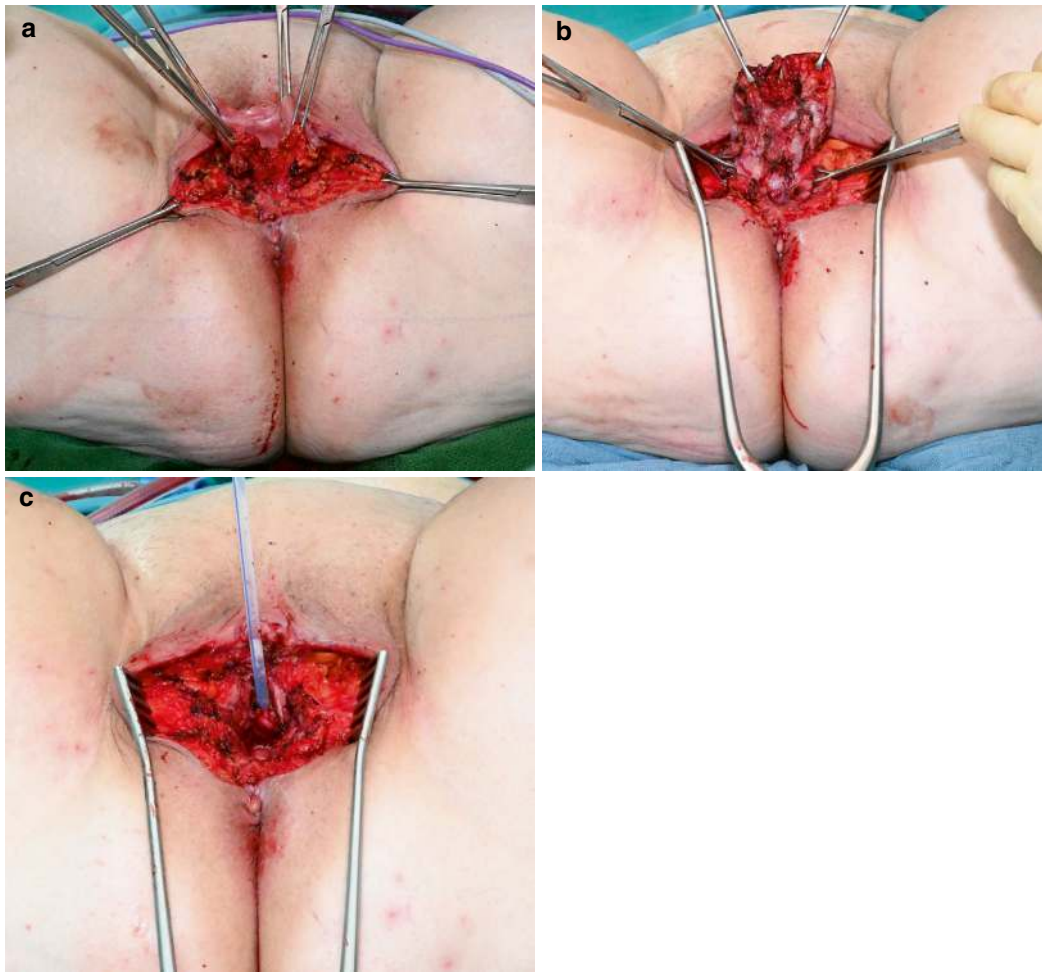

Fig. 11.23 Cancer field resection of the sinus vagina as part of a centrally extended VFR. (**a**) The anterior circumference of the anal sphincter muscle and lower medial margins of the bulbi vestibulares with overlying bulbospongiosus muscles are exposed. (**b**) The bulbospongiosus muscle-bulbi vestibulares-urogenital diaphragm complexes (grasped with Babcock clamps) have been mobilized laterally to expose the complete posterior sinus vagina, allowing the proximal incision (colpotomy) posteriorly. (**c**) Resection of the sinus vagina is completed

vestibulum distal to the hymenal margin. The anterior circumference of the sphincter ani muscles and the medial margins of the bulbi vestibulares and overlying bulbospongiosus muscles are exposed by dissection along the central perineal tendon (Fig. 11.23a). The proceeding surgical steps correspond to those of centrally extended VFR with the transection of the urogenital diaphragm medial to the bulbi vestibulares. The composite tissue complex of bulbospongiosus muscles, bulbi vestibulares, and diaphragma urogenitale adhering to the medial margins of the levator ani muscles is mobilized laterally to expose the posterior and lateral sinus vagina over a length of about 5 cm (Fig. 11.23b).

The proximal central incision is also carried out as described for centrally extended VFR at the estimated level of the urethrovesical transition (approximately 3–4 cm proximal to the hymenal margin) (Fig. 11.23c).

11.15 Postoperative Management

With regard to the perineal surgical wound, postoperative care is described in Chap. 12 as it relates predominantly to reconstructive procedures. The suction drains of the inguinal wounds are removed when the 24-h flow volume is repeatedly less than 50 mL. The exit sites of the drains are inspected daily for signs of infection and are prophylactically treated with disinfective solutions. Skin staples are taken off partially on day 10 and completely on day 12 postsurgery.

11.16 Management of Complications

Herein, only complications of the lymph node dissection are considered. Complication management of the perineal surgery is described in Chap. 12.

Postsurgical bleeding must be treated by immediately reopening the wound, rinsing, and eventually controlling the bleeding vessels. If bleeding vessels cannot be identified, the complete removal of blood and blood clots is important. After the placement of a new suction drain, the wound is closed again with interrupted skin sutures.

Clinical symptoms of infected drainage stab wounds mandate the withdrawal of the drains, irrespective of their present flow volume. Infection of the inguinal wound diagnosed from clinical signs of inflammation is an indication to open and spread the wound and clear it from contaminated fluid and pus. Germ-specific antibiotic medication is used as a supplement and to prevent erysipelas. Daily wound lavage or vacuum treatment is done. After the infection is cleared, the wound is readapted with skin sutures or left for secondary healing. Wound margin necrosis necessitates tissue debridement to obtain capillary bleeding at all wound sites.

Inguinal wounds are prone to developing lymphoceles. In order to prevent iatrogenic infection by puncturing the closed lymphocele with a syringe, it is recommended to focally incise the wound and let the fluid spill out. Infected lymphoceles necessitate the broad opening and lavaging of the wounds. Spontaneous early closure of the wound must be prevented by barrier devices until the infection is eliminated.

Lymphedema of the legs is still an unpreventable long-term complication of lymph node dissection in some patients. Its management with manual decongestive therapy, the use of compression garments, and surgical options such as lymphovenous anastomoses, gastroepiploic vascularized lymph node transfer, and suction-assisted lipectomy are beyond the scope of this textbook. In order to avoid aggravation by erysipelas, patients are advised to ask for prophylactic antibiotic treatment in the case of even minor lower extremity skin injuries.

12 Surgical Reconstruction of the Vulva Following Vulvar Field Resection and Extended Regional Treatment

Except for focal vulvar field resection (VFR) (see Chap. 11), we consider immediate surgical reconstruction with local skin flaps after cancer field surgery for vulvar carcinoma an essential element of the treatment. Dispensing with flap reconstruction for either the primary closure or the secondary healing of the perineal soft-tissue defect should be based on anatomical and medical reasons (see below) as well as on the discretion of the patient. However, for extended soft-tissue defects resulting from the resection of locoregionally advanced and recurrent vulvar carcinoma, primary closure or secondary healing is no option. In this chapter, we briefly discuss local random and axial pattern skin flaps designed by plastic surgeons and describe in more detail modified and specified procedures, which fulfill the criteria that we have set up for optimizing the *anatomical reconstruction* of the vulva after different types of vulvar field resection (VFR). These criteria are as follows:

1. The plastic restoration of the gross contour of the vulva by two symmetrical vertical skin flaps.
2. The ability of undisturbed micturition, cohabitation, and defecation.
3. The restoration of near-normal vulvar sensation mediated by the pudendal and genitofemoral nerves.

Although local skin flap reconstruction techniques can also be useful in traditional surgery for vulvar cancer, the flap techniques described herein are optimized to be combined with the different types of VFR. The reconstruction of major perineal and pubic inguinal soft-tissue defects resulting from the surgical treatment of locoregionally advanced and postirradiation recurrent tumors often mandates the application of distant musculofasciocutaneous flaps, such as tensor fasciae latae, gracilis, gluteal thigh, and rectus abdominis flaps [1]. Their procedural presentation is beyond the scope of this textbook. However, the gluteopudendal thigh flap developed by the author for surgical reconstruction after extended VFR is included in this chapter.

Any surgery performed on the female perineum is threatened by wound infection and its consequences in terms of dehiscence and tissue necrosis due to the unavoidable contamination of the surgical field from the vagina and the anus. For reconstruction with local flaps, this risk relates to the donor sites as well. The dislocation and necrosis of the infected flaps can significantly hamper the reconstructive goals. For the planning of the reconstruction, one must therefore be aware of this risk, and the optimal techniques have to be selected accordingly. The most important risk factor for failure is morbid obesity. Long-term and poorly treated diabetes mellitus

M. Höckel et al., *Cancer Field Surgery in Gynecologic Oncology*,
https://doi.org/10.1007/978-3-031-83030-3_12

and a history of smoking are also associated with a high probability of healing complications. The presence of any of these conditions in severe expression or a combination of these is considered a contraindication for flap reconstruction in general or in particular (see below). Previous perineal irradiation is a strict contraindication for the use of local skin flaps. Previous surgery within or related to the potential donor site may also spoil the application of certain flap techniques. A temporary loop colostomy at the time of VFR to prevent massive feces contamination of the early perineal wound in patients with a high risk of infectious wound breakdown can be considered for extended VFR for advanced vulvar carcinoma. Fortunately, according to our observations, secondary healing in flap reconstruction does not lead to inferior reconstructive results in the majority of patients compared to primary healing, although it takes a much longer time.

The skin flaps suitable for anatomical reconstruction after vulvar field surgery are either of the random type or of the axial pattern type based on vascular territories. Suitable random flaps for anatomical vulvar reconstruction are as follows:

- The pubolabial V-Y advancement flap [2].
- The gluteal fold V-Y advancement flap [3].
- The Limberg flap [4].
- Axial pattern flaps to be used for anatomical reconstruction, with multiple designs, are supplied by terminal branches of the internal pudendal vessels. They are known as:
- Pudendal thigh flaps [5].

An algorithm for planning flap reconstruction is presented in Chap. 13. The pubolabial V-Y advancement flap is useful for reconstruction after anterior VFR. Alternatively, bilateral paralabial island flaps, a modification of the pudendal thigh flap optimized for this application, can be chosen. Lateral VFR defects are well substituted by ipsilateral pudendal thigh flaps, either in the island or in the peninsula version. Bilateral perianal Limberg flaps sharing the midline sites ("open book" design) are favored for posterior VFR. Larger posterior defects can be treated with pudendal thigh flaps of the peninsula design. Total VFR tissue defects demand either bilateral peninsular pudendal thigh flaps or a combination of a pubolabial V-Y advancement flap and two perianal Limberg flaps in the open book design. Which of these flaps can be expected to achieve the best reconstructive results has to be decided for individual patients intraoperatively. The flap combination of pubolabial V-Y and Limberg flaps is limited by the maximum size of the Limberg flaps. Another option to reconstruct perineal defects after total VFR is bilateral V-Y advancement flaps from the gluteal fold region. With regard to contour and introital tissue compliance, these flaps are inferior to the other two alternatives, but for high-risk patients with regard to wound infection, dehiscence, and flap necrosis, the gluteal fold V-Y flaps offer a better course in the case of secondary healing. Depending on the amount of tissues that have to be included in extended VFRs, reconstruction may still be possible with the techniques described for total VFR; otherwise, it is better achieved with bilateral gluteopudendal thigh flaps.

Figure 12.1 provides a schematic overview of the flap techniques modified, specified, or designed by the author. These are presented in more detail below.

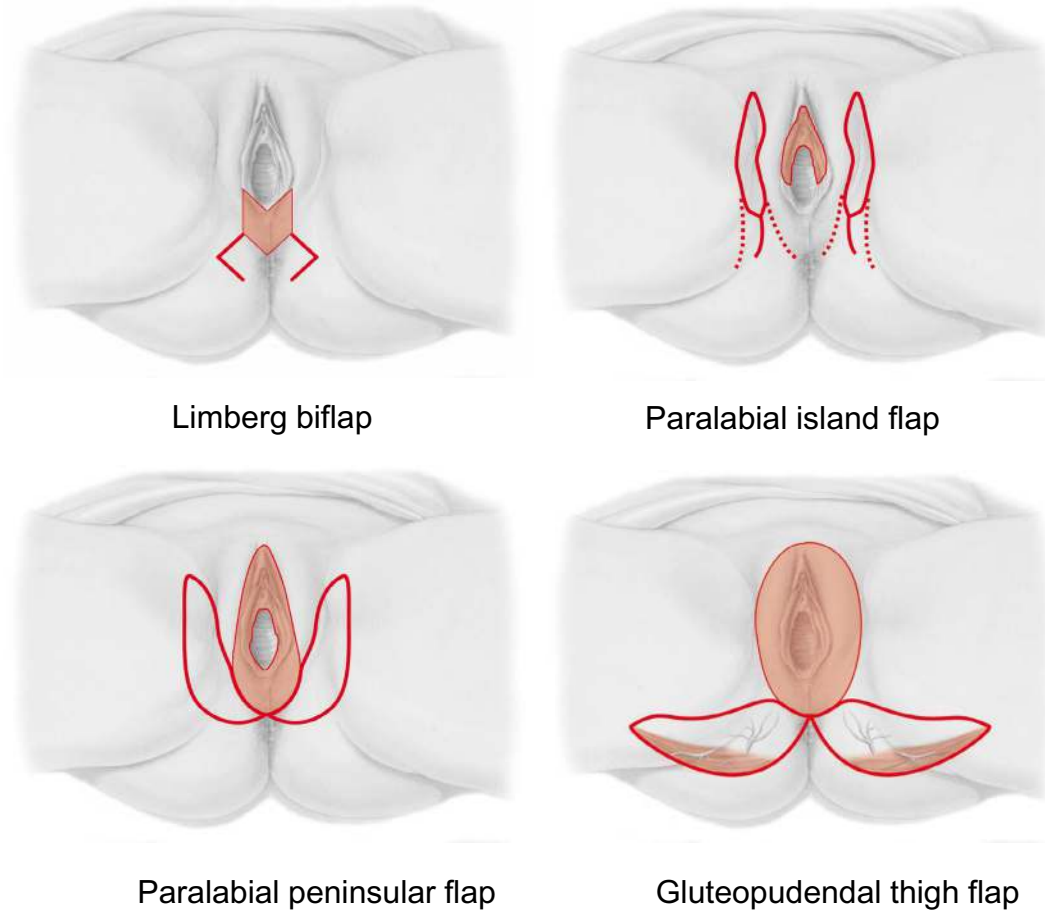

Fig. 12.1 Overview of different local skin flaps for anatomical reconstruction after cancer field resection of vulvar carcinoma

12.1 Equipment

The surgical equipment necessary for anatomical reconstruction with local skin flaps corresponds to that recommended for VFR (see Chap. 11, Table 11.1).

12.2 Patient Preparation and Positioning

The essentials of preoperative patient management for VFR are given in Chap. 11. If a temporary loop colostomy is planned, potential suitable positions should be marked on the sitting patient's hypo- and epigastric abdominal skin. Lithotomy positioning of the patient for reconstructive surgery corresponds to the VFR part.

12.3 Surgical Techniques

Planning, elevation, transposition, eventual trimming and refinement, as well as fixation of the flaps and donor site closure are described for the perianal Limberg biflaps; the paralabial flaps, both in the peninsular and in the island versions; and the gluteopudendal thigh flap.

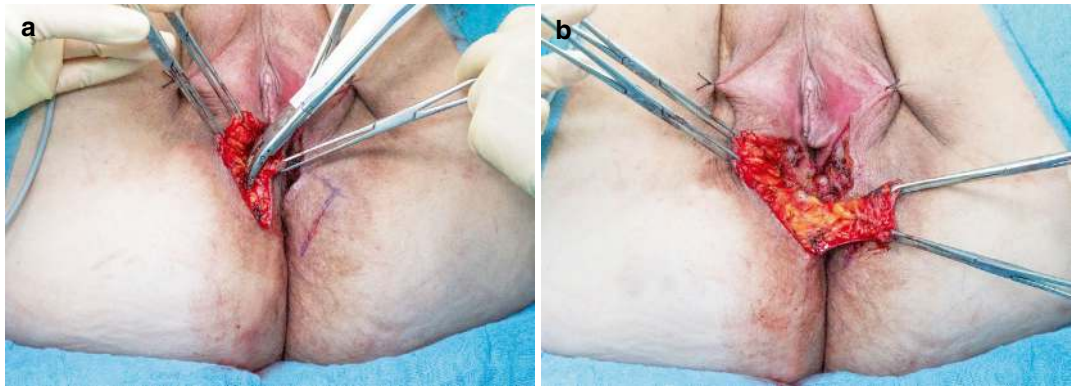

Fig. 12.2 Perianal Limberg biflap elevation. (**a**, **b**) The right skin flap is raised from distal to proximal with a subcutaneous layer of 1–2 cm thickness

Fig. 12.3 Perianal Limberg biflap transposition. The right lateral proximal donor site is pulled with a Gillies hook further laterally, and the flap is rotated medially to the sagittal midline

12.4 "Open Book" Limberg Biflaps (Figs. 12.2, 12.3, and 12.4)

Posterior VFR for oT1 vulvar carcinoma up to about 2 cm in size, located at the posterior intermediate subcompartment, can be performed primarily with regard to optimal reconstruction by perianal Limberg biflaps. A paper template indicates the skin incision figure. The side length of the birhomboid is determined by the distance from the distal vagina at 6 o'clock to the anus at 12 o'clock (see Chap. 11).

12.4.1 Flap Planning (Fig. 11.19)

The paper template is exactly adapted to the defect, and lines advancing the axis between the 120° angles of the two rhomboids for the side length are drawn on the perineal-perianal skin. At a 60° downward angle, a second line of the side length completes the bilateral flap design.

12.4.2 Flap Elevation (Figs. 11.20c and 12.2)

The skin is incised along the marked lines, and the rhomboid flaps are raised within the subcutaneous layer from the apex to the base, integrating a fat thickness of about 1–2 cm.

12.4.3 Flap Transposition (Fig. 12.3)

With lateral traction by a Gillies hook at the 60° angles of the donor sites, both Limberg flaps are rotated inward and fixed with their upper medial margin to the 6 o'clock position of the vaginal wound.

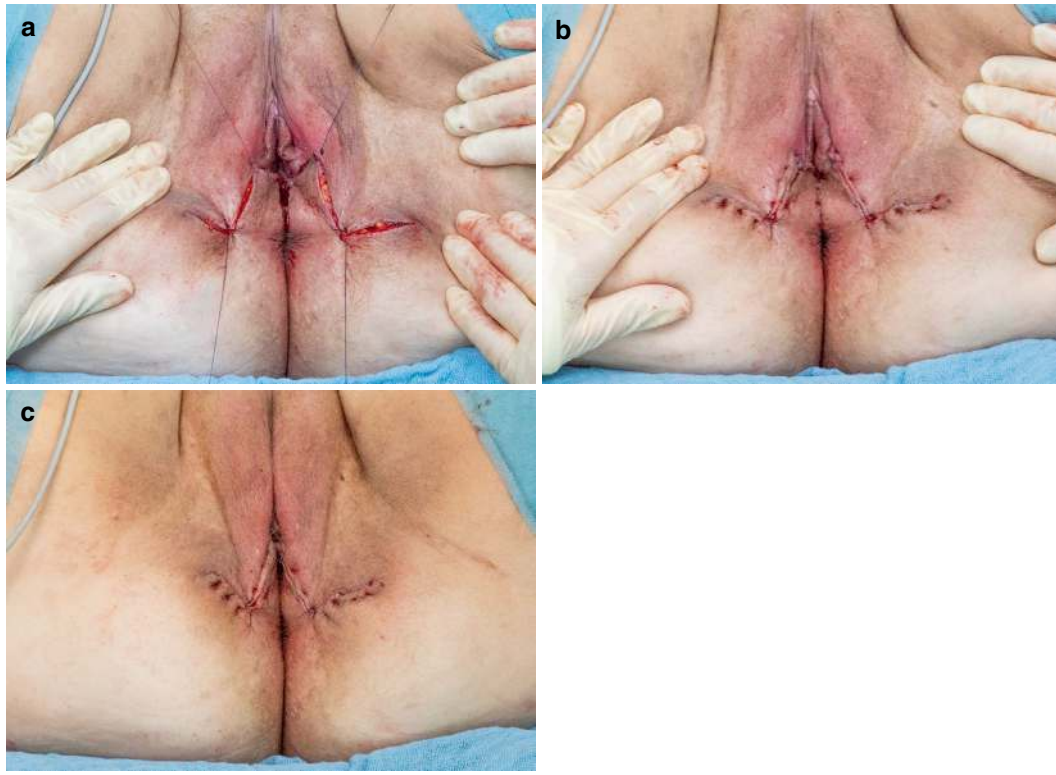

Fig. 12.4 Perianal Limberg flap fixation and donor site closure. (**a**) The transposed flaps are fixed with stay sutures, which also close the donor defects. (**b**, **c**) Anatomical vulvar reconstruction after posterior VFR completed

12.4.4 Flap Fixation and Donor Site Closure (Fig. 12.4)

The 120° angles of the donor sites are approximated and fixed with stay sutures (Fig. 12.4a). A third stay suture adapts the vulvar wound margin to the upper lateral edge of each Limberg flap. The donor sites are closed with interrupted sutures, followed by the completion of the adaptation of the flaps to the vaginal and vulvar wound margins. Finally, both flaps are sutured together in the midline from the vaginal to the anal margins. No drains are used (Fig. 12.4b).

12.5 Pudendal Thigh Flaps

Pudendal thigh flaps can be successfully applied for anatomical reconstruction following partial, total, and extended VFR. These axial pattern flaps are elevated with an island skin paddle for reconstruction after anterior VFR and in the peninsular design after lateral, posterior, total, and extended VFRs. A unilateral pudendal thigh flap in an island or peninsular design is applied for reconstruction after lateral VFR. Bilateral peninsular flaps are used for posterior vulvar defects if they exceed the reconstructive potential of Limberg flaps. Pudendal thigh flaps can be raised from the proximal inner thigh skin region at any axis between the genitocrural and gluteal folds. The author has optimized the design of both island and peninsular flaps from the paralabial region-genitocrural fold with regard to anatomical vulvar reconstruction after partial and total VFR and donor site morbidity.

12.6 Paralabial Island Flap

12.6.1 Flap Planning (Fig. 12.5)

A horizontal line is drawn from the palpated ischial tuberosity to the anus at 12 o'clock. The pivot point of the flap is located at the lateral third

of its length. Next, the width necessary for the skin paddle corresponding to the distance between the external and internal incision lines of the VFR is measured. The genitocrural fold or the lateral margin of the labium majus, as the medial flap border, is marked with a pen, and a parallel line at a distance of the determined half flap width is drawn further laterally as the flap axis. A third parallel line indicates the lateral flap border. The length of the skin paddle is ascertained with a suture fixed at the pivot point of the flap. The flap length is limited to the projection of the adductor longus muscle. The distances from this point to the lower and upper poles of the soft-tissue defect are marked on the flap axis. These markings, with consideration of the individual anatomy of the donor sites and the shape of the soft-tissue defect, serve to establish the definitive design of the skin paddle. From the posterior pole of the skin paddle, a line is drawn toward the point of rotation, centrally overlying the further future fat tissue pedicle.

Fig. 12.5 Bilateral paralabial island flap planning. Both skin paddles have been designed to exactly match the soft-tissue defect after anterior VFR. They are located in the bilateral genitocrural regions, with their medial sides abutting the lateral margins of the labia majora. The most proximal points of the skin paddles are equidistant to the most dorsal points of the resection with respect to the points of rotation (stars)

12.6.2 Flap Elevation (Fig. 12.6).

The skin paddle is incised to the fascia apically, laterally, and medially. At the base of the paddle, the depth of the incision is limited to the dermis. The skin above the pedicle is incised at the marked midline, and the medial and lateral skin flaps are developed, corresponding to the width of the pedicle (Fig. 12.6a). At the apex of the skin paddle, the fascia is cut in the projection of the flap, which is then mobilized as a fasciocutaneous tissue entity from apical to basal, with permanent visualization of the projected course of the internal pudendal vessels (Fig. 12.6b).

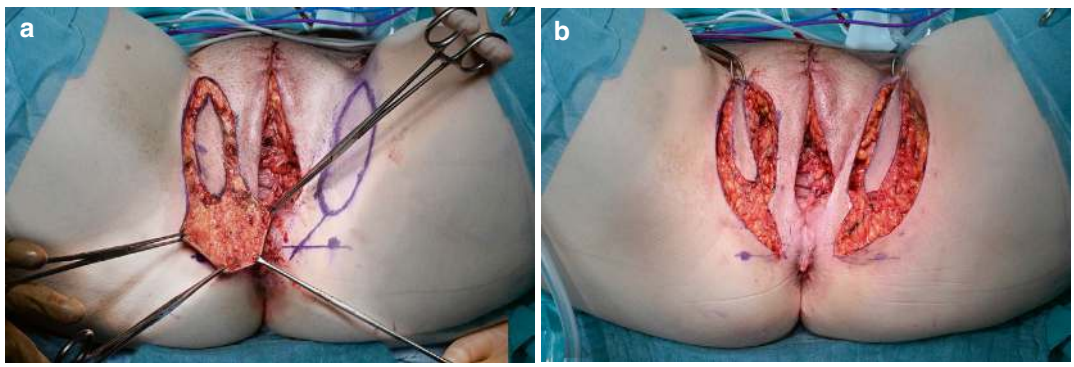

Fig. 12.6 Bilateral paralabial island flap elevation. (**a**) Skin incision of the right paddle and pedicle. (**b**) Both flaps with skin paddles and fibrofatty pedicles containing the pudendal vessels have been raised

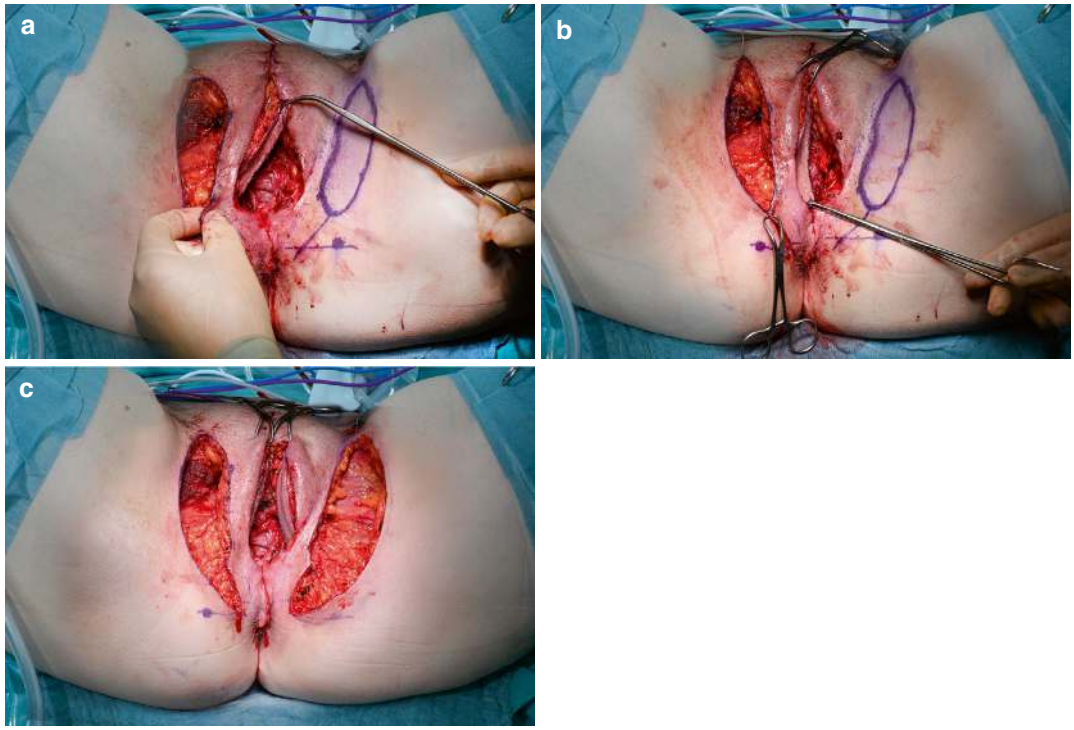

Fig. 12.7 Bilateral paralabial island flap transposition. (**a**, **b**) The right island flap has been rotated medially underneath the right labium majus. (**c**) Both island flaps have been rotated medially. The skin island exactly covers the bilateral soft-tissue defects of the anterior VFR

12.6.3 Flap Transposition (Fig. 12.7)

For the medial rotation of an island flap, the labium majus is undermined below the Dartos fat layer to create a tunnel of sufficient size.

12.6.4 Flap Fixation, Refinement, and Donor Site Closure (Fig. 12.8)

The donor site is closed first. The lateral wound margin is mobilized to enable tension-free approximation to the medial margin. A suction drain is placed, and the donor site defect is closed with interrupted skin sutures, keeping the wound linear with tension at its ventral and dorsal poles (Fig. 12.8a). Each flap is set into the correct position and sutured to the vulvar defect margins proceeding from dorsal to ventral. When the dorsal part of the flap is fixed, a Scherbak vaginal speculum is inserted to ensure the creation of a sufficiently wide vaginal introitus by the ventral flap fixation. Bilateral flaps are united in the midline above the anus and the urethra. Eventual skin surplus at the tip of the flap is excised. A primary closure of the previous anterior commissure of the vulva over a short (1–2 cm) distance may be necessary in some cases (Fig. 12.8b, c).

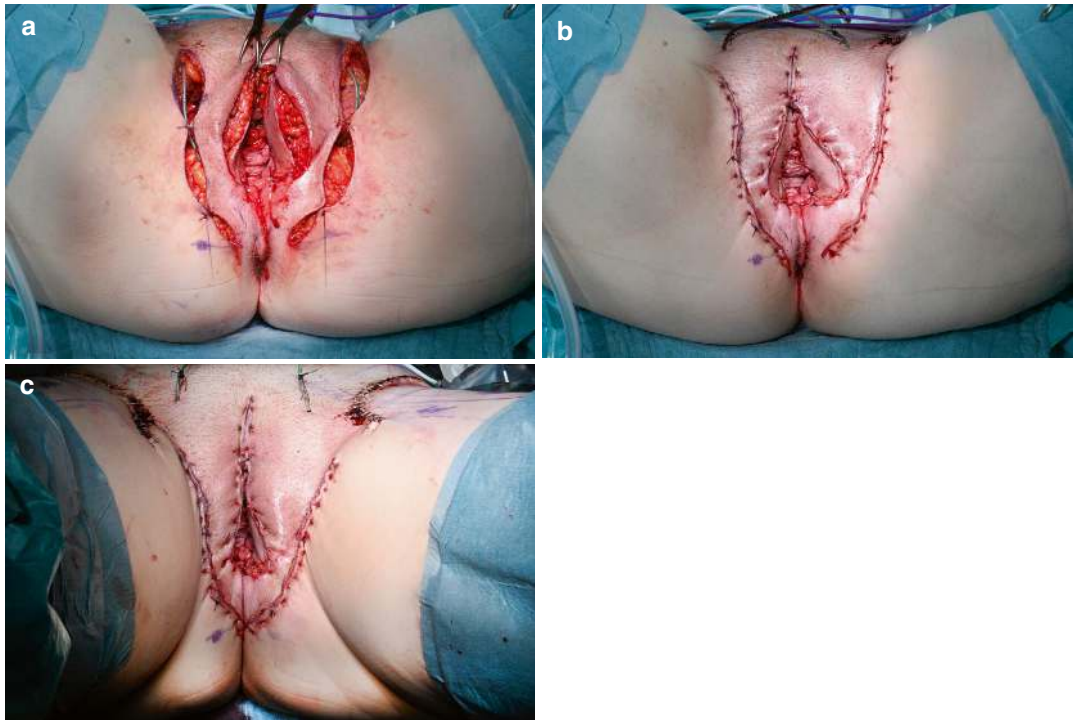

Fig. 12.8 Bilateral paralabial island flap fixation refinement. (**a**) Primary closure of the donor sites. (**b**, **c**) Anatomical reconstruction after anterior VFR completed.

12.7 Paralabial Peninsular Flap

12.7.1 Flap Planning (Fig. 12.9)

Marking the point of rotation and measuring the adequate flap width to cover the defect is done as described for the island flap. Likewise, the necessary length of the flap is determined with a suture temporarily fixed to the point of rotation and to the upper pole of the defect. As with the island flap, the length is limited to the projection of the adductor longus muscle. A line representing the midflap axis is drawn lateral to the genitocrural fold, starting from the pivot point over the determined flap length. The final flap design, with respect to length, width, and position, is then drawn on the skin. At the flap base, the axis of the pedicle ending at the pivot point may deviate laterally from the skin paddle axis as the latter has to be placed at a distance of half of the flap width from the lateral margin of the defect.

Fig. 12.9 Bilateral paralabial peninsular flap planning. The flap size of the right and left skin paddles has been adjusted to the corresponding soft-tissue defects after total VFR. Their medial sites are determined by the genitocrural folds. Stars mark the points of rotation

12.7.2 Flap Elevation (Fig. 12.10)

The skin is incised around the flap perimeter (Fig. 12.10a). The incision is deepened to the fascia lata, which is included in the flap (Fig. 12.10b). Flap elevation proceeds from apical to basal. At the flap base, the incision stops at the subcutaneous fatty tissue (Fig. 12.10c).

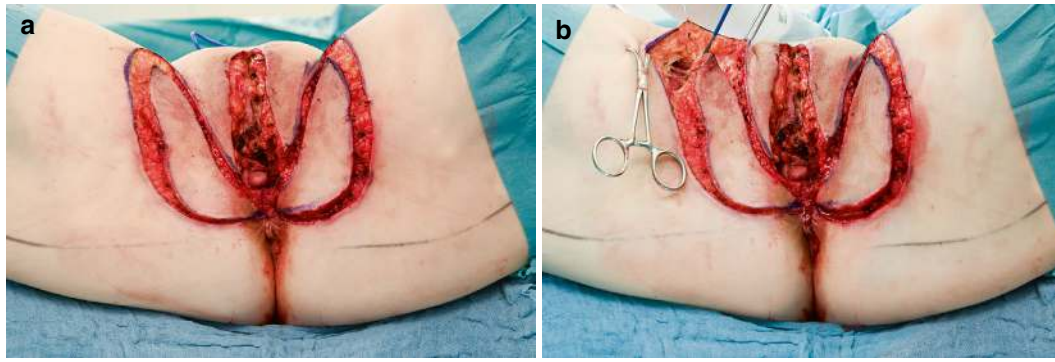

Fig. 12.10 Bilateral paralabial peninsular flap elevation. (**a**) Skin incision along the drawn flap perimeter. (**b**) The right flap is beginning to be elevated from apical to basal, including the fascia lata. Below the points of rotation, the skin incision is deepened only to the subcutaneous fatty tissue

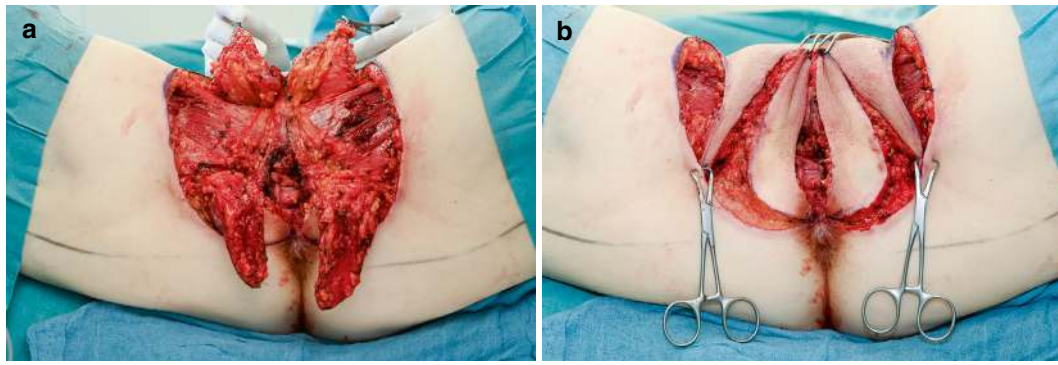

Fig. 12.11 Bilateral paralabial peninsular flap transposition. (**a**) In addition to the elevation of the two paralabial peninsular flaps, the labium majus-genitocrural skin flaps have been mobilized ventrally to the level of the pubic bones. (**b**) Paralabial peninsular flaps are rotated medially and labium majus-genitocrural flaps laterally, preliminarily fixed with Backhaus clamps

12.7.3 Flap Transposition (Fig. 12.11)

The ipsilateral labium majus-genitocrural skin fat flap is mobilized ventrally (Fig. 12.11a) and rotated laterally to enable the medial rotation of the paralabial peninsular flap, which is preliminarily fixed with clamps (Fig. 12.11b).

12.7.4 Flap Fixation, Refinement, and Donor Site Closure (Fig. 12.12)

The transposed paralabial peninsular flaps are united midsagitally at their bases and sutured to the distal dorsal vaginal wall to restore the gynecologic midperineum (Fig. 12.12a).

The next step corresponds to the maneuver with the island flap as described above. The sharp edge of the lateralized labium majus-genitocrural skin flap should be somewhat rounded to prevent focal necrosis (Fig. 12.12b, c).

12.8 Gluteopudendal Flap

This musculofasciocutaneous flap with double blood supply from the descending branch of the inferior gluteal artery and the internal pudendal arteries has been designed by the author to cover large perineal defects after extended VFR with the aim of anatomical vulvar reconstruction. The gluteopudendal thigh flap is also applicable for postradiation recurrences or persistence of

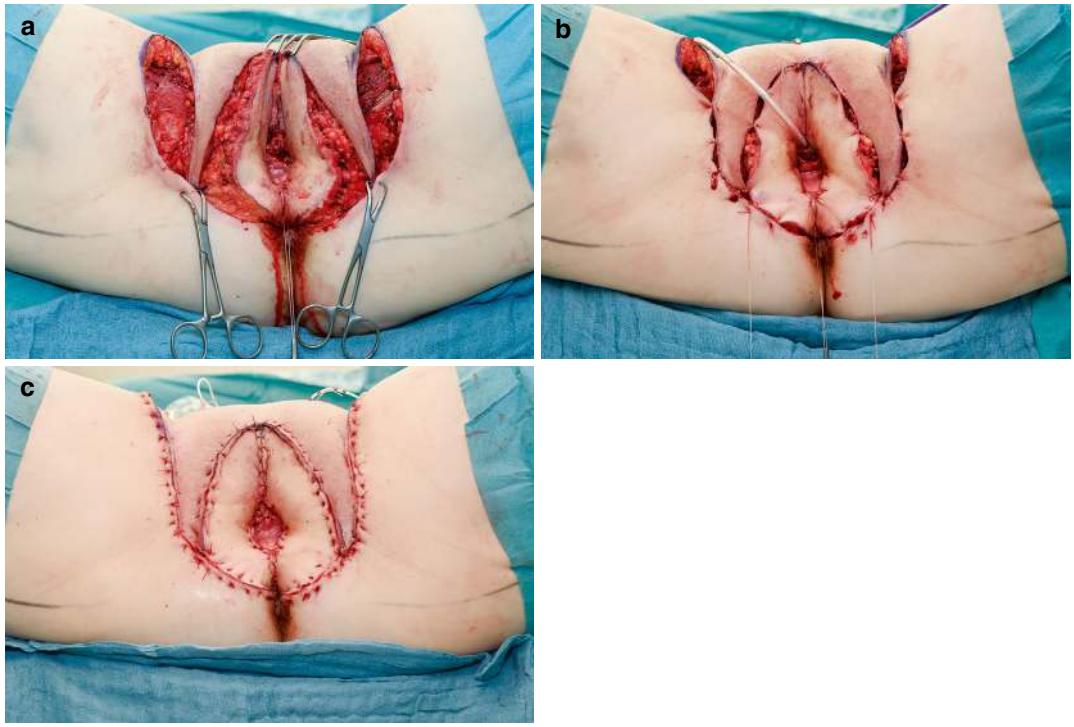

Fig. 12.12 Bilateral paralabial peninsular flap fixation and donor site closure. (**a**) Both paralabial peninsular flaps are adapted in the sagittal midline and sutured to the distal dorsal vagina to form a gynecologic midperineum of about 3 cm in width. (**b**) Fixation of the four flaps with stay sutures. The distal tips of the labium majus-genitocrural skin flaps have been shortened. (**c**) Anatomical vulvar reconstruction after total VFR with bilateral paralabial peninsular flaps completed

vulvar carcinoma when local skin flaps are not indicated due to the radiotherapy-induced micro-angiopathia and impaired healing potential (see above).

12.8.1 Flap Planning (Fig. 12.13)

Prior to the operation, the course of the descending branches of the bilateral inferior gluteal arteries projected to the posterior thigh skin should be marked on the standing patient. The lines run from a point at the gluteal crease midway between the greater trochanter and the ischial tuberosity to the middle of the popliteal fossa. In the lithotomy position, these lines shift lateralward; therefore, they have to be drawn preoperatively. The lines

Fig. 12.13 Bilateral gluteopudendal flap planning. The concave midline axes of the flaps run from the projection of the ischial tuberosity to a point at the midline of the posterior thighs distal to the gluteal crease. The dimensions of the flaps are determined by the perineal soft-tissue defects. The ischial tuberosities mark the pivot points of the flap (stars)

indicate the longitudinal axes from their distal ends to the genital crease. Proximally, the flap axes bend toward the center of the anus (or of its former location if the anorectum had to be included in the extended VFR). The apical, lateral, and medial borders of the flaps are then drawn, respecting the flap axis and the dimensions of the tissue defect. The pivot point at the base of the flaps is at the level of the ischial tuberosities.

12.8.2 Flap Elevation (Fig. 12.14)

The skin is incised at the flap perimeter, and the incision is deepened into the fascia lata (Fig. 12.14a). The genitocrural and medial thigh skin flaps ventral to the gluteopudendal flaps are mobilized (Fig. 12.14b). At the gluteopudendal flap's apex, just below the fascia, the descending branch of the inferior gluteal artery, which is

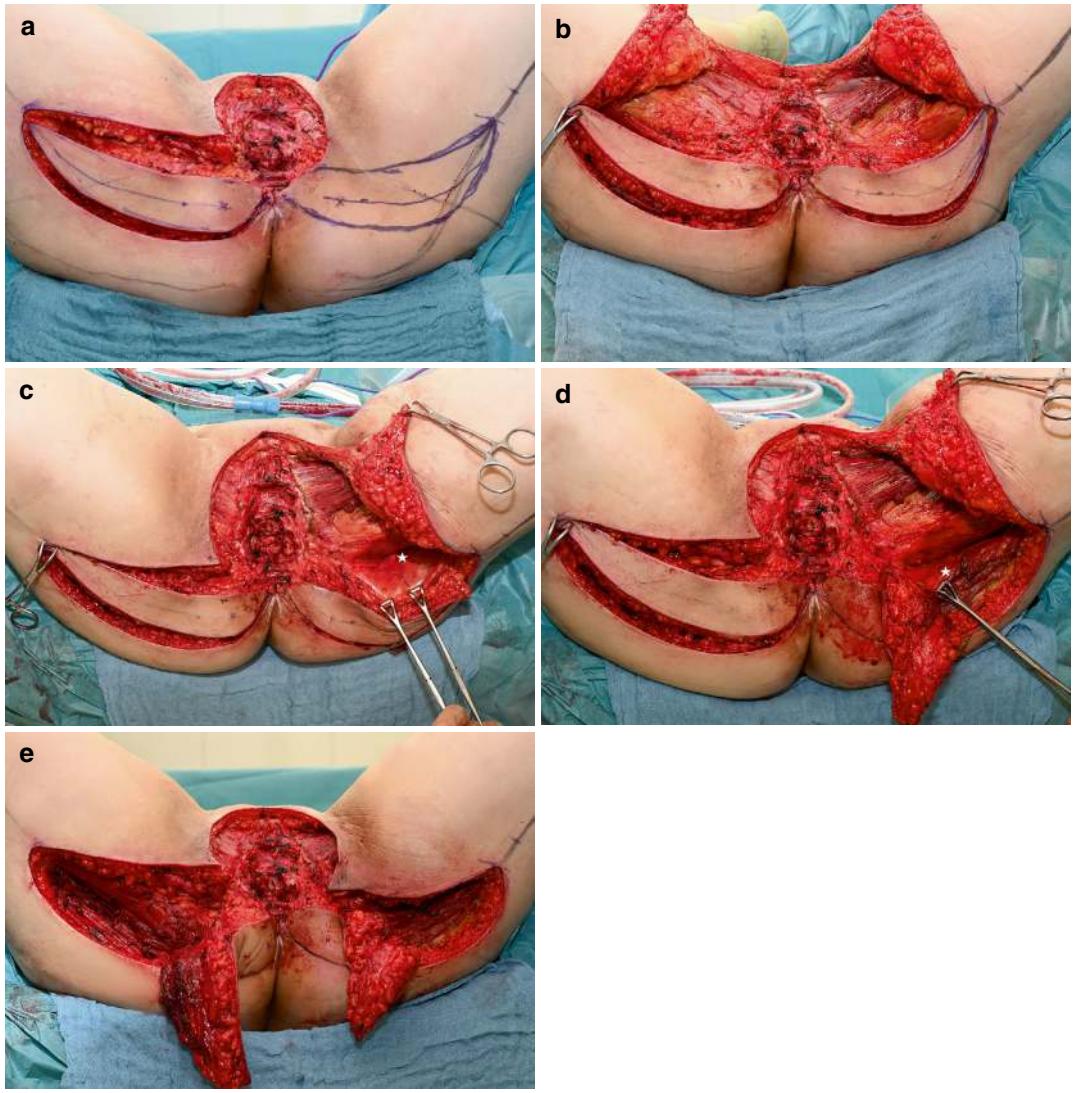

Fig. 12.14 Bilateral gluteopudendal flap elevation. (**a**) The skin and subcutaneous tissue along the right flap perimeter has been incised. (**b**) Both genitocrural and medial thigh skin flaps, including the subcutaneous fat and fascia lata ventral to the gluteopudendal flaps, have been mobilized. (**c**) The left inferior gluteal vessels (star) appear below the semitendinosus-biceps femoris muscles. (**d**) The left gluteus maximus muscle is incised to keep the part of it containing the inferior gluteal vessels within the gluteopudendal flap. (**e**) Both gluteopudendal flaps are raised to their pivot points at the ischial tuberosities

Fig. 12.15 Bilateral gluteopudendal flaps for anatomical perineal reconstruction after extended VFR completed

accompanied by the posterior thigh cutaneous nerve, is identified, sealed, and cut. The elevation of the fasciocutaneous part of the flap proceeds proximally following the course of this neurovascular pedicle (Fig. 12.14c). At the level of the gluteal crease, the appearing gluteus maximus muscle has to be split laterally and medially toward the sciatic foramen to mobilize the musculofasciocutaneous part of the flap to its point of rotation at the level of the ischial tuberosity (Fig. 12.14d, e).

12.8.3 Flap Transposition, Fixation, and Donor Site Closure (Fig. 12.15)

This corresponds to the pudendal thigh flap as described above. Closure of the donor sites should be supported by fasciocutaneous mattress sutures to relax tissue tension.

12.9 Reconstruction Following Extended Regional Treatment

Advanced regional disease caused by the extracapsular spread of lymph node metastases may necessitate the resection of the fascia lata and/or significant amounts of inguino-pubo-perineal skin and subcutaneous fatty tissue. If the femoral vessels are exposed within the femoral triangle, their coverage by an ipsilateral sartorius muscle flap is an effective means to prevent major complications in the case of infectious wound dehiscence (Fig. 12.16a, b). Major inguino-pubo-perineal soft-tissue defects are best covered by an ipsilateral tensor fasciae latae flap.

12.10 Postoperative Management

At the end of each perineal reconstructive procedure applying skin flaps, the position of the urethral opening related to the perineum is marked to facilitate postsurgical catheterization. Indwelling catheters should be avoided to prevent apical necrosis of the flaps, which can result if the catheter compresses the flap under unnoticed tension. The perineal wounds may be sealed with acryl glue after suture to reduce postsurgical bacterial contamination.

Patients who received flaps raised from the gluteal region (gluteopudendal flaps and gluteal fold V-Y advancement flaps) should lie on antidecubitus mattresses and sit on ring cushions in the early postoperative period to avoid pressure-induced wound dehiscence.

After 48 h, all perineal and donor site wounds are antiseptically cleaned twice daily and following each defecation. Drains are removed when fluid production per 24 h is repeatedly less than 50 mL and in all situations with signs of infection at the entry site. The patients are mobilized as soon as they are able to walk. The sutures are removed successively at 12 and 14 days.

12.11 Management of Complications

As perineal surgery in the female cannot be performed aseptically, infectious wound complications are frequent. The clinical spectrum spans from minor wound dehiscence to the complete breakdown of all wounds, infectious tissue necrosis, and flap displacement.

Moreover, partial flap necrosis, due to insufficient perfusion of the distal portion despite proper performance of the surgery, may also occur due

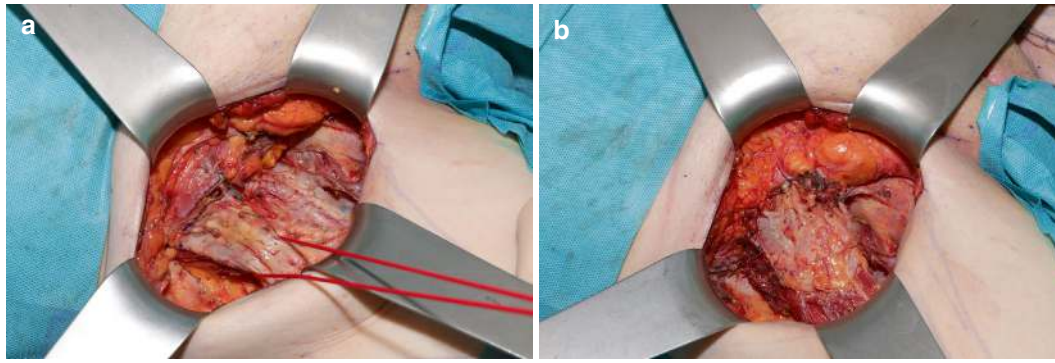

Fig. 12.16 Sartorius muscle flap. (**a**) The right sartorius muscle has been undermined just distal to its origin and grasped with an elastic loop. The muscle will be transected at its origin and rotated medially to cover and protect the denuded proximal femoral vessels. (**b**) The transposed right sartorius muscle flap has been sutured to the inguinal ligament

to infection. The management principles of these complications are regular wound toilet, i.e., rinsing the perineum with disinfecting solutions and debridement of all avital tissue. Surgical debridement has to ensure capillary bleeding at all wound sites. If partial flap necrosis is due to primary ischemia without signs of gross infection, the demarcation of the avital tissue should be awaited prior to debridement. Coping with situations of severe infectious perineal wound breakdown necessitates a temporary loop colostomy.

Antibiotic medication may supplement the local therapy. It is indicated if the infection spreads as erysipelas or cellulitis. Once the local infection is cleared—clinically evident with non-secreting (clean) wounds generating granulation tissue—it must be decided whether leaving the wounds for secondary healing or surgical readaptation of the wound margins would be the best option. Displacement of the flaps mandates the latter procedure.

Late complications caused by the scarring of the perineal wounds may result in functional disturbances of micturition, cohabitation, defecation, and deviations from the desired neovulvar tissue contours. Most of these problems have to be addressed by surgical revision. Only in highly motivated patients manual self-treatment with vaginal dilatators may overcome introital stenosis.

Some patients report pain due to scar formation at donor sites in the gluteal region, particularly when sitting. A ring cushion can usually relieve the discomfort. In most cases, this complication disappears within a few months postoperatively. Persistent numbness, paresthesia, and (neo)vulvodynia are more difficult to handle. Treatment with antidepressive medication can be helpful in these relatively infrequent situations.

As verified by validated questionnaires, the majority of patients reported satisfaction with the reconstructive outcomes obtained through the surgical techniques introduced herein.

References

1. Strauch B, Vasconez LO, Hall-Findlay EJ. Editors. Grabb's encyclopedia of flaps. Vol. III torso, pelvis, and extremities. Boston: Little Brown & Comp; 1990.
2. Moschella F, Cordova A. Innervated Island flaps in morphofunctional vulvar reconstruction. Plast Reconstr Surg. 2000;105:1649–57. https://doi.org/10.1097/00006534-200004050-00008.
3. Lee PK, Choi MS, Ahn ST, Oh DY, Rhie JW, Han KT. Gluteal fold V-Y advancement flap for vulvar and vaginal reconstruction: a new flap. Plast Reconstr Surg. 2006;118:401–6. https://doi.org/10.1097/01.prs.0000227683.47836.28.
4. Lister GD, Gibson T. Closure of rhomboid skin defects: the flaps of limberg and dufourmentel. Br J Plast Surg. 1972;25:300–14. https://doi.org/10.1016/S0007-1226(72)80067-5.
5. Wee JTK, Joseph VT. A new technique of vaginal reconstruction using neurovascular pudendal-thigh flaps: a preliminary report. Plast Reconstr Surg. 1989;83:701–9. https://doi.org/10.1097/00006534-198904000-00018.

Treatment Algorithms and Clinical Results

13

In this chapter, management directives for gynecologic malignancies to be treated with cancer field surgery and the clinical results obtained with these procedures at the University Hospitals in Leipzig and Essen are presented. Details of the diagnostic process for the clinical assessment of the disease and step-by-step illustrations of the procedures are given in Chaps. 7–12.

Although the algorithms can serve as guidelines, modifications of the proposed surgical management may be necessary due to unexpected intraoperative findings, such as noncancer pathologic conditions, anatomical variations, and anomalies. The principles that govern cancer field surgery can no longer be properly applied in situations when previous surgery or pathologies have distorted or destroyed the ontogenetic tissue borders necessary to define the dissection planes.

The diagnostic criteria that determine the treatment with cancer field surgery are established pre- and intraoperatively. Generally, the final pathological report is expected to confirm the disease evaluation on which the surgical management was founded. With accurate procedural performance, any findings in the final histopathological report that necessitate additional actions to achieve the goals of locoregional tumor control should be the exception. Optimal intraoperative communication and cooperation with the pathologist is therefore essential. Treatment algorithms and clinical results are given for carcinomas of the vulva, vagina, cervix, and endometrium. It is assumed that cancer field surgery with immunologic defense line-directed lymph node dissection (iLND) can also be successfully adapted for the management of early tubal and ovarian carcinoma and, without lymph node dissection, for sarcomas of the genital tract. However, due to the rareness of these entities, we only have anecdotal experience with them and cannot give data-based recommendations.

13.1 Carcinoma of the Vulva

A diagnostic prerequisite for planning the treatment with cancer field surgery is determining the ontogenetic (oT) stage of the histologically proven invasive carcinoma, its size, and its exact location. Moreover, the perineum should have been clinically assessed for lichen sclerosus, and the results of the ontogenetic vulvar mapping, considering the multifocality of the cancer and additional dysplastic lesions, must be known. Clinical inguinal and, in case of suspicious findings, pelvic magnetic resonance imaging (MRI) supplements the preoperative diagnostics. Pelvic MRI is also recommended to assess oT > 2 carcinomas with deep tissue infiltration. The patient's history taking must include previous surgeries of the inguinal and perineal regions. Intraoperatively, distinct lymph nodes and topographically defined resection margins have to be examined by the pathologist. Details of the diagnostic management

M. Höckel et al., *Cancer Field Surgery in Gynecologic Oncology*,
https://doi.org/10.1007/978-3-031-83030-3_13

are described in Chap. 7. The vulvar reconstruction is tentatively planned preoperatively from the evaluation of the oncological and anatomical features, of information on nononcological morbidity, and of the patient's preferences. The local, regional, and reconstructive management algorithms for vulvar carcinoma are shown in Fig. 13.1a–c. Unifocal very early (oT1, pT1a) vulvar carcinomas are treated with focal vulva field resection (VFR), i.e., wide tumor excision within the corresponding ontogenetic vulvar subcompartment. oT1/2, pT1b vulvar carcinomas are locally controlled with partial VFR, unless the cancer is multifocal or covers more than one sector of the vulvar compartment. In these situations, total VFR is indicated (Fig. 13.1a). Likewise, total VFR is recommended if differentiated (d-)VIN is diagnosed remotely from the invasive lesion. The extension of total VFR is defined by the individual ontogenetic vulvar compartment to be identified from its anatomical landmarks (see Chap. 4). Partial VFR should ascertain the wide excision of the carcinoma *within* the infiltrated subcompartment(s) and the inclusion of noninfiltrated adjacent subcompartment(s). oT > 2 tumors necessitate extended VFR for local control. Extended VFR includes parts of abutting nonvulvar compartments to achieve a wide local tumor excision outside of the vulvar compartment.

For the planning of the regional treatment (Fig. 13.1b), the oT and clinical nodal stages must be known. Clinically suspicious inguinal lymph nodes are an indication for pelvic MRI to evaluate the downstream iliac lymph node regions. For oT1 carcinomas with clinically unsuspicious inguinal regions, radionuclide-guided sentinel lymph node biopsy is an option. Alternatively and in the case of noninformational radioactive marking, anatomically guided superomedial quadrant lymph node dissection is performed (see Chap. 6). With oT1 tumors in the peripheral subcompartment, the inferomedial quadrant should additionally be removed corresponding to the complete first-line lymph node dissection. Since we detected inguinal metastases in two of 14 (14%) pT1a cases, we also recommend sentinel lymph node biopsy for pT1a vulvar carcinomas. oT2 and oT > 2 tumors and all tumors with clinically suspicious lymph nodes are primarily treated with first- and second-line (with respect to the vulvar compartment) lymph node dissection, which includes the superomedial, inferomedial, and superolateral quadrants of the femoral triangle. If the intraoperative frozen section assessment does not find lymph node metastases, regional treatment is accomplished.

When lymph node metastases are histologically confirmed by frozen section assessment, the following further management is recommended: With up to two non-Rosenmüller lymph node metastases and no evidence of pelvic lymph node metastases in the MRI, therapeutic lymph node dissection is completed. A metastatic Rosenmüller node is an indication to extirpate the ipsilateral lacunar nodes. Likewise, the diagnosis of enlarged lymph nodes by MRI in the case of two or more non-Rosenmüller lymph node metastases justifies the incision of the inguinal ligament to excise the pelvic (lacunar) lymph nodes. Multiple (>2) inguinal lymph node metastases excluding the Rosenmüller node are associated with a 10% (three of 30) risk of pelvic (lacunar) metastases referring to both ipsilateral and contralateral sites. According to our results, only in the case of >2 inguinal lymph node metastases the inferolateral quadrant of the superficial inguinal lymph nodes has to be removed for regional tumor control. We never detected metastases in the deep inguinal region. However, this lymph node region may be at risk for metastasis in oT > 2 carcinomas infiltrating deep perineal tissues.

Recommendations for anatomical vulvar reconstruction are compiled in Fig. 13.1c. Arguments for the indication of skin flap reconstruction versus primary wound closure or secondary healing by primary intention are discussed in Chap. 12. Likewise, criteria for the selection of the optimal flap type are given there.

The analysis of surgical complications according to the Clavien-Dindo score [1] of 115 consecutive patients with vulvar carcinoma treated

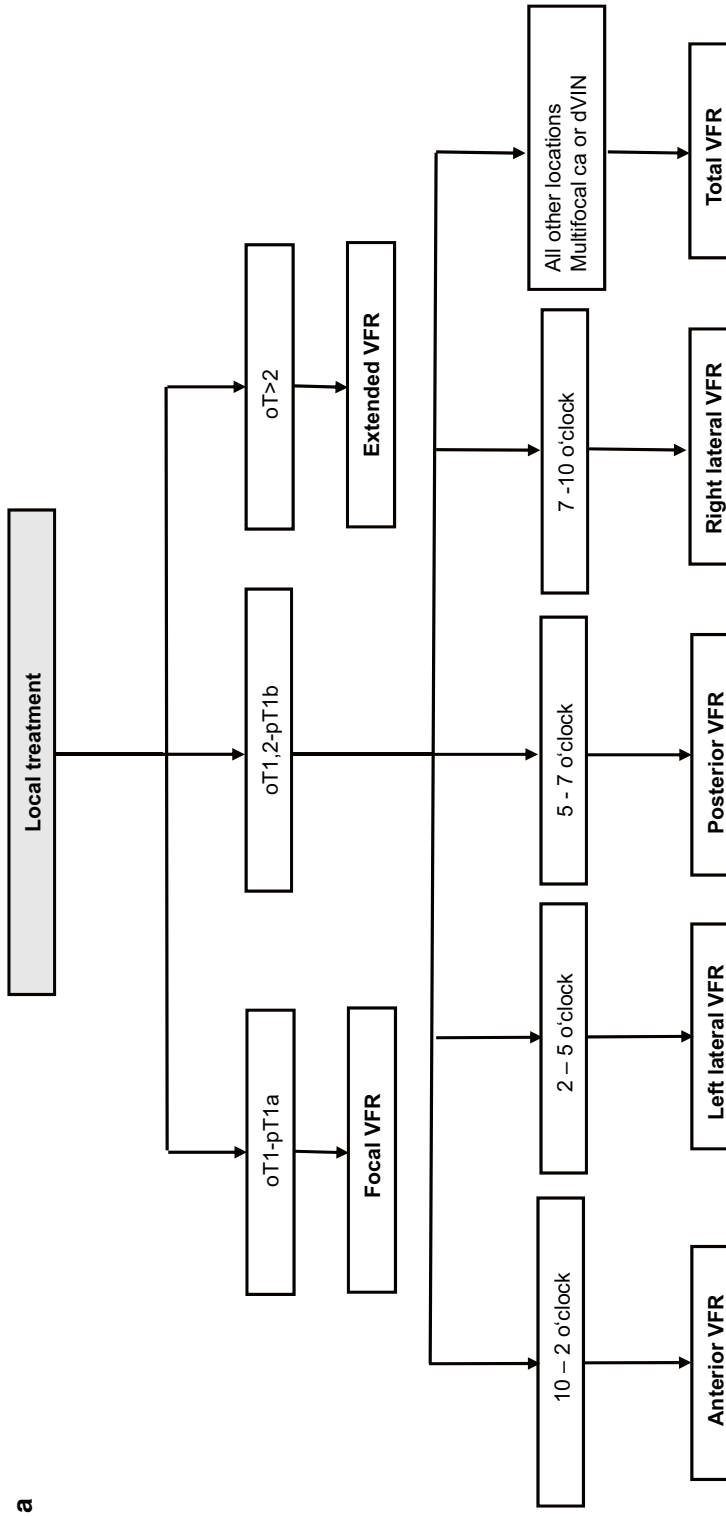

Fig. 13.1 Local (**a**), regional (**b**), and reconstructive (**c**) treatment algorithms for vulvar carcinoma with cancer field surgery. VFR, vulvar field resection; SNL, sentinel node biopsy; FL, SL, TL, first line, second line, third line; IPT, inguinopelvic transition

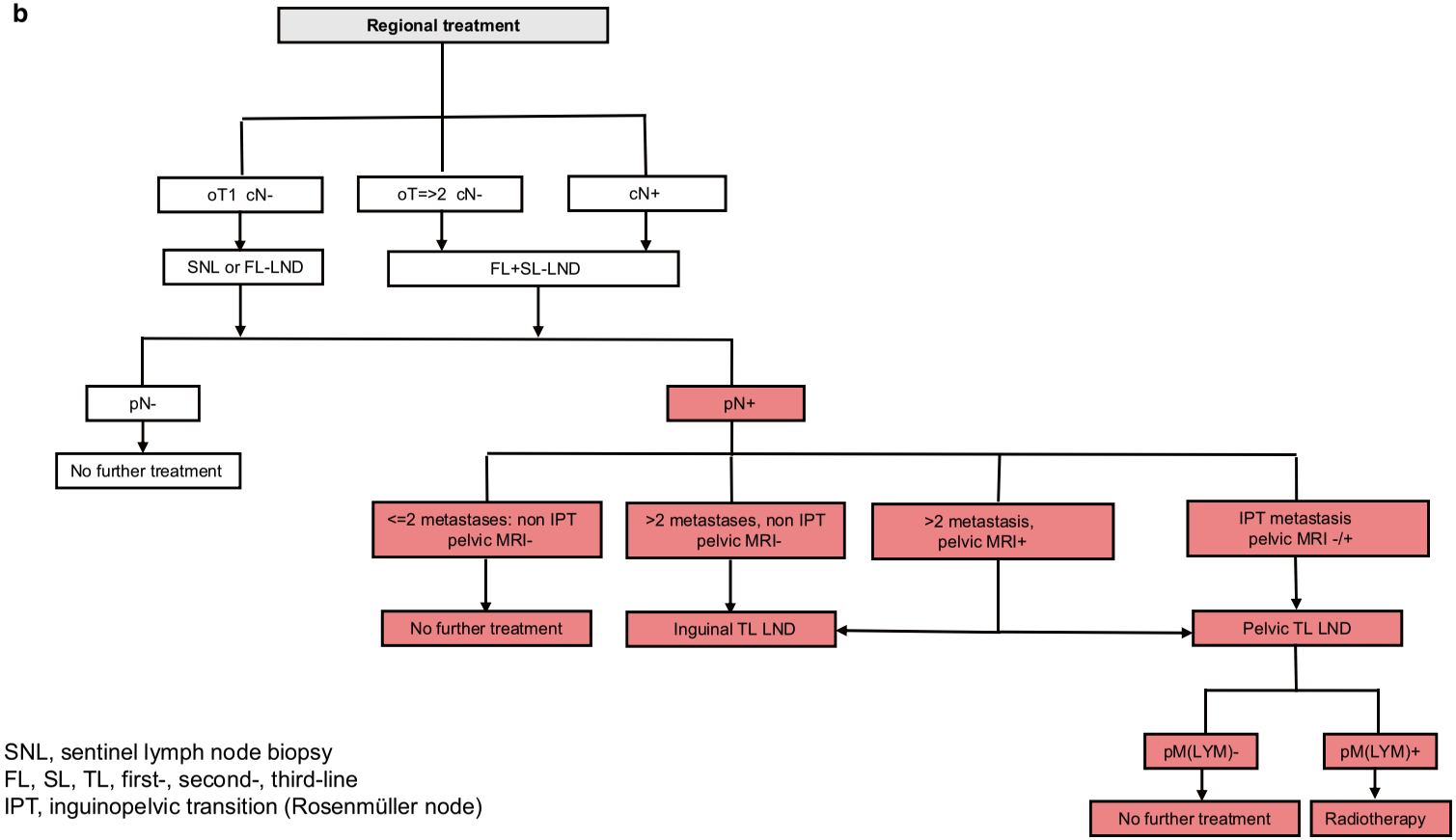

Fig. 13.1 (continued)

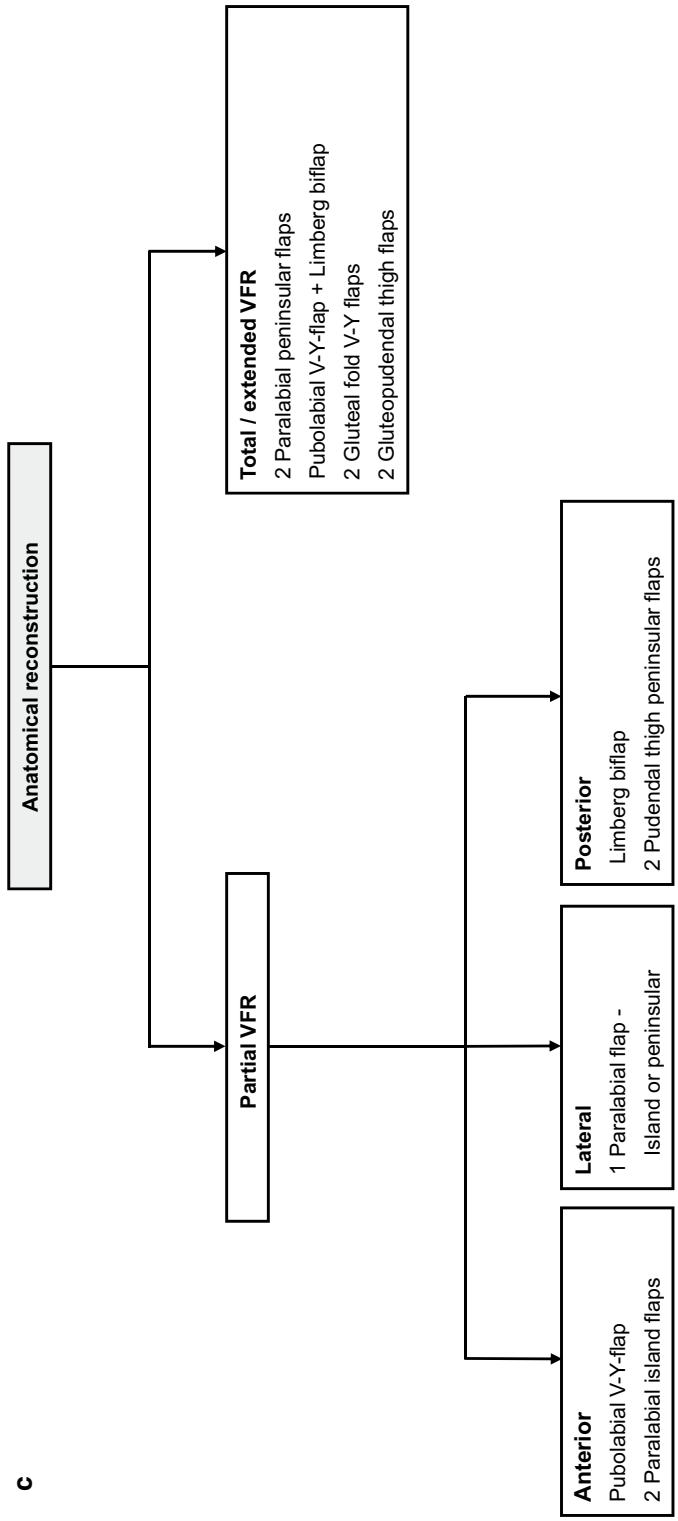

Fig. 13.1 (continued)

with VFR from 2017 to 2023 resulted in 34 patients (30%) without any complication. The most severe (IIIb) complications occurred in 29 (25%) patients. Infectious wound breakdown was the major treatment-related morbidity. Fortunately, secondary healing after this complication did not spoil the functional and aesthetic results in the majority of patients compared to primary healing, although it prolonged the treatment time significantly.

Lymphedema formation in patients who had to undergo therapeutic lymph node dissection because of lymph node metastases cannot be avoided. In our first series of 97 patients, ten patients developed significant and 16 patients moderate lymphedema of the lower limbs [2]. Microsurgical treatment, such as lymphovenous anastomosis or vascularized lymph node transfer [3, 4], which is possible in the unirradiated patient, has been successfully performed in VFR patients.

The analysis of failures performed with 212 consecutive unselected patients treated between 2009 and 2023 with cancer field surgery for vulvar carcinoma oT stages 1–3 at a median follow-up of 56 (34–108) months revealed distant metastases or a distant component in 17 of the 35 patients with known tumor relapses. Locoregional recurrences occurred mainly in disease states characterized by primary carcinomas, with cancer fields exceeding the extent of possible surgical resection. Secondary carcinomas that originated in a cancerization field were observed in six patients. Control of locoregional relapses was achieved in 13 patients with secondary surgery or radiotherapy. Recurrence-free and disease-specific survival at 5 years was 84% (95% CI 79–89) and 88% (95% CI 84–93). For nodal-negative vulvar carcinomas, recurrence-free and disease-specific survival was 94% (95% CI 90–98) and 99% (95% CI 97–100) at 5 years. Nodal-positive patients had recurrence-free and disease-specific survival probabilities of 60% (95% CI 48–74) and 63% (95% CI 51–77) at 5 years. Recurrence-free and disease-specific survival after cancer field surgery without adjuvant radiotherapy is strikingly superior to standard treatment performed under optimal conditions [5].

13.2 Carcinoma of the Vagina

Our experience with conservative (i.e., preservation of bladder and rectum) cancer field surgery of primary vaginal carcinoma is limited to 18 patients. Three patients had carcinomas of the sinus vagina, and in 15 patients, the cancer originated in the suprasinus vagina. Cancer field surgery for the treatment of carcinoma of the sinus vagina was subcompartment resection and inguinal first- and second-line lymph node dissection (see Chap. 11). Patients with carcinomas of the suprasinus vagina underwent abdominoperineal total or extended mesometrial resection (TMMR/EMMR) and immunologic defense line-directed lymph node dissection (iLND) (see Chap. 8). The diagnostic management and treatment directives of the latter correspond to cervix cancer (see below). Preoperative evidence for oT3 and higher stages of the disease excludes a patient from conservative cancer field surgery. Anterior laterally extended endopelvic resection (LEER) would be necessary, which is not indicated if there is a radiotherapeutic option. However, in patients with vaginal carcinoma who had received radiotherapeutic treatment for cervix cancer—representing a significant number of all patients with this disease—LEER may even be mandatory for lower oT stages. This is due to the risk of vesico- or rectovaginal fistula formation if abdominoperineal TMMR is performed. Restoration of the vaginal function is possible for the unirradiated patient. Distal vaginal reconstruction is accomplished with bilateral pudendal thigh flaps (see Chap. 12). Alternatively, split-thickness skin transplants can be applied. Early in our series, we offered the patients sigmoid colon flaps for suprasinus vaginal reconstruction. However, since one out of four patients developed a massive mucosal prolapse, which could not be successfully treated with supporting nets, and finally had her neovagina removed and another patient permanently complained about excessive discharge, we stopped this reconstructive treatment. Five-year disease-specific survival of 15 oT1 and oT2 patients with vaginal carcinoma treated with cancer field surgery was 93% (95% CI 80–100).

13.3 Stage I–II Carcinoma of the Uterine Cervix

Very early stages of cervix carcinoma (i.e., pT1a1, pT1a2, pT1b <2 cm) are usually diagnosed from a cone biopsy. With more advanced tumors, the patients should undergo the diagnostic process as outlined in Chap. 7, including examination under anesthesia with simultaneous pelvic MRI displayed in the operating room. The treatment algorithm for this heterogeneous disease group is shown in Fig. 13.2a. Patients with microinvasive cervix carcinoma pT1a1 without lymph vascular space involvement (L0) are subjected to wide tumor excision by conization if they wish to preserve their uterus. The application of the cancer field model for the fertility-preserving treatment of cervix carcinoma pT1a1; L1, pT1a2; pT1b1, <2 cm demands the determination of the nodal state first. This should be performed as a minimally invasive marker-guided sentinel lymph node biopsy or first-line lymph node dissection (see Chaps. 6 and 8). In the most probable (about 95%) case of nodal negativity, local tumor control through wide excision is boosted by a second conization adjusted to the location of the tumor within the first cone. The resection of the first cone's scar may also eliminate occult cancer cells. The identification of lymph node metastases excludes fertility preservation, rendering the patient a candidate for TMMR. Very early stages of cervix carcinoma allowing conservative treatment are excluded from the prospective mesometrial resection trial. They are not considered here further.

From the principles of cancer field surgery, cervix carcinomas of ontogenetic stages oT1 and 2 are optimal candidates for TMMR as the complete cancer field is surgically removed with this procedure. Patients with oT > 2 cervix cancer can also benefit from TMMR or EMMR, as demonstrated by the clinical results of our series. However, contrary to oT1 and oT2 carcinomas, it is not established how TMMR and EMMR, which do not cover the complete cancer field, compare to chemoradiotherapy in the treatment of oT > 2 cervix carcinoma.

Patients with FIGO (2009) stages IB1–IB2 and IIA1–IIA2 cervix carcinomas, including all cases of pN+ and pT2b states, should undergo cancer field surgery without adjuvant radiation. Vaginal infiltration detectable preoperatively is an indication to perform the colpotomy about 2 cm below the macroscopically identified caudal tumor or to include the complete vagina in the TMMR specimen. The decision for TMMR or EMMR can only be made intraoperatively. Microscopic subepithelial cancer infiltration of the vagina that cannot be noticed preoperatively but can be found out by the pathologist from the frozen section evaluation mandates additional resection of vaginal tissue. Ovariectomy is only indicated in oT > 2 cancers and in the case of multiple lymph node metastases. It is also performed in patients with an established risk for ovarian neoplasms or if they ask for it after having been informed about the potential consequences.

The treatment algorithm for immunologic defense line-directed basin lymph node dissection in oT1 and 2 cervix carcinoma is presented with Fig. 13.2b. It is based on the tumor size and intraoperative findings of the first-line lymph nodes. In case of metastases in the latter, the nodal state of the aortic bifurcation determines the further management (see below). As mentioned earlier (Chaps. 6 and 7), all intercalated lymph nodes at risk for metastases for oT1 and 2 cervix carcinomas are resected with TMMR/EMMR. If pre- or intraoperative diagnostics confirm an oT > 2 stage, lymph node dissection always includes the first- and second-line basin lymph node regions, as well as the resection of the aortic bifurcation nodes as an upstream third-line region. In the case of metastasis in the latter region, complete mesenteric and lumbar periaortic (third-line) lymph node dissection is performed (see Chap. 6). Subserous and serous tumor infiltration of the uterine corpus mandates the resection of infundibulopelvic ligaments with the ovarian vessels up to their origins, respectively estuaries, as well as mesenteric periaortic lymph node dissection.

The treatment-related complications of TMMR and iLND assessed for the first 357 FIGO stage IB and IIA cervix carcinoma patients with the Franco-Italian glossary [6] include 58 (16%) moderate and ten (3%) severe events [7]. EMMR and iLND treatment was associated with a higher

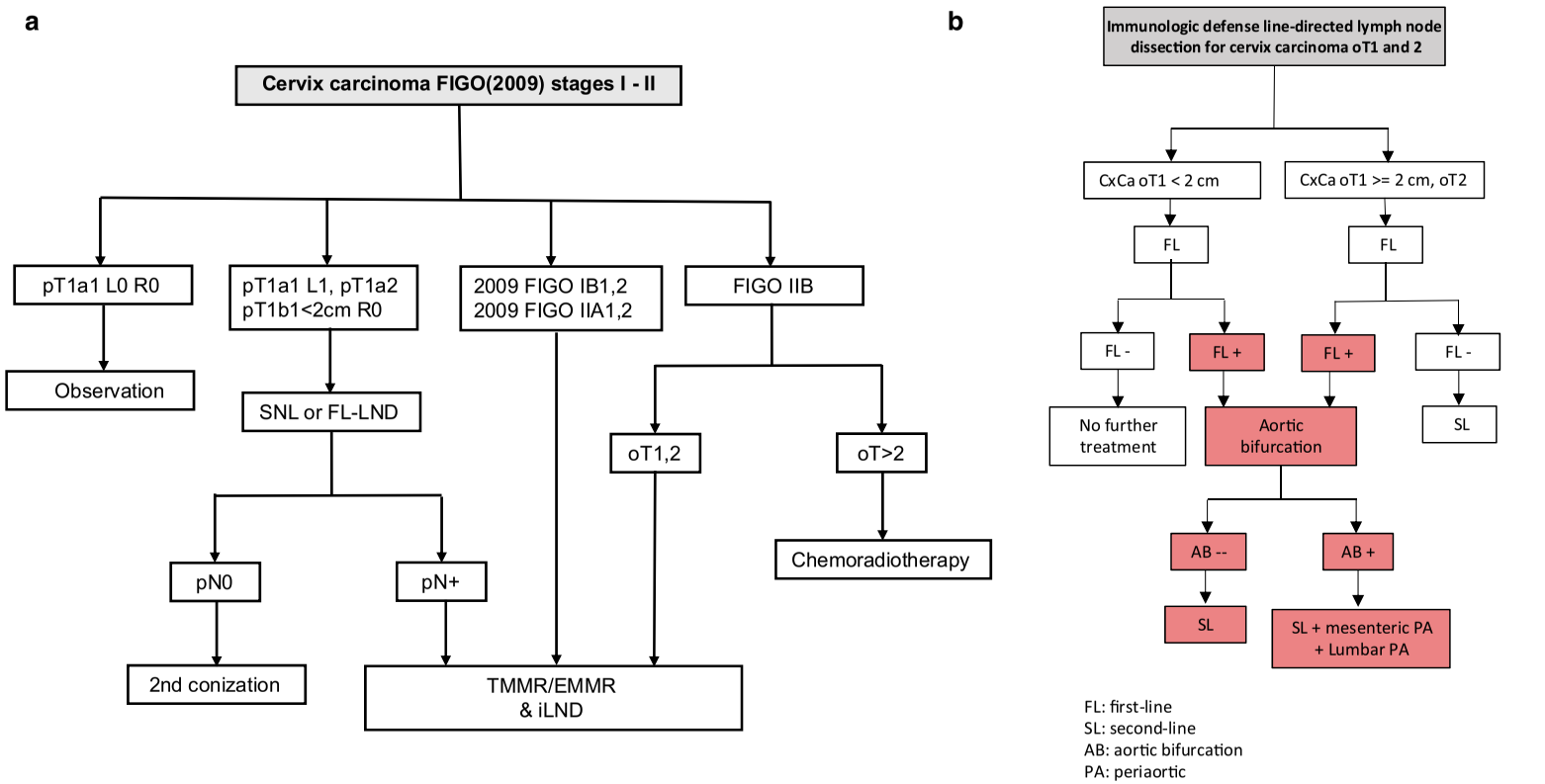

Fig. 13.2 (**a**) Treatment recommendations for patients with cervix carcinoma FIGO (2009) stages I–II according to the cancer field model. (**b**) Immunologic defense line-directed lymph node dissection algorithm for cervix carcinomas oT1 and 2. TMMR/EMMR, total/extended mesometrial resection; *SNL* sentinel node biopsy, *FL, SL* first line, second line, *iLND* immunologic defense line-directed lymph node dissection, *PA* periaortic

rate of complications (34% moderate, 4% severe) [8]. The moderate and severe urinary complications of TMMR could be reduced to 1% with increased experience. Leg edema is the most significant complication of cancer field surgery for cervix carcinoma. A retrospective investigation of 100 representative patients treated with TMMR/EMMR and iLND revealed stage 1 grade 1 edema in 43 patients and stage 1 grade 2 edema in 12 patients. Two patients had stage 2 edemas [9]. As with the patients who underwent iLND for vulvar carcinoma, improvements in coping with leg edema are also expected for these patients from the new microsurgical procedures.

Patients with FIGO stages IB and IIA cervix carcinomas strongly benefit from cancer field surgery without radiotherapy as compared to traditional treatment, including postoperative chemoradiation. This has been substantiated by an analysis of large patient cohorts from Sweden and Germany.

Five-year disease-free survival of patients with FIGO stage IB and IIA low-risk tumors (pT1b1, 2a, pN0) at a median follow-up period of 129 months (74–187) was 96.6%, $n = 173$. The corresponding high-risk cohort (pT2b, pN1) had a 5-year overall survival rate of 89.4% (82.7–96.6), $n = 101$ [10]. Patients with FIGO stage IB3 cervix carcinoma had a 92.1% (85–99.8) overall survival rate at 5 years, $n = 53$. Five-year recurrence-free and overall survival of early-stage cervical carcinoma with FIGO 2009 stage IB1 and IIA1 was 91.2% and 93.3% in the TMMR cohort versus 81.8% and 90.3% in the cohort receiving standard treatment ($p = 0.002$ and $p= 0.034$) [10]. The first survival analysis of a European multicenter study based on 116 patients with cervix carcinoma FIGO (2009) stages IB–IIA, followed for a median observation period of 24 months (6–80), confirmed the results from Leipzig University [11].

In our patient series, FIGO stage IIB cervix carcinomas represent oT1–2 and oT > 2 stages in 39% and 61% of the cases, respectively. Five-year overall survival was 84% (74–96) for oT1–2 cases. It dropped to 59% (48–73) for oT > 2 cases in line with the cancer field model, which indicates that the cancer fields of these stages exceed the extent of the surgical treatment [7].

Current diagnostic means, including pelvic MRI, are not accurate enough to distinguish oT1–2 from oT > 2 carcinomas of FIGO stage IIB. We have established criteria based on clinical and MRI findings, to be tested prospectively for this discrimination. Until this diagnostic dilemma is settled, we inform the patients with FIGO IIB cervix carcinomas about the uncertainties and provide counseling and eventual treatment by the radio-oncologist.

Analysis of the type of relapse based on the complete follow-up of 589 unselected consecutive patients treated for cervix carcinoma FIGO (2009) stages IB–IIB with TMMR/EMMR and iLND revealed 39 (6.6%) pelvic, 23 (3.5%) pelvic and distant, and 33 (5.9)% distant recurrences at a median observation time of 73 months (IQR 47–135). The majority of pelvic recurrences originated from the discontinuous spread of cancer cells, rendering the importance of resection margins neglectable with cancer field surgery, which achieved R0 state in >99%. The pathoanatomy of the pelvic recurrences confirmed the model of ontogenetic cancer fields that has been elaborated from the primary tumors. Forty percent of the patients with pelvic recurrences could be saved, mainly by chemoradiotherapy.

13.4 Carcinoma of the Endometrium

The therapeutic management of endometrial carcinoma according to the cancer field model is directed by pre- and intraoperative diagnostic findings (see Chaps. 7 and 9). Both conventional and ontogenetic local tumor staging systems are important here. According to arguments given in Chap. 9, the minimally invasive approach by robotic assistance is advantageous for the treatment with peritoneal mesometrial resection (PMMR) in the majority of endometrial carcinoma patients. Only types B and AB PMMR are currently considered to be optimally performed through a midline laparotomy.

As with the other gynecologic cancer entities, cancer field surgery of endometrial carcinoma should completely dispense with adjuvant radiotherapy for locoregional tumor control. Systemic treatment respecting molecular markers is important for oT4 disease with peritoneal carcinosis, which is, however, outside the scope of cancer field surgery discussed here. Likewise, any adjuvant systemic therapy is not considered in this context.

Suspected endometrial carcinoma is verified by histopathological assessment of tissue extracted from the uterine cavity and cervical canal by hysteroscopy and curettage during the examination under anesthesia (see Chap. 7). Gynecologic inspection, palpation, and assessment with ultrasound, as well as biopsies from additional sites, such as cervical stroma or vagina, complete the diagnostic procedure. If these findings indicate significant infiltration of the cervical stroma, pT3b stage (i.e., tumor involvement of the parametria or vagina), peritoneal carcinosis, or lymph node macrometastases, further diagnostic information by pelvic MRI with T2-weighted transverse and sagittal scans should be obtained.

The local treatment algorithm for endometrial carcinoma applying cancer field surgery is shown in Fig. 13.3a. Deep (>50%) cervix stroma infiltration and parametrial or vaginal infiltration may demand cancer field surgery to be performed as an open procedure. Otherwise—representing the vast majority of the patients with endometrial carcinoma—the procedures are executed endoscopically with robotic assistance. Peritoneal exploration, in the case of suspicious findings supplemented by frozen section histopathologic assessment, is the next diagnostic step. If tumor infiltration of subserosal or serosal tissues can be excluded clinically, standard PMMR should be done. Proven infiltration of any part of the genital peritoneum (see Chap. 7) corresponding to an oT3a stage demands type A extended PMMR. This procedure also removes the peritoneal tissues of the oT3b cancer field and may achieve local tumor control. However, tumor infiltration of the intestinal (including omental) and parietal peritoneum, which represents an oT4 stage, is no longer compatible with this goal. Patients with oT4 disease are no candidates for cancer field surgery but may benefit from surgical cytoreduction.

Regarding regional tumor control, cancer field surgery aims to be diagnostic, and in the case of histologically proven lymph node metastasis, it is therapeutic as well. Figure 13.3b demonstrates the treatment algorithm. For the rare situation of endometrial carcinoma exhibiting large-volume lymph node metastases or metastatic conglomerates demonstrated with pelvic MRI or abdominal CT, laparotomy is preferred. Immunologic defense line-directed lymph node dissection (iLND) is then performed according to the algorithm for cervix carcinoma (Fig. 13.2b). The vast majority of endometrial cancer patients do not present large-volume lymph node metastases, allowing endoscopic surgery for regional tumor control, which is performed as lymph collector-guided pelvic first-line lymph node dissection in all cases and gonadomesenteric lymph node dissection if the genital peritoneum appears to be involved at intraoperative inspection. If lymph node metastases are histologically proven in these first-line regions, complete resection of the second-line and eventually third-line nodes is carried out as indicated for cervix cancer (Fig. 13.2b).

The first results of cancer field surgery for the locoregional control of endometrial carcinoma have been published with 51 patients [12]. Follow-up of 135 patients who received PMMR and lymph collector-guided first-line node dissection eventually extended to iLND at a median observation time of 27.5 months showed an overall recurrence rate of 8.1%, with only two (1.5%) locoregional relapses. The rate of postoperative irradiation, which would have been 50.4% according to international guidelines, could be reduced to 10.4%. Overall survival was 97.2% for patients with FIGO I and II and 88.5% for FIGO III and IV carcinomas. Intraoperative complications for the 135 procedures included one vessel lesion, one bladder lesion, and six bowel lesions, five of which were only serosal defects. No conversion to laparotomy was mandatory. Postoperative complications, graded according to the Clavien-Dindo score, were nine (6.7%) grade I, nine (6.7%) grade II, five (3.7%) grade III, one (0.7%) grade IV, and one (0.7%) grade V. The

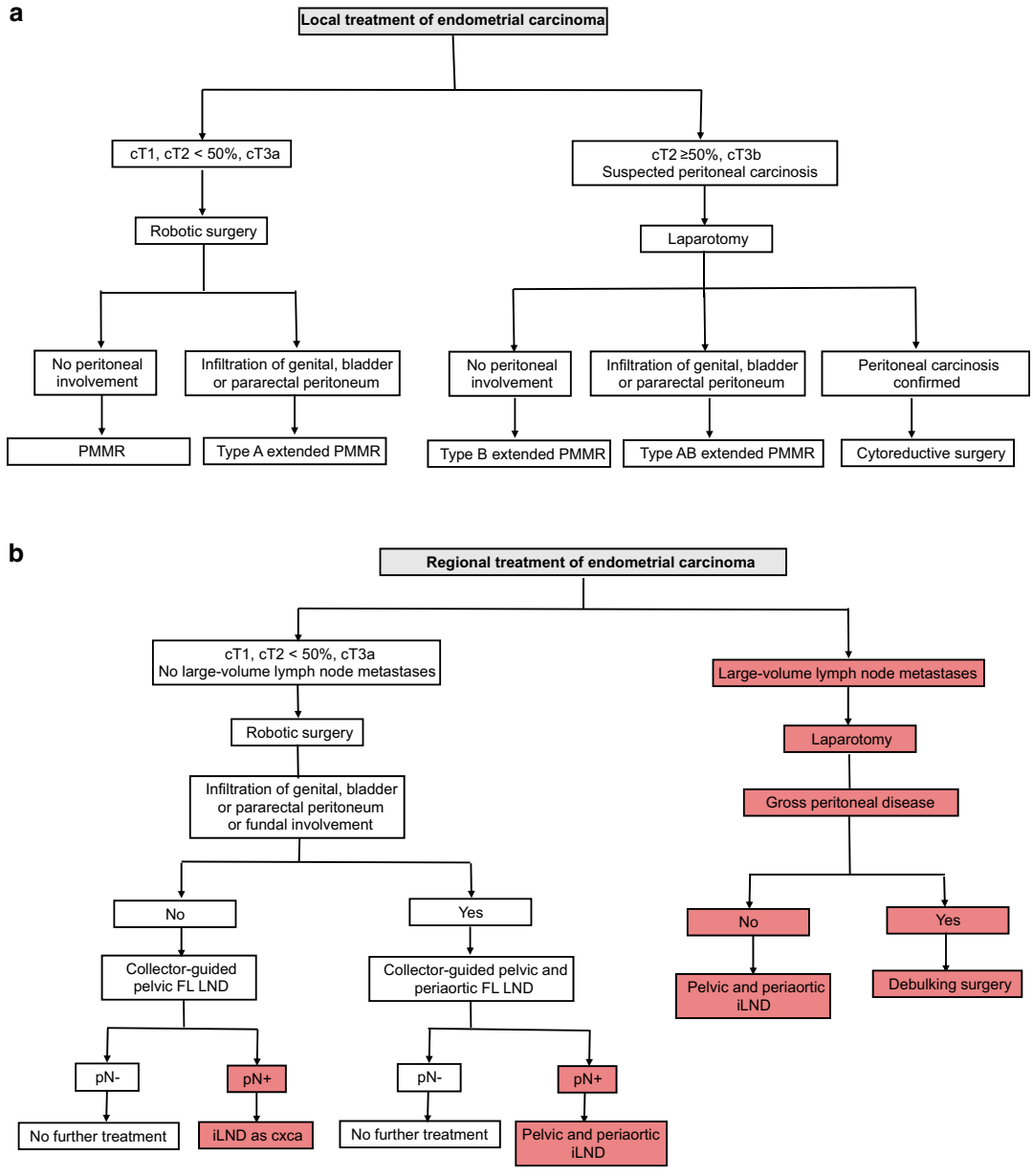

Fig. 13.3 Treatment recommendations for patients with endometrial carcinoma according to the cancer field model. (**a**) Local treatment. (**b**) Regional treatment. *PMMR* peritoneal mesometrial resection, *FL* first line, *iLND* immunologic defense line-directed lymph node dissection

majority of postoperative complications were caused by infection, with only one patient exhibiting impaired wound healing.

13.5 Locally Advanced Cervicovaginal Carcinoma

Ascertaining whether a patient suffering from locally advanced cervicovaginal carcinoma would benefit from multivisceral cancer field surgery, such as anterior or total (anteroposterior) laterally extended endopelvic resection (LEER), demands the following:

- Accurate information about the patient's medical history, particularly details of previous cancer treatment in patients with recurrences.
- Ontogenetic locoregional tumor staging by examination under anesthesia and high-resolution MRI displayed during an examination, as described in Chap. 7.
- Whole-body screening for distant metastases, e.g., with positron emission tomography-computed tomography (PET-CT).
- Detailed counseling of the patient, considering the procedure, postoperative course, treatment-related morbidity, and curative chance.

The general criteria we have set up to offer treatment with LEER to a patient are as follows:

- Achievement of locoregional tumor control with a significant chance of cure.
- No radiotherapeutic treatment alternative.
- The patient's presumed ability to cope with the treatment sequelae.

These conditions are met for nonfragile, motivated patients with pelvic recurrences or secondary primaries of cervicovaginal carcinoma after pelvic irradiation, as specified below. Unirradiated patients exhibiting FIGO IVA tumors with an existing or high probability of developing urinary or fecal fistulas are potential candidates as well. Alternatively, primary IVA cancers may undergo chemoradiation after surgical urinary and/or fecal diversion. The existing clinical data do not allow a conclusion on the superiority of LEER or radiotherapy after diversion in these cases. Distant metastases have to be excluded in all patients to be considered for LEER treatment.

As described in Chap. 10, LEER procedures remove the complete cancer fields of oT3a and oT3b cervicovaginal cancers. Patients with oT4 carcinomas are eligible for cancer field surgery if the tumor invasion of somatic pelvic tissues, i.e., fascio-musculo-skeletal and parietal neurovascular structures, can be excluded. Both hydronephrosis and tumor fixation to the pelvic wall are not per se indicative of somatic involvement. However, sciatic pain and malignant leg edema are clinical correlates of somatic tumor involvement. Tumor infiltration of somatic pelvic tissues has to be proven by MRI (Figs. 7.18 and 7.19). Lymph node metastases, both in the pelvis and in the periaortic regions, decrease but do not completely abolish the patient's chance to be cured with LEER (see below).

LEER is planned to be an anterior or total (anteroposterior) procedure based on the diagnostic findings. Anterior LEER is indicated for oT3a cancers and total LEER for oT3b/4 cancers without infiltration of somatic pelvic wall tissues (Fig. 13.4).

As deduced from the regional cancer field model, complete first-, second-, and third-line lymph node dissection has to be combined with LEER treatment for regional tumor control in advanced ontogenetic stages. Whereas LEER can be executed step-by-step as described in Chap. 10 for postirradiation and primary disease states, previous surgical locoregional therapy may have significantly changed the peritoneal, retroperitoneal, and subperitoneal anatomy. The surgeon is forced to adapt the locoregional treatment goals to the massively disturbed anatomical situation. Very often, tissue mobilization can only be achieved by means of periosteal dissectors.

Options for the restoration of vital pelvic functions, i.e., micturition and defecation, depend mainly on the pretreatment—particularly whether the patient had received pelvic and periaortic irradiation—and on the experience of the multidisciplinary surgical team.

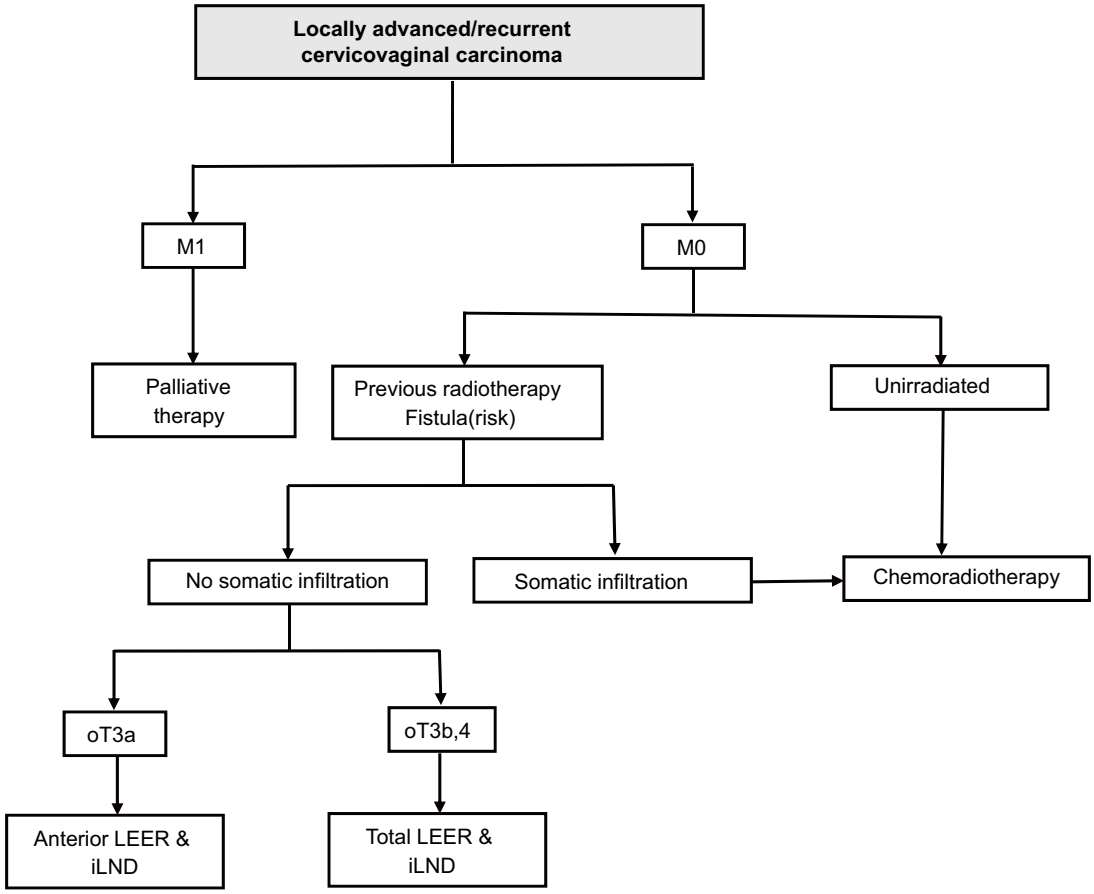

Fig. 13.4 Treatment recommendations for locally advanced and recurrent cervicovaginal carcinoma according to the cancer field model. *LEER* laterally extended endopelvic resection, *iLND* immunologic defense line-directed lymph node dissection

LEER leads to significant treatment-related morbidity, mainly with regard to reconstructive procedures. The treatment of 100 patients with cervicovaginal carcinoma was associated with 53% moderate and 7% severe complications. Five-year disease-specific survival was 50% (40–62) at a median follow-up of more than 10 years. Survival was not significantly different for primary or recurrent disease states and with or without tumor fixation at the pelvic wall. Lymph node metastases dropped 5-year survival to 27% (15–49), irrespective of their location. The survival of the 51 patients in the cohort who had no therapeutic alternative to LEER treatment was 46% (34–62) [13].

References

1. Dindo D, Demartines N, Clavien P-A. Classification of surgical complications. A new proposal with evaluation in a cohort of 6336 patients and results of a survey. Ann Surg. 2004;240:205–13. https://doi.org/10.1097/01.sla.0000133083.54934.ae.
2. Höckel M, Trott S, Dornhöfer N, Horn L-C, Hentschel B, Wolf B. Vulvar field resection based on ontogenetic cancer field theory for surgical treatment of vulvar carcinoma: a single-Centre, single-group, prospective trial. Lancet Oncol. 2018;19:537–48. https://doi.org/10.1016/S1470-2045(18)30109-8.
3. Lin WC, Safa B, Buntic RF. Approach to lymphedema management. Semin Plast Surg. 2022;36:260–73. https://doi.org/10.1055/s-0042-1758691.
4. Meuli JN, Guiotto M, Elmers J, Mazzolai L, di Summa PG. Outcomes after microsurgical treatment of lymphedema: a systematic review and meta-

analysis. Int J Surg. 2023;109:1360–72. https://doi.org/10.1097/JS9.0000000000000210.
5. Te Grootenhuis NC, van der Zee AGJ, van Doorn HC, van der Velden J, Vergote J, Zanagnolo V, et al. Sentinel nodes in vulvar cancer: long-term follow-up of the GROningen international study on sentinel nodes in vulvar cancer (GROINSS-V). Gynecol Oncol. 2016;140:8–14. https://doi.org/10.1016/j.ygyno.2015.09.077.
6. Chassagne D, Sismondi P, Horiot JC, Sinistrero G, Bey P, Zola P, et al. A glossary for reporting complications of treatment in gynecological cancers. Radiother Oncol. 1993;26:195–202. https://doi.org/10.1016/0167-8140(93)90260-F.
7. Höckel M, Wolf B, Schmidt K, Mende M, Aktas B, Kimmig R, et al. Surgical resection based on ontogenetic cancer field theory for cervical cancer: mature results from a single-Centre, prospective, observational, cohort study. Lancet Oncol. 2019;20:1316–26. https://doi.org/10.1016/S1470-2045(19)30389-4.
8. Wolf B, Ganzer R, Stolzenburg J-U, Hentschel B, Horn L-C, Höckel M. Extended mesometrial resection (EMMR): surgical approach to the treatment of locally advanced cervical cancer based on the theory of ontogenetic cancer fields. Gynecol Oncol. 2017;146:292–8. https://doi.org/10.1016/j.ygyno.2017.05.007.
9. Höckel M, Horn L-C, Tetsch E, Einenkel J. Pattern analysis of regional spread and therapeutic lymph node dissection in cervical cancer based on ontogenetic anatomy. Gynecol Oncol. 2012;125:168–74. https://doi.org/10.1016/j.ygyno.2011.12.419.
10. Falconer H, Norberg-Hardie A, Salehi S, Alfonzo E, Weydandt L, Dornhöfer N, et al. Oncologic outcomes after total mesometrial resection (TMMR) or treatment according to current international guidelines in FIGO (2009) stages IB1-IIB cervical cancer: an observational study. The Lancet eClinicalMedicine. 2024;73:102696. https://doi.org/10.1016/j.eclinm.2024.102696.
11. Buderath P, Stukan M, Ruhwedel W, Strutas D, Feisel-Schwickardi G, Wimberger P, et al. Total mesometrial resection (TMMR) for cervical cancer FIGO IB-IIA: first results from the multicentric TMMR register study. J Gynecol Oncol. 2022;33:e9. https://doi.org/10.3802/jgo.2022.33.e9.
12. Buderath P, Rusch P, Mach P, Kimmig R. Cancer field surgery in endometrial cancer: peritoneal mesometrial resection and targeted compartmental lymphadenectomy for locoregional control. J Gynecol Oncol. 2021;33:e7. https://doi.org/10.3802/jgo.2021.32.e7.
13. Höckel M, Wolf B, Hentschel B, Horn L-C. Surgical treatment and histopathological assessment of advanced cervicovaginal carcinoma: a prospective study and retrospective analysis. Eur J Cancer. 2017;70:99–110. https://doi.org/10.1016/j.ejca.2016.10.016.

Epilogue: The Paradox and the Order of Cancer: Clues from the Ontogenetic Cancer Field Model

The ontogenetic cancer field model outlined in this book was deduced from topographical data of human developmental anatomy and from the pathoanatomy of more than 1000 gynecologic carcinomas. The model claims general validity and is very briefly discussed in a broader context in this epilogue.

The cancer field model for locoregional propagation of carcinomas can be summarized in ten theses:

1. Multicellular animals develop from one totipotent immature cell. Cancer, a universal disease of multicellular animals, develops from one transformed mature cell, suggesting common biological mechanisms of morphogenesis and tumorigenesis.
2. The development of multicellular animals can be described by a pedigree of branched trajectories of cell type differentiation from the zygote to the many cell types of the mature organism. Each step during the differentiation pathway is represented by a temporarily stable cell type with increased specificity at the cost of reduced plasticity compared to its preceding cell type.
3. A cell type and its habitat, i.e., the anatomically distinct environment of its population, exhibit a circular relationship: the cell type generates its habitat and the habitat dictates the cell type. The fixed relation between a cell type and its anatomical location mandates a cell type-specific topoanatomical identity. However, the plasticity of immature cell types, which enables the transdifferentiation of a cell type upon contact with adjacent habitats of other cell types, extends their permissive territory to a morphogenetic field encompassing several cell type habitats.
4. Cell type de-differentiation followed by redifferentiation is a canonical response of multicellular organisms to tissue injury or disruption of tissue homeostasis.
5. Persistent uncontrolled proliferation of the transformed mature cell type (cancer cell) causes permanent disturbance of tissue homeostasis ("non-healing wound"), which induces de-differentiation of the cells at the site of damage including the cancer cells themselves. De-differentiation of the cancer cells extends their permissive territory by decreasing the topoanatomical specificity and thus increases the magnitude of tissue disturbance, which triggers further cancer cell de-differentiation. This vicious circle represents the malignant progression of cancer leading to the death of the organism, unless halted by therapeutic intervention. The de-differentiation response of cancer cells in order to repair the disrupted homeostasis exaggerates their destructive potential representing the *cancer paradox.*
6. Like de-differentiation for tissue repair, pathological de-differentiation during malignant progression reverses the cell type differentiation trajectory of the transformed cells and their topoanatomical identity. However, the

M. Höckel et al., *Cancer Field Surgery in Gynecologic Oncology*,
https://doi.org/10.1007/978-3-031-83030-3

conserved sequence of states during differentiation and de-differentiation establishes a *principle of order.*

7. The order of cancer cell de-differentiation brings about a spatial order of tissues permissive for local tumor spread, i.e., cancer fields. The topography of these cancer fields is determined by the mature derivatives of the morphogenetic fields during the differentiation trajectory of the corresponding normal cell type.
8. As a consequence of the local tissue damage caused by the solid cancer, both peripheral autoantigens and tolerized tumor antigens are presented in the draining regional (first-line) lymph nodes initiating priming, activation, and clonal proliferation of cognate regulatory T cells (Tregs). In the lymph node, the primed Tregs are imprinted with the topoanatomical information of the tumor bed.
9. Proliferating Tregs transmit the topoanatomical information related to their cognate antigens in complementary form to the lymph node environment, including the extracellular matrix, and equips the draining lymph node with focal cancer fields, which can be exploited for proliferation by transformed epithelial (carcinoma) cells with the corresponding topoanatomical identity.
10. Tolerized tumor antigens of a lymph node metastasis are presented to the downstream (second-line) lymph node and activate Treg memory cells with the topoanatomical information of the local tumor. Thus, the cancer field is also extended to the second-line lymph node enabling further regional metastases.

Putative Biological Mechanisms: Transitions of Gene Regulatory Networks

The cell as the smallest living unit in the multicellular animal comprises a multilayered gene regulatory network (GRN) dynamically interacting with the cellular and extracellular environment during its lifetime [1]. Functional network layers or modules include a myriad of biological programs of information processing [2]. During the development from the zygote to the mature cell type, the GRN transits through distinct temporarily stable inheritable epigenetic states.

Continuous cell proliferation, migration, and cell death as driving forces of ontogenesis change the number of cells in a particular environment. This destabilizes the current GRN state of a cell type and moves it towards a new state, increasing the spatial order and complexity at the cost of lower plasticity for territorial colonization during the developmental period. Cell type differentiation continues to the exhaustion of its potential, which characterizes the mature cell type in homeostasis.

Tissue injury disrupts the anatomical homeostasis and destabilizes the GRN states of mature cell types at the site of damage. Temporary stabilization is achieved by de-differentiation to a conserved previous state of increased plasticity and decreased specificity. The extent of cell type de-differentiation and subsequent re-differentiation accompanied by controlled cell division depends on the magnitude of tissue injury and on the species.

Progressive tissue injury due to unrestricted proliferation of a transformed cell type causes permanent destabilization of the cancer cell's GRN. Its temporarily stable states are driven towards greater immaturity exhibiting more and more plasticity. As a consequence, more and more tissues are prone to the destructive activities of the cancer cells.

In a more abstract view, the model of ontogenetic cancer fields can be conceived as describing a self-organizing complex adaptive system during the construction process. In a stepwise trajectory, the system gains order whereas the constructive potential decreases. The process continues until exhaustion of the finite constructive potential, which marks the completeness of the construction at maximum order.

A damage of the completed system will perturb the state of maximum order. If the system is not destroyed altogether, it has to regain constructive potential. Reversing the stepwise

trajectory of the construction process restores a finite constructive potential.

Supramolecular substrate of the gene regulatory system is the 3D organized genome, termed chromatin, a complex hierarchy including nucleosome-entwisted methylated DNA at increasing scales: folded in loops and aggregations, topologically associated domains (TADs), euchromatin and heterochromatin compartments, and finally chromosomes adhering to the nucleic lamina [3–5].

Gene regulation in multicellular animals is linked to the state of 3D chromatin conformation by the approximation of distant enhancers to promoters in the presence of transcription factors and non-coding RNAs [6]. Transitions in the differentiation trajectory of a cell type are associated with global changes in the 3D chromatin conformation. These manifest themselves predominantly at the level of the TADs, which are translocated between heterochromatin and euchromatin compartments [7–10]. As a result of these epigenetic mechanisms of cell type differentiation, genetic programs that are demanded for alternative cell fates and positions are suppressed and programs for distinct cellular functions, for the placement at distinct anatomical locations, and for morphogenetic actions are activated. Cell type de-differentiation for tissue repair and regeneration in normal cells and paradoxically in transformed cells during malignant progression follows from the reversal of these conserved epigenetic states. Heterochromatin and euchromatin compartments are translocated to their previous positions increasing cell type plasticity and widening the permissive territory.

The reactivation of developmental programs during malignant progression has been demonstrated by transcriptome analyses of human cancer [11–13]. Moreover, cancer initiation through epigenetic alterations during development without mutation of genes has been experimentally achieved in Drosophila [14].

Although our work is not based on molecular and supramolecular clues, the apparent association between epigenomic state transitions during development, regeneration, and malignant tumors in multicellular animals strongly supports the topological link between the developmental anatomy and the pathoanatomy of carcinoma propagation, which is the foundation of the ontogenetic cancer field paradigm. As shown for gynecologic cancers in this book, the clinical translation of the cancer field model into ontogenetic anatomy, ontogenetic staging, cancer field surgery, and immunologic defense line-directed lymph node dissection holds great potential for further success in the fight against malignant solid tumors.

References

1. Kauffman S. Homeostasis and differentiation in random genetic control networks. Nature. 1969;224:177–8. https://doi.org/10.1038/224177a0.
2. Erwin DH, Davidson EH. The evolution of hierarchical gene regulatory networks. Nat Rev Genet. 2009;10:141–8. https://doi.org/10.1038/nrg2499.
3. Bonev B, Cavalli G. Organization and function of the 3D genome. Nat Rev Genet. 2016;17:661–78. https://doi.org/10.1038/nrg.2016.112.
4. Lieberman-Aiden E, van Berkum NL, Williams L, Imakaev M, Ragoczy T, Telling A, et al. Comprehensive mapping of long-range interactions reveals folding principles of the human genome. Science. 2009;326:289–93. https://doi.org/10.1126/science.1181369. https://www.science.org/toc/science/326/5950.
5. Stevens TJ, Lando D, Basu S, Atkinson LP, Cao Y, Lee SF, et al. 3D structures of individual mammalian genomes studied by single-cell hi-C. Nature. 2017;544:59–64. https://doi.org/10.1038/nature21429.
6. Heinz S, Romanoski CE, Benner C, Glass CK. The selection and function of cell type-specific enhancers. Nat Rev Mol Cell Biol. 2015;16:144–54. https://doi.org/10.1038/nrm3949.
7. Dixon JR, Jung I, Selvaraj S, Shen Y, Antosiewicz-Bourget JE, Lee AY, et al. Chromatin architecture reorganization during stem cell differentiation. Nature. 2015;518:331–6. https://doi.org/10.1038/nature14222.

8. Nicetto D, Donahue G, Jain T, Peng T, Sidoli S, Sheng L, et al. H3K9me3-heterochromatin loss at protein-coding genes enables developmental lineage specification. Science. 2019;363:294–7. https://doi.org/10.1126/science.aau0583.
9. Stadhouders R, Filion GJ, Graf T. Transcription factors and 3D genome conformation in cell-fate decisions. Nature. 2019;569:345–54. https://doi.org/10.1038/s41586-019-1182-7.
10. Yadav T, Quivy J-P, Almouzni G. Chromatin plasticity: a versatile landscape that underlies cell fate and identity. Science. 2018;361:1332–6. https://doi.org/10.1126/science.aat8950.
11. Ge Y, Gomez NC, Adam RC, Nikolova M, Yang H, Verma A, et al. Stem cell lineage infidelity drives wound repair and cancer. Cell. 2017;169:636–50. https://doi.org/10.1016/j.cell.2017.03.042.
12. Pomerantz MM, Qiu X, Zhu Y, Takeda DY, Pan W, Baca SC, et al. Prostate cancer reactivates developmental epigenomic programs during metastatic progression. Nat Genet. 2020;52:790–9. https://doi.org/10.1038/s41588-020-0664-8.
13. Sharma A, Blériot C, Currenti J, Ginhoux F. Oncofetal reprogramming in tumour development and progression. Nat Rev Cancer. 2022;22:593–602. https://doi.org/10.1038/s41568-022-00497-8.
14. Parreno V, Loubiere V, Schuettengruber B, Fritsch L, Rawal CC, Erokhin M, et al. Transient loss of Polycomb components induces an epigenetic cancer fate. Nature. 2024;629:688–96. https://doi.org/10.1038/s41586-024-07328-w.

Glossary

Specific Terms[1]

Cell type—cytotype—differentiation trajectory—determination A *cell type* of a multicellular animal is characterized by a (temporarily) stable somatically inheritable epigenetic state of the cellular genome, specific for an individual organism. All mature cell types of the organism develop from the fertilized egg (zygote) cell through branched *trajectories* of states of *cell type differentiation* with increasing functional specificity and decreasing plasticity. Likewise, each state of cell type differentiation exhibits linear or branched *cytotype* differentiation trajectories towards increased specificity and decreased plasticity. Cytotypes at increasing states of differentiation comprise stem cells, progenitor cells, and terminally differentiated cells. However, cell types may also exist exclusively as differentiated cytotypes. When a cell type trajectory has reached the state of *determination*, the cell type's potential of trans-differentiation into another cell type when facing a corresponding microenvironment abrogates. The branched cell type differentiation trajectory proceeds until anatomical maturity. Overall, post-phylotypic cellular development in a multicellular animal organism occurs at two phases—pre-determination and post-determination—and at two scales: cell type and cytotype.

Habitat—topoanatomical identity and plasticity—morphogenetic field—compartment—subcompartment—ontogenetic anatomy—topoanatomical code At each state of development, the population of a (pattern forming) cell type generates its *habitat* at a distinct anatomical location of the organism. This *topoanatomical identity* is established by interaction with the microenvironment and is memorized by the cell type and the habitat. Prior to determination, cells of a distinct cell type exert *topoanatomical plasticity* to a variable extent. By entering the habitat of an adjacent population of a different cell type, the cell can adopt the topoanatomical identity of the neighboring cell type by trans-differentiation. The habitat of a pre-determination cell type together with the habitats of adjacent cell types with trans-differentiation potential constitute an anatomically distinct *morphogenetic field* of the developing organism. After determination, the morphogenetic fields of cell types at proceeding states of differentiation correspond to their anatomically distinct habitats. The habitat of the first determined cell type is termed *ontogenetic compartment*, the habitats of its progeny are referred to as *ontogenetic subcompartments*.

The mature tissue derivatives of the morphogenetic fields for each state of the cell type differentiation trajectory from the post-phylotypic state to maturity are mapped to

[1]The following terms have a specific meaning within the paradigm of ontogenetic cancer fields. They are used exclusively in the designated semantic sense throughout the book.

M. Höckel et al., *Cancer Field Surgery in Gynecologic Oncology*,
https://doi.org/10.1007/978-3-031-83030-3

specify the ontogenetic anatomy of a cell type. The mature cell types are proposed to exhibit topoanatomical codes specifying their topoanatomical identity.

Normal and transformed cell type de-differentiation—cancer paradox Disruption of tissue homeostasis in metazoa initiates a canonical repair−regeneration response of the organism that includes local cell type de-differentiation and local and regional Treg cell activation and proliferation. Permanent disruption of tissue homeostasis by uncontrolled proliferating cancer cells (non-healing wound) causes their cell type de-differentiation. This further increases their permissive territory and expands the disruptive area. This vicious circle drives the (epigenetic) process of malignant progression.

Cancer fields—local cancer field model—order of cancer—ontogenetic tumor staging—cancer field surgery Cancer fields are anatomical territories, which are permissive for the colonization (proliferation and migration) of a transformed cell type. The local cancer field model relates them to the mature tissues derived from the morphogenetic fields of the normal cell type, which are mapped by ontogenetic anatomy.

Malignant progression of the cancer cell as stepwise epigenetic de-differentiation of the transformed cell type establishes an order by reversing the hierarchy of the differentiation trajectory of the normal cell type. The decreasing specificity of the topoanatomical identity and increasing plasticity of the cancer cell lead to a successive expansion of the cancer fields in a predictable sequence, the order of cancer.

The cancer field already occupied by tumor cells at the time of diagnosis of the disease indicates the malignant progression expressed as *ontogenetic tumor stage (oT)*. The aim of *cancer field surgery* is the complete resection of the ontogenetic tumor stage-associated cancer field or the wide excision of the tumor within the borders of its cancer field.

Regional cancer field model—peripheral immunological defense lines—first-, second-, third-line lymph nodes—regional cancer field surgery—immunologic defense line-directed lymph node dissection According to the *regional cancer field model*, the potential pattern of lymph node metastasis for a carcinoma of a distinct transformed cell type is deduced from the ontogenetic stage-associated cancer field of the carcinoma and its tumor bed, i.e., the tissue actually colonized by the cancer cells as tributary tissue of the draining lymphatic network. The latter represents distinct peripheral immunological defense lines by intercalated and basin lymph nodes at defined anatomical locations. Consequently, *first-, second-,* and *third-line lymph node regions* are anatomically specified for an individual carcinoma. *Regional cancer field surgery* designated as *immunologic defense line-directed lymph node dissection (iLND)* primarily resects the first-line lymph node region(s). Depending on the metastatic state of the first-line nodes, second- and third-line nodes are removed with the aim of complete regional tumor control without adjuvant radiation.

Anterior cloacal mesenchyme (ACM) Homogenous cell population located between the anterior and anterolateral endoderm of the future cloaca, the cloacal membrane, and the ectoderm of the caudal pole of the embryo as visible at Carnegie stage 11. The ACM cell population cannot be discriminated phenotypically from the adjacent mesenchymal cell type population at that stage.

Splanchnic and somatic coelom mesoderm Corresponds to the splanchnopleuric and somatopleuric mesoderms to designate both the epithelial mesothelial and mesenchymal medial and lateral walls of the lower coelom cavity.

Sinus and suprasinus vagina The sinus vagina is the most caudal subcompartment of the Müllerian system. It is completely encased

by mesenchyme derivatives of the proximal splanchnic ACM. Caudally, it abuts to the vestibulum of the vulva, and cranially it is continuous with the suprasinus subcompartment of the Müllerian system. Together sinus and suprasinus vagina represent the complete organ.

Müllerian adventitia Subserous and subperitoneal tissue mantle encasing the vagina, uterus, and uterine tubes containing blood vessels and fibrous but not fatty tissue.

Vascular mesometrium and mesocolpos Part of the urogenital mesentery derived from proximal splanchnic ACM containing the uterine and vaginal vessels, lymph collectors, and intercalated lymph nodes embedded in fibrofatty tissue. The distal ureter-mesureter complex transgresses the mesometrium-mesocolpos complex dividing it into the supraureteral mesometrium and the infraureteral mesocolpos. Multiple branches of the inferior hypogastric plexus (Frankenhäuser's plexus) radiate into the tissue complex. The urogenital mesentery includes the bladder mesentery with the superior and inferior bladder vessels, lymph collectors, and intercalated lymph nodes.

Ligamentous mesometrium and mesocolpos, peritoneal mesometrium Tissue derivatives of the genital coelom mesoderm. The ligamentous mesometria and mesocolpoi form a dorsally directed horseshoe-shaped fibrous structure that connects the cervical and suprasinus vaginal subcompartment to the rectum shaping the early urorectal pouch. Anteriorly, the bilateral ligamentous mesometria and mesocolpoi are continuous with the vascular mesometria and mesocolpoi. Posteriorly, they extend into the pararectal fascia. Cranially, the ligamentous mesometria transit into the vaginocervical serosa centrally and into the bilateral peritoneal mesometria covered by genital peritoneum.

Phallic urogenital sinus surface Precursor cell type of the vulva compartment in the female covering the external and internal surfaces of the hollow genital tubercle in the sexually indifferent state.

Pubogenitocrural ectoderm Craniolateral skin regions adjacent to the phallic urogenital sinus ectosurface covering the genital swellings, inguinal region, and pubic region.

Dissection and transection Techniques of cancer field surgery designating tissue mobilization along ontogenetic borders (dissection) and cutting through continuous tissue structures (transection).

Anatomical sentinel biospy Relates to the resection of the first-line lymph nodes of a cancer field.

Anatomical reconstruction Designates the surgical restoration of plastic, functional, and sensory aspects.

Vaginal introitus Designates the contact and fusion zone between the vestibulum of the vulva and the sinus vagina corresponding to the hymen.

Paravisceral lymph node region Lymph nodes containing fat pad adjacent to the anterior internal iliac, obturator, internal pudendal vessels, obturator internus muscle, and ventral urogenital mesentery.

Mesenteric and lumbar periaortic lymph node regions Basin lymph nodes from the mesenteric and lumbar lymph sacs. Mesenteric periaortic lymph nodes are mainly located ventral to the abdominal aorta and inferior vena cava and at the infrarenal left side of the aorta. Lumbar periaortic nodes are mainly located dorsal to the large vessels.

General Terms

Metazoa Multicellular animals

Topographic anatomy Depiction of the morphological relationships among the tissue structures in the organism.

Carnegie stages System of 23 chronologic stages of the human embryonic period encompassing the first eight weeks of development.

Fetal period Post-embryonic prenatal period of development in the human.

Early and late fetal periods comprising 9-24 weeks and 25-40 weeks, respectively.

Phylotypic stage/period Developmental stage or period when embryos of different species within a phylum have similar morphologies.

In the human, it corresponds to Carnegie stage 11 indicating the beginning of organogenesis.

Somites Bilateral blocks of paired paraxial mesoderm forming along the craniocaudal axis in the embryogenesis of segmented animals.

In vertebrates, somites give rise to skeletal muscle and other tissues.

Epigenetic states Temporary stable and somatically inheritable states of the cell genome with distinct patterns of gene expression associated with alterations of the 3D genome conformation at multiple scales.

Epigenome Overall epigenetic states of a cell.